

Heteroatom-modified polymer immobilised ionic liquid-stabilised metal nanoparticles: Synthesis and applications

Tom Backhouse



A thesis submitted for the degree of
Doctor of Philosophy in Chemistry

School of Natural and Environmental Sciences

Newcastle University

June 2019

Abstract

The exponentially increasing demand for synthetic commodities has fuelled the development of new methodologies to improve the sustainability of existing chemical processes. The use of robust, scalable and highly efficient catalyst technologies that integrate bioderived feedstock will be crucial to achieve this. In this light, chapter 1 discusses the unique physicochemical properties of ionic liquids (ILs) that have linked them to this goal, their incorporation into functional materials and their applications in metal nanoparticle (NP) catalysed transformations.

Chapter 2 details the synthesis of IL and heteroatom-functionalised polymer supports which were used to support and stabilise PdNPs. Both systems are extremely efficient catalysts for the Suzuki-Miyaura cross-coupling and the TOF of 16,300 h⁻¹ obtained with PdNP@PPh₂-PEGPIILP under mild conditions is the highest reported on comparison with the literature.

Chapter 3 reports that PdNP@PPh₂-PEGPIILP is the most efficient system for the aqueous phase Pd-catalysed hydrogenation of α,β -unsaturated carbonyls. Catalyst modifications revealed that the phosphine, IL and PEG act in a synergistic manner, which is crucial for selectivity.

In chapter 4, tris(*p*-vinylphenyl)phosphine was incorporated into the polymer to limit the Pd-P interaction through extensive cross-linking and thereby increase the surface area for catalysis. These systems were less active than their lightly cross-linked counterparts and were unable to catalyse the hydrogenation of heteroaromatic nitroarenes. Poisoning experiments and FD-XAS analysis indicated that these substrates deactivate the catalyst.

In chapter 5, PIIL-supported AuNPs were shown to be efficient catalysts for the partial reduction of nitroarenes. To this end, AuNP@PPh₂-PEGPIILP catalyses the solvent-dependent selective reduction of nitrobenzene to afford commodity chemicals; *N*-phenylhydroxylamine, azoxybenzene or aniline as the sole product.

Chapter 6 describes a series of heteroatom-functionalised PEGylated PIILP-stabilised RuNPs which are highly efficient catalysts for the selective hydrogenation of model and bioderived carbonyls. The heteroatom donor was crucial for optimum performance, likely due to interfacial electronic effects.

Acknowledgements

First and foremost, I would like to thank Dr Simon Doherty for not just improving my knowledge through efficient day to day supervision, but for inspiring me to learn and gain confidence in my own ability. Your guidance and motivation were pivotal and have driven me to pursue my career in the chemical industry. I would like to thank Julian Knight for giving me a sound and robust knowledge of all things chemistry. The problem sessions were worth it!

I would like to thank my mam and dad (or as what I am led to believe they are called - Jane and Neil), their partners and my grandparents, who never stopped believing in me and supported me in every way possible. I was very fortunate that I was reminded 3-4 times daily that I had a thesis to write. A thankyou is also due to my cats, Jasper and Evie, who despite being my biggest critics, proved to be extremely useful as very early morning battery-free alarms during the write-up process.

To my partner Laura, you have supported me through thick and thin, although unfortunately I'm more on the thicker side at the minute, you never stopped being the driving force to see things through in the face of adversity.

I would also like to give some heart felt recognition to my colleagues from the Doherty and Errington research groups, who became to me what some people would call friends – your encouragement was uplifting throughout my three years in the group. To Phil Layford, Tina Tran and Francesca Stals who witnessed many tantrums and flying objects, but also learnt a few extra words during our time in the lab together. To Kate Phipps, who was instrumental in ensuring I ate my lunch no later than 12 noon every day and who always enjoyed my rendition of John Williams' classic piece - the Jurassic Park theme tune. I would also like to thank past member of the group, Dr Einas Abood, who helped in the early stages of the project as well as Hind, Abdul, Hussam, Nawaf and Nuha.

A further thanks to academic collaborators whose expertise was crucial to this work. Dr Tom Chamberlain and Dr Richard Bourne (Leeds University), for their hard work providing endless materials characterisation (TEM, TGA and DLS) which supported the entire project, and for the use of continuous flow apparatus in chapter 4. Dr Kevin Lovelock, who provided XPS spectra for chapter 5 and Dr David Apperley (Durham University) and Dr Nick Rees (Oxford University), for providing solid state NMR spectra for chapters 2-4, and 5/6, respectively.

Table of Contents

| | |
|--|---------------|
| Chapter 1 Introduction..... | 1 |
| 1.1 Ionic Liquids..... | 1 |
| 1.2 Ionic Liquids in Catalysis..... | 4 |
| 1.2.1 ILs for conversion of biomass..... | 5 |
| 1.2.2 Heteroatom donor functionalised ILs..... | 8 |
| 1.2.3 Ionic liquids in biphasic catalysis – charge tagged ligands (CTLs) and thermoregulated ILs..... | 10 |
| 1.3 Nanoparticles for Catalysis..... | 16 |
| 1.3.1 Nanoparticle synthesis and stabilisation..... | 16 |
| 1.3.2 IL stabilised NPs..... | 22 |
| 1.4 Supported Ionic Liquids..... | 26 |
| 1.4.1 SILP Catalysis..... | 27 |
| 1.5 Polymer Immobilised Ionic Liquid Phase Catalysis..... | 32 |
| 1.6 Project aims..... | 36 |
| 1.7 References..... | 37 |
| Chapter 2 Synthesis of PIILP Materials and Application in the Suzuki-Miyaura Cross Coupling Reaction..... | 41 |
| 2.1 Introduction..... | 41 |
| 2.2 Results and Discussion..... | 43 |
| 2.2.1 Monomer Synthesis..... | 43 |
| 2.2.2 Synthesis and characterisation of PIILs..... | 45 |
| 2.2.3 Synthesis and characterisation of PIIL Supported Palladium Nanoparticles (PdNP@PIILP)..... | 50 |
| 2.3 Application of PIILP-Based Catalysts for Suzuki-Miyaura Cross-Coupling..... | 58 |
| 2.3.1 Preliminary results and catalyst optimisation..... | 59 |
| 2.3.2 Solvent optimisation..... | 60 |
| 2.3.3 Base optimisation..... | 63 |
| 2.3.4 Substrate screening..... | 64 |

| | |
|--|----|
| 2.3.5 Catalyst poisoning and deactivation in the presence of heteroaromatics | 69 |
| 2.3.6 Kinetic studies..... | 70 |
| 2.3.7 Longevity and recycle studies..... | 72 |
| 2.3.8 Probing the nature of the reaction..... | 75 |
| 2.3.9 Comparison with a commercial catalyst..... | 77 |
| 2.4 Conclusion..... | 78 |
| 2.5 References..... | 79 |

Chapter 3 Application of PIILP materials to the selective hydrogenation of α,β - unsaturated aldehydes and ketones.....82

| | |
|--|-----|
| 3.1 Introduction..... | 82 |
| 3.2 Results and Discussion..... | 85 |
| 3.2.1 Comparative catalyst testing..... | 85 |
| 3.2.2 Effect of temperature..... | 88 |
| 3.2.3 Effect of pressure..... | 90 |
| 3.2.4 Effect of base..... | 91 |
| 3.2.5 Catalysis with in-situ generated NPs..... | 94 |
| 3.2.6 Recycling studies..... | 95 |
| 3.2.7 Probing the role of the support functionality..... | 97 |
| 3.2.8 Comparison with commercial catalyst..... | 105 |
| 3.3 Conclusion..... | 106 |
| 3.4 References..... | 107 |

Chapter 4 Application of PIILP Catalysts to the selective reduction of nitroarenes.....109

| | |
|--|-----|
| 4.1 Introduction..... | 109 |
| 4.2 Results and Discussion..... | 112 |
| 4.2.1 Synthesis of highly crosslinked phosphine functionalised PIILPs..... | 112 |
| 4.2.2 Characterisation of highly crosslinked PIILP stabilised PdNPs..... | 114 |

| | |
|--|-----|
| 4.3 Optimisation of the reaction conditions for PdNP@PIILP catalysed hydrogenation of nitroarenes..... | 122 |
| 4.3.1 Substrate screening..... | 125 |
| 4.3.2 Recycling studies..... | 128 |
| 4.3.3 Comparison with other PIILP systems and commercial catalysts..... | 130 |
| 4.4 PdNP@PIILP catalysed transfer hydrogenation of nitroarenes..... | 131 |
| 4.4.1 Reaction optimisation..... | 132 |
| 4.4.2 Towards elucidating the reaction mechanism..... | 135 |
| 4.4.3 Substrate screening..... | 137 |
| 4.4.4 Catalyst deactivation..... | 141 |
| 4.4.5 One pot synthesis of biaryl amines..... | 143 |
| 4.4.6 Transfer hydrogenation in flow..... | 144 |
| 4.5 Conclusion..... | 145 |
| 4.6 References..... | 147 |

| | |
|--|------------|
| Chapter 5 Synthesis of PIILP stabilised gold nanoparticles and application in the selective reduction of nitroarenes..... | 149 |
| 5.1 Introduction..... | 149 |
| 5.2 Results and Discussion..... | 154 |
| 5.2.1 Catalyst synthesis and characterisation..... | 154 |
| 5.3 Initial optimisation..... | 161 |
| 5.3.1 Comparative catalyst testing..... | 164 |
| 5.3.2 Substrate screening..... | 168 |
| 5.4 Optimisation for selective formation of aniline..... | 169 |
| 5.5 Optimisation for the selective formation of azoxybenzene..... | 171 |
| 5.6 Conclusion..... | 175 |
| 5.7 References..... | 178 |

| | |
|---|------------|
| Chapter 6 Synthesis of PIILP-stabilised ruthenium nanoparticles and application in the hydrogenation of bioderived feedstock and model substrates..... | 180 |
| 6.1 Introduction..... | 180 |
| 6.1.1 Aqueous phase ruthenium catalysed hydrogenation..... | 181 |
| 6.1.2 Heteroatom promoted catalysis with electron-rich ruthenium nanoparticles..... | 184 |
| 6.2 Results and discussion..... | 186 |
| 6.3 Catalyst synthesis and characterisation..... | 187 |
| 6.3.1 Monomer synthesis..... | 187 |
| 6.3.2 Immobilisation of RuNPs within PIILP frameworks..... | 188 |
| 6.3.3 Characterisation of RuNP@R-PEGPIILP materials..... | 188 |
| 6.4 Comparative catalyst testing..... | 192 |
| 6.5 Reaction optimisation..... | 193 |
| 6.5.1 Solvent screen..... | 193 |
| 6.5.1 Additive screen..... | 195 |
| 6.5.2 Effect of Pressure..... | 198 |
| 6.5.3 Catalyst comparison..... | 201 |
| 6.5.4 Substrate scope..... | 202 |
| 6.5.5 Catalyst poisoning..... | 208 |
| 6.5.6 Recycling..... | 209 |
| 6.5.7 Complete reduction of acetophenone..... | 212 |
| 6.6 Application of RuNP@R-PIILP catalysts for the hydrogenation of bioderived substrates..... | 213 |
| 6.6.1 PIILP-supported RuNP-catalysed hydrogenation of furfural..... | 213 |
| 6.6.2 Levulinic acid and its ethyl ester..... | 216 |
| 6.7 Conclusion..... | 223 |
| 6.8 Outlook..... | 225 |
| 6.9 References..... | 228 |

| | |
|---|-----|
| Chapter 7 Experimental | 229 |
| 7.1 Chapter 2 experimental..... | 230 |
| 7.1.1 <i>Synthesis of methyl octaethylene glycol chloride (2.1)</i> | 230 |
| 7.1.2 <i>Synthesis of 2-methyl-1-(2,5,8,11,14,17,20,23-octaoxapentacosan-25-yl)-1H-imidazole (2.2)</i> | 230 |
| 7.1.3 <i>Synthesis of 1-bromomethyl-4-vinyl-benzene (2.3)</i> | 231 |
| 7.1.4 <i>Synthesis of 2-methyl-1-(2,5,8,11,14,17,20,23-octaoxapentacosan-25-yl)-3-(4-vinylbenzyl)-1H-3λ4-imidazolium chloride (2.4)</i> | 231 |
| 7.1.5 <i>Synthesis of 1,2-dimethyl-3-(4-vinylbenzyl)-1H-imidazol-3-ium chloride. (2.5)</i> | 231 |
| 7.1.6 <i>Synthesis of 2-methyl-1-(4-vinylbenzyl)-1H-imidazole (2.6)</i> | 232 |
| 7.1.7 <i>Synthesis of 2-methyl-1,3-bis(4-vinylbenzyl)-1H-imidazol-3-ium chloride. (2.7)</i> | 232 |
| 7.1.8 <i>Synthesis of diphenyl(4-vinylphenyl)phosphine (2.8)</i> | 233 |
| 7.1.9 <i>General procedure for polymerisations</i> | 234 |
| 7.1.10 <i>General procedure for impregnation of PIILs with Na₂[PdCl₄]</i> | 234 |
| 7.1.11 <i>General procedure for chemical reduction of [PdCl₄]²⁻ loaded PIILs with NaBH₄</i> | 234 |
| 7.1.12 <i>General procedure for the Suzuki-Miyaura coupling</i> | 235 |
| 7.1.13 <i>General procedure for Suzuki-Miyaura mercury poisoning experiments</i> | 235 |
| 7.1.14 <i>General procedure for Suzuki-Miyaura heteroaromatic poisoning experiments</i> | 235 |
| 7.2 Chapter 3 Experimental..... | 236 |
| 7.2.1 <i>General procedure for the Pd catalysed hydrogenation of α,β-unsaturated aldehydes and ketones</i> | 236 |
| 7.2.2 <i>Synthesis of 1-(4-vinylphenyl)-2,5,8,11,14,17,20,23,26-nonaoxaheptacosane (para-PEG-styrene, for catalysis with modified neutral polymer supports)</i> | 236 |
| 7.2.3 <i>Synthesis of PdNP@PPh₂-PEGPIILP via reduction of PdCl₄@PPh₂-PEGPIILP with hydrogen</i> | 237 |
| 7.3 Chapter 4 experimental..... | 237 |
| 7.3.1 <i>Synthesis of tris(4-vinylphenyl)phosphine</i> | 237 |
| 7.3.2 <i>Synthesis of highly crosslinked polymers 4.2 and 4.3</i> | 238 |
| 7.3.3 <i>General procedure for the catalytic hydrogenation of nitroarenes</i> | 238 |

| | |
|--|-----|
| 7.3.4 General procedure for the catalytic transfer hydrogenation of nitroarenes..... | 239 |
| 7.3.5 Continuous flow reduction of nitrobenzene..... | 239 |
| 7.4 Chapter 5 experimental..... | 240 |
| 7.4.1 General procedure for impregnation of PIIL supports with $K[AuCl_4]$ | 240 |
| 7.4.2 General procedure for the selective transfer hydrogenation of nitroarenes to the corresponding arylhydroxylamine..... | 240 |
| 7.4.3 General procedure for the selective transfer hydrogenation of nitrobenzene to azoxybenzene..... | 240 |
| 7.4.4 General procedure for the selective transfer hydrogenation of nitroarenes to the corresponding arylamines..... | 241 |
| 7.5 Chapter 6 experimental..... | 241 |
| 7.5.1 Synthesis of <i>N</i> -[(4-vinylphenyl)methyl]phthalimide (6.1)..... | 241 |
| 7.5.2 Synthesis of (4-vinylphenyl)methanamine (6.2)..... | 242 |
| 7.5.3 Synthesis of NH_2 -PEGPIILP (6.3)..... | 242 |
| 7.5.4 Synthesis of PEGPIILP (6.4)..... | 242 |
| 7.5.5 General procedure for synthesis of PIIL-stabilised RuNPs..... | 242 |
| 7.5.6 General procedure for the selective hydrogenation of model aldehydes and ketones..... | 243 |
| 7.5.7 General procedure for the hydrogenation of acetophenone to cyclohexylethanol..... | 243 |
| 7.5.8 General procedure for the selective hydrogenation of furfural to furfuryl alcohol..... | 244 |
| 7.5.9 General procedure for the hydrogenation of levulinic acid to γ -valerolactone..... | 244 |
| 7.5.10 General procedure for the hydrogenation of ethyl levulinate to γ -valerolactone..... | 245 |

Appendices

| | |
|---|-----|
| A1 TEM images (a) and the associated particle size distribution (b) of PdNPs generated by the <i>in situ</i> reduction of PdCl ₄ @PPh ₂ -PIILP (2.11) with phenyl boronic acid. Scale bars are 5 nm (white) and 25 nm (black)..... | 249 |
| A2 TEM images (a) and the associated particle size distribution (b) of PdNPs generated from <i>in situ</i> reduction of PdCl ₄ @PPh ₂ -PIILP (2.12) with phenyl boronic acid. Scale bars are 5 nm (white) and 25 nm (black)..... | 249 |
| A3 TGA curve for PPh ₂ PEGstyrene wt% v temperature (green) and (b) derivative wt% v temperature (blue). Heating rate of 10 °C..... | 250 |
| A4 SEM images of PPh ₂ PEGstyrene..... | 250 |
| A5 Solid state ³¹ P NMR spectrum of PPh ₂ PEGstyrene..... | 251 |
| A6 TGA curve for PEGPIILP wt% v temperature (green) and (b) derivative wt% v temperature (blue). Heating rate of 10 °C..... | 251 |
| A7 SEM images of PEGPIILP..... | 252 |
| A8 TGA curve for PPh ₂ styrene wt% v temperature (green) and (b) derivative wt% v temperature (blue). Heating rate of 10 °C..... | 252 |
| A9 SEM images of PPh ₂ styrene..... | 253 |
| A10 Solid state ³¹ P NMR spectrum of PPh ₂ styrene..... | 253 |
| A11 TGA curve for PIILP wt% v temperature (green) and (b) derivative wt% v temperature (blue). Heating rate of 10 °C..... | 254 |
| A12 SEM images of PIILP..... | 254 |
| A13 Pd 3d core level XPS spectrum of [PdCl ₂ (MeCN) ₂]@PPh ₂ PEGstyrene referenced to the hydrocarbon C 1s at 284.8 eV..... | 255 |
| A14 SEM images of [PdCl ₂ (MeCN) ₂]@PPh ₂ PEGstyrene..... | 255 |
| A15 Solid state ³¹ P NMR spectrum of [PdCl ₂ (MeCN) ₂]@PPh ₂ PEGstyrene..... | 256 |
| A16 Pd 3d core level XPS spectrum of [PdCl ₄]@PEGPIILP referenced to the hydrocarbon C 1s at 284.8 eV..... | 256 |
| A17 SEM images of [PdCl ₄]@PEGPIILP..... | 257 |
| A18 Pd 3d core level XPS spectrum of [PdCl ₂ (MeCN) ₂]@PPh ₂ styrene referenced to the hydrocarbon C 1s at 284.8 eV..... | 257 |
| A19 SEM images of [PdCl ₂ (MeCN) ₂]@PPh ₂ styrene..... | 258 |
| A20 Solid state ³¹ P NMR spectrum of [PdCl ₂ (MeCN) ₂]@PPh ₂ styrene..... | 258 |

| | |
|--|-----|
| A21 Pd 3d core level XPS spectrum of [PdCl ₄]@PIILP referenced to the hydrocarbon C 1s at 284.8 eV..... | 259 |
| A22 SEM images of [PdCl ₄]@PIILP..... | 259 |
| A23 Pd 3d core level XPS spectrum of PdNP@PPh ₂ PEGstyrene (2.15) referenced to the hydrocarbon C 1s at 284.8 eV..... | 260 |
| A24 TEM micrographs (a-d) and associated particle size distribution (e) of PdNP@PPh ₂ PEGstyrene (2.15). Scale bars are 25 nm (black) and 5 nm (white)..... | 260 |
| A25 Solid state ³¹ P NMR spectrum of [PdNP]@PPh ₂ PEGstyrene (2.15)..... | 261 |
| A26 SEM images of PdNP@PPh ₂ PEGstyrene (2.15)..... | 261 |
| A27 Pd 3d core level XPS spectrum of PdNP@PEGPIILP (2.16) referenced to the hydrocarbon C 1s at 284.8 eV..... | 262 |
| A28 TEM micrographs (a-d) and the associated particle size distribution (e) of PdNP@PEGPIILP (2.16). Scale bars are 25 nm (black) and 5 nm (white)..... | 262 |
| A29 SEM images of PdNP@PEGPIILP (2.16)..... | 263 |
| A30 Pd 3d core level XPS spectrum of PdNP@PPh ₂ styrene (2.17) referenced to the hydrocarbon C 1s at 284.8 eV..... | 263 |
| A31 TEM micrographs (a-d) and the associated particle size distribution (e) of PdNP@PPh ₂ styrene (2.17). Scale bars are 25 nm (black) and 5 nm (white)..... | 264 |
| A32 Solid state ³¹ P NMR spectrum of [PdNP]@PPh ₂ styrene (2.17)..... | 264 |
| A33 SEM images of PdNP@PPh ₂ styrene (2.17)..... | 265 |
| A34 Pd 3d core level XPS spectrum of PdNP@PIILP (2.18) referenced to the hydrocarbon C 1s at 284.8 eV..... | 265 |
| A35 TEM micrographs (a-d) and the associated particle size distribution (e) of PdNP@PIILP (2.18). Scale bars are 25 nm (black) and 5 nm (white)..... | 266 |
| A36 SEM images of PdNP@PIILP (2.18)..... | 266 |
| A37 XRD spectra of 2.13 - 2.18 | 267 |
| A38 TGA curve for P(Sty) ₃ -PIILP (4.2)..... | 267 |
| A39 SEM images of P(Sty) ₃ -PIILP (4.2)..... | 268 |
| A40 Solution state ³¹ P NMR spectrum of P(Sty) ₃ -PIILP (4.2)..... | 268 |
| A41 TGA curve for P(Sty) ₃ -PEGPIILP (4.3)..... | 269 |
| A42 SEM images of P(Sty) ₃ -PEGPIILP (4.3)..... | 269 |
| A43 Solid state ³¹ P NMR spectrum of P(Sty) ₃ -PEGPIILP (4.3)..... | 270 |
| A44 XRD spectrum for PdNP@P(Sty) ₃ -PIILP (4.6)..... | 270 |

| | |
|---|-----|
| A45 XRD spectrum for PdNP@P(Sty) ₃ -PEGPIILP (4.7)..... | 271 |
| A46 Time-composition profiles for the transfer hydrogenation of nitrobenzene catalysed by 2.13 (top), 4.6 (middle), and 4.7. Reactions conditions: 1 mmol nitrobenzene, 0.047 mol% catalyst, 2.5 mmol NaBH ₄ , RT, 2 mL water..... | 271 |
| A47 N 1s core level XPS spectrum of [AuCl ₄]Cl@PPh ₂ PIILP (5.3) referenced to the hydrocarbon C 1s at 284.8 eV..... | 272 |
| A48 P 2p core level XPS spectrum of [AuCl ₄]Cl@PPh ₂ -PIILP (5.3) referenced to the hydrocarbon C 1s at 284.8 eV..... | 272 |
| A49 SEM images of freshly prepared [AuCl ₄]Cl@PPh ₂ PIILP (5.3)..... | 273 |
| A50 N 1s core level XPS spectrum of [AuCl ₄]Cl@PPh ₂ -PEGPIILP (5.4) referenced to the hydrocarbon C 1s at 284.8 eV..... | 273 |
| A51 P 2p core level XPS spectrum of [AuCl ₄]Cl@PPh ₂ -PEGPIILP (5.4) referenced to the hydrocarbon C 1s at 284.8 eV..... | 274 |
| A52 SEM images of freshly prepared [AuCl ₄]Cl@PPh ₂ -PEGPIILP (5.4)..... | 274 |
| A53 N 1s core level XPS spectrum of [AuCl ₄]Cl@PIILP (5.5) referenced to the hydrocarbon C 1s at 284.8 eV..... | 275 |
| A54 SEM images of freshly prepared [AuCl ₄]Cl@PIILP (5.5)..... | 275 |
| A55 N 1s core level XPS spectrum of [AuCl ₄]Cl@PEGPIILP (5.6) referenced to the hydrocarbon C 1s at 284.8 eV..... | 276 |
| A56 SEM images of freshly prepared [AuCl ₄]Cl@PEGPIILP (5.6)..... | 276 |
| A57 N 1s core level XPS spectrum of AuNP@PPh ₂ -PIILP (5.7) referenced to the hydrocarbon C 1s at 284.8 eV..... | 277 |
| A58 P 2p core level XPS spectrum of AuNP@PPh ₂ -PIILP (5.7) referenced to the hydrocarbon C 1s at 284.8 eV..... | 277 |
| A59 N 1s core level XPS spectrum of AuNP@PEGPPH ₂ -PIILP (5.8) referenced to the hydrocarbon C 1s at 284.8 eV..... | 278 |
| A60 P 2p core level XPS spectrum of AuNP@PPh ₂ -PEGPIILP (5.8) referenced to the hydrocarbon C 1s at 284.8 eV..... | 278 |
| A61 N 1s core level XPS spectrum of AuNP@PIILP (5.9) referenced to the hydrocarbon C 1s at 284.8 eV..... | 279 |
| A62 TEM micrographs (a-d) and the associated particle size distribution (e) and EDX spectrum confirming the presence of Au in AuNP@PIILP (5.9). Scale bars are 25 nm (black) and 5 nm (white)..... | 279 |
| A63 N 1s core level XPS spectrum of AuNP@PEGPIILP (5.10) referenced to the hydrocarbon C 1s at 284.8 eV..... | 280 |

| | |
|--|-----|
| A64 TEM micrographs (a-d) and the associated particle size distribution (e) and EDX spectrum confirming the presence of Au in AuNP@PEGPIILP (5.10). Scale bars are 25 nm (black) and 5 nm (white)..... | 280 |
| A65 TGA curve for NH ₂ -PEGPIILP (6.3)..... | 281 |
| A66 SEM images of NH ₂ -PEGPIILP (6.3)..... | 282 |
| A67 XRD spectrum of RuNP@PPh ₂ -PEGPIILP (6.5)..... | 283 |
| A68 XRD spectrum of RuNP@NH ₂ -PEGPIILP (6.6)..... | 283 |
| A69 XRD spectrum of RuNP@PEGPIILP (6.7)..... | 283 |
| A70 Solid state ¹³ C NMR spectrum of RuNP@PEGPIILP (6.7)..... | 284 |

List of Figures

Chapter 1

Figure 1: Schematic representation of the possible interactions in ILs.

Figure 2: An ionic liquid-organic based biphasic catalysis system.

Figure 3: Representation of the aqueous biphasic thermoreversibility profile for *N,N*-dimethyl-*N*-(*N'*,*N'*-dimethylaminoethyl) ammonium octanoate, PPG and water (orange square is the initial mixture composition).

Figure 4: Different stabilisation methods for nanoparticles.

Figure 5: TEM image and electron-diffraction pattern of Fe₂O₃ nanobars prepared in [omim][BF₄]/DMF (1:1.5). (b) TEM image of Fe₂O₃ nanowires prepared in [omim][BF₄]/DMF (1:3). (c) TEM image of the IONs prepared in [cmim][BF₄]/DMF (1:1.5). (d) TEM image of the IONs prepared in [bmim][BF₄]/DMF (1:1.5). Published by Kim *et al.*

Figure 6: Schematic representation of SILP catalysis.

Figure 7: Schematic representation of different SILP based materials (left to right) immersion method, covalent anchoring method, covalently bound catalyst using anchored method, solid catalyst with ionic liquid layer (SCILL method).

Chapter 2

Figure 8: Solution ¹H NMR spectrum of PPh₂-PEGPIILP in CDCl₃ (left) and PPh₂-PIILP in MeOD (right).

Figure 9: Selected SEM images of freshly prepared PIILPs **2.10** (top) and **2.9** (bottom).

Figure 10: Solid state ³¹P NMR spectrum of **2.10** (left) and **2.9** (right).

Figure 11: TGA/DSC curves for **2.10** (left) and **2.9** (right).

Figure 12: SEM images of PdCl₄@PPh₂-PIILP (top left), PdCl₄@PPh₂-PEGPIILP (top right), PdNP@PPh₂-PIILP (bottom left), PdNP@PPh₂-PEGPIILP (bottom right).

Figure 13: Solid state ³¹P NMR spectrum of PdCl₄@PPh₂-PIILP (top left), PdCl₄@PPh₂-PEGPIILP (top right), PdNP@PPh₂-PIILP (bottom left) and PdNP@PPh₂-PEGPIILP (bottom right).

Figure 14: XPS spectrum of PdCl₄@PPh₂-PIILP (top left), PdCl₄@PPh₂-PEGPIILP (top right), PdNP@PPh₂-PIILP (bottom left) and PdNP@PPh₂-PEGPIILP (bottom right).

Figure 15: HRTEM images of PdNP@PPh₂-PIILP (a-d) and PdNP@PPh₂-PEGPIILP (f-i) with the associated histograms (e and j) showing particle size distribution based on >100 particles. Scale bars are 25 nm (black) and 5 nm (white).

Figure 16: XRD spectra of PdNP@PPh₂-PEGPIILP (top) and PdNP@PPh₂-PIILP (bottom).

Figure 17: a) DLS measurements showing intensity vs. particle size for 1.5 mg of PdCl₄@PPh₂-PEGPIILP in 2.4 mL of water (green), ethanol (red) and a water/ethanol mixture (50:50, blue). b) Depiction of solutions containing 1.5 mg of PdCl₄@PPh₂-PEGPIILP in 2.4 mL of (left to right) near H₂O, H₂O/ethanol (75:25), H₂O/ethanol (50:50), H₂O/ethanol (25:75) and neat ethanol. c) Summary of calculated average aggregate sizes for 1.5 mg of PdCl₄@PPh₂-PEGPIILP in 2.4 mL of water, ethanol and a water/ethanol mixture recorded at 25 °C (average of 10 runs).

Figure 18: Conversion as a function of pyridine addition time. Reaction Conditions: 0.1 mol% catalyst, 1 mmol pyridine, 1 mmol 4-bromoacetophenone, 1.13 mmol phenylboronic acid, 1.2 mmol K₂CO₃, 1.2 mL H₂O, 1.2 mL ethanol, RT, conversion determined by GC with 1 mmol decane std, average of 2 runs.

Figure 19: Time conversion plots for the Pd^(X)@PPh₂-RPIILP catalysed Suzuki-Miyaura cross coupling between 4-bromobenzonitrile and phenylboronic acid.

Figure 20: Time-conversion plot for the Pd^(X)@PPh₂-PEGPIILP catalysed Suzuki-Miyaura cross coupling of 2-bromotoluene and phenylboronic acid.

Figure 21: TEM image of spent PdNP@PPh₂-PEGPIILP isolated after catalysing the Suzuki-Miyaura coupling of 2-bromotoluene and phenylboronic acid, reaction time = 6 hours. Scale bars are 25 nm (black) and 5 nm (white).

Figure 22: Recycling profile for the Suzuki-Miyaura coupling between 4-bromoacetophenone and phenyl boronic acid catalysed by 0.1 mol% **2.14**.

Figure 23: Results of the Hg poisoning study. Reaction Conditions: 0.1 mol% catalyst, mercury (400 eq. to catalyst), 1 mmol 4-bromotoluene, 1.13 mmol phenylboronic acid, 1.2

mmol K_2CO_3 , 1.2 mL EtOH, 1.2 mL H_2O , RT, 6 h, conversion determined by GC with 1 mmol decane std, average of 2 runs.

Figure 24: Results of the reaction dilution study. Reaction Conditions: 0.1 mol% catalyst, 1 mmol 4-bromotoluene, 1.13 mmol phenylboronic acid, 1.2 mmol K_2CO_3 , RT, 6 h, conversion determined by GC with 1 mmol decane std, average of 2 runs.

Chapter 3

Figure 24: Temperature screening of the PdNP@PPh₂-PEGPIILP catalysed hydrogenation of cinnamaldehyde. Reaction conditions: 1 mmol cinnamaldehyde, 0.5 mol% catalyst, 13 mL water, 70 psi H_2 , time = 30 mins. Yields and selectivities determined by 1H NMR spectroscopy and GC analysis using 1,3- dinitrobenzene and *n*-decane as an internal standards respectively. Average of three runs. Selectivity for 3-phenylproprionaldehyde = [% 3-phenylproprionaldehyde / (% 3-phenylproprionaldehyde + % cinnamyl alcohol + % 3-phenyl-1-propanol)].

Figure 25: Temperature screening of the PdNP@PPh₂-PIILP catalysed hydrogenation of cinnamaldehyde. Reaction conditions: 1 mmol cinnamaldehyde, 0.5 mol% catalyst, 13 mL water, 70 psi H_2 , time = 30 mins. Yields and selectivities determined by 1H NMR spectroscopy and GC analysis using 1,3- dinitrobenzene and *n*-decane as an internal standards respectively. Average of three runs. Selectivity for 3-phenylproprionaldehyde = [% 3-phenylproprionaldehyde / (% 3-phenylproprionaldehyde + % cinnamyl alcohol + % 3-phenyl-1-propanol)].

Figure 26: Conversion and selectivity for the PdNP@PPh₂-PEGPIILP catalysed hydrogenation of cinnamaldehyde as a function of equivalents of K_2CO_3 additive. Selectivity for 3-phenylproprionaldehyde = [% 3-phenylproprionaldehyde / (% 3-phenylproprionaldehyde + % cinnamyl alcohol + % 3-phenyl-1-propanol)].

Figure 27: Recycling study for the hydrogenation of cinnamaldehyde catalysed by PdNP@PPh₂-PIILP **2.12** (top) and PdNP@PPh₂-PEGPIILP **2.14** (bottom) accompanied with visual depiction of the extraction procedure demonstrating that **2.14** remains in the aqueous layer and **2.12** sits at the interface. Reaction conditions: 1 mmol cinnamaldehyde, 0.5 mol% catalyst, 10 mol% K_2CO_3 , 13 mL water, 70 psi H_2 , room temperature, reaction time for PdNP@PPh₂-PIILP = 1.25 hours, reaction time for PdNP@PPh₂-PEGPIILP = 45 mins. Yields and selectivities determined by 1H NMR spectroscopy and GC analysis using 1,3-

dinitrobenzene and *n*-decane as an internal standard, respectively. Average of three runs. Selectivity for 3-phenylpropionaldehyde = [% 3-phenylpropionaldehyde / (% 3-phenylpropionaldehyde + % cinnamyl alcohol + % 3-phenyl-1-propanol)].

Figure 288: a) HRTEM micrographs and b) particle size distribution of PdNP@PPh₂-PEGPIILP isolated after 7 runs. Scale bars are 25 nm (black) and 5 nm (white).

Figure 29: Structures of additional PIILP based catalysed synthesised to explore the effect of the PPh₂ and IL moieties.

Figure 30: a-d) HRTEM micrographs and e) particle size distribution of PdNP@PPh₂-PEGStyrene. Scale bars are 25 nm (black) and 5 nm (white).

Figure 31: a-d) HRTEM micrographs and e) particle size distribution of PdNP@PEGPIILP. Scale bars are 5 nm.

Figure 32: Depiction of the cinnamaldehyde adsorption modes on Pd₄ clusters (a and b) and on a flat Pd(111) surface (c and d), with their relative energies reported by Liu *et al.*

Chapter 4

Figure 33: Solid state ³¹P NMR spectrum of **4.6** (top) and **4.7** (bottom). Star indicates signals associated with free phosphine.

Figure 34: XPS spectrum of PdCl₄@P(Sty)₃-PIILP (**4.4**).

Figure 35: XPS spectrum of PdCl₄@P(Sty)₃-PEGPIILP (**4.5**).

Figure 36: XPS spectrum of PdNP@P(Sty)₃-PIILP (**4.6**).

Figure 37: XPS spectrum of PdNP@P(Sty)₃-PEGPIILP (**4.7**).

Figure 38: FD-XAS spectrum showing the Pd L_{III} edges of PdCl₄@PPh₂-PIILP (red), PdCl₄@PPh₂-PEGPIILP (blue), PdCl₄@P(Sty)₃-PIILP (green), PdCl₄@P(Sty)₃-PEGPIILP (yellow) and NaPdCl₄ (purple). Raw data (black) has been included on smoothed lines.

Figure 39: FD-XAS spectrum showing the Pd L_{III} edges of PdNP@PPh₂-PIILP (red), PdNP@PPh₂-PEGPIILP (blue), PdNP@P(Sty)₃-PIILP (green), PdNP@P(Sty)₃-PEGPIILP (yellow) and Pd/C (purple). Raw data (black) has been included on smoothed lines.

Figure 40: TEM images (a-d) and histogram showing particle size distribution (e) of **4.6** based on analysis of >100 particles. Scale bars are 20 nm (black) and 5 nm (white).

Figure 41: TEM images (a-d) and histogram showing particle size distribution (e) of **4.7** based on analysis of >100 particles. Scale bars are 20 nm (black) and 5 nm (white).

Figure 42: Reaction profile as a function of pressure for the **2.14** catalysed hydrogenation of nitrobenzene. Reaction conditions: 1.0 mmol nitrobenzene, 0.47 mol % **2.14**, RT, 13 mL water. Conversion and selectivity determined by ^1H NMR spectroscopy with dioxane as the internal standard. Selectivity for aniline = [% aniline / (% aniline + % *N*-phenylhydroxylamine)].

Figure 43: Recycling profile for the hydrogenation of nitrobenzene catalysed by **2.14**. Reaction conditions: 1 mmol substrate, 0.47 mol % **2.14**, RT, 70 psi H_2 , reaction time = 60 mins.

Figure 44: Recycling profile for the hydrogenation of nitrobenzene catalysed by **4.6**. Reaction conditions: 1 mmol substrate, 0.47 mol % **2.14**, RT, 70 psi H_2 , reaction time = 60 mins.

Figure 45: Conversion and selectivity as a function of the NaBH_4 :substrate ratio for the reduction of nitrobenzene catalysed by **2.14**. Reaction conditions: 1 mmol nitrobenzene, 0.047 mol % **2.14**, 2 mL water, RT reaction time = 2 hours. Yields calculated using ^1H NMR spectroscopy using dioxane as the internal standard and GC analysis using decane as the internal standard, average of minimum 3 runs. Selectivity for aniline = [% aniline / (% aniline + % *N*-phenylhydroxylamine)].

Figure 46: Conversion and selectivity as a function of the NaBH_4 :substrate ratio for the reduction of nitrobenzene catalysed by **2.14**. Reaction conditions: 1 mmol substrate, 0.047 mol % **2.14**, 2 mL water, RT, reaction time = 20 min. Yields calculated using ^1H NMR spectroscopy using dioxane as the internal standard and GC analysis using decane as the internal standard, average of minimum 3 runs. Selectivity for aniline = [% aniline / (% aniline + % *N*-phenylhydroxylamine)].

Figure 47: Conversion-time profile for reduction of nitrobenzene catalysed by 0.047 mol % **2.14** in water in the presence of 2.5 equivalents of NaBH_4 at room temperature.

Figure 48: Conversion-time profile for reduction of nitrobenzene catalysed by 0.047 mol % **2.14** in the presence of 1.0 equivalent of NaBH_4 at room temperature.

Figure 49: HRTEM images of PdNPs formed by *in situ* reduction of **2.12** (a-d), and the associated particle size distribution (e) based on >100 particles. Average particle size = 3.05 ± 0.86 nm. Scale bars are 25 nm (black) and 5 nm (white).

Figure 50: HRTEM images of PdNPs formed by *in situ* reduction of **4.5** (a-d), and the associated particle size distribution (e) based on >100 particles. Average particle size = 2.55 ± 0.97 nm. Scale bars are 25 nm (black) and 5 nm (white).

Figure 51: Conversion-time profile for reduction of nitrobenzene catalysed by 0.047 mol % **2.14** in the presence 1 mmol pyridine using 2.5 equivalents of NaBH₄ at room temperature in water.

Figure 52: FD-XAS spectrum showing the Pd L_{III} edges of PPh₂-PEGPIILP (red), PdCl₄@PPh₂-PEGPIILP (green), PdNP@PPh₂-PEGPIILP (blue) and PdNP@PPh₂-PEGPIILP after treatment with pyridine (orange). Raw data (black) has been included on smoothed lines.

Chapter 5

Figure 53: ³¹P Solid state NMR spectra of **5.3** (left) and **5.4** (right).

Figure 54: Au 4f core level XPS spectra for [AuCl₄]Cl@PPh₂-PIILP (a), [AuCl₄]Cl@PPh₂-PEGPIILP (b), [AuCl₄]Cl@PIILP (c), [AuCl₄]Cl@PEGPIILP (d) all referenced to the C 1s alkyl peak at 284.8 eV.

Figure 55: Au 4f core level XPS spectra for AuNP@PPh₂-PIILP (a), AuNP@PPh₂-PEGPIILP (b), AuNP@PIILP (c), AuNP@PEGPIILP (d) all referenced to the C 1s alkyl peak at 284.8 eV.

Figure 56: HRTEM micrographs with the observed atomic spacing (parallel white lines confirming the presence of metallic Au) of **5.7** (a-b) and **5.8** (d-e), and the associated particle size distributions based on >100 particles. Scale bars are 25 nm (black) and 1 nm (white).

Figure 57: Left: Aqueous solution containing AuNPs left to right: AuNP@Citrate, AuNP@PPh₂-PEGPIILP, AuNP@PPh₂-PIILP, AuNP@PEGPIILP, AuNP@PIILP. Right: combined UV-vis spectra.

Figure 58: Reaction profile as a function of the NaBH₄:substrate ratio for the transfer hydrogenation of nitrobenzene catalysed by **5.7**. Reaction conditions: 1 mmol nitrobenzene, 0.005 mol% **5.7**, 2 mL water, RT, reaction time = 30 mins. Conversion and selectivity determined using ¹H NMR spectroscopy using dioxane as the internal standard. Selectivity

for *N*-phenylhydroxylamine = [% *N*-phenylhydroxylamine / (% *N*-phenylhydroxylamine + % aniline + % azoxybenzene + % azobenzene)]. Average of three runs.

Figure 59: Time-composition profile for the reduction of nitrobenzene to *N*-phenylhydroxylamine catalysed by **5.7**, **5.8** and AuNP@Citrate. Reaction conditions: 1 mmol nitrobenzene, 2.5 mmol NaBH₄, 0.005 mol% catalyst, 2 mL water, RT. Conversion and selectivity determined using ¹H NMR spectroscopy with dioxane as the internal standard. Selectivity for *N*-phenylhydroxylamine = [% *N*-phenylhydroxylamine / (% *N*-phenylhydroxylamine + % aniline + % azoxybenzene + % azobenzene)].

Figure 60: Time-composition profile for the reduction of nitrobenzene catalysed by **5.8**. Reaction conditions: 1 mmol nitrobenzene, 5.0 mmol NaBH₄, 0.005 mol% **5.8**, 2 mL water, 60 °C. Relative composition determined by ¹H NMR spectroscopy using dioxane as the internal standard. Average of three runs. Selectivity for aniline = [% aniline / (% aniline + % *N*-phenylhydroxylamine)].

Figure 61: Time-composition profile for the reduction of nitrobenzene catalysed by **5.7**. Reaction conditions: 1 mmol nitrobenzene, 5.0 mmol NaBH₄, 0.005 mol% **5.7**, 2 mL water, 60 °C. Relative composition determined by ¹H NMR spectroscopy using dioxane as the internal standard. Average of three runs. Selectivity for aniline = [% aniline / (% aniline + % *N*-phenylhydroxylamine)].

Figure 62: Time-composition profile for the reduction of nitrobenzene to azoxybenzene catalysed by 0.005 mol% **5.8**. Reaction conditions: 1 mmol nitrobenzene, 2.5 mmol NaBH₄, 2 mL ethanol, RT. Relative composition determined by ¹H NMR spectroscopy using dioxane as the internal standard. Average of three runs. Selectivity for azoxybenzene = [% azoxybenzene / (% azoxybenzene + % aniline + % *N*-phenylhydroxylamine + % azobenzene)].

Figure 63: ¹H NMR spectra of nitrobenzene (a) and the post reaction mixtures of the reactions catalysed by **5.8** (b-d), showing the reduction products obtained selectively. Reaction conditions are; b) water, 2.5 equivalents NaBH₄, 0.005 mol % catalyst, inert atmosphere, RT, 40 min. c) dry ethanol, 2.5 equivalents NaBH₄, 0.005 mol % catalyst, inert atmosphere, RT, 150 min. d) water 5 equivalents of NaBH₄, 0.005 mol % catalyst, inert atmosphere, 50 °C, 6 hours.

Chapter 6

Figure 64: Schematic demonstration of the production of fuel and platform chemicals from bioderived resources.

Figure 65: (left to right) SEM images of RuNP@PPh₂-PEGPIILP (**5.5**), RuNP@NH₂-PEGPIILP (**5.6**) and RuNP@PEGPIILP (**5.7**).

Figure 66: ¹³C solid state NMR spectrum of NH₂-PEGPIILP (left) and RuNP@NH₂-PEGPIILP (right).

Figure 67: ³¹P solid state NMR spectrum of PPh₂-PEGPIILP (left) and RuNP@PPh₂-PEGPIILP (right).

Figure 68: HRTEM images of a) RuNP@NH₂-PEGPIILP **6.6**, b) RuNP@PPh₂-PEGPIILP **6.5**, and c) RuNP@PEGPIILP **6.7**. Average particle sizes of 1.0 ± 0.2 nm, 2.2 ± 0.6 nm and 1.5 ± 0.4 nm were determined based on >100 particles for a), b) and c) respectively. Scale bars are 25 nm (black) and 5 nm (white).

Figure 69: Conversion and selectivity for the hydrogenation of acetophenone as a function of solvent. Reaction conditions: 1 mmol acetophenone, 0.1 mol% RuNP@PPh₂-PEGPIILP (**6.5**), 70 psi H₂, 50°C, 13 mL solvent, reaction time = 3 hours. Conversion and selectivity determined by ¹H NMR spectroscopy with 1,3-dinitrobenzene as the internal standard. Selectivity for 1-phenylethanol = [% 1-phenylethanol / (% 1-phenylethanol + % cyclohexylethanol)].

Figure 70: Conversion and selectivity for the hydrogenation of acetophenone as a function of solvent. Reaction conditions: 1 mmol acetophenone, 0.1 mol% RuNP@NH₂-PEGPIILP (**6.6**), 70 psi H₂, 50°C, 13 mL solvent, reaction time = 3 hours. Conversion and selectivity determined by ¹H NMR spectroscopy with 1,3-dinitrobenzene as the internal standard. Selectivity for 1-phenylethanol = [% 1-phenylethanol / (% 1-phenylethanol + % cyclohexylethanol)].

Figure 71: Reaction conditions: 1 mmol acetophenone, 0.1 mol% RuNP@PPh₂-PEGPIILP, 0.1 mmol additive, 13 mL water, 50°C, 70 psi H₂, reaction time = 3 hours. Conversion and selectivity determined by ¹H NMR spectroscopy with 1,3-dinitrobenzene as the internal standard. Selectivity for 1-phenylethanol = [% 1-phenylethanol / (% 1-phenylethanol + % cyclohexylethanol)].

Figure 72: Reaction conditions: 1 mmol acetophenone, 0.1 mol% RuNP@NH₂-PEGPIILP, 0.1 mmol additive, 13 mL water, 50°C, 70 psi H₂, reaction time = 3 hours. Conversion and selectivity determined by ¹H NMR spectroscopy with 1,3-dinitrobenzene as the internal standard. Selectivity for 1-phenylethanol = [% 1-phenylethanol / (% 1-phenylethanol + % cyclohexylethanol)].

Figure 73: Conversion and selectivity for the hydrogenation of acetophenone catalysed by **6.5** in the presence of varying amounts of K₂CO₃. Reaction conditions: 1 mmol acetophenone, 0.1 mol% RuNP@PPh₂-PEGPIILP (**6.5**), 13 mL water, 50°C, 70 psi H₂, reaction time = 3 hours. Conversion and selectivity determined by ¹H NMR spectroscopy with 1,3-dinitrobenzene as the internal standard. Selectivity for 1-phenylethanol = [% 1-phenylethanol / (% 1-phenylethanol + % cyclohexylethanol)].

Figure 74: Conversion and selectivity for the hydrogenation of acetophenone catalysed by **6.5** in the presence of varying amounts of K₂CO₃. Reaction conditions: 1 mmol acetophenone, 0.1 mol% RuNP@NH₂-PEGPIILP (**6.6**), 13 mL water, 50°C, 70 psi H₂, reaction time = 3 hours. Conversion and selectivity determined by ¹H NMR spectroscopy with 1,3-dinitrobenzene as the internal standard. Selectivity for 1-phenylethanol = [% 1-phenylethanol / (% 1-phenylethanol + % cyclohexylethanol)].

Figure 75: Conversion and selectivity for the hydrogenation of acetophenone as a function of hydrogen pressure. Reaction conditions: 1 mmol acetophenone, 0.1 mol% RuNP@PPh₂-PEGPIILP (**6.5**), 0.1 mmol K₂CO₃, 13 mL water, 50°C, reaction time = 45 mins. Conversion and selectivity determined by ¹H NMR spectroscopy with 1,3-dinitrobenzene as the internal standard. Selectivity for 1-phenylethanol = [% 1-phenylethanol / (% 1-phenylethanol + % cyclohexylethanol)].

Figure 76: Conversion and selectivity for the hydrogenation of acetophenone as a function of hydrogen pressure. Reaction conditions: 1 mmol acetophenone, 0.1 mol% RuNP@NH₂-PEGPIILP (**6.6**), 0.1 mmol K₂CO₃, 13 mL water, 50°C, reaction time = 45 mins. Conversion and selectivity determined by ¹H NMR spectroscopy with 1,3-dinitrobenzene as the internal standard. Selectivity for 1-phenylethanol = [% 1-phenylethanol / (% 1-phenylethanol + % cyclohexylethanol)].

Figure 77: Recycling profile for the hydrogenation of benzaldehyde catalysed by **6.5**. Reaction conditions: 1 mmol substrate, 0.1 mol % RuNP@PPh₂-PEGPIILP, 0.1 mmol K₂CO₃, 13

mL water, 50°C, 70 psi H₂, reaction time = 90 mins. Conversion and selectivity determined by ¹H NMR spectroscopy with 1,3-dinitrobenzene as the internal standard. Selectivity for benzyl alcohol = [% benzyl alcohol / (% benzyl alcohol+ % other products)].

Figure 78: Recycling profile for the hydrogenation of benzaldehyde catalysed by **6.6**.

Reaction conditions: 1 mmol substrate, 0.1 mol % RuNP@NH₂-PEGPIILP, 0.1 mmol K₂CO₃, 13 mL water, 50°C, 70 psi H₂, reaction time = 90 mins. Conversion and selectivity determined by ¹H NMR spectroscopy with 1,3-dinitrobenzene as the internal standard. Selectivity for benzyl alcohol = [% benzyl alcohol / (% benzyl alcohol+ % other products)].

Figure 79: Conversion and selectivity for the hydrogenation of furfural as a function of pressure. Reaction conditions: 1 mmol substrate, 0.1 mol % RuNP@PPh₂-PEGPIILP, 13 mL water, 50°C, reaction time = 90 mins. ^b Conversion and selectivity determined by ¹H NMR spectroscopy with 1,3-dinitrobenzene as the internal standard. Selectivity for furfuryl alcohol = [% furfuryl alcohol / (% furfuryl alcohol+ % tetrahydrofurfuryl alcohol)].

Figure 80: Product distribution for the hydrogenation of levulinic acid catalysed by 0.1 mol% **6.5** as a function of time. Reaction conditions: 1 mmol substrate, 0.1 mol % catalyst, 13 mL water, 110°C, 420 psi H₂. Conversion and selectivity determined by ¹H NMR spectroscopy with 1,3-dinitrobenzene as the internal standard.

Figure 81: Product distribution for the hydrogenation of levulinic acid catalysed by 0.1 mol% **6.5** with base additive as a function of time. Reaction conditions: 1 mmol substrate, 0.1 mol % catalyst, 0.1 mmol K₂CO₃, 13 mL water, 110°C, 420 psi H₂. Conversion and selectivity determined by ¹H NMR spectroscopy with 1,3-dinitrobenzene as the internal standard.

Figure 82: Product distribution for the hydrogenation of ethyl levulinate catalysed by **6.5** with base additive as a function of time. Reaction conditions: 1 mmol substrate, 0.1 mol % catalyst, 0.1 mmol K₂CO₃, 13 mL water, 110°C, 420 psi H₂. Conversion and selectivity determined by ¹H NMR spectroscopy with 1,3-dinitrobenzene as the internal standard.

Figure 83: Product distribution for the hydrogenation of levulinic acid catalysed by 0.1 mol % **6.5** in the absence of base additive as a function of time. Reaction conditions: 1 mmol substrate, 0.1 mol % catalyst, 13 mL water, 110°C, 420 psi H₂. Conversion and selectivity determined by ¹H NMR spectroscopy with 1,3-dinitrobenzene as the internal standard.

List of Tables

Chapter 1

Table 1: IL stabilised RuNP catalysed hydrogenation of bioderived compounds Reaction conditions: Ru@[C₁₂MIM][BTA], 2 h, 120°C 120 bar; c(Ru) = 0.05 mol L⁻¹. Ru/substrate ratio 1:100.

Chapter 2

Table 2: Pd content of PIILP materials as determined by ICP-OES.

Table 3: Optimisation for the PdNP@PIILP catalysed Suzuki-Miyaura cross-coupling between 4-bromoacetophenone and phenylboronic acid.

Table 4: Optimisation of the water/ethanol ratio.

Table 5: Optimisation of the base for PdNP@PIILP catalysed Suzuki-Miyaura cross coupling between 4-bromoacetophenone and phenylboronic acid.

Table 6: Substrate screening for the PdNP@PIILP catalysed Suzuki-Miyaura cross coupling reaction.

Table 7: Comparative catalyst testing with commercially available catalysts for the Suzuki-Miyaura couplings of aryl bromides with phenyl boronic acid.

Chapter 3

Table 8: Optimisation of the reaction solvent for the PdNP@PIILP catalysed hydrogenation of cinnamaldehyde. NB analysis of the reaction mixture gave no evidence of the formation of cinnamyl alcohol.

Table 9: Hydrogenation of cinnamaldehyde to 3-phenylproprionaldehyde catalysed by **2.14** prepared *via* hydrogen reduction or chemical reduction with NaBH₄.

Table 10: Effect of pressure on the hydrogenation of cinnamaldehyde.

Table 11: Optimisation of base additive for the Pd catalysed hydrogenation of cinnamaldehyde.

Table 12: hydrogenation of cinnamaldehyde catalysed by PdNPs formed *in situ* from PdCl₄@PPh₂-PEGPIILP.

Table 13: hydrogenation of cinnamalehyde catalysed by PdNPs supported on a range of functionalised polymeric supports.

Table 14: Hydrogenation of cinnamalehyde catalysed PdNPs supported on a range of functionalised polymeric supports in the absence of base.

Table 15: Hydrogenation of a series of α,β -unsaturated aldehydes and ketones catalysed by **2.14**.

Table 16: Comparison of different catalyst systems for the hydrogenation of cinnamaldehyde to 3-phenylpropionaldehyde.

Chapter 4

Table 17: Pd content of PIILP catalysts as determined by ICP-OES.

Table 18: Average particles sizes of PIILP supported PdNPs determined by measuring >100 particles.

Table 19: Optimisation of the reaction solvent for the PdNP@PIILP catalysed hydrogenation of nitrobenzene.

Table 20: Hydrogenation of various substituted nitroarenes and heteroaromatic nitros catalysed by 2.14.

Table 21: Comparison of modified PdNP@PIILP catalysts and Pd/C to determine the influence of support functionality.

Table 22: Optimisation of the reaction conditions for the Pd catalysed NaBH₄ mediated transfer hydrogenation of nitrobenzene.

Table 23: Comparison of different PIILP catalyst systems for the transfer hydrogenation of nitrobenzene using *in situ* and *ex situ* generated PdNPs.

Chapter 5

Table 24: Gold loading of PIILP catalysts as determined by ICP-OES.

Table 25: Au 4f core level binding energies for [AuCl₄]⁻ loaded precursors and reduced catalysts relative to the C1s alkyl peak at 248.8 eV.

Table 26: Optimisation of the reaction conditions for the Au catalysed reduction of nitrobenzene.

Table 27: Comparison catalyst testing for the reduction of nitrobenzene to *N*-phenylhydroxylamine.

Table 28: Reduction of selected nitroarenes to the corresponding *N*-phenylhydroxylamines catalysed by **5.8**.

Table 29: Reduction of selected nitroarenes to the corresponding anilines catalysed by **5.8**.

Table 30: Optimisation of the relative ethanol/water content for the selective reduction of nitrobenzene to azoxybenzene catalysed by **5.8**.

Chapter 6

Table 31: Comparison of different metal phases for the hydrogenation of propanal.

Table 32: Ruthenium content of PIILP catalysts as determined by ICP-OES.

Table 33: Effect of H₂ pressure on selectivity for the 6.5 catalysed hydrogenation of acetophenone to 1-phenylethanol at high conversion.

Table 34: Comparison of catalysts for the Ru catalysed hydrogenation of acetophenone to 1-phenylethanol.

Table 35: Selective hydrogenation of aromatic and heteroaromatic ketones and aldehydes catalysed by PIILP supported RuNPs.

Table 36: Hydrogenation of further aromatic aldehydes and ketones catalysed by 6.5.

Table 37: Results of catalyst poisoning studies for the hydrogenation of acetophenone and benzaldehyde in the presence of amines and nitriles.

Table 38: Comparison of Ru catalysts for the selectivity hydrogenation of acetophenone to 1-cyclohexylethanol.

Table 39: Optimisation of the reaction parameters for the selective hydrogenation of furfural to furfuryl alcohol catalysed by **6.5**.

Table 40: Results of the Ru catalysed hydrogenation of levulinic acid.

Table 41: Results of the Ru catalysed hydrogenation of ethyl levulinate.

List of Schemes

Chapter 1

Scheme 1: A selection of common IL cations and anions a) imidazolium, b)pyrrolidinium, c) pyridinium, d) ammonium, e) phosphonium, f) sulfonium, g) halide, h) dicyanamide, i) tetrafluoroborate, j) hexafluorophosphate, k) alkylsulfate, l) thiocyanate.

Scheme 1: Structure of 1st, 2nd and 3rd generation ionic liquids.

Scheme 2: Synthesis of IL stabilised RuNPs used as catalysts for the hydrogenation of bioderived aldehydes and ketones.

Scheme 3: Proposed mechanism for the IL assisted Ru catalysed hydrogenation of CO₂ yielding formic acid.

Scheme 4: Tuneable behaviour of PFIL stabilised ruthenium nanoparticle catalysts.

Scheme 5: Ionic tagged phosphine ligands synthesised by Dupont *et al.*

Scheme 6: Charge tagged triphenylphosphine ligand synthesised by Williams *et al.* for the Pd catalysed Heck reaction in aqueous/IL media.

Scheme 7: the Ostwald ripening process for nanoparticles.

Scheme 8: Method for synthesising small ligand stabilised metal nanoparticles.

Scheme 9: Schematic representation of the ligand effect of trialkyl phosphines explored by Chaudret *et al.*

Scheme 10: PdNPs encapsulated within amino functionalised graphene oxide nanosheet layers as an efficient catalyst for the Suzuki cross coupling developed by Wang.

Scheme 11: Bifunctional catalyst comprised of RuNPs immobilised on acidic imidazolium functionalised silica developed by Leitner and Luska for the hydrodeoxygenation of phenols.

Scheme 12: Switchable selectivity in the Selective hydrogenation of a bioderived furan using Ru and FeRuNP catalysts.

Scheme 13: General synthetic protocol for the preparation of PIIL stabilised NPs.

Scheme 14: Peroxometallate PIILP catalyst developed by Doherty/Knight group for epoxidation of allylic alcohols and oxidation of sulphides.

Chapter 2

Scheme 16: Pd catalysed carbon-carbon bond forming cross coupling reactions (X = Cl, Br or I).

Scheme 17: Representation of various functions in PIILP materials.

Scheme 18: Target monomers; a hydrophilic PEGylated imidazolium monomer (**2.4**), dimethylimidazolium monomer (**2.5**), phosphino functionalised monomer (**2.8**) and dibenzylimidazolium crosslinking monomer (**2.7**).

Scheme 19: Synthesis of PEGylated hydrophilic monomer **2.4**.

Scheme 20: Synthesis of monomer **2.5** and cationic crosslinker **2.7**.

Scheme 21: Synthesis of phosphine functionalised monomer **2.8**.

Scheme 22: Synthesis of PPh₂ functionalised PIILPs via AIBN initiated free radical polymerisation.

Scheme 23: Synthetic route used for impregnation of PIILP materials with [PdCl₄]²⁻ and reduction to NPs with NaBH₄.

Scheme 24: Catalytic cycle involving both homogeneous and heterogeneous pathways for the palladium catalysed Suzuki-Miyaura cross coupling reaction.

Scheme 25: **2.14** catalysed Suzuki-Miyaura cross-coupling reaction between 2-bromotoluene and phenylboronic acid in the presence of pyridine.

Scheme 26: Suzuki-Miyaura cross coupling reaction between 4-bromobenzonitrile and phenylboronic acid catalysed by **2.14**.

Scheme 27: Suzuki-Miyaura cross coupling between 4-bromoacetophenone and phenylboronic acid at reduced catalyst loading.

Scheme 28: Suzuki-Miyaura cross coupling between 2-bromotoluene and phenylboronic acid catalysed by **2.12** or **2.14**.

Chapter 3

Scheme 29: General mechanism for the hydrogenation of alkenes over heterogeneous Pd catalysts.

Scheme 30: PdNPs supported on propylamine functionalised silica developed by Rossi *et al.*

Scheme 31: Possible products of the Pd catalysed hydrogenation of *trans*-cinnamaldehyde.

Scheme 32: General scheme for investigating the effect of temperature on the PdNP@PIILP catalysed hydrogenation of cinnamaldehyde.

Scheme 33: Schematic representation of the suggested roles of PIILP modifications.

Scheme 34: Efficacy of PdNP@PPh₂-PEGPIILP on comparison with commercially available Pd/C.

Chapter 4

Scheme 35: Direct (a) and condensation (b) reaction pathways for the reduction of nitrobenzene to aniline.

Scheme 36: Strategy developed by Lipschutz *et al.* for the safe and selective reduction of nitroarenes.

Scheme 37: Synthesis of monomer **4.1**.

Scheme 38: Composition of PIIL supports.

Scheme 39: Reaction conditions for optimisation of the hydrogen pressure.

Scheme 40: Activation of hydrogen over PdNPs supported on phosphine functionalised PIILPs and different reaction pathways for the **2.14** catalysed reduction of nitrobenzene according to the Haber mechanism showing their dependency on the NaBH₄:substrate ratio.

Scheme 41: One-pot tandem Suzuki-Miyaura cross-coupling hydrogenation sequence for the synthesis of biaryl amines catalysed by **2.14**.

Scheme 42: Continuous flow set up for the transfer hydrogenation of nitrobenzene catalysed by **2.14**.

Scheme 43: Summary of results for the hydrogenation and transfer hydrogenation of nitroarenes catalysed by **2.14**.

Chapter 5

Scheme 44: Schematic representation of AuNPs supported on anatase edges for the chemoselective hydrogenation of nitroarenes.

Scheme 45: Two-step one-pot method for obtaining azoxybenzene with an Au/TiO₂ catalyst.

Scheme 46: Three possible products obtainable from the reduction of substituted nitrobenzenes over mesoporous ceria supported AuNPs.

Scheme 47: Composition of polymers **2.9** and **2.10**, preparation of [AuCl₄][−] loaded catalyst precursors and PIILP-stabilised AuNPs.

Scheme 48: Product distribution for the transfer hydrogenation of nitrobenzene catalysed by **5.7** in air.

Scheme 49: Product distribution for the transfer hydrogenation of nitrobenzene catalysed by **5.7** under an N₂ atmosphere.

Scheme 50: Addition of water to a solution of azoxybenzene in water resulting in no reaction.

Scheme 51: Formation of two equivalents of *N*-phenylhydroxylamine *via* hydrolysis of azoxybenzene and reduction of nitrosobenzene.

Scheme 52: Differences in the Pd and Au catalysed reduction of nitroarenes.

Chapter 6

Scheme 53: Stepwise deoxygenation of glucose yielding potential biofuel DMF.

Scheme 54: Isotopic labelling experiments demonstrating the incorporation of deuterium into gamma valerolactone.

Scheme 55: Hydrogenation of levulinic acid to γ -valerolactone catalysed by *i*-Ru–NH₂– γ -Al₂O₃.

Scheme 56: Synthesis of 4-(vinylphenyl)methanamine **6.2**.

Scheme 57: Synthesis and schematic representation of RuNP@R-PEGPIILP catalysts.

Scheme 58: Possible products from the hydrogenation of acetophenone.

Scheme 59: Catalyst screening of base and Lewis acid additives for the selective hydrogenation of acetophenone.

Scheme 60: Reaction scheme for the hydrogenation of acetophenone with varied hydrogen pressure

Scheme 61: Products of the Ru catalysed hydrogenation of furfural.

Scheme 62: Possible products of the Ru catalysed hydrogenation of levulinic acid.

Scheme 63: Products of the Ru catalysed hydrogenation of ethyl levulinate.

List of symbols and abbreviations

| | |
|----------------|---|
| AIBN | Azobisisobutyronitrile |
| BET | Brunauer-Emmett-Teller |
| CNT | carbon nanotubes |
| DLS | Dynamic light scattering |
| DRIFTS | Diffuse Reflectance Infrared Fourier Transform Spectroscopy Analysis. |
| DSC | Differential Scanning Calorimetry |
| DVB | divinylbenzene |
| ee | enantiomeric excess |
| FD-XAS | Fluorescence Detected X-ray Absorption Spectroscopy |
| FT-IR | Fourier Transform InfraRed |
| ICP-OES | Inductively Coupled Plasma Optical Emission Spectrometry |
| IL | Ionic liquid |
| NHC | <i>N</i> -heterocyclic carbene |
| NMR | Nuclear magnetic resonance |
| NP | nanoparticle |
| PEG | polyethylene glycol |
| PIIL | Polymer-Immobilised Ionic Liquid |
| PIILP | Polymer-Immobilised Ionic Liquid Phase |
| PIL | polyionic liquid |
| ppm | parts per million |
| PS | polystyrene |
| RAFT | Reversible addition-fragmentation chain-transfer |
| ROMP | Ring-Opening Metathesis Polymerisation |
| SCILL | Solid Catalyst with Ionic Liquid Layer |
| SEM | Scanning Electron Microscopy |
| SILP | Supported Ionic Liquid Phase |
| TEM | Transmission Electron Microscopy |
| TGA | Thermal Gravimetric Analysis |
| TOF | turnover frequency |
| TON | turnover number |
| Triflate (OTf) | trifluoromethanesulfonate |

| | |
|------|----------------------------------|
| TSIL | Task specific ionic liquid |
| XAS | X-ray Absorption Spectroscopy |
| XPS | X-ray Photoelectron Spectroscopy |
| XRD | X-ray Diffraction |

Publications

S. Doherty, J. G. Knight, M. A. Carroll, A. R. Clemmet, J. R. Ellison, **T. Backhouse**, N. Holmes, L. A. Thompson and R. A. Bourne "Efficient and selective oxidation of sulfides in batch and continuous flow using styrene-based polymer immobilised ionic liquid phase supported peroxotungstates", *RSC Adv.*, 2016, **6**, 73118-73131.

S. Doherty, J. G. Knight, **T. Backhouse**, E. Abood, H. Alshaikh, I. J. S. Fairlamb, R. A. Bourne, T. W. Chamberlain and R. Stones "Highly efficient aqueous phase chemoselective hydrogenation of α,β -unsaturated aldehydes catalysed by phosphine-decorated polymer immobilized IL-stabilized PdNPs" *Green Chem.*, 2017, **19**, 1635-1641.

S. Doherty, J. G. Knight, **T. Backhouse**, A. Bradford, F. Saunders, R. A. Bourne, T. W. Chamberlain, R. Stones, A. Clayton and K. Lovelock "Highly efficient aqueous phase reduction of nitroarenes catalyzed by phosphine-decorated polymer immobilized ionic liquid stabilized PdNPs" *Catal. Sci Technol.*, 2018, **8**, 1454-1467.

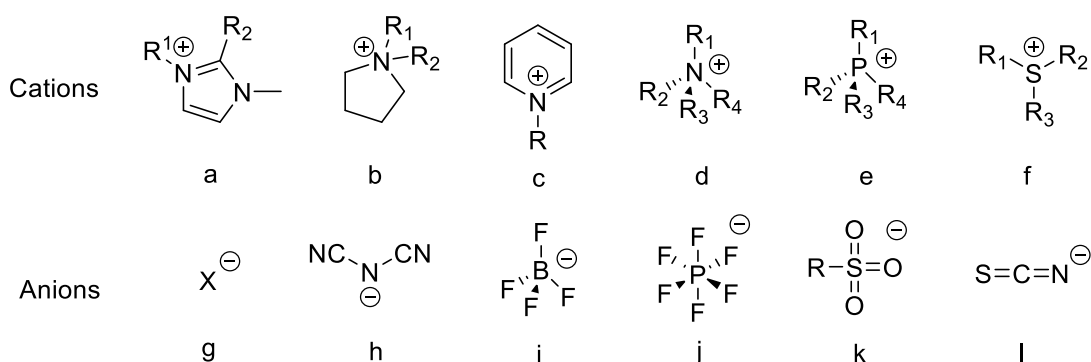
S. Doherty, J. G. Knight, **T. Backhouse**, E. Abood, H. Al-shaikh, A. R. Clemmet, J. R. Ellison, R. A. Bourne, T. W. Chamberlain, R. Stones, N. J. Warren, I. J. S. Fairlamb and K. R. J. Lovelock "Heteroatom Donor-Decorated Polymer-Immobilized Ionic Liquid Stabilized Palladium Nanoparticles: Efficient Catalysts for Room-Temperature Suzuki-Miyaura Cross-Coupling in Aqueous Media" *Adv. Synth. Catal.*, 2018, **360**, 3716-3731.

S. Doherty, J. G. Knight, **T. Backhouse**, R.J. Summers, E. A. Abood, W. Simpson, W. Paget, R.A. Bourne, T. W. Chamberlain, R. Stones, K. R. J. Lovelock, J.M. Seymour, M.A. Isaacs, C. Hardacre, H. Daly, N.H. Rees, "Highly Selective and Solvent-Dependent Reduction of Nitrobenzene to *N*-Phenylhydroxylamine, Azoxybenzene and Aniline Catalyzed by Phosphino-Modified Polymer Immobilised Ionic Liquid-Stabilized AuNPs" *ACS Catal.*, 2019, **9**, 4777-4791.

Chapter 1 Introduction

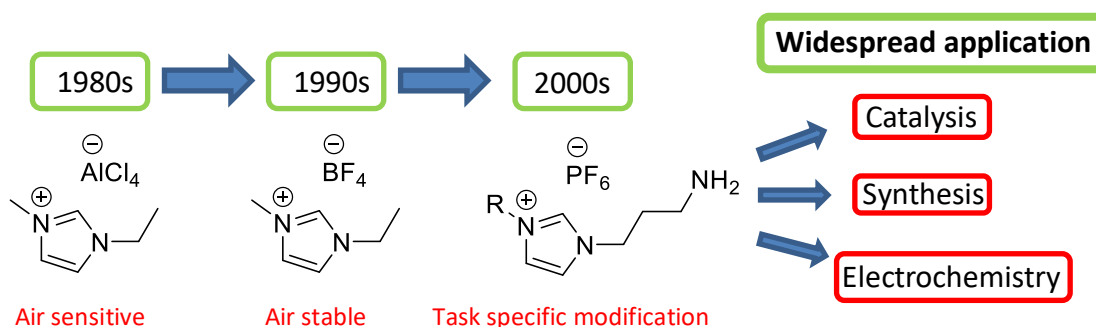
1.1 Ionic Liquids

Ionic liquids (ILs) are defined as compounds comprised entirely of ions that due to their tendency to form weakly coordinating ion pairs, exhibit a low lattice energy and therefore a low melting point, conventionally below 100°C.¹ The intriguing physicochemical properties of ILs such as polarity, viscosity, hydrophobicity and density have afforded a wealth of research throughout the academic literature in recent years due to the fact that these fundamental properties may be finely tuned, fuelling a range of scientific curiosities.¹⁻³ Furthermore, owing to their high ionic conductivity, thermal stability and broad electrochemical window, ILs can easily be modulated to possess finite properties to optimise their performance in many different chemical applications.⁴ Through virtue of their organic composition, there is huge scope for synthetic functionalisation of these dynamic fluids, including the design of ILs that are miscible with organic/aqueous solution providing the ability to form unique ionic microenvironments. Moreover, ILs have been referred to as potential 'green' alternatives to conventional organic solvents due to their ability to solvate a wide range of compounds as well as their low volatility and non-flammability.⁵ The most commonly used ILs are based on the dialkylimidazolium cation due to their lower viscosity, stability to oxidative and reductive reaction conditions as well as their facile derivatisation. However, the field is rapidly expanding, and more recent work has utilised combinations of a range of anions and cations; a selection of some common ions is shown in Scheme 1.



Scheme 1: A selection of common IL cations and anions a) imidazolium, b) pyrrolidinium, c) pyridinium, d) ammonium, e) phosphonium, f) sulfonium, g) halide, h) dicyanamide, i) tetrafluoroborate, j) hexafluorophosphate, k) alkylsulfate, l) thiocyanate.⁶

It is now widely acknowledged that Walden's observations on the interesting physical properties of ethylammonium nitrate (mp, 13-14°C) in 1914 was the first ever reported ionic liquid.⁷ Despite this, the emergence of modern ILs began with the pioneering work conducted on 'first generation' ILs based on 1-alkyl-3-methylimidazolium salts bearing the moisture sensitive tetrachloroaluminate anion.⁸ The same group 10 years later developed air-stable second generation ILs by replacement of the tetrachloroaluminate anion with the hydrolytically more stable tetrafluoroborate anion.⁹ The ease of handling these substances has fuelled their application as reaction media for a range of organic and inorganic transformations and paved the way for the introduction of third generation 'task specific' ionic liquids (TSILs); much of the early work in this area was conducted by Davis who developed amine functionalised ILs with applications in the separation of organic compounds and catalysis.¹⁰ Since then, significant progress in the area has allowed the application of ILs to spread over a range of chemical and biological disciplines (Scheme 2).¹¹



Scheme 2: Structure of 1st, 2nd and 3rd generation ionic liquids.

Since the development of stable ILs, there has been a great deal of reports published describing the application of imidazolium-based ILs as green solvents for catalysis.¹² The interest in ILs as 'green' solvents is derived from their low vapour pressure and high thermal stability in comparison to conventional organic solvents. These properties not only allow for safe storage of the IL, but also facilitate separation of product, recovery of the catalyst and recycling of the solvent. Because ILs are composed completely of ions, they possess unique solvent-solute and solvent-catalyst interactions in the IL microphase. By judicious selection of the anion and cation, ILs have been shown to enhance reaction rates and play a positive role in the reaction by stabilizing reactive catalytic species or intermediates, which has led to unprecedented enhancements in reaction selectivity.¹³

Whilst most ionic compounds are extremely polar, ILs exhibit only moderate polarity due to their largely organic composition with dielectric constants ranging from 8-15. Interestingly,

this parameter appears to be largely dependent on the nature of the anion, with the general trend of $[\text{OTf}]^- > [\text{BF}_4]^- > [\text{PF}_6]^-$.¹⁴ Whilst the dielectric constant is a well-established quantitative method of measuring polarity, the fact that ILs can solvate a broad range of organic and inorganic species suggests that there are many other factors that influence the nature of the solvent-solute interactions. Therefore, as previously discussed, it should be possible to modify ILs to optimise interactions between the IL and solute for use as designer reaction media. Modern scientific technologies have enabled researchers to study the complex nature of ILs which have shown that the intriguing bulk material properties are dictated through many synergistic intermolecular interactions. For example, considering the common dialkylimidazolium-based ILs as a model, many interactions are possible such as van der Waals forces, through incorporating hydrophobic alkyl chains, hydrogen bonding through the imidazolium aromatic protons, π -stacking through the aromatic ring as well as various other coulombic interactions details of which are depicted in Figure 1.¹⁵

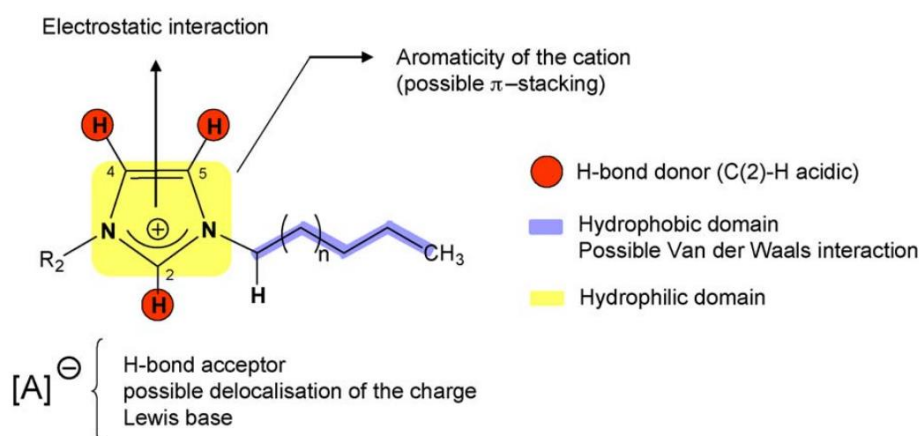


Figure 1: Schematic representation of the possible interactions in ILs.¹⁵

One of the key differences between ILs and conventional organic solvents is that the dominant attractive intermolecular forces in molecular liquids are either van der Waals, dipolar or hydrogen bonding forces. The implication of this is that because these forces are known to be orientated in a specific direction, these compounds form well-ordered structures across small distances. However, the addition of dynamic coulombic forces in ILs gives rise to larger and more sophisticated assemblies and ordered mesoscopic structures.¹⁶ For example, polymeric structures of 1,3-dialkylimidazolium salts have been observed using multinuclear NMR.¹⁷

Whilst it is accepted that ILs are capable of forming exclusive regions of hydrophilicity or hydrophobic domains due to alkyl substituents, recent work has shown that ILs are often

randomly distributed on the molecular scale.^{16, 18} This phenomenon is intrinsically difficult to quantify due to the complexity of the interactions involved. As an example of the cooperative nature of the competing interactions in ILs, Hardacre *et al.* recently conducted an elegant study probing the nature of the ion pairing between the 1-ethyl-3-methylimidazolium cation ([EMIM]⁺) and the acetate ([OAc]⁻) and bis(trifluoromethane)sulfonimide ([TFSI]⁻) anion using pulsed field gradient NMR (PFG NMR). The authors compared the diffusion activation energies of the two ILs and found that [EMIM][OAc] had a higher activation energy of diffusion compared with [EMIM][TFSI] (35-38 kJ mol⁻¹ vs 25-26 kJ mol⁻¹), which agrees with their relative viscosities. Furthermore, when comparing the self-diffusion coefficients of the anions in the respective ILs, the larger [TFSI]⁻ anion had a faster diffusion coefficient. This result demonstrated that the rate of the diffusion does not reflect the ionic radius of the anion and rather, that coulombic interactions play a pivotal role in determining the ionic mobility. Since the cation remains the same in both ILs, the authors suggested that the difference in diffusion rates are derived from the nature of the anion. The authors further suggested that the higher charge density of the [OAc]⁻ anion may result in stronger coordination to the [EMIM]⁺ cation preventing diffusion. It is also noteworthy that after dissolution of glucose into [EMIM][OAc], the rate of diffusion was markedly slower as diffusion was disrupted by interfering ion pairs formed through strong H-bonds; this reinforces the complex nature of the relatively simple system.¹⁹

1.2 Ionic Liquids in Catalysis

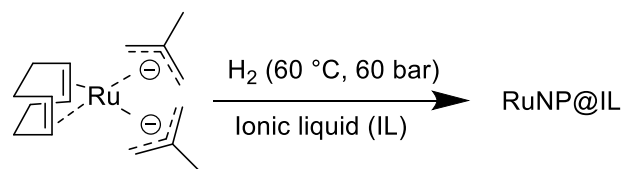
The global consumption of a range of essential raw materials has seen an exponential increase over the last few decades triggered by the increasing world population and new availability of such resources from improvements in modern technology.¹¹ Driven by governmental legislation and academic interest, chemists are striving to develop greener, more sustainable, efficient and cleaner routes for the production of food products, bioactive ingredients, agrochemicals and other fine chemicals. The field of green chemistry has received much attention since its beginning in the early 1990s as researchers continue to use innovative methods in order to advance current technologies.²⁰ To accommodate increasing demands in a sustainable manner, catalysis has been a vital tool not only on a molecular level but also in engineering environmentally benign protocols to improve the efficiency of chemical processes.²¹ In addition to their benefits as green solvents, ILs have several desirable properties that have attracted their use in catalysis. As discussed previously, the range of

available cations and anions and the various permutations means that the volatility and interactions with the substrate and/or catalyst may be tuned and optimised for a given application; this is especially important for catalysis, as strategic development of tailored or 'task specific' ILs can substantially improve catalyst lifetime, activity and selectivity.²² Specifically, most of the literature concerning the use of ILs in catalysis has described their ability to improve reaction kinetics either by activating the catalyst or tailoring the substrate-solvent interaction such that reactants can be directed within close proximity of the catalyst. Generally, improvements in selectivity can be observed either by a specific interaction between the IL and catalyst, thus modifying its activity or affinity for a given reactive site, or secondly, the ability to design ILs with discreet regions that promote removal of the desired product from the active site to prevent further reaction. Many proficient and informative reviews have described in detail the progress made in this rapidly evolving area of research.^{1, 6, 12, 22-26} The short section of this review that follows will highlight the key aspects of this research that have inspired the work in this project.

1.2.1 ILs for conversion of biomass

A key goal for the future of green chemistry is targeting molecules crucial to industrial processes that may be retrosynthetically linked to bioderived feedstock. Such processes lend themselves to a large-scale improvement on their sustainable output by adapting protocols in order to incorporate renewable sources. The defunctionalisation of highly oxygenated substrates is a challenging transformation that must be addressed to realise the potential of using biomass as a renewable source of carbon. Drawing from their green credentials, tuneable physical properties and ability to solvate highly oxygenated species, ILs have been strongly linked to this goal. Moreover, the high thermal stability of ionic liquids makes them a useful medium for the upgrading of biomass, as the reaction temperatures required for these processes exceed those of common organic solvent.

Naturally occurring carbohydrates, which constitute the largest fraction of terrestrial biogenic carbon sources, serve as a potential source for various useful platform molecules possessing huge scope for facile synthetic diversification.²⁷ In one of the most profound examples of the use of ILs in green chemistry, Leitner demonstrated that ILs could act as both reaction media and stabiliser for the selective RuNP-catalysed hydrogenation of bioderived aldehydes and ketones. By varying the nature of the IL, in particular the anion, the selectivity towards C=C, C=O, arenes and heteroaromatics could be finely tuned.²⁸



Scheme 3: Synthesis of IL stabilised RuNPs used as catalysts for the hydrogenation of bioderived aldehydes and ketones.

The size of the nanoparticles was demonstrated to be dependent on the nature of the IL, and the unique interactions with the particles are responsible for the high catalyst activity which was comparable to those of homogenous systems, but with the advantage that the catalyst could be recycled using supercritical CO₂.

Table 1: IL stabilised RuNP catalysed hydrogenation of bioderived compounds Reaction conditions: Ru@[C₁₂MIM][BTA], 2 h, 120 °C 120 bar; c(Ru) = 0.05 mol L⁻¹. Ru/substrate ratio 1:100.

| Substrate | Product | Yield (%) |
|-----------|---------|-----------|
| | | 99 |
| | | 95 |
| | | 99 |

Amongst a host of commercially important transformations is the selective hydrogenation of CO₂ to formic acid (FA). Due to the demand for reducing CO₂ levels globally, this reaction has received a great deal of attention as CO₂ serves as the feedstock, inherently causing its depletion as well as utilising it as a source of organic carbon. Commonly synthesised by carbonylation of methanol, followed by hydrolysis of the resulting formate ester, commercial FA production is close to 600,000 tons per year. Therefore, metal catalysed hydrogenation of CO₂ has been highlighted as a sustainable alternative as this one-step transformation would improve the overall efficiency by removing the need to separate the product from intermediate formate-based by-products in addition to making use of abundant reagents and

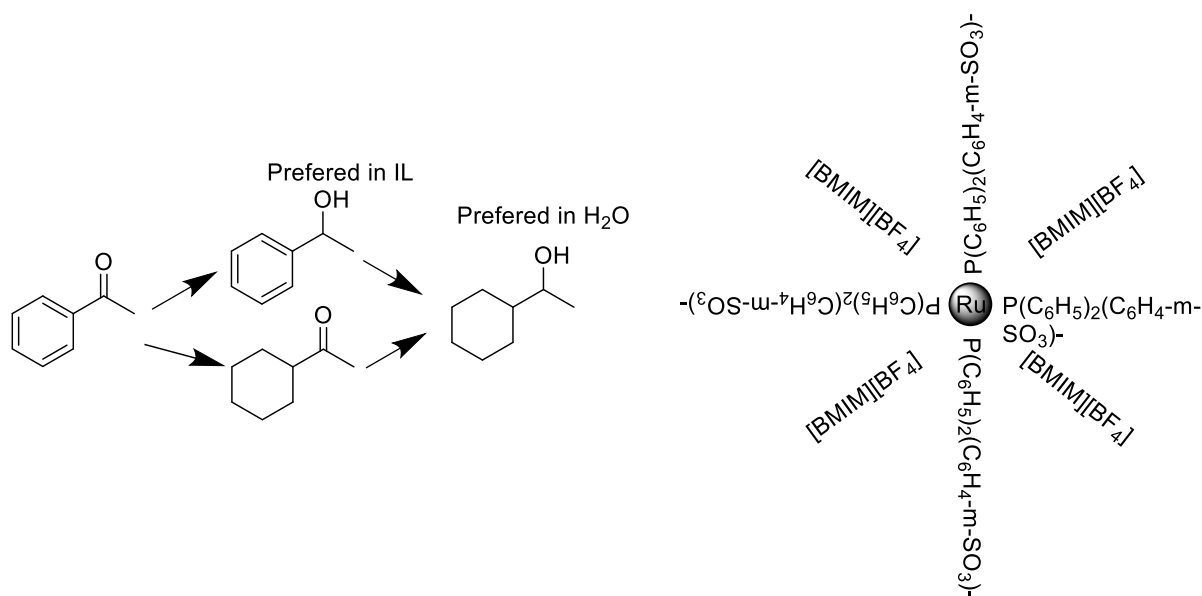
requiring less intensive resources. A very recent study by Dupont *et al.* demonstrated the multifunctional use of imidazolium acetate-based ILs as reaction solvent with catalysts derived from $[\text{Ru}_3(\text{CO})_{12}]$, which are able to overcome the high kinetic and thermodynamic barriers associated with the reduction of CO_2 .²⁹ The authors showed that the synergistic combination of ILs designed with basic anions allow the reaction to occur under base-free conditions, which prevents the formation of unwanted formate-based by-products. As well as enhancing the reactivity of the catalyst, the IL plays a crucial role by forming a critical carbonate intermediate which facilitates the formation of the product (Scheme 4). The basic nature of the IL also drives the reaction by acting as a buffer and preventing catalyst deactivation through protonation. Removal of the IL resulted in quantitative recovery of starting material confirming the role played by the IL.

Scheme 4: Proposed mechanism for the IL assisted Ru catalysed hydrogenation of CO₂ yielding formic acid.

of the β - isomer can be suppressed using stoichiometric amounts of toxic or expensive additives, the authors suggested that the IL plays a crucial role in facilitating an ionic reaction pathway by promoting favourable electrostatic interactions with the substrate; this strategy was effective for a range of different substrates and allowed the target products to be obtained in high yield.

1.2.2 Heteroatom donor functionalised ILs

The ability to easily functionalise ILs has led to their decoration with heteroatom donors. This concept has been widely explored as the advantageous aspects of ILs may be combined with the positive effects that donors may provide by altering the electronic properties of the catalyst. In this regard, reactions using donor-modified ILs as the solvent media have been shown to dramatically improve many benchmark transformations. For example, Dyson reported that nitrile-functionalised ILs improve the efficiency and selectivity of palladium catalysed hydrogenations through a strong interaction with the active PdNPs. The ability of the IL to act as a ligand also enables the active Pd catalyst to be retained during reaction workup.³² Shreeve *et al.* prepared 2,2-biimidazole-functionalised ILs that proved to be efficient reaction media for the palladium catalysed Suzuki-Miyaura cross-coupling. Significant improvements in recyclability of the catalyst was suggested to be due to strong coordination of the IL to the catalyst preventing leaching of palladium.³³ An interesting study from Jiang demonstrated that phosphine-functionalised ILs (PFILs) can exhibit switchable chemoselectivity for the ruthenium NP catalysed hydrogenation of functionalised aromatic carbonyls. The PFILs were shown to stabilise the Ru particles against aggregation and demonstrated switchable selectivity as two different products could be isolated selectively by using either 1-butyl-2,3-dimethylimidazolium or water as the reaction media (Scheme 5).



Scheme 5: Tuneable behaviour of PFIL stabilised ruthenium nanoparticle catalysts.

Carbanion-functionalised ILs capture CO with remarkable efficiency and the resulting IL-CO mixture has been used for a Pd catalysed carbonylation reaction yielding a range of useful platform molecules.³⁴ Whilst thought to be challenging due to the high bond dissociation energy, the authors demonstrated using quantum mechanical calculations and spectroscopic investigations that the unique solvation properties of the IL are responsible for the efficient absorption of CO. Their strategy is to essentially make use of the supernucleophilicity of carbanions to reversibly bind the π -acidic CO and facilitate reaction. The ability of the IL to also encapsulate the reactants is key to the efficacy of the reaction.

Although the use of ionic liquids as solvents for catalysis is an extremely diverse area of research encompassing a wide range of chemical transformations, there are many practical limitations that hamper their applications. As described above, despite their ability to enhance the rate and/or selectivity of a reaction, the intrinsic disadvantages of ILs include their high viscosity, which limits access of the reactants onto the catalyst surface, and the tendency of ILs to leach during reaction workup means regular replenishment of the IL is required. Furthermore, as a result of their low volatility, energy intensive purification of the IL may be required after the reaction. In recent years, there has been a great deal of interest in the design of more innovative systems to utilise the advantageous aspects of ILs including biphasic liquid-ionic liquid catalysis as well as multiphase reactions. Moreover, advances in materials science has inspired the immobilisation of ILs onto a solid surface to facilitate recovery and recycling of the IL as well as the development of continuous flow processes. Expanding on

their use as solvents, ILs have also been utilised as stabilisers for metal nanoparticles (NPs) which are evolving as a highly efficient class of catalyst for carbon-carbon and carbon-heteroatom bond formation as well as a host of hydrogenations and oxidations. The primary aim of the following sections will be to inform and describe selected examples of such work and related areas relevant to this PhD study.

1.2.3 Ionic liquids in biphasic catalysis – charge tagged ligands (CTLs) and thermoregulated ILs

One of the biggest challenges facing synthetic chemists is the isolation of products and recovery of active catalysts on a large scale. One significant advantage of using an IL as solvent is that simple synthetic modifications can enable facile and selective recovery of the desired product. In this regard, by employing hydrophilic ILs under biphasic conditions, organic products can be readily separated from reaction mixtures by simple decantation or organic extraction while the catalyst is retained in the IL layer, thus allowing the IL and active catalyst to be recycled. This concept allows the high activity achievable in homogenous catalysis to be combined with the ease of recycling of a heterogeneous catalyst (Figure 2).¹² This is particularly important when considering the aspects of scale-up or the design of industrial processes as the IL and catalyst inherently constitute the bulk of the cost coupled with the fact that ILs are often the products of multistep syntheses.

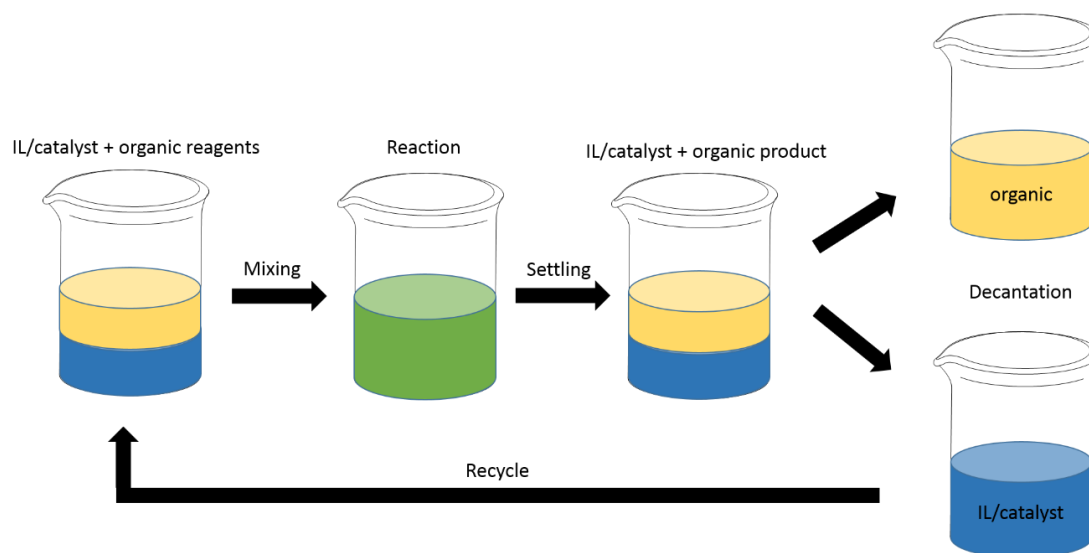


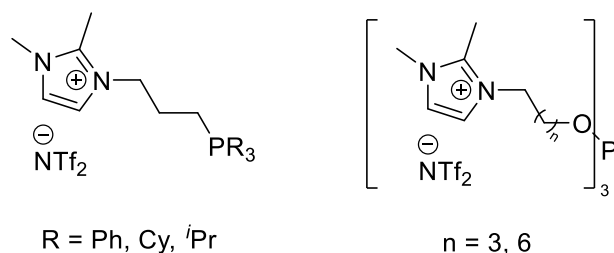
Figure 2: An ionic liquid-organic based biphasic catalysis system.

When considering the use of ILs in biphasic catalysis, there are certain criteria that must be adhered to in order to design viable reaction systems. Firstly, the IL layer must be able to solvate the catalyst in order to effectively immobilise it in the IL phase. This prevents leaching

of the catalyst during the reactions and avoids downstream removal of toxic metal waste from product streams and accumulative catalyst attrition. Secondly, the IL must not exhibit any detrimental effects due to catalyst deactivation. Furthermore, the reactants should be soluble in the IL phase to allow rapid mass transfer to the catalyst. Finally, it is important that the solubility of the IL is finely tuned in order to allow liberation of the product from the IL layer.²³ Whilst this seems a convenient method of affording sustainable and scalable processes, in reality, these systems can suffer drawbacks derived from mass transfer effects imposed by the high viscosity of ILs, slowing diffusion of the substrate to the active site, as well as the diffusion of the substrate between the organic and IL phases.³⁵ Moreover, leaching of the IL or solvent often occurs during workup as a large excess of organic solvent is often required to extract products that have high miscibility with the IL. In this regard, a great deal of research has been devoted to the design of 'ionic tagged' commercially important ligand systems.³⁶ It is well-established that in classical homogenous catalysis, the ligands have a profound effect on catalyst performance. As such, incorporation of an ionic fragment on to a ligand scaffold has been shown to be a powerful tool for immobilising catalysts in the IL layer by improving the solubility properties of the overall complex.

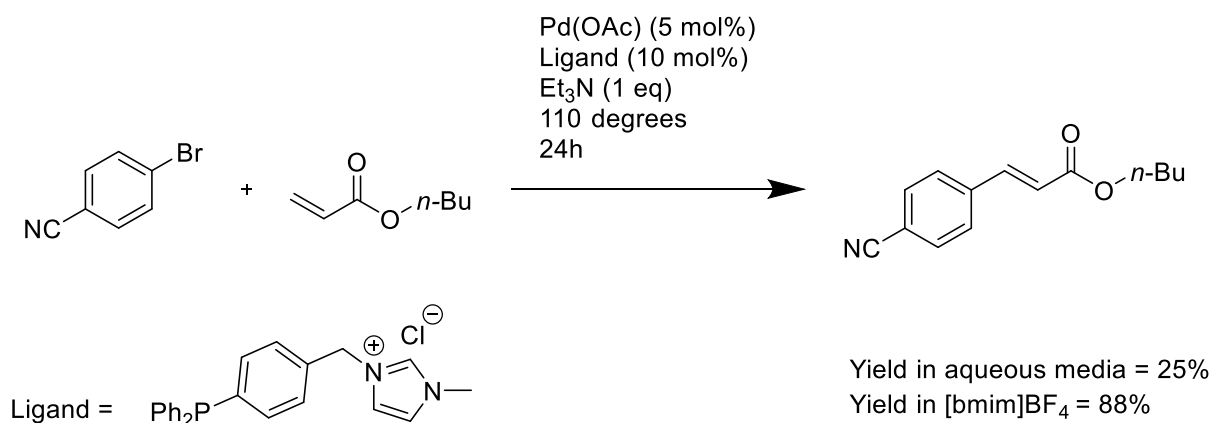
In a recent study, Dupont *et al.* demonstrated that $[\text{RuHCl}(\text{CO})(\text{PPh}_3)_3]$ was a highly active catalyst for the isomerization of estragole to *trans*-anethole.³⁷ Under the optimized reaction conditions, a catalyst loading of 4×10^{-3} mol % gave 100% conversion of estragole with a turnover number (TON) of 25,000, which corresponds to a turnover frequency (TOF) of 500 min^{-1} at 80°C in toluene. Although there was a dramatic influence of the solvent on catalyst efficacy, the phosphine was key to the high catalyst activity. This system was then successfully transposed into a biphasic IL system using $[\text{nPr}(\text{OH})\text{MI}][\text{NTf}]$ as the bulk solvent. Initially, this facilitated efficient separation of the products from the reaction mixture by decantation, however, ICP analysis of the organic layer showed that 160 ppm of the original 216 ppm Ru was present, suggesting substantial leaching of the catalyst. The authors postulated that the use of designer ionic phosphines and phosphites (shown in Scheme 6) may well a) exhibit an increase in the observed catalyst activity by virtue of the steric and electronic ligand effects observed in molecular catalysis, and b) coordinate strongly to the catalyst and prevent leaching of metal into the product phase due to the increase in affinity for the IL phase. Indeed, the use of ionic phosphines did enable the IL to retain the catalyst, however, they did observe

a drop in the reaction rate, which was reported to be due to mass transfer limitations given the poor solubility of the substrate in the IL.



Scheme 6: Ionic tagged phosphine ligands synthesised by Dupont *et al.*

Williams and co-workers recently designed a modular synthesis to generate a range of ionophilic phosphate and imidazolium-tagged phosphines in high yield from readily available starting materials.³⁸ These ligands were then used to generate highly active Pd catalysts derived from Pd(OAc)₂ which were employed for Suzuki-Miyaura cross coupling and Heck reactions in aqueous media and ionic liquid (Scheme 7). Whilst moderate conversions were obtained in aqueous media, the reaction rate was markedly enhanced in ILs. The benefits of these systems lie in the reusability of the catalyst as reactions conducted in 1-butyl-3-imidazolium tetrafluoroborate could be recycled 5 times with no loss in activity. Furthermore, no Pd black formed indicating that the ligands form stable complexes. Additionally, the absence of ligands or palladium in the organic phase also further confirms that the ionic nature of the ligands successfully immobilises the catalyst in the IL layer.



Scheme 7: Charge tagged triphenylphosphine ligand synthesised by Williams *et al.* for the Pd catalysed Heck reaction in aqueous/IL media.

The ability to tag virtually any organic substituent has allowed researchers to extend the applications of CTLs. For example, Nehra *et al.* recently prepared an imidazolium-tagged zinc complex for the aqueous phase synthesis of bis(indoyl)methanes.³⁹ The same complex was

also useful for DNA cleavage and exhibited excellent antifungal and antibacterial activities against a broad range of bacteria. Furthermore, charge-tagged triazole based Pd-NHC complexes synthesised via postmodification with ammonium head groups form efficient catalysts for Suzuki-Miyaura cross-coupling reactions in molten tetrabutylammonium bromide.⁴⁰ The synthetic postmodification approach yielded rare examples of 1,2,4-triazole based NHCs and each rotamer was identified using ¹H NMR spectroscopy.

Despite the clear advantages of using ionic liquids as solvents there still remains obvious problems with catalyst/IL leaching, which is especially the case for neutral/uncharged catalysts. While the development of CTLs has made steps toward overcoming this problem in many cases there is an equilibrium between bound and unbound metal which provides a pathway for metal leaching. Additionally, the challenge of handling ILs in such systems due to their high viscosity is well-documented.^{13, 41, 42}

The operational problems associated with determining physical parameters of reactions is derived from the large solvent friction and this effect has been investigated by Kumar and Pawar, who reported that the high viscosity of 1,3-dialkylimidazolium-based ILs severely hamper a range of simple intermolecular Diels-Alder reactions.⁴³ The rate constants for three different Diels-Alder cycloadditions were determined which revealed a clear relationship between viscosity and reaction rate. The authors found that addition of methanol as a cosolvent dramatically increased the reaction rate most likely due to the substantial decrease in viscosity of the bulk solvent. Kukawka and coworkers also reported that the high viscosity of phosphonium-based ILs hampers the rhodium and platinum catalysed hydrosilation of octane.⁴⁴ Zhao *et al.* reported that amino functionalised ILs exhibited excellent CO₂ absorption profiles as well as good stability but suffered strongly from mass transfer effects in batch and as such, prolonged reaction times and high catalyst loadings were required which limited the efficiency of the system.⁴⁵

More recently, in attempt to address the problems associated with mass transfer limitations in viscous ILs, it has been shown that a judicious choice of IL and cosolvent can allow both efficient mixing and extraction of products by tuning the properties of the IL such that the compatibility with the cosolvent is switchable under specific conditions. Whilst it is also possible to facilitate product extraction in biphasic media using a reversible reaction with CO₂ to alter miscibility,^{46, 47} these systems are limited as they require specialist technical

equipment which has hampered their applications on larger scale. Recently, Passos *et al.* developed polypropylene glycol (PPG) modified ammonium-based ionic liquids, from readily available and cheap organic acids and bases. These systems undergo temperature-induced phase transitions in aqueous solution that allow reactions to be conducted in the homogenous phase and the product to be separated by cooling to form a biphasic system.⁴⁸ To demonstrate proof of principle, these substances were utilised for the separation of commercially important proteins. The novelty of these systems is that the nature of these ILs render them highly sensitive to temperature and as such, only small changes in the applied temperature are required to induce phase separation. Of the ILs tested, *N,N*-dimethyl-*N*-ethylammonium phenylacetate and *N,N*-dimethyl-*N*-(*N'*,*N'*-dimethylaminoethyl) ammonium octanoate, bearing large hydrophobic groups were unable to form aqueous biphasic systems with PPG. In contrast, more hydrophilic ILs did, as the increased affinity for water facilitated formation of crucial hydrates.

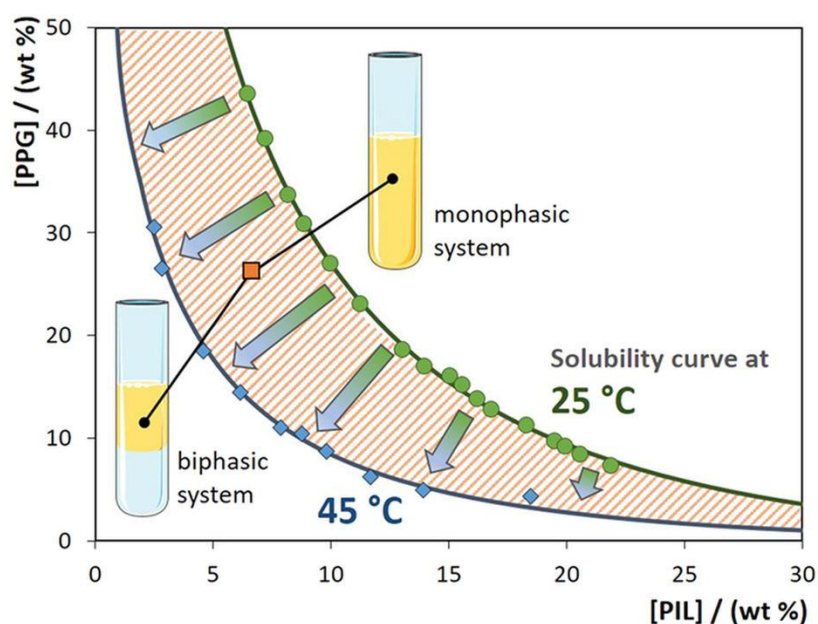


Figure 3: Representation of the aqueous biphasic thermoreversibility profile for *N,N*-dimethyl-*N*-(*N'*,*N'*-dimethylaminoethyl) ammonium octanoate, PPG and water (orange square is the initial mixture composition).⁴⁸

The concept of thermoregulated ILs has been applied widely throughout the literature and many reviews have documented recent work.^{49, 50} Hou and co-workers reported the use of polyethylene-glycol (PEG) functionalised alkyl imidazolium-based ILs bearing phosphine-functionalised anions coupled with ethyl acetate as a non-toxic organic cosolvent for the Pd and Rh nanoparticle catalysed hydrogenation of α,β -unsaturated aldehydes.⁵¹ Besides stabilisation of the nanoparticles, the authors reported that the use of $[P(C_6H_4-m-SO_3)_3]^{3-}$ was

crucial for achieving high selectivity due to the electronic changes induced on the surface of the particles after coordination through the phosphorus. The thermomorphic properties of this system enable reactions to be conducted in a single phase at high temperature, which readily formed a biphasic mixture upon cooling. This in turn allowed the catalyst to be recycled 10 times without any loss in activity. Wang *et al.* utilised carboxylic acid functionalised imidazolium based ILs for the acid catalysed dehydration of fructose to yield commercially important 5-hydroxymethylfurfural.⁵² In this case, the active catalyst is covalently attached to the IL which allowed reaction parameters such as catalyst loading and concentration to be varied, while thermoregulation of IL miscibility in isopropanol facilitated separation of the products. Beyond the select examples described above, the area of thermoregulated ILs for biphasic catalysis has encompassed a wide range of transformations including hydrosilation,⁵³ Heck reactions,⁵⁴ hydrogenations,⁵⁵ and oxidations.⁵⁶

While most examples of biphasic catalysis with ILs are restricted to batch studies Yang *et al.* have recently reported the use of tetrabutylphosphonium stearate and n-tetradecane as a biphasic system for the PdNP-catalysed hydrochlorination of acetylene in continuous flow.⁵⁷ The unique combination of IL and cosolvent facilitated the formation of discrete self-assembled nanostructures that stabilise the metal nanoparticles. In this biphasic system, a continuous flow of organic solvent and gaseous reagent promoted the formation of small IL droplets that served as microreactors by housing catalytically active PdNPs. TEM analysis of the solution demonstrated that the PdNPs formed *in situ* by reduction with the carboxylate group were successfully confined inside IL droplets. Under the optimum conditions, at 180°C and a catalyst loading of 0.038 mol/L, 98% conversion and 99.5% selectivity for the vinylchloride monomer was obtained and the system exhibited a stable profile over 72 hours. For comparison, a dramatic drop in reaction rate was observed when the same reaction was conducted in ionic liquid. Through the formation of droplets, only a small amount of IL is required, and the mass transport of heat and reactant is increased. Moreover, as the system can be operated in continuous flow, the economics of the entire process are improved.

In summary, the examples described above clearly demonstrate the versatile nature of ILs as solvents in catalysis. Whilst the tuneable nature of ILs has allowed them to evolve as useful solvents or additives in diverse range of applications, the complex nature of these dynamic fluids renders them difficult to model and thus, there is still a need to develop a detailed understanding of their role in catalytic reactions. Although there are clear benefits associated

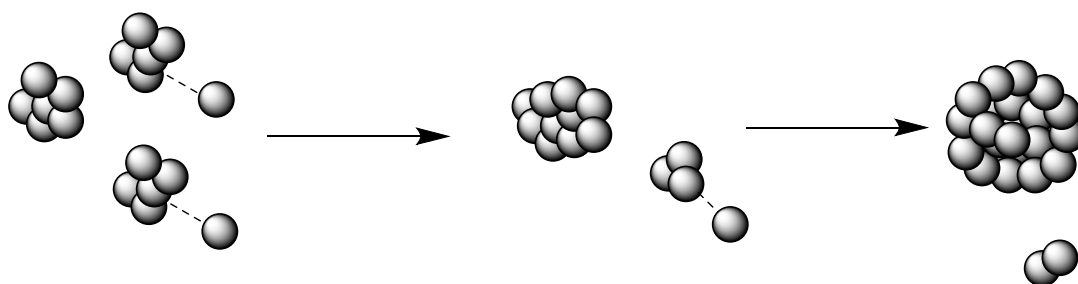
with the use of ionic liquids in catalysis such as efficient catalyst activation, enhancements in activity and selectivity and ease of recovery, there are numerous drawbacks related to their high viscosity, cost and viability for operational use. This has fuelled research into developing new structures and materials, in order to utilise the advantageous aspects of ILs and further bridge the gap between homogenous reactions and heterogeneous separation, which will be discussed in section 1.4.

1.3 Nanoparticles for Catalysis

Transition metal nanoparticle (NP) catalysis is evolving as an extremely versatile and powerful technology. Due to their nanoscale size dimensions (1-100 nm) and the quantum confinement effect, they possess discrete unique physical profiles, which has also fuelled their applications in electrochemistry,⁵⁸ medicine,⁵⁹ biotechnology,⁶⁰ drug delivery⁶¹ and fuel cells.⁶² Their extraordinary catalytic activity is derived from their large surface area to volume ratio when compared to their bulk counterparts, which in turn increases the amount of exposed active sites accessible for catalysis.⁶³ Due to their small size and high catalytic activity, NPs are considered as the interface between homogenous and heterogeneous catalysis. During the last decade, an enormous number of publications have appeared that document a wide range of synthetic methodologies that have been strategically designed to generate NPs with controllable size and surface properties, which represents a new era of heterogeneous catalysis. Further to this, NPs can be immobilised and incorporated into a range of materials facilitating their reuse and improving their 'green' credentials.

1.3.1 Nanoparticle synthesis and stabilisation

One of the key challenges in NP catalysis is to prevent aggregation under reaction conditions. NPs are kinetically unstable and tend to agglomerate into larger particles which necessarily results in a decrease in catalytic activity. This process, termed 'the Ostwald ripening principle' is due to the low stability of the co-ordinately unsaturated surface atoms relative to those of the bulk, which are highly ordered and have a high coordination number. Therefore, to lower the energy of the overall system, the particles will aggregate to form more thermodynamically stable larger particles by detachment of atoms from small particles and reattachment onto larger particles (Scheme 8).⁶⁴



Scheme 8: the Ostwald ripening process for nanoparticles.

As nanoparticles have a large ratio of surface atoms to bulk, they require additional stabilisation which has classically been achieved by surface ligating anions, surfactants or donor ligands. The design of stabilisers for NPs has revolutionised their use in catalysis as stabilisers often offer multimodal use with regards to improving NP solubility or isolation, however, it is important that the stabiliser does not inhibit access of the substrate to the catalyst surface.²²

There are two main approaches for the synthesis of metal NPs and optimising the preparation of such protocols is a key aspect for heterogeneous catalysis. In this regard, it is possible to improve the efficacy of the approach by lowering the total expensive precious metal content as well as achieving increased thermal and kinetic stability of the particles through favourable interactions with the support or stabiliser.⁶⁵ Firstly, the ‘top down’ approach involves disintegration of bulk metal into nanoparticles either by chemical, thermal or mechanical means. However, the more practical and common ‘bottom up approach’ is conventionally achieved via reduction or decomposition of organometallic precursors in the presence of stabilisers followed by aggregation into nanoparticles. The latter enables a more rational catalyst design due to the ability to control the nanoparticle shape, size and dispersity – factors that can ultimately govern the activity and selectivity of the newly formed catalyst.⁶³ Moreover, this method is more amenable to scale-up for industrial production.⁶⁶ Thus, the stabilisation of metal nanoparticles is an integral aspect crucial to the generation of highly selective and active catalysts. Whilst there is currently a wealth of research concerning the development of designer nanoparticle stabilisers such as; organic heteroatom donor functionalised polymers,⁶⁷⁻⁶⁹ metal organic frameworks,⁷⁰ ionic liquids,⁷¹ fullerenes,⁷² carbon nanotubes⁷³ and inorganic polyoxometallates,⁷⁴ the fundamental principles associated with their stabilisation all fall within three main subcategories (Figure 4).

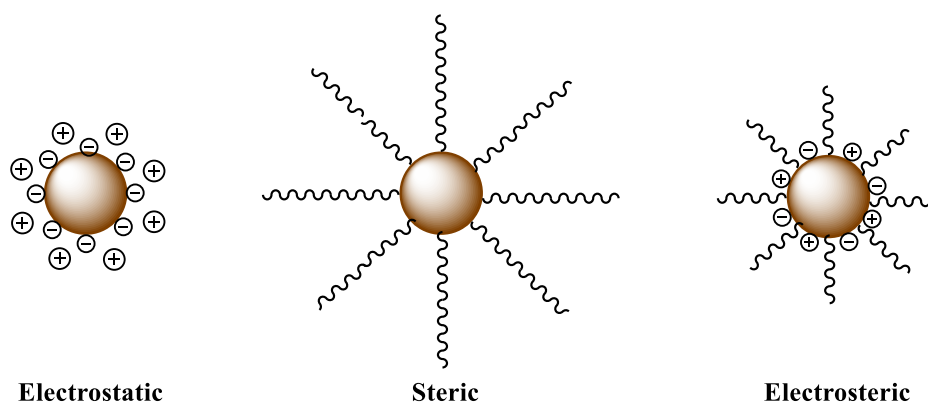


Figure 4: Different stabilisation methods for nanoparticles.

i) Electrostatic stabilisation

The DLVO (Derjaguin–Landau–Verwey–Overbeek) theory aims to rationalise the stability of colloids. This suggests that in the presence of ionic media, anions are adsorbed onto the electrophilic surface of the NPs, this protective anionic layer then provides coulombic repulsion between neighbouring particles. The unfavourable electrostatic repulsion interactions therefore prevent agglomeration with other nearby particles.⁷⁵ This type of stabilisation can be achieved using a range of salts dissolved in solution or more intuitively, with the use of task specific ILs, which will be discussed more thoroughly in section 1.3.2.

ii) Steric stabilisation

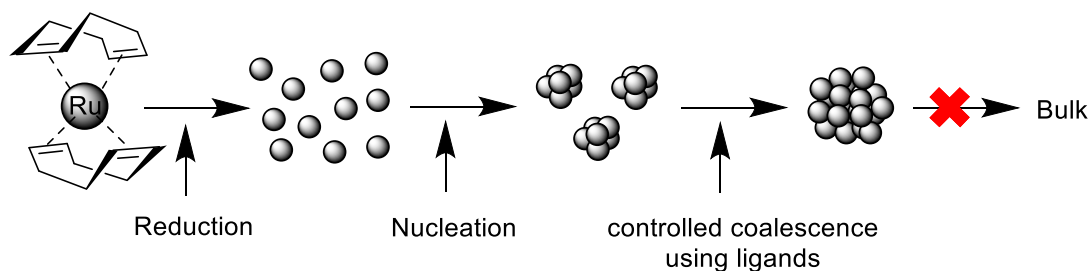
Steric stabilisation of NPs can be achieved either by performing the reduction step in the presence of large bulky protecting groups or designer supramolecular material; this will prevent aggregation by limiting the proximity of neighbouring particles. For example, Hutchings prepared bimetallic Au/Pd nanoparticles stabilised by graphene oxide (GO) which were excellent catalysts for the selective oxidation of alcohols.⁷⁶ Variation of the metal-GO ratio was used to fine tune the particle size by limiting space for particle growth in the cavities between the GO sheets. Additionally, by incorporating TiO as a templating agent, activity can be enhanced by forming a two-dimensional GO layer to prevent aggregation of the particles under catalysis conditions. The benefit of this strategy is that there is no requirement for organic surfactants which may limit the accessibility of the active site. Chamberlain *et al.* developed single-walled carbon nanotubes (SWNTs) that served as microreactors and facilitated formation of metal nanoclusters of the formula $[M_6I_{14}]^{2-}$.⁷⁷ The advantage of this approach is that the size of the SWNT cavity controls the particle growth to give clusters with a discrete size. A range of electron microscopy techniques coupled with Raman spectroscopy

revealed that the SWNTs were crucial to the reactivity of the particles by acting as electron reservoirs during reaction and that unique guest-host interactions were responsible for the stabilisation of the nanoparticles. Steric protection of NPs has also been achieved by incorporating NPs into polymer matrices^{78, 79} or by the use of various other capping agents such as dendrimers^{80, 81} or silanes.⁸²

iii) Electrosteric stabilisation

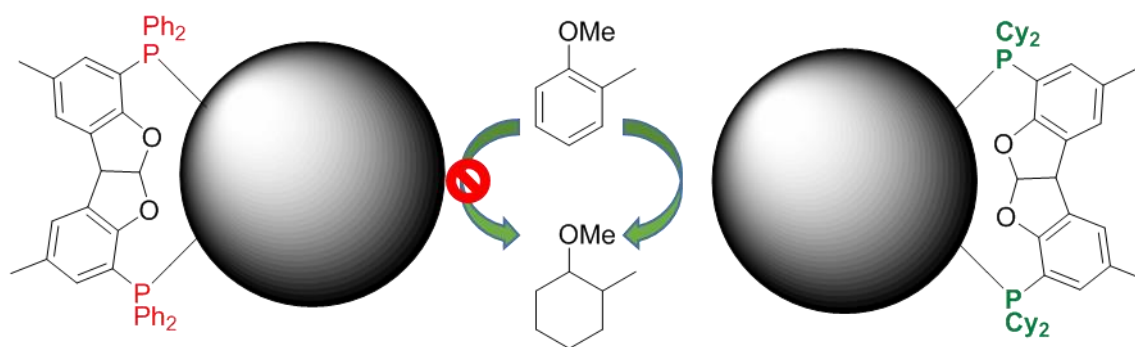
The functionalisation of large molecules with ionic/polar head groups provides a combination of electrostatic and steric stabilisation. This is classically achieved using amphiphilic polymers,⁸³ polyacrylate dispersions⁸⁴ and designer ionic liquids bearing long alkyl chains that can encapsulate NPs.⁸⁵ This form of stabilisation involves an electrostatic type protective layer at the surface of the particle combined with a hydrophobic sterically hindered outer layer.

Although not conventionally referred to as electrostatic stabilisation, the design of heteroatom modified materials or surfactants has been demonstrated as a method to control or modify particle size and surface structure and optimise the electronic properties of the catalyst as well as provide additional stabilising forces. In classical coordination chemistry and homogeneous catalysis, the electronic nature of the ligands exerts a significant influence on catalyst performance, hence, there has recently been increasing interest in exploring the influence of incorporating heteroatom donors into supports for heterogeneous catalyst. In such systems, dramatic improvements in catalyst selectivity and lifetime have been obtained by virtue of the coordinative nature of heteroatom donors such as amines, phosphines or oxides. In a recent insightful account, Chaudret demonstrated that the fundamental principles of metal-ligand interactions in homogeneous catalysis remain true for the coordination of ancillary ligands to the surface of metal nanoparticles.⁸⁶ The shape, size and reactivity of metal nanoparticles can be modulated through a judicious choice of ligand additive (Scheme 9), which has been shown to exhibit dynamic coordinative behaviour classically seen in molecular systems using NMR spectroscopy. For example, the use of organometallic Ru precursors that decompose into RuNPs under mild conditions without leaving organic residues on the NP surface allowed the authors to observe that ligands with stronger donors afforded smaller RuNPs. In this study, alcohol ligands afforded the largest RuNPs, whereas diphosphines and *N*-heterocyclic carbenes afforded the smallest.



Scheme 9: Method for synthesising small ligand stabilised metal nanoparticles.

This concept is particularly important for heterogeneous catalysis, as many commercially available supports can be modified with heteroatom donors to improve catalyst performance. For example, Hutchings *et al.* designed acidic oxygen functionalised carbon nanofibers (CNFs) in order to capture and stabilise PdAu nanoparticles.⁸⁷ These materials showed superior activity for suppression of hydrogenation and decomposition of H_2O_2 during its synthesis than other supports and metals, and also enhanced the overall productivity of H_2O_2 . Dong *et al.* examined the influence of amine modified hyperbranched polymers on the AuNP catalysed reduction of nitrophenol.⁸⁸ The authors reported that interactions between the support and the metal surface were crucial to achieving high catalytic activity. Chaudret and co-workers reported a pronounced ligand effect for the ruthenium nanoparticle catalysed hydrogenation of arenes.⁸⁹ Small phosphine stabilised RuNPs were obtained by controlled decomposition of $[\text{Ru}(\text{COD})(\text{COT})]$ in THF containing various phosphines. Comparative catalyst testing revealed that triaryl phosphine-stabilised catalysts were inactive whereas trialkyl phosphine-based catalysts were highly active for the hydrogenation of *o*-methylanisole (Scheme 10).



Scheme 10: Schematic representation of the ligand effect of trialkyl phosphines explored by Chaudret *et al.*

In related work, Glorius *et al.* synthesised N-heterocyclic carbene (NHC) modified $\text{Ru}/\text{K-Al}_2\text{O}_3$ catalysts by impregnation of $\text{Ru}/\text{K-Al}_2\text{O}_3$ with *in-situ* generated NHCs.⁹⁰ A broad range of surface characterisation techniques were employed to explore the role of the ligand. As evidenced by ^{13}C solid state NMR spectroscopy, the authors report that the carbene

coordinates to the RuNPs and alters the electronic structure of the surface; this was further confirmed by XPS analysis of the nitrogen 1s region. Preliminary catalyst testing for the hydrogenation of phenylacetylene revealed that in the absence of NHC, quantitative yields of the fully reduced ethylcyclohexane were obtained, however, equimolar amounts of ethyl benzene and ethylcyclohexane were obtained in the presence of 1.0 equiv. of NHC. A further increase in the amount of NHC resulted in an improvement in chemoselectivity to 92% for ethylbenzene; demonstrating the advantages of incorporating homogeneous ligands into heterogeneous structures. The same group also demonstrated that post modification of Pd/Al₂O₃ catalysts with N-heterocyclic substituted NHCs induces electronic changes to the catalyst surface which activates that system for Buchwald-Hartwig aminations.⁹¹ The unmodified catalyst was inactive under the same conditions and a combination of DFT calculations and detailed structural analysis revealed that the pronounced electronic changes to the PdNPs are due to the strong σ -donor ability of the NHCs. This interaction lowers the barrier for C-Br cleavage required for the rate limiting oxidative addition step in the catalytic cycle and highlights possible opportunities to design more selective catalyst systems via the introduction of additional donors into the support.

Despite advances in physical techniques available to chemists, there is still a need obtain fundamental insights into the complex processes involved during nanoparticle formation. Whilst it is well established that synergistic and cooperative effects of stabiliser and preparatory method can modulate particle morphology, little is known about the kinetics of nanoparticle formation. To this end, Catlow and Hardacre *et al.* have recently used a combination of diffuse reflectance infrared Fourier transform spectroscopy (DRIFTS) and advanced X-ray absorption fine structure (XAFS) spectroscopy studies to probe the formation of PdO NPs during the calcination of a range of metal loaded oxide supports.⁶⁶ The decomposition of two Pd precursors, Pd(NO₃)₂ and Pd(NH₃)₄(OH)₂ were examined using time-resolved DRIFTS, and the NH₃ ligands were shown to be oxidised to N₂O and NO while the NO₃ ligands formed bridged structures with Pd centres. The relative nucleation rates of each precursor were determined using XAFS and it was found that the coordinative nature of the NO₃ ligand assists the formation of larger particles. In stark contrast, decomposition of Pd(NH₃)₄(OH)₂ favours the formation of well isolated Pd-Pd sites that were anchored to the support. The smaller NPs formed from the ammonia complex therefore possess better

dispersity across the support, hence, more step edges resulting in improved performance for the oxidation of methane.

1.3.2 IL stabilised NPs

The use of ILs to protect nanoparticles is well-documented in many informative reviews.^{6, 22, 92} Whilst the DLVO theory is largely accepted as a reasonable model for the interaction of NP surfaces with isolated ions, this was not designed to account for more complex systems such as ILs that are often composed of sterically demanding ionic aggregates. As such, investigations into IL stabilised NPs have drawn much attention over the last decade. The benefits of using ionic liquid as stabilisers lies in their ability to exhibit a unique microenvironment, where through the various interactions discussed in section 1.1, it is possible to modulate the physicochemical properties of the NPs to improve catalyst performance and recyclability. From a green perspective, the positive influence on the catalytic properties of the NPs from fine-tuning of the composition of the IL, offers a ligand free synthesis of active catalysts often with switchable activity, as discussed earlier. Moreover, IL stabilised NPs form homogenous dispersions which avoids mass transport issues, however, the active site is composed of metal surfaces rather than single sites, placing these systems at the interface of homogenous and heterogeneous catalysis.⁹³ Importantly, ILs often exhibit more facile dissociation from the active site during catalysis than other stabilisers which results in a more active catalyst.²⁸

As discussed earlier, the complex interactions within ILs can induce the formation of sophisticated structural organisations. Often the properties of ILs are a result of extensive networks rather than the isolated ions. By forming exclusive regions of different polarity, it is possible to selectively capture solutes in a predetermined domain. This is particularly important for NP-IL dispersions as use of an appropriate metal precursor can enable modulation of the NP size and shape by altering the volume of these nanoregions.⁹² Despite the wealth of examples of IL stabilised NPs, it is difficult to elucidate the crucial aspects that govern the size and shape of the resulting nanomaterials. However, there appears to be a synergy between the nature and concentration of the metal precursor, as the possible by-products that may form aggregates on the metal surface, as well as method of reduction and type of IL used, which play a key role in the kinetics of NP formation.⁹⁴

Kim *et al.* prepared ionic liquid coated iron oxide nanoparticles (IONs) by thermal decomposition of $\text{Fe}(\text{CO})_5$ in a solution of DMF/1,3-dialkylimidazolium based ILs.⁹⁵ Modulating the chain length of the alkyl substituent on the imidazolium as well as the ratio of organic solvent to IL was shown to regulate the size and shape of the NPs formed and influence the relative decomposition rates of the iron precursors (Figure 5). This strategy was used to design discrete nanostructures for different applications. For example, one dimensional Fe_2O_3 nanobars prepared in 1-*n*-octyl-3-methylimidazolium tetrafluoroborate ([omim][BF₄]) exhibited superparamagnetic behaviour in the presence of an external magnetic field and demonstrated a contrast enhancement effect in a MR scanner, whereas Fe_2O_3 spherical particles prepared in 1-*n*-cetyl-3-methylimidazolium tetrafluoroborate ([cmim][BF₄]) were ineffective under the same conditions.

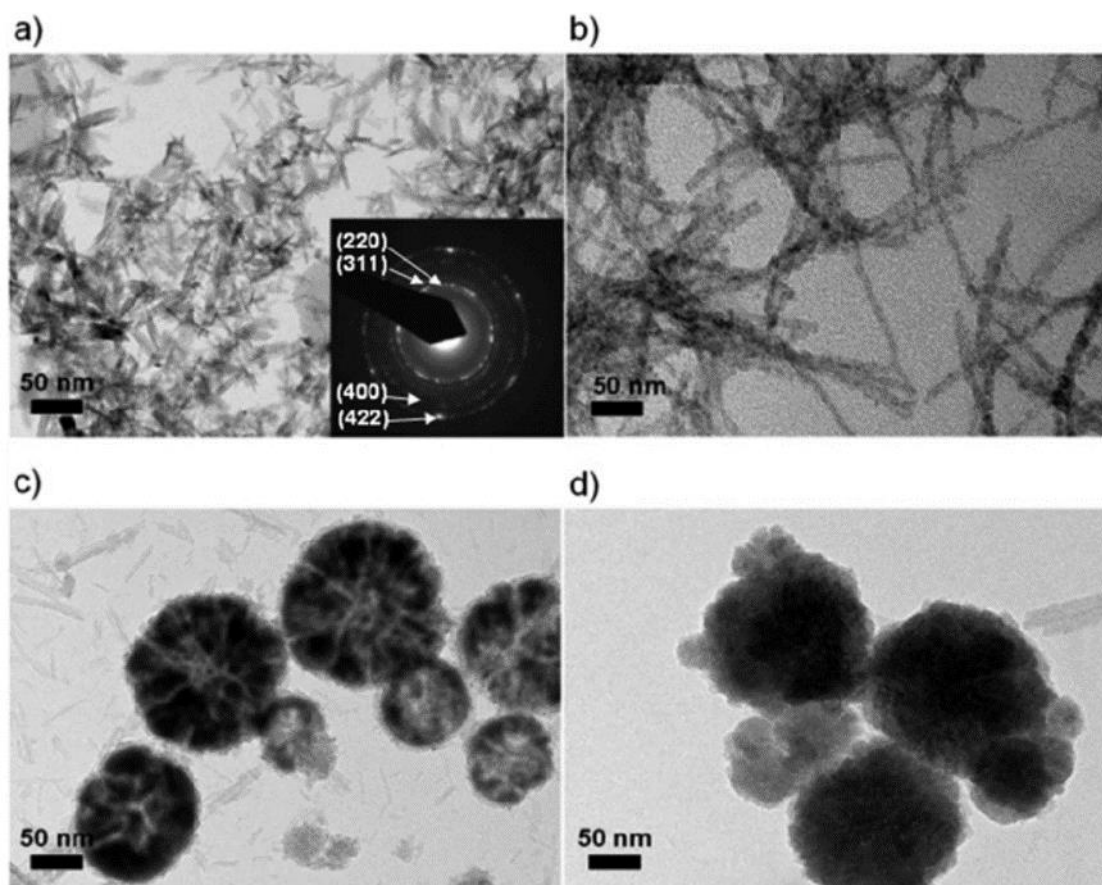
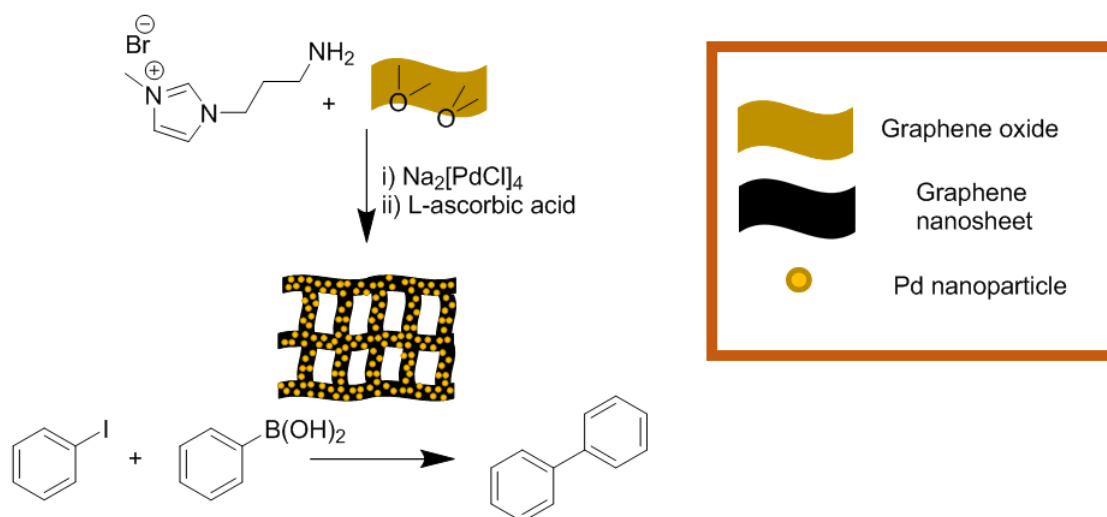


Figure 5: TEM image and electron-diffraction pattern of Fe_2O_3 nanobars prepared in [omim][BF₄]/DMF (1:1.5). (b) TEM image of Fe_2O_3 nanowires prepared in [omim][BF₄]/DMF (1:3). (c) TEM image of the IONs prepared in [cmim][BF₄]/DMF (1:1.5). (d) TEM image of the IONs prepared in [bmim][BF₄]/DMF (1:1.5). Published by Kim *et al.*⁹⁵

As well as acting as stabilising media for the dispersion of NPs, ILs can be chemically grafted onto the surface which can give rise to materials with novel properties whilst retaining the advantageous features of the ILs or NPs. These materials, termed ‘nanoparticle-ionic liquid

hybrids' are of increasing interest due to the ability to optimise the unique properties of the bulk material. For example, Mutin *et al.* demonstrated that grafting phosphonic acid functionalised ILs onto the surface of TiO₂ nanoparticles facilitates the phase transfer of the particles from an aqueous solution into an ionic liquid. This technique allows the formation of small NPs and enables them to be efficiently separated from the medium they are synthesised in and redispersed in another for a specific application.⁹⁶ The strong M-O-P bonds formed from the phosphonic acids were crucial for their selective extraction and this enabled TiO₂ NPs to be redispersed in [emim][NTf₂], enabling the possibility for their subsequent use in other fields such as catalysis, energy storage or separation technology. Archer *et al.* reported that imidazolium grafted SiO₂ nanoparticles dispersed in 1-butyl-3-methylpyrrolidinium bis(trifluoromethyl sulfonyl) imide (BmpyrTFSI) form ionogels for applications in electrochemical conversion.⁹⁷ While BmpyrTFSI has a tendency to crystallise which somewhat limits its applications, doping of the solution with imidazolium grafted SiO nanoparticles forms novel ionogels that have a minimal effect on the IL transport properties. Interactions between the IL and the NP-IL hybrid were proposed to disrupt crystallisation of the IL by coupling of the anion with the IL grafted cation demonstrating that IL grafted NPs can manipulate the properties of bulk ILs.

Furthermore, nanoparticle-ionic liquid hybrids can be designed whereby NPs are chemically incorporated into a preformed IL-based structure that is already optimised for a given application, therefore improving the versatility and efficiency of the overall system. For example, Wang *et al.* prepared NH₂- functionalised imidazolium-based ILs that were incorporated into the three dimensional structure of graphene via a 'green reduction inducing self-assembly method'.⁹⁸ The NH₂-IL fragments embedded within the architecture were proposed to prevent restacking of graphene sheets which increased surface area and improved catalytic activity. PdNPs were incorporated through anion exchange of [PdCl₄]²⁻ with the bromide of the IL followed by reduction of the resulting Pd^(II) precursor. TEM and BET analysis demonstrated that this method yields well dispersed and small PdNPs with a large surface area throughout the macroporous structure. The catalyst operates efficiently under extremely mild conditions for the Pd catalysed Suzuki cross-coupling giving TOFs up to 800 h⁻¹. Furthermore, no decrease in activity was observed even after 10 recycles, which the authors attribute to the stabilising effects and robust nature of the amino-modified support.



Scheme 11: PdNPs encapsulated within amino functionalised graphene oxide nanosheet layers as an efficient catalyst for the Suzuki cross coupling developed by Wang.

Yang *et al.* synthesised bimetallic Pd/Au NPs confined inside imidazolium functionalised single walled carbon nanotubes (SWCNTs).⁹⁹ The highly conjugated aromatic surface of the SWCNTs was modified with imidazolium-based ILs which participate in π - π stacking interactions to afford robust nanotubes. Wet impregnation of the resultant materials with $\text{K}_2[\text{PdCl}_4]$, $\text{H}[\text{AuCl}_4]$ and NaH_2PO_2 in various ratios followed by reduction gave small $\text{Pd}_4\text{Au}_1\text{-P}$ clusters stabilised and anchored by the ILs within the nanotubes (denoted as $\text{Pd}_4\text{Au}_1\text{-P/PDIL-CNTs}$). Favourable interaction with the imidazolium cations embedded within the scaffold facilitated the dispersion of both the nanotubes in water during impregnation, and the metal salt throughout the nanotubes which gives small and well dispersed NPs. The synergistic relationship between the IL with Au, Pd and P within the nanotubes enhances the kinetics and promotes the efficient catalytic performance of the $\text{Pd}_4\text{Au}_1\text{-P/PDIL-CNTs}$ for ethanol electrooxidation. Furthermore, the ILs within the structure also facilitates efficient charge transfer between the surface of the electrode and the electrolyte.

To summarise, nanoparticles have a diverse array of potential applications in various fields of science. For catalysis, NPs have been demonstrated to be extremely active catalysts and allow the advantageous aspects of both homogenous and heterogeneous catalysis to be combined, representing a green alternative to both. Through surface modulation, it is possible to optimise their catalytic behaviour for a range of transformations. ILs can further enhance the physical and chemical properties of NPs as dispersive media, forming a protective layer against aggregation whilst facilitating recycling and dictating the solubility, shape and reactivity of the NPs. Furthermore, the balance of several interactions can be finely tuned for novel

applications with the use of nanoparticle-ionic liquid hybrids, where pre-existing chemical functionality and mesoscopic properties can be combined with the advantageous of NPs in order to observe synergistic effects that can further improve the materials properties.

1.4 Supported Ionic Liquids

The unique combination of properties of ILs has enabled them to enhance catalyst activity and, selectivity as well as improve recyclability. Furthermore, their high thermal stability and nonvolatility have seen them emerge as suitable candidates as biphasic reaction media in order to utilise the advantageous properties of ILs on a larger scale.¹⁰⁰ Despite the success in this area, biphasic systems generally require a large volume of ionic liquid which can increase the overall cost of a process. Combined with undesired leaching of the IL during reaction workup, the high viscosity of ILs can impose severe mass transfer limitations on the reaction and whilst this problem may be overcome with intense stirring, the energetic input required can be impractical and may be unviable in certain protocols. Due to this, there has been considerable drive to design more robust recyclable systems. In this regard, the concept of supported ionic liquid phase (SILP) catalysis initially pioneered by Menhert for rhodium catalysed hydroformylation¹⁰¹ was developed to address such limitations. In SILP catalysis, the advantageous of homogenous catalysis may be combined with those of heterogeneous catalysis as the IL is immobilised on a solid matrix in the form of a thin film thereby enabling facile product separation, reuse of the catalyst and ease of handling.

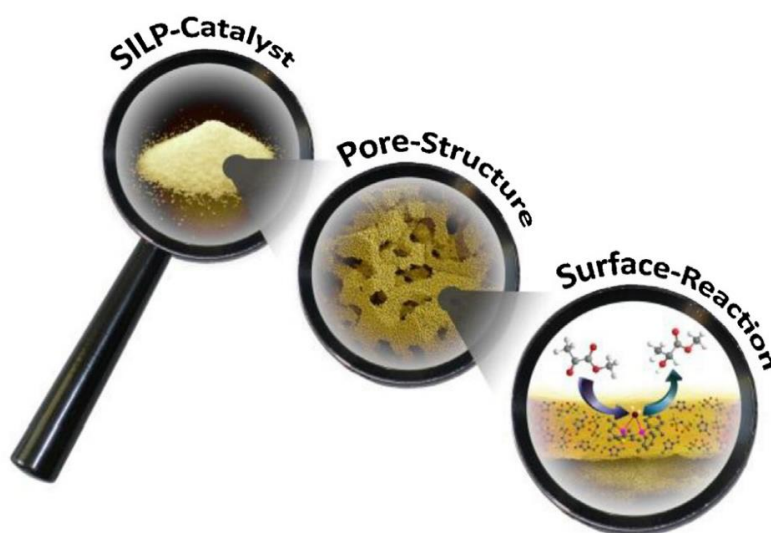


Figure 6: Schematic representation of SILP catalysis.¹⁰²

1.4.1 SILP Catalysis

SILP catalysis consists of a bulk catalyst phase in which the primary diffusional layer contains the active catalyst, IL and substrate. This high dispersion of IL across the surface of the solid support facilitates dissolution of the reactants to the catalyst surface. Furthermore, the IL exists as a thin layer at the support surface, enabling more efficient use, therefore significantly lower ionic content and catalyst loading is required to achieve high activity.¹⁰⁰ Moreover, SILP technology facilitates more efficient recovery of the catalyst via simple filtration by virtue of the robust solid nature of the material; this also improves its amenability to scale-up and continuous flow operation for example, in a fixed-bed reactor. More recently, SILPs have been utilised as dual stabiliser and support for nanoparticle catalysts in which the metal precursor is adsorbed onto the surface and then reduced/decomposed to generate NPs. In these systems the substrate is dispersed in a thin film of ionic liquid and is necessarily in close proximity to the catalyst; this can overcome the problems associated with the high viscosity of ILs and result in rate enhancements compared with IL-based biphasic systems.¹⁰³ Much progress has been made in the area of SILP catalysis, however, it is still in its infancy and there are still several limitations such as irreproducibility, leaching of the IL or catalyst and pore blocking of the inorganic support, which can result in catalyst deactivation. There is a clear need to develop a more detailed understanding of the effect of the support-catalyst interactions on performance.¹⁰⁴

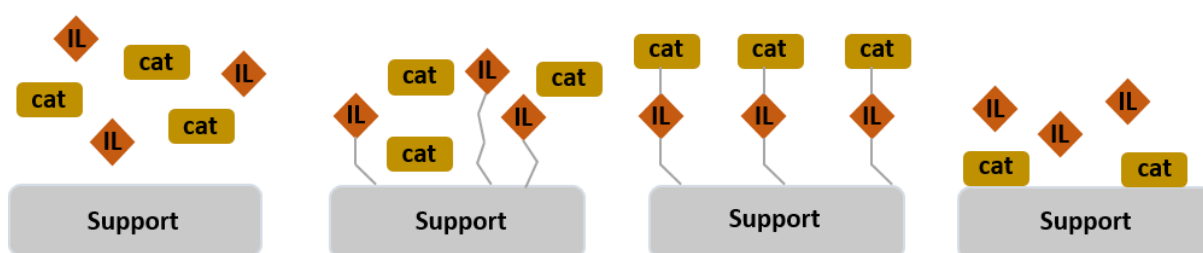
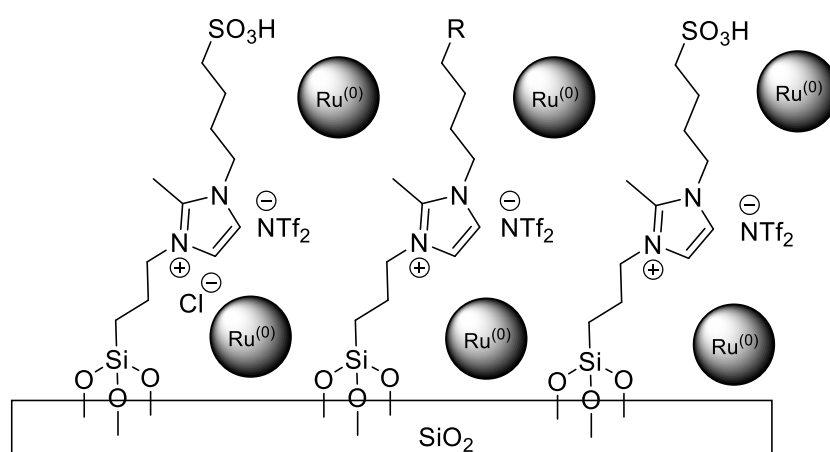


Figure 7: Schematic representation of different SILP based materials (left to right) immersion method, covalent anchoring method, covalently bound catalyst using anchored method, solid catalyst with ionic liquid layer (SCILL method).

Conventionally, the preparation of SILP materials involves the dispersion of the active catalyst into IL solution followed by immersion of a preformed highly porous solid support. This method results in adsorption of the IL/catalyst onto the surface of the support which is then isolated as an insoluble material which can be easily reused (Figure 7).¹⁰⁵ In this regard, dispersion of the catalyst in an ionic liquid environment can give homogenous type activity on a molecular scale, while allowing the catalyst to be recovered in the same manner as a

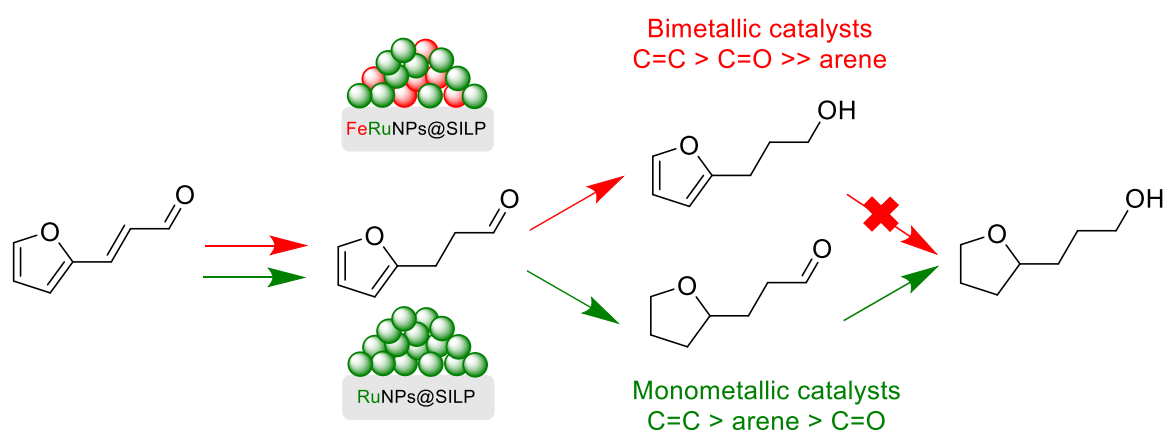
heterogeneous system. The use of this methodology has been widely reported, for instance, Hardacre *et al.* synthesised dimeric Ru complexes using 4'-azulenyl-2,2':6',2''-terpyridine as the ligand in a solution of methanol/IL followed by immobilisation onto silica and evaporation of the solvent to yield the active SILP.¹⁰⁶ The materials are efficient catalysts for the direct oxidation of amines to nitriles and gave activities comparable to their homogeneous counterparts. Haumann immobilised catalytically active *Candida Antarctica* Lipase B enzymes in 1-octyl-3-methylimidazolium tetrafluoroborate [OMIM][BF₄] supported inside a hybrid cellulose-2.5-acetate/polymer monolith for the continuous gas-phase transesterification of vinyl propionate using supercritical CO₂ as the transport medium. The robust nature of the system allowed the catalyst to operate for >700 hours with no observable deactivation and under the optimum conditions, a TON of 2.4×10^8 mol substrate/mol_{CALB}⁻¹ was obtainable; this corresponded to a maximum productivity of 340 μmol/mg_{CALB}⁻¹ h⁻¹. Kirchner prepared Fe^(III) PNP pincer complexes by dissolution of an active iron hydride complex in 1-butyl-2,3-dimethyl-imidazolium bis(trifluoromethylsulfonyl) ([bm₂im][NTf₂]) and absorption onto powdered silica; the resulting catalyst was used for the chemoselective hydrogenation of aldehydes to alcohols.¹⁰⁷ Under conditions of catalysis, the complex remained in the surface-tethered IL layer and under mild conditions (25 °C, 10–50 bar H₂ pressure), TOFs up to 4000 h⁻¹ could be obtained. Similar methodologies using a wide range of inorganic supports have been reported, for example, [bmim][BF₄] and PdOAc immobilised on chitosan is highly active for palladium-catalysed allylations.¹⁰⁸ [Ru(CO)₃Cl₂]₂ dispersed in commercially available [C₄C₁C₁Im][OTf] immobilised on aluminium oxide (γ-Al₂O₃) has been reported to be highly active for the water-gas shift reaction.¹⁰⁹ The ability to incorporate a wide variety of ILs from the large pool of possible structures offers innumerable potential applications and, as such, SILP methodology has been applied for a wide range of transformations.²³ As previously mentioned, whilst the preparation of SILPs by the immersion method may be synthetically facile, it can lead to loss of metal and IL into the reaction phase. Using the IL [bmim][PF₆], Mehnert *et al.* prepared SILP materials incorporating [HRh(CO)(tppti)₃] (tppti = tri(m-sulfonyl)triphenyl phosphine tris(1-butyl-3-methyl-imidazolium)) for Rh catalysed hydroformylations.¹⁰⁴ The SILP system improved selectivity and activity on comparison with the corresponding biphasic IL/organic solvent system. However, as the reaction progressed, the high concentration of product altered the polarity of the organic phase resulting in leaching of the catalyst. To suppress metal loss, productivity had to be limited and additional phosphine was required, lowering the overall efficiency of the process.

In order to overcome such limitations, the ‘anchoring method’ was developed in which the IL is covalently attached to the support. In this approach a suitable support such as silica, activated carbon or alumina is modified by covalent attachment of an ionic liquid, impregnated with a homogenous catalyst in solution to enable absorption of the catalyst on the thin layer of IL film and the solvent removed to afford the SILP.¹¹⁰ However, this method is less economically viable and can be synthetically challenging which limits its applications on a larger scale. Despite this, the anchoring method provides a convenient approach to supporting and stabilising nanoparticles for recycling and as such, has been widely used throughout the literature.²³ Luska and Leitner designed bifunctional SILP catalysts in which sulfonic acid functionalised imidazolium moieties were tethered to a silica support and the resulting immobilised ruthenium nanoparticles catalysed the hydrodeoxygenation of phenols.¹¹¹ The design of such bifunctional catalysts is a rapidly evolving area of interest as multi-step reactions can be conducted in a single process to access a wider range of products. The authors report that using this approach enables optimisation of the synergistic relationship between the RuNPs and pendant acid groups such that the rate of the overall transformations, comprised of sequential hydrogenation and acid catalyst dehydration, are enhanced on comparison to the separate steps catalysed by each individual functionality. Furthermore, the relative ratio of the components can be tuned using a molecular ‘bottom up’ strategy to generate highly active and selective catalysts. The authors postulate that the intimate contact between the metal and proximal acid sites is responsible for the superior activity of the SILP catalysts due to a cooperative effect.



Scheme 12: Bifunctional catalyst comprised of RuNPs immobilised on acidic imidazolium functionalised silica developed by Leitner and Luska for the hydrodeoxygenation of phenols.

Bimetallic SILPs containing Au^{3+} and Cu^{2+} ions immobilised in 1-propyl-3-methylimidazolium chloride supported on activated carbon have been reported as efficient catalysts for the hydrochlorination of acetylene.¹¹² The SILP material was employed in a fixed-bed reactor and under the optimum conditions 99.8% selectivity for the vinyl chloride monomer was obtained; this corresponds to a total TOF of 168.5 h^{-1} . ICP analysis confirmed negligible leaching of the catalyst which showed a stable activity profile over 500 hours. The Cu doped material substantially outperformed the corresponding monometallic gold-based SILP system and the authors proposed that a Cu-mediated redox reaction allowed efficient adsorption of the reactants on Au^{3+} surfaces as well as re-oxidation of the Au^0 formed in the catalytic cycle. Interestingly, Leitner and Chaudret have demonstrated that the formation, shape and size of bimetallic FeRu nanoparticles can be controlled on imidazolium based ILs tethered to a silica support.¹¹³ The authors proposed that this method allowed both facile access and removal of the organic reactants and products from the metal site and that the SILP material provided enhanced stabilisation of the NPs through electrosteric protection from the silica as well as tuneable reactivity derived from the IL functionalisation. Furthermore, the Fe:Ru ratio could be varied to tailor the catalyst selectivity for the hydrogenation of heteroaromatic α,β -unsaturated ketones. Dilution of Ru with Fe resulted in stark differences in catalyst activity and selectivity and ultimately, could reverse functional group preference under the appropriate conditions. Hot filtration experiments demonstrated that no leaching of Ru occurred and the SILP could be recovered from the reaction by filtration.



Scheme 13: Switchable selectivity in the Selective hydrogenation of a bioderived furan using Ru and FeRuNP catalysts.

In 2007 Kernchen reported a new concept for the preparation of SILP materials whereby a heterogeneous catalyst is coated with a thin layer of ionic liquid to form a solid catalyst with an ionic liquid layer (SCILL).¹¹⁴ A commercially available nickel catalyst (Ni on SiO_2) coated with

[BMIM][n-C₈H₁₇OSO₃] showed enhanced selectivity from 40% to 70% for the sequential hydrogenation of cyclooctadiene (COD) to cyclooctene (COE) and cyclooctane with no leaching of the IL. Furthermore, as this method does not require complete solvation of complex inorganic structures, a range of different supports can be easily modified. To this end, Parvulescu and Hardacre recently coated the surface of platinum and ruthenium NPs supported on silica, carbon and OMS-2 and the resulting SCILLs were efficient catalysts for the aerobic oxidative coupling of 1-butanethiol and thiophenol to dibutyl disulfide and diphenyl disulphide, respectively, under extremely mild conditions using air as the oxidant.¹¹⁵ A range of imidazolium-based ILs containing the (bis(trifluoromethylsulfonyl)imide anion were deposited onto the surface of the catalysts and even though these systems were less active than IL-free catalysts, the ionic liquid disrupted the strong metal-sulfur interactions that cause deactivation, thereby improving the long term stability. However, whilst this method has resulted in enhanced selectivities in many reactions, it is limited to biphasic conditions where the reactant product and organic phase are immiscible with the IL which somewhat hampers its applications. Furthermore, Pd/C coated with a thin film of the Lewis acid IL [BMIM]Cl/AlCl₃ as well as a liquid coordination complex (LCC) urea/AlCl₃ catalysed the hydrogenation of various aromatics.¹¹⁶ However, despite improvements in activity observed at low volumes of IL, larger volumes were shown to deactivate the catalyst due to pore blocking of the support.

In summary, supported ionic liquid phase catalysis aims to combine the advantageous aspects of both homogenous and heterogenous catalysis and thereby improve catalyst performance, reuse and product extraction. Furthermore, this methodology can reduce the required amount of IL quite significantly compared with biphasic systems and improve the economic viability of catalysis in ILs, which makes SILP an attractive technology for future applications. One of the most desirable attributes of SILP catalysis is its application in fixed-bed reactors in continuous gas phase reactions for industrial processes. In a recent example, SILP technology was used for the continuous gas phase methoxycarbonylation of ethylene with a significant improvement in overall catalyst turnover and space time yields on comparison to commercially available catalysts.¹⁰³ However, there is still scope for improvement on the current systems due to some intrinsic limitations. For example, from the examples described above, the application of SILP catalysis in gas phase reactions is operationally facile, whereas liquid phase reactions often require careful consideration of the polarity of the reaction components to avoid leaching of the catalyst or IL. Moreover, detailed mechanistic studies are

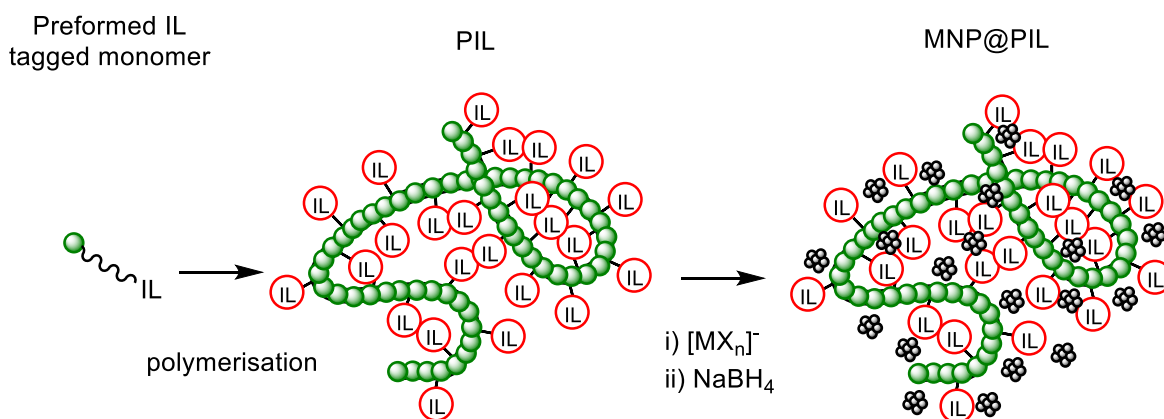
required to determine the nature of the active species in SILP catalysis as there is a clear synergy between the influence of the support and nature of the IL on the catalyst performance.

1.5 Polymer Immobilised Ionic Liquid Phase Catalysis

Polyionic liquids (PILs) are an intriguing new class of polymers that comprise a polymer backbone tagged with an IL moiety which gives rise to novel morphologies and structures that would generally be inaccessible from the two individual constituents.⁵⁰ PILs are extremely diverse as these materials allow the tuneable properties of ionic liquids to be combined with the favourable attributes of polymers.⁵⁰ One particularly attractive feature of using PILs over their SILP counterparts is their flexibility and swelling properties in solution. In this regard, PILs offer an alternative reaction environment to conventional heterogeneous inorganic materials. Swelling of the polymer support enables facile access of the substrate to non-surface catalytically active sites, which would not be possible in rigid SILP systems.¹¹⁷ Furthermore, the modular construction of PILs enables a variety of IL-tagged monomers and neutral task specific monomers to be incorporated to control the ionic microenvironment and its function. In this regard, optimisation of the physical properties of polymers such as flexibility through the degree of crosslinking, thermal stability and compatibility with a range of solvents enables control over their dynamic behaviour in solution which has fuelled their applications in a range of scientific disciplines including biotechnology,¹¹⁸ fuel cell applications,¹¹⁹ energy materials,¹²⁰ and drug delivery.¹²¹ As an extension of SILP, the concept of polymer immobilised ionic liquid (PIIL) catalysis has revolutionised the field of heterogeneous catalysis and is emerging as an extremely versatile class of support and stabiliser for metal nanoparticles. As such, PIIL materials are now well documented in the field of catalysis, in particular the embedding of metal nanoparticles into polymer matrices is frequently reported due to the convenient synthesis,¹²² and will therefore be the primary area of discussion in this section.

Whilst there are numerous methods for the construction of polymeric materials, the most common method of preparing PIIL stabilised NPs is through the rational design of ionic liquid-like monomers that can be combined with neutral comonomers through polymerisation.⁵⁰ Whilst it is possible to fabricate PIILs by post polymerisation modification of imidazole functionalised polymers, this method can often be non-quantitative and present challenges with product purification. Furthermore, the straightforward synthesis of styrenic imidazolium monomers provides a facile method of preparing IL-based polystyrene. The PIIL can then be

impregnated with an appropriate metal precursor before reduction with H_2 or molecular reducing agents to afford the corresponding metal nanoparticles. In this strategy, the PIL can provide electrosteric protection of the NPs against aggregation through weak interactions between the IL and surface of the nanoparticle surface as well as steric protection from the large polymer backbone. Tuning of the polymer composition has been used to control the nature of the interactions at the polymer-catalyst interface and thereby achieve enhancements in rate as well as drastic improvements in selectivity through various interactions with the substrate.⁵¹



Scheme 14: General synthetic protocol for the preparation of PIL stabilised NPs.

For example, carboxylic acid functionalised imidazolium-based IL monomers copolymerised with divinyl benzene form a mesoporous polyionic liquid capable of supporting and stabilising Pd nanoparticles (NPs) for the efficient aqueous phase catalytic oxidation of benzyl alcohol to benzaldehyde using O_2 gas as the oxidant.¹²³ The authors suggest that the PIL plays a crucial role in the catalysis as the hydrophilic sites within the ionic framework possess a strong affinity for water, which allows the chemisorption of the solvent onto the IL moiety. The -OH groups present at the interface allow facile diffusion of the poorly soluble substrate to the catalyst surface through H-bond interactions. Furthermore, once the product is formed, the increased miscibility with water facilitates its removal from the active site which avoids further oxidation and improves selectivity. The authors also state that the low concentration of product at the active site increases the reaction rate through an equilibrium shift. Anisotropic poly ionic liquid membranes impregnated with Pd are efficient catalysts for the Suzuki-Miyaura cross coupling.¹²⁴ In this system, poly(vinylbenzyl chloride) was effectively layered onto a membrane and surface benzylchloride groups were quaternised with *N*-butylimidazole to generate a layer of PIL on the surface, which was complexed with $PdCl_2$. The selective solubility

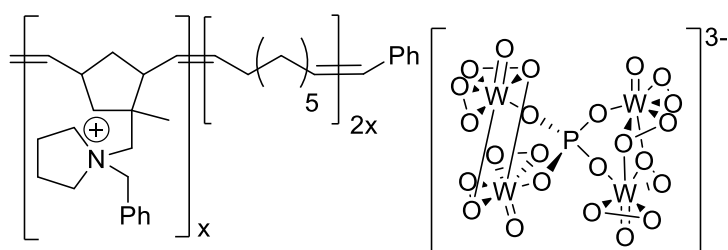
of the hybrid catalyst-membrane material enabled the product to be separated from the phenyl boronic acid reactant solution by diffusion through the IL layer while the phenylboronic acid remained in the reaction phase. Furthermore, the IL phase is immiscible with the bulk solvent, a water-ethanol mix, which prevented leaching of the catalyst. The practical viability of this system allowed for the development of continuous flow protocol which showed a stable profile and a total TOF of 154 h^{-1} . Functionalisation of the surface of carbon nanotubes (CNTs) with imidazolium based polyionic liquids has been shown to overcome problems associated metal leaching in CNTs for catalysis.¹²⁵ The PIL on the surface facilitates encapsulation and stabilisation of PtRu NPs by significantly increasing the potential binding sites for the metal precursors. Furthermore, the uniform dispersion of metal precursor across the PIL decorated CNTs was responsible for formation of the small NPs which showed improved performance for the electrooxidation of methanol compared with the non-functionalised CNTs. *N*-Heterocyclic carbene functionalised PILs have recently been shown to be capable of controlling the size of metal nanoparticles.¹²⁶ In this approach, polytriazolium-derived PILs functionalised with hexyl side chains appear to induce the spontaneous formation of PIL nanovesicles which limits the size of particle growth. Additionally, the incorporation of neutral carbenes in the polymer architecture provides extra stabilisation of the NPs, controls the ionic microenvironment by decreasing the overall charge density and enhances the activity of the NP catalysts. For example, rhodium NPs prepared in this manner outperform state of the art catalysts for the methanolysis of ammonia borane.

The modular synthesis of PILs has also been used to prepare bifunctional catalysts, for example, sulfonic acid-tethered imidazolium-based PIL stabilised PdNPs.¹²⁷ In this system, the sulfonic acid groups promote efficient dissolution of the polymer in water, allowing the reaction to be conducted in an environmentally responsible medium. The catalysts exhibited extremely high activity and selectivity in the hydrogenation of phenol to cyclohexanone. The high selectivity was attributed to the ability of the PIL support to form hydrophilic cages heavily decorated with sulfonic acids and ions that effectively induce i) enrichment of the phenol concentration through favourable interactions, ii) a highly uniform dispersion of the PdNPs inside the cavity and iii) removal of the product, enhancing the rate of reaction.

The work described in this thesis is based on a recent initiative developed by the Doherty/Knight group to explore and develop the concept of polymer immobilised ionic liquid phase (PIILP) catalysis in an attempt to address the limitations that ILs pose in

homogenous/biphasic catalysis. The modular synthesis of PIILs allows ionic liquid-like monomers and task specific monomers to be incorporated into the polymer backbone; cross-linking can also be readily introduced to improve integrity and modify porosity. The appropriate homogenous catalyst or catalyst precursor is embedded into the polymer and thereby heterogenized to facilitate recovery and separation of products. The novelty of this strategy is that polymer properties such as porosity, ionic microenvironment and microstructure, stability, durability and structural integrity can be fine-tuned in a rational and systematic manner through a judicious choice of monomer, co-monomer and cross-linker. Furthermore, this technique also allows the catalyst-support interactions and substrate accessibility to be optimised to tailor the catalyst activity and selectivity across a broad range of transformations.

To this end, the Doherty/Knight group have already demonstrated that linear pyrrolidinium-based PIILPs synthesised by ROMP are capable of immobilising a peroxophosphotungstate catalyst which was extremely efficient for the epoxidation of allylic alcohols and alkenes.¹²⁸ Comparative catalyst testing revealed that the PIILP systems substantially outperformed the parent $[\text{PW}_{12}\text{O}_{40}][\text{NEt}_4]_3$ validating the role of the polymer support. The PIILP catalyst could be recycled 4 times in an operationally straightforward protocol with only a minor drop in activity. Additionally, no evidence of metal leaching was demonstrated by obtaining ICP analysis of the solvent after filtration and recovery of the catalyst. The versatility of this approach was later demonstrated as similar systems were shown to be remarkably efficient catalysts for the oxidation of sulfides in batch and continuous flow under extremely mild conditions.¹²⁹ The robust nature of these PIILP systems enabled a stable activity-selectivity profile over 8 hours to be obtained under continuous flow conditions yielding a total TON of 46,428.



Scheme 15: Peroxometallate PIILP catalyst developed by Doherty/Knight group for epoxidation of allylic alcohols and oxidation of sulphides.

The group also prepared PIILP catalysts by AIBN-initiated radical copolymerisation of styryl functionalised pyrrolidinium-based ILs with styrene and divinyl benzene crosslinkers for the immobilisation of chiral copper(II)-bis(oxazoline) complexes.¹³⁰ The introduction of chirality into the polymer architecture yielded catalysts that were highly efficient and selective for the Diels–Alder reaction between N-acryloyloxazolidinone and cyclopentadiene. In order to assess the relative merits of the PIILs, the active catalyst was also immobilised on common inorganic SILP supports such as SiO₂ and multiwalled carbon nanotubes. Comparative catalyst testing revealed that higher activities and ees were obtained using the PIILP supports. Moreover, the PIILP systems showed substantial improvements in recycling experiments which was proposed to be derived from the increased binding affinity of the catalyst within the ionic polymer network. Moreover, 99% ee was achieved for the cycloadduct *endo*-(2S) product using a pyrrolidinium-functionalised styrene support which is the highest reported in the literature for a Cu(II)-catalysed reaction of this substrate combination at room temperature under heterogeneous or homogeneous conditions. It was proposed that the unique ionic microenvironment provided by the polymer support surrounding the metal triflate was responsible for the differences in activities.

1.6 Project aims

This work will begin by harnessing the concept of PIILP previously developed by the Doherty group and will initially focus on styrene-based heteroatom donor-modified PIILs for the stabilisation of metal nanoparticles. There are many viable methods for the fabrication of polymeric structures such as living radical polymerisation which may give additional control with regards to polymer growth and polydispersity, however, the requirement of expensive RAFT agents and their limited tolerance to functional groups may limit the scope of monomers available for polymerisation.⁵⁰ Furthermore, whilst step polymerisation has been shown to be a convenient method of producing various polymers and oligomers, the reactive end groups needed for sequential reactions again limits the scope of monomers available and requires further synthetic steps. The practical advantages associated with the modular synthesis of styrene-based imidazolium monomers presents a more attractive method of synthesising PIILs. The innovation and timeliness of this project lies in the introduction of additional functionality into the polymer immobilised ionic liquid to rationally modulate the catalyst-support interactions to elucidate factors that improve catalyst lifetime, selectivity profile and recyclability in a range of industrially relevant transformations. The introduction of neutral

heteroatom donors into the backbone may allow control over the morphological growth and activity of the NPs derived from the ligand effects described previously, as well as exert additional control over the ionic microenvironment by modulating charge density. It will therefore be necessary to undertake detailed investigations in order to identify optimum property-performance profiles of the supported nanoparticle catalysts. A key goal for this project is the development of novel and innovative catalyst technology concerned with improving the efficacy of the conversion of biomass derived substrates into potential fuels and platform chemicals in a viable and green manner. In this regard, research in this area is devoted to the improvement of industrial-based catalysts in order to increase sustainability by reducing the number of reagents and developing systems that operate efficiently under mild conditions. To this end we propose to develop PIIL stabilised NP catalysts that operate efficiently in the aqueous phase and that are highly active and selective for the hydrogenation of model and biomass derived substrates. Due to its low toxicity, flammability and volatility, water is generally considered an environmentally benign solvent and as such aqueous phase catalysis offers many attractive features, as the highly oxygenated reactants which are water-miscible remain in the catalyst phase, whereas the deoxygenated products may be collected by simple extraction techniques.

1.7 References

1. Z. Lei, B. Chen, Y.-M. Koo and D. R. MacFarlane, *Chem. Rev.*, 2017, **117**, 6633-6635.
2. P. M. Shem, R. Sardar and J. S. Shumaker-Parry, *Langmuir*, 2009, **25**, 13279-13283.
3. T. Tsukasa, T. Tetsuya, O. Ken - ichi and K. Susumu, *Adv. Mater.*, 2010, **22**, 1196-1221.
4. A. A. C. Toledo Hijo, G. J. Maximo, M. C. Costa, E. A. C. Batista and A. J. A. Meirelles, *ACS Sustainable Chem. Eng.*, 2016, **4**, 5347-5369.
5. L. Zhang, Y. Cui, C. Zhang, L. Wang, H. Wan and G. Guan, *Ind. Eng. Chem. Res.*, 2012, **51**, 16590-16596.
6. J. P. Hallett and T. Welton, *Chem. Rev.*, 2011, **111**, 3508-3576.
7. S. Sugden and H. Wilkins, *J. Chem. Soc.*, 1929, 1291-1298.
8. J. S. Wilkes, J. A. Levisky, R. A. Wilson and C. L. Hussey, *Inorg. Chem.*, 1982, **21**, 1263-1264.
9. J. S. Wilkes and M. J. Zaworotko, *J. Chem. Soc., Chem. Commun.*, 1992, 965-967.
10. J. H. Davis Jr, *Chem. Lett.*, 2004, **33**, 1072-1077.
11. R. L. Vekariya, *J. Mol. Liq.*, 2017, **227**, 44-60.
12. J. Dupont, R. F. de Souza and P. A. Z. Suarez, *Chem. Rev.*, 2002, **102**, 3667-3692.
13. S. Mallakpour and M. Dinari, in *Green Solvents II: Properties and Applications of Ionic Liquids*, eds. A. Mohammad and D. Inamuddin, Springer Netherlands, Dordrecht, Editon edn., 2012, pp. 1-32.
14. C. Wakai, A. Oleinikova, M. Ott and H. Weingärtner, *J. Phys. Chem. B*, 2005, **109**, 17028-17030.
15. H. Olivier-Bourbigou, L. Magna and D. Morvan, *Appl. Catal., A*, 2010, **373**, 1-56.
16. H. Chen, X. Chen, J. Deng and J. Zheng, *Chem. Sci.*, 2018, **9**, 1464-1472.
17. J. Dupont, *J. Braz. Chem. Soc.*, 2004, **15**, 341-350.
18. T. L. Greaves, D. F. Kennedy, S. T. Mudie and C. J. Drummond, *J. Phys. Chem. B*, 2010, **114**, 10022-10031.
19. D. A. Carmine, D. M. Mick, L. M. Claire, H. Christopher and F. G. Lynn, *ChemPhysChem*, **0**.
20. P. Anastas and N. Eghbali, *Chem. Soc. Rev.*, 2010, **39**, 301-312.
21. P. T. Anastas, M. M. Kirchhoff and T. C. Williamson, *Appl. Catal. A*, 2001, **221**, 3-13.
22. V. I. Pârvulescu and C. Hardacre, *Chem. Rev.*, 2007, **107**, 2615-2665.
23. H.-P. Steinrück and P. Wasserscheid, *Catal. Lett.*, 2015, **145**, 380-397.

24. P. Wasserscheid and W. Keim, *Angew. Chem.*, 2000, **39**, 3773-3789.
25. K. T. Prabhu Charan, N. Pothanagandhi, K. Vijayakrishna, A. Sivaramakrishna, D. Mecerreyes and B. Sreedhar, *Eur. Polym. J.*, 2014, **60**, 114-122.
26. K. Anderson, P. Goodrich, C. Hardacre and D. W. Rooney, *Green Chem.*, 2003, **5**, 448-453.
27. G. W. Huber, S. Iborra and A. Corma, *Chem. Rev.*, 2006, **106**, 4044-4098.
28. J. Julis, M. Holscher and W. Leitner, *Green Chem.*, 2010, **12**, 1634-1639.
29. A. Weilhard, M. I. Qadir, V. Sans and J. Dupont, *ACS Catal.*, 2018, **8**, 1628-1634.
30. M. Filice, O. Romero, O. Abian, B. de las Rivas and J. M. Palomo, *RSC Adv.*, 2014, **4**, 49115-49122.
31. J. Mo, L. Xu and J. Xiao, *J. Am. Chem. Soc.*, 2005, **127**, 751-760.
32. D. Zhao, Z. Fei, R. Scopelliti and P. J. Dyson, *Inorg. Chem.*, 2004, **43**, 2197-2205.
33. J.-C. Xiao and J. n. M. Shreeve, *J. Org. Chem.*, 2005, **70**, 3072-3078.
34. T. Duan - Jian, C. Feng - Feng, T. Zi - Qi, H. Kuan, M. M. Shannon, J. De - en and D. Sheng, *Angew. Chem.*, 2017, **129**, 6947-6951.
35. M. Potdar, G. Kelso, L. Schwarz, C. Zhang and M. Hearn, *Molecules*, 2015, **20**, 16788.
36. J. Limberger, B. C. Leal, A. L. Monteiro and J. Dupont, *Chem. Sci.*, 2015, **6**, 77-94.
37. B. C. Leal, G. L. P. Aydos, P. A. Netz and J. Dupont, *ACS Omega*, 2017, **2**, 1146-1155.
38. V. L. van Zyl, A. Muller and D. B. G. Williams, *Tetrahedron Lett.*, 2018, **59**, 918-921.
39. P. Nehra, B. Khungar, R. P. Singh, S. C. Sivasubramanian, P. N. Jha and V. Saini, *Inorg. Chim. Acta*, 2018, **478**, 260-267.
40. V. H. Nguyen, M. B. Ibrahim, W. W. Mansour, B. M. El Ali and H. V. Huynh, *Organometallics*, 2017, **36**, 2345-2353.
41. M. Shawn, D. P. Harry and M. A. Travis, *Molecular Informatics*, 2017, **36**, 1600125.
42. M. J. Climent, A. Corma and S. Iborra, *Green Chem.*, 2014, **16**, 516-547.
43. A. Kumar and S. S. Pawar, *Science China Chemistry*, 2012, **55**, 1633-1637.
44. M. Jankowska-Wajda, R. Kukawka, M. Smiglak and H. Maciejewski, *New J. Chem.*, 2018, **42**, 5229-5236.
45. Z. Yanfei, Y. Bo, Y. Zhenzhen, Z. Hongye, H. Leiduan, G. Xiang and L. Zhimin, *Angew. Chem. Int. Ed.*, 2014, **53**, 5922-5925.
46. Y. Park, K.-Y. A. Lin, A.-H. A. Park and C. Petit, *Frontiers in Energy Research*, 2015, **3**.
47. i. Anugwom, P. Mäki-Arvela, P. Virtanen, P. Damlin, R. Sjöholm and J.-P. Mikkola, *Switchable Ionic liquids (SILs) based on glycerol and acid gases*, 2011.
48. H. Passos, A. Luís, J. A. P. Coutinho and M. G. Freire, *Scientific Reports*, 2016, **6**, 20276.
49. Y. Qiao, W. Ma, N. Theyssen, C. Chen and Z. Hou, *Chem. Rev.*, 2017, **117**, 6881-6928.
50. W. Qian, J. Texter and F. Yan, *Chem. Soc. Rev.*, 2017, **46**, 1124-1159.
51. Z. Wenwen, Y. Yinyin, Y. Hanmin, H. Li, Q. Yunxiang, Z. Xiuge and H. Zhenshan, *Chem. Eur. J.*, 2013, **19**, 2059-2066.
52. Y. Ma, S. Qing, L. Wang, N. Islam, S. Guan, Z. Gao, X. Mamat, H. Li, W. Eli and T. Wang, *RSC Adv.*, 2015, **5**, 47377-47383.
53. D. Wang, J. Li, J. Peng, Y. Bai and G. Lai, *Phosphorus, Sulfur, and Silicon and the Related Elements*, 2011, **186**, 2258-2266.
54. E. Rafiee and M. Kahrizi, *J. Mol. Liq.*, 2016, **218**, 625-631.
55. J. L. Fiorio, N. López and L. M. Rossi, *ACS Catal.*, 2017, **7**, 2973-2980.
56. G. F. De Gregorio, R. Prado, C. Vriamont, X. Erdocia, J. Labidi, J. P. Hallett and T. Welton, *ACS Sustainable Chem. Eng.*, 2016, **4**, 6031-6036.
57. Y. Lifeng, Y. Qiwei, H. Jingyi, B. Zongbi, S. Baogen, Z. Zhiguo, R. Qilong and X. Huabin, *AIChE J.*, **0**.
58. L. Rassaei, F. Marken, M. Sillanpää, M. Amiri, C. M. Cirtiu and M. Sillanpää, *TrAC, Trends Anal. Chem.*, 2011, **30**, 1704-1715.
59. D. Mrinmoy, S. G. Partha and M. R. Vincent, *Adv. Mater.*, 2008, **20**, 4225-4241.
60. E. Blanco, H. Shen and M. Ferrari, *Nat. Biotechnol.*, 2015, **33**, 941.
61. O. S. Adeyemi and F. A. Sulaiman, *J. Bio. Res.*, 2015, **29**, 145-149.
62. R. Benavides, L. W. Oenning, M. M. S. Paula and L. Da Silva, *Int. J. Hydrogen Energy*, 2015, **40**, 17413-17420.
63. M. Zahmakıran and S. Özkır, *Metal nanoparticles in liquid phase catalysis; from recent advances to future goals*, 2011.
64. P. W. Voorhees, *J. Stat. Phys.*, 1985, **38**, 231-252.
65. S. Ojala, N. Bion, A. Baylet, M. Tarighi, R. Keiski and D. Duprez, *Correlations between oxygen activation and methane oxidation over Pd/γ-Al₂O₃ catalysts prepared by nitrite method*, 2011.
66. E. K. Dann, E. K. Gibson, R. A. Catlow, P. Collier, T. Eralp Erden, D. Gianolio, C. Hardacre, A. Kroner, A. Raj, A. Goguet and P. P. Wells, *Chem. Mater.*, 2017, **29**, 7515-7523.
67. H.-y. Jiang and X.-x. Zheng, *Catal. Sci. Technol.*, 2015, **5**, 3728-3734.
68. P. M. Uberman, C. S. Garcia, J. R. Rodriguez and S. E. Martin, *Green Chem.*, 2017, **19**, 739-748.

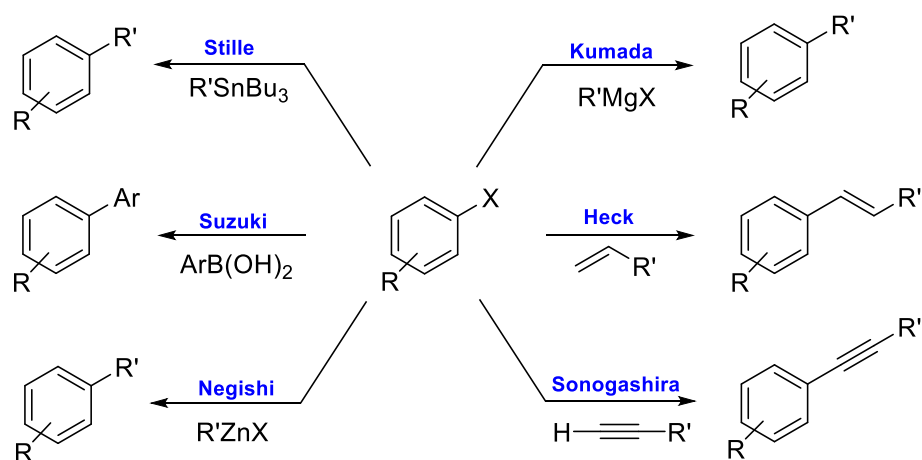
69. D. K. Mishra, A. A. Dabbawala and J.-S. Hwang, *Catal. Commun.*, 2013, **41**, 52-55.
70. W. Dong, L. Zhang, C. Wang, C. Feng, N. Shang, S. Gao and C. Wang, *RSC Adv.*, 2016, **6**, 37118-37123.
71. S. Doherty, J. G. Knight, T. Backhouse, E. Abood, H. Alshaikh, I. J. S. Fairlamb, R. A. Bourne, T. W. Chamberlain and R. Stones, *Green Chem.*, 2017, **19**, 1635-1641.
72. M. T. Islam, S. K. Molugu, P. H. Cooke and J. C. Noveron, *New J. Chem.*, 2015, **39**, 5923-5926.
73. X. Jin, B. He, J. Miao, J. yuan, Q. Zhang and L. Niu, *Carbon*, 2012, **50**, 3083-3091.
74. L. Suo, W. Gao, Y. Du, R. Wang, L. Wu and L. Bi, *New J. Chem.*, 2016, **40**, 985-993.
75. H. Ohshima, in *Biophysical Chemistry of Biointerfaces*, John Wiley & Sons, Inc., Editon edn., 2010, pp. 420-430.
76. J. Wang, S. A. Kondrat, Y. Wang, G. L. Brett, C. Giles, J. K. Bartley, L. Lu, Q. Liu, C. J. Kiely and G. J. Hutchings, *ACS Catal.*, 2015, **5**, 3575-3587.
77. A. Botos, J. Biskupek, T. W. Chamberlain, G. A. Rance, C. T. Stoppiello, J. Sloan, Z. Liu, K. Suenaga, U. Kaiser and A. N. Khlobystov, *J. Am. Chem. Soc.*, 2016, **138**, 8175-8183.
78. M. K. Corbierre, N. S. Cameron, M. Sutton, S. G. J. Mochrie, L. B. Lurio, A. Rühm and R. B. Lennox, *J. Am. Chem. Soc.*, 2001, **123**, 10411-10412.
79. I. Medina-Ramirez, S. Bashir, Z. Luo and J. L. Liu, *Colloids and Surfaces B: Biointerfaces*, 2009, **73**, 185-191.
80. X. Liu, D. Gregurec, J. Irigoyen, A. Martinez, S. Moya, R. Ciganda, P. Hermange, J. Ruiz and D. Astruc, *Nat. Comm.*, 2016, **7**, 13152.
81. S. R. Barman, A. Nain, S. Jain, N. Punjabi, S. Mukherji and J. Satija, *J. Mater. Chem. B*, 2018, **6**, 2368-2384.
82. D. S. Gaikwad, K. A. Undale, D. B. Patil, D. M. Pore and A. A. Kamble, *Res. Chem. Intermed.*, 2018, **44**, 265-275.
83. G. Fritz, V. Schädler, N. Willenbacher and N. J. Wagner, *Langmuir*, 2002, **18**, 6381-6390.
84. J. Hang, L. Shi, X. Feng and L. Xiao, *Powder Technol.*, 2009, **192**, 166-170.
85. M. Qu, S. Chen, W. Ma, J. Chen, K. Kong, F. Zhang, H. Li, Z. Hou and X.-M. Zhang, *Langmuir*, 2016, **32**, 13746-13751.
86. L. M. Martínez-Prieto and B. Chaudret, *Acc. Chem. Res.*, 2018, **51**, 376-384.
87. A. Villa, S. J. Freakley, M. Schiavoni, J. K. Edwards, C. Hammond, G. M. Veith, W. Wang, D. Wang, L. Prati, N. Dimitratos and G. J. Hutchings, *Catal. Sci. Technol.*, 2016, **6**, 694-697.
88. D. Hui, D. Yu, Z. Xiaojin, Z. Zhenguo, F. Shuangli and Z. Zhenlin, *Nanotechnology*, 2018, **29**, 055705.
89. D. González-Gálvez, P. Nolis, K. Philippot, B. Chaudret and P. W. N. M. van Leeuwen, *ACS Catal.*, 2012, **2**, 317-321.
90. J. B. Ernst, S. Muratsugu, F. Wang, M. Tada and F. Glorius, *J. Am. Chem. Soc.*, 2016, **138**, 10718-10721.
91. J. B. Ernst, C. Schwermann, G.-i. Yokota, M. Tada, S. Muratsugu, N. L. Doltsinis and F. Glorius, *J. Am. Chem. Soc.*, 2017, **139**, 9144-9147.
92. J. Dupont and J. D. Scholten, *Chem. Soc. Rev.*, 2010, **39**, 1780-1804.
93. Z. He and P. Alexandridis, *Adv. Colloid Interface Sci.*, 2017, **244**, 54-70.
94. J. Dupont, G. S. Fonseca, A. P. Umpierre, P. F. P. Fichtner and S. R. Teixeira, *J. Am. Chem. Soc.*, 2002, **124**, 4228-4229.
95. C.-M. Lee, H.-J. Jeong, S. T. Lim, M.-H. Sohn and D. W. Kim, *ACS Appl. Mater. Interfaces*, 2010, **2**, 756-759.
96. R. Bhandary, J. G. Alauzun, P. Hesemann, A. Stocco, M. In and P. H. Mutin, *Soft Matter*, 2017, **13**, 8023-8026.
97. S. S. Moganty, S. Srivastava, Y. Lu, J. L. Schaefer, S. A. Rizvi and L. A. Archer, *Chem. Mater.*, 2012, **24**, 1386-1392.
98. Y. Huang, Q. Wei, Y. Wang and L. Dai, *Carbon*, 2018, **136**, 150-159.
99. H. Yang, Z. Yu, S. Li, Q. Zhang, J. Jin and J. Ma, *J. Catal.*, 2017, **353**, 256-264.
100. R. Anders, F. Rasmus, H. Marco and W. Peter, *Eur. J. Inorg. Chem.*, 2006, **2006**, 695-706.
101. C. P. Mehnert, R. A. Cook, N. C. Dispenziere and M. Afeworki, *J. Am. Chem. Soc.*, 2002, **124**, 12932-12933.
102. M. J. Schneider, M. Haumann and P. Wasserscheid, *J. Mol. Catal. A: Chem.*, 2013, **376**, 103-110.
103. G. Khokarale Santosh, J. García - Suárez Eduardo, R. Fehrmann and A. Riisager, *ChemCatChem*, 2017, **9**, 1824-1829.
104. A. Riisager, R. Fehrmann, M. Haumann and P. Wasserscheid, *Eur. J. Inorg. Chem.*, 2006, **2006**, 695-706.
105. T. Selvam, A. Machoke and W. Schwieger, *Appl. Catal. A*, 2012, **445-446**, 92-101.
106. O. D. Pavel, P. Goodrich, L. Cristian, S. M. Coman, V. I. Parvulescu and C. Hardacre, *Catal. Sci. Technol.*, 2015, **5**, 2696-2704.
107. J. Brüinig, Z. Csendes, S. Weber, N. Gorgas, R. W. Bittner, A. Limbeck, K. Bica, H. Hoffmann and K. Kirchner, *ACS Catal.*, 2018, **8**, 1048-1051.

108. R. Moucel, K. Perrigaud, J. M. Goupil, P. J. Madec, S. Marinel, E. Guibal, A. C. Gaumont and I. Dez, *Adv. Synth. Catal.*, 2010, **352**, 433-439.
109. T. Bauer, R. Stepic, P. Wolf, F. Kollhoff, W. Karawacka, C. R. Wick, M. Haumann, P. Wasserscheid, D. M. Smith, A.-S. Smith and J. Libuda, *Catal. Sci. Technol.*, 2018, **8**, 344-357.
110. C. Van Doorslaer, J. Wahlen, P. Mertens, K. Binnemans and D. De Vos, *Dalton Trans.*, 2010, **39**, 8377-8390.
111. L. Luska Kylie, P. Migowski, S. El Sayed and W. Leitner, *Angew. Chem. Int. Ed.*, 2015, **54**, 15750-15755.
112. J. Zhao, Y. Yu, X. Xu, S. Di, B. Wang, H. Xu, J. Ni, L. Guo, Z. Pan and X. Li, *Appl. Catal. B*, 2017, **206**, 175-183.
113. K. L. Luska, A. Bordet, S. Tricard, I. Sinev, W. Grünert, B. Chaudret and W. Leitner, *ACS Catal.*, 2016, **6**, 3719-3726.
114. U. Kernchen, B. Etzold, W. Korth and A. Jess, *Chem. Eng. Technol.*, 2007, **30**, 985-994.
115. O. D. Pavel, I. Podolean, V. I. Parvulescu, S. F. R. Taylor, H. G. Manyar, K. Ralphs, P. Goodrich and C. Hardacre, *Faraday Discuss.*, 2018, **206**, 535-547.
116. M. Lijewski, J. M. Hogg, M. Swadzba-Kwasny, P. Wasserscheid and M. Haumann, *RSC Adv.*, 2017, **7**, 27558-27563.
117. B. Corain, M. Zecca and K. Jeřábek, *J. Mol. Catal. A: Chem.*, 2001, **177**, 3-20.
118. J. Venugopal, S. Ramakrishna, *Biotechnol. Appl. Biochem.*, 2005, **125**, 147-157.
119. S. Liu, L. Zhou, P. Wang, F. Zhang, S. Yu, Z. Shao and B. Yi, *ACS Appl. Mater.*, 2014, **6**, 3195-3200.
120. N. Ajjan Fátima, M. Ambrogio, A. Tiruye Girum, D. Cordella, M. Fernandes Ana, K. Grygiel, M. Isik, N. Patil, L. Porcarelli, G. Rocasalbas, G. Vendramientto, E. Zeglio, M. Antonietti, C. Detrembleur, O. Inganäs, C. Jérôme, R. Marcilla, D. Mecerreyes, M. Moreno, D. Taton, N. Solin and J. Yuan, *Polym. Int.*, 2017, **66**, 1119-1128.
121. M. Omedes Pujol, D. J. L. Coleman, C. D. Allen, O. Heidenreich and D. A. Fulton, *J. Controlled Release*, 2013, **172**, 939-945.
122. K. Manojkumar, A. Sivaramakrishna and K. Vijayakrishna, *J. Nanopart. Res.*, 2016, **18**, 103.
123. Q. Wang, X. Cai, Y. Liu, J. Xie, Y. Zhou and J. Wang, *Appl. Catal. B*, 2016, **189**, 242-251.
124. M. Wilson, R. Kore, A. W. Ritchie, R. C. Fraser, S. K. Beaumont, R. Srivastava and J. P. S. Badyal, *Colloids Surf. A.*, 2018, **545**, 78-85.
125. B. Wu, D. Hu, Y. Kuang, B. Liu, X. Zhang and J. Chen, *Angew. Chem.*, 2009, **121**, 4845-4848.
126. J.-K. Sun, Z. Kochovski, W.-Y. Zhang, H. Kirmse, Y. Lu, M. Antonietti and J. Yuan, *J. Am. Chem. Soc.*, 2017, **139**, 8971-8976.
127. A. Chen, G. Zhao, J. Chen, L. Chen and Y. Yu, *RSC Adv.*, 2013, **3**, 4171-4175.
128. S. Doherty, J. G. Knight, J. R. Ellison, D. Weekes, R. W. Harrington, C. Hardacre and H. Manyar, *Green Chem.*, 2012, **14**, 925-929.
129. S. Doherty, J. G. Knight, M. A. Carroll, A. R. Clemmet, J. R. Ellison, T. Backhouse, N. Holmes, L. A. Thompson and R. A. Bourne, *RSC Adv.*, 2016, **6**, 73118-73131.
130. S. Doherty, J. G. Knight, J. R. Ellison, P. Goodrich, L. Hall, C. Hardacre, M. J. Muldoon, S. Park, A. Ribeiro, C. A. N. de Castro, M. J. Lourenco and P. Davey, *Green Chem.*, 2014, **16**, 1470-1479.

Chapter 2 Synthesis of PIILP Materials and Application in the Suzuki-Miyaura Cross Coupling Reaction

2.1 Introduction

The application of heteroatom donor modified transition metal nanoparticles in catalysis is as discussed in Chapter one, well documented. In this regard, due to its high activity and versatility, palladium is often used as the active component for a range of heterogeneously catalysed processes.¹ Amongst the most common transformations reported for polyionic liquid-stabilised Pd nanoparticles are hydrogenations² and various carbon-carbon bond forming reactions (Scheme 16).³⁻⁵ Combined with the advantageous of catalyst reuse and enhanced activity, the use of supported PdNPs also offers a ligand free synthesis which further reduces costs. As such, the development of highly selective and efficient heteroatom-functionalised PdNP-based catalysts that operate under mild conditions has led to remarkable achievements in synthetic organic chemistry. In particular, Pd catalysed aryl-aryl and aryl-heteroaryl bond formation is of critical importance in the pharmaceutical industry as the synthesis of biaryl motifs is a key transformation.⁶

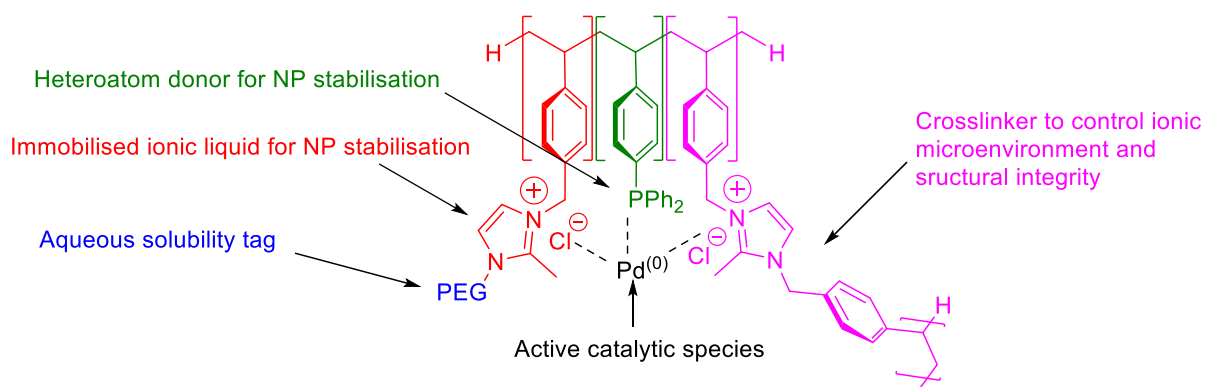


Scheme 16: Pd catalysed carbon-carbon bond forming cross coupling reactions ($\text{X} = \text{Cl}, \text{Br}$ or I).

As previously described, many different ligand structures have been successfully incorporated into catalyst systems including carbenes⁷ and amines⁸ in order to improve the performance and stability of a range of transition metal nanoparticles. Due to their tuneable electronic and steric properties, phosphines are perhaps the most widely applied ligand scaffold in homogenous catalysis, of which the most profound examples include; biaryl monophosphines developed by Buchwald,⁹ the Doherty-Knight KITPHOS monophosphines¹⁰ and Zhang's triazole derived monophosphines.¹¹ However, despite their high activities, they suffer

numerous drawbacks as they are prone to oxidation, require expensive multi-step synthesis and are often challenging to recover and recycle. To overcome these limitations there has been a great deal of research into the fabrication of phosphine-functionalised heterogeneous supports in order to combine the favourable metal-phosphine interactions with facile recovery of the catalyst for recycling. For example, Das and Sahu prepared PPh_2 -modified silica as a recyclable support for PdNPs that were highly active for aqueous phase Suzuki-Miyaura cross coupling.¹ Furthermore, phosphine donors have been shown to enable control over NP size and modulate selectivity in the rhodium-catalysed hydrogenation of substituted arenes.¹² Coordination of triphenyl phosphine and diphenylphosphinobutane onto the surface of RuNPs has been shown to increase selectivity in the hydrogenation of aromatic ketones.¹³ Additionally, the introduction of polyethylene glycol (PEG) into a catalyst support has been reported to increase the hydrophilicity and thus improve aqueous phase compatibility. For example, Lipshultz *et al.* has demonstrated that the weak interaction of PEG groups not only provides additional stabilisation of metal NPs, but also mediates efficient dispersion of the hydrophilic supports in aqueous solution, which facilitates recycling of the aqueous phase in a safe and sustainable protocol.¹⁴⁻¹⁶

Using PIILP catalysis the favourable aspects of phosphines may be combined with ILs within a sophisticated macromolecular polymer network. This strategy aims to provide unique stabilisation of the NPs within the IL/phosphine microenvironment, influence the kinetics of NP formation to modulate particle growth and enhance catalytic activity and selectivity. To this end, this chapter will describe the synthetic methodology developed in order to generate highly active, stable and recyclable PdNP catalysts based on PPh_2 decorated PILs.



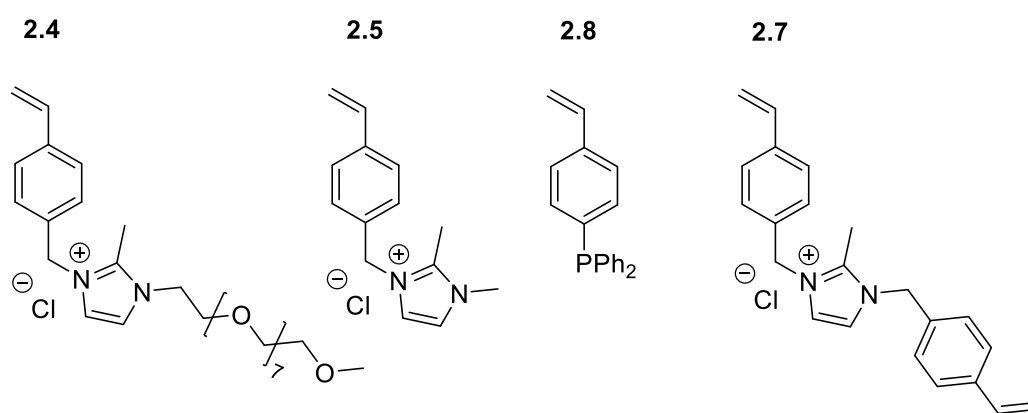
Scheme 17: Representation of various functions in PIILP materials.

Furthermore, it is hoped that the introduction of PEG within the ionic liquid framework may improve catalyst performance due to the additional stabilising forces as well as increased

swelling/dispersion of the polymer in aqueous media facilitating access of substrate to the active site. As such, the relative merits of PEGylated phosphine-functionalised PIILPs will be evaluated against its non-PEGylated counterpart for comparative catalyst testing in the Pd catalysed Suzuki-Miyaura cross coupling.

2.2 Results and Discussion

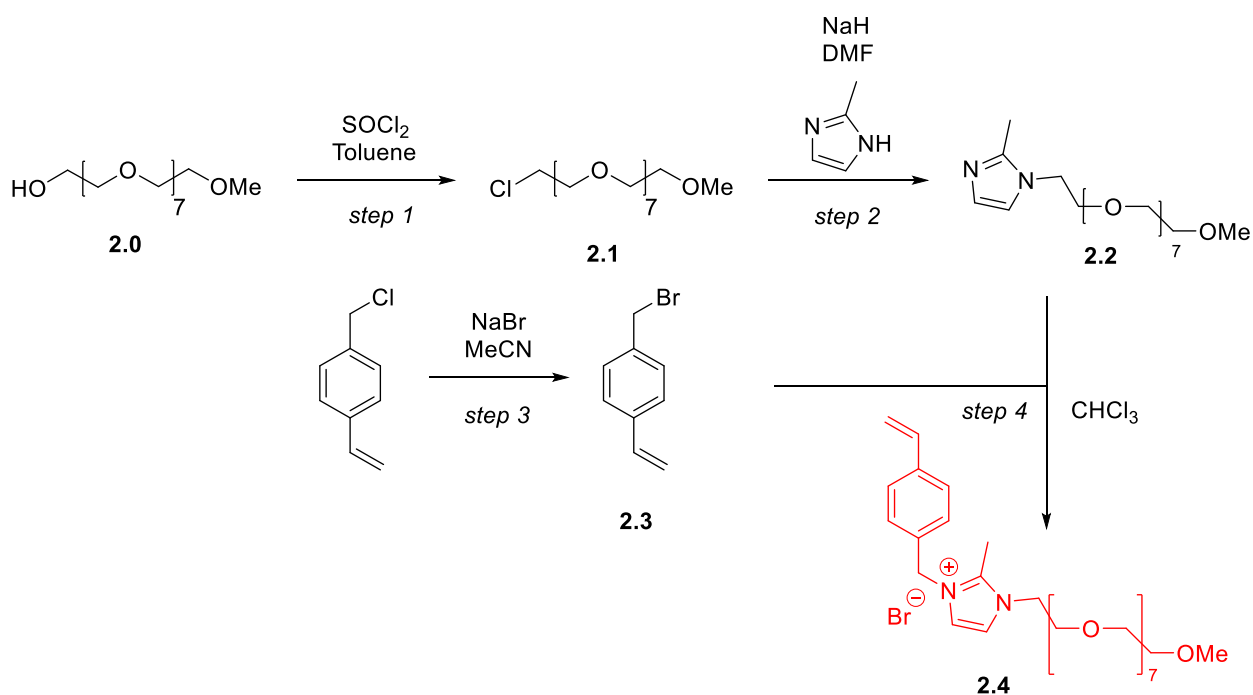
A series of monomers were targeted in order to incorporate the required functionality into the PIILP materials (Scheme 18). Variation of the 'R' group on the imidazolium-based IL-like monomers will enable the role of the PEG group to be systematically evaluated with respect to materials properties (swelling/dispersion/structural integrity) and catalyst efficiency.



Scheme 18: Target monomers; a hydrophilic PEGylated imidazolium monomer (2.4), dimethylimidazolium monomer (2.5), phosphino functionalised monomer (2.8) and dibenzylimidazolium crosslinking monomer (2.7).

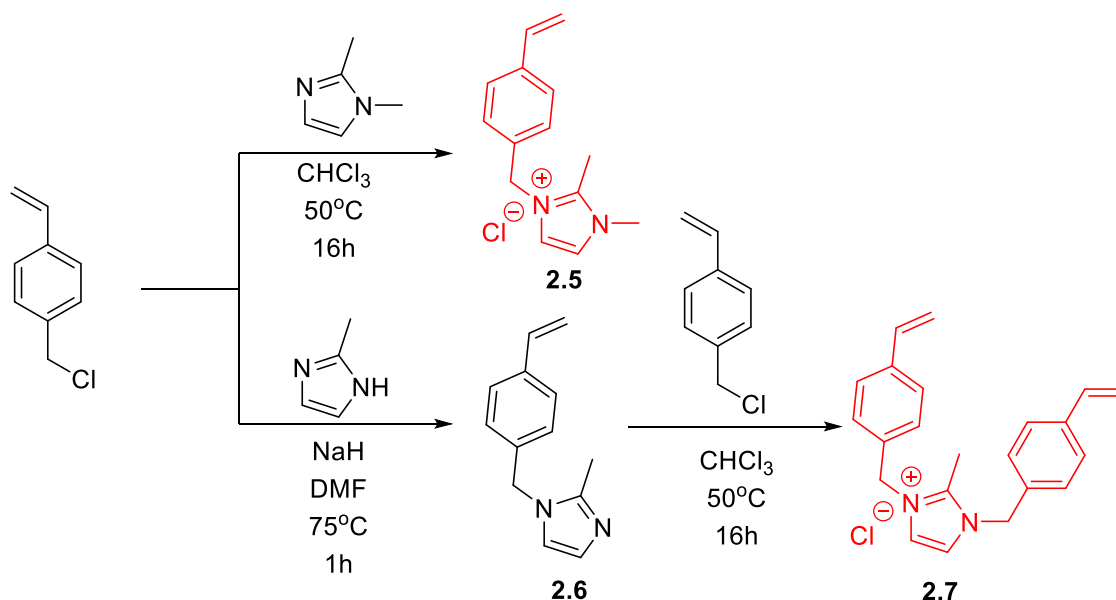
2.2.1 Monomer Synthesis

Monomer **2.4** was synthesised *via* a convergent 4 step protocol (Scheme 19). Poly(ethyleneglycol)monomethyl-350 ether (**2.0**) was chosen as a source of PEG as it is inexpensive and commercially available. Treatment of **2.0** with SOCl_2 in refluxing toluene for 3 days afforded the chlorinated product **2.1** in 87% yield. In step 2, reaction of **2.1** with 2-methylimidazolide, generated by deprotonation of 2-methylimidazole with NaH in DMF, results in rapid substitution of chloride to afford **2.2** as a viscous yellow oil. In Step 3, a Finkelstein reaction was employed to exchange chloride in 4-chloromethylstyrene for bromide which enabled quaternisation with **2.2** to be conducted in chloroform under milder conditions to avoid chloride assisted dealkylation of the PEG group in step 4. The desired monomer was obtained in 94% yield as a viscous pale-yellow oil after induced precipitation of a concentrated methanol solution into diethyl ether.



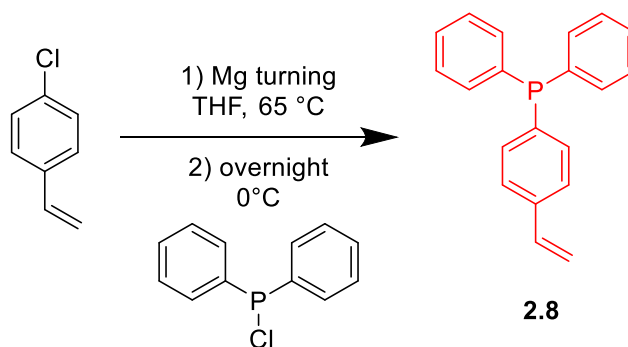
Scheme 19: Synthesis of PEGylated hydrophilic monomer 2.4.

2.5 was obtained by stirring 1,2-dimethylimidazole and 4-chloromethylstyrene at 50°C overnight (Scheme 20). After removal of the solvent and washing the residue with ethyl acetate to remove the neutral starting material, the product was obtained in virtually quantitative yield. The two step synthesis of crosslinker **2.7** was adapted from Jingson *et al.*¹⁷ In the first step, 2-methylimidazole was deprotonated using NaH, before dropwise addition of the resulting imidazolide to a DMF solution of 4-chloromethylstyrene. After stirring for 45 minutes, the intermediate monobenzylated imidazole **2.6** was isolated as a colourless oil. Following this, quaternisation was achieved by stirring **2.6** with 4-chloromethylstyrene in chloroform overnight to afford **2.7** as a white powder in 97% yield.



Scheme 20: Synthesis of monomer **2.5** and cationic crosslinker **2.7**.

The Grignard reaction required for the synthesis of 4-diphenylphosphinostyrene **2.8** was adapted from the synthesis reported by Marcus and Rabinowitz.¹⁸ Due to the sensitivity of the phosphine, the aqueous workup procedure was performed exclusively under a N_2 atmosphere using degassed solvents. Using this method, a white crystalline solid was obtained which showed a single peak in the ^{31}P NMR spectrum at δ -6.7 ppm indicating successful isolation of spectroscopically pure product.

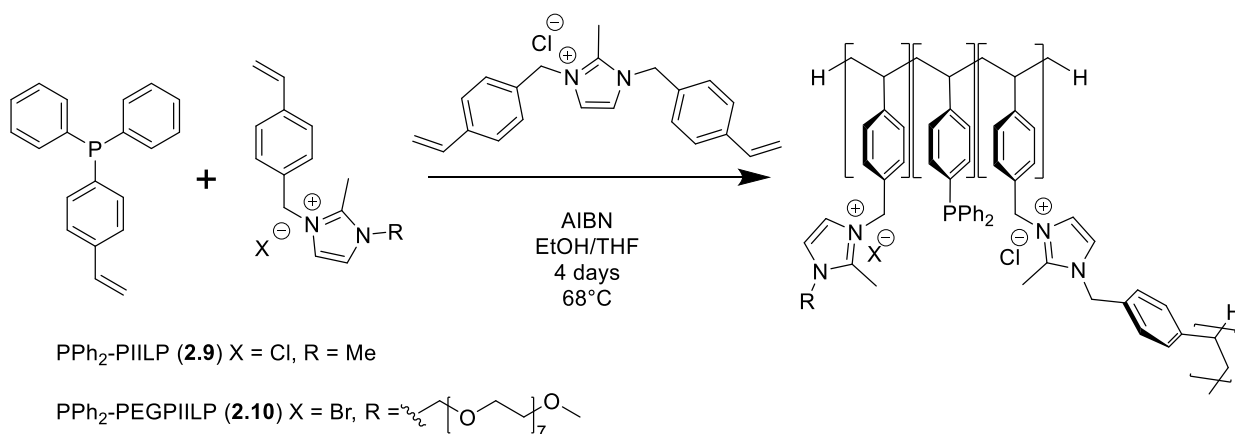


Scheme 21: Synthesis of phosphine functionalised monomer **2.8**.

2.2.2 Synthesis and characterisation of PIILs

Two phosphino-decorated polystyrene PIILP supports were prepared by AIBN-initiated free radical copolymerisation of **2.5**, **2.8** and **2.7** (PPh_2 -PIILP) and **2.4**, **2.8** and **2.7** (PPh_2 -PEGPIILP). The ratio of the IL-like, phosphine-functionalised and crosslinking comonomers was chosen to be 1.86:1:0.14, respectively, such that the overall charge ratio of the repeat unit is 2:1 IL-like monomer to neutral phosphine. Furthermore, complete exchange of halide for

tetrachloropalladate would give a palladium to phosphine ratio of 1. The monomers were dissolved in anhydrous ethanol/THF and 5 mol% AIBN was added. The solution was then degassed using the freeze thaw method to ensure oxygen was removed from the system; the resulting mixture was then heated at 70°C for 4 days. To avoid the use of challenging purification methods, after this time a further 5 mol% AIBN was added and the mixture was stirred for 24 hours to ensure complete consumption of the monomers.



Scheme 22: Synthesis of PPh₂ functionalised PIILPs via AIBN initiated free radical polymerisation.

Caution must be taken in the case of copolymerisations to consider the relative rates of polymerisation of monomers as dissimilarity can lead to the formation of discrete regions of isolated functionality. However it has been reported that variation of the substituents of styrene based monomers in the para position has only a negligible effect on the relative unimolecular polymerisation rates or initiation periods.¹⁹ Ziegler reported that phosphonic acid functionalised styrene monomers showed a slight increase in polymerisation rate on comparison with styrene, however, this was attributed to the low solubility of styrene in aqueous solution.²⁰ Based on these findings it was assumed that under the conditions employed the PIILP materials would have efficient incorporation and dispersion of the monomers within the polymer backbone. A sample of the crude post reaction mixture was analysed by ¹H NMR spectroscopy and the absence of any vinylic signals was taken as a clear indication that all of the monomers had been consumed. Due to the random nature of the polymer and the tumbling effects associated with polymer molecules in solution, the signals exhibit substantial peak broadening, further confirming the reaction had ran to completion (Figure 8). After concentration of the reaction mixtures *in vacuo*, both phosphino-functionalised PIILs **2.9** and **2.10** were obtained in 98 and 99% yield, respectively, as off-white powders by induced precipitation into diethyl ether from a concentrated methanol solution.

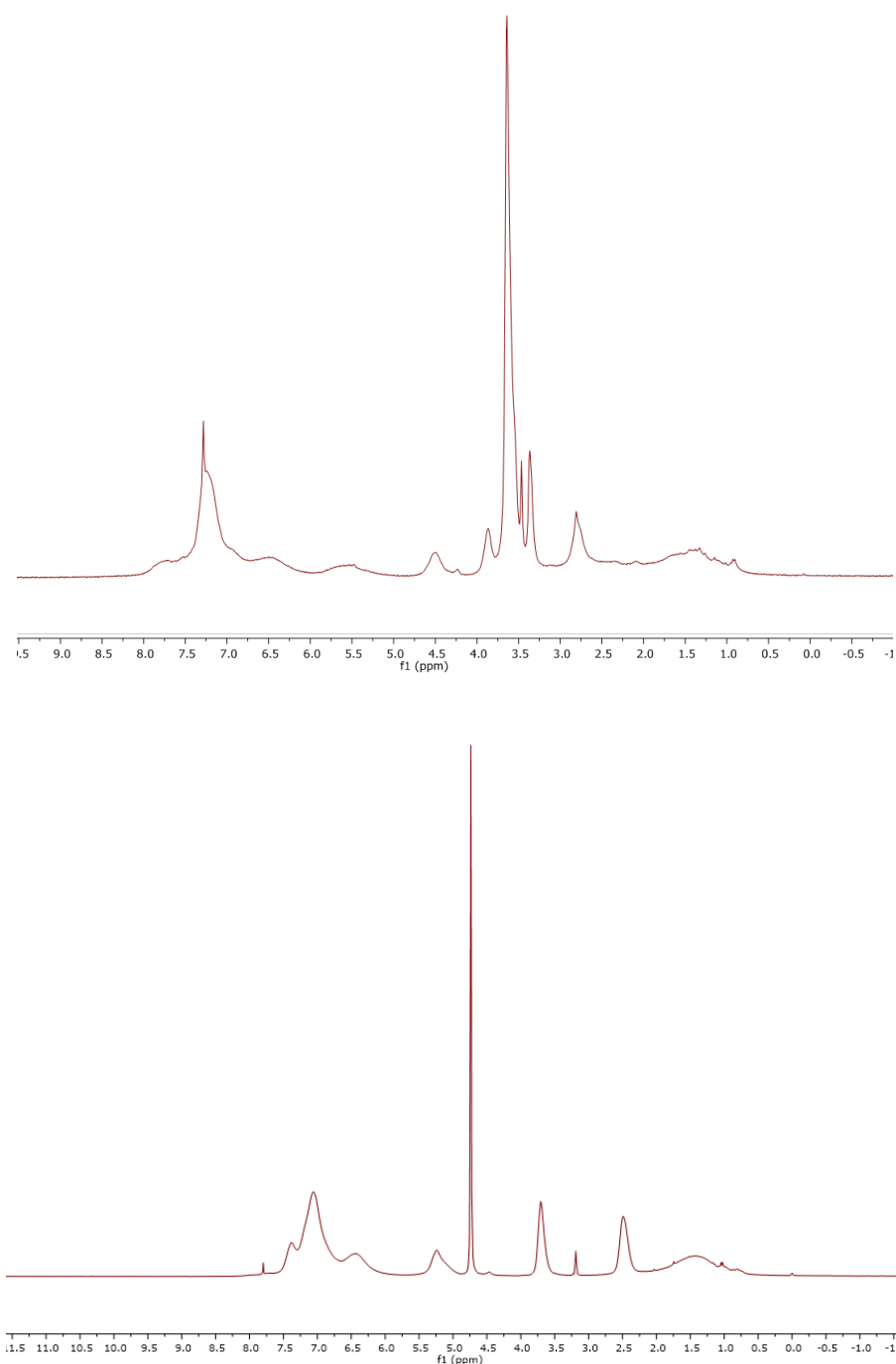


Figure 8: Solution ^1H NMR spectrum of PPh₂-PEGPIILP in CDCl₃ (top) and PPh₂-PIILP in MeOD (bottom).

Unfortunately, it proved challenging to completely eradicate all of the residual solvent due to the complex nature of the crosslinked polymer network. The hydrophilicity and inherent porosity of the materials may cause a degree of solvent trapping and as such, elemental analysis was considered unreliable for determination of the composition. SEM analysis was conducted to examine the morphology of the polymer surfaces (Figure 9). Both polymers appear to have smooth surfaces with only small areas of non-uniform porous nature which

may well indicate that the hydrophilicity of PIIL composites facilitates a degree of hygroscopic swelling derived from absorption of alcoholic solvents during the polymerisation.

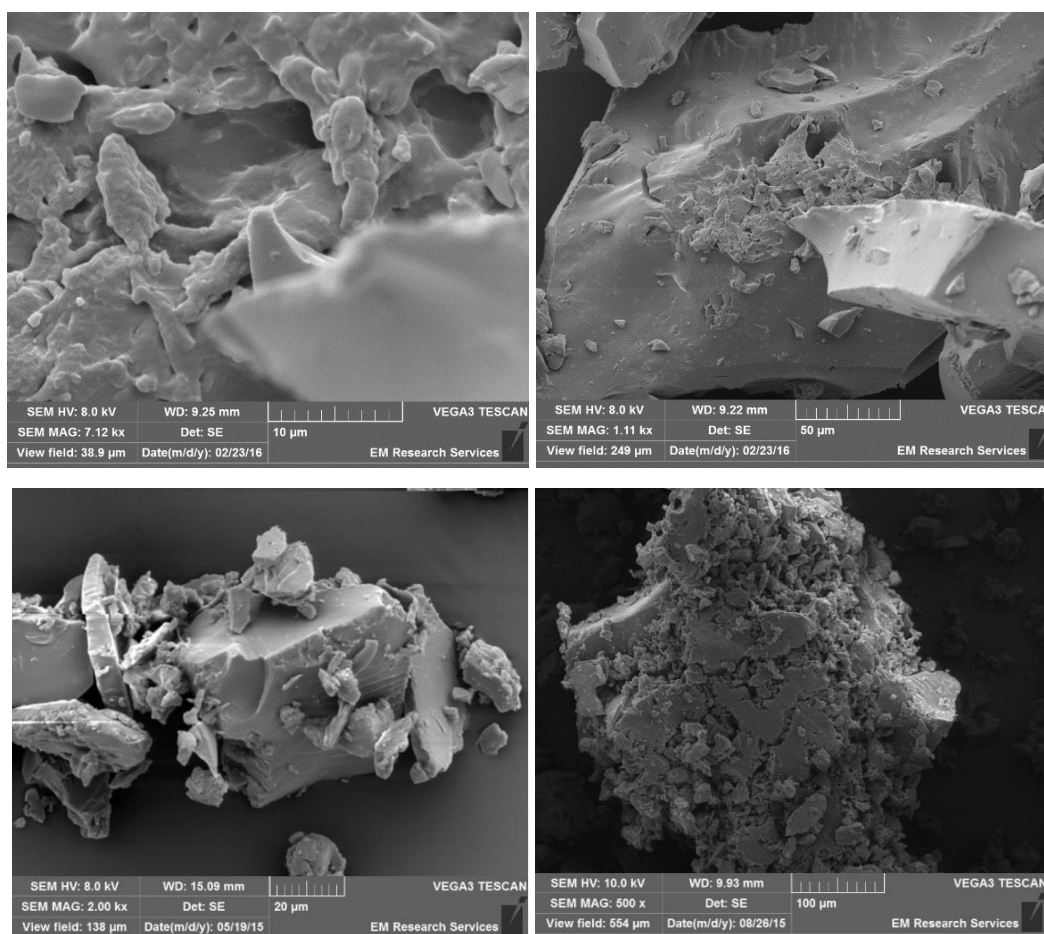


Figure 9: Selected SEM images of freshly prepared PIILPs **2.10** (top) and **2.9** (bottom).

Figure 10 shows the solid-state ^{13}P NMR spectrum of PPh_2 -PIILP, **2.9** and its PEGylated counterpart, **2.10**, respectively. Both spectra demonstrate that product is the major component (approx. δ -6 and -7 ppm respectively) with spinning side bands. There is also an indication that a small amount of phosphine oxide (approx. δ 23 and 21 ppm) was incorporated into the polymer, which was most likely generated during the workup. The spectrum of PPh_2 -PIILP (**2.9**) also shows another resonance of lower intensity at δ -28 which is attributed to a minor phosphorus containing impurity. These values are in agreement with the values reported by Iwai *et al.* for the synthesis of threefold crosslinked triphenylphosphine functionalised polystyrene supports.²¹

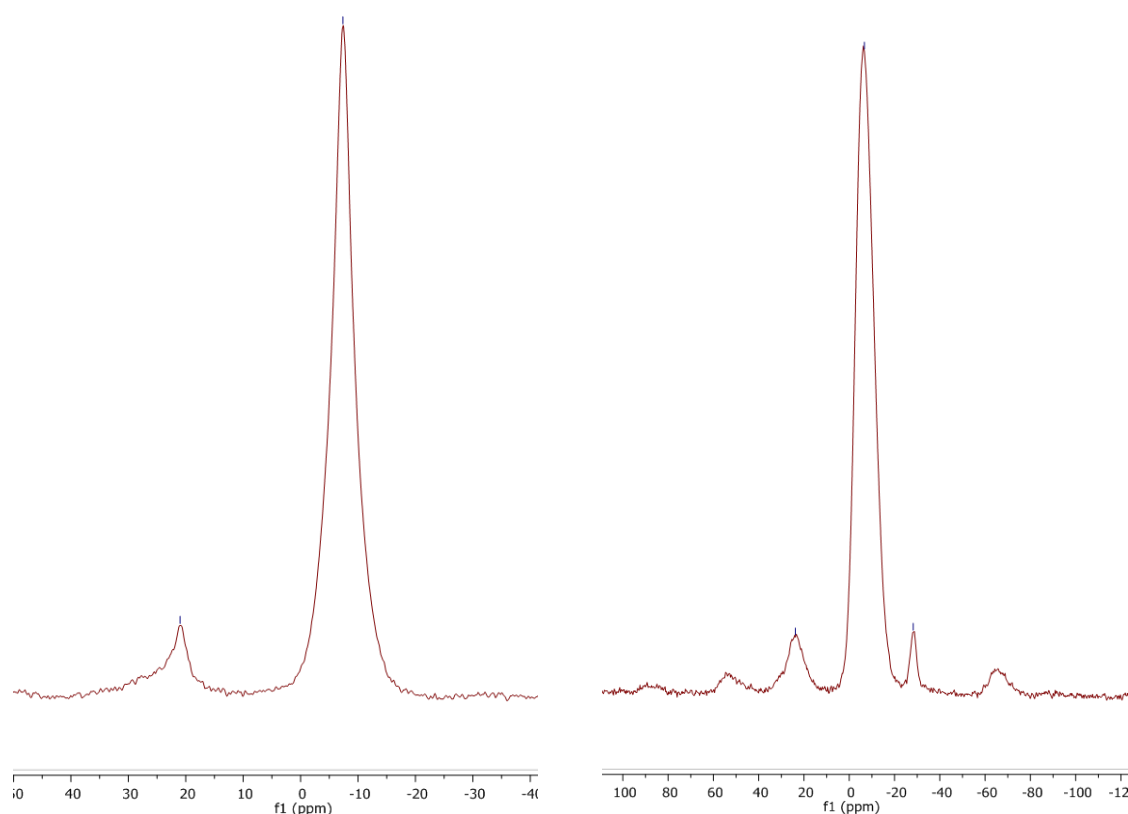


Figure 10: Solid state ^{31}P NMR spectrum of 2.10 (left) and 2.9 (right).

Thermogravimetric analysis was used to investigate the thermal stability of the polymers. The small initial degradation pathway at approximately 100°C is attributed to the loss of water physisorbed on the support indicating a small degree of solvent adsorption. Quantitatively, the water content is equivalent to approximately 5 and 8 wt% for $\text{PPh}_2\text{-PEGPIILP}$ and $\text{PPh}_2\text{-PIILP}$, respectively. After removal of residual solvent, both polymers undergo three similar degradation stages. Degradation of the polystyrene backbone is known to occur at approximately 550°C ,²² which is evident in both spectra. The first pathway is attributed to the decomposition of the imidazolium fragment at $\sim 270^\circ\text{C}$, which has been shown to occur through dealkylation and carbene formation,²³ followed by the PPh_2 moiety at $370\text{--}400^\circ\text{C}$. As the onset of degradation of the PIILP materials does not occur until $\sim 270^\circ\text{C}$, which is well above the temperatures required for liquid phase catalysis, both polymers are sufficiently stable for use as catalyst supports.

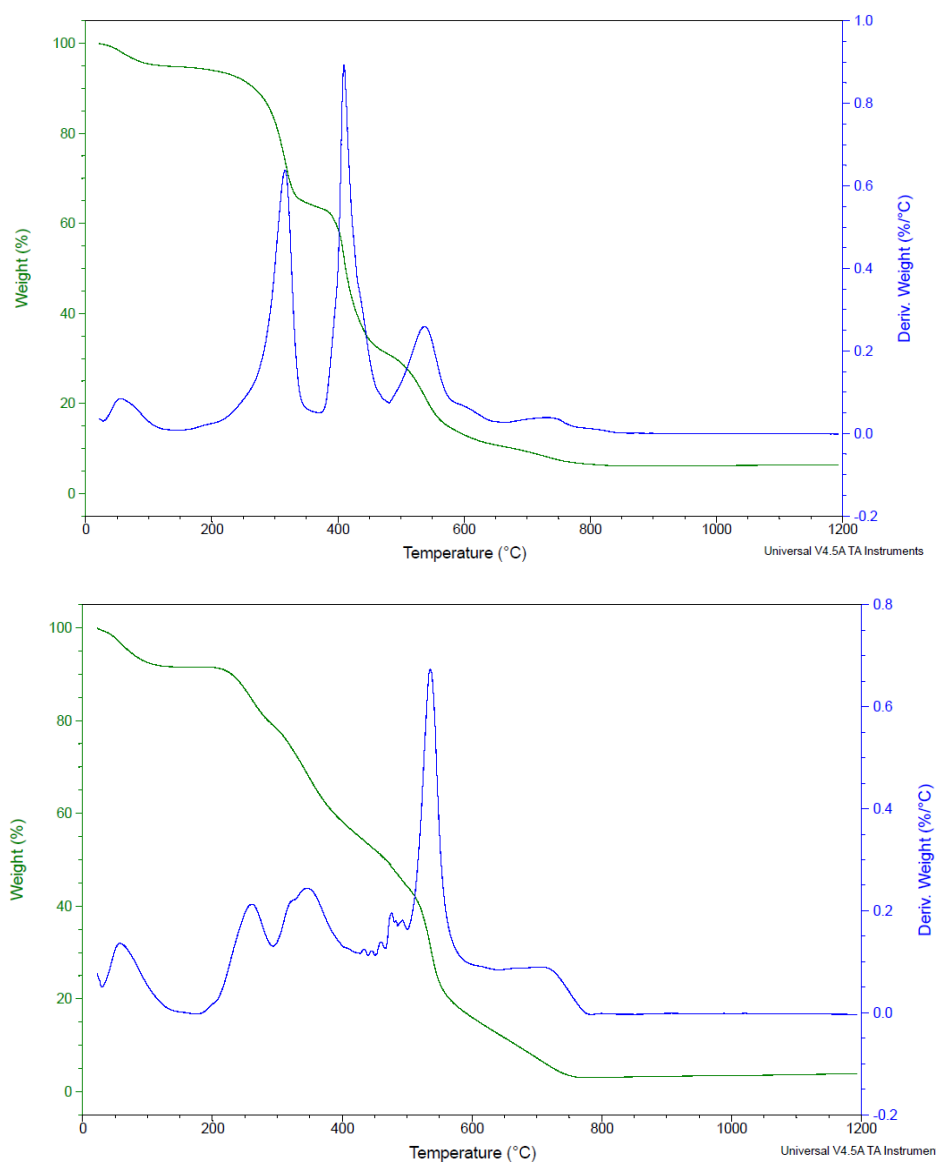
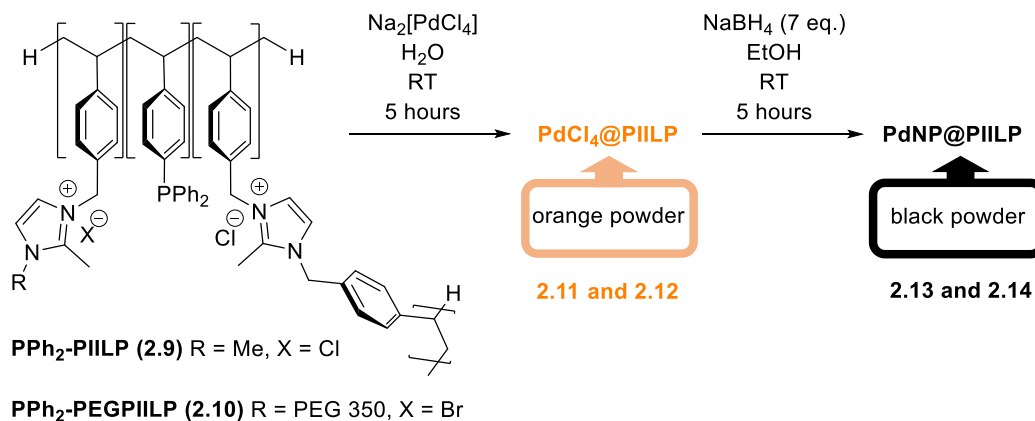


Figure 11: TGA/DSC curves for **2.10** (top) and **2.9** (bottom).

2.2.3 Synthesis and characterisation of PIIL Supported Palladium Nanoparticles (PdNP@PIILP)

Using an ion exchange method, PdNPs were embedded within the polymer network following a simple protocol (Scheme 23). Stoichiometric exchange of the halide anions with $[\text{PdCl}_4]^{2-}$ was achieved by adding the polymer to an aqueous solution of commercially available $\text{Na}_2[\text{PdCl}_4]$. A strong electrostatic attraction is to be expected between the imidazolium cations and the negatively charged Pd salt which should facilitate efficient immobilisation of the Pd within the polymer. After stirring at room temperature 5 hours, the $[\text{PdCl}_4]^{2-}$ impregnated materials **2.11** and **2.12** were isolated as orange solids in good yield (>90%) after filtration and drying under vacuum. The corresponding PIIL-supported nanoparticles were synthesised by reduction of the Pd^{II} precursor with excess NaBH_4 . The mixture instantly changed colour from orange to

black signifying that reduction from Pd^{II} to Pd⁰ is almost instantaneous. After stirring for 5 hours, the mixture was centrifuged and filtered, yielding **2.13** and **2.14** as black powders in near-quantitative yield which were carefully washed with water to remove excess salts, before washing with ethanol and diethyl ether.



Scheme 23: Synthetic route used for impregnation of PIILP materials with [PdCl₄]²⁻ and reduction to NPs with NaBH₄.

SEM analysis of the freshly prepared materials revealed stark differences in the surface morphology of both [PdCl₄]²⁻ loaded polymers and pre-reduced samples compared to the parent polymers. In this case, the samples have a more granular texture which is most likely due to the extra processing steps required during the impregnation and reduction.

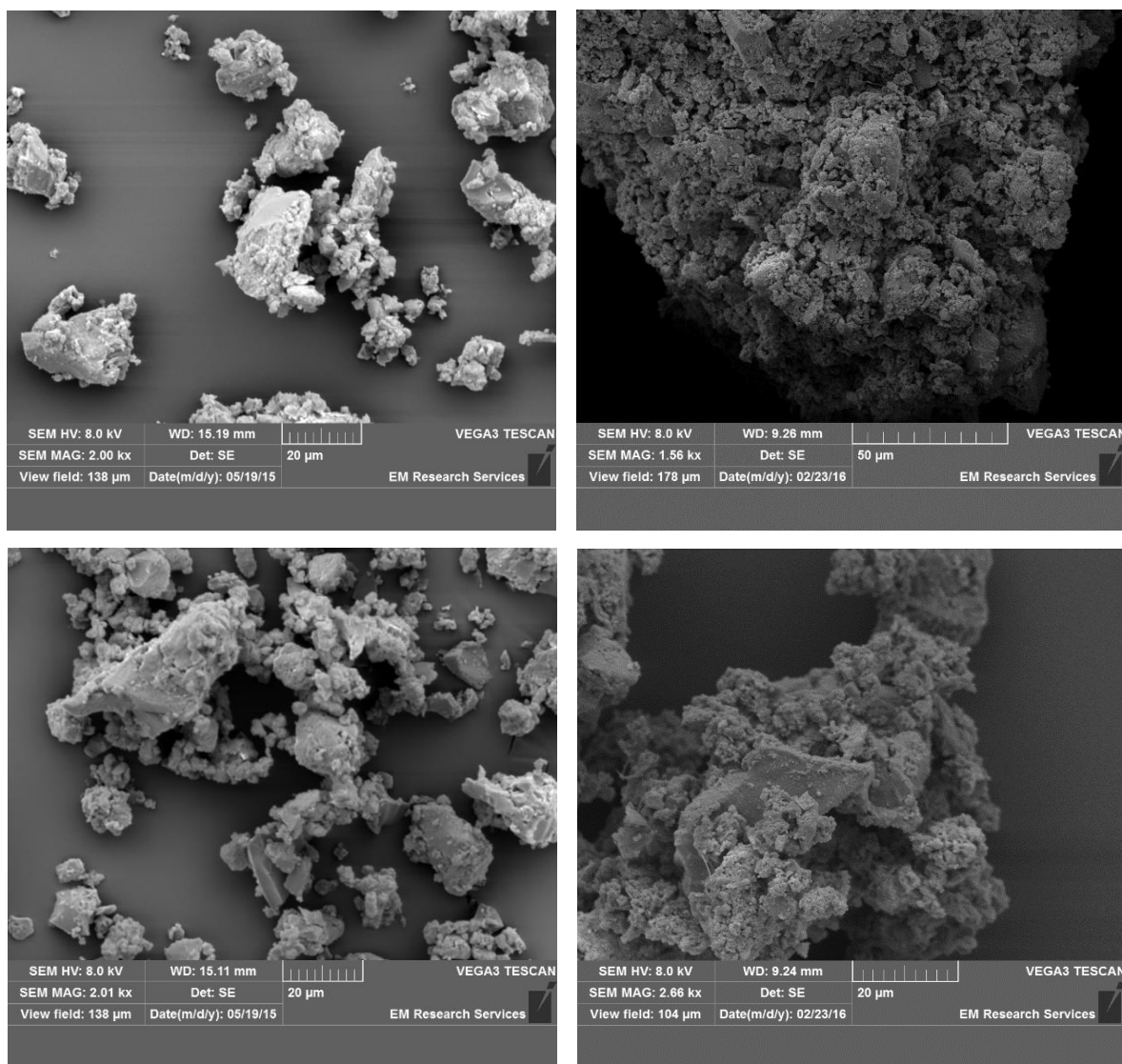


Figure 12: SEM images of PdCl₄@PPh₂-PIILP (top left), PdCl₄@PPh₂-PEGPIILP (top right), PdNP@PPh₂-PIILP (bottom left), PdNP@PPh₂-PEGPIILP (bottom right).

Solid state ³¹P NMR analysis of PdCl₄@PPh₂-PIILP (**2.11**) and PdCl₄@PPh₂-PEGPIILP (**2.12**) confirmed the presence of the Pd-P interaction as evident from the large downfield shift from δ -6 and -7 ppm to δ 27 and 26 ppm for **2.11** and **2.12**, respectively. The single product peak and disappearance of peaks associated with the starting material indicates that there is no remaining free phosphine. The solid state ³¹P NMR spectrum of PdNP@PPh₂-PEGPIILP (**2.14**) contained two peaks, possibly due to the presence of Pd^(II) as confirmed by XPS (*vide infra*), with the major component at δ 29 ppm and the minor at δ 24 ppm. The small downfield shift of 3 ppm may be due in part, to the coordination of the phosphine to the more electron rich Pd⁰ clusters. Whilst the spectrum of PdNP@PPh₂-PIILP (**2.13**) showed that the product is the major component which is also shifted slightly downfield at δ 28 ppm, smaller resonances are observed at δ 10 and 0 ppm. This may well be due to the generation of the phosphine oxide

during synthesis or as a result of the many possible binding modes of phosphine functionalised supports with the non-uniform nanoparticle surface as opposed to isolated Pd atoms. Iwai *et al.* reported the various binding modes of highly crosslinked PPh₂ modified polystyrene supports which can bind to the surface of PdNPs in mono-, bi- and tridentate fashion.²¹ Both of the PdNP@PIILP catalysts showed no peaks corresponding to the starting material which suggests that the NP surface is decorated with phosphine.

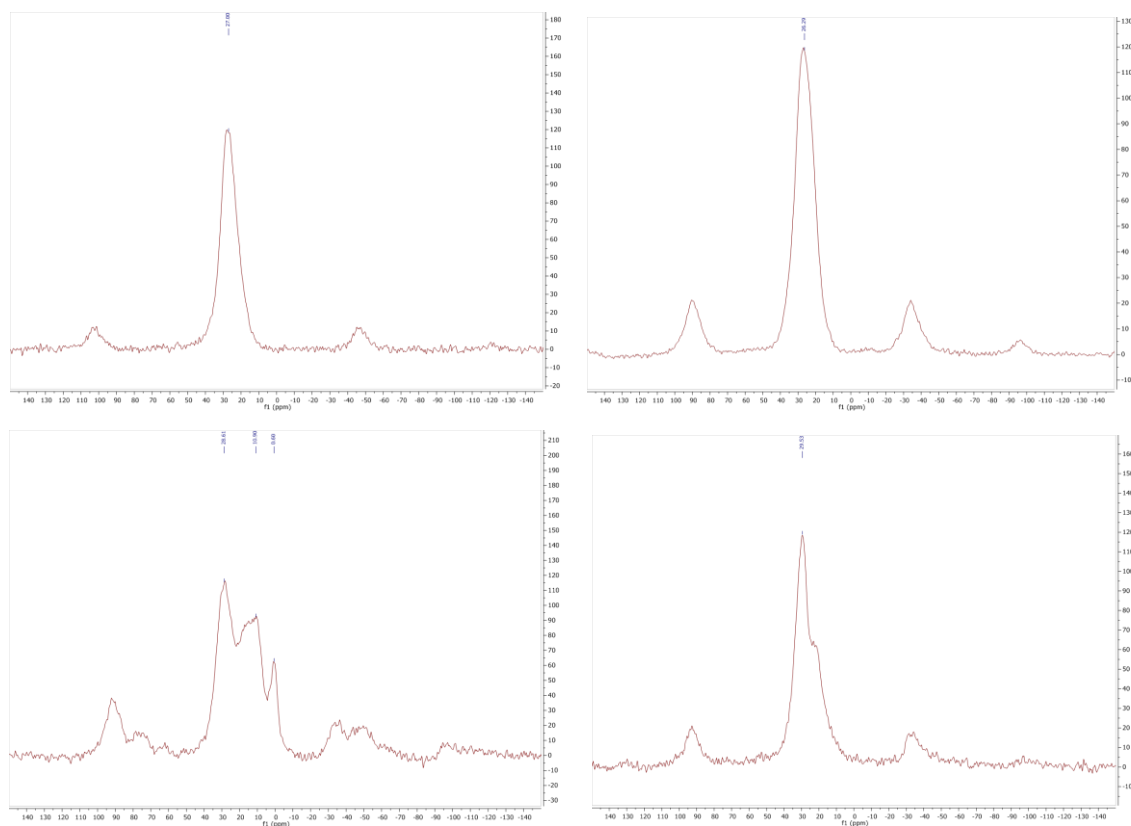


Figure 13: Solid state ³¹P NMR spectrum of PdCl₄@PPh₂-PIILP (top left), PdCl₄@PPh₂-PEGPIILP (top right), PdNP@PPh₂-PIILP (bottom left) and PdNP@PPh₂-PEGPIILP (bottom right).

The Pd content of the catalysts was determined using ICP-OES analysis and the calculated Pd concentrations are listed in Table 2. In all cases lower Pd content is reported for catalysts containing the PEG functionality which may be associated with absorbed solvent. By virtue of their hydrophilic nature, PEGylated materials are intrinsically more hygroscopic and as such, even after extensive drying some solvent may remain in the sample. Alternatively, extraction of Pd may occur during isolation and washing of the material.

Table 2: Pd content of PIILP materials as determined by ICP-OES.

| Catalyst | mmol Pd/ g PIILP | Pd wt% |
|--|------------------|--------|
| PdCl₄@PPh₂-PIILP | 0.58 | 6.2 |
| PdCl₄@PPh₂-PEGPIILP | 0.86 | 9.1 |
| PdNP@PPh₂-PIILP | 1.1 | 10.9 |
| PdNP@PPh₂-PEGPIILP | 0.36 | 3.8 |

Surface characterisation of the Pd-loaded materials was carried out using X-ray photoelectron spectroscopy (XPS). As the Pd 3d region contains highly resolved spin-orbit components with good separation, analysis of the Pd 3d_{3/2} and Pd 3d_{5/2} doublets provides a convenient method to assess the oxidation state of the Pd-loaded materials after both impregnation and reduction. Peak fitting and deconvolution was carried out using CasaXPS software. The relative binding energies of the Pd components were calibrated based on the binding energy of the C1s at 284.8 eV. Both [PdCl₄]²⁻ loaded polymers show more than one Pd environment. The major doublets corresponding to the Pd^{II} oxidation state were found at binding energies of 342.93 eV and 342.63 eV for the Pd_{3/2} and at 337.63 eV and 337.78 eV for the Pd_{5/2} for **2.11** and **2.12** respectively. The low intensity peaks in the spectrum correspond to Pd in a reduced form. In this instance, it is likely from partial reduction during the synthesis – possibly from the use of alcoholic solvents. Analysis of the Pd 3d region of the chemically reduced samples **2.13** and **2.14** showed that both catalysts contain a mixture of Pd^(III) and Pd⁽⁰⁾, the former is most likely due to either the formation of PdO derived from oxidation in air, or incomplete reduction of the Pd^{II} precursors. Given that the binding energies of the Pd^(III) peaks are similar to those of the precursor, and that signals corresponding to PdO are generally found at slightly lower binding energies (approx. 337.0 eV),²⁴ these resonances are more likely associated with incomplete reduction. In this regard, it is possible that if the [PdCl₄]²⁻ precursor is embedded deep within the polymer, it may be difficult for the reducing agent to access the tetrachloropalladate. Ejection of an electron from more electron rich centres is a more facile process and as such the Pd 3d peaks associated with metallic Pd are shifted to lower binding energies of 340.68 (Pd_{3/2}) and 335.38 (Pd_{5/2}) eV for PdNP@PPh₂-PIILP and 340.21 (Pd_{3/2}) and

334.90 (Pd_{5/2}) eV for PdNP@PPh₂-PEGPIILP. These values are in close agreement with recently reported PdNPs immobilised on a heptazine based porous framework.²⁵

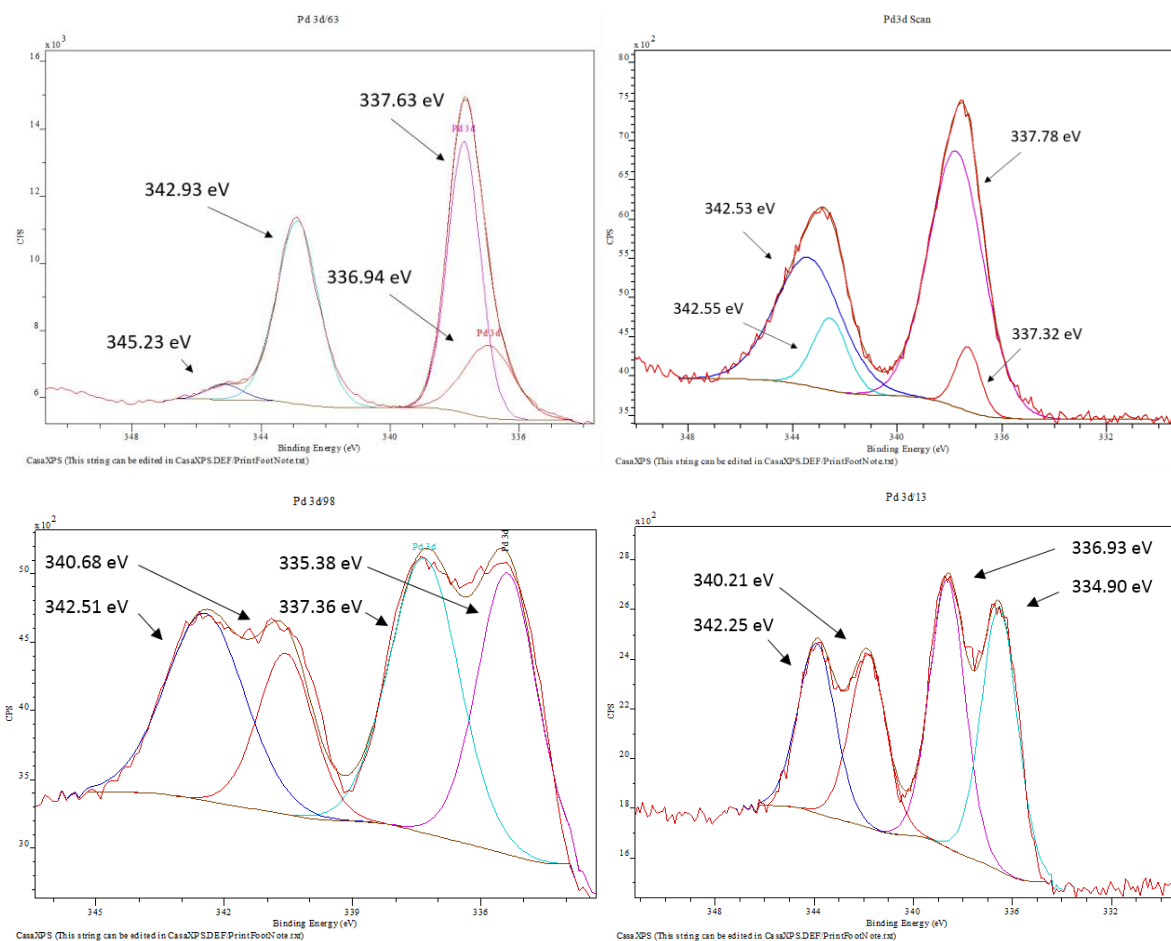


Figure 14: XPS spectrum of PdCl₄@PPh₂-PIILP (top left), PdCl₄@PPh₂-PEGPIILP (top right), PdNP@PPh₂-PIILP (bottom left) and PdNP@PPh₂-PEGPIILP (bottom right).

HRTEM analysis of the as-synthesised catalysts was performed in order to assess the size and shape of the NPs. Figure 15 shows the HRTEM micrographs which revealed that both catalysts consist of small, spherical and near-monodisperse NPs. The NPs are well-dispersed throughout the polymer most likely due to strong association with the cation decorated composites and the partial negative charge that arises on the NP surface. The average diameter was determined based on >100 NPs and was calculated as 2.29 ± 0.96 and 1.93 ± 0.67 nm for PdNP@PPh₂-PIILP and PdNP@PPh₂-PEGPIILP, respectively. Interestingly, it appears that the introduction of PEG yields smaller NPs with a narrower size distribution. This may be as a result of the additional stabilisation against agglomeration which can be achieved through coordination of the oxygen donors to the NP surface. Additionally, the increased hydrophilicity may enable better dispersion of the polymer in solution, facilitating a more uniform dispersion of Pd throughout the support during impregnation. For comparison, average particle sizes of

4.0 nm were reported for PdNPs supported on bioderived hydroxyapatite,²⁶ and Taylor reported PdNPs of 3 nm supported on TiO₂ for the selective hydrogenation of furfural.²⁷

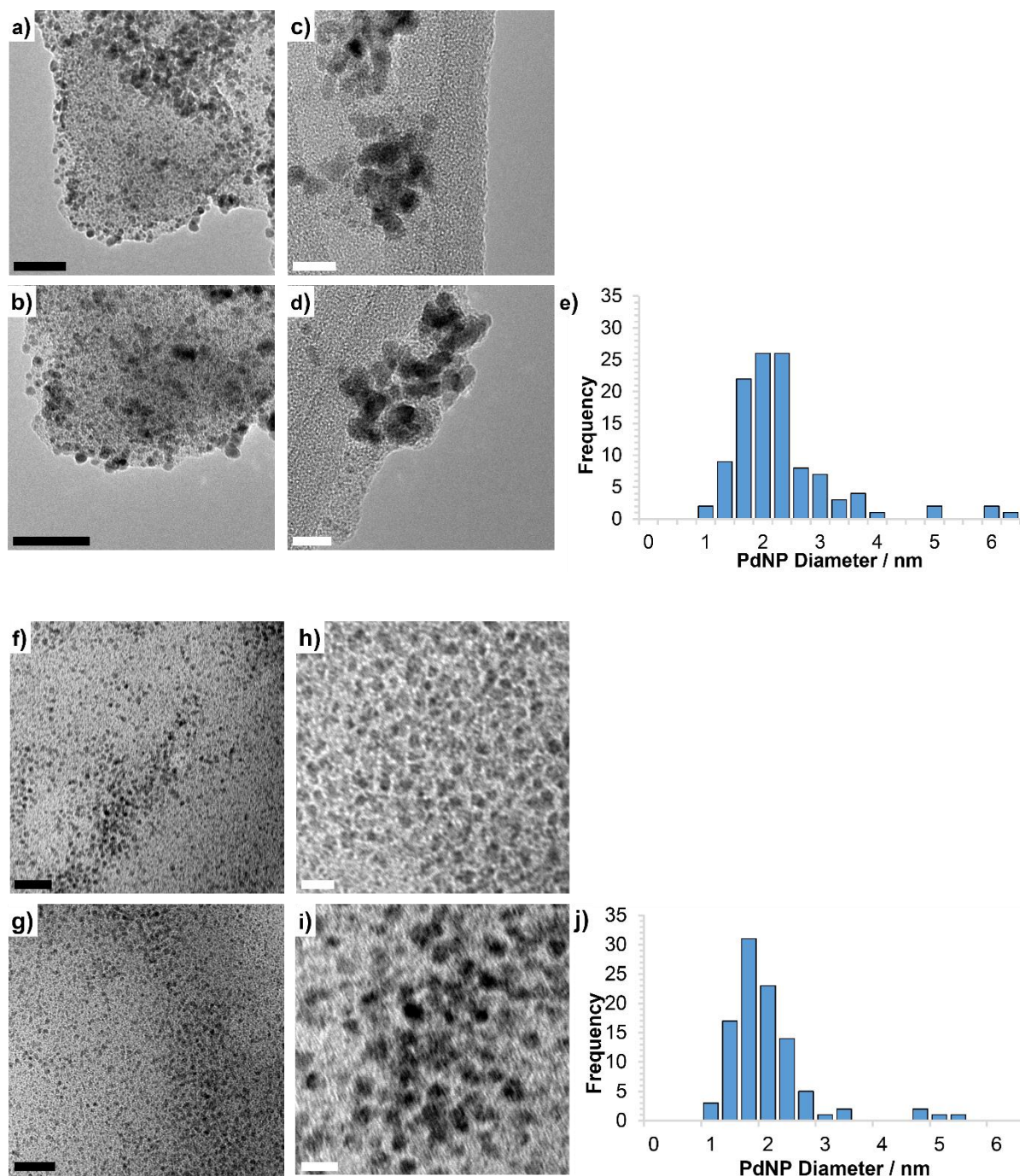


Figure 15: HRTEM images of PdNP@PPh₂-PIILP (a-d) and PdNP@PPh₂-PEGPIILP (f-i) with the associated histograms (e and j) showing particle size distribution based on >100 particles. Scale bars are 25 nm (black) and 5 nm (white).

XRD analysis of PdNP@PPh₂-PEGPIILP showed no evidence of crystalline Pd phases which further suggests that the PdNPs are small and well-dispersed over the amorphous polymer support and any crystalline Pd content is below the threshold of detection (Figure 16, top). The spectrum also shows numerous peaks which are most likely associated with the residual

borate salts resulting from contamination during the NaBH_4 reduction. Removal of the salts with water is challenging due to the high hydrophilicity of the support as excessive washing extracts the polymer. Metal nanoparticles often cause peak-broadening due to a decrease in crystallinity of the cluster on comparison with isolated crystallites. Furthermore, smaller particles exhibit increased peak broadening as the random orientations of Pd atoms within the particles becomes more significant. A similar effect was reported by Shen *et al.* where PdNPs generated by reduction of $\text{Pd}(\text{acac})_2$ were highly dispersed over the support and as such the Pd peaks were below the limit of detection of the XRD instrument.²⁶ In stark contrast, a small peak at approximately 40° for 2θ is observed in the spectrum of PdNP@PPh₂-PIILP which corresponds to the (111) crystal plane of face-centered cubic Pd nanoparticles (Figure 16, bottom). This is in agreement with the TEM data presented above as the average particle size is larger for the non-PEGylated catalyst. Furthermore, the decrease in hydrophilicity of the non-PEGylated support enabled the borate salts to be removed by exhaustive washing.

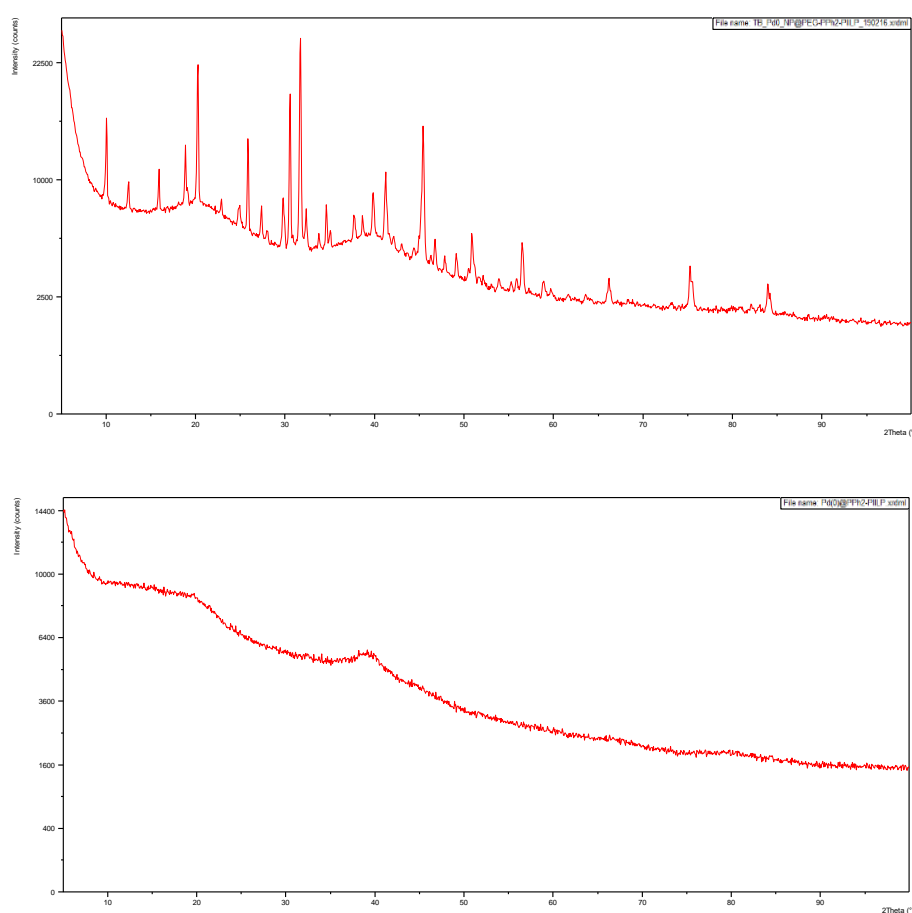
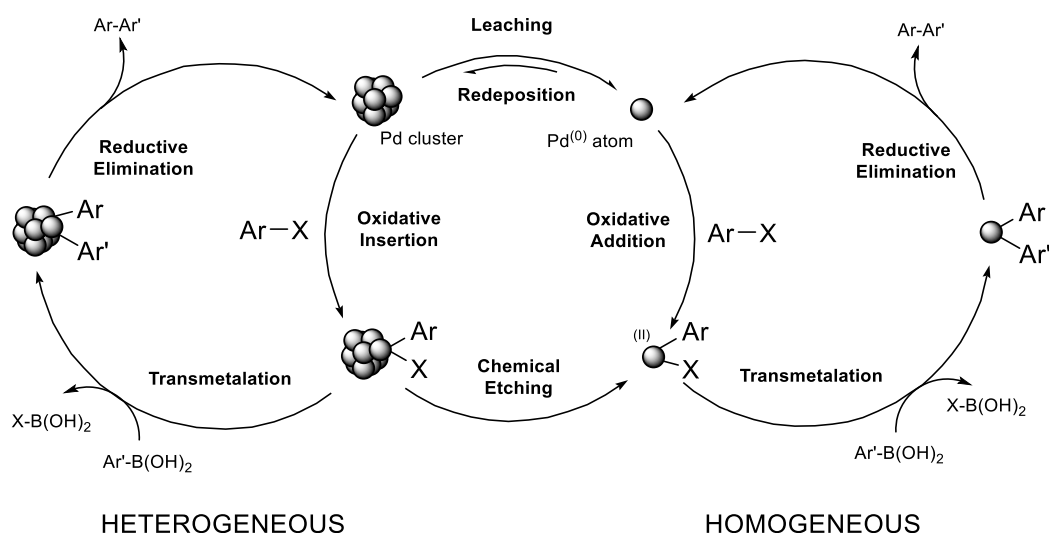


Figure 16: XRD spectra of PdNP@PPh₂-PEGPIILP (top) and PdNP@PPh₂-PIILP (bottom).

2.3 Application of PIILP-Based Catalysts for Suzuki-Miyaura Cross-Coupling

The efficacy of both PdNP-loaded phosphine-decorated PIILP catalysts **2.13** and **2.14** were examined for the Pd catalysed Suzuki-Miyaura cross coupling. Since its discovery, the Suzuki-Miyaura cross coupling reaction has become the most convenient and adaptable method for the synthesis of symmetrical and non-symmetrical biaryl units.⁵ Characterised by the coupling of a boronic acid or its derivative with an aryl halide, the Suzuki-Miyaura reaction is the most widely used method for expanding the carbon framework of organic molecules. The versatility of the reaction is derived from its tolerance to a range of solvents and boronic acids which are often simple to synthesise. Furthermore, due to the high activity of heterogeneous Pd catalysts, high TONs can be achieved under relatively mild conditions without the formation of toxic by-products which has led to remarkable progress in industrial synthetic organic chemistry.²⁸ As such, the reaction provides a useful benchmark to evaluate the efficacy of the newly developed PIILP systems. Despite the advances in cross-coupling catalyst technology, whilst the series of fundamental transformations involved in the catalytic cycle are largely accepted, the exact mechanism has been the subject of academic debate with regards to the true nature of the active species and whether it occurs via a homogeneous or heterogeneous pathway (Scheme 24). In order to provide mechanistic insight, a range of experiments were conducted in order to elucidate the nature of the active species in PIILP catalysis which will be discussed later in this chapter. An informative review published by Ananikov and Beletskaya gives a detailed current perspective on C-C and C-heteroatom bond forming reactions and their mechanisms with regards to single site, homogeneous and heterogeneous metal surface catalysis as well as the possibility of a parallel mechanism.²⁹ Rothenberg has proposed that supported PdNPs simply act as a reservoir of Pd and that leaching of soluble molecular Pd from clusters is caused as Pd is continuously etched away.³⁰ A U-tube permeation cell reactor designed to allow selective extraction of molecular Pd and physical exclusion of nanoparticles into the reaction mixture demonstrated that leached Pd was the active species in the Pd catalysed homogenous Heck coupling reaction. However, Bernini reported that catalysis mostly likely takes place at defect sites or 'steps' on a nanoparticle surface.³¹ If leached Pd was responsible for the activity, it is conceivable that the morphology of the PdNPs would be subject to change causing a decline in catalyst activity. However, after numerous recycles no drop in activity was observed and TEM analysis of the PdNPs showed they remained unchanged suggesting that this is not the case.



Scheme 24: Catalytic cycle involving both homogeneous and heterogeneous pathways for the palladium catalysed Suzuki-Miyaura cross coupling reaction.³²

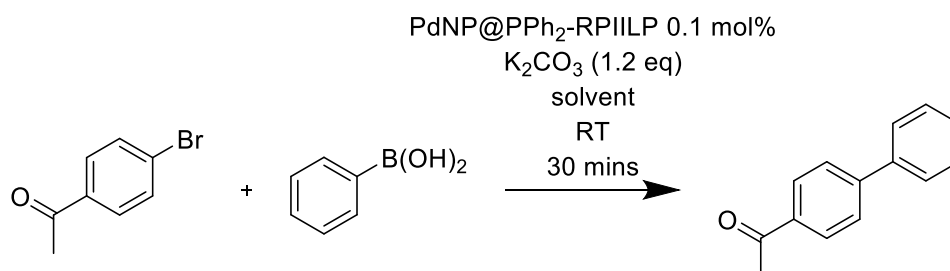
2.3.1 Preliminary results and catalyst optimisation

Optimisation of the various reaction parameters was initially carried out to establish the ideal conditions for catalysis. Throughout the literature 4-bromoacetophenone is widely used as a model aryl halide with phenylboronic acid as the coupling partner due to the short reaction times required to achieve high conversions. As such, this was chosen as a suitable benchmark for comparative catalyst testing in the presence of a small excess of K_2CO_3 as the base at a catalyst loading of 0.1 mol% at room temperature.

2.3.2 Solvent optimisation

Solvents are known to play a key role in reactions and can have a dramatic effect on catalyst performance. In heterogeneous catalysis, the solvent plays a crucial role in mediating and dictating the interaction between the reactants and the catalyst surface. As such a solvent screen was undertaken to assess the performance of PdNP@PPh₂-PIILP and its PEGylated counterpart in a range of protic, aprotic, polar and non-polar solvents.

Table 3: Optimisation for the PdNP@PIILP catalysed Suzuki-Miyaura cross-coupling between 4-bromoacetophenone and phenylboronic acid.



| Entry ^a | Solvent | PdNP@PPh ₂ -PEGPIILP conversion (%) ^b | PdNP@PPh ₂ -PIILP conversion (%) ^b |
|--------------------|----------------------|--|---|
| 1 | Water | 32 | 10 |
| 2 | Ethanol | 28 | 24 |
| 3 | Toluene | 3 | 3 |
| 4 | THF | 1 | 2 |
| 5 | DMF | 20 | 12 |
| 6 | Water/Ethanol 1:1 | 100 | 98 |
| 7 | THF/Water 1:1 | 15 | 10 |

^aReaction Conditions: 0.1 mol% catalyst, 1 mmol aryl halide, 1.13 mmol phenylboronic acid, 1.2 mmol K_2CO_3 , 2.4 mL solvent, RT, 0.5 h. ^b Determined by GC with 1 mmol decane std, average of 2 runs.

The results in Table 3 reveal that varying the solvent has a dramatic effect on performance for both catalysts. In all cases the PEGylated catalyst outperforms its less hydrophilic counterpart. Furthermore, whilst reactions conducted in polar aprotic organic solvents gave very poor conversions in both cases (entries 4 and 5), slightly higher activity is achieved using ethanol as a polar protic solvent (entry 2). The low conversion obtained in organic solvents may be a result of the low solubility of the inorganic base. Gratifyingly, under purely aqueous conditions the PEGylated catalyst gave a markedly higher conversion than its non-PEGylated counterpart,

most likely due to the increase in hydrophilicity and water compatibility; however, conversions were low for both (entry 1). Again, the limited solubility of the organic reagents in water may impose mass transfer limitations during the reaction yielding low conversion. A THF-water cosolvent mixture also gave low conversions in both cases despite this solvent system being widely applied in homogenous palladium catalysed couplings.³³ Remarkably, high conversions were obtained with both catalysts in a water/ethanol mixture, with the PEGylated system again slightly outperforming its non-PEGylated counterpart. Furthermore, the nature of IL on the support is likely highly compatible in ethanol-water mixtures and may form a liquid-like monolayer on the support surface creating a favourable microenvironment for catalysis. Water-promoted Suzuki-Miyaura couplings are now well-cited in the literature,³⁴ therefore on this basis an investigation into the ethanol/water ratio was conducted to identify the optimum solvent composition.

Table 4: Optimisation of the water/ethanol ratio.

| Entry ^a | Water/Ethanol ratio | PdNP@PPh ₂ -PEGPIILP conversion (%) ^b | PdNP@PPh ₂ -PIILP conversion (%) ^b |
|--------------------|---------------------|--|---|
| 1 | 1:3 | 66 | 70 |
| 2 | 1:1 | 100 | 98 |
| 3 | 3:1 | 39 | 29 |

^aReaction Conditions: 0.1 mol% catalyst, 1 mmol aryl halide, 1.13 mmol phenylboronic acid, 1.2 mmol K₂CO₃, 2.4 mL solvent, RT, 0.5 h. ^b Determined by GC with 1 mmol decane std, average of 2 runs.

The results in Table 4 show that addition of small amounts of water results in a stark increase in conversion. For example, using as little as a 1:3 water-ethanol mixture results in an increase from 28% and 24% in neat ethanol to 66% and 70% for PdNP@PPh₂-PEGPIILP and PdNP@PPh₂-PIILP respectively (entry 1). The optimum ratio is reached with a 50:50 mixture, as virtually quantitative conversion is achieved in both cases (entry 2). However, further dilution with water results in a dramatic drop in conversion (entry 3).

Dynamic light scattering measurements were undertaken to investigate the morphological and solubility changes associated with the dispersion of the PEGylated supported catalyst in each of the solvent mixtures. The results in Figure 17 revealed a stark contrast in average aggregate size in different solvent mixtures. In neat ethanol or water, cloudy solutions with

large aggregates were observed whereas the 50:50 mixture gave a homogenous solution with smaller defined aggregates of 115 nm. Whilst the largely spherical PdNPs may act as a template and facilitate organised aggregation of the flexible support around the particles, most of the IL fragments may not participate in metal-support interactions. Therefore, such fragments are amenable to interact with other functionality in the support. Thus, changes in the solvent composition may give rise to various different interparticle associations between the free imidazolium motifs resulting in large differences in particle size. While it is difficult at this stage to establish a relationship between aggregate size and catalyst activity, there is a clear solvent dependant morphological change to the support.

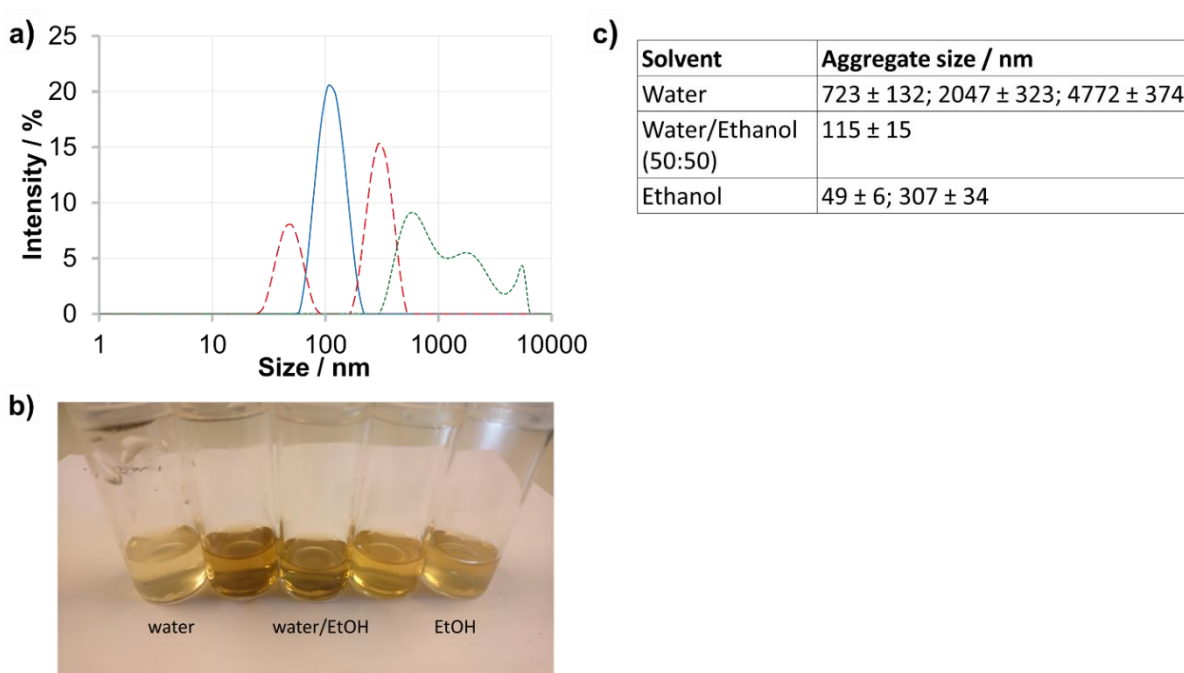


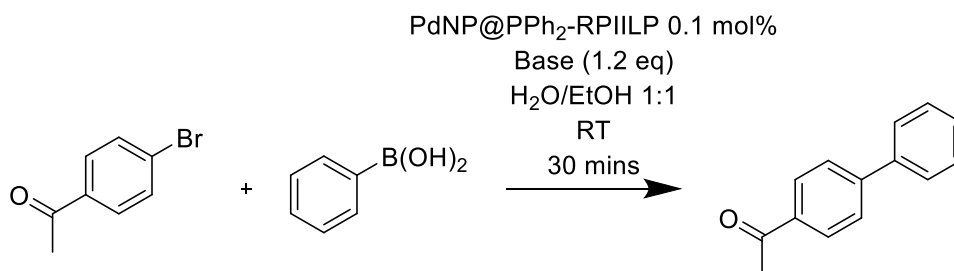
Figure 17: a) DLS measurements showing intensity vs. particle size for 1.5 mg of PdCl₄@PPh₂-PEGPIILP in 2.4 mL of water (green), ethanol (red) and a water/ethanol mixture (50:50, blue). b) Depiction of solutions containing 1.5 mg of PdCl₄@PPh₂-PEGPIILP in 2.4 mL of (left to right) near H₂O, H₂O/ethanol (75:25), H₂O/ethanol (50:50), H₂O/ethanol (25:75) and neat ethanol. c) Summary of calculated average aggregate sizes for 1.5 mg of PdCl₄@PPh₂-PEGPIILP in 2.4 mL of water, ethanol and a water/ethanol mixture recorded at 25 °C (average of 10 runs).

Despite the advantages associated with facile selective extraction of the products from a purely aqueous system, the substantial improvement in catalyst performance achieved using an ethanol cosolvent renders this solvent system more viable. Moreover, recently considered as ‘aqueous media’, the benefits and desirable green credentials of ethanol-water mixtures has led to their frequent use as a nontoxic and cheap reaction media for nanoparticle-based heterogeneous catalysis.^{35, 36} As such, this solvent system provides a suitable benchmark to compare PIILP systems with the literature (*vide infra*).

2.3.3 Base optimisation

Although preliminary catalyst testing was carried out using potassium carbonate as the base, a series of batch reactions were carried out with several inorganic bases as well as tributylamine in order to determine the most suitable base for this system. The results are presented in Table 5.

Table 5: Optimisation of the base for PdNP@PIILP catalysed Suzuki-Miyaura cross coupling between 4-bromoacetophenone and phenylboronic acid.



| Entry ^a | Base | PdNP@PPh ₂ -PIILP (2.13) conversion (%) ^b | PdNP@PPh ₂ -PEGPIILP (2.14) conversion (%) ^b |
|--------------------|---------------------------------|--|---|
| 1 | K ₂ CO ₃ | 98 | 100 |
| 2 | Na ₂ CO ₃ | 83 | 74 |
| 3 | Cs ₂ CO ₃ | 75 | 92 |
| 4 | NaOAc | 7 | 9 |
| 5 | CsOAc | 11 | 11 |
| 6 | K ₃ PO ₄ | 62 | 66 |
| 7 | CsF | 22 | 27 |
| 8 | NBu ₃ | 2 | 5 |

^aReaction Conditions: 0.1 mol% catalyst, 1 mmol aryl halide, 1.13 mmol phenylboronic acid, 1.2 mmol base, 1.2 mL H₂O, 1.2 mL ethanol, RT, 0.5 h. ^b Determined by GC with 1 mmol decane std, average of 2 runs.

For both catalysts, varying the base had a dramatic effect on efficacy. The most drastic was obtained with organic base tributylamine (Table 5, entry 8) as the conversion dropped to 2% and 5% with **2.13** and **2.14**, respectively. As expected, good conversions were obtained with

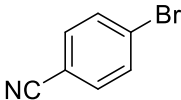
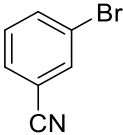
other metal carbonates for both catalysts (entries 2 and 3), whereas the use of metal acetates gave poor conversions (entries 4 and 5). Of the carbonates, the best performance was achieved with the potassium salt (entry 1). Despite being the most basic, use of the caesium salt resulted in poorer performance, which may result from lower solubility in the ethanol-water mix. Whilst likely to be the most soluble, the use sodium carbonate as the base also resulted in lower conversion (entry 2). However this is the least basic of the three carbonates.

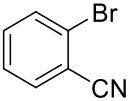
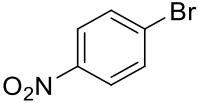
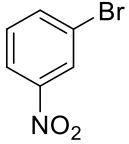
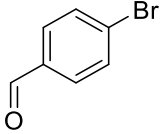
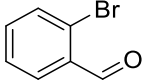
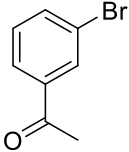
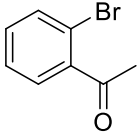
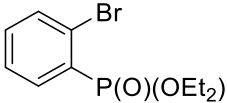
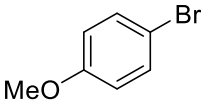
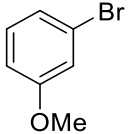
Surprisingly, potassium phosphate only gave moderate conversions (entry 6), and caesium fluoride gave poor conversion (entry 7). As such, potassium carbonate was identified as the base of choice as it is cheap and readily available.

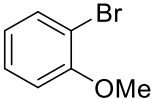
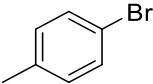
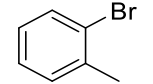
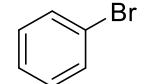
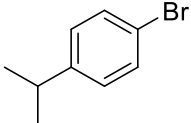
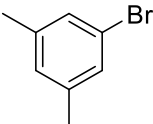
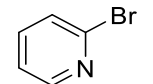
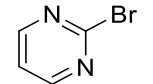
2.3.4 Substrate screening

Having identified the optimum conditions, comparative catalyst testing was conducted using a broad range of sterically and electronically disparate electrophiles to assess the scope of the newly prepared catalysts. Furthermore, as the preformed catalysts **2.13** and **2.14** are generated from their tetrachloropalladate precursors $\text{PdCl}_4\text{@PPh}_2\text{-PIILP}$ (**2.11**) and $\text{PdCl}_4\text{@PPh}_2\text{-PEGPIILP}$ (**2.12**) by chemical reduction, it was envisaged that NPs could be formed *in situ* by phenyl boronic acid-mediated reduction prior to the addition of substrate. In this regard, this strategy presents numerous practical advantages as further processing can be avoided as well as the need to isolate and store potentially sensitive NP catalysts. Furthermore, this would enable a more operationally straightforward protocol for scale up. Thus, the substrate screen was undertaken by generating catalyst *in-situ* immediately prior to addition of substrate and comparing their efficacy with ex-situ generated PdNP-catalysts.

Table 6: Substrate screening for the PdNP@PIILP catalysed Suzuki-Miyaura cross coupling reaction.

| Entry ^a | Substrate | Time (hours) | 2.11 (%) ^b | 2.13 (%) ^b | 2.12(%) ^b | 2.14(%) ^b |
|--------------------|---|-----------------|-----------------------|-----------------------|----------------------|----------------------|
| 1 |  | 0.5 | 95 | 96 | 99 | 99 |
| 2 |  | 3 | 80 | 96 | 99 | 99 |

| | | | | | | |
|-----------|---|-----|----|----|----|----|
| 3 |  | 5 | 81 | 95 | 98 | 99 |
| 4 |  | 2 | 89 | 96 | 91 | 98 |
| 5 |  | 1 | 96 | 95 | 99 | 99 |
| 6 |  | 0.5 | 95 | 97 | 97 | 99 |
| 7 |  | 16 | 93 | 83 | 98 | 92 |
| 8 |  | 16 | 95 | 81 | 99 | 99 |
| 9 |  | 16 | 58 | 34 | 99 | 91 |
| 10 |  | 6 | 89 | 57 | 99 | 92 |
| 11 |  | 5 | 62 | 45 | 97 | 93 |
| 12 |  | 5 | 31 | 31 | 89 | 96 |

| | | | | | | |
|-----------|---|----|----|----|----|----|
| 13 |  | 16 | 89 | 91 | 99 | 94 |
| 14 |  | 6 | 96 | 85 | 90 | 89 |
| 15 |  | 16 | 67 | 60 | 80 | 78 |
| 16 |  | 6 | 80 | 87 | 49 | 69 |
| 17 |  | 16 | 47 | 62 | 74 | 79 |
| 18 |  | 16 | 55 | 67 | 64 | 81 |
| 19 |  | 16 | 22 | 17 | 80 | 19 |
| 20 |  | 16 | 34 | 28 | 18 | 23 |

^aReaction Conditions: 0.1 mol% catalyst, 1 mmol aryl halide, 1.13 mmol phenylboronic acid, 1.2 mmol K₂CO₃, 1.2 mL H₂O, 1.2 mL ethanol, RT, variable reaction time. ^b Determined by GC with 1 mmol decane std, average of 2 runs. **2.12** = PdCl₄@PPh₂-PEGPIILP, **2.14** = PdNP@PPh₂-PEGPIILP, **2.11** = PdCl₄@PPh₂-PIILP, **2.11** = PdNP@PPh₂-PIILP.

Initial screening with 4-bromoacetophenone as the electrophile and using catalysts generated *in situ* from the Pd^(III) loaded precursors were encouraging as conversions of 96% and 100% were obtained under identical reaction conditions for **2.11** and **2.12**, respectively, which is comparable with their pre-reduced counterparts. A sample of the *in-situ* prepared NPs were submitted for TEM analysis which revealed that these catalysts consist of monodisperse particles (see appendix A1 and A2 for images and figures). For comparison, PdNPs obtained from *in situ* reduction of **2.11** were found to be 2.61 ± 0.38 nm which is comparable to the mean diameter of the PdNPs in the prereduced catalyst **2.13**, which were 2.29 ± 0.96 nm.

However, the average diameters of PdNPs generated *in situ* from **2.12** were calculated as 3.36 ± 0.61 nm, which are larger than that generated *ex situ* which had a mean diameter of 1.93 ± 0.67 nm.

A full substrate screen demonstrated the efficacy of the PIILP catalysts as the results presented in Table 6 reveal that moderate to good yields can be achieved with both electron donating and electron withdrawing substituted aryl bromides as well sterically hindered substrates. With the exception of 2- and 3-bromotoluene (Table 6 entries 15 and 16), the PEGylated catalysts outperformed the non-PEGylated catalysts which highlights the benefits of the PEG modification on the polymer support. Encouragingly, in general, comparable results were obtained between *ex-situ* and *in-situ* prepared nanoparticles with their respective catalyst supports, however, slightly higher activity is generally achieved using the Pd^(II) loaded precursors for electron deficient substrates which is most evident in the case of 2-bromoacetophenone, 2-bromoanisole and 3-bromotoluene (entries 9, 11 and 16). Aryl bromides bearing *para*-substituted activating electron withdrawing groups such as cyano, nitro and formyl groups gave excellent conversions for all catalysts (entries 1, 4 and 6) after a reaction time of only 30 minutes. However, aryl bromides bearing *para*-substituted electron donating groups required longer reaction times to achieve comparable conversions. For example, 4-bromoanisole (entry 11) and 4-bromotoluene (entry 14) required 5 and 6 hours, respectively, for all catalysts. This effect is perhaps not surprising as electron withdrawing substituents are favoured during the rate-limiting oxidative addition step in the catalytic cycle. In comparison, the corresponding *meta*-electron withdrawing substituted aryl bromides were not as active. For example, 3-bromobenzonitrile required a reaction time of 3 hours to reach a comparable conversion to its *para*-substituted counterpart (entry 2), while 3-bromoacetophenone was particularly sluggish and required the reaction time to be extended from 30 mins to 16 hours to achieve comparable conversions (entry 8). Although moderate conversions were achieved with 3-bromotoluene (entry 16) and 3-bromoanisole (entry 12) at the same reaction time, the conversions were lower than those obtained with their 4-substituted derivatives (entries 14 and 11 respectively). The decrease in activity may be attributed to a decrease in polarisation of the C-Br bond derived from substitution at the *meta*-position; this may result in a slightly stronger bond which would slow the oxidative addition step.

As expected in the case of *ortho*-substituted electrophiles, longer reaction times were required to achieve good conversions as a result of the unfavourable steric interactions on coordination of the reactants to the particle surface. The most evident example is that of 2-bromobenzaldehyde (entry 7) which required 16 hours to achieve >90% conversion whereas the *para*-substituted derivative reached near-quantitative conversion after only 30 mins for each catalyst. A similar reaction profile is also observed in the case of 2-bromobenzonitrile (entry 3), 2-bromoacetophenone (entry 9), 2-bromoanisole (entry 13) and 2-bromotoluene (entry 15). Furthermore, the sterically cumbersome substrates 4-*tert*-butylbromobenzene (entry 17) and 3,5-dimethylbromobenzene (entry 18) required the longest reactions times to reach even moderate conversions due to the severe steric intolerance of the substrate.

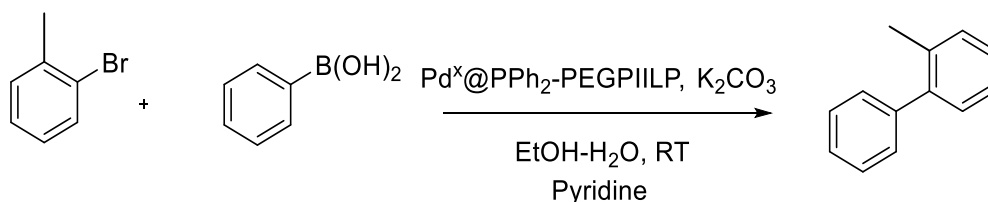
Finally, 2-bromopyridine (entry 19) and 2-bromopyrimidine (entry 20) were chosen as model heteroaryl bromides. Using the same protocol, only minor conversions were obtained even after prolonged reaction times and heating. Furthermore, after extending the reaction time to 3 days, no increase in conversion was observed suggesting that the heteroaromatic may well poison the catalyst; this would most likely occur via binding and saturation of the active site *via* the nitrogen lone pair. Whilst it is clear that all of the phosphine is covalently attached to the catalyst surface, as evidenced by ^{31}P solid state NMR, the high activity observed in the Suzuki-Miyaura coupling of a range of aryl bromides suggest that either i) the surface is not entirely covered i.e. the surface is not coordinatively saturated with phosphorus or ii) dissociation of coordinated phosphine during catalysis to assist substrate binding is a facile process. On this basis, it may be possible that the presence of 1000 equivalents of heteroaryl donor may saturate the surface irreversibly, therefore rapidly diminishing activity and eventually causing complete deactivation. In this regard, a series of model poisoning experiments were conducted, details of which are presented in the following section.

2.3.5 Catalyst poisoning and deactivation in the presence of heteroaromatics

To develop an understanding of the effect of nitrogen donors on the catalyst activity, **2.14** was pre-stirred with pyridine. Whilst it would be difficult to mimic such a complex dynamic system, it was envisaged that this model may provide some fundamental mechanistic detail on the nature of catalyst deactivation. Following this, two initial experiments were conducted whereby the Suzuki-Miyaura coupling between 4-bromoacetophenone and phenylboronic acid was carried out in the presence of **2.14** after pre-treatment with pyridine for 1 hour and 16 hours. Deactivation was evident as in both cases only 6% conversion was obtained after a

reaction time 30 minutes (*c.f.* 100% without pre-treatment) which further suggests that saturation of the catalyst surface may be responsible for the lack of catalytic activity for *N*-heterocyclic donor substrates.

To examine the rate of deactivation and establish a deactivation-time profile, the Suzuki-Miyaura coupling of 2-bromotoluene and phenylboronic acid in the presence of 0.1 mol% **2.14** was monitored as a function of pyridine addition. To this end, a series of batch reactions were conducted in parallel and 1 mmol of pyridine was added at the appropriate intervals and the conversion determined after a total reaction time of 8 hours. The electrophile 2-bromotoluene was chosen as this substrate requires a prolonged reaction time, therefore it was envisaged that this would allow the onset of deactivation to be more accurately interpreted.



Scheme 25: **2.14** catalysed Suzuki-Miyaura cross-coupling reaction between 2-bromotoluene and phenylboronic acid in the presence of pyridine.

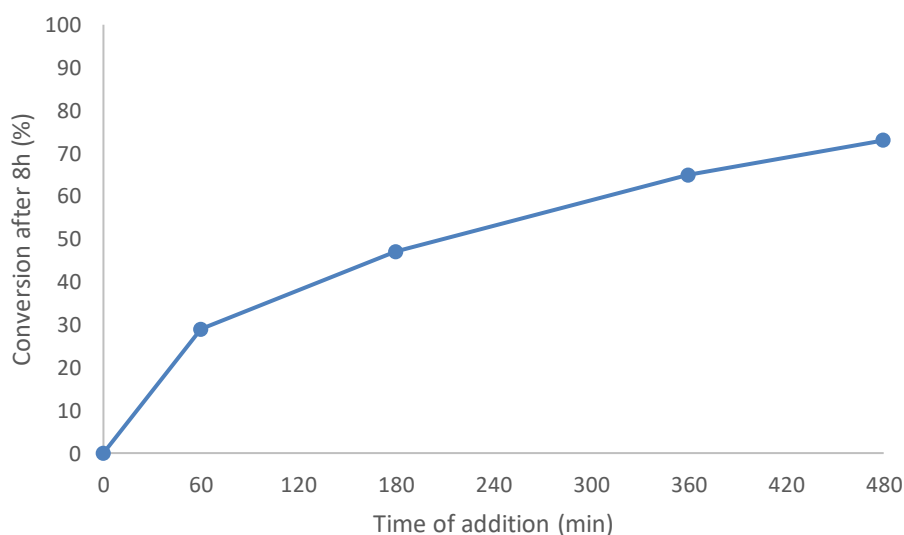


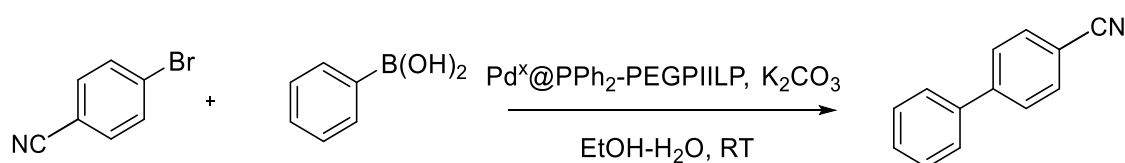
Figure 18: Conversion as a function of pyridine addition time. Reaction Conditions: 0.1 mol% catalyst, 1 mmol pyridine, 1 mmol 4-bromoacetophenone, 1.13 mmol phenylboronic acid, 1.2 mmol K_2CO_3 , 1.2 mL H_2O , 1.2 mL ethanol, RT, reaction time = 8 hours. Conversion determined by GC with 1 mmol decane std, average of 2 runs.

The profile depicted in Figure 18 shows that addition of pyridine at $T=0$ induces complete deactivation and quenching of the reaction. Furthermore, the addition of pyridine at later

stages of the reaction allows the reaction to proceed further before quenching which again suggests that deactivation is most likely due to poisoning by the addition of nitrogen donors.

2.3.6 Kinetic studies

The results in Table 6 clearly demonstrate that the PEG modification improves the catalyst efficiency across a range of substrates. To explore this phenomenon in more detail, the Suzuki-Miyaura coupling between 4-bromobenzonitrile and phenylboronic acid catalysed by **2.13** and **2.14**, along with NPs generated by *in situ* reduction of the corresponding precursors was monitored as a function of time. This substrate was chosen as an activated substrate with a relatively short reaction time.



Scheme 26: Suzuki-Miyaura cross coupling reaction between 4-bromobenzonitrile and phenylboronic acid catalysed by **2.14**.

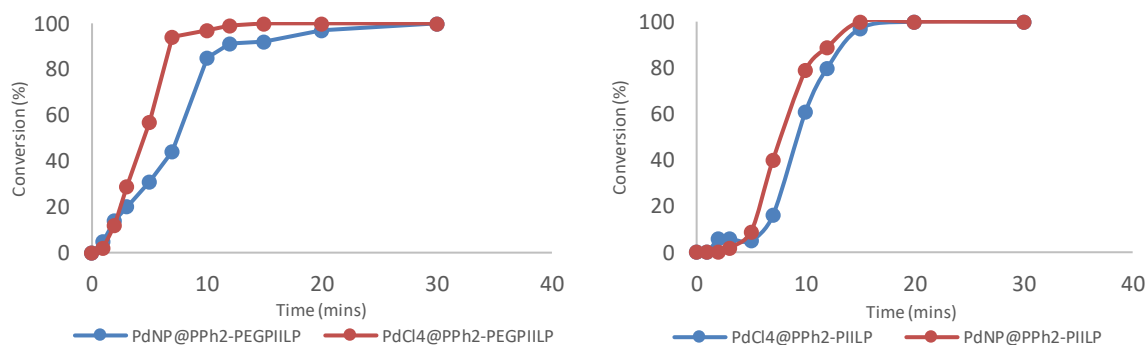


Figure 19: Time conversion plots for the Pd^(X)@PPh₂-RPIILP catalysed Suzuki-Miyaura cross coupling between 4-bromobenzonitrile and phenylboronic acid.

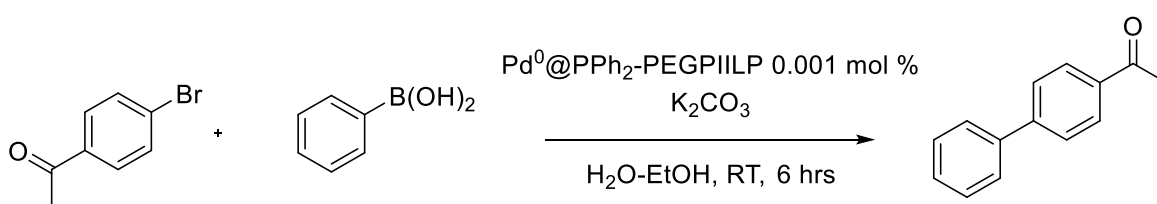
The time-conversion profiles in Figure 19 demonstrate that PdNP@PPh₂-PEGPIILP (**2.14**) exhibits a shorter induction period (< 1 min vs. 5 min) than PdNP@PPh₂-PIILP (**2.13**) and that the PEGylated catalyst reaches full conversion at approx. 10 mins whereas 15 mins is required to achieve full conversion for its non-PEGylated counterpart. This may well be associated with the increased hydrophilicity of the support facilitating access of the substrate to the active Pd species. Furthermore, the increased hydrophilicity may facilitate increased solubility or swelling of the support enabling a better dispersion of the NPs in the reaction mixture, which

correlates with the DLS data presented in section **1.2.2**. To investigate whether the induction period is a result of changes in polymer morphology due to dispersion in solution, it would be useful to monitor the induction period as a function of time for prestirring the catalyst prior to the addition of substrate. After 1 minute, 9% conversion is achieved for the PEGylated catalysts, after which rapid conversion of the remaining starting material occurs and the reaction is almost complete after 10 minutes. A similar profile depicting rapid conversion over a ca. 5 min period was obtained for the reaction catalysed by **2.11** and **2.13** which occurs after an initial induction period and consequently, full conversion is achieved after approximately 15 minutes.

Additionally, both catalysts generated *in-situ* from **2.11** and **2.12** show a similar reaction profile to that of their preformed counterpart suggesting that reduction of the $[\text{PdCl}_4]^{2-}$ loaded precursor is facile and does not have a profound effect on the kinetic profiles. Whilst this clearly demonstrates the advantages of the PEG functionality, a more thorough investigation based on a range of substrates with varied electronic and steric properties would need to be conducted in order to ultimately understand the different reaction profiles.

2.3.7 Longevity and recycle studies

To examine the robustness of the catalyst, the Suzuki-Miyaura coupling between phenylboronic acid and 4-bromoacetophenone was conducted in the presence of PdNP@PPh₂-PEGPIILP at a reduced catalyst loading of 0.001 mol% under the optimum conditions.

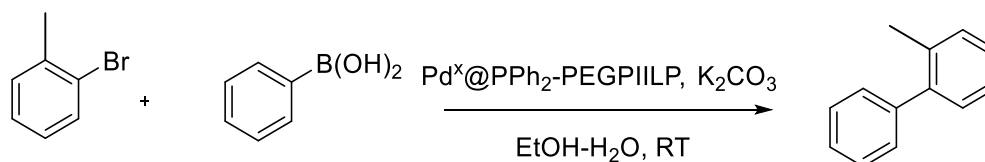


Scheme 27: Suzuki-Miyaura cross coupling between 4-bromoacetophenone and phenylboronic acid at reduced catalyst loading.

Remarkably, after a reaction time of 6 hours the conversion reached 98% which corresponds to a turnover number (TON) of 98,000 and an average turnover frequency (TOF) of 16,300 h⁻¹. A review of literature revealed that PIILP systems substantially outperform many designer systems for this type of transformation including water soluble sulfonated PEPPSI-Pd-NHC catalysts which gave a TOF of 412 h⁻¹,³⁷ palladium nanoparticles stabilised by 3,4-

dihydropyridine functionalised Fe_3O_4 nanoparticles which gave a TOF of 6000 h^{-1} ,³⁸ and PdNPs immobilised in Schiff base-functionalised multiwalled carbon nanotubes which gave a TOF of $2,400 \text{ h}^{-1}$.³⁶ Furthermore, the efficacy of PdNP@PPh₂-PEGPIILP is comparable to that of PdNPs supported on cyclodextrin reported recently which gave a TOF of $16,000 \text{ h}^{-1}$ based on 32% conversion.³⁹

Interestingly, even after prolonged reaction times, the conversion of 2-bromotoluene did not increase above the 80% and 78% obtained with **2.12** and **2.14**, respectively in 16 hours. To examine the reaction kinetics and investigate catalyst longevity, comparative catalyst testing was conducted to generate a conversion-time profile for the Suzuki-Miyaura coupling between 2-bromotoluene and phenylboronic acid in the presence of 0.1 mol% *in-situ* generated and *ex-situ* prepared PdCl₄@PPh₂-PEGPIILP (**2.12**) and PdNP@PPh₂-PEGPIILP (**2.14**).



Scheme 28: Suzuki-Miyaura cross coupling between 2-bromotoluene and phenylboronic acid catalysed by **2.12** or **2.14**.

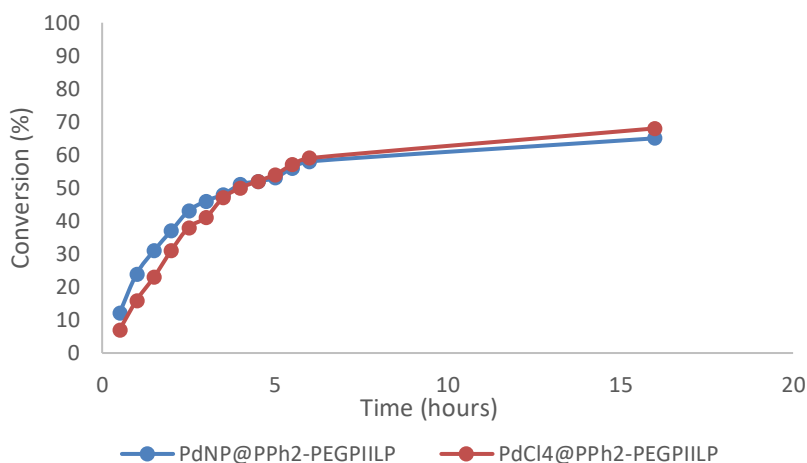


Figure 20: Time-conversion plot for the Pd^(X)@PPh₂-PEGPIILP catalysed Suzuki-Miyaura cross coupling of 2-bromotoluene and phenylboronic acid.

The plot in Figure 20 reveals that both catalysts show a similar activity profile and that the optimum conversion is effectively achieved at approximately 5 hours. This may be due to the fact that during the early stages of the reaction the solution is homogeneous, however, as the reaction proceeds, the biaryl product precipitates from the solution which may begin to hamper the efficiency of stirring as the reaction is reasonably concentrated (0.42 mol dm^{-3}).

However, given that high conversions can be obtained with other biaryls that precipitate during the reaction, there may well be other factors that contribute to the progressive catalyst deactivation.

TEM analysis of PdNP@PPh₂-PEGPIILP isolated after the reaction revealed that whilst the NPs remained near monodisperse, they suffered significant agglomeration and the average diameter increased from 1.93 ± 0.67 nm before catalysis to 3.72 ± 0.58 nm after the reaction (Figure 21). Its possible that under the reaction conditions Pd may leach into solution and form larger aggregates over the course of the study. In order to assess the activity of the spent catalyst, a single batch reaction was conducted, the product extracted, and the aqueous phases recharged with a further equivalent of 2-bromotoluene, phenylboronic acid and potassium carbonate. After a reaction time of 6 hours, 42% conversion was achieved which represents a 16% drop in conversion. However, at this stage it is difficult to attribute this drop in activity solely to a change in size of the NP. For instance, as the catalyst cannot be directly isolated from the solution via filtration, it is possible that accumulation of boronic acid and potassium carbonate derived by-products may saturate the solution and/or block active sites on the NPs.

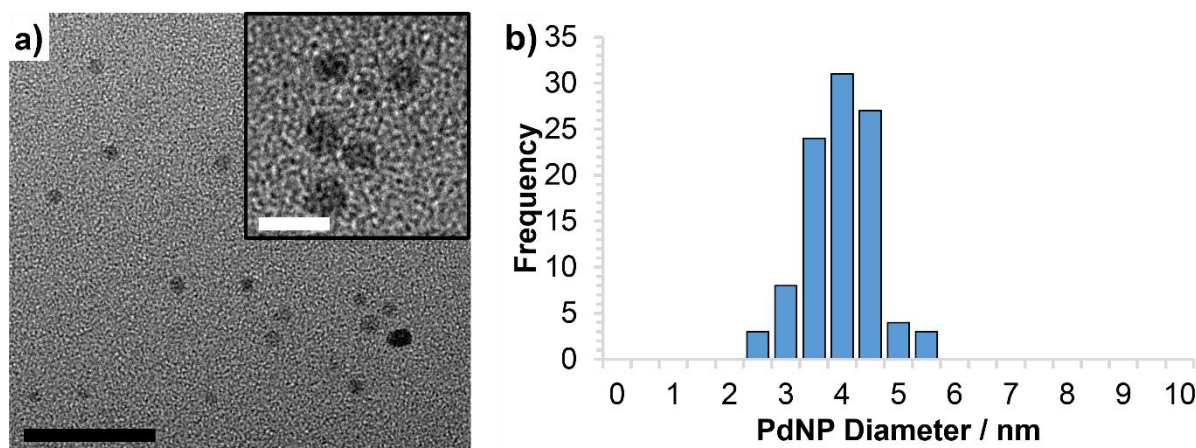


Figure 21: TEM image of spent PdNP@PPh₂-PEGPIILP isolated after catalysing the Suzuki-Miyaura coupling of 2-bromotoluene and phenylboronic acid, reaction time = 6 hours. Scale bars are 25 nm (black) and 5 nm (white).

To further investigate the longevity of the catalyst, a series of batch recycle studies were conducted. To this end, the PdNP@PPh₂-PEGPIILP catalysed Suzuki-Miyaura cross-coupling between 4-bromoacetophenone and phenylboronic acid was chosen due to the short reaction times. As discussed earlier, due to the nature of the reaction, neither the inorganic by-products nor the PEGylated catalyst can be directly isolated from the reaction mixture, therefore after initiation of the reaction by addition of the substrate, the organic products

were extracted after the appropriate time before recharging with more potassium carbonate, phenylboronic acid and 4-bromoacetophenone.

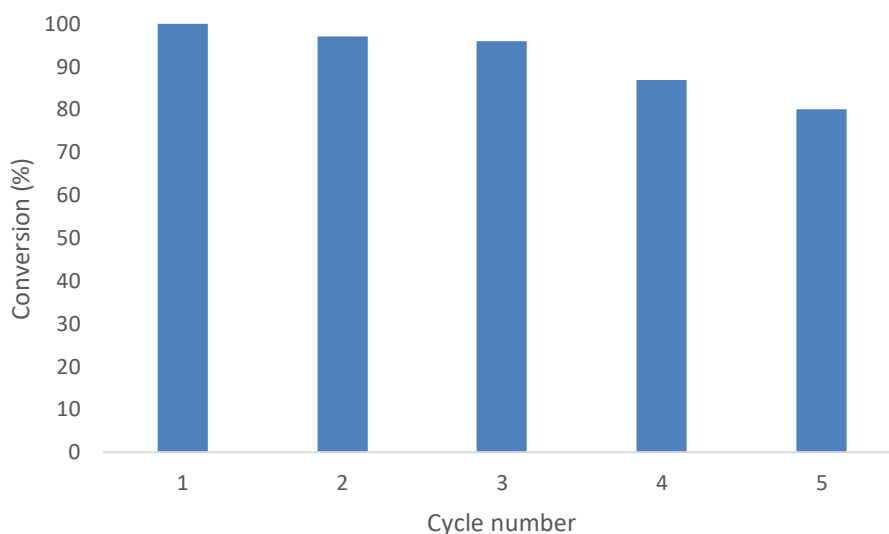


Figure 22: Recycling profile for the Suzuki-Miyaura coupling between 4-bromoacetophenone and phenyl boronic acid catalysed by 0.1 mol% 2.14.

The results in Figure 22 show that there was only a minor drop in conversion from 99% to 96 % after three runs, although the reaction time was extended from 30 minutes to 1 h after the first run to achieve comparable activity. However, conversions dropped quite dramatically after the fifth run and only 80% conversion was obtained after 1 hour. TEM analysis of the catalyst isolated after the fifth run revealed a substantial increase in average particle size from 1.93 ± 0.67 nm to 4.85 ± 0.98 nm which suggests that either i) the NPs lose stability and agglomerate into less active species under the conditions of catalysis or that ii) Pd leaches from the support and is later recaptured, forming larger particles. Although more information is clearly required to elucidate the mechanism of deactivation, a more robust and efficient protocol is needed for catalyst recovery and reuse. Furthermore, after multiple runs, the solution becomes heavily saturated with inorganic by-products which may well impose severe mass transport limitations. Although ultimately a continuous flow process would be a more efficient way to monitor and assess the longevity of the catalyst, this system presents some intrinsic challenges due to the difficulty of ensuring the reactants and products remain in a single solution phase which would require bespoke engineering of the process.

2.3.8 Probing the nature of the reaction

As previously mentioned, the true nature of the active species in PdNP catalysed cross-couplings is still the subject of academic debate; partly due to the challenges associated with obtaining definitive results. In this regard, a series of experiments were conducted in attempt to probe the nature of PdNP@PIILP systems. ICP analysis of the organic extract revealed no leaching of Pd as the palladium content was below the threshold of the apparatus. However, the possibility that catalysis occurs over soluble molecular Pd before redeposition (i.e. a 'catch and release' mechanism) cannot be discounted. Therefore, a series of mercury poisoning tests were conducted with the optimum system. In this regard, if the catalyst was heterogeneous in nature, i.e. catalysis occurring on defect sites, the addition of mercury would induce quenching of the reaction by forming a mercury-palladium amalgam; this would inhibit chemisorption of the substrates and essentially deactivate the catalyst. To this end, the Suzuki-Miyaura coupling of 4-bromotoluene and phenylboronic was identified as a suitable reaction to model this effect as high conversion is achieved over 6 hours, enabling sufficient time for the onset of deactivation to be established. Thus, the *ex-situ* and *in-situ* prepared catalysts **2.14** and **2.12**, respectively, were stirred under the optimum conditions with 400 equivalents of mercury for a series of different times prior to the addition of the substrate. Figure 23 shows that immediate addition of the substrate results in a drop in conversion from 80% and 90% for the *in situ* and *ex situ* catalysts, respectively, to 46% and 52%, respectively. Furthermore, a non-linear decrease in activity is observed for both catalysts with increasing exposure to mercury prior to addition of the substrate. Finally, after stirring with mercury for 24 hours, the reaction is almost completely quenched and only 6% conversion is achieved.

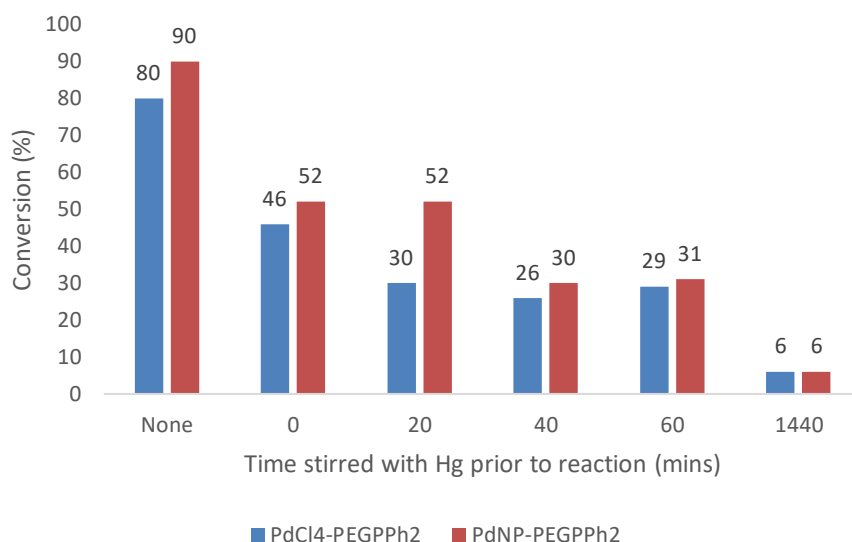


Figure 23: Results of the Hg poisoning study. Reaction Conditions: 0.1 mol% catalyst, mercury (400 eq. to catalyst), 1 mmol 4-bromotoluene, 1.13 mmol phenylboronic acid, 1.2 mmol K₂CO₃, 1.2 mL EtOH, 1.2 mL H₂O, RT, 6 h, conversion determined by GC with 1 mmol decane std, average of 2 runs.

In order to further investigate the nature of the catalyst, a series of reactions were conducted varying the solvent volume. In typical homogenous systems, dilution of the reaction mixture would effectively reduce the catalyst concentration which should result in a drop in activity. Contrary to this, for a heterogeneous system, the same loss of activity is not likely to be observed on the basis that particles are statistically less likely to aggregate under the reaction conditions and high surface area can be maintained.

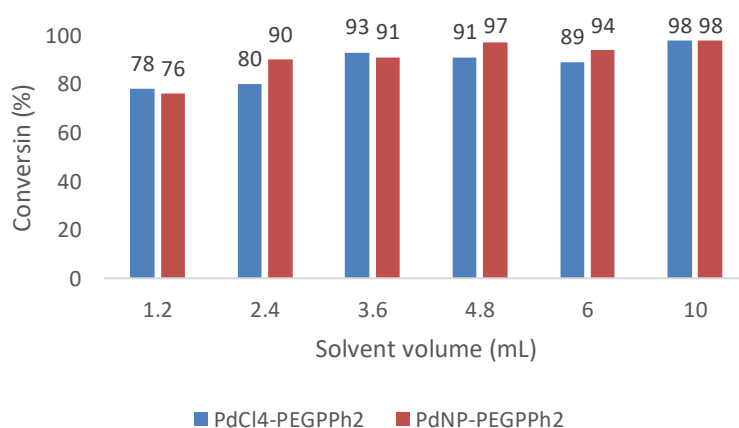


Figure 24: Results of the reaction dilution study. Reaction Conditions: 0.1 mol% catalyst, 1 mmol 4-bromotoluene, 1.13 mmol phenylboronic acid, 1.2 mmol K₂CO₃, RT, 6 h, conversion determined by GC with 1 mmol decane std, average of 2 runs.

The results in Figure 24 reveal a slight drop in conversion for both catalysts as the reaction volume is reduced from 2.4 mL to 1.2 mL. Interestingly, there was a gradual increase in conversion as the reaction volume was diluted such that almost quantitative conversion was obtained with a reaction volume of 10 mL. Whilst these results coupled with the mercury poisoning experiments may indicate that the major species responsible for the catalysis is heterogeneous, the addition of mercury to a heterogeneous catalyst is often reported to result in instantaneous passivation.³⁷ Additionally, the limited solubility of mercury in the ethanol-water mixture may hamper its dispersion, which may explain the profile depicted in Figure 23. Furthermore, Jones *et al.* reported that the addition of mercury can also inhibit molecular Pd⁽⁰⁾ catalysts and as such an alternative homogenous pathway cannot be completely discounted.⁴⁰

2.3.9 Comparison with a commercial catalyst

The efficiency of the two *ex situ* prepared PIILP catalysts was compared to three commercial samples of Pd/C. Gratifyingly, under the optimum conditions, both PIILP systems substantially outperformed their commercially available alternatives for a representative set of three substrates. Interestingly, there appears to be a substantial variation in the activity between different commercial samples of Pd/C which was most evident for 2-bromoanisole with a 31% variation across the three samples. Although the role of the various functionality within the support is complex, and at this stage not fully understood, these results present PIILP technology as a viable alternative for Suzuki-Miyaura couplings in aqueous media under extremely mild conditions.

Table 7: Comparative catalyst testing with commercially available catalysts for the Suzuki-Miyaura couplings of aryl bromides with phenyl boronic acid.

| Entry ^a | R | Time hours | PdNP@PPh ₂ - PIILP ^b | PdNP@PPh ₂ - PEGPIILP ^b | Pd/C 10% (Sigma) ^b | Pd/C 5% (Sigma) ^b | Pd/C 5% (Alpha) ^b |
|--------------------|----------|---------------|---|--|-------------------------------------|------------------------------------|---------------------------------------|
| 1 | 4-C(O)Me | 0.5 | 98 | 100 | 6 | 9 | 1 |
| 2 | 3-Me | 6 | 87 | 69 | 53 | 61 | 65 |
| 3 | 2-OMe | 16 | 91 | 94 | 51 | 39 | 70 |

^aReaction conditions: 1 mmol substrate, 0.1 mol% catalyst, 1.13 mmol phenylboronic acid, 1.2 mmol K₂CO₃, 1.2 mL water, 1.2 mL EtOH, RT. conversion determined by GC with 1 mmol decane std, average of 2 runs.

2.4 Conclusion

Palladium nanoparticles supported on two different phosphine functionalised imidazolium-based lightly crosslinked polymer immobilised ionic liquids; PdNP@PPh₂-PIILP and PdNP@PPh₂-PEGPIILP, have been prepared via radical polymerisation and extensively characterised using a variety of physical techniques. The monomer synthesis is modular and can easily be adapted to incorporate additional functionality to diversify the support e.g. for use in bifunctional catalysis. TGA analysis of the materials revealed that both PIILs were stable up to around 250°C and SEM analysis revealed slightly different morphology of the polymer surface most likely due to increased swelling of the hydrophilic PEGylated support. The polymers were readily impregnated with tetrachloropalladate and reduced by NaBH₄ to afford the corresponding PIIL-stabilised PdNPs. Analysis of the materials by solid state ³¹P NMR spectroscopy confirmed the presence of a Pd-P interaction and that all the phosphine was coordinated to Pd. XPS analysis revealed incomplete reduction of the Pd^(III) precursor for both catalysts, and TEM analysis demonstrated the presence of well dispersed, small spherical Pd nanoparticles with the PEGylated system having slightly smaller NPs. At this stage it is difficult to pinpoint the roles of the functionality on the support, nevertheless, the use of phosphine-functionalised ionic liquid-modified supports is clearly beneficial, as both PdNP@PPh₂-PIILP and PdNP@PPh₂-PEGPIILP are remarkably efficient catalysts for the Suzuki-Miyaura cross-coupling under extremely mild conditions at low catalyst loadings. Catalyst testing revealed that the PEGylated system consistently outperformed its non-PEGylated counterpart across a range of substrates; this improvement in efficacy is most likely attributed to an increase in dispersity/solvation of the support in aqueous media facilitating access to the active site. While high conversions were obtained with both systems, the catalyst appears to be deactivated by heteroaromatics which was further supported by poisoning experiments using pyridine as a model heteroaromatic. Furthermore, nanoparticles generated *in-situ* by reduction of the [PdCl₄]²⁻ loaded precursor with excess phenylboronic acid were as efficient as their *ex-situ* prepared counterparts; kinetic studies with a range of electronically disparate substrates revealed that there was also no induction period indicating that reduction of the Pd^(III) is facile.

Mercury poisoning and dilution studies strongly suggest that the major species is heterogeneous, however, further in-depth surface studies will be required to validate this.

Finally, both PIILP systems substantially outperformed a range of commercially available heterogeneous catalysts and the TOF of 16,300 h⁻¹ obtained for the benchmark coupling between 4-bromoacetophenone and phenylboronic acid with PdNP@PPh₂-PEGPIILP is to the best of our knowledge the most efficient system to be reported in the literature.

It is hoped that these encouraging results, coupled with previous studies by the Doherty/Knight group with other heteroatom donors, may provide a lead for future catalyst design. It may be possible to further tune the properties of the support to ultimately optimise surface interactions and develop systems that i) are extremely efficient and operate under environmentally preferred conditions, and ii) uphold the appropriate materials properties to facilitate their incorporation into larger scale production i.e. continuous flow protocols and iii) are useful for a range of other transformations.

2.5 References

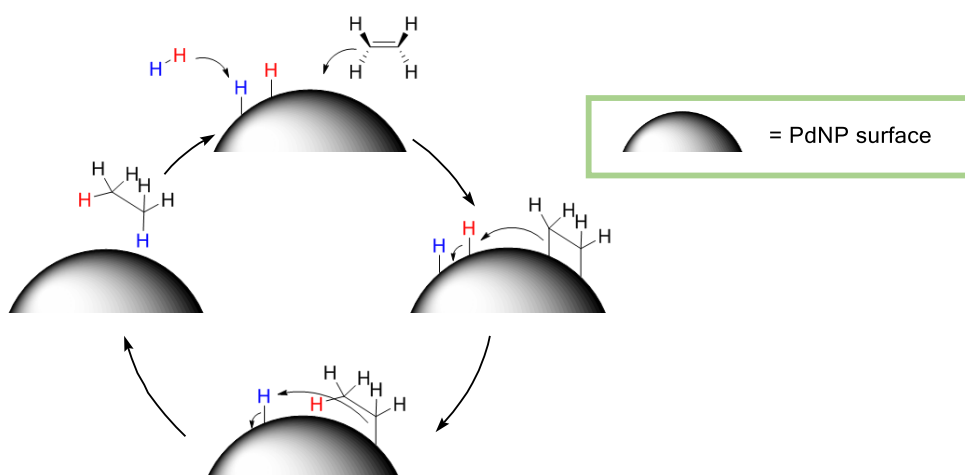
1. D. Sahu and P. Das, *RSC Adv.*, 2015, **5**, 3512-3520.
2. A. Chen, G. Zhao, J. Chen, L. Chen and Y. Yu, *RSC Adv.*, 2013, **3**, 4171-4175.
3. Y. Huang, Q. Wei, Y. Wang and L. Dai, *Carbon*, 2018, **136**, 150-159.
4. C. Pavia, E. Ballerini, L. A. Bivona, F. Giacalone, C. Aprile, L. Vaccaro and M. Gruttadauria, *Adv. Synth. Catal.*, 2013, **355**, 2007-2018.
5. S. Paul, M. M. Islam and S. M. Islam, *RSC Adv.*, 2015, **5**, 42193-42221.
6. K. C. Nicolaou, G. Bulger Paul and D. Sarlah, *Angew. Chem. Int. Ed.*, 2005, **44**, 4442-4489.
7. A. Rühling, K. Schaepe, L. Rakers, B. Vonhören, P. Tegeder, B. J. Ravoo and F. Glorius, *Angew. Chem. Int. Ed.*, 2016, **55**, 5856-5860.
8. D. Hui, D. Yu, Z. Xiaojin, Z. Zhenguo, F. Shuangli and Z. Zhenlin, *Nanotechnology*, 2018, **29**, 055705.
9. H. G. Lee, P. J. Milner, M. S. Placzek, S. L. Buchwald and J. M. Hooker, *J. Am. Chem. Soc.*, 2015, **137**, 648-651.
10. S. Doherty, J. G. Knight, N. A. B. Ward, D. M. Bittner, C. Wills, W. McFarlane, W. Clegg and R. W. Harrington, *Organometallics*, 2013, **32**, 1773-1788.
11. Q. Dai, W. Gao, D. Liu, L. M. Kapes and X. Zhang, *J. Org. Chem.*, 2006, **71**, 3928-3934.
12. J. L. Castelbou, A. Gual, E. Mercade, C. Claver and C. Godard, *Catal. Sci. Technol.*, 2013, **3**, 2828-2833.
13. J. Llop Castelbou, E. Bresó - Femenia, P. Blondeau, B. Chaudret, S. Castillón, C. Claver and C. Godard, *ChemCatChem*, 2014, **6**, 3160-3168.
14. J. Feng, S. Handa, F. Gallou and B. H. Lipshutz, *Angew. Chem. Int. Ed.*, 2016, **55**, 8979-8983.
15. E. D. Slack, C. M. Gabriel and B. H. Lipshutz, *Angew. Chem. Int. Ed.*, 2014, **53**, 14051-14054.
16. H. Pang, F. Gallou, H. Sohn, J. Camacho-Bunquin, M. Delferro and B. H. Lipshutz, *Green Chem.*, 2018, **20**, 130-135.
17. W. Chen, Y. Zhang, L. Zhu, J. Lan, R. Xie and J. You, *J. Am. Chem. Soc.*, 2007, **129**, 13879-13886.

18. R. Rabinowitz and R. Marcus, *J. Org. Chem.*, 1961, **26**, 4157-4158.
19. K. F. O'Driscoll and P. J. White, *J. Pol. Sci. A.*, 1965, **3**, 283-299.
20. A. Ziegler, K. Landfester and A. Musyanovych, *Colloid. Polym. Sci.*, 2009, **287**, 1261.
21. T. Iwai, T. Harada, K. Hara and M. Sawamura, *Angew. Chem. Int. Ed.*, 2013, **52**, 12322-12326.
22. S. Montolio, C. Vicent, V. Aseyev, I. Alfonso, M. I. Burguete, H. Tenhu, E. García-Verdugo and S. V. Luis, *ACS Catal.*, 2016, **6**, 7230-7237.
23. S.D Chambreau, A.C. Schenk, A.J. Sheppard, G.R. Yandek, G.L Vaghjiani, J. Maciejewski, C.J. Koh, A. Golan and S.R. Leone, *J. Phys. Chem. A*, 2014, **118**, 11119-11132.
24. M. Peuckert, *J. Phys. Chem.*, 1985, **89**, 2481-2486.
25. Z.-L. Du, Q.-Q. Dang and X.-M. Zhang, *Ind. Eng. Chem. Res.*, 2017, **56**, 4275-4280.
26. Y. Shen, X. Bo, Z. Tian, Y. Wang, X. Guo, M. Xie, F. Gao, M. Lin, X. Guo and W. Ding, *Green Chem.*, 2017, **19**, 2646-2652.
27. R. Albilali, M. Douthwaite, Q. He and S. H. Taylor, *Catal. Sci. Technol.*, 2018, **8**, 252-267.
28. N. Mejías, R. Pleixats, A. Shafir, M. Medio-Simón and G. Asensio, *Eur. J. Org. Chem.*, 2010, **2010**, 5090-5099.
29. V. P. Ananikov and I. P. Beletskaya, *Organometallics*, 2012, **31**, 1595-1604.
30. B. Thathagar Mehul, E. ten Elshof Johan and G. Rothenberg, *Angew. Chem. Int. Ed.*, 2006, **45**, 2886-2890.
31. R. Bernini, S. Cacchi, G. Fabrizi, G. Forte, F. Petrucci, A. Prastaro, S. Niembro, A. Shafir and A. Vallribera, *Green Chem.*, 2010, **12**, 150-158.
32. P. Taladriz-Blanco, P. Hervés and J. Pérez-Juste, *Top. Catal.*, 2013, **56**, 1154-1170.
33. R. Chemler Sherry, D. Trauner and J. Danishefsky Samuel, *Angew. Chem. Int. Ed.*, 2001, **40**, 4544-4568.
34. B. Van Vaerenbergh, K. De Vlieger, K. Claeys, G. Vanhoutte, J. De Clercq, P. Vermeir and A. Verberckmoes, *Appl. Catal. A*, 2018, **550**, 236-244.
35. I. Hoffmann, B. Blumenroder, S. Onodi nee Thumann, S. Dommer and J. Schatz, *Green Chem.*, 2015, **17**, 3844-3857.
36. H. Veisi, R. Azadbakht, F. Saeidifar and M. R. Abdi, *Catal. Lett.*, 2017, **147**, 976-986.
37. R. Zhong, A. Pothig, Y. Feng, K. Riener, W. A. Herrmann and F. E. Kuhn, *Green Chem.*, 2014, **16**, 4955-4962.
38. M. pirhayati, H. Veisi and A. Kakanejadifard, *RSC Adv.*, 2016, **6**, 27252-27259.
39. Y. Guo, J. Li, X. Shi, Y. Liu, K. Xie, Y. Liu, Y. Jiang, B. Yang and R. Yang, *Appl. Organomet. Chem.*, 2017, **31**, e3592.
40. T. S. Phan Nam , M. Van Der Sluys and W. C. Jones, *Adv. Synth. Catal.*, 2006, **348**, 609-679.

Chapter 3 : Application of PIILP materials to the selective hydrogenation of α,β - unsaturated aldehydes and ketones

3.1 Introduction

Metal nanoparticle catalysed hydrogenation is an extremely powerful and enabling technology. In particular, the design and fabrication of catalysts that facilitate the selective reduction of unsaturated moieties in the presence of other reactive fragments is of crucial importance. This is typically achieved on batch scale using homogenous catalysts in transfer hydrogenation solvents,¹ however, the use of supported heterogeneous catalysts would vastly improve the efficiency and allow the design of more efficient, sustainable and scalable protocols. In this regard, the selective hydrogenation of α,β - unsaturated aldehydes over heterogeneous catalysts is a key challenge as the resulting products are often valuable intermediates in the pharmaceutical and fine chemical industries.² Palladium based catalysts are the most widely reported due to their high selectivity for the reduction of the thermodynamically and kinetically more accessible C=C bond over the C=O.³ The fundamental mechanistic framework is largely accepted whereby the crucial role of the metal is to firstly mediate the absorption and dissociation of gaseous hydrogen across the surface, forming chemisorbed surface hydrogen atoms (Scheme 29).



Scheme 29: General mechanism for the hydrogenation of alkenes over heterogeneous Pd catalysts.

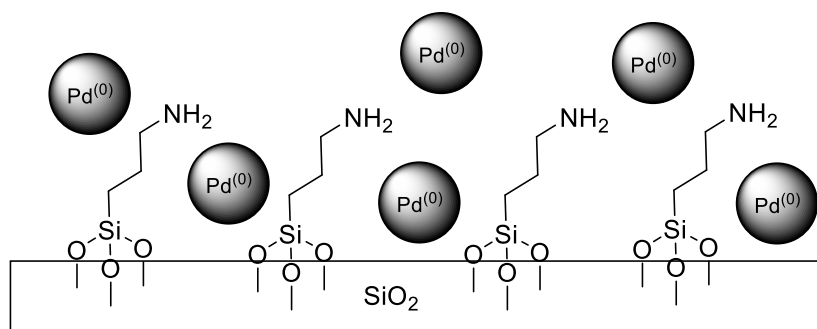
Following this, the metal facilitates stepwise addition of hydrogen across an adsorbed unsaturated substrate, firstly forming a surface-coordinated alkyl fragment before liberating the fully hydrogenated product. Although initially proposed for the alkene model, it is largely accepted that same the basic idea applies to other unsaturated substrates.³ Whilst this hypothesis is supported by many calculations, this oversimplifies the complex nature of

supported metal catalysts under catalytic conditions and recent advances in surface chemistry have highlighted the integral role of other factors, such as the role of carbonaceous deposits,⁴ and the competing adsorption modes of various substrates on non-uniform catalytic surface sites.⁵

The most widely accepted adsorption mode is that alkenes initially coordinate to metal surfaces in an extrinsic π -bonded manner, as this idea is based on the more realistic notion that catalysis occurs on non-ideal surfaces and accounts for molecules adsorbing on top of other surface bound species.⁶ Furthermore, the extrinsic π -bonded intermediate has been characterised using various *in situ* experiments under catalytic conditions.⁷ It is suggested that this intermediate may then rehybridise to form a di- σ type arrangement (depicted above), thereby forming two surface metal-carbon bonds before stepwise insertion of two chemisorbed hydrogen atoms and formal reductive elimination.⁸ However, it is clear the exact nature of the insertion step is not well known, as numerous recent reports have discovered evidence that the π -bonded intermediate may abstract two hydrogen atoms simultaneously.⁹⁻¹¹ Additionally, it has been suggested that changes in NP size can alter the initial absorption modes of the substrate, which can exert profound effects on the selectivity. Moreover, it has been shown that for α,β -unsaturated aldehydes, smaller nanoparticles favour adsorption of the C=C bond over the C=O.¹² Although the role of carbonaceous deposits on the surface of transition metal nanoparticles is still yet to be validated, there is a body of research that has documented their presence. Zaera characterised surface bound alkylidyne on Pt(111) single crystal surfaces using operando techniques which are proposed to be surface artefacts rather than hydrogenation intermediates.¹³ Similar findings have been reported by Wilde *et al.* on PdNP catalysts.¹⁴ Whilst both authors acknowledge that the role of these species in catalysis is not well understood, they propose that it is the presence of these species that is responsible for inhibiting side reactions such as dehydrogenations and/or modulating the electronic nature of the metal, which can strongly influence catalyst activity.

Additionally, catalyst-support interactions have been shown to modulate catalyst performance and enable optimisation of the catalyst activity by varying the support functionality. In this regard, Rossi *et al.* reported that PdNPs supported on various amine-modified silicas improved selectivity such that propylamine-functionalised silica-stabilised PdNPs catalysed the semi-hydrogenation of a range of alkynes with complete selectivity for the alkene.¹⁵ The amine modification was proposed to be crucial as it offered i) ligand assisted

catalysis at the PdNP active site to enhance selectivity, ii) improved Pd uptake during impregnation and iii) provided additional stabilisation of the particles to improve catalyst lifetime. Taylor *et al.* also demonstrated that the role of the support can drastically alter the product distribution in the palladium catalysed hydrogenation of bioderived furaldehyde and that whilst Pd/C was more active, PdNPs supported on TiO₂ were much more selective towards the production of tetrahydrofurfuryl alcohol compared with MgO, Al₂O₃, Fe₂O₃ and carbon-based supports.¹²



Scheme 30: PdNPs supported on propylamine functionalised silica developed by Rossi *et al.*¹⁵

Many reports document the high catalyst activity and tuneable selectivity of supported homogeneous catalysts and nanoparticle-based systems.^{16, 17} In particular, if used on a larger scale, these systems can reduce waste production and improve on overall product turnover. However, in reality, hydrogenative transformations on an industrial scale are classically conducted in the vapour phase using heterogeneous catalysts.¹⁸ The implementation of vapour phase technology presents many practical advantages from an engineering perspective with regards to reactor design, increased hydrogen solubility and mass transfer as well as facile product isolation and catalyst reuse which currently outweighs the benefits of large-scale homogeneous methods. However, despite the intrinsic advantages of vapour phase hydrogenation, the high pressure and temperatures required for operating under these conditions (usually in excess of 300°C) impose economic limitations on such processes and can lead to coking or deactivation of sensitive catalysts, especially over longer periods of time.¹⁹

As such, there is considerable drive towards the development of heterogeneous catalysts that operate efficiently under mild conditions in the aqueous phase, as water is considered an environmentally benign, cheap and non-toxic alternative to conventional organic solvent. Furthermore, the use of two-phase systems is desirable as the organic reactant/product phase can easily be extracted from the aqueous phase containing the catalyst which would facilitate

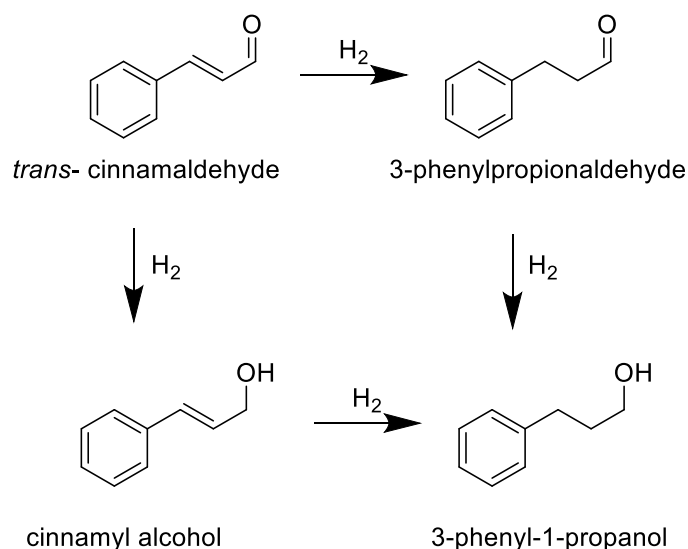
recycling.²⁰ There are a number of potential green credentials associated with supported aqueous phase catalysis, however, new separation technologies and strategies must be developed if the benefits of this approach are to be fully realised. Yet the potential benefits associated with low temperature aqueous phase catalyst would present a significant improvement in sustainability.

Additionally, a number of reports document an activating role of water in catalysis, however, this effect is currently not well understood due to the difficulty in obtaining unambiguous data. Nevertheless, this is generally attributed to either i) the hydrophobic effect whereby water-immiscible organic reagents are directed to the active catalyst due to the driving force associated with favourable interactions with the support or ii) chemisorbed water molecules on the catalyst surface participating in the reaction. For example, Riisager reported that deuterium was incorporated in to the product during D₂O labelling studies on the Pd-catalysed transfer hydrogenation of furfural.²¹ Furthermore, Shirai *et al.* reported that the addition of small amounts of water to the Pd catalysed hydrogenation of acetophenone resulted in a remarkable improvement in activity of 25% under otherwise identical conditions.²²

3.2 Results and Discussion

3.2.1 Comparative catalyst testing

As described in section 3.1, the less challenging selective hydrogenation of the C=C bond over the C=O moiety present in α,β -unsaturated aldehydes over palladium nanoparticles is now widely reported. Based on this precedent and the encouraging results presented in Chapter 1, it was reasoned that the newly developed catalysts PdNP@PPh₂-PIILP (**2.13**) and PdNP@PPh₂-PEGPIILP (**2.14**) could be efficient and selective catalysts for the aqueous phase production of various saturated aldehydes from their α,β -unsaturated counterparts. Based on literature precedent, *trans*-cinnamaldehyde was chosen as a suitable model to examine the relative merits of the PIILP systems as it is widely accepted as the benchmark substrate for this transformation and the products shown in Scheme 31 are all valuable intermediates with applications in the pharmaceutical and fragrance industries.²³



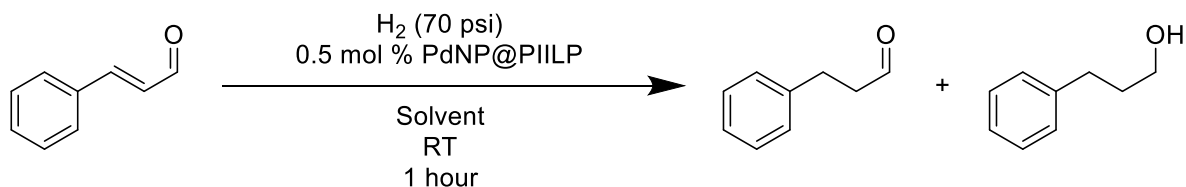
Scheme 31: Possible products of the Pd catalysed hydrogenation of *trans*-cinnamaldehyde.

Effect of solvent

A series of batch reactions were conducted using a benchtop 50 mL reactor equipped with a magnetically coupled stirrer and temperature controller to identify the optimum conditions for catalysis. Solvent choice is of crucial importance for heterogeneously catalysed hydrogenations as solvents have been widely reported to compete with adsorption of the substrate, thus, effecting the observed selectivity of the catalyst.²⁴ In an initial foray, it appeared that variance of the solvent had a dramatic effect on catalyst activity and selectivity for **2.13** and **2.14** (Table 8). In all cases, the major product formed was 3-phenylpropionaldehyde with the 3-phenyl-1-propanol as the minor and only other product. Whilst both catalysts perform poorly in conventional organic solvent (entries 1-4), activity improved in both cases in hydrogen bonding solvents - neat ethanol (entry 5) and ethanol water mixtures (entry 6). Although a slightly higher activity was obtained using the non-PEGylated catalyst in an ethanol-water mixture, gratifyingly, the highest selectivity was obtained under purely aqueous conditions with the PEGylated catalyst (entry 7). In the interests of green chemistry, the design of highly selective catalysts is crucial for waste reduction. Therefore, prompted by the efficacy of the PEGylated catalyst coupled with the sustainable green credentials and the practical advantages of using purely aqueous phase catalysis, water was chosen as the optimum solvent for the remainder of the studies. Although this result is most likely due to the increased hydrophilicity of the PEGylated support improving dispersion of the catalyst in solution, it is also possible that the organic framework

may serve as a medium for the build-up of hydrogen and organic substrate in solution, both of which have limited solubility in water.

Table 8: Optimisation of the reaction solvent for the PdNP@PIILP catalysed hydrogenation of cinnamaldehyde. NB analysis of the reaction mixture gave no evidence of the formation of cinnamyl alcohol.



| Entry ^a | Solvent | 2.13 | 2.13 | 2.14 | 2.14 |
|--------------------|-------------------|------------------|------------------|------------------|------------------|
| | | Conversion | Selectivity | Conversion | Selectivity |
| | | (%) ^b | (%) ^b | (%) ^b | (%) ^b |
| 1 | Toluene | 0 | 0 | 23 | 78 |
| 2 | Hexane | 35 | 58 | 52 | 82 |
| 3 | 2-Methyl-THF | 22 | 59 | 35 | 62 |
| 4 | Ethyl Acetate | 10 | 58 | 29 | 84 |
| 5 | Ethanol | 57 | 69 | 54 | 76 |
| 6 | Ethanol/Water 1:1 | 92 | 72 | 75 | 74 |
| 7 | Water | 75 | 74 | 81 | 85 |

^aReaction conditions: 1 mmol cinnamaldehyde, 0.5 mol% catalyst, 13 mL solvent, 70 psi H₂, time = 1 h, room temperature.

^bYields and selectivities determined by ¹H NMR spectroscopy and GC analysis using 1,3- dinitrobenzene and *n*-decane as an internal standard, respectively. Average of three runs. Selectivity for 3-phenylpropanaldehyde = [% 3-phenylpropanaldehyde / (% 3-phenylpropanaldehyde + % cinnamyl alcohol + % 3-phenyl-1-propanol)].

Furthermore, even at similar conversions, PdNP@PPh₂-PEGPIILP (**2.14**) is always more selective than **2.13** for partial reduction. Fundamentally, the selectivity is governed by the relative rates of the first and second reduction therefor it could be assumed that for **2.14**, the second reduction is slower than for **2.13** as more saturated alcohol is produced even at lower conversion for the **2.13** catalysed hydrogenation. Although the origin of this difference in selectivity is not clear, the PEGylated catalyst has smaller nanoparticles which have been shown to increase selectivity for selective C=C reduction.²⁵ In addition, it is also possible the

oxygen atoms in the PEG chain could bind to the NP surface in a donor fashion and thus induce electronic or structural changes of the active Pd surface.

Additionally, as hydrogenation is a convenient method for the fabrication of palladium nanoparticles from a Pd^(III) precursor, a sample PdCl₄@PPh₂-PEGPIILP (**2.12**) was suspended in ethanol, heated to 60 °C and subjected to 20 bar of hydrogen overnight. After this time, a black solid was obtained after removal of the solvent. Comparative catalyst testing with the NaBH₄ reduced catalyst revealed that PdNPs obtained via hydrogenation were significantly less active and selective (Table 9). The stark difference in performance between the two may well be associated with the harsh reaction conditions required for reduction *via* hydrogenation whereas NaBH₄ reduction occurs smoothly at room temperature. Alternatively, NaBH₄ mediated reduction occurs almost instantaneously, whereas hydrogen reduction is a slower process which may influence the kinetics of nanoparticle formation. As nanoparticles are prone to agglomeration under higher temperature and at slower reduction rates due to an increase in nucleation, aggregation into larger and thus less active particles may be responsible for the drop in activity, however, TEM analysis would be required to enable any differences in particle size and/or morphology to be identified.

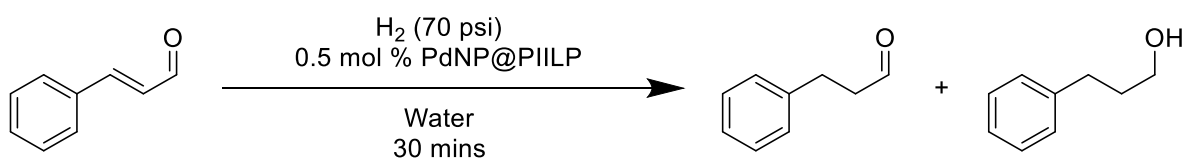
Table 9: Hydrogenation of cinnamaldehyde to 3-phenylpropionaldehyde catalysed by 2.14 prepared *via* hydrogen reduction or chemical reduction with NaBH₄.

| Entry ^a | Reductant | PdNP@PPh ₂ -PEGPIILP Conversion (%) ^b | PdNP@PPh ₂ -PEGPIILP Selectivity (%) ^b |
|--------------------|-------------------|--|---|
| 1 | NaBH ₄ | 81 | 85 |
| 2 | H ₂ | 69 | 69 |

^aReaction conditions: 1 mmol cinnamaldehyde, 0.5 mol% catalyst, 13 mL water, 70 psi H₂, time = 1 h, room temperature. ^b Yields and selectivities determined by ¹H NMR spectroscopy and GC analysis using 1,3- dinitrobenzene and *n*-decane as internal standards respectively. Average of three runs. Selectivity for 3-phenylpropionaldehyde = [% 3-phenylpropionaldehyde / (% 3-phenylpropionaldehyde + % cinnamyl alcohol + % 3-phenyl-1-propanol)].

3.2.2 Effect of temperature

The effect of temperature on catalyst efficacy was first studied with PdNP@PPh₂-PEGPIILP (**2.14**) and the reaction time was decreased from 1 hour to 30 mins to ensure full consumption of the starting material did not occur.



Scheme 32: General scheme for investigating the effect of temperature on the PdNP@PIILP catalysed hydrogenation of cinnamaldehyde.

As expected, from the results in Figure 24, an increase in temperature gave an increase in conversion, although the increase is marginal after 40°C. This trend may reflect changes in mass transfer of the substrate at different temperatures i.e. the reaction is diffusion controlled with respect to cinnamaldehyde up until 40°C. Perhaps unexpectedly, an increase in temperature also resulted in a slight increase in selectivity (85% to 92%). This observation is interesting as a higher temperature may be expected to enable the more challenging C=O reduction to occur. In this regard it would be instructive to conduct a full kinetic study on the hydrogenation of cinnamaldehyde and 3-phenylpropionaldehyde separately using **2.14** as the catalyst to determine the relative rates and temperature dependence of each hydrogenation.

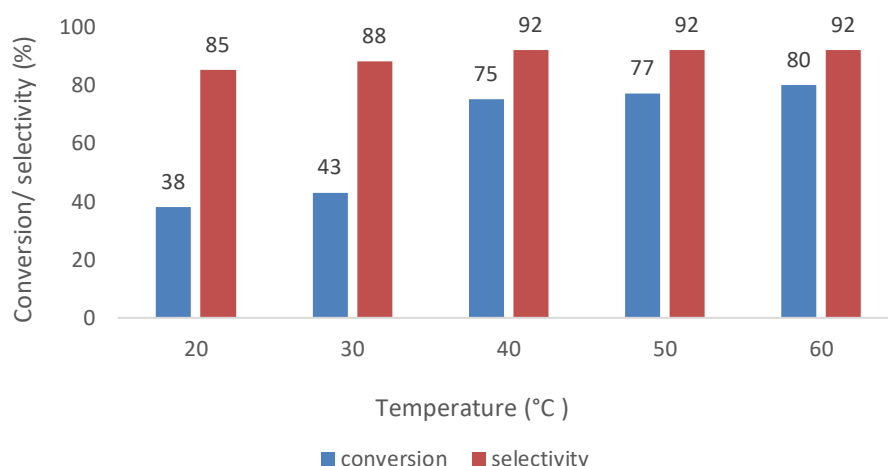


Figure 24: Temperature screening of the PdNP@PPh₂-PEGPIILP catalysed hydrogenation of cinnamaldehyde. Reaction conditions: 1 mmol cinnamaldehyde, 0.5 mol% catalyst, 13 mL water, 70 psi H₂, time = 30 mins. Yields and selectivities determined by ¹H NMR spectroscopy and GC analysis using 1,3- dinitrobenzene and *n*-decane as internal standards respectively. Average of three runs. Selectivity for 3-phenylpropionaldehyde = [% 3-phenylpropionaldehyde / (% 3-phenylpropionaldehyde + % cinnamyl alcohol + % 3-phenyl-1-propanol)].

A similar effect was also observed for the PdNP@PPh₂-PIILP catalyst (Figure 25) although the effect was less pronounced with an increase in selectivity from 84% at 30 °C to 91% at 60 °C. Furthermore, the diffusion of the substrate is likely dominating the reaction kinetics at lower temperatures. Overall, the non-PEGylated catalyst gives comparable selectivity, but this may be associated with the clear and marked decrease in conversion on comparison with PdNP@PPh₂-PEGPIILP. As good conversion and selectivity were obtained with PdNP@PPh₂-

PEGPIILP at room temperature, this was chosen as the optimum temperature for further optimisation.

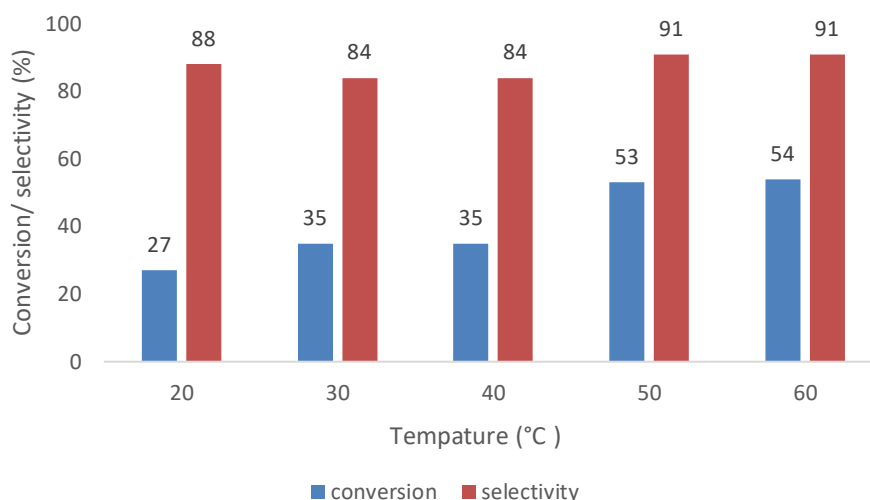


Figure 25: Temperature screening of the PdNP@PPh₂-PIILP catalysed hydrogenation of cinnamaldehyde. Reaction conditions: 1 mmol cinnamaldehyde, 0.5 mol% catalyst, 13 mL water, 70 psi H₂, time = 30 mins. Yields and selectivities determined by ¹H NMR spectroscopy and GC analysis using 1,3- dinitrobenzene and *n*-decane as internal standards respectively. Average of three runs. Selectivity for 3-phenylpropionaldehyde = [% 3-phenylpropionaldehyde / (% 3-phenylpropionaldehyde + % cinnamyl alcohol + % 3-phenyl-1-propanol)].

At this stage it is difficult to rationalise the reaction profile as changes in temperature may well induce structural changes to the polymer support which may have an intrinsic effect on catalyst performance. Furthermore, Lashdaf *et al.* reported that an increase in temperature for the RuNP catalysed hydrogenation of cinnamaldehyde had a profound effect on the product distribution and reasoned that at higher temperatures residual metal oxide species present on the catalyst surface are removed.²⁶ This again highlights the various challenges associated with interpreting results during the optimisation process with a heterogeneous catalyst due to the complex and often non-ideal nature of the particle surface under reaction conditions.

3.2.3 Effect of pressure

Although the system performs efficaciously at a relatively low hydrogen pressure, it may be possible that reducing the pressure may afford higher selectivity as further reduction of the desired product may be suppressed. Preliminary pressure studies revealed that this was not the case and selectivity decreased by 7%, accompanied by an expected dramatic drop in conversion to 37% (entry 1). Interestingly, a tenfold increase in the hydrogen pressure had only negligible effects on catalyst performance as only a marginal increase in conversion was achieved with no change in selectivity (entry 3).

Table 10: Effect of pressure on the hydrogenation of cinnamaldehyde.

| Entry ^a | H ₂ Pressure (PSI) | PdNP@PPh ₂ -PEGPIILP Conversion (%) ^b | PdNP@PPh ₂ -PEGPIILP Selectivity (%) ^b |
|--------------------|-------------------------------|--|---|
| 1 | 40 | 37 | 78 |
| 2 | 70 | 82 | 85 |
| 3 | 800 | 95 | 85 |

^aReaction conditions: 1 mmol cinnamaldehyde, 0.5 mol% catalyst, 13 mL water, time = 1 h, room temperature. ^b Yields and selectivities determined by ¹H NMR spectroscopy and GC analysis using 1,3- dinitrobenzene and *n*-decane as an internal standard, respectively. Average of three runs. Selectivity for 3-phenylpropionaldehyde = [% 3-phenylpropionaldehyde / (% 3-phenylpropionaldehyde + % cinnamyl alcohol + % 3-phenyl-1-propanol)].

As a good conversion and selectivity was obtained at 70 psi, and neither experiment gave a substantial change in selectivity, all further experiments were conducted at this pressure.

3.2.4 Effect of base

The addition of base to the hydrogenation of cinnamaldehyde has been frequently documented to have a positive effect. Presently, the role of the base is not yet fully understood, however, it is possible that an improvement in selectivity may be electronically promoted *via* partial poisoning of the catalyst, hampering the second and more challenging reduction or, that the base may compete with the substrate for adsorption on the catalyst surface. Winterbottom reported that the addition of strong bases substantially improved the activity of platinum-based catalysts for the hydrogenation of cinnamaldehyde,²⁷ while Leng recently reported that addition of amine bases improved the efficiency of ruthenium nanoparticles for the selective hydrogenation of cinnamaldehyde to cinnamyl alcohol.²⁸ Chandalia reported a substantial improvement in selectivity using a two phase toluene-aqueous KOH mixture as reaction media for selective hydrogenation of citral.²⁹ In this case the authors postulated that KOH partially deactivated the catalyst by blocking adsorption of the intermediate and thereby suppressing further reduction.

Table 11: Optimisation of base additive for the Pd catalysed hydrogenation of cinnamaldehyde.

| Entry ^a | Base | 2.13 | 2.13 | 2.14 | 2.14 |
|--------------------|---------------------------------|--------------------------------|---------------------------------|--------------------------------|---------------------------------|
| | | Conversion (%) ^b | Selectivity (%) ^b | Conversion (%) ^b | Selectivity (%) ^b |
| 1 | K ₂ CO ₃ | 27 | 90 | 100 | 100 |
| 2 | NaOH | 43 | 95 | 97 | 100 |
| 3 | NEt ₃ | 24 | 91 | 90 | 91 |
| 4 | K ₃ PO ₄ | 49 | 93 | 94 | 100 |
| 5 | H ₂ KPO ₄ | 39 | 92 | 84 | 95 |
| 6 | None | 95 | 75 | 100 | 85 |

^aReaction conditions: 1 mmol cinnamaldehyde, 0.5 mol% catalyst, 70 psi H₂, 13 mL water, 10 mol% base, time = 75 mins, room temperature. ^bYields and selectivities determined by ¹H NMR spectroscopy and GC analysis using 1,3-dinitrobenzene and *n*-decane as internal standards, respectively. Average of three runs. Selectivity for 3-phenylproprionaldehyde = [% 3-phenylproprionaldehyde / (% 3-phenylproprionaldehyde + % cinnamyl alcohol + % 3-phenyl-1-propanol)].

In this regard, a series of organic and inorganic bases were screened and compared against the standard conditions identified above. Preliminary investigations using PdNP@PPh₂-PEGPIILP revealed that the catalyst may well be partially inhibited as only 69% conversion was achieved using K₂CO₃ as the base (*cf.* 81% in the absence of base), therefore the reaction time was extended to 75 minutes. For PdNP@PPh₂-PIILP, the addition of base resulted in a substantial drop in activity from 95% to less than 50% for each base examined, however, in each case selectivity improved quite dramatically with sodium hydroxide giving the best improvement to 95% (entry 2). Both catalysts performed poorly in the presence of the organic base trimethylamine (entry 3), possibly due to catalyst deactivation as the addition of large excesses of amines have been frequently reported to reduce catalyst activity.^{15, 30, 31} As expected the PEGylated catalyst outperformed its non-PEGylated counterpart in all cases and remarkably, the addition of 10 mol % potassium carbonate to the reaction mixture resulted in marked improvement for PdNP@PPh₂-PEGPIILP such that quantitative conversion and 100% selectivity for 3-phenylproprionaldehyde was achieved (entry 1). Furthermore, further hydrogenation of the product is also completely suppressed in the presence of NaOH (entry 2) and K₃PO₄ (entry 4).

For comparison, Hutchings *et al.* recently prepared bimetallic Pd/Au nanoparticles on TiO₂ supports, and tuned the selectivity for 3-phenylpropionaldehyde by varying the Au/Pd ratio and obtained a maximum selectivity of 82%.³² Chilukuri achieved 93% selectivity for 3-phenylpropionaldehyde at 100% conversion using PdNPs embedded within nitrogen doped mesoporous carbon,²³ and Giambastiani reported 97% selectivity at 100% conversion using a Pd/ γ -Al₂O₃ catalyst,³³ however, the reaction required 3 hours heating at 100 °C with 20 bar H₂ using organic solvent. In contrast, PdNP@PPh₂-PEGPIILP operates efficiently at room temperature in water under extremely mild conditions. Whilst early pioneering work from Hardacre and Goodrich *et al.* demonstrated that almost 100% selectivity can be achieved using commercially available Pd/C in a range of ionic liquids,³⁴ the reactions were particularly slow and the use of designer ILs in solvent quantity presents economic problems. Remarkably, a further survey of the literature revealed that PdNP@PPh₂-PEGPIILP is the most active and selective catalyst for this class of substrate, under aqueous phase conditions, presenting PIILP technology as an extremely efficient and viable tool for the selective reduction of unsaturated carbonyl compounds.

To examine in more detail the effect of the base, a series of reactions were conducted using the optimum system and the conversion and selectivity were monitored as a function of the amount of base (Figure 26).

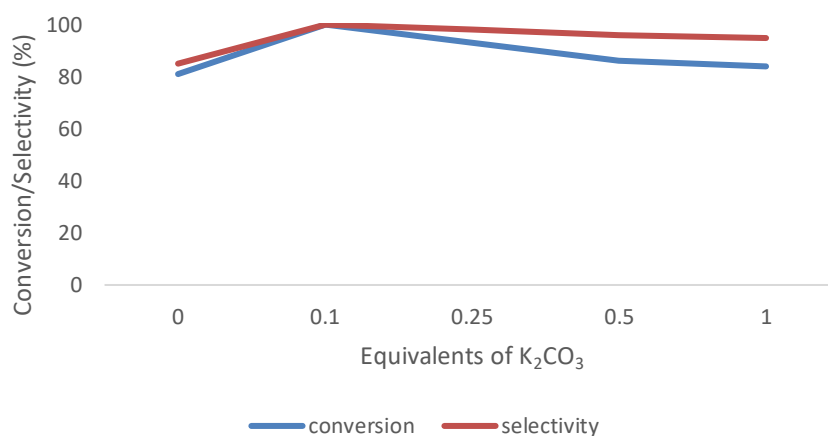


Figure 26: Conversion and selectivity for the PdNP@PPh₂-PEGPIILP catalysed hydrogenation of cinnamaldehyde as a function of equivalents of K₂CO₃ additive. Selectivity for 3-phenylpropionaldehyde = [% 3-phenylpropionaldehyde / (% 3-phenylpropionaldehyde + % cinnamyl alcohol + % 3-phenyl-1-propanol)].

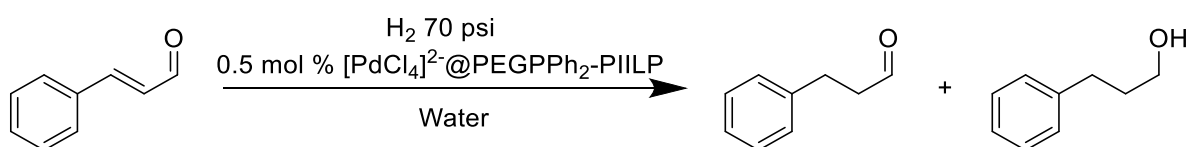
The data in Figure 26 shows that optimum performance is achieved using 0.1 equivalents of base and that whilst selectivity remained at 100% a further increase the amount of base is detrimental to activity. Whilst this profile may well suggest that the improvement in selectivity

may be due to partial inhibition of the catalyst, the possibility that any surface bound carbonate may also alter the electronic properties of the catalyst cannot be discounted. Given the efficacy of the system, there is a clear rationale for further investigations into this effect. In particular, the use of advanced *in situ* surface techniques may provide more convincing results about the nature of the active site under conditions of catalysis.

3.2.5 Catalysis with *in-situ* generated NPs

Despite the poor performance obtained with PdNPs obtained via hydrogenation, as nanoparticles could potentially be generated *in situ* under the milder reaction conditions, and that this strategy would enable a more streamlined approach, a comparative study was conducted using the Pd^(III) precursor for the optimum system (**2.12**).

Table 12: hydrogenation of cinnamaldehyde catalysed by PdNPs formed *in situ* from PdCl₄@PPh₂-PEGPIILP.



| Entry ^a | Time (mins) | PdCl ₄ @PPh ₂ -PEGPIILP Conversion (%) ^b | PdCl ₄ @PPh ₂ -PEGPIILP Selectivity (%) ^b |
|--------------------|-------------|--|---|
| 1 | 30 | 40 | 47 |
| 2 | 45 | 75 | 45 |
| 3 | 60 | 100 | 44 |
| 4 | 120 | 100 | 45 |

^aReaction conditions: 1 mmol cinnamaldehyde, 0.5 mol% catalyst, 13 mL water, 70 psi H₂, room temperature. ^b Yields and selectivities determined by ¹H NMR spectroscopy and GC analysis using 1,3- dinitrobenzene and *n*-decane as an internal standard respectively. Average of three runs. Selectivity for 3-phenylpropionaldehyde = [% 3-phenylpropionaldehyde / (% 3-phenylpropionaldehyde + % cinnamyl alcohol + % 3-phenyl-1-propanol)].

The results in Table 12 reveal that reduction of the precursor is facile, as full conversion is also achieved after 60 minutes and whilst the activity of the *in situ* generated NPs are comparable with the preformed NPs, there is a marked drop in selectivity. As both catalysts have similar activity, the stark difference in selectivity suggests that *in situ* activation of the catalyst exerts significant impact on the properties of the catalyst.

Initially, it was considered that HCl generated during the reduction of the impregnated $[\text{PdCl}_4]^{2-}$ may activate the C=O functionality *via* protonation, which would generate more alcohol. To examine this possibility, varying concentrations of HCl were added to the reaction catalysed by the preformed catalyst **2.14**, however, the selectivity remained constant at 45% across a range of substrate:HCl ratios from 0.1-1 equivalents thus, any activating role was essentially eliminated. However, as even 0.1 mmol HCl is also sufficient enough to induce protonation of the $-\text{PPh}_2$ moiety on the support, this may suggest that the phosphine is integral for the efficiency in catalyst performance. Whilst this is purely speculative, the use of *in situ* XPS or FTIR techniques may provide further information about the phosphorus environments under conditions of catalysis. Furthermore, it should be noted that even after prolonged reaction times of up to 24 hours, no increase in conversion to the fully saturated 3-phenyl-1-propanol was obtained.

3.2.6 Recycling studies

As discussed earlier, one of the practical advantages of aqueous phase catalysis is facile separation and recovery of the organic products and recycling of the aqueous phase containing the catalyst. In this regard, it was envisaged that the ionic and hydrophilic nature of the support may allow the catalyst to be efficiently retained in the aqueous layer after removal of the reactants and products *via* extraction. Therefore, a series of sequential batch reactions were conducted whereby the organics were extracted with ethyl acetate in a dropping funnel after the reaction and the aqueous phase was recharged with a further 1 mmol of cinnamaldehyde and the reaction repeated.

Unfortunately, recycling with **2.13** proved challenging as there was a significant drop in conversion of 24% (96% to 72%) after the first cycle (Figure 27); this was followed by a gradual decline such that after 7 runs a conversion of only 7% was achieved. The increase in selectivity is attributed to the low conversion i.e. lower concentration of saturated aldehyde intermediate present for further reduction. ICP analysis of the aqueous phase and TEM analysis of the spent catalyst would ideally be required to establish whether the gradual loss of activity is derived from catalyst deactivation or accumulative attrition. Visually, on extraction of the organic products, it appears that the non-PEGylated catalyst sits at the organic-aqueous interface, which may present challenges with efficient recovery and reuse and, in this regard, it was hoped that the PEGylated system would offer a more efficient and streamlined protocol.

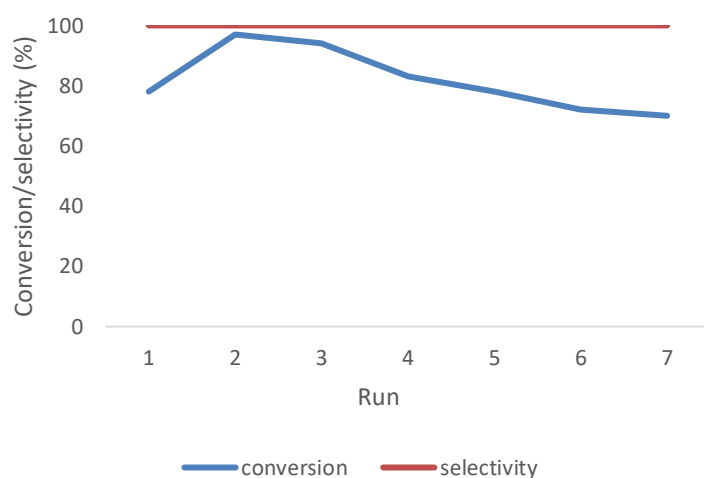
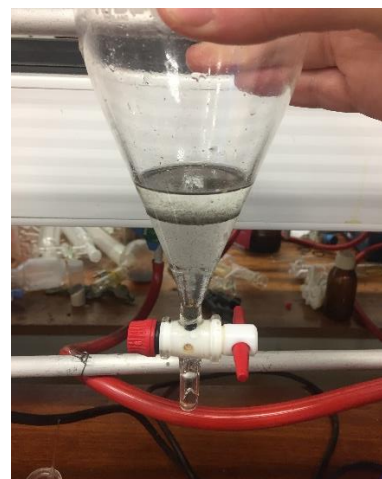
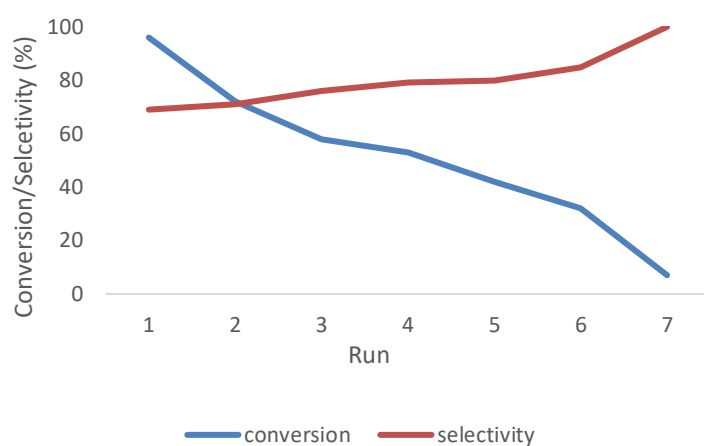


Figure 27: Recycling study for the hydrogenation of cinnamaldehyde catalysed by PdNP@PPh₂-PIILP 2.12 (top) and PdNP@PPh₂-PEGPIILP 2.14 (bottom) accompanied with visual depiction of the extraction procedure demonstrating that 2.14 remains in the aqueous layer and 2.12 sits at the interface. Reaction conditions: 1 mmol cinnamaldehyde, 0.5 mol% catalyst, 10 mol% K₂CO₃, 13 mL water, 70 psi H₂, room temperature, reaction time for PdNP@PPh₂-PIILP = 1.25 hours, reaction time for PdNP@PPh₂-PEGPIILP = 45 mins. Yields and selectivities determined by ¹H NMR spectroscopy and GC analysis using 1,3- dinitrobenzene and *n*-decane as an internal standard, respectively. Average of three runs. Selectivity for 3-phenylproprionaldehyde = [% 3-phenylproprionaldehyde / (% 3-phenylproprionaldehyde + % cinnamyl alcohol + % 3-phenyl-1-propanol)].

Indeed, in stark contrast, recycling studies on the hydrogenation of cinnamaldehyde catalysed by PdNP@PPh₂-PEGPIILP revealed an encouraging profile, and that even after seven runs the selectivity remained at 100%. Interestingly, after the initial run, the catalyst appears to be activated and an increase in conversion is observed (78% to 97%); this was followed by a slight but steady decrease in conversion such that after the seventh run a conversion of 70% was obtained. The origin of this profile is difficult to rationalise but could be due to morphological changes to the support after exposure to the reaction conditions and continuous agitation; this may enable more facile substrate access to the active site. Alternatively, under the reaction conditions, any residual surface Pd^(III) may be successively reduced to metallic Pd over runs 1-3 providing more surface area for catalysis. Whilst ICP analysis of the organic phase

revealed no evidence for leached Pd, ICP analysis of the aqueous phase after the 7th run revealed a drop in Pd content from 44 ppm (0.5 mol %) to 28 ppm which corresponds to an overall loss of 38%. Therefore the drop over runs 4-7 is most likely due to catalyst attrition during workup protocol rather than passivation or leaching and would account for the gradual drop in activity. Furthermore, TEM analysis of the catalyst isolated after the seventh run revealed negligible change in the particle size and morphology (1.93 ± 0.67 nm before and 1.97 ± 0.38 nm after catalysis) of the spent catalyst.

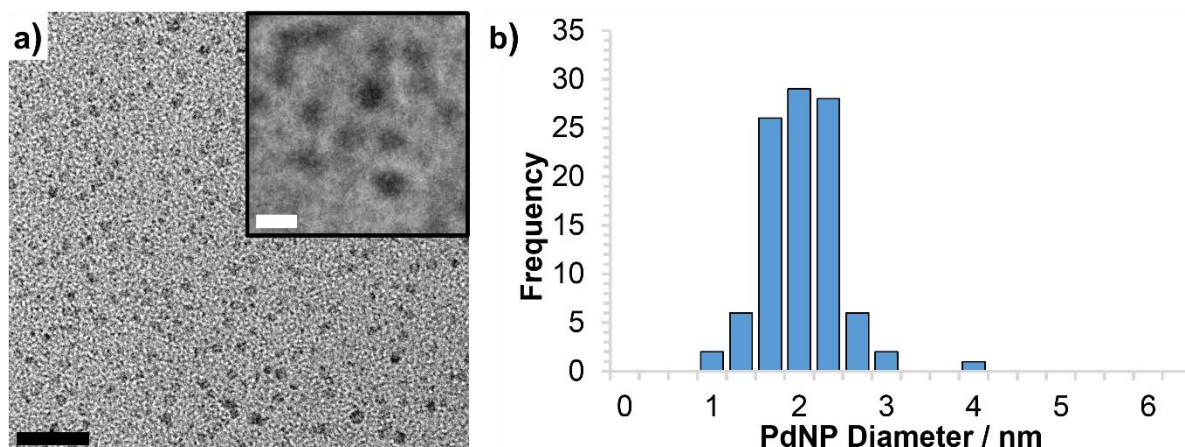


Figure 28: a) HRTEM micrographs and b) particle size distribution of PdNP@PPh₂-PEGPIILP isolated after 7 runs. Scale bars are 25 nm (black) and 5 nm (white).

Additionally, retention of the NP structure and size may also suggest that leaching and redeposition of molecular Pd is unlikely to occur and that catalysis is more likely to occur *via* a heterogeneous mechanism. To this end, hot filtration and recharging the aqueous filtrate with a further equivalent of substrate revealed that some catalyst activity was retained, as 23% conversion was achieved under the same conditions. However, the PEGylated hydrophilic polymer may well help solubilise a small amount of the catalyst on warming of the solution. In this regard, more in depth studies would be required to more accurately elucidate the mechanism of catalysis.

3.2.7 Probing the role of the support functionality

In attempt to investigate the influence of the various constituents within the polymer scaffold on catalyst efficacy, a series of modified PIILP-based catalysts were synthesised using the general protocol discussed in Chapter 2. Preliminary investigations involved the preparation and comparative catalyst testing of **2.15** and **2.16** (Figure 29) against **2.14**, in order to systematically investigate the role of the PPh₂ and the immobilised imidazolium fragments,

respectively. Full details of the synthesis and characterisation are provided in the experimental section and appendix (A23-29), respectively.

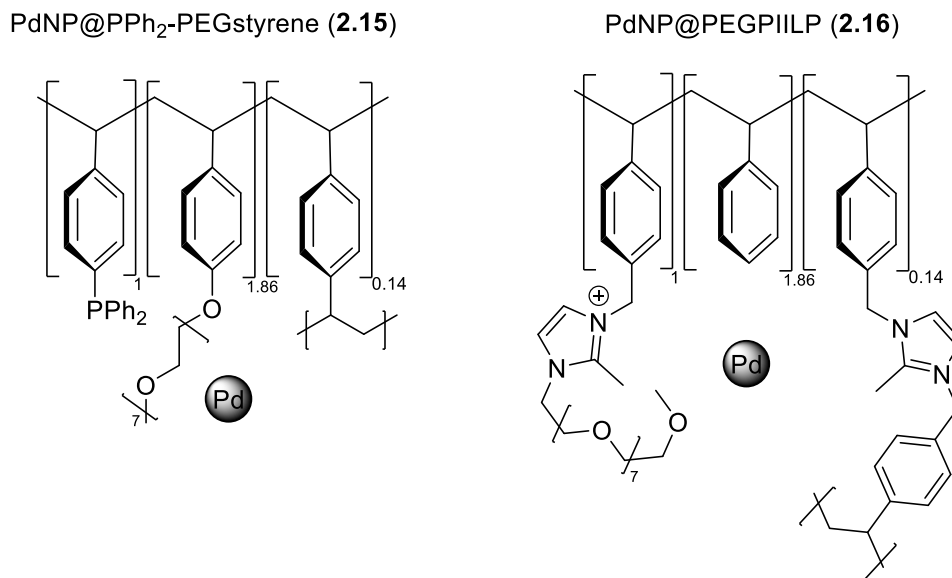


Figure 29: Structures of additional PIILP based catalysed synthesis to explore the effect of the PPh₂ and IL moieties.

To assess how the composition of the support influences the particle morphology, comparative TEM analysis was conducted which revealed a marked difference in nanoparticle size between the two newly fabricated supports. Removal of the ionic liquid from the optimum support appears to have negligible effects on the particle size as the mean diameter of 1.83 ± 0.44 determined for **2.15** was comparable to that of 1.93 ± 0.67 for **2.14**.

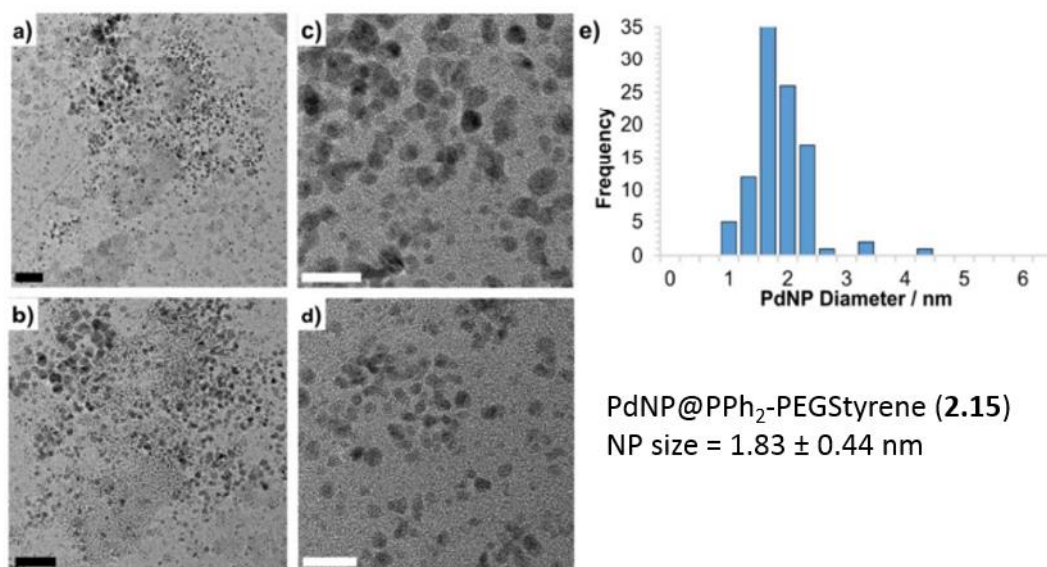


Figure 30: a-d) HRTEM micrographs and e) particle size distribution of PdNP@PPh₂-PEGStyrene. Scale bars are 25 nm (black) and 5 nm (white).

In stark contrast, removal of the phosphine yielded significantly larger particles for the imidazolium-functionalised support (Figure 31), which may suggest that the phosphine is integral for stabilisation and/or efficient dispersion of the NPs.

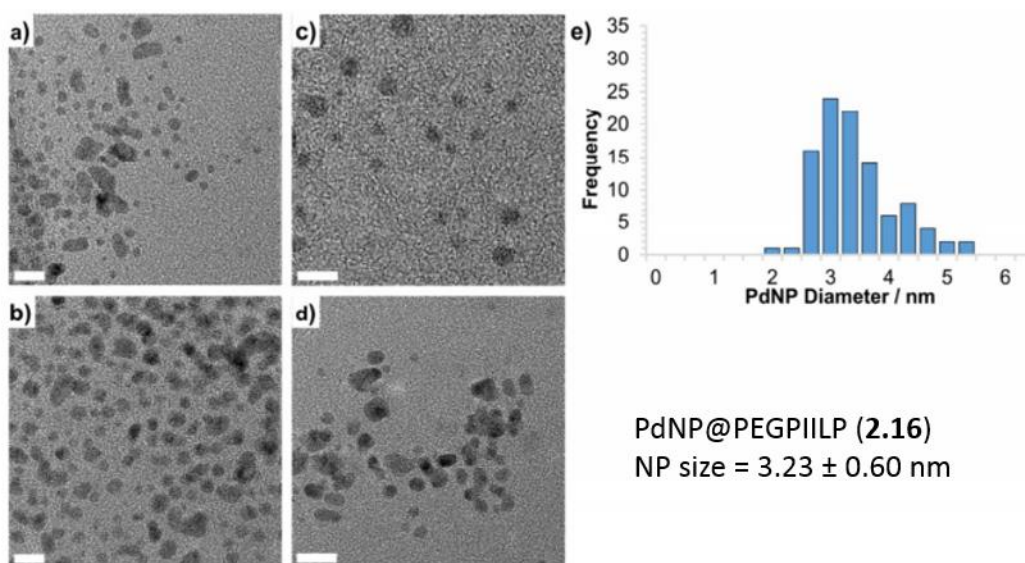


Figure 31: a-d) HRTEM micrographs and e) particle size distribution of PdNP@PEGPIILP. Scale bars are 5 nm.

To determine the influence on catalyst performance, both catalysts were screened under the optimum conditions identified for **2.14**. Comparative catalyst testing revealed that high selectivity was maintained when the ionic group was removed in **2.15** (Table 13, entry 2), however, this was accompanied by a marked drop in activity as a reaction time of 2 hours was required to reach only 72% conversion. In contrast, **2.16** retained high activity at the normal reaction time of one hour (entry 3) i.e. removal of the phosphine had no effect on activity, however, selectivity dropped quite dramatically. The effect of the support on selectivity is even more profound without the base additive as **2.15** reached 86% selectivity which is comparable with **2.14**, however, **2.16** was much less selective and only reached 56% selectivity under the same conditions. Whilst further investigations would be required to elucidate whether the change in activity and selectivity is size-dependant or due to electronic modification of the catalyst surface, it is tentatively suggested that phosphine modification may be crucial to achieving high selectivity (entries 1 and 2) and that the IL modification appears to improve activity (entries 1 and 3).

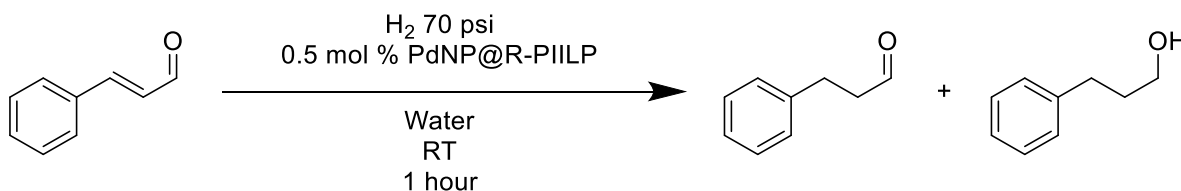
Table 13: hydrogenation of cinnamaledehyde catalysed by PdNPs supported on a range of functionalised polymeric supports.

| Entry ^a | Support | Time | NP size (nm) | Conversion (%) ^b | Selectivity (%) ^b |
|--------------------|-----------------------------------|---------|--------------|-----------------------------|------------------------------|
| 1 | PPh ₂ -PEGPIILP (2.14) | 75 min | 1.92 | 100 | 100 |
| 2 | PPh ₂ Styrene (2.15) | 120 min | 1.83 | 72 | 96 |
| 3 | PIILP (2.16) | 75 min | 3.23 | 96 | 83 |

^aReaction conditions: 1 mmol substrate, 0.5 mol% cat, 10 mol % K₂CO₃ 13 mL water, 70 psi H₂, room temperature. ^b Yields and selectivities determined by ¹H NMR spectroscopy and GC analysis using 1,3- dinitrobenzene and *n*-decane as internal standards, respectively. Average of three runs. Selectivity for 3-phenylpropionaldehyde = [% 3-phenylpropionaldehyde / (% 3-phenylpropionaldehyde + % cinnamyl alcohol + % 3-phenyl-1-propanol)].

To provide a more comprehensive study, the series of supports was extended to include all possible combinations of PEG, PPh₂ and IL. Comparative catalyst testing was carried out under the optimum conditions in the absence of potassium carbonate to avoid any potential poisoning effects.

Table 14: Hydrogenation of cinnamaledehyde catalysed PdNPs supported on a range of functionalised polymeric supports in the absence of base.



| Entry ^a | Support | Functionality | NP size (nm) | Conversion (%) ^b | Selectivity (%) ^b |
|--------------------|---------|----------------------------|--------------|-----------------------------|------------------------------|
| 1 | 2.13 | PPh ₂ , IL | 2.29 ± 0.96 | 75 | 74 |
| 2 | 2.14 | PPh ₂ , IL, PEG | 1.93 ± 0.67 | 81 | 85 |
| 3 | 2.15 | PPh ₂ , PEG | 1.83 ± 0.44 | 65 | 86 |
| 4 | 2.16 | IL, PEG | 3.23 ± 0.61 | 74 | 56 |
| 5 | 2.17 | PPh ₂ | 1.38 ± 0.18 | 60 | 82 |

| | | | | | |
|---|------|----|-------------|----|----|
| 6 | 2.18 | IL | 3.00 ± 0.62 | 70 | 46 |
|---|------|----|-------------|----|----|

^aReaction conditions: 1 mmol substrate, 0.5 mol% cat, 13 mL water, 70 psi H₂, room temperature. ^b Yields and selectivities determined by ¹H NMR spectroscopy and GC analysis using 1,3- dinitrobenzene and *n*-decane as an internal standard, respectively. Average of three runs. Selectivity for 3-phenylpropionaldehyde = [% 3-phenylpropionaldehyde / (% 3-phenylpropionaldehyde + % cinnamyl alcohol + % 3-phenyl-1-propanol)].

The results in Table 14 revealed that the mean diameters of NPs stabilised by PPh₂-modified supports are smaller than those stabilised by their non-phosphine containing polymers. Furthermore, all PPh₂ modified supports produced PdNPs with average particles sizes that fell below 2 nm with the exception of **2.13**, which had a mean diameter of 2.29 ± 0.96. This observation further suggests that the PPh₂ modification is crucial and most likely the primary stabilising force as removal of the phosphine results in larger NPs (entries 4 and 6). Interestingly, all catalysts stabilised by a phosphine containing support showed a marked improvement in selectivity on comparison with the non-phosphine functionalised counterparts. Furthermore, in all cases, removal of the IL resulted in an obvious drop in conversion (entries 3 and 5), again further suggesting the IL is key for high catalyst activity, which is not surprising given the discussion on the benefits of ILs in catalysis in Chapter 1. Whilst the PEG modification appears to have little effect on NP size, all of the PEGylated catalysts are more active than their non-PEGylated counterparts.

Traditionally, catalysis involving hydrogenation of unsaturated bonds has been classified as ‘structure insensitive’, however, fuelled by advances in modern nanotechnology, more recent work has demonstrated that reaction selectivity can be tuned through the size and shape of the NP and thus the substrate-surface interactions.³⁵ For example, this size effect is particularly profound for Pd catalysed dehydrogenations as ‘reactive hydride phases’ have been proposed to form on isolated Pd crystallites as a result of hydrogen diffusion into octahedral lattice vacancies within the NPs, which may be integral to the catalytic performance.³⁶ Moreover, the accessibility of such lattice vacancies has been proposed to be directly related to the NP size, therefore modulation of the particle size should play a crucial role in determining catalyst selectivity.³⁷ Lee *et al.* reported the improved selectivity for hydrogenation of the carbonyl in cinnamaldehyde was attributed to reduced steric crowding on the surface of the larger PtNPs prompting reorientation of surface bound cinnamaldehyde.³⁸ Furthermore, Liu *et al.* reported PdNPs with tuneable particle sizes achieved *via* the manipulation of strong metal-support interactions (SMSIs) of different Pd precursors on a TiO₂ support, and that smaller NPs favoured hydrogenation of the C=C bond

in cinnamaldehyde over the C=O. The authors also conducted DFT calculations to help elucidate the particle size effect and demonstrated that on smaller particles (modelled by a Pd₄ atom cluster), initial adsorption of cinnamaldehyde occurs through the C=C bond, however, the barrier for C=C adsorption is higher for larger particles and C=O adsorption becomes more favoured (Figure 32).²⁵

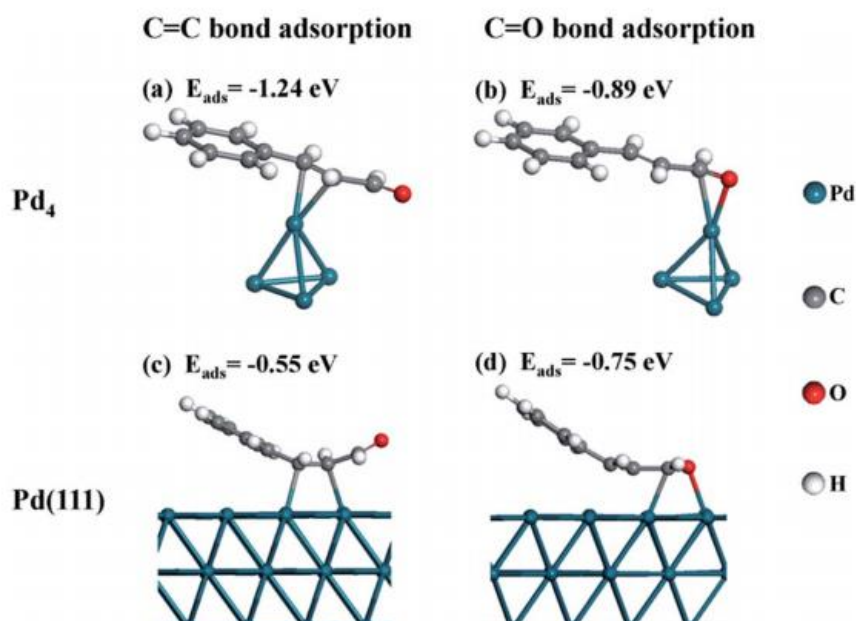
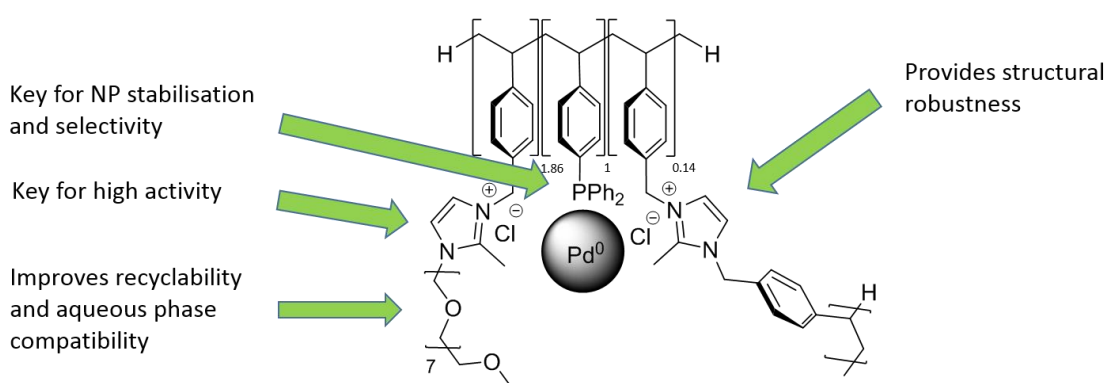


Figure 32: Depiction of the cinnamaldehyde adsorption modes on Pd₄ clusters (a and b) and on a flat Pd(111) surface (c and d), with their relative energies reported by Liu *et al.*²⁵

Whilst further analysis of the electronic changes imposed on the PdNPs from metal-support interactions in this work is still required, it appears that there is a cooperative effect from each of the PEG, PPh₂ and imidazolium modifications and that **2.14** still remains the optimum system. Moreover, the differences in catalyst performance may well also be associated with the physicochemical changes imposed on the polymer by the various modifications i.e. dispersability, solubility or flexibility of the respective supports.



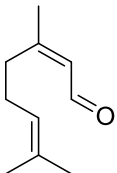
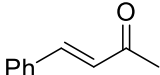
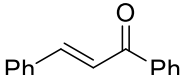
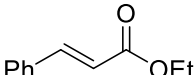
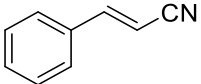
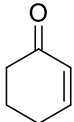
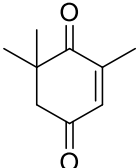
Scheme 33: Schematic representation of the suggested roles of PIILP modifications.

Substrate screening

A range of α,β -unsaturated carbonyls were screened under the optimum conditions identified above to explore the efficacy of PdNP@PPh₂-PEGPIILP. Gratifyingly, **2.14** was extremely efficient and selective for hydrogenation of the C=C bond in both α,β -unsaturated aldehydes and ketones, albeit at longer reaction times for the latter.

Table 15: Hydrogenation of a series of α,β -unsaturated aldehydes and ketones catalysed by **2.14**.

| Entry ^a | Substrate | Time (mins) | Conversion (%) ^b | Selectivity (%) ^b |
|--------------------|-----------|-------------|-----------------------------|------------------------------|
| 1 | | 75 | 98 | 97 |
| 2 | | 75 | 99 | 98 |
| 3 | | 75 | 98 | 100 |
| 4 | | 75 | 99 | 100 |
| 5 | | 75 | 97 | 67 |

| | | | | |
|-----------|---|-----|-----|-----|
| 6 |  | 75 | 99 | 100 |
| 7 |  | 240 | 94 | 100 |
| 8 |  | 240 | 98 | 100 |
| 9 |  | 360 | 99 | 100 |
| 10 |  | 120 | 96 | 100 |
| 11 |  | 120 | 99 | 100 |
| 12 |  | 240 | 100 | 92 |

^aReaction conditions: 1 mmol substrate, 0.5 mol% PdNP@PPh₂-PEGPIILP, 13 mL water, 70 psi H₂, 10 mol% K₂CO₃ room temperature. ^b Yields and selectivities determined by ¹H NMR spectroscopy and GC analysis using 1,3- dinitrobenzene and *n*-decane as an internal standard, respectively. Average of three runs. Selectivity towards reduction of the conjugated C=C bond. Relative selectivity = [% desired product / (% desired product + % undesired product)].

The results in Table 15 demonstrate that modification of the phenyl ring of cinnamaldehyde with electron donating groups is not detrimental to catalysis as high conversion and selectivity was achieved for the hydrogenation of dimethylaminocinnamaldehyde (entry 1) and 4-methoxycinnamaldehyde (entry 2) in the same reaction time. Furthermore, saturated aliphatic aldehydes were obtained as the sole product in excellent yield from *trans*-pentenal (entry 3) and 3-methylcrotonaldehyde (entry 4). The presence of three unsaturated sites within the citral structure has led to its wide use as a model substrate for the design of efficient and selective catalysts. Gratifyingly, the hydrogenation of citral catalysed by **2.14** afforded citronellal as the sole product in excellent yield and the isolated C=C bond remained fully intact

(entry 6). This result may suggest that a difference in binding mode of the α,β -unsaturated functionality with regards to the isolated alkene may be responsible for the high selectivity. Hydrogenation of 3-(furan-2-yl)acrolein was more challenging and only achieved 67% selectivity to the corresponding saturated aldehyde at 97% conversion and 3-tetrahydrofuran-2-yl-propionaldehyde was identified as the minor product resulting from reduction of the furan ring. For comparison, Monflier *et al.* reported selectivities of 87-96% for hydrogenation of 3-(2-furyl)acrolein to 3-(2-furyl)propionaldehyde using RuNPs stabilised by a poly(citric acid- β -cyclodextrin) polymer, however, these values were only obtained at low conversion (8-38%), in which the concentration of the intermediate saturated aromatic aldehyde would be low.³⁹ Complete selectivity was achieved for all of the ketone substrates which is expected, as the carbonyl functionality is intrinsically less reactive. *Trans*-chalcone and benzylidene acetone required longer reaction times which is not surprising as the additional R group on the ketone is clearly more sterically cumbersome than the corresponding aldehyde proton, however saturated ketones were still obtained as the sole product in high yield (entries 7 and 8). Near-quantitative yields of saturated ketone and ester were also obtained from cyclohexenone (entry 11) and ethyl cinnamate (entry 9), respectively, and hydrogenation of cinnamionitrile yielded 100% chemoselectivity for the saturated nitrile (entry 10). Interestingly, hydrogenation of ketoisophorone afforded the saturated dione levodione in 92% selectivity (entry 12) with minor amounts of 4-hydroxy-3,3,5-trimethylcyclohexanone and 4-hydroxy-3,5,5-trimethyl-cyclohex-2-enone. Of the two other products, the major component was 4-hydroxy-3,5,5-trimethyl-cyclohex-2-enone, i.e. in this case, hydrogenation of the more sterically hindered ketone *ortho*- to the methyl substituents occurred before hydrogenation of the C=C bond. Baiker *et al.* reported similar observations for the Pd/Al₂O₃ catalysed hydrogenation of ketoisophorone and reasoned that the unusual chemoselectivity observed on comparison with other α,β -unsaturated ketones is that the influence of a second α -ketone renders the C=C bond less electron deficient.⁴⁰ Moreover, the authors state that the adsorption of the unsaturated alcohol product on the catalyst is much weaker than the starting material and therefore it does not react further. Additionally, for ketoisophorone, the effect of base on the selectivity is particularly pronounced, as only 50% selectivity for levodione was obtained in the absence of potassium carbonate.

3.2.8 Comparison with commercial catalyst

In order to compare the relative merits of PIILP systems against a commercially available alternative, a sample of Pd/C (10 wt% obtained from Sigma, product number: 520888) was screened under the optimum conditions. Gratifyingly, **2.13** and **2.14** both outperformed commercial Pd/C by quite some margin (Table 16, entries 1 and 2), as reactions catalysed by Pd/C required heating at 60 °C to reach a similar conversion to that obtained with **2.13** (entry 3), which is substantially lower than the quantitative conversion obtained with the optimum catalyst **2.14** (entry 1). Furthermore, the selectivity still falls short of 100% obtained with **2.14** (entry 1), which verifies the efficacy of PIILP systems for this transformation. The active role of the catalyst was confirmed as quantitative amounts of cinnamaldehyde were obtained in the presence of only the unloaded PIILP support (entry 4).

Table 16: Comparison of different catalyst systems for the hydrogenation of cinnamaldehyde to 3-phenylpropionaldehyde.

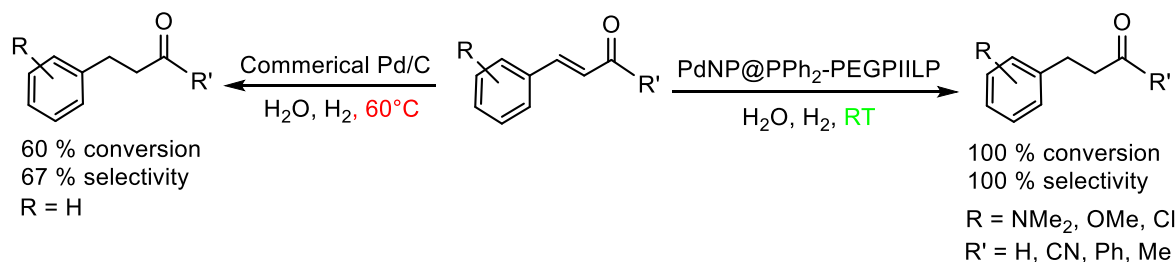
| Entry ^a | Catalyst | Conversion with base (without) ^b (%) ^c | Selectivity with base (without) ^b (%) ^c |
|--------------------|---|---|--|
| 1 | PdNP@PPh ₂ -PEGPIILP (2.14) | 100 (100) | 100 (85) |
| 2 | PdNP@PPh ₂ -PIILP (2.13) | 43 (75) | 95(74) |
| 3 | Pd/C ^d | 42 (60) | 93 (67) |
| 4 | PPh ₂ -PEGPIILP | 0 | 0 |

^aReaction conditions: 1 mmol cinnamaldehyde, 0.5 mol% catalyst, 10 mol% base, 13 mL water, 70 psi H₂, room temperature reaction time = 1 hour. ^b Reaction ran for 75 mins. ^c Yields and selectivities determined by ¹H NMR spectroscopy and GC analysis using 1,3- dinitrobenzene and *n*-decane as an internal standard, respectively. Average of three runs. ^d Reaction conducted at 60 °C. Selectivity for 3-phenylpropionaldehyde = [% 3-phenylpropionaldehyde / (% 3-phenylpropionaldehyde + % cinnamyl alcohol + % 3-phenyl-1-propanol)].

3.3 Conclusion

The results presented in this chapter have demonstrated that phosphine-functionalised PIILP catalysts **2.13** and its PEGylated counterpart **2.14** are highly efficient and selective catalysts for the aqueous phase partial hydrogenation of α,β -unsaturated carbonyls, with **2.14** yielding saturated aldehydes and ketones often in quantitative yield. Optimisation studies revealed that addition of 10 mol% K₂CO₃ gave remarkable improvements in selectivity, which may be due to partial inhibition of the PdNPs. Furthermore, **2.14** appears to be the most efficient catalyst for this type of transformation, outperforming commercially available Pd/C and other

reported designer systems in the literature whilst operating in water under extremely mild conditions.



Scheme 34: Efficacy of PdNP@PPh₂-PEGPIILP on comparison with commercially available Pd/C.

The efficacy of these catalysts in water may be due to the hydrophobic effect, and the PEG functionality on the support was key to enabling efficient recycling of the catalyst *via* simple organic extraction techniques. Most interestingly, investigations into the roles of each modification suggested that the PPh₂ was crucial for generating small NPs which were highly selective, whereas removal of the PPh₂ yielded significantly larger particles which were much less selective for C=C hydrogenation. Moreover, whilst removal of the IL appeared to have only a negligible effect on the mean diameters of the NPs, this rendered these catalysts markedly less active. Therefore, PIILP methodology appears to be a convenient method of developing catalysts with tuneable activity-selectivity profiles. In future studies, the effect of the support on catalyst performance will be explored by preparing and immobilising NPs with a well-defined and predetermined size (using a well-established methodology) as this will allow a more accurate assessment of any interfacial electronic effects by eliminating NP size effects. Given the high efficacy, stability and robustness of PIILP systems, the development and engineering of bespoke continuous flow systems would be desirable in order to demonstrate commercial viability, and this will form the basis of future developments in the group. Additionally, the implementation of continuous flow systems may also allow more accurate analysis of the relative rates in order to deconvolute the intricate relationships between support functionality and overall catalyst performance, with particular emphasis on generating highly selective catalysts. Finally, having identified suitable reaction parameters, the work presented in this chapter may hopefully also serve as a platform for the development of catalysts to tackle challenges in more diverse applications such as hydrogenative transformations of bioderived feedstock to afford value added platform chemicals and fuel additives.

3.4 References

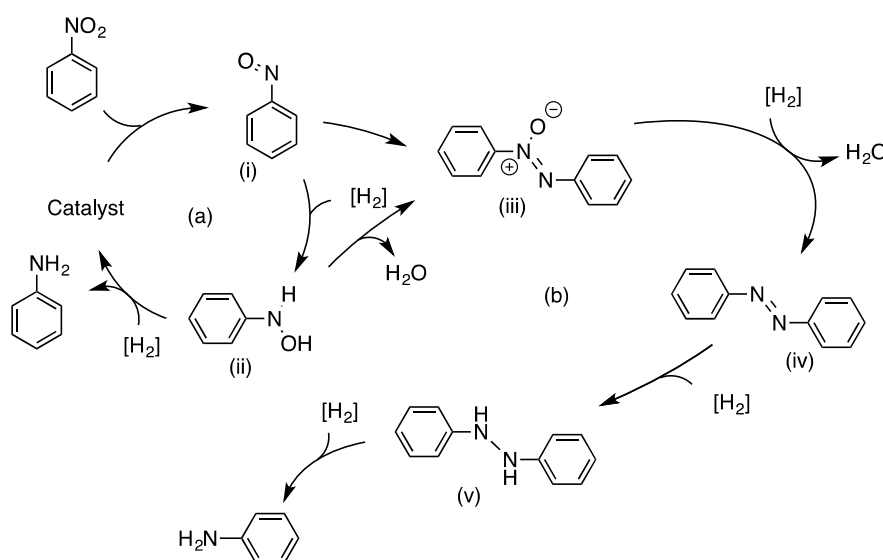
1. S. N. Coman, V. I. Parvulescu, M. De Bruyn, D. E. De Vos and P. A. Jacobs, *J. Catal.*, 2002, **206**, 218-229.
2. J. C. Serrano-Ruiz, A. López-Cudero, J. Solla-Gullón, A. Sepúlveda-Escribano, A. Aldaz and F. Rodríguez-Reinoso, *J. Catal.*, 2008, **253**, 159-166.
3. M. S. Ide, B. Hao, M. Neurock and R. J. Davis, *ACS Catal.*, 2012, **2**, 671-683.
4. Z. Ma and F. Zaera, *Surf. Sci. Rep.*, 2006, **61**, 229-281.
5. D. Stacchiola and W. T. Tysoe, *Surf. Sci.*, 2002, **513**, L431-L435.
6. H. Öfner and F. Zaera, *J. Phys. Chem. B*, 1997, **101**, 396-408.
7. I. Lee and F. Zaera, *J. Phys. Chem. C*, 2007, **111**, 10062-10072.
8. N. Sheppard and C. De La Cruz, *Catal. Today*, 2001, **70**, 3-13.
9. Y. Dong, M. Ebrahimi, A. Tillekaratne, J. P. Simonovis and F. Zaera, *PCCP*, 2016, **18**, 19248-19258.
10. R. Zhou, E. W. Zhao, W. Cheng, L. M. Neal, H. Zheng, R. E. Quiñones, H. E. Hagelin-Weaver and C. R. Bowers, *J. Am. Chem. Soc.*, 2015, **137**, 1938-1946.
11. W. Zhao Evan, R. Maligal - Ganesh, C. Xiao, T. W. Goh, Z. Qi, Y. Pei, E. Hagelin - Weaver Helena, W. Huang and R. Bowers Clifford, *Angew. Chem. Int. Ed.*, 2017, **56**, 3925-3929.
12. M. J. Taylor, L. J. Durndell, M. A. Isaacs, C. M. A. Parlett, K. Wilson, A. F. Lee and G. Kyriakou, *Appl. Catal. B*, 2016, **180**, 580-585.
13. A. Tilekaratne, J. P. Simonovis, M. F. López Fagúndez, M. Ebrahimi and F. Zaera, *ACS Catal.*, 2012, **2**, 2259-2268.
14. M. Wilde, K. Fukutani, W. Ludwig, B. Brandt, J. H. Fischer, S. Schauer mann and H. J. Freund, *Angew. Chem. Int. Ed.*, 2008, **47**, 9289-9293.
15. F. P. da Silva, J. L. Fiorio and L. M. Rossi, *ACS Omega*, 2017, **2**, 6014-6022.
16. M. Králik and A. Biffis, *J. Mol. Catal. A: Chem.*, 2001, **177**, 113-138.
17. A. Riisager, R. Fehrmann, M. Haumann and P. Wasserscheid, *Eur. J. Inorg. Chem.*, 2006, **2006**, 695-706.
18. D. J. Cole-Hamilton, *Science*, 2003, **299**, 1702-1706.
19. M. Thomas Sir John, *ChemCatChem*, 2010, **2**, 127-132.
20. G. Franciò, U. Hintermair and W. Leitner, *Phil. trans. A.*, 2015, **373**, 20150005.
21. H. Li, W. Zhao, S. Saravanamurugan, W. Dai, J. He, S. Meier, S. Yang and A. Riisager, *Commun. Chem.*, 2018, **1**, 32.
22. N. Hiyoshi, O. Sato, A. Yamaguchi and M. Shirai, *Chem. Commun.*, 2011, **47**, 11546-11548.
23. A. S. Nagpure, L. Gurralla, P. Gogoi and S. V. Chilukuri, *RSC Adv.*, 2016, **6**, 44333-44340.
24. A. Stolle, T. Gallert, C. Schmoger and B. Ondruschka, *RSC Adv.*, 2013, **3**, 2112-2153.
25. F. Jiang, J. Cai, B. Liu, Y. Xu and X. Liu, *RSC Adv.*, 2016, **6**, 75541-75551.
26. M. Lashdaf, A. O. I. Krause, M. Lindblad, M. Tiitta and T. Venäläinen, *Appl. Catal. A*, 2003, **241**, 65-75.
27. W. Koo-amornpattana and J. M. Winterbottom, *Catal. Today*, 2001, **66**, 277-287.
28. F. Leng, I. C. Gerber, M. R. Axet and P. Serp, *Comptes Rendus Chimie*, 2017.
29. V. Satagopan and B. Chandalia Sampatraj, *J. Chem. Technol. Biotechnol.*, 1994, **59**, 257-263.
30. D. Hui, D. Yu, Z. Xiaojin, Z. Zhenguoguo, F. Shuangli and Z. Zhenlin, *Nanotechnology*, 2018, **29**, 055705.
31. E. H. Boymans, P. T. Witte and D. Vogt, *Catal. Sci. Technol.*, 2015, **5**, 176-183.
32. S. Cattaneo, S. J. Freakley, D. J. Morgan, M. Sankar, N. Dimitratos and G. J. Hutchings, *Catal. Sci. Technol.*, 2018, **8**, 1677-1685.

33. A. M. R. Galletti, C. Antonetti, A. M. Venezia and G. Giambastiani, *Appl. Catal. A*, 2010, **386**, 124-131.
34. K. Anderson, P. Goodrich, C. Hardacre and D. W. Rooney, *Green Chem.*, 2003, **5**, 448-453.
35. F. Zaera, *PCCP*, 2013, **15**, 11988-12003.
36. F. Zaera, *ACS Catal.*, 2017, **7**, 4947-4967.
37. N. K. Nag, *J. Phys. Chem. B*, 2001, **105**, 5945-5949.
38. L. J. Durndell, C. M. A. Parlett, N. S. Hondow, M. A. Isaacs, K. Wilson and A. F. Lee, *Scientific Reports*, 2015, **5**, 9425.
39. R. Herbois, S. Noel, B. Leger, S. Tilloy, S. Menuel, A. Addad, B. Martel, A. Ponchel and E. Monflier, *Green Chem.*, 2015, **17**, 2444-2454.
40. M. von Arx, T. Mallat and A. Baiker, *J. Mol. Catal. A: Chem.*, 1999, **148**, 275-283.

Chapter 4 Application of PIILP Catalysts to the selective reduction of nitroarenes

4.1 Introduction

Aryl amines are an immensely important class of compound with diverse applications in pharmaceuticals, dyes and agrochemical compounds.¹ Amongst many synthetic options including the reduction of imines and nitriles or N-arylation, the palladium catalysed reduction of nitroarenes represents the most versatile and operationally straightforward protocol.² However, limitations such as the requirement for stoichiometric metal reagent, toxic additives, high catalyst loadings, use of volatile flammable solvents and low product selectivity must still be addressed for the large scale production of functionalised anilines.³ Additionally, residual organic solvent, leached precious metal and, in particular, the successive accumulation of toxic azo-based by-products regularly contaminate product streams thereby detracting from the sustainability of any industrial processes. The origin of these unwanted azo-based products is derived from the formation of condensation intermediates during the reaction.⁴ Scheme 35 depicts the accepted and complex reaction network postulated by Haber for the reduction of nitrobenzene involving two often competing pathways namely, the direct (a) and condensation (b) pathways.⁵



Scheme 35: Direct (a) and condensation (b) reaction pathways for the reduction of nitrobenzene to aniline.

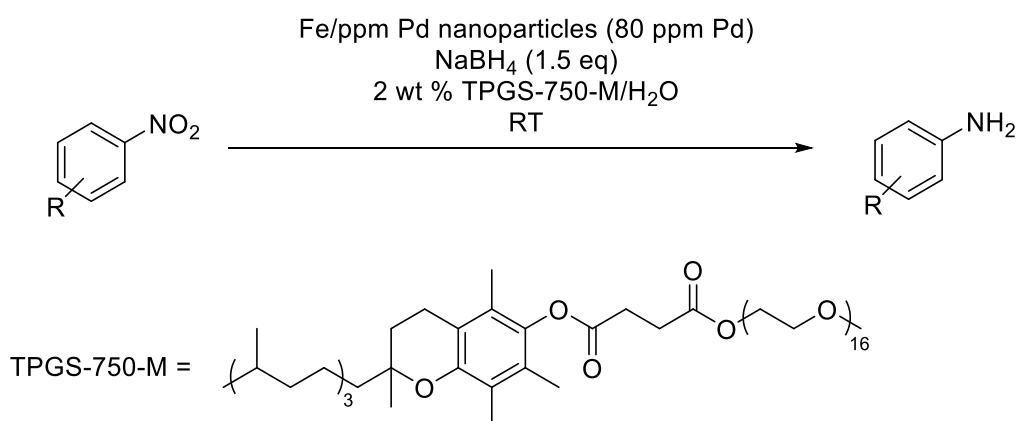
The first step involves the addition of a single chemisorbed molecule of H₂ to nitrobenzene present on the catalyst surface and loss of water affording nitrosobenzene (i), which rapidly

accepts another equivalent of H_2 to form thermally unstable *N*-phenylhydroxylamine (ii). In the direct pathway, *N*-phenylhydroxylamine is further hydrogenated to liberate the fully reduced amine, which is the most commonly reported pathway for Pd based catalysts.⁶ However, under certain conditions, *N*-phenylhydroxylamine molecules can accumulate on the catalyst surface, facilitating the formation of azoxy benzene (iii) *via* a condensation reaction. Králik *et al.* reported that low concentration of reductant and/or substrate may favour this path.⁷ Subsequently, a cascade of two further sequential hydrogenations proceed *via* azobenzene (iv) and diphenyl hydrazine (v), before yielding aniline as the final product. In total, a possible six different products can be generated under any given reaction conditions, highlighting the need for selective catalysts that afford a single product in high yield, if challenging purification methods are to be avoided.

Advances in liquid phase hydrogenation have since improved the selectivity, atom efficiency and industrial compatibility of heterogeneous catalysts, due to the emergence of various tuneable designer catalyst technologies that utilise the unique properties of metal nanoparticles.⁸ Despite this, many of these systems still suffer from either harsh reaction conditions or strongly acidic/basic additives which results in poor functional group tolerance in the presence of sensitive or highly functionalised substrates.⁹ For example, while Fe_2O_3 nanoparticle based catalysts supported on nitrogen doped carbon are highly selective for the complete reduction of nitrobenzene to aniline,^{10, 11} energetically intense conditions and prolonged reaction times were required to achieve good activity which limits the practicality as well as the scope to substrates to those that are thermally stable.

Based on the above discussion, there is clearly a strong incentive to develop more intuitive methods and design more chemoselective catalysts with industrially desirable and 'green' credentials. In this scenario, the ideal system would operate at room temperature, have low catalyst loadings, exhibit high selectivity, require short reaction times, utilise operationally simple strategies for catalyst reuse and finally, improve sustainability by eradicating the need for organic solvent. Many reported systems have met the majority of these criteria, including Pd/ZrP-based catalysts prepared by Tuteja,⁹ electrochemically prepared PVP-stabilised PdNPs,⁶ carbon nanofiber-supported Pd and PtNPs,¹ AuNPs supported on phosphate-functionalised nanosheets,¹² and Pd nanoclusters supported on porous CeO_2 nanorods,¹³ however, none achieve all of the desired criteria exclusively.

Pioneering work by the Lipschutz group over the past few years now constitutes the only example so far that adheres to all of these parameters, thus delivering a safe and environmentally responsible method for the selective reduction of nitroarenes.¹⁴ This group discovered that the designer surfactant TPGS-750-M, forms discrete nanomicelles that encapsulate PdNPs,¹⁵ and the resulting system catalysed the reduction of nitroarenes to anilines under safe and mild conditions.



Scheme 36: Strategy developed by Lipschutz et al. for the safe and selective reduction of nitroarenes.

The role of the designer surfactant is twofold; as the pendant polyethylene glycol (PEG) chains are mobile in aqueous solution and aggregate around the active PdNPs, they prevent unwanted aggregation and simultaneously form discrete nanoreactors. Furthermore, utilising the hydrophobic effect, these self-assemblies also act as the effective reaction solvent, whereby the surfactant also mediates the delivery of water immiscible substrates to the active site. A unique combination of the surfactant, which dictates colloidal properties, and the FeCl₃ additive which acts as a geometric promoter, facilitating dispersion of small and highly active Pd clusters, enables traditionally challenging reactions to occur at room temperature in water. Furthermore, recycling of the entire aqueous phase allows the catalyst to be reused up to five times without any sign of deactivation.

Based on the superior performance of PEG-modified PIILP catalysts for aqueous phase hydrogenations in Chapter 3, it is possible that the same synergistic solvent-support interactions may promote similar macromolecular assemblies in PIILP catalysis. Subsequently, as an extension, the work in this chapter explores the catalytic performance of the same systems for the chemoselective aqueous phase reduction of nitroarenes, many of which are insoluble solids. As discussed earlier, the phosphine donor, PEG modification and the

immobilised IL appear to be essential to achieve optimum performance and this investigation will probe whether the same modifications are responsible for determining the activity of the catalysts for other reductive transformations. Moreover, it is hoped that *via* systematic and logical catalyst design and optimisation, it could be possible to develop an alternative versatile, scalable and environmentally responsible tool for this type of reaction.

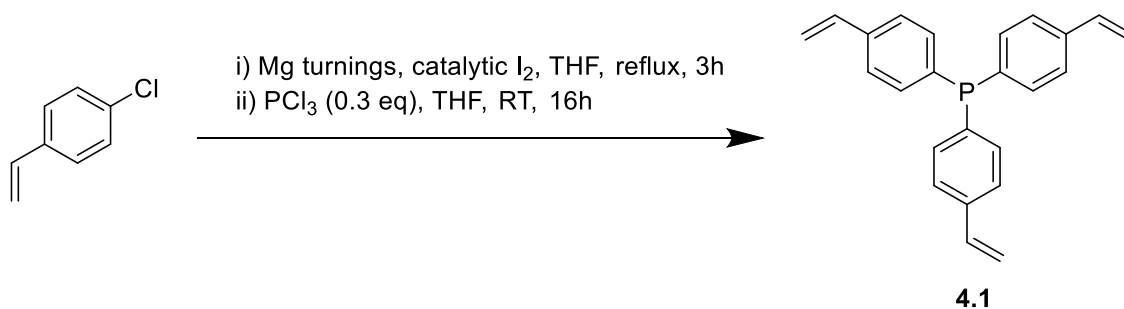
Toward this, another aspect of this project aims to explore the influence of introducing tris(*p*-vinylphenyl)phosphine (**4.1**) into the polymer scaffold on the basis that reducing flexibility about the central P atom using extensive cross-linking may promote site isolation and limit the possible Pd-P interactions. This work is based on the original findings of Iwai *et al.* who reported that threefold cross-linking, achieved *via* incorporating **4.1** into a polystyrene backbone, significantly increased the density of the polymer backbone around the PPh₃ core. By constraining the Pd-P interaction to a monodentate fashion, more of the active site will be exposed for substrate adsorption, which may result in an enhancement in catalyst activity.¹⁶ Conversely, decreasing the cross-linking around the PPh₃ core increases the effective mobility of the donors - these systems were characterised by more regular bi and tridentate type binding to the PdNPs, as evidenced by solid state ³¹P NMR spectroscopy, which proved to be detrimental to catalysis.

In this manner, by incorporating **4.1** into PIILP based catalysts, it may also be possible to rationalise the nature and effects of the Pd-P interaction on the kinetics of nanoparticle formation. Furthermore, it is envisaged that site isolation of the phosphine in these systems may also promote the formation of coordinatively unsaturated PdNPs embedded within the support leaving a larger surface area available for catalysis.

4.2 Results and Discussion

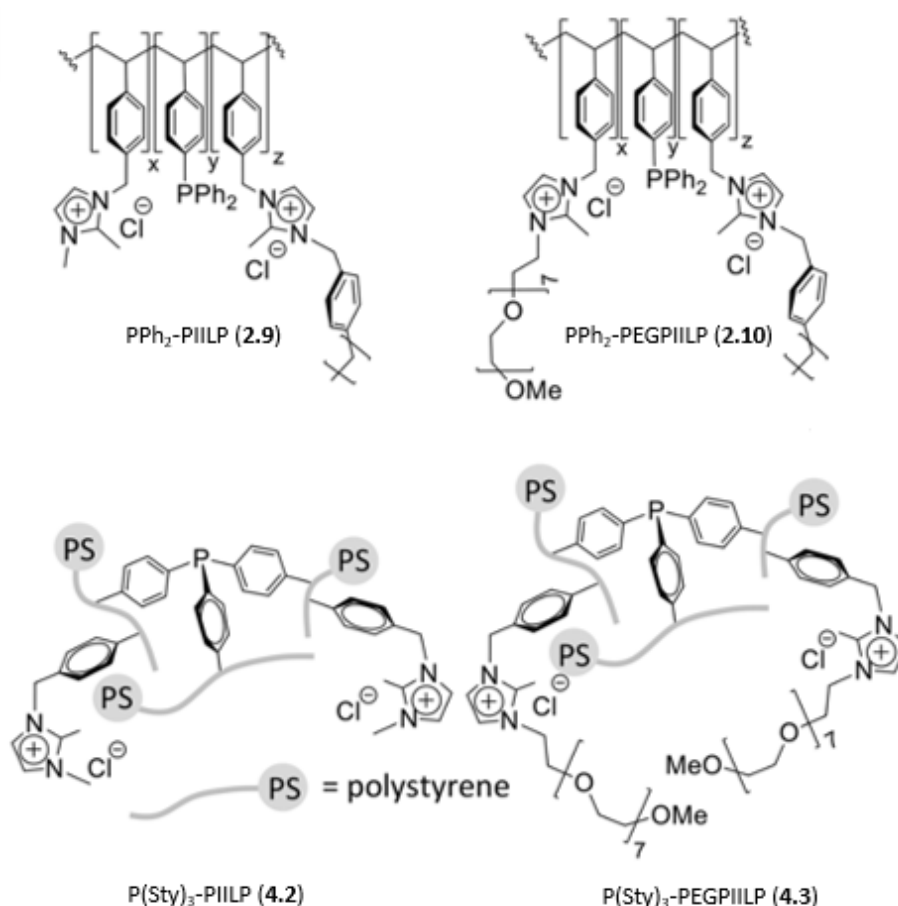
4.2.1 Synthesis of highly crosslinked phosphine functionalised PIILPs

Monomer **4.1** was prepared using an adaptation of a recently reported procedure.¹⁶ A solution of 4-chloromethylstyrene in THF was added to Mg turnings suspended in THF along with a crystal of iodine, generating the Grignard reagent *in situ* after refluxing for 3 hours. Following this, the Grignard reagent was then added slowly *via* cannula transfer to a solution of PCl₃ dissolved in THF, and the mixture was stirred overnight under an inert atmosphere.



Scheme 37: Synthesis of monomer **4.1**.

The product was obtained as a white solid in 67% yield after performing an aqueous workup under N₂ using degassed solvents. **4.1** was then subsequently deemed spectroscopically pure based on analysis of the ¹H, ¹³C and ³¹P NMR spectra and was taken forward without further purification. The two highly cross-linked cation decorated polymers; P(Sty)₃-PIILP (**4.2**) and P(Sty)₃-PEGPIILP (**4.3**), were then prepared by AIBN initiated radical polymerisation using the general method discussed in Chapter 2, maintaining the stoichiometric ratio of 2:1 IL to phosphine. Both PIILPs were obtained in >90% yield and characterised by TGA, SEM and ³¹P solid state NMR spectroscopy, which can be found in the appendix (A40 and A43); no significant changes to the support properties were observed.



Scheme 38: Composition of PIIL supports.

Highly cross-linked phosphine functionalised PIILP stabilised PdNP catalysts **4.6** and **4.7** were then prepared as discussed previously *via* ion exchange with $\text{Na}_2[\text{PdCl}_4]$ and subsequent chemical reduction of $\text{Pd}^{\text{(III)}}$ loaded catalyst precursors **4.4** and **4.5** with NaBH_4 .

4.2.2 Characterisation of highly crosslinked PIILP stabilised PdNPs

The ^{31}P solid state NMR spectra of **4.4** and **4.5** revealed that in contrast to lightly cross-linked phosphine modified PIILPs, both PIILPs consist of two distinct phosphine environments. The major peaks at δ 26.8 and 27.9 ppm for **4.4** and **4.5**, respectively, correspond to a significant downfield shift of δ 31.1 and 35.4 ppm after impregnation, which is indicative of coordination of the phosphine to Pd. Interestingly, site isolation of the PPh_3 core appears to indeed limit the Pd-P interaction. The minor resonances at δ -4.1 and -4.8 ppm for **4.4** and **4.5**, respectively, are upfield shifted, in the region consistent with free phosphine which may be due to the reduced mobility of the phosphine. Integration of the relative peak areas revealed that these resonances correspond to a total of 6 and 14 % free phosphine for **4.4** and **4.5**, respectively. After reduction, the major peaks undergo a slight downfield shift to δ 29.5 and 28.8 ppm for **4.6** and **4.7**, respectively, as a result of coordination to the more electron rich $\text{Pd}^{(0)}$ particles.

The minor resonances attributed to uncoordinated phosphine remain at δ -4.1 and -6.9 ppm and correspond to 13 and 7%, respectively.

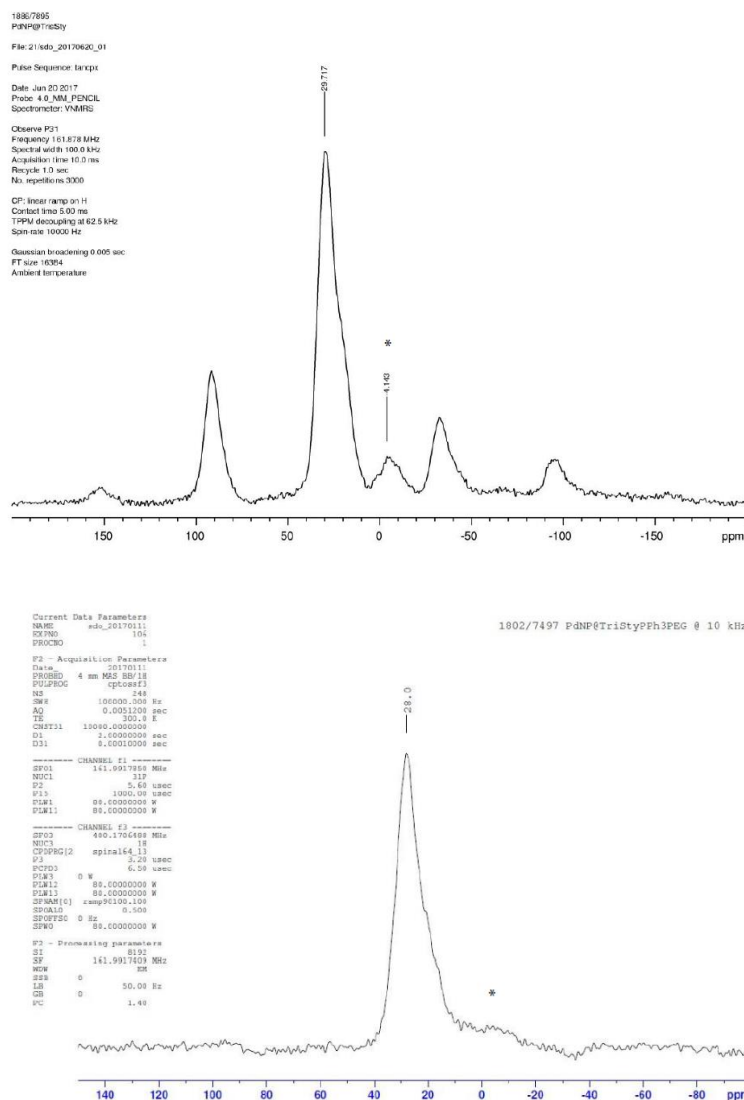


Figure 33: Solid state ^{31}P NMR spectrum of 4.6 (top) and 4.7 (bottom). Star indicates signals associated with free phosphine.

The relative Pd contents of the *ex situ* prepared catalysts and their respective precursors was determined using ICP-OES analysis. There was a substantial difference in Pd loading between the two catalyst precursors, as the Pd content of **4.4** was determined to be 0.30 mmol g^{-1} which was ca. 7-fold higher than that of 0.04 mmol g^{-1} for **4.5** (entry 1 and 2). In this regard, the disparate values may not be accurate representations of the actual Pd content, and the significantly low Pd content of **4.5** may be due to poor digestion during the sample preparation process. Additionally, the increased hydrophilicity of the PEGylated support is likely to have a higher affinity for absorption of water molecules within the pores of the support architecture, further lowering the effective Pd wt%. Despite this, after further processing and drying, the

final catalysts appear to have similar Pd loadings at around 5 wt% (entry 3 and 4); this enabled a more straightforward comparison of the relative merits of the two supports for catalysis.

Table 17: Pd content of PIILP catalysts as determined by ICP-OES.

| Entry | Catalyst | mmol Pd/ g PIILP | Pd wt% |
|-------|--|---------------------|--------|
| 1 | PdCl ₄ @P(Sty) ₃ -PIILP (4.4) | 0.30 | 3.21 |
| 2 | PdCl ₄ @P(Sty) ₃ -PEGPIILP (4.5) | 0.04 | 0.41 |
| 3 | PdNP@P(Sty) ₃ -PIILP (4.6) | 0.49 | 5.23 |
| 4 | PdNP@P(Sty) ₃ -PEGPIILP (4.7) | 0.50 | 5.39 |

Surface characterisation studies of the Pd in the newly prepared highly crosslinked catalysts was performed using XPS analysis of the Pd 3d_{3/2} and Pd 3d_{5/2} spin-orbit components (Figures 34-37).

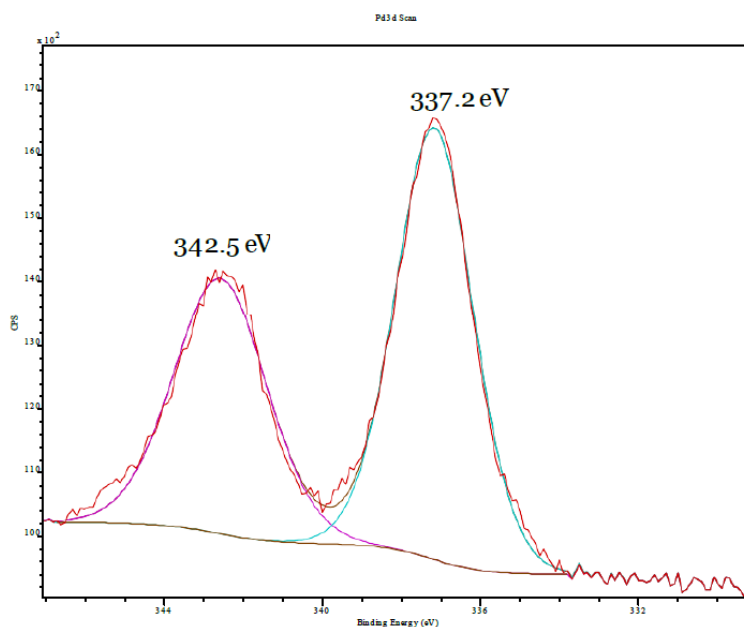


Figure 34: XPS spectrum of PdCl₄@P(Sty)₃-PIILP (4.4).

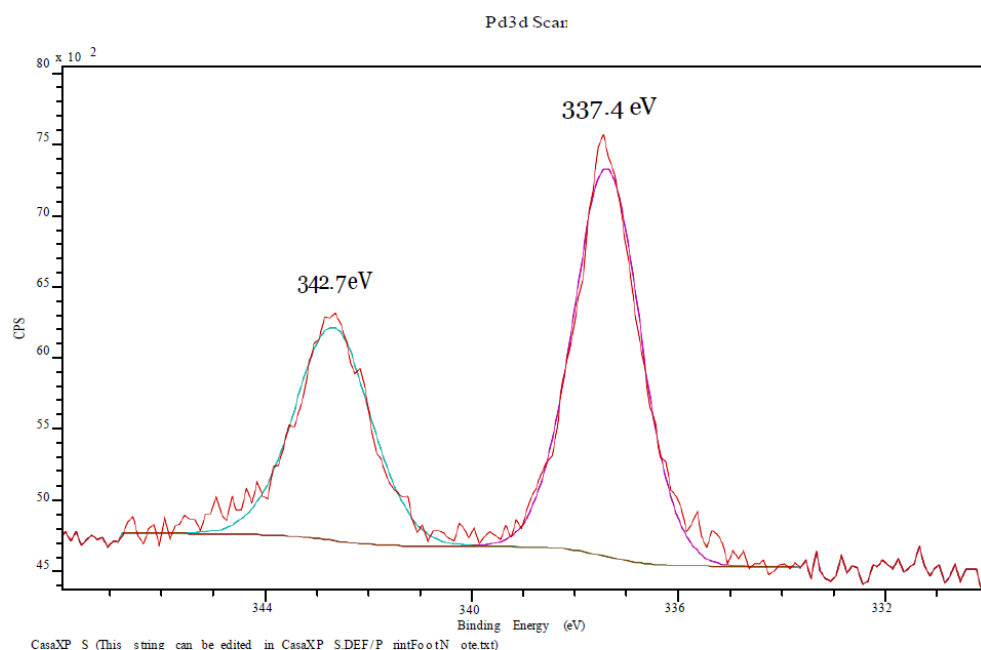


Figure 35: XPS spectrum of PdCl₄@P(Sty)₃-PEGPIILP (4.5).

The XPS spectra of **4.4** and **4.5** demonstrated that both precursors consist of a single Pd environment. The Pd3d binding energies of 337.2 and 342.5 eV for **4.4**, and 337.4 and 342.7 eV for **4.5** indicate that only Pd^(II) is present the surface.

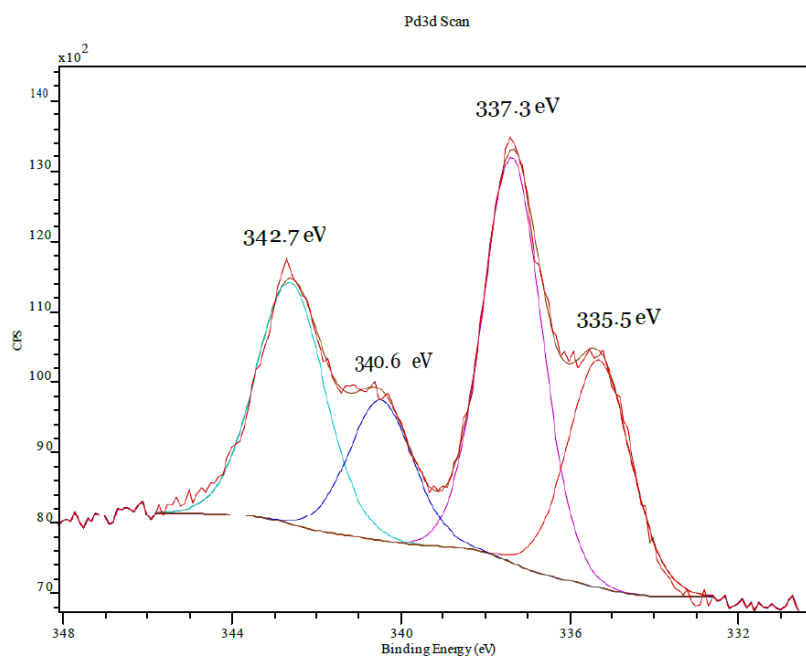


Figure 36: XPS spectrum of PdNP@P(Sty)₃-PIILP (4.6).

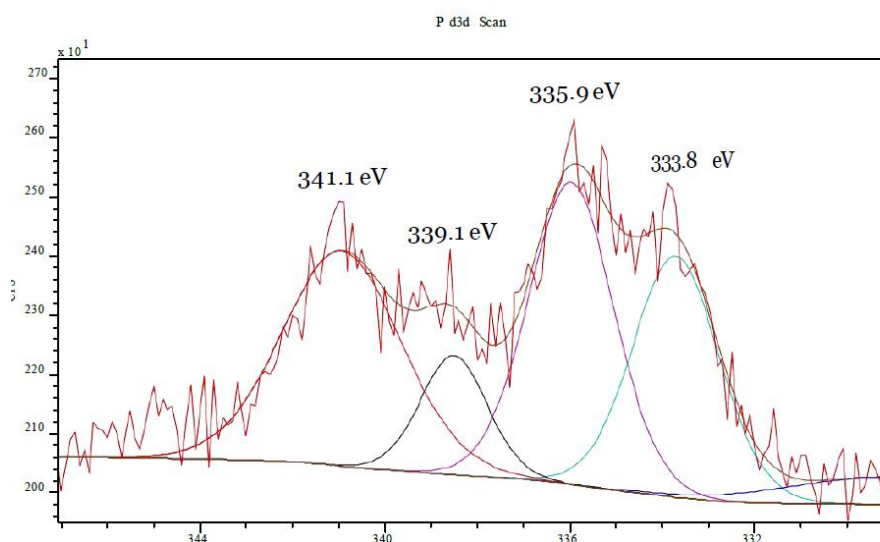


Figure 37: XPS spectrum of PdNP@P(Sty)₃-PEGPIILP (**4.7**).

Similar to observations described in Chapter 2 for the lightly crosslinked PIILP systems, the spectra of **4.6** and **4.7** clearly show two separate environments consistent with the presence of both Pd^(III) and Pd⁽⁰⁾. The former is possibly the result of reoxidation of the metallic Pd to the corresponding oxide in air. Alternatively, the Pd^(III) signals may be a result of incomplete reduction due to limited diffusion of the reducing agent through the support during the chemical reduction step, which may be more likely given the resistance of the noble metals to oxidation and the large increase in crosslinking of the polymer. More detailed XPS depth profiling studies may provide more definitive evidence as to the origin of surface Pd^(III) and demonstrate either a surface oxide layer or reveal a gradient as a result of diffusion limitations. For **4.6**, the peaks corresponding to Pd^(III) are centred at 337.3 and 342.7 eV, and those shifted to lower binding energies of 335.5 and 340.6 eV are attributed to the more electron rich metallic Pd on the surface. Similarly, for **4.7**, peaks associated with Pd^(III) are observed at 335.9 and 341.1 eV, whereas the lower binding energy peaks associated with Pd in the reduced state appear at 333.8 and 339.1 eV. Qualitatively, non-PEGylated **4.6** clearly consists of proportionately more oxidised Pd, which may indicate that diffusion limitations are responsible for the incomplete reduction, given that **4.4** is completely insoluble in the reduction reaction media and as such does not disperse as well as **4.5**.

Fluorescence-detected X-ray absorption spectroscopy (FD-XAS) was then used to probe the surface electronics of the newly prepared catalysts. To compare the influence of the support, analysis of Pd L_{III} edge energy was measured relative to Na₂[PdCl₄] or Pd/C on the basis that in these systems there is no interaction with any donors and limited interaction with the support.

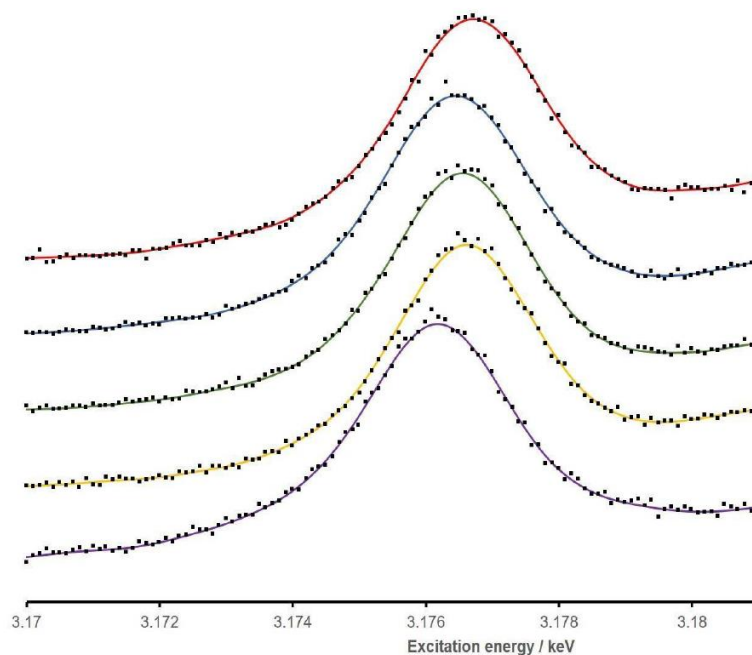


Figure 38: FD-XAS spectrum showing the Pd L_{III} edges of PdCl₄@PPh₂-PIILP (red), PdCl₄@PPh₂-PEGPIILP (blue), PdCl₄@P(Sty)₃-PIILP (green), PdCl₄@P(Sty)₃-PEGPIILP (yellow) and NaPdCl₄ (purple). Raw data (black) has been included on smoothed lines.

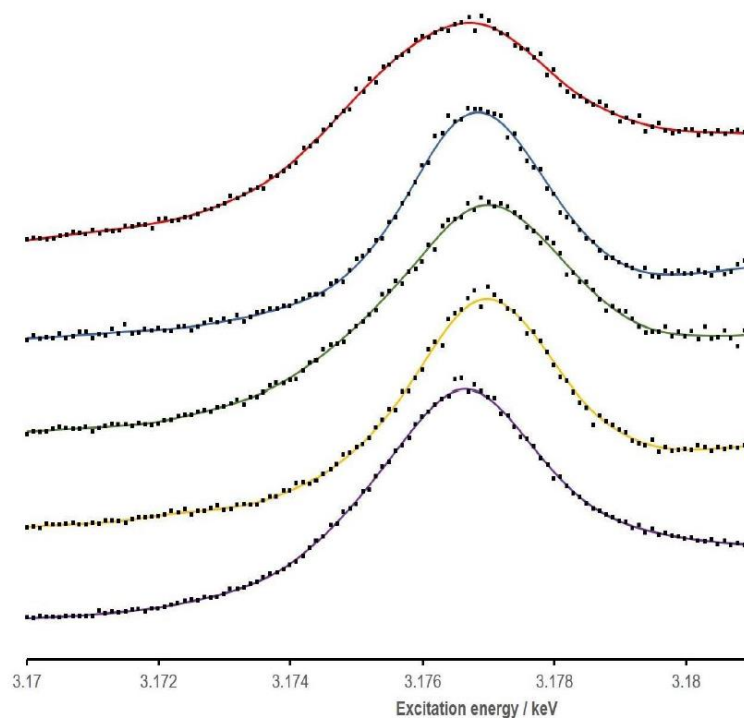


Figure 39: FD-XAS spectrum showing the Pd L_{III} edges of PdNP@PPh₂-PIILP (red), PdNP@PPh₂-PEGPIILP (blue), PdNP@P(Sty)₃-PIILP (green), PdNP@P(Sty)₃-PEGPIILP (yellow) and Pd/C (purple). Raw data (black) has been included on smoothed lines.

The results gathered show a general increase in the Pd L_{III} edge energy for PIILP-supported PdNPs on comparison with the reference materials, suggesting a small decrease in electron

density at the metal. This is perhaps not unprecedented given that PIILP materials consist largely of cation decorated regions which would withdraw electron density away from the Pd atoms. Interestingly, in contrast to XPS analysis, the change in white line energy for PEGylated catalysts **2.14** and **4.7** upon reduction is significantly smaller than that for **2.13** and **4.6**, which is likely a reflection of the surface sensitive nature of XPS. Moreover, this also suggests that the PEG modification also strongly interacts with the Pd surface as well as improving catalyst dispersion.

Comparative TEM analysis was conducted to investigate whether the alternative binding modes as dictated by the nature of the support influence the size and shape of the PdNPs. TEM micrographs revealed an average Pd particle size of 3.67 ± 0.67 and 4.01 ± 1.11 nm for highly cross-linked systems **4.6** and **4.7**, respectively (entries 3 and 4). Interestingly, these values are somewhat larger than those immobilised on the lightly crosslinked supports (entries 1 and 2). From these stark differences it could be inferred that site isolation of the phosphine donor through extensive crosslinking exerts a significant influence on the particle morphology. Two possible reasons for this is that either the particles are more prone to aggregation due to the decrease in stabilising Pd-P electrostatic interactions, or that the large extent of crosslinking may limit diffusion of the Pd precursor and reducing agent during preparation, ultimately limiting the dispersion of Pd and the kinetics of nanoparticle formation. To this end, further studies in the group are currently underway to vary the Pd-P ratio and extent of crosslinking to more accurately model the factors that govern NP formation. These observations, in conjunction with solid state NMR data, further suggest that the primary stabilisation of the NPs is through interaction with the PPh_2 unit.

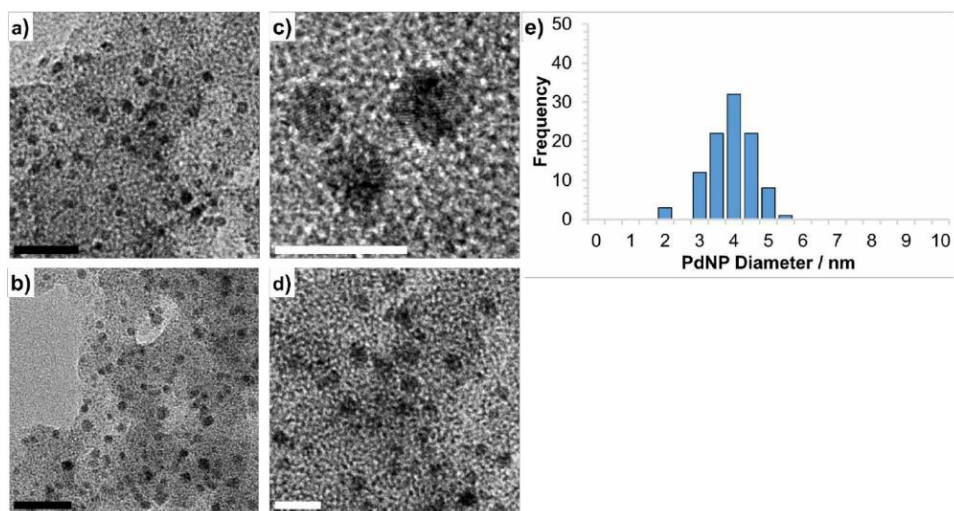


Figure 40: TEM images (a-d) and histogram showing particle size distribution (e) of 4.6 based on analysis of >100 particles. Scale bars are 20 nm (black) and 5 nm (white).

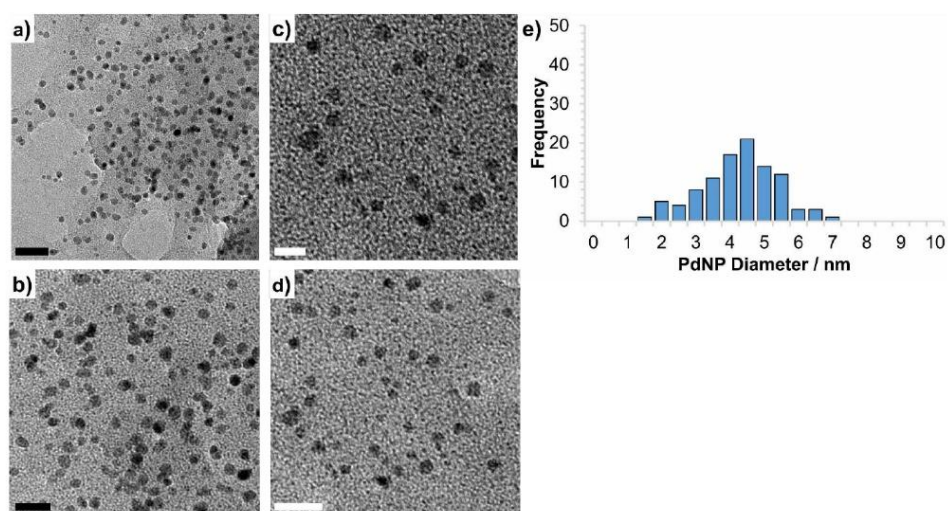


Figure 41: TEM images (a-d) and histogram showing particle size distribution (e) of 4.7 based on analysis of >100 particles. Scale bars are 20 nm (black) and 5 nm (white).

Table 18: Average particles sizes of PIILP supported PdNPs determined by measuring >100 particles.

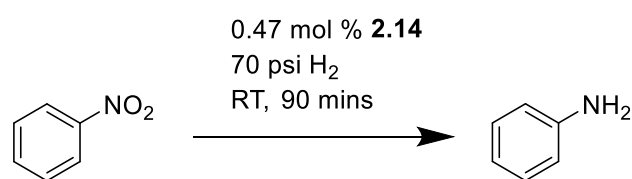
| Entry | Catalyst | Mean particle diameter (nm) |
|-------|------------------------------------|-----------------------------|
| 1 | PdNP@PPh ₂ -PIILP | 2.29 ± 0.96 |
| 2 | PdNP@PPh ₂ -PEGPIILP | 1.93 ± 0.67 |
| 3 | PdNP@P(Sty) ₃ -PIILP | 3.67 ± 0.67 |
| 4 | PdNP@P(Sty) ₃ -PEGPIILP | 4.01 ± 1.11 |

The XRD spectra (available in the appendix A44) for **4.6** contained diffraction peaks at $2\theta = 40.1, 46.3, 68.5, 82.1$ and 86.0 which index to the (111), (200), (220), (311) and (222) lattice planes of face centred cubic Pd, and the clear line-broadening indicates that these atoms likely exist in nanoassemblies. This observation further confirms the TEM observations and more subtly, differences in the catalyst-support interaction, as lightly crosslinked PIILP stabilised NPs were undetectable, suggesting they consist of small and highly dispersed PdNPs. In stark contrast, despite a larger average particle size, the XRD spectra of **4.7** (available in the appendix A45) contains no evidence of any diffraction peaks associated with metallic palladium. In this instance, it may be that the peaks corresponding to crystalline phases of borate salt by-product produced during the reduction step overlap with and are higher intensity than any Pd resonances; the by-product remained as washing of the PEGylated catalyst was difficult due to the hydrophilic nature of the support.

4.3 Optimisation of the reaction conditions for PdNP@PIILP catalysed hydrogenation of nitroarenes

Having characterised and identified differences in support/catalyst properties, optimisation studies were conducted to investigate how they influence catalyst performance. To this end, reactions were carried out in a stirred benchtop reactor under mild conditions (room temperature, 70 psi H₂) and at a catalyst loading of 0.47 mol % using nitrobenzene as the standard substrate.

Table 19: Optimisation of the reaction solvent for the PdNP@PIILP catalysed hydrogenation of nitrobenzene.



| Entry ^a | Solvent | 2.13 | 2.14 | 4.6 | 4.7 |
|--------------------|-------------------|------------------------|------------------------|------------------------|------------------------|
| | | Yield (%) ^b | Yield (%) ^b | Yield (%) ^b | Yield (%) ^b |
| 1 | Water | 60 | 100 | 81 | 72 |
| 2 | Water/EtOH | 47 | 99 | 77 | 76 |
| 3 | Ethanol | 33 | 83 | 74 | 66 |

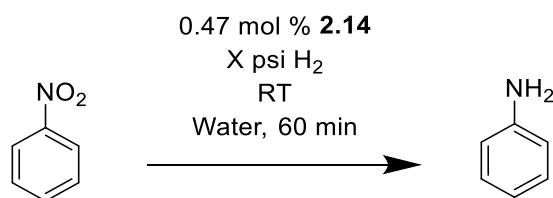
| | | | | | |
|----------|----------------------|---|----|----|----|
| 4 | Ethyl acetate | 4 | 18 | 11 | 12 |
| 5 | Toluene | 4 | 5 | 7 | 7 |
| 6 | MeCN | 3 | 7 | 2 | 6 |

^aReaction conditions: 1 mmol substrate, 0.47 mol % catalyst, 13 mL water, RT, 70 psi H₂, reaction time = 90 minutes.

^bConversion as determined by ¹H NMR spectroscopy using dioxane as the internal reference standard. Average of at least 3 runs.

A survey of the reaction solvent revealed that the highest conversion was achieved in water for all catalysts (entry 1), and aniline was obtained as the sole product. This further suggests that the hydrophobic effect, driven by the lipophilic polystyrene backbone, may promote enhancement of the reaction considering the limited solubility of the substrate in aqueous solution. The unique ionic microenvironment also appears to influence the relative performance, as modification of the support with PEG in the case of **2.14**, offers a marked improvement on comparison with **2.13**. Whilst this is likely to improve the swelling and dispersive properties of the support, comparative DLS measurements and other more detailed studies on the dynamic solution behaviour of the support/catalyst would be required to confirm this. Interestingly, this is not the case for the highly crosslinked systems as **4.6** had higher activity than **4.7** suggesting that in these systems dispersibility may not be the dominant factor. High conversions were also obtained in a 1:1 ethanol water mix suggesting that hydrogen bonding is a key factor for high activity (entry 2); interestingly the order of catalyst activity followed the same trend. Reactions performed in conventional organic solvent were much slower and gave lower conversion (entries 3-6). Given the high solubility of nitrobenzene in these solvents, this may simply be due to poor dispersion of the catalyst. In this manner, the 'hydrophobic effect' driving force no longer is significant and ultimately, the concentration of reactant within close proximity to the active site is substantially lower.

Given the practical and environmental advantages of aqueous phase catalysis, water was chosen as the solvent for the remainder of the studies. To investigate the effect of H₂ concentration on the reaction rate, the hydrogenation of nitrobenzene catalysed by **2.14** was monitored as a function of hydrogen pressure at a reaction time of 30 minutes.



Scheme 39: Reaction conditions for optimisation of the hydrogen pressure.

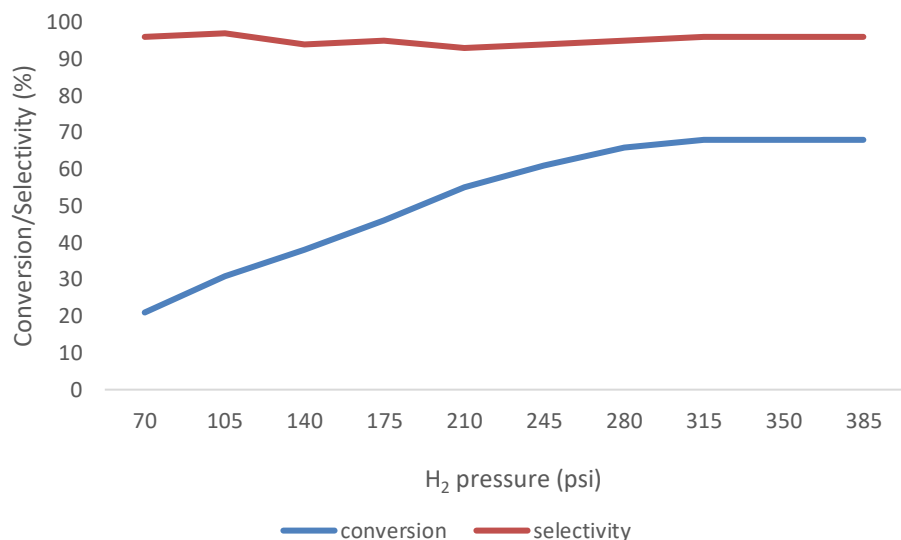


Figure 42: Reaction profile as a function of pressure for the **2.14** catalysed hydrogenation of nitrobenzene. Reaction conditions: 1.0 mmol nitrobenzene, 0.47 mol % **2.14**, RT, 13 mL water. Conversion and selectivity determined by ¹H NMR spectroscopy with dioxane as the internal standard. Selectivity for aniline = [% aniline / (% aniline + % *N*-phenylhydroxylamine)].

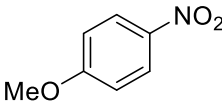
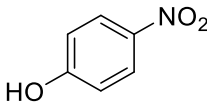
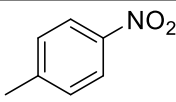
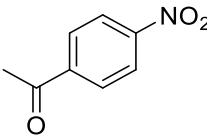
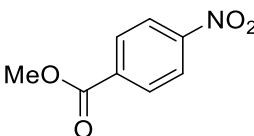
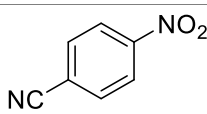
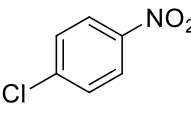
The graph in Figure 42 shows that increasing the pressure results in a near-linear increase in conversion from 21% at 70 psi, up to 68% at 315 psi where a plateau is reached, corresponding to TOFs of 89 h⁻¹ and 289 h⁻¹, respectively (measured as moles of product per mole catalyst per hour). This profile clearly signifies that the reaction is limited by H₂ diffusion in aqueous medium at lower H₂ pressures. However, diffusion control will realistically still dominate and impede the reaction kinetics due to the poor dispersion and inhomogeneity of the substrate and catalyst. However, to fully investigate how the reaction kinetics are affected by hydrogen diffusion, it would be necessary to measure conversion as a function of stirring speed. Reducing the catalyst loading tenfold to 0.047 mol % resulted in conversions of 15% and 24% at 70 psi and 315 psi which corresponds to TOFs of 638 h⁻¹ and 1021 h⁻¹, respectively, indicating that indeed the reaction is diffusion limited under these conditions. Interestingly, during this study, minor amounts of *N*-phenylhydroxylamine were observed as the only intermediate suggesting that reduction of this species is slow, and the reaction proceeds *via* the direct route as described earlier. Since quantitative conversion can be obtained at reaction

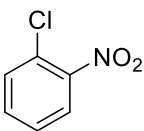
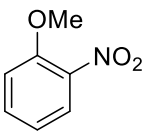
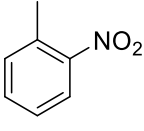
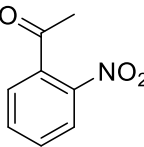
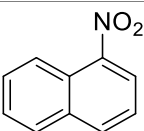
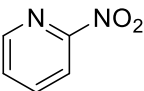
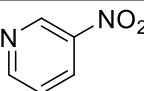
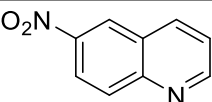
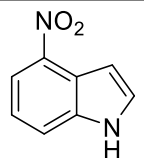
times as short as 90 mins under a mild pressure of 70 psi, all subsequent reactions were performed under these conditions by adjusting the reaction time accordingly.

4.3.1 Substrate screening

The optimised conditions were then applied to a range of substituted nitroarenes and nitro substituted heteroarenes to examine the scope of **2.14**; selected examples were compared against **2.13**, **4.6** and **4.7** for comparison.

Table 20: Hydrogenation of various substituted nitroarenes and heteroaromatic nitros catalysed by **2.14**.

| Entry ^a | Substrate | Time (min) | 2.14 yield ^b |
|--------------------|---|------------|---|
| 1 |  | 90 | 98 (98 ^c 97 ^d 94 ^e) |
| 2 |  | 150 | 98 |
| 3 |  | 150 | 93 |
| 4 |  | 60 | 99 (92 ^c 94 ^d 89 ^e) |
| 5 |  | 90 | 93 |
| 6 |  | 150 | 86 |
| 7 |  | 720 | 98 ^f |

| | | | |
|-----------|---|-----|---|
| 8 |  | 720 | 99 ^f |
| 9 |  | 210 | 86 (62 ^c 47 ^d 52 ^e) |
| 10 |  | 150 | 74 |
| 11 |  | 150 | 85 |
| 12 |  | 960 | 73 (51 ^c 33 ^d 34 ^e) |
| 13 |  | 150 | 98 (98 ^c 99 ^d 98 ^e) |
| 14 |  | 240 | 84 |
| 15 |  | 150 | 93 |
| 16 |  | 150 | 27 |

^aReaction conditions: 1 mmol substrate, 0.47 mol % 2.14, 13 mL water, RT, 70 psi H₂. ^bYields calculated by ¹H NMR spectroscopy using dioxane as the internal standard and GC analysis using decane as the internal standard, average of minimum 3 runs. ^cReaction catalysed by 0.47 mol % 2.13. ^dReaction catalysed by 0.47 mol % 4.6. ^eReaction catalysed by 0.47 mol % 4.7. ^fYield of aniline as a result of hydrodehalogenation.

Nitro compounds substituted with electron donating groups such as 4-nitroanisole, 4-nitrophenol and 4-nitrotoluene were converted to the corresponding aryl amines in excellent

yield in relatively short reaction times (entries 1-3). For comparison, good conversions were also obtained with 4-nitroanisole for the reaction catalysed by **2.13**, **4.6** and **4.7** (entry 1). Substrates containing electron withdrawing groups were also tolerated, and the reaction proceeded with 100% chemoselectivity as ester, cyano and acetyl functionalised amines were obtained in near-quantitative yield, which was also the case for the other catalysts examined (entries 4-6). Unexpectedly, no direct hydrogenation products were obtained for the **2.14** catalysed hydrogenation of 4-chloro-1-nitrobenzene or 2-chloro-1-nitrobenzene; aniline was obtained in high yield as the sole product indicating that the competing hydrodechlorination is fast under these conditions (entries 7 and 8). Interestingly, competing dehalogenation is often reported but usually yields aniline as only a minor side product,⁶ and so further studies will be required to elucidate the reaction path for this and ascertain which factors influence the relative rates of hydrogenation vs dehalogenation. Substitution around the 2- position enabled *ortho*- substituted amines to be obtained in high yield at relatively short reaction times, despite the inherent increase in steric congestion around the nitro substituent for reactions catalysed by **2.14** (entries 9-11). However, the efficacy of **2.13**, **4.6** and **4.7** for the hydrogenation of 2-nitroanisole was lower, especially for the highly crosslinked systems. The hydrogenation of 1-nitronaphthalene proved to be significantly more challenging and a reaction time of 16 hours was required to achieve 73% conversion (entry 12). Under these conditions, the catalyst was resistant to poisoning by heteroaromatics as the corresponding amines were obtained from the reduction of 2 and 3-nitropyridine as well as 6-nitroquinoline in high yield (entries 13-15). Similarly, the hydrogenation of 2-nitropyridine catalysed by **2.13**, **4.6** and **4.7** proceeded smoothly in short reaction times (entry 13). However, the same activity was not exhibited in the presence of 4-nitroindole as only 27% conversion was obtained using **2.14** (entry 16), although higher yields could be obtained by extending the reaction time.

4.3.2 Recycling studies

As presented in Chapter 3, further benefits of aqueous phase catalysis lie in the implementation of facile recycling procedures and catalyst recovery. To this end, recycling experiments were conducted by extracting the products and any remaining starting material into ethyl acetate prior to recharging the aqueous phase with a further equivalent of nitrobenzene and reintroducing hydrogen into the system.

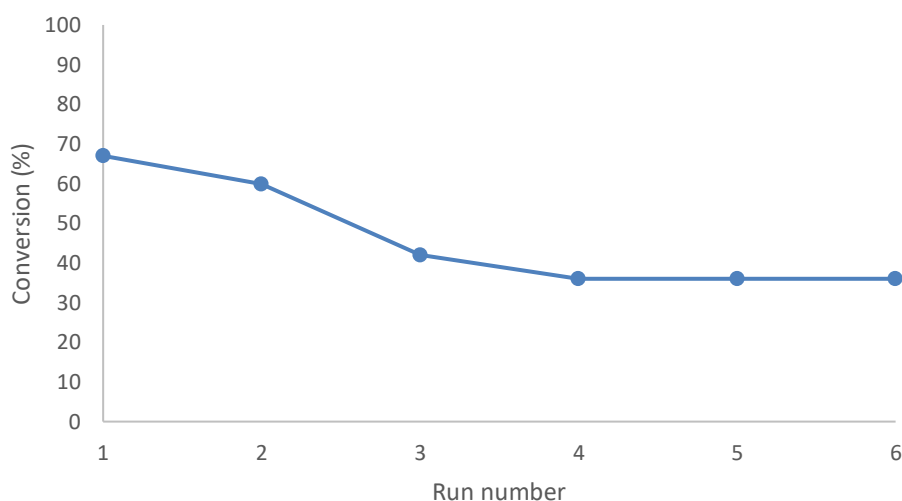


Figure 43: Recycling profile for the hydrogenation of nitrobenzene catalysed by **2.14**. Reaction conditions: 1 mmol substrate, 0.47 mol % **2.14**, RT, 70 psi H₂, reaction time = 60 mins.

As the most active and most likely to disperse efficiently, **2.14** was initially chosen to investigate catalyst reusability. The data in Figure 43 shows that in contrast to the **2.14** catalysed hydrogenation of α,β -unsaturated aldehydes, in which the catalyst appeared to be activated in the early stages of the study, activity drops over runs 1-3 before reaching a stable conversion profile. The Pd content of the aqueous phase after the 6th run revealed a significant drop in Pd content of 39%, which may be responsible for the loss of activity rather than catalyst deactivation. However, ICP analysis of the combined organic phases demonstrated that leaching of the Pd was negligible, as the Pd content was below the detection limit. In this regard, catalyst may have been lost from adhesion to glassware during the separation and recovery procedure or deposition onto the sides of the reactor; since small amounts of catalyst are used (10-15 mg) a small loss may result in dramatic reduction in Pd content. Alternatively, since the aqueous catalyst solution only becomes visually homogeneous after the first three runs, the possibility of a parallel homogeneous mechanism involving soluble Pd cannot be discounted. TEM analysis of the catalyst recovered after the final run showed an increase in the average particle size from 1.93 ± 0.67 nm in the freshly prepared sample to 3.05 ± 0.86

nm corresponding to an overall drop of ca. 35% in surface area, which may also be responsible for the drop in activity.

Catalyst **4.6** was also investigated under the same conditions to provide an insightful comparison on the basis that it exhibited similar activity yet the relative dispersibility properties are markedly different.

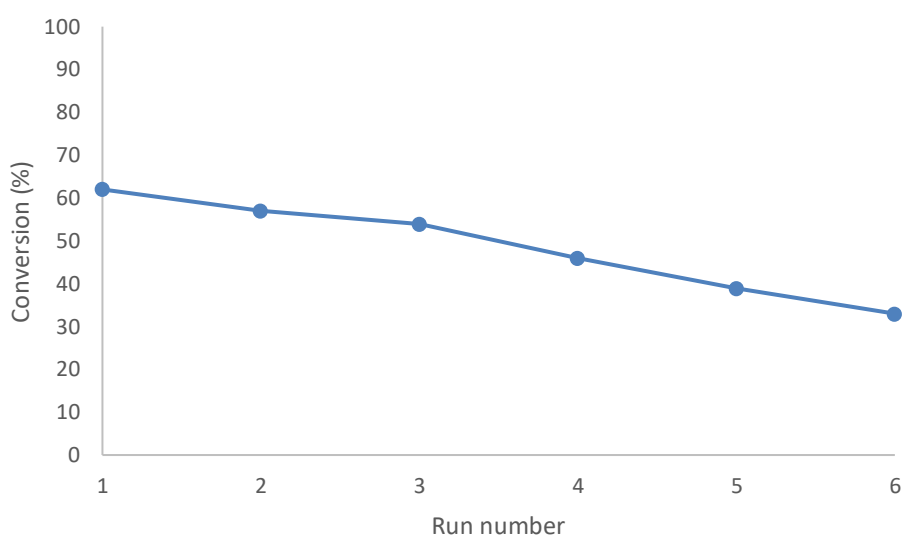


Figure 44: Recycling profile for the hydrogenation of nitrobenzene catalysed by **4.6**. Reaction conditions: 1 mmol substrate, 0.47 mol % **2.14**, RT, 70 psi H₂, reaction time = 60 mins.

The profile in Figure 44 demonstrates that extensive crosslinking has a negative effect on the recyclability of the catalyst. Similar to **2.14**, activity drops over runs 1-3 however, rather than reach a steady state, activity continues to decline on subsequent reuse over runs 4-6. This profile is indicative of continuous catalyst loss or attrition, most likely through adhesion. In this regard, the physical properties of the support may be the dominant factor as the highly crosslinked systems are more difficult to solubilise, increasing the potential for losses through adhesion during recovery.

To further probe the potential intrinsic turnover rate of **2.14**, the catalyst loading was lowered to 0.0018 mol %. Under the same conditions as described above, the conversion reached 65% after a reaction time of 15 hours; this corresponds to a TON of 36,100 and TOF of 2400 h⁻¹. This is likely to be a more realistic indication of catalyst efficiency given that further reducing the catalyst loading to 0.001 mol % resulted in only a marginal increase in TOF to 2466 h⁻¹. On this basis, this system may be suitable for use in a continuous flow system to harvest the high efficiency in a more convenient and scalable process.

4.3.3 Comparison with other PIILP systems and commercial catalysts

To explore the influence of the phosphine, surface ionic liquid and PEG modifications on catalysis, comparative catalyst testing was performed using the library of PIILP based catalysts discussed in the previous chapter, and their respective compositions are described in Table 21. The data gathered in Table 21 demonstrates that selective removal of the hydrophilic PEG group results in a decrease in activity for all the lightly crosslinked systems. This result is not unprecedented given that the positive effects are likely derived from the additional surface stabilising interactions with the PdNPs in the respective ionic microenvironments. Furthermore, the dispersibility, and as a result, the effective surface area of the microenvironment for catalysis is also improved through use of the PEG modification. In contrast, introduction of the PEG modification did not improve the performance for the highly cross-linked system (entries 7 and 8) and resulted in a drop in overall catalyst turnover. In this respect these systems are intrinsically more difficult to homogenise due to their structural robustness, and this observation is probably associated with the relative particle sizes rather than dispersibility.

Table 21: Comparison of modified PdNP@PIILP catalysts and Pd/C to determine the influence of support functionality.

| Entry ^a | Catalyst | Functionality | Conversion (%) ^b | TOF (h ⁻¹) ^c | Average NP size (nm) |
|--------------------|----------|-------------------------------|-----------------------------|-------------------------------------|----------------------|
| 1 | 2.13 | PPh ₂ , IL | 38 | 43 | 2.29 ± 0.96 |
| 2 | 2.14 | PPh ₂ , IL, PEG | 66 | 140 | 1.93 ± 0.67 |
| 3 | 2.15 | PPh ₂ , PEG | 34 | 69 | 1.83± 0.44 |
| 4 | 2.16 | IL, PEG | 38 | 44 | 3.23± 0.61 |
| 5 | 2.17 | PPh ₂ | 21 | 62 | 1.38 ± 0.18 |
| 6 | 2.18 | IL | 44 | 23 | 3.00 ± 0.62 |
| 7 | 4.6 | P(Sty) ₃ , IL | 55 | 122 | 3.67 ± 0.67 |
| 8 | 4.7 | P(Sty) ₃ , IL, PEG | 45 | 56 | 4.01 ± 1.11 |

| | | | | | |
|-----------|-------------------------|-----|----|----|-----|
| 9 | Pd/C^d | n/a | 21 | 40 | n/a |
| 10 | None | n/a | 0 | 0 | n/a |

^aReaction conditions: 1 mmol substrate, catalyst, 13 mL water, RT, 70 psi H₂, reaction time = 60 minutes. ^b Conversion as determined by ¹H NMR spectroscopy using dioxane as the internal reference standard. Average of at least 3 runs. ^c Calculated as moles of product/mole catalyst per hour based on Pd content as determined by ICP-OES analysis. ^d 0.47 mol % catalyst.

The role of the IL in catalysis was validated by removing the IL functionality from the support to afford **2.15**. The reaction conducted in the presence of **2.15** resulted in a significant decrease in TOF from 140 h⁻¹ to 69 h⁻¹ (entry 3). This is likely due to the removal of potential sites for solvent and reagent interaction close to the active site, as well as solubilising effects from the ionic nature, rather than a stabilising effect as the NP sizes of **2.15** are comparable with **2.14**. Removal of the PPh₂ from the optimum system is reflected in the performance of **2.16** and was demonstrated to be detrimental to catalysis as the TOF decreased quite significantly from 140 h⁻¹ to 44 h⁻¹ (entry 4). Given that a combination of PEG and IL would likely result in a highly dispersible catalyst in aqueous solution, this drop in TOF may well be associated with the increase in particle size from 1.93 ± 0.67 nm to 3.23 ± 0.61 nm as a result of PPh₂ removal, as the two systems are otherwise identical.

At this stage the results demonstrate a clear dependence on all three aspects, which was further demonstrated by removal of two components (entries 5 and 6), which resulted in a higher drop in activity on comparison with **2.14**. To more accurately rationalise these effects, more studies would be required utilising *in situ* and surface-based techniques to establish the effect that each component has on the particle surface electronics and morphology, as well as the overall materials properties that contribute to catalysis.

Gratifyingly, the commercially purchased sample of Pd/C proved to be less active than any PIILP systems in this study and exhibited over a threefold decrease in activity based on the results obtained with the reaction catalysed by **2.14** (entry 9) and finally, no reduction products were observed for the reaction conducted in the absence of catalyst (entry 10).

4.4 PdNP@PIILP catalysed transfer hydrogenation of nitroarenes

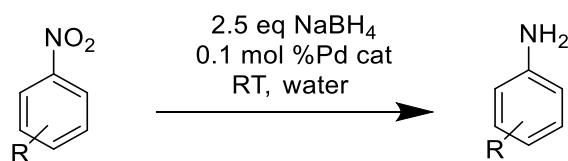
An alternative strategy for the reduction of nitroarenes is *via* catalytic transfer hydrogenation (CTH), in which rather than high pressure hydrogen gas, potential hydrogen ‘donors’ act as a pseudo source of hydrogen through metal mediated decomposition to generate chemisorbed

hydrogen or metal hydride-like species on the catalyst surface.⁹ This method has many advantages, as the problems associated with low solubility of hydrogen in liquid phase are no longer significant and the apparatus required is more straightforward and less costly since a specialist gas phase reactor is not required.

4.4.1 Reaction optimisation

Using the methodology reported by Lipschutz discussed earlier as a lead, a series of batch experiments using nitrobenzene as the benchmark nitroarene were conducted to investigate the efficacy of **2.13**, **2.14**, **4.6** and **4.7**. Reactions were conducted in the presence of NaBH₄ as the reducing agent as it is cheap, readily available and widely used, providing reasonable scope for comparison. Furthermore, as a water-soluble reagent, the reducing agent and the associated by-products can be easily separated from the organic products during post reaction processing.

Table 22: Optimisation of the reaction conditions for the Pd catalysed NaBH₄ mediated transfer hydrogenation of nitrobenzene.



| Entry ^a | Catalyst | Solvent | Hydrogen source | Conversion (%) ^b | Selectivity (%) ^b |
|--------------------|-------------|----------------|----------------------------------|-----------------------------|------------------------------|
| 1 | 2.14 | Water | NaBH ₄ | 100 | 100 |
| 2 | 2.14 | Ethanol | NaBH ₄ | 40 | 14 |
| 3 | 2.14 | Ethanol/Water | NaBH ₄ | 77 | 17 |
| 4 | 2.14 | Methanol | NaBH ₄ | 33 | 27 |
| 5 | 2.14 | Methanol/Water | NaBH ₄ | 91 | 27 |
| 6 | 2.14 | Water | NH ₃ .BH ₃ | 87 | 94 |
| 7 | 2.13 | Water | NaBH ₄ | 99 | 99 |

| | | | | | |
|-----------|-------------|-------|-------------------|----|-----|
| 8 | 4.6 | Water | NaBH ₄ | 82 | 82 |
| 9 | 4.7 | Water | NaBH ₄ | 92 | 92 |
| 10 | Pd/C | Water | NaBH ₄ | 63 | 63 |
| 11 | None | Water | NaBH ₄ | 0 | n/a |

^aReaction conditions: 1 mmol substrate, 0.047 mol % catalyst, 2 mL solvent, RT, 2.5 mmol reducing agent. ^bYields calculated using ¹H NMR spectroscopy using dioxane as the internal standard and GC analysis using decane as the internal standard, average of minimum 3 runs. Selectivity for aniline = [% aniline / (% aniline + % *N*-phenylhydroxylamine + % azoxybenzene + % azobenzene)].

Reactions were conducted at room temperature using a catalyst loading of 0.047 mol %. For the initial screening, **2.14** was chosen as the benchmark as this was the optimum catalyst identified for hydrogenation. The results above demonstrate that the reaction proceeds smoothly and most efficiently in water (Table 22, entry 1). As well as the hydrophobic effect, the high solubility of the reducing agent in aqueous solution is probably responsible for the high activity. Furthermore, as the solubility of NaBH₄ is much higher than molecular H₂ in water, the concentration of catalyst can be lowered tenfold whilst retaining comparable productivity. As expected, changing to alcoholic solvents resulted in a marked decrease in activity (entries 2 and 4). Under these conditions, reaction selectivity also dropped quite dramatically, as significant amounts of intermediates from both the direct (*N*-phenylhydroxylamine) and condensation (azoxybenzene and azobenzene) routes were identified. This suggests that their decomposition into aniline is slower under these conditions in comparison with those of hydrogenation, and in these cases, the major product of partial reduction was *N*-phenylhydroxylamine. Activity was enhanced by dilution of the alcoholic solvents with water (entries 3 and 5) however, the reaction selectivity remained similar, suggesting that the presence of alcohol may impede subsequent reduction of the intermediates. Using ammonia borane as an alternative water soluble reducing agent gave good conversion but did not match the efficiency of NaBH₄ (entry 6). Interestingly, under the conditions examined the performance of **2.13** matches that of **2.14** and as expected, both lightly crosslinked systems outperformed their highly crosslinked counterparts (entries 8 and 9). However, all the PIILP systems outperformed commercially available Pd/C (entry 10). Finally, quantitative amounts of starting material were recovered in the reaction conducted in the absence of Pd catalyst confirming its active role (entry 11).

The efficacy of these systems is evident as the majority of reported PdNP-based systems typically require a larger excess of reducing agent (>10 eq.),¹⁴ whereas PIILP based catalysts appear to operate efficiently in the presence of only 2.5 equivalents of NaBH₄ and give good conversions in short reaction times with low catalyst loadings at room temperature.

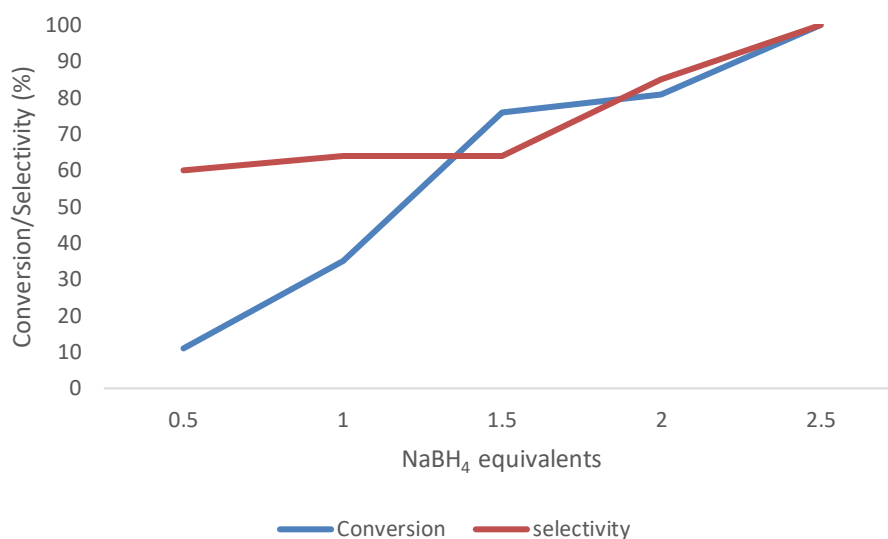


Figure 45: Conversion and selectivity as a function of the NaBH₄:substrate ratio for the reduction of nitrobenzene catalysed by 2.14. Reaction conditions: 1 mmol nitrobenzene, 0.047 mol % 2.14, 2 mL water, RT reaction time = 2 hours. Yields calculated using ¹H NMR spectroscopy using dioxane as the internal standard and GC analysis using decane as the internal standard, average of minimum 3 runs. Selectivity for aniline = [% aniline / (% aniline + % *N*-phenylhydroxylamine)].

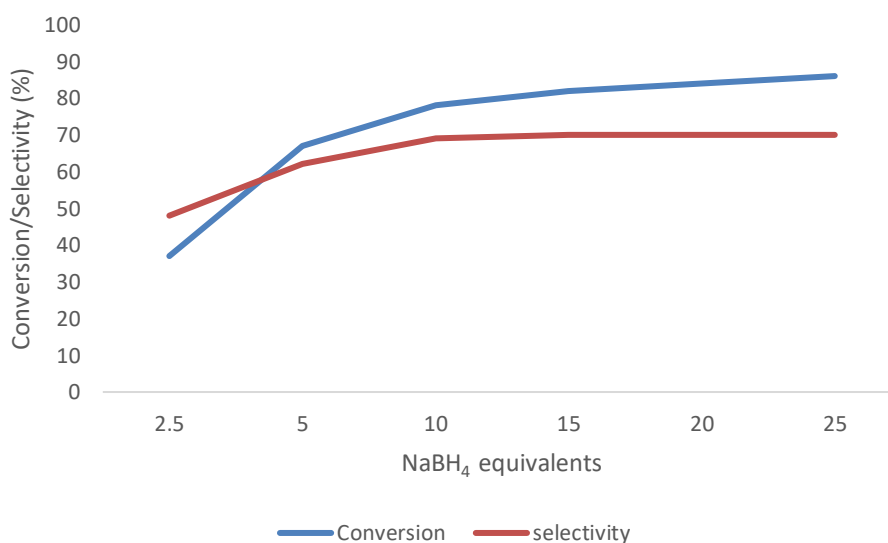


Figure 46: Conversion and selectivity as a function of the NaBH₄:substrate ratio for the reduction of nitrobenzene catalysed by 2.14. Reaction conditions: 1 mmol substrate, 0.047 mol % 2.14, 2 mL water, RT, reaction time = 20 min. Yields calculated

using ^1H NMR spectroscopy using dioxane as the internal standard and GC analysis using decane as the internal standard, average of minimum 3 runs. Selectivity for aniline = [% aniline / (% aniline + % *N*-phenylhydroxylamine)].

No products were obtained conducting the reaction in the absence of NaBH_4 , confirming that the reducing agent is likely the primary source of hydrogen rather than water. The profile in Figure 45 demonstrates that decreasing the NaBH_4 :substrate ratio below 2.5 resulted in a dramatic decrease in activity and accordingly, the selectivity for aniline. Furthermore, by decreasing the reaction time appropriately, it was demonstrated that increasing the NaBH_4 :substrate ratio from 2.5 to 10 results in a marked increase in activity of 41% (Figure 46). The conversion continues to increase above this ratio, albeit only marginally, until 25 equivalents at which point the solution is presumably saturated with NaBH_4 . At this point, conversion reaches 86% with 70% selectivity for aniline. This profile is a clear indication that when using 2.5 equivalents of NaBH_4 , the reaction is operating under mass transfer limitations. Despite this, given that 100% yield of aniline is obtainable with 2.5 equivalents in only 2 hours, this was taken forward for the remainder of the studies as this would significantly reduce the accumulation of inorganic alkali metal by-product waste. Furthermore, reducing the catalyst loading to 0.00035 mol % afforded aniline in 96% yield and 96% selectivity after only 16 hours, which corresponds to a TON of 274,000 and TOF of $17,125\text{ h}^{-1}$. While this activity is still capped by mass transfer limitations, comparison with the most active systems in the literature reveals that under these conditions, **2.14** is the most efficient system for this type of transformation, and by using a low excess of reducing agent, delivers a safe and sustainable protocol.^{8, 17, 18}

4.4.2 Towards elucidating the reaction mechanism

As several intermediates were identified under the reaction conditions, a series of time-conversion profiles were conducted to investigate the factors that influence the reaction pathway with the aim of determining the primary pathway for the transfer hydrogenation of nitrobenzene catalysed by **2.14**.

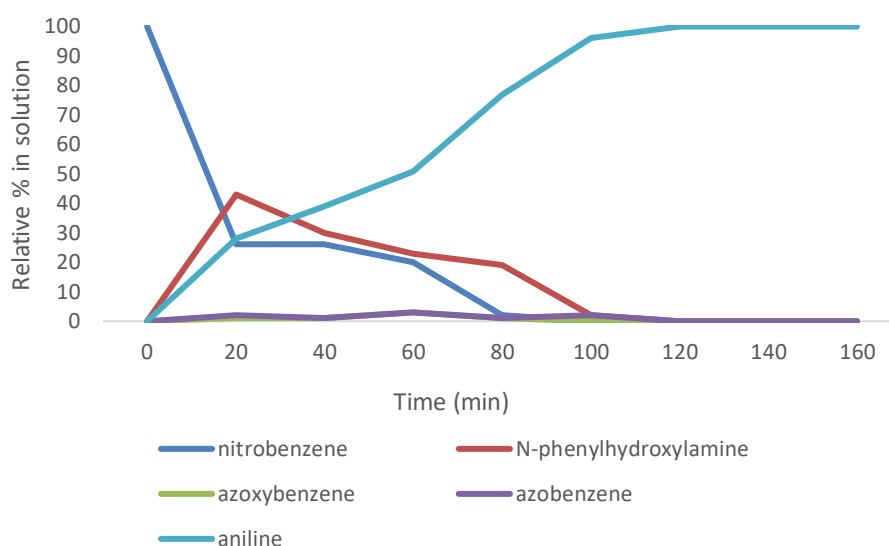


Figure 47: Conversion-time profile for reduction of nitrobenzene catalysed by 0.047 mol % **2.14** in water in the presence of 2.5 equivalents of NaBH₄ at room temperature.

The plot in Figure 47 demonstrates that the major intermediate is *N*-phenylhydroxylamine and thus, **2.14** appears to catalyse the transfer hydrogenation of nitrobenzene *via* the direct route. The concentration of this species reaches its peak after 20 minutes at which time *N*-phenylhydroxylamine comprises 43% of the reaction mixture, and only trace amounts of azoxybenzene (4%) and azobenzene (3%) are present. Following this, these intermediates are consumed through further reduction to aniline and the reaction proceeds to completion after approximately 100 minutes. Similar profiles were obtained for the reactions catalysed by **2.13**, **4.6** and **4.7** which are available in the appendix (A46).

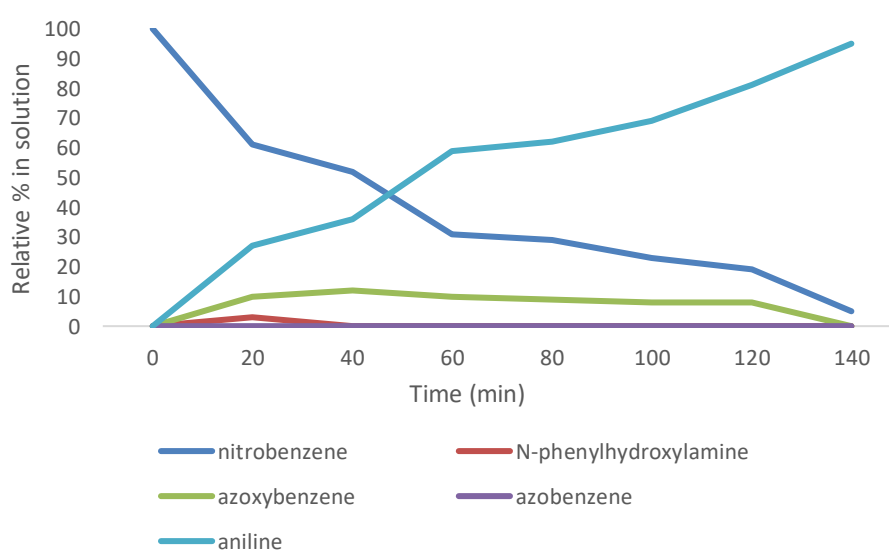
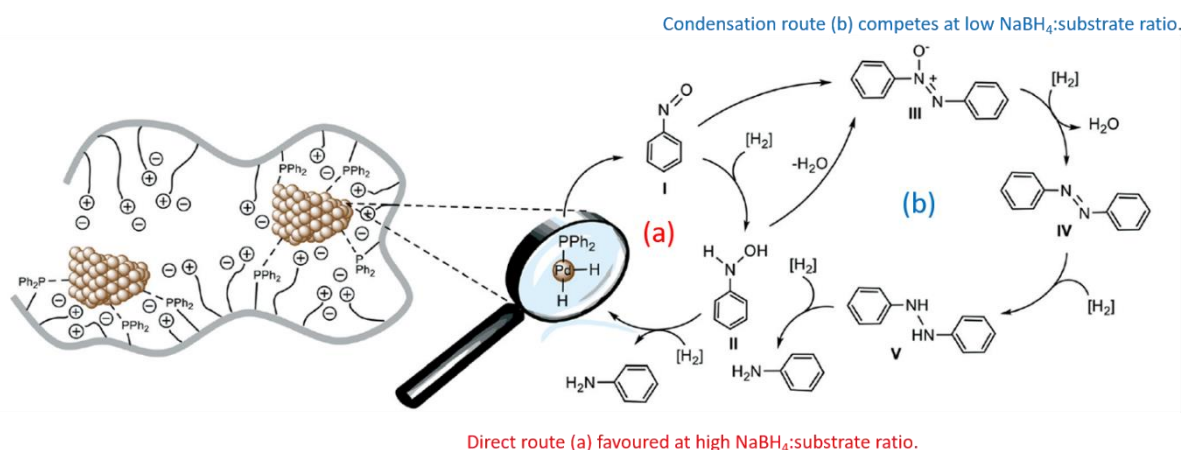


Figure 48: Conversion-time profile for reduction of nitrobenzene catalysed by 0.047 mol % **2.14** in the presence of 1.0 equivalent of NaBH₄ at room temperature.

As it has been reported that a low concentration of reducing agent may favour the condensation route,⁷ the reduction of nitrobenzene catalysed by **2.14** using only 1 equivalent of NaBH₄ was monitored as a function of time. Under these conditions the reaction was markedly slower, as the maximum yield of aniline was 95% at a reaction time of 140 mins. Interestingly, under these conditions, azoxybenzene was the major intermediate and only trace amounts of *N*-phenylhydroxylamine were observed; this suggests that reduction may occur *via* the condensation pathway under these conditions. While there is not sufficient evidence to rationalise these observations, under optimised conditions and under the assumption that the PdNP surface is heavily populated with large PPh₂ donors, condensation of two chemisorbed *N*-phenylhydroxylamine molecules may be disfavoured. However, as the amount of NaBH₄ is reduced, the reaction rate inherently decreases as a result of a decrease in activated hydrogen concentration. Therefore, the rate of condensation may now surpass the rate of hydrogenation, giving rise to the formation of azoxy-based intermediates.

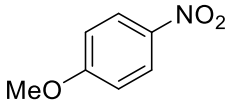
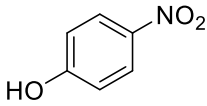
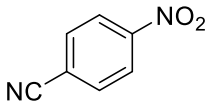
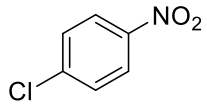
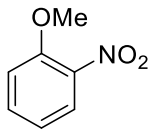
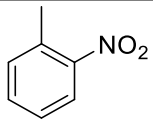
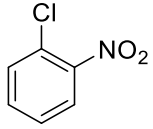
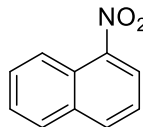


Scheme 40: Activation of hydrogen over PdNPs supported on phosphine functionalised PIILPs and different reaction pathways for the **2.14** catalysed reduction of nitrobenzene according to the Haber mechanism showing their dependency on the NaBH₄:substrate ratio.

4.4.3 Substrate screening

Having identified the optimum reaction conditions, several substrates were screened to fully evaluate the efficacy of the newly developed catalysts. Furthermore, as reactions are conducted in the presence of NaBH₄, catalysts were also generated *in situ* by reduction of the respective tetrachloropalladate-loaded precursor. This approach has many distinct benefits as the extra synthetic steps involved in preparing NPs *ex situ* are avoided. Additionally, catalysts can be stored safely under ambient conditions without any reoxidation.

Table 23: Comparison of different PIILP catalyst systems for the transfer hydrogenation of nitrobenzene using *in situ* and *ex situ* generated PdNPs.

| Entry ^a | Substrate | Time (min) | 2.13 yield ^b (2.11) ^b | 2.14 yield ^b (2.12) ^b | 4.6 yield ^b (4.4) ^b | 4.7 yield ^b (4.5) ^b |
|--------------------|---|---------------|--|--|---|--|
| 1 |  | 120 | 99 (99) | 99 (99) | 93 (99) | 95 (99) |
| 2 |  | 120 | 99 (70) | 99 (90) | 80 (63) | 70 (99) |
| 3 |  | 120 | 75 (77) | 87 (86) | 57 (65) | 52 (52) |
| 4 ^c |  | 360 | 91 (92) | 93 (95) | 95 (96) | 94 (96) |
| 5 |  | 300 | 94 (89) | 86 (97) | 76 (92) | 91 (97) |
| 6 |  | 120 | 95 (84) | 99 (97) | 49 (86) | 91 (92) |
| 7 ^c |  | 360 | 34 (31) | 39 (34) | 40 (67) | 52 (67) |
| 8 |  | 360 | 77 (69) | 79 (94) | 62 (58) | 53 (62) |

^aReaction conditions: 1 mmol substrate, 0.047 mol % catalyst, 2 mL water, RT, 2.5 mmol NaBH₄. ^bYields calculated using ¹H NMR spectroscopy using dioxane as the internal standard and GC analysis using decane as the internal standard, average of minimum 3 runs. ^c Remaining mass balance corresponds to aniline.

The results presented in Table 23 show that a range of functionalised nitroarenes can be reduced with PIILP catalysts to give good yields of the corresponding amines under mild conditions. Nitroarenes bearing electron donating substituents, 4-nitroanisole, 4-nitrophenol

and 2-nitrotoluene were tolerated and the products were isolated in excellent yields (entries 1, 2 and 6). Substitution around the *ortho*- position resulted in a slower reaction as the reduction of 2-nitroanisole required an extra 180 minutes to achieve a conversion comparable to its *para*- substituted counterpart (entry 5). Reduction of sterically cumbersome 1-nitronaphthalene proceeded well with lightly cross-linked catalysts **2.13** and **2.14** albeit the reaction was substantially slower than the other substrates examined (entry 8). Furthermore, highly cross-linked catalysts **4.6** and **4.7** proved to be even less effective for this substrate. Sites of other reducible functionality were preserved as the reduction of 4-nitrobenzonitrile yielded 4-aminobenzonitrile as the sole product (entry 3). Full conversion of the starting material occurred for the hydrogenation of 1-chloro-4-nitrobenzene with each of the catalysts, however, minor amounts of aniline were obtained as a product of hydrodechlorination (entry 4). In contrast, hydrodechlorination was much more facile in the case of 1-chloro-2-nitrobenzene as conversions reached 100% but yields of 2-chloroaniline varied between 34-52% due to competitive dehalogenation to give aniline (entry 7). Interestingly, hydrodechlorination occurred to a lesser extent for the reactions catalysed by highly cross-linked catalysts **4.6** and **4.7**. This may well be a result of the lower activity, rendering hydrogenation relatively more accessible than hydrodechlorination.

PdNPs formed via *in situ* reduction from the corresponding Pd^(II) precursors proved to be equally as efficient for most substrates tested, indicating that reduction is quick and facile. TEM analysis of PdNPs generated under the reaction conditions revealed mean particle diameters of 3.05 ± 0.86 nm and 2.55 ± 0.97 nm for **2.14** and **4.7**, respectively, which represents a change in surface area of approximately 40% for each catalyst.

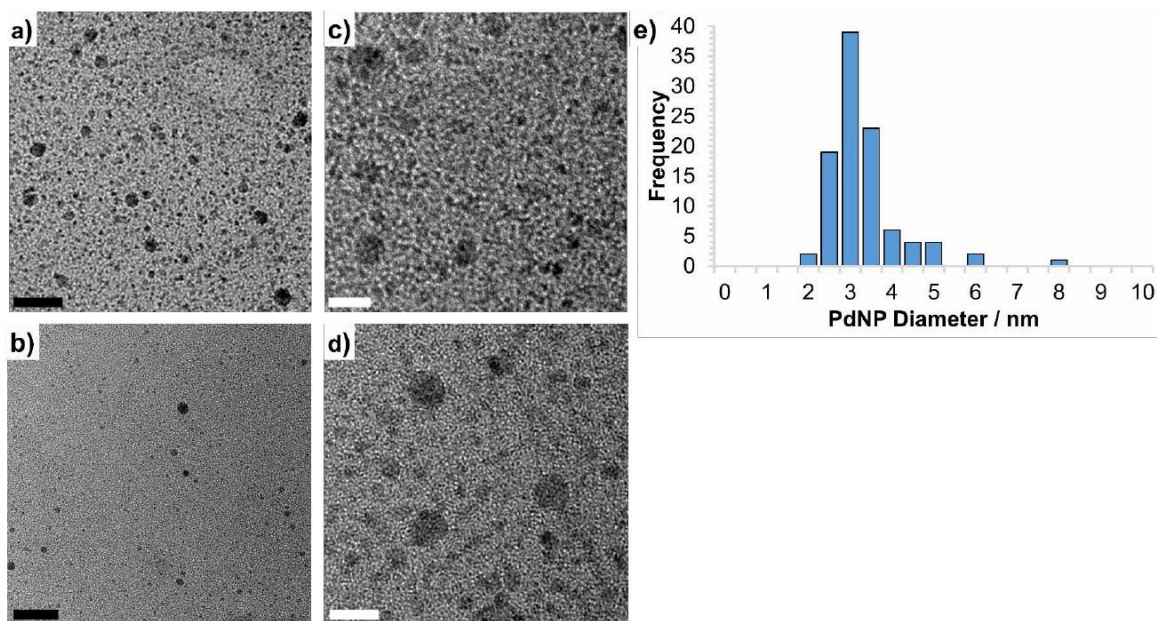


Figure 49: HRTEM images of PdNPs formed by *in situ* reduction of 2.12 (a-d), and the associated particle size distribution (e) based on >100 particles. Average particle size = 3.05 ± 0.86 nm. Scale bars are 25 nm (black) and 5 nm (white).

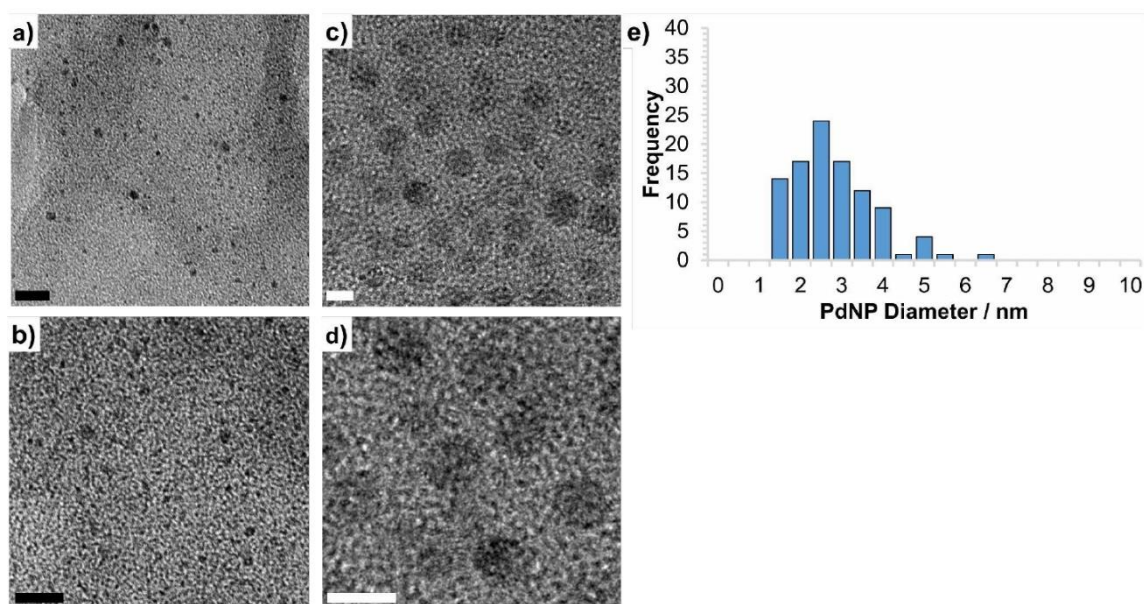


Figure 50: HRTEM images of PdNPs formed by *in situ* reduction of 4.5 (a-d), and the associated particle size distribution (e) based on >100 particles. Average particle size = 2.55 ± 0.97 nm. Scale bars are 25 nm (black) and 5 nm (white).

Clearly this drastic change in surface area does is not reflected in catalytic activity, which may suggest that surface electronic changes induced by functionality on the support may be a more influential factor rather than particle size, although this would require further investigation to verify. Overall, the comparative performance of PdNPs generated *in situ*, indicate that this would be a viable method for improving the step economy of the whole process.

4.4.4 Catalyst deactivation

To gain further insight into the how heteroaromatics may induce poisoning or inhibition of the catalyst, **2.14** was treated with of pyridine and the reduction of nitrobenzene monitored as a function of time. To this end, a sample of **2.14** was stirred with 1 mmol (1 equivalent with regards to the substrate) of pyridine for 10 minutes prior to the addition of nitrobenzene and the reducing agent.

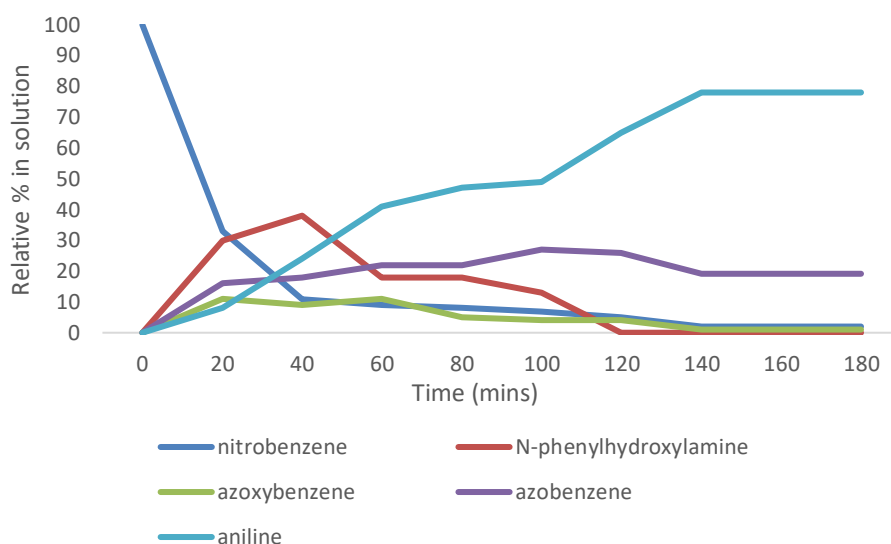


Figure 51: Conversion-time profile for reduction of nitrobenzene catalysed by 0.047 mol % **2.14** in the presence 1 mmol pyridine using 2.5 equivalents of NaBH₄ at room temperature in water.

The resulting time-conversion profile in Figure 51 revealed a stark difference derived from the presence of pyridine in the system. As described above, in the absence of pyridine the reaction proceeds primarily through the direct route and reaches completion after 120 mins, whereas only 78% aniline together with azoxybenzene (4%) and azobenzene (26%) is obtained after 180 min after treatment with pyridine. During the early stages of the reaction, significant amounts of *N*-phenylhydroxylamine form, but as the reaction progresses the concentration of condensation intermediates increases, before the reaction begins to plateau at 140 minutes. This observation indicates that the addition of pyridine severely hampers the intrinsic reaction rate as the reaction proceeds and as a result, condensation of the intermediates occurs. Furthermore, given that at the later stages of the reaction, the concentration of aniline and azo-based intermediates begins to plateau, this profile may suggest that aniline may only form *via* the direct route, although further experiments would be required to validate this. To extend this study, the reduction of 2-nitrotoluene in the presence of **2.14** after pre-treatment with a solution of 5-nitroindole was also investigated. Under these conditions, only 4%

conversion was obtained after 1 hour. For comparison, under the same conditions but in the absence of 5-nitroindole, 46% conversion to 2-aminotoluene was obtained in the same time. Furthermore, the addition of 5-nitroindole to the NaBH_4 -mediated reduction of 2-nitrotoluene after 1 hour resulted in no further reaction as the conversion remained at 46% after aging for a further 1 hour, demonstrating immediate inhibition.

To further probe the effects of the interaction between pyridine and the PdNP surface, a sample of fresh **2.14** and a sample obtained after pre-treatment with pyridine was analysed using FD-XAS in collaboration with Leeds University. Analysis of the Pd L_{III} edge revealed an increase in the Pd L_{III} edge energy after treatment with pyridine from 3.175874 KeV to 3.176196 KeV, which is in keeping with a reduction in electron density on the Pd surface.

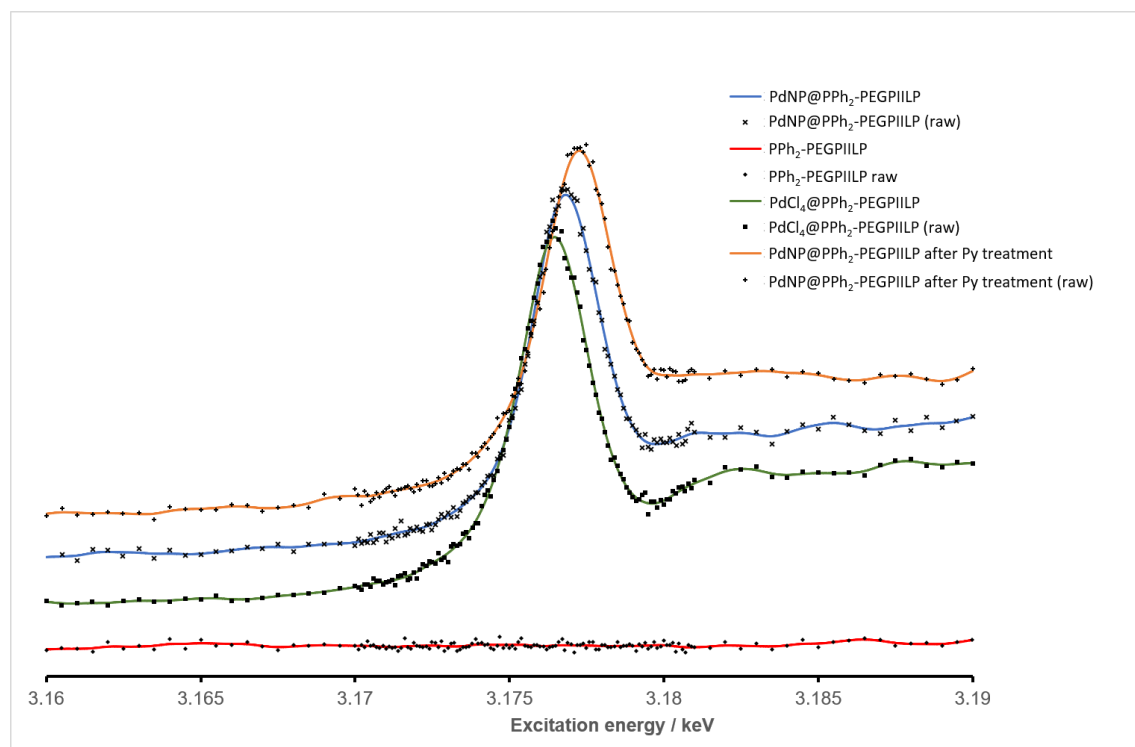


Figure 52: FD-XAS spectrum showing the Pd L_{III} edges of PPh_2 -PEGPIILP (red), PdCl_4 @ PPh_2 -PEGPIILP (green), PdNP@ PPh_2 -PEGPIILP (blue) and PdNP@ PPh_2 -PEGPIILP after treatment with pyridine (orange). Raw data (black) has been included on smoothed lines.

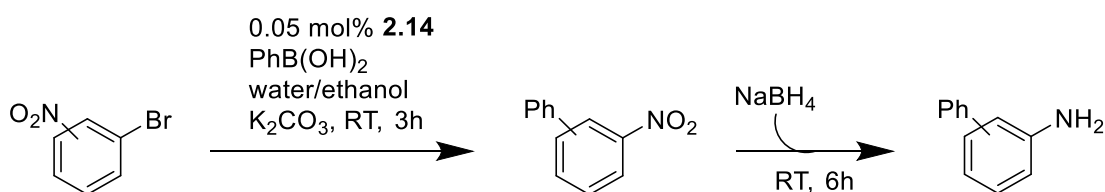
On this basis, and given that under the reaction conditions, the heteroaromatic substrate is present in >2000-fold excess with regards to Pd, it is tentatively suggested that pyridine irreversibly coordinates to the PdNPs and saturates the surface which consequently renders the catalyst inactive. Additionally, as surface analysis suggests a decrease in electron density, this may also suggest displacement of the surface ligated PPh_2 , as nitrogen donors are classically regarded as weaker electron donors than phosphines. In this regard, whilst these

methods provide valuable insight towards rationalising experimental observations, further surface-based *in situ* techniques would be required to substantiate this interpretation and hereby assist in the design of more robust systems capable of catalysing the reduction of nitro-functionalised heteroaromatics.

4.4.5 One pot synthesis of biaryl amines

The efficiency of **2.14** as a catalyst for the transfer hydrogenation of nitroarenes as well as the Suzuki-Miyaura cross coupling reaction (Chapter 2) inspired the development of a tandem reaction sequence which could be conducted in a single vessel. In this regard, such methods would significantly improve sustainability of the process, as intermediary purification and product isolation would not be necessary, therefore combined waste and processing steps would be drastically reduced.

To this end, **2.14** is ideally suited to practically harvest the benefits of this proposed strategy, as both reactions have been demonstrated to occur under similar conditions. Therefore, the reactions could proceed without requiring the addition of activating ligands, modifiers or additives between steps, and no changes in reaction temperature or pH would be required downstream.



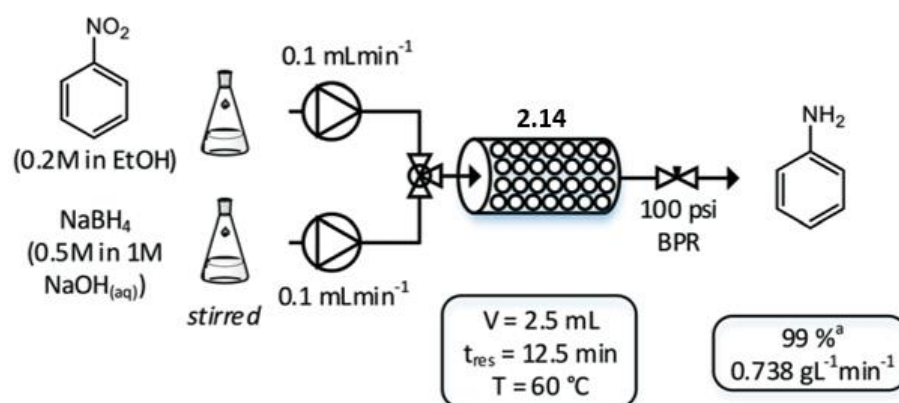
Scheme 41: One-pot tandem Suzuki-Miyaura cross-coupling hydrogenation sequence for the synthesis of biaryl amines catalysed by **2.14**.

Using the reaction conditions identified in Chapter two, a two-step, one-pot sequence was developed. In the first step, the Suzuki-Miyaura coupling reaction between 3- or 4-nitro bromobenzene and phenyl boronic acid catalysed by 0.47 mol% **2.14** yielded the corresponding 3- or 4-nitrobiphenyl products in virtually quantitative yield after a reaction time of 3 hours at room temperature using a water-ethanol mix as the solvent. Following this, an aqueous solution of 2.5 equivalents of NaBH₄ was added directly into the reaction mixture, and the resulting 3 or 4-aminobiphenyl products were obtained in yields of 91 and 93%, respectively, after stirring for 6 hours. The robustness of the system is reflected in this activity as the reduction of the biaryl nitroarenes occurs smoothly in high yield despite the presence

of borate by-products associated with the initial coupling protocol. Inspection of the literature revealed that this is the first example of a one-pot tandem C-C coupling-hydrogenation sequence that operates at room temperature in an aqueous medium. Although there are two reports of similar sequences, these systems required organic solvent and/or much higher reaction temperatures or catalyst loadings to achieve comparable activity.^{6, 19}

4.4.6 Transfer hydrogenation in flow

Another practical feature of this technology, in line with the principles of green chemistry, is the ability to integrate **2.14** into a continuous flow process as this would increase productivity, enable implementation of reaction modelling, facilitate scale-up, and reduce overall waste accumulation. In collaboration with Leeds University, a continuous process was engineered using **2.14** as catalyst for the transfer hydrogenation of nitrobenzene based on the optimum conditions identified in batch reactions.



Scheme 42: Continuous flow set up for the transfer hydrogenation of nitrobenzene catalysed by **2.14**.

All testing for continuous flow operation was conducted by Adam Clayton under the supervision of Dr Richard Bourne at Leeds University. To achieve this efficiently, it was necessary to adjust the original reaction conditions identified for batch reactions. A 1:1 solution of ethanol and water was required to homogenise the mixture and ensure efficient flow and mixing of the reagents. A 0.2M solution of nitrobenzene in ethanol was mixed with a solution of NaBH₄ dissolved in 1M NaOH(aq) at pH 14, as this has been reported to significantly reduce the rate of hydrolysis of the reducing agent (half-life = 426 days compared to 3.7 seconds at pH 7).²⁰ Additionally, to compensate for the subsequent reduction in reaction rate, the reaction temperature was increased to 60 °C.

In summary, as depicted in Scheme 42, 92 mg of **2.14**, equivalent to 3.81 wt% Pd, was packed with sand inside a 2.5 mL aluminium packed-bed reactor tube. Under the conditions described

above with a resonance time of 12.5 min and flow rate of 0.1 mL min⁻¹ for both reactants, a total yield of 99% was achieved for aniline. Moreover, activity was maintained throughout the study after a total time on line of 250 minutes, corresponding to precisely 20 full reactor volumes, indicating that the catalyst was stable towards deactivation over this period. The overall space-time yield of 0.738 g L⁻¹ min⁻¹ represents a twofold increase in activity compared to that achieved in batch (0.384 g L⁻¹ min⁻¹). Based on these encouraging results, future studies are now underway in collaboration with researchers at Leeds University to extend this to a tandem sequence and employ an automated method for screening of the reaction conditions to more rapidly optimise turnover and sustainability metrics.

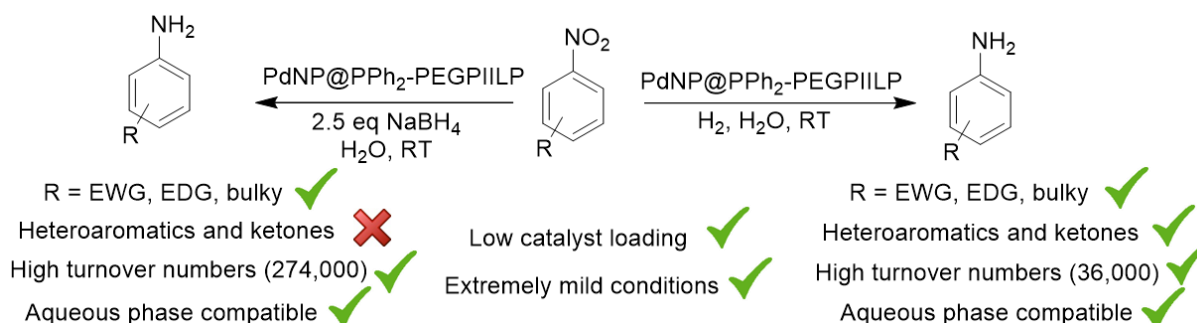
4.5 Conclusion

Two new highly crosslinked PIILP-stabilised PdNP based catalysts **4.6** and **4.7** were fabricated with the aim of improving catalyst performance on the basis that site isolation of the PPh₂ core would limit Pd-P interactions and thus increase surface area available for substrate activation. The increase in crosslinking induced structural changes in the catalysts, which were characterised using various physical analytical techniques. In this regard, ³¹P solid state NMR analysis revealed the presence of uncoordinated phosphine indicating that that site isolation does limit the Pd-P interaction. Following this, TEM analysis of the chemically reduced materials demonstrated that these catalysts consist of larger nanoparticles on comparison with their lightly crosslinked counterparts. However, at this stage further experiments would be required to deduce whether changes in physical properties of the support or electrostatic stabilising interactions govern the kinetics of nanoparticle formation, hence particle size and morphology.

The newly prepared highly crosslinked materials were then tested alongside previously prepared **2.13** and **2.14** for the catalytic hydrogenation and transfer hydrogenation of nitroarenes. Gratifyingly, all the PIILP catalysts were highly active and outperformed commercially available samples of Pd/C. However, intensifying the crosslinking to promote site isolation of the phosphine did not improve catalyst activity as **2.14** outperformed both **4.6** and **4.7** by quite some margin. Although more studies will be required to ascertain the underlying reasons for the observed loss in activity, at this stage is it tentatively attributed to either a reduction in favourable stabilising forces through site isolation of the PPh₂ unit, or that the increased degree of crosslinking imposes mass transport and diffusion limitations on the reaction kinetics. Furthermore, since both highly crosslinked systems appeared similar in

comparison with **2.13** this may suggest that dispersibility is crucial to achieve the best activity. To rationalise this effect, future studies will focus on monitoring the catalyst activity with respect to the degree of site isolation and crosslinking.

Despite this, the optimum system, **2.14**, proved to be remarkably efficient and selective, achieving higher TOFs than any reported systems in the literature. In this respect, despite operating under dissolution control, hydrogenation with molecular H₂ occurred smoothly and efficiently under extremely mild conditions. On this basis, **2.14** may well prove to be a versatile catalyst for the aqueous phase hydrogenation of functionalised aryl and heteroaryl amines in a clean, sustainable and atom efficient manner. Mechanistically, the reaction appears to proceed *via* the direct route as small amounts of *N*-phenylhydroxylamine were observed during the optimisation. Lowering the catalyst loading to 0.001 mol% resulted in a TON of 37,000 corresponding to a TOF of 2466 h⁻¹. The results of recycling studies with **2.14** suggested that a steady state could be reached, although more studies would be required to investigate catalyst lifetime using more appropriate apparatus. Finally, a series of experiments demonstrated that a combination of the phosphine, IL and PEG modifications are crucial for the activity of **2.14**.



Scheme 43: Summary of results for the hydrogenation and transfer hydrogenation of nitroarenes catalysed by **2.14**.

The same systems also catalysed the transfer hydrogenation of nitroarenes using NaBH₄ as the reducing agent proved and near quantitative yields of anilines could be obtained in short reaction times, at room temperature and at remarkably low catalyst loadings. Furthermore, the TOF of 17,125 h⁻¹ obtained with **2.14** appears to be the highest reported to date for this type of transformation. Sampling of the reaction revealed that reduction proceeds primarily *via* the direct route, however, at lower concentration of NaBH₄, the condensation route appears to compete. One drawback of this system is the inability to catalyse the reduction of heteroaromatic nitro compounds. In this respect, poisoning experiments and FD-XAS was used

to probe changes in the surface electronic structure of **2.14** using pyridine as a model heteroaromatic and analysis of the Pd L_{III} edge revealed a decrease in electron density after exposure. This was attributed to displacement of the phosphine by the nitrogen within the aromatic ring and saturation of the surface was considered to be responsible for rendering the catalyst inactive.

Encouraging results were obtained during preliminary studies using a packed bed reactor maintaining continuous flow operation over a period of 250 minutes. A stable profile was reached, and the space-time yield was a significant improvement on that obtained in batch. In addition, **2.14** catalyses tandem Suzuki-Miyaura cross-coupling-nitro reduction to afford biaryl amines in a single-pot protocol and future studies will extend this to further Pd catalysed tandem sequences in batch and continuous flow. This work provides a platform to develop alternative PIILP systems incorporating different metals and/or support functionality in order to diversify the range of transformations and/or tailor the reaction selectivity.

4.6 References

1. M. Takasaki, Y. Motoyama, K. Higashi, S.-H. Yoon, I. Mochida and H. Nagashima, *Org. Lett.*, 2008, **10**, 1601-1604.
2. C. W. Cheung and X. Hu, *Nature Comm.*, 2016, **7**, 12494.
3. A. Saha and B. Ranu, *J. Org. Chem.*, 2008, **73**, 6867-6870.
4. J. Wisniak and M. Klein, *Ind. Eng. Chem.*, 1984, **23**, 44-50.
5. F. Haber, in *Z. Phys. Chem.*, Editon edn., 1900, vol. 32U, p. 193.
6. P. M. Uberman, C. S. Garcia, J. R. Rodriguez and S. E. Martin, *Green Chem.*, 2017, **19**, 739-748.
7. M. Turáková, T. Salmi, K. Eränen, J. Wärnå, D. Y. Murzin and M. Králik, *Appl. Catal. A*, 2015, **499**, 66-76.
8. M. Orlandi, D. Brenna, R. Harms, S. Jost and M. Benaglia, *Org. Proc. Res. Dev.*, 2018, **22**, 430-445.
9. J. Tuteja, S. Nishimura and K. Ebitani, *RSC Adv.*, 2014, **4**, 38241-38249.
10. R. V. Jagadeesh, K. Natte, H. Junge and M. Beller, *ACS Catal.*, 2015, **5**, 1526-1529.
11. R. V. Jagadeesh, A.-E. Surkus, H. Junge, M.-M. Pohl, J. Radnik, J. Rabeah, H. Huan, V. Schünemann, A. Brückner and M. Beller, *Science*, 2013, **342**, 1073-1076.
12. X. Gao, G. Xu, Y. Zhao, S. Li, F. Shi and Y. Chen, *RSC Adv.*, 2015, **5**, 88045-88051.
13. S. Zhang, C.-R. Chang, Z.-Q. Huang, J. Li, Z. Wu, Y. Ma, Z. Zhang, Y. Wang and Y. Qu, *J. Am. Chem. Soc.*, 2016, **138**, 2629-2637.
14. J. Feng, S. Handa, F. Gallou and B. H. Lipshutz, *Angew. Chem. Int. Ed.*, 2016, **55**, 8979-8983.
15. B. H. Lipshutz, S. Ghorai, A. R. Abela, R. Moser, T. Nishikata, C. Duplais, A. Krasovskiy, R. D. Gaston and R. C. Gadwood, *J. Org. Chem.*, 2011, **76**, 4379-4391.
16. T. Iwai, T. Harada, K. Hara and M. Sawamura, *Angew. Chem. Int. Ed.*, 2013, **52**, 12322-12326.

17. C. Wang, R. Ciganda, L. Salmon, D. Gregurec, J. Irigoyen, S. Moya, J. Ruiz and D. Astruc, *Angew. Chem. Int. Ed.*, 2016, **55**, 3091-3095.
18. H. Pang, F. Gallou, H. Sohn, J. Camacho-Bunquin, M. Delferro and B. H. Lipshutz, *Green Chem.*, 2018, **20**, 130-135.
19. A. Kumar, K. Purkait, S. K. Dey, A. Sarkar and A. Mukherjee, *RSC Adv.*, 2014, **4**, 35233-35237.
20. R. Retnamma, A. Q. Novais and C. M. Rangel, *Int. J. Hydrogen Energy*, 2011, **36**, 9772-9790.

Chapter 5 : Synthesis of PIILP stabilised gold nanoparticles and application in the selective reduction of nitroarenes

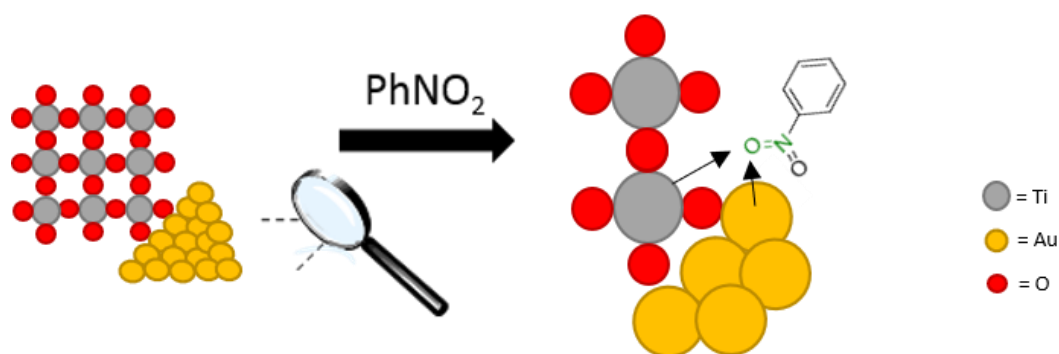
5.1 Introduction

Reports documenting the applications of gold nanoparticles in catalysis have exponentially increased over the past decade as improvements in nanotechnology has highlighted the remarkable properties of nanoscale gold clusters.¹ Despite accessibility of its various oxidation states, gold was for many years considered catalytically inert due to the high stability of its metallic state, and was thought to be virtually inactive with regards to activation of molecular hydrogen or oxygen.² However, the evidence of several detailed DFT studies now suggest that the 'low frequency-factor' of catalytically active species on the surface due to slow H₂ dissociation is rate-limiting, rather than an inaccessible H₂ activation barrier. This effect is derived from only partial filling of the *d*-band at moderate temperatures thus, only a low concentration H₂ is ever present on the particle surface. Furthermore, studies have shown that in contrast to other precious metals, the H₂ activation capacity of gold increases in response to increases in temperature.³

In this regard, the tuneable reactivity and rates of substrate activation of heterogeneous gold nanoparticle (AuNP) catalysts lies in the synergistic interactions between the unique nature of the metal with the support and reaction media.⁴ As a result, unprecedented enhancements in selectivity compared to conventional Pd, Pt and Ru based catalysts have been obtained, which has presented a platform for the development of new and sustainable catalyst technology. For example, Dupont and co-workers recently reported that three different distinct H₂ activation pathways over AuNPs are accessible dependant on the nature of the metal-support interaction.⁵ H₂ cleavage occurs heterolytically over 'naked' AuNPs as a result of cooperative behaviour between the particles and the oxide support. However, in contrast, the addition of an IL layer disrupted the metal-support interactions and promoted homolytic cleavage and enabled substrate discrimination in the partial hydrogenation of model unsaturated aldehydes, yielding highly selective AuNP catalysts that outperformed other group 8-10 metals. For example, AuNPs supported on a γ -Al₂O₃-IL hybrids prepared *via* reaction of the support with 1-*n*-butyl-3-(trimethoxysilylpropyl)imidazolium chloride catalysed the selective hydrogenation of cyclohexenone to cyclohexanone with 99% selectivity.

One of the most studied model transformations of AuNP based catalysts is the reduction of nitroarenes. Whilst Pd catalysts are the conventional choice, a host of supported AuNP based

systems have been reported as efficient and highly selective catalysts for this reduction. For example, Wang *et al.* developed a novel method to support AuNPs on the ‘edges’ of TiO₂, (Scheme 44).⁶ This provided a unique adsorption mode for the nitro substituent on the gold surface and high chemoselectivity over other sensitive functional groups was obtained with TOFs up to 279 h⁻¹ for the production of anilines under mild conditions. Additionally, nanocrystalline MgO supported AuNPs proved to be a highly selective catalyst for the reduction of nitroarenes to anilines in the presence of other reducible functionality without the need for additional promoters.⁷

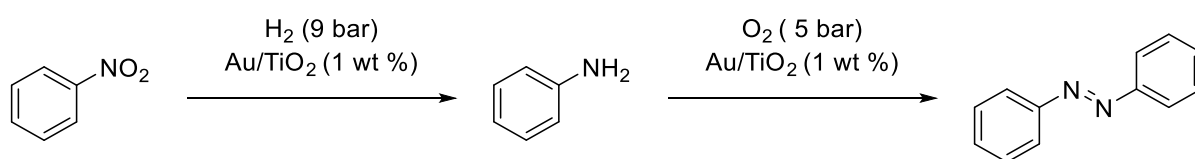


Scheme 44: Schematic representation of AuNPs supported on anatase edges for the chemoselective hydrogenation of nitroarenes.

In order to efficiently optimise catalyst systems, clearly it would be useful to gain insight into the reaction mechanism, enabling a ‘bottom up’ approach to catalyst optimisation. As discussed in Chapter 4, there are several proposals for the mechanism of metal catalysed nitroarene reduction, however, ultimately there is no general consensus. Systematic and kinetic analysis conducted by Lu *et al.* demonstrated that the Au-SiO₂ catalysed reduction of nitrobenzene proceeds *via* the direct route.⁸ *In-situ* IR analysis revealed the presence of *N*-phenylhydroxylamine in the mixture and independent studies on the Au-SiO₂ catalysed reduction of azoxybenzene ruled out the condensation route. Similarly, Corma employed *in-situ* IR techniques in combination with macrokinetic experiments which led to the proposal of a novel reaction sequence for the titanium oxide-supported AuNP-catalysed reduction of nitroarenes.⁹ A series of batch reactions were conducted and analysis of the reaction mixture revealed that aniline was the sole product in solution. Whilst this provided no insight into the true mechanism, time-resolved IR spectroscopy revealed the presence of nitrosobenzene and *N*-phenylhydroxylamine on the surface. Furthermore, using a feed of nitrosobenzene as the

reactant, azoxybenzene was the only species present in solution, suggesting that its reduction to aniline is extremely slow, further confirming that the direct route is favoured.

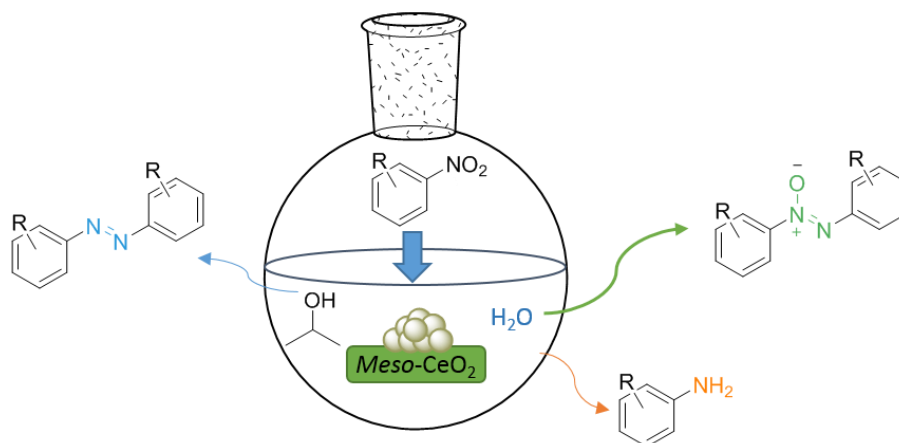
Being one of the most fundamental catalytic transformations in organic chemistry, the production of functionalised anilines via metal catalysed hydrogenation of nitroarenes is now well documented.² However, unsurprisingly, reports documenting the more challenging task of selective partial reduction of nitroarenes to the corresponding hydroxylamine or azoxy-based intermediates are limited. The use of various additives to promote poisoning of the catalyst has been demonstrated to modulate selectivity, however, this method often requires toxic reagents and can severely hamper catalyst turnover. For example, manipulation of the surface electronics of Pt nanowires using an ethylenediamine coating enabled the selective reduction of nitroarenes to industrially relevant hydroxylamines to occur under ambient conditions.¹⁰ However, despite selectivity enhancements, the catalyst exhibited reduced activity on comparison with unmodified Pt black. In an alternative approach, Corma *et al.* used a two-step one-pot reaction sequence.¹¹ In this strategy, AuNPs supported on TiO₂ catalysed the reduction of nitroarenes to the corresponding anilines, which were subsequently aerobically oxidised to the corresponding azo-based compounds. The amino group itself acted as a reservoir of electrons, and simultaneous activation of oxygen on the gold surface facilitated the oxidation. However, harsh reaction conditions (100°C, 5 bar O₂ pressure), use of organic solvent and high catalyst loadings may limit the applicability of the process on an industrial scale.



Scheme 45: Two-step one-pot method for obtaining azoxybenzene with an Au/TiO₂ catalyst.

Therefore, to maximise efficiency and reduce additional processing steps, the ideal catalyst would be a robust and recyclable system that is highly selective toward the desired product using only a single reaction step whilst operating under well-defined conditions. However, for the partial reduction of nitroarenes, this can be challenging due to the intrinsic instability of the products under the reaction conditions, as they are thermally sensitive. Based on the catalytic properties and surface plasmon resonance (SPR) effects exhibited by AuNPs, Zhu and co-workers facilitated selective and direct photo catalytic reduction of nitroarenes to the

corresponding azoxy intermediates at room temperature using AuNPs supported on a ZrO_2 semiconductor.¹² On irradiation, the AuNPs are able to harvest significant amounts of UV absorption causing excitation of the abundant conduction electrons at the AuNP surface, which in turn provides a source of electrons to drive the reduction of the nitroarene. This technique allows the reaction to proceed efficiently at room temperature, preventing thermal degradation of the intermediates and as a result, quantitative yields of azoxy intermediate were obtained. However, the extensive set-up required for photocatalytic reductions may impair the scalability of this protocol. More recently, Cao and co-workers demonstrated that fine-tuning of the reaction media can promote switchable catalytic behaviour of AuNPs supported on *meso*-structured ceria ($\text{Au}/\text{meso-CeO}_2$).¹³ Moreover, the reactions can be conducted in a more operationally simplistic manner using mild 'green' conditions. A range of substituted azoxybenzenes were obtained from the corresponding nitroarenes in excellent yield (90-100%) in a 5:1 isopropanol/water mixture under mild conditions. Moreover, the composition of the reaction medium had a dramatic effect on the reduction such that further reduction to azobenzenes could be obtained using a 1:1 isopropanol/water mixture. Furthermore, full reduction to the aniline could also be obtained by increasing the temperature to 90°C and removing the base additives; under these conditions yields between 91-99% were obtained.



Scheme 46: Three possible products obtainable from the reduction of substituted nitrobenzenes over mesoporous ceria supported AuNPs.

Whilst the ability to recover three different target products using a single catalyst system represents a significant achievement, long reaction times (10 hours), high catalyst loadings (cat/substrate ratio = 1:100) and requirement for basic additives limits the overall practicality and atom efficiency of this process.

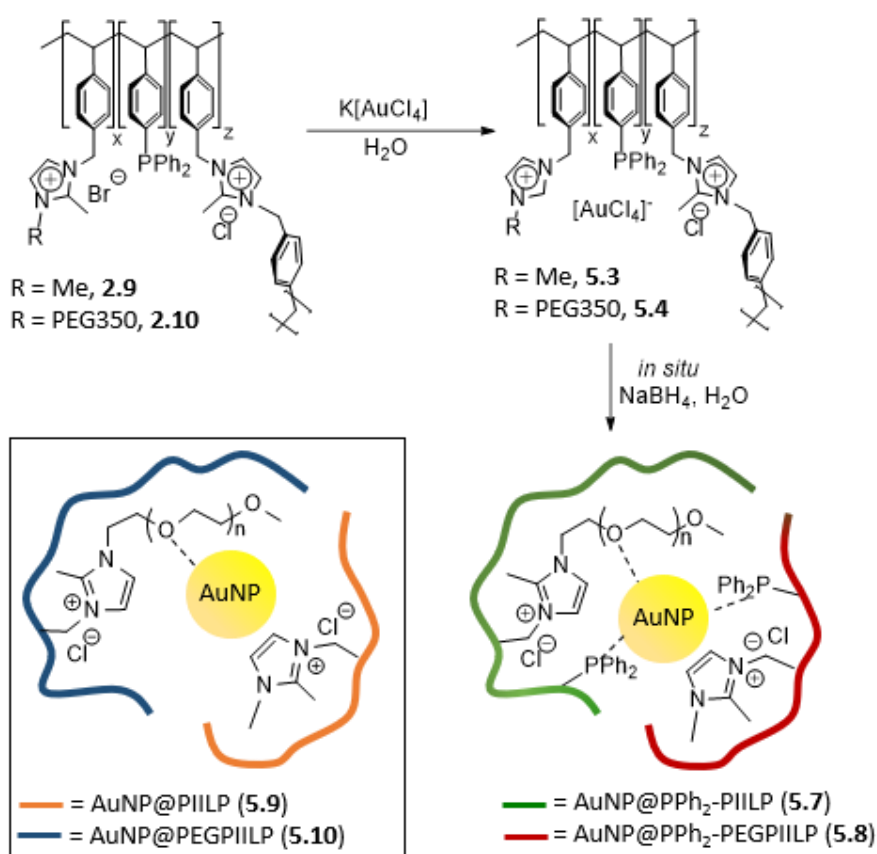
Lykakis *et al.* found that AuNPs supported on mesoporous titania (AuNP/MTA) catalysed the partial reduction of nitro compounds to hydroxylamines, however, the substrate scope was severely limited, as only aromatic carbonyl or aliphatic hydroxylamines were recovered.¹⁴ The group later demonstrated that activation of ammonia-borane complexes with AuNPs/MTA enabled the partial reduction of a wide range of nitroarenes to hydroxylamines to occur in short reaction times,¹⁵ however, a high catalyst loading was required to achieve reasonable yields (substrate/catalyst ratio = 1:25).

Based on the select examples discussed, the activity and selectivity of AuNP based catalysts is extremely sensitive to the surrounding environment. In this regard, it may be possible to utilise the unique properties of AuNPs and develop innovative and tuneable catalyst technology to enable various nitro-based intermediates to be obtained selectively using a single catalyst system by carefully modulating the reaction conditions. Such a system would represent a significant step towards optimising and improving the economic potential of industrial processes in a sustainable manner. Results presented in this thesis so far have demonstrated that using the concept of PIILP catalysis, the favourable attributes of ILs such as their ability to stabilise NPs, ability to enhance reaction rate and improve selectivity may be upheld - even in catalytic quantities without loss of the IL. Introduction of the PEG functionality has been shown to enhance activity, selectivity and recyclability. Furthermore, simple synthetic modification of the styrene backbone with heteroatom donors can also improve catalyst performance utilising the strong covalent interaction of the donor to the metal surface. While initially employed to provide additional stabilisation and prolong catalyst lifetime under reaction conditions, the results presented so far suggest that the incorporation of a phosphine donor may also modulate the surface electronic structure and influence selectivity. In this regard, a judicious choice of the support functionality in PIILP may enable some degree of control over particle nucleation or surface electron density, and thereby allow the size and morphology to be controlled and catalyst selectivity to be optimised. Thus, the aim of this project was to prepare and examine the efficacy of PIILP stabilised AuNP-based catalysts for the selective reduction of nitroarenes on the basis that the nature of the particles i.e. differences in electronic composition of the metallic state in comparison with PIILP-stabilised PdNPs may give differences in catalyst activity and/or selectivity.

5.2 Results and Discussion

5.2.1 Catalyst synthesis and characterisation

The general synthetic route and relative compositions of the polymers, catalyst precursors and corresponding PIILP stabilised AuNPs prepared in this study are shown in Scheme 47. The tetrachloroaurate loaded catalyst precursors were synthesised by impregnation of previously prepared supports; PPh₂-PIILP (**2.9**), PPh₂-PEGPIILP (**2.10**), PIILP (**5.1**), and PEGPIILP (**5.2**) with potassium tetrachloroaurate, *via* the addition of an aqueous solution of K[AuCl₄] to a suspension of the polymer in water. These supports were chosen to determine the influence that the various modifications have on the catalyst activity and selectivity. After stirring for 6 hours, filtering, washing and drying, precatalysts **5.3**, **5.4**, **5.5** and **5.6** were obtained as yellow powders in good yields.



Scheme 47: Composition of polymers **2.9** and **2.10**, preparation of [AuCl₄]⁻ loaded catalyst precursors and PIILP-stabilised AuNPs.

Having successfully isolated the precatalysts, ICP-OES analysis was used to determine the respective gold loadings which are presented in Table 24. As seen throughout, lower metal loadings were obtained with the PEGylated supports likely due to the increase in solvent absorption.

Table 24: Gold loading of PIILP catalysts as determined by ICP-OES.

| Entry | Catalyst | mmol Au/ g PIILP | Au wt% |
|-------|--|---------------------|--------|
| 1 | [AuCl ₄]Cl@PPh ₂ -PIILP (5.3) | 0.16 | 3.1 |
| 2 | [AuCl ₄]Cl @PPh ₂ -PEGPIILP (5.4) | 0.037 | 0.73 |
| 3 | [AuCl ₄]Cl @PIILP (5.5) | 0.128 | 2.5 |
| 4 | [AuCl ₄]Cl @PEGPIILP (5.6) | 0.080 | 1.6 |

A Au-P interaction between the support and the immobilised gold precursor was detected using ³¹P solid state NMR spectroscopy for phosphine-functionalised **5.3** and **5.4**. The downfield shift from δ -5 and -10.4 ppm to δ 27.1 and 24.5 ppm is similar to those obtained in related Pd systems and is consistent with coordination of the phosphine to the gold surface.¹⁶ The absence of peaks corresponding to the starting material confirmed that all the phosphine is coordinated to the metal.

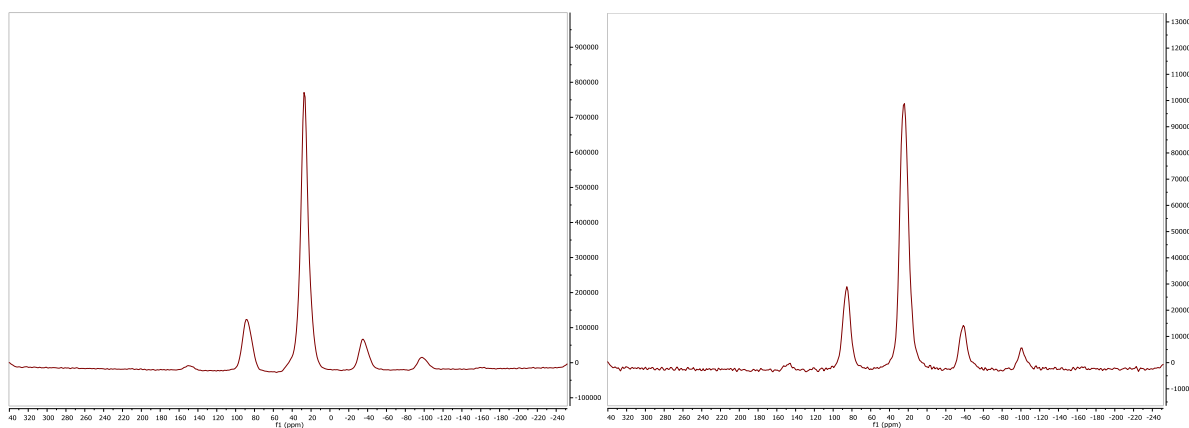


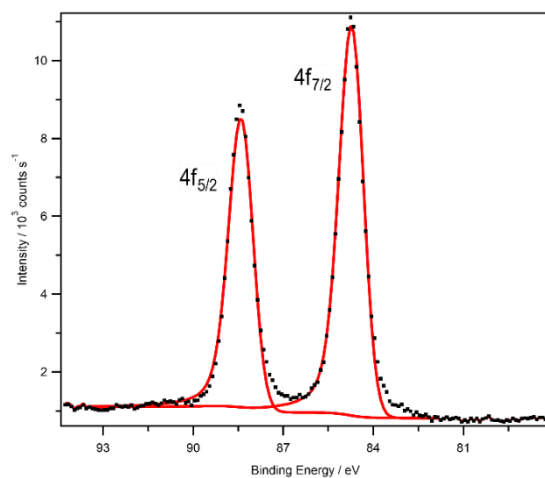
Figure 53: ³¹P Solid state NMR spectra of 5.3 (left) and 5.4 (right).

Given that in Chapter 4, PdNPs generated *in situ* by reduction of the [PdCl₄]²⁻ loaded precursors with NaBH₄ were equally as efficient as the corresponding *ex situ* prepared catalysts, precursors **5.3**, **5.4**, **5.5** and **5.6** were used directly for catalyst optimisation studies. However, to compare how the polymer composition influences the properties of the respective AuNPs, samples of the corresponding AuNP@PIILP catalysts, **5.7-5.10** were

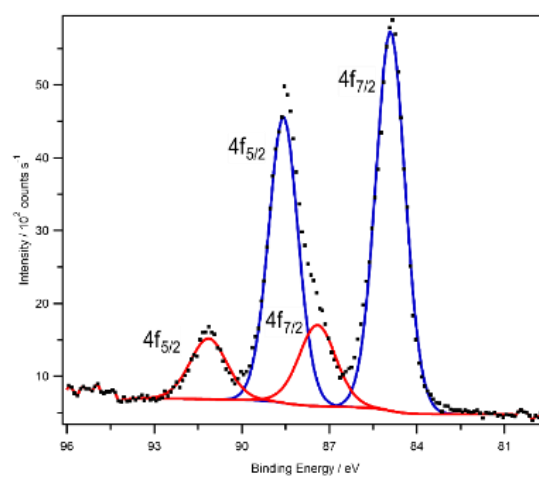
generated under pseudo reaction conditions to obtain XPS and TEM data that would be more representative of the active species.

XPS analysis of the tetrachloroaurate-loaded precursors revealed that **5.4**, **5.5** and **5.6** contain two different Au oxidation states (Figure 54). The Au 4f_{7/2} binding energies of 87.4-87.6 eV (Table 25 entries 2-4) are consistent with the presence of the Au³⁺.¹⁷ The Au 4f_{7/2} doublets shifted to lower binding energies in the region of 84.7-85 eV (entries 1-4) are assigned to the presence of a Au^(I) species as a result of decomposition caused by excessive exposure to the X-ray source.¹⁸ This theory was further supported by analysis of the N1s region, which showed evidence of the imidazolium signals as well as signals at lower binding energies attributed to neutral and anionic nitrogen species as a result of such damage (available in the appendix A47-63).¹⁹ Interestingly, the spectrum for **5.3** contains a single resonance associated with the Au^(I) oxidation state, indicating that the [AuCl₄]⁻ precursor had fully decomposed during acquisition. The XPS spectra of the chemically reduced catalysts indicate these compounds consist of a single Au environment (Figure 55) and the shift in the Au 4f_{7/2} doublets to lower binding energies of 83.7-83.8 eV is indicative of metallic Au (entries 5-8).²⁰ Seemingly, there is no evidence for the Au-P interactions previously identified by ³¹P solid-state NMR spectroscopy as the binding energies corresponding to Au^(III) or Au⁽⁰⁾ were similar for all the systems (see appendix A47-A63).

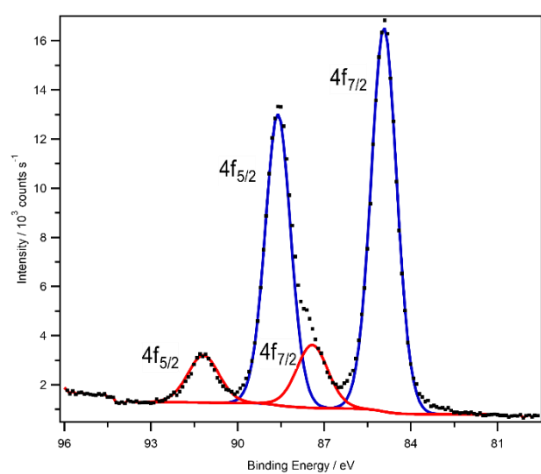
(a) 5.3



(b) 5.4



(c) 5.5



(d) 5.6

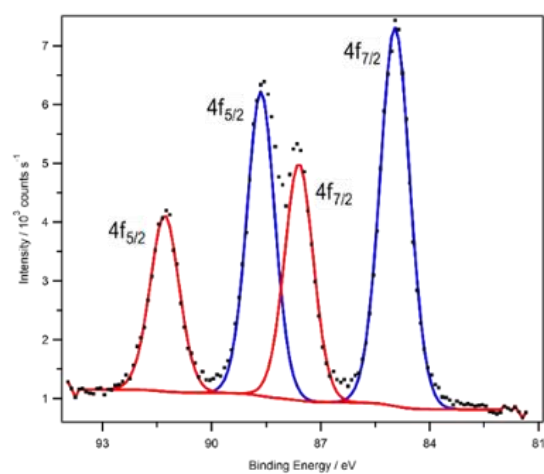


Figure 54: Au 4f core level XPS spectra for $[\text{AuCl}_4]\text{Cl}@P\text{Ph}_2\text{-PIILP}$ (a), $[\text{AuCl}_4]\text{Cl}@P\text{Ph}_2\text{-PEGPIILP}$ (b), $[\text{AuCl}_4]\text{Cl}@PIILP$ (c), $[\text{AuCl}_4]\text{Cl}@PEGPIILP$ (d) all referenced to the C 1s alkyl peak at 284.8 eV.

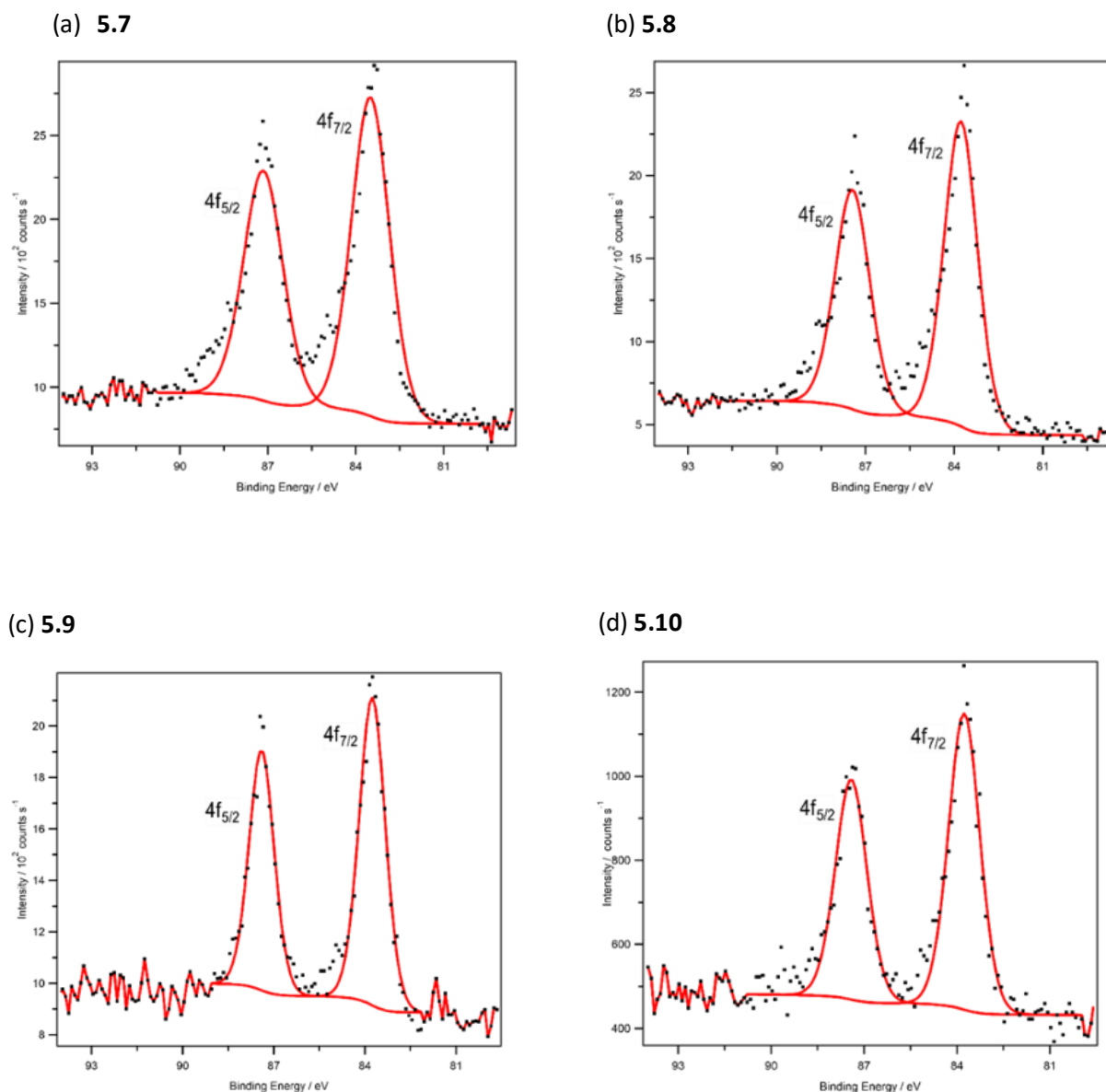


Figure 55: Au 4f core level XPS spectra for AuNP@PPh₂-PIILP (a), AuNP@PPh₂-PEGPIILP (b), AuNP@PIILP (c), AuNP@PEGPIILP (d) all referenced to the C 1s alkyl peak at 284.8 eV.

Table 25: Au 4f core level binding energies for [AuCl₄]⁻ loaded precursors and reduced catalysts relative to the C1s alkyl peak at 248.8 eV.

| Entry ^a | Catalyst | Au 4f _{5/2} (eV) | Au 4f _{7/2} (eV) | Difference (eV) |
|--------------------|----------|------------------------------|---------------------------|--------------------|
| 1 | 5.3 | 88.4 | 84.7 | 3.7 |
| 2 | 5.4 | 91.1/88.6 | 87.4/84.9 | 3.5 |
| 3 | 5.5 | 91.2/88.6 | 87.4/84.9 | 3.7 |

| | | | | |
|----------|-------------|-----------|-----------|-----|
| 4 | 5.6 | 91.3/88.6 | 87.6/85.0 | 3.7 |
| 5 | 5.7 | 87.4 | 83.7 | 3.6 |
| 6 | 5.8 | 87.4 | 83.8 | 3.7 |
| 7 | 5.9 | 87.4 | 83.8 | 3.6 |
| 8 | 5.10 | 87.4 | 83.8 | 3.6 |

TEM micrographs of **5.7** and **5.8** obtained from *in situ* reduction of the corresponding $[\text{AuCl}_4]^-$ loaded precursors confirmed the presence of near-monodisperse AuNPs with average particle sizes of 3.4 ± 0.9 and 2.5 ± 0.6 nm, respectively (Figure S6). These values are similar to those of PIILP-supported PdNPs presented earlier which follow the same trend, as the PEGylated catalyst consisted of proportionately smaller NPs. Thus, it appears that the number of and nature of the heteroatom donor does influence the particle size. However, the data does not differentiate as to whether the disparate sizes are a result of additional stabilising interactions preventing agglomeration, or differences in relative dispersion which may alter the relative kinetics of NP growth. For comparison, **5.9** and **5.10** consist of particles with mean diameters of 3.4 ± 1.1 and 3.3 ± 0.9 nm, respectively, which are essentially the same as **5.7** (appendix A62 and 64). Whilst unexpected, this result may help rationalise differences in catalyst performance solely as a result of the Au-support interaction.

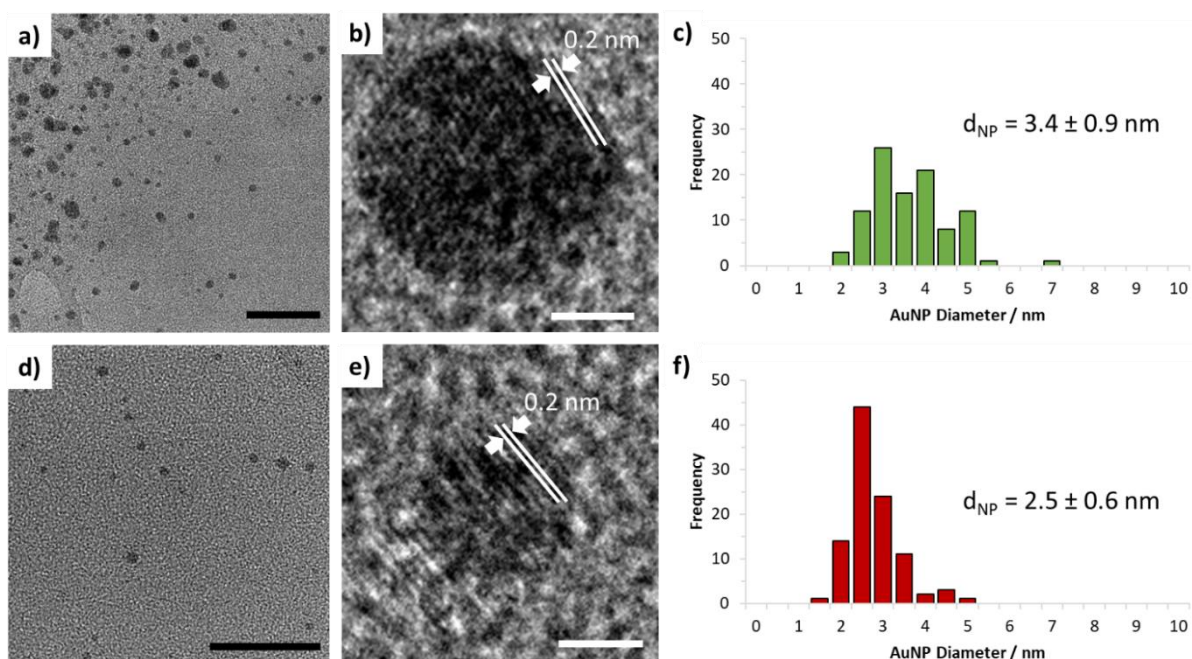


Figure 56: HRTEM micrographs with the observed atomic spacing (parallel white lines confirming the presence of metallic Au) of **5.7** (a-b) and **5.8** (d-e), and the associated particle size distributions based on >100 particles. Scale bars are 25 nm (black) and 1 nm (white).

As discussed earlier, AuNPs tend to be highly sensitive to the local environment. The surface plasmon resonance (SPR) absorption for AuNPs has been shown to depend on many factors including the morphology of the particle itself, as well as the dielectric constant of the medium.²¹ The strong SPR bands of the two phosphine-modified catalysts **5.7** and **5.8** were found at 519 nm while λ_{max} for **5.9** was found at 517 nm, which is consistent with the formation of spherical particles.²² Interestingly, the value of λ_{max} for **5.10** was red shifted to 525 nm. For PIIL stabilised AuNPs, the polymer support would influence the nature of the AuNP surface electronics, and the resultant marked difference in λ_{max} for **5.10** may well be due to differences in the metal-support interactions, as **5.10** is the only system without a heteroatom donor. Moreover, the differences in λ_{max} do not reflect the average NP sizes as evidenced by TEM analysis as **5.7**, **5.9**, and **5.10** were morphologically identical, further highlighting the influence of the metal-support interactions.

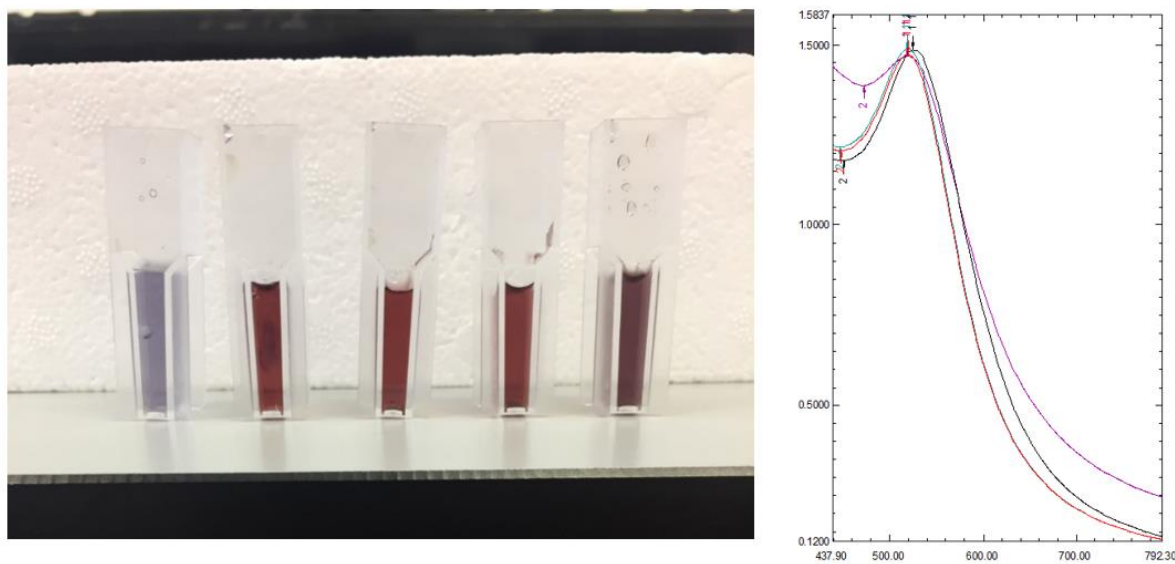
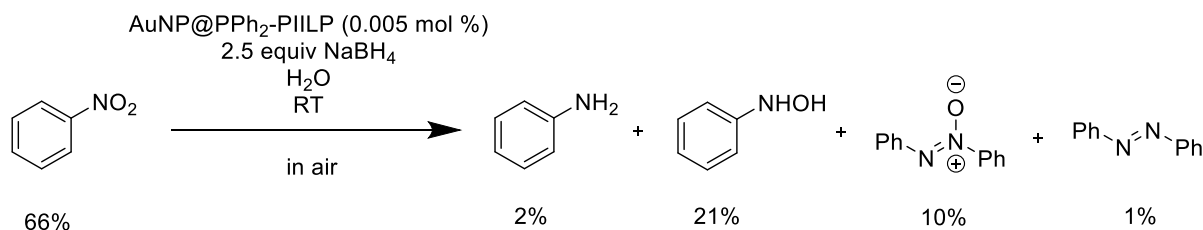


Figure 57: Left: Aqueous solution containing AuNPs left to right: AuNP@Citrate, AuNP@PPh₂-PEGPIILP, AuNP@PPh₂-PIILP, AuNP@PEGPIILP, AuNP@PIILP. Right: combined UV-vis spectra.

5.3 Initial optimisation

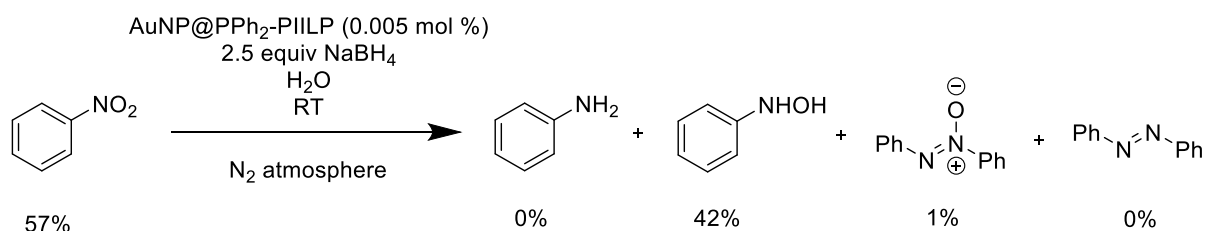
Preliminary studies were conducted following the protocol developed for the PIILP-stabilised PdNP-catalysed transfer hydrogenation of nitroarenes discussed in Chapter 4 as a lead. The reduction of nitrobenzene catalysed by 0.005 mol % of AuNP@PPh₂-PIILP (**5.7**) generated *in situ* from **5.3**, was conducted at room temperature in water using 2.5 equivalents of NaBH₄ as the reducing agent. Analysis of the post reaction mixture after a reaction time of 40 minutes revealed only 34% conversion and only trace amounts (2%) of aniline (AN). Interestingly, the major species was identified as *N*-phenylhydroxylamine (NPHA) which represented 21% of the mixture, corresponding to 62% selectivity. The remainder of the reaction mixture comprised of 10% azoxybenzene (AXB) and a trace amount (1%) of the further reduction product azobenzene (AZB).



Scheme 48: Product distribution for the transfer hydrogenation of nitrobenzene catalysed by **5.7** in air.

This initial observation highlights an intrinsic fundamental difference in reaction kinetics of PIILP-stabilised AuNPs compared with their Pd counterparts, as under these conditions the reduction of NPHA to AN is markedly slower, allowing the accumulation of NPHA. Given that

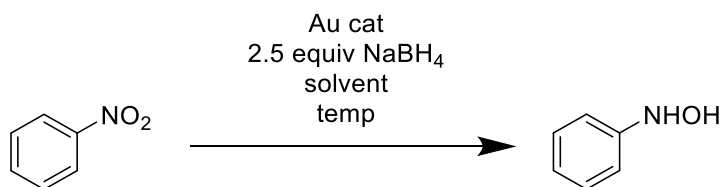
the reduction of nitrosobenzene to NPHA was extremely fast, the presence of substantial amounts of condensation products was not anticipated. In this regard, speculating that the reduction of nitrosobenzene to NPHA may be reversible in air, which would provide a pathway to condensation products, the reaction was then performed under the same conditions but under a nitrogen atmosphere.



Scheme 49: Product distribution for the transfer hydrogenation of nitrobenzene catalysed by 5.7 under an N_2 atmosphere.

Interestingly, the exclusion of atmospheric air resulted in a remarkable improvement as selectivity for NPHA increased dramatically to 97% and the conversion increased to 43%. Furthermore, extending the reaction time to 2 hours gave 100% conversion with 96% selectivity for NPHA with small amounts of aniline as the only by-product. This observation is completely unprecedented given the low stability of NPHA under reductive conditions. This result also indicates that the formation of condensation products is likely derived from oxidation of NPHA and that under nitrogen the reaction is no longer reversible, hence condensation is virtually suppressed. Moreover, exposing the post reaction mixture to air and monitoring the composition of the solution over time using 1H NMR spectroscopy revealed an increase in the relative concentration of azoxybenzene at the expense of NPHA, further supporting this theory.

Table 26: Optimisation of the reaction conditions for the Au catalysed reduction of nitrobenzene.



| Entry ^a | Catalyst | Mol % | Solvent | Temp (°C) | Time (min) | Conversion (%) ^b | Selectivity (%) ^b |
|--------------------|----------|-------|--------------------------|--------------|---------------|--------------------------------|---------------------------------|
| 1 | 5.7 | 0.005 | water | 25 | 40 | 43 | 97 |
| 2 | 5.7 | 0.005 | EtOH | 25 | 40 | 32 | 100 ^c |
| 3 | 5.7 | 0.005 | EtOH/H ₂ O | 25 | 40 | 34 | 92 |
| 4 | 5.7 | 0.005 | 2-MeTHF | 25 | 40 | 1 | 100 |
| 5 | 5.7 | 0.005 | 2-MeTHF/H ₂ O | 25 | 40 | 17 | 98 |
| 6 | 5.7 | 0.005 | water | 50 | 40 | 100 | 83 |
| 7 | 5.7 | 0.025 | water | 25 | 40 | 81 | 92 |

^aReaction conditions: 1 mmol nitrobenzene, catalyst, 2 mL solvent, temperature, time, 2.5 mmol NaBH₄. ^b Conversion and selectivity determined using ¹H NMR spectroscopy using dioxane as the internal standard, average of at least three runs. ^c Selectivity for azoxybenzene.

A survey of the reaction solvent revealed that water is the best solvent for optimum performance as activity and selectivity decreased significantly using 2-methyltetrahydrofuran, a 1:1 ethanol/water mixture or a 1:1 mixture of 2-methyltetrahydrofuran/water (Table 26, entries 3-5). Interestingly, switching the solvent to ethanol resulted in a complete change in reaction selectivity as azoxybenzene was obtained as the sole product (*vide infra*) in 32% conversion (entry 2). Increasing the reaction temperature resulted in an increase in conversion accompanied with a marked drop in selectivity for NPHA due to the formation of aniline (entry 6). Analysis of the post reaction mixture showed that aniline was the major by-product (14%) together with trace amounts of AZB (2%). This result indicates that the energy barrier for the reduction of NPHA under these conditions is significantly higher than that for the formation of NPHA itself, which reflects the high selectivity achieved by conducting the reaction at room temperature. Furthermore, whilst an increase in the catalyst loading to 0.025 mol% enhanced

the reaction rate, increasing amounts of aniline formed which lowered the selectivity (entry 7).

As activity for the PdNP@R-PIILP catalysed reduction of nitroarenes proved to be partially dependant on the NaBH₄:substrate ratio, the reduction of nitrobenzene catalysed by **5.7** was monitored as a function of NaBH₄ equivalents. The plot in Figure 58 shows that conversion dropped significantly to 9% on lowering the NaBH₄:substrate ratio to 1:1, while conversions increased linearly before reaching a plateau at 15 equivalents. As for the Pd systems, this profile indicates that the reaction is mass transfer-limited with regards to the reducing agent. However, the overall turnover is still likely to be mass transfer-limited given the limited solubility of the substrate. Therefore, to improve atom efficiency and reduce waste, 2.5 equivalents was chosen as the best compromise, as high conversions and selectivity could be achieved in relatively short reaction times.

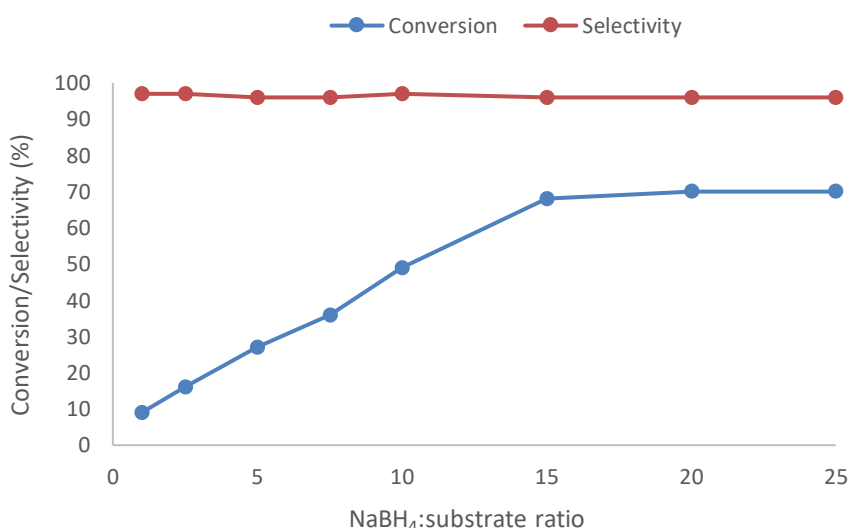
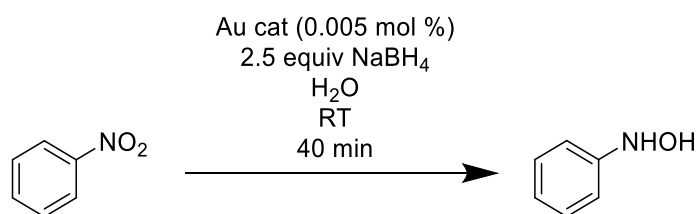


Figure 58: Reaction profile as a function of the NaBH₄:substrate ratio for the transfer hydrogenation of nitrobenzene catalysed by **5.7**. Reaction conditions: 1 mmol nitrobenzene, 0.005 mol% **5.7**, 2 mL water, RT, reaction time = 30 mins. Conversion and selectivity determined using ¹H NMR spectroscopy using dioxane as the internal standard. Selectivity for *N*-phenylhydroxylamine = [% *N*-phenylhydroxylamine / (% *N*-phenylhydroxylamine + % aniline + % azoxybenzene + % azobenzene)]. Average of three runs.

5.3.1 Comparative catalyst testing

Having identified optimum conditions, comparative catalyst testing was conducted to examine the influence of the PEG and phosphine modifications which have previously proved crucial for activity and selectivity. A series of reactions were performed under the conditions described above but for a reduced reaction time of 40 minutes to enable differences in catalyst performance to be more easily identified and quantified.

Table 27: Comparison catalyst testing for the reduction of nitrobenzene to *N*-phenylhydroxylamine.



| Entry ^a | Catalyst | Mol % | Solvent | Temp (°C) | Time (min) | Conversion (%) ^b | Selectivity (%) ^b |
|--------------------|--------------|-------|---------|--------------|---------------|--------------------------------|---------------------------------|
| 1 | 5.7 | 0.005 | water | 25 | 40 | 43 | 97 |
| 2 | 5.8 | 0.005 | water | 25 | 40 | 100 | 100 |
| 3 | 5.9 | 0.005 | water | 25 | 40 | 27 | 97 |
| 4 | 5.10 | 0.005 | water | 25 | 40 | 55 | 96 |
| 5 | AuNP@Citrate | 0.005 | water | 25 | 40 | 23 | 83 |

^aReaction conditions: 1 mmol substrate, catalyst, 2.5 mmol NaBH₄, 2 mL water, RT, reaction time = 40 mins. ^b Conversion and selectivity determined using ¹H NMR spectroscopy using dioxane as the internal standard, average of at least three runs. Selectivity for *N*-phenylhydroxylamine = [% *N*-phenylhydroxylamine / (% *N*-phenylhydroxylamine + % aniline + % azoxybenzene + % azobenzene)].

Integrating the PEG moiety into the support resulted in a remarkable improvement in performance such that quantitative amounts of *N*-phenylhydroxylamine were obtained after a reaction time of only 40 minutes (entry 2). In addition to the smaller NPs, this marked improvement in activity may also attributed to the dispersive effects of the hydrophilic chain which would improve access to the active site in aqueous solution. The origin of the improvement in selectivity is more challenging to rationalise but may be associated with the additional electronic interactions between the oxygen donors in the PEG chain which would surround the AuNP surface, causing alterations in the relative reaction barriers. Alternatively, the reactivity could also be governed by the disparate dispersibilities, hence accessibility of the respective active sites of **5.7** and **5.8**, which would consequently drastically alter the reaction kinetics. Removal of the PPh₂ from **5.7** resulted in a significant drop in activity as the reaction catalysed by AuNP@PIILP, **5.9**, gave 27% conversion and 97% selectivity (entry 3). Similarly, removal of the PPh₂ modification from **5.8** also resulted in a dramatic drop in conversion from 100% to 55% (entry 4). Interestingly, the advantages of the PEG modification

are also reflected in the relative performances of **5.9** and **5.10** as, despite consisting of similar average particle sizes (3.4 ± 1.1 and 3.3 ± 0.9 nm, respectively), the conversion of 55% obtained with **5.10** was double that of 27% obtained with **5.9**. The favourable stabilising and rate-enhancing effects of the PIILP supports were investigated with comparative testing against AuNPs generated *in situ* by reduction of potassium tetrachloroaurate with sodium citrate (entry 5). Under otherwise identical conditions, the reaction catalysed by AuNP@Citrate gave a conversion of only 23% and a markedly lower selectivity of 83% due to the formation of azoxybenzene (2%) and aniline (2%).

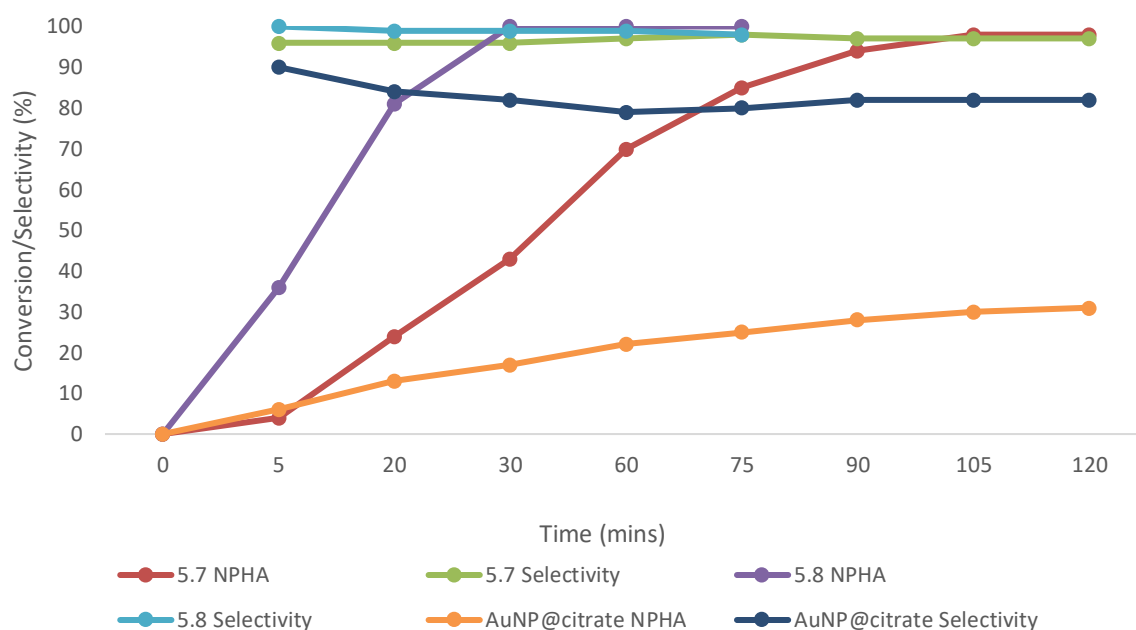


Figure 59: Time-composition profile for the reduction of nitrobenzene to *N*-phenylhydroxylamine catalysed by **5.7**, **5.8** and AuNP@Citrate. Reaction conditions: 1 mmol nitrobenzene, 2.5 mmol NaBH₄, 0.005 mol% catalyst, 2 mL water, RT. Conversion and selectivity determined using ¹H NMR spectroscopy with dioxane as the internal standard. Selectivity for *N*-phenylhydroxylamine = [% *N*-phenylhydroxylamine / (% *N*-phenylhydroxylamine + % aniline + % azoxybenzene + % azobenzene)].

The comparative time-conversion profile for the reduction of nitrobenzene catalysed by **5.7**, **5.8** and AuNP@Citrate highlights the marked differences in the rates of formation of *N*-phenylhydroxylamine. The efficiency of **5.8** was further demonstrated as a reduction in the catalyst loading to 0.0002 mol % afforded NPHA as the sole product in 22% conversion after 90 minutes, which corresponds to a TON of 110,000 and a TOF of 73,000 h⁻¹. This is probably more representative of the true activity, as reducing the catalyst loading by a further 50% resulted in a negligible increase in TON to 112,000. While there are many nanoparticle-based systems that catalyse the reduction of nitroarenes, reports documenting the selective production of *N*-arylhydroxylamines are extremely scarce. These few systems include titania

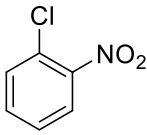
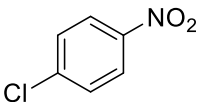
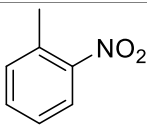
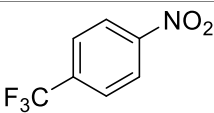
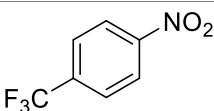
supported AuNPs²³ or AgNPs,²⁴ polystyrene supported RuNPs²⁵ and PtNPs supported on amberlite.²⁶ In these cases, selectivity has mainly been attributed to interfacial electronic effects of the stabilisers or additives that render the competitive adsorption of the electron rich NPHA intermediate slower than the reactant. However, in comparison to **5.8**, these systems suffer from the need for high catalyst loadings, toxic additives and reducing agents, organic solvent and low selectivity.

In this regard, the remarkable TOFs and selectivity for the reduction of nitrobenzene to NPHA catalysed by **5.8** under extremely mild conditions and in the absence of toxic additives is completely unprecedented and a seminal discovery given the challenging nature of this selective reduction. Interestingly, selectivity in the AuNP catalysed reduction of nitroarenes to anilines has been suggested to be modulated by electrostatic interactions between the AuNPs and various surface-modifiers. Ammonium-modified thiolates present on the surface of AuNPs were shown to promote channelling of the substrate to the active site through favourable electrostatic interactions and proved to be efficient for the reduction of various nitroarenes.²⁷ In contrast, their negatively charged counterparts, carboxylate-modified thiolates, proved to be inactive for the same transformations. It is possible that use of the IL in PIILP systems may promote similar interactions with the charged starting material, enhancing the reaction rate and altering the reaction kinetics. Whilst the results presented with PIILP systems clearly substantiate the support modifications in these instances, further modifications and structure-activity relationship studies will be required to accurately deconvolute the factors that govern catalyst performance and elucidate the origin of this unprecedented selectivity

5.3.2 Substrate screening

The optimum conditions were then applied to selected substrates to assess the versatility of **5.8**, the results of which are presented in Table 28.

Table 28: Reduction of selected nitroarenes to the corresponding *N*-phenylhydroxylamines catalysed by **5.8**.

| Entry ^a | Substrate | Time (hours) | Conversion (%) ^b | Selectivity (%) ^b |
|--------------------|---|-----------------|--------------------------------|---------------------------------|
| 1 |  | 2 | 98 | 95 |
| 2 |  | 2 | 80 | 93 |
| 3 |  | 2 | 99 | 97 |
| 4 |  | 2 | 99 | 97 |
| 5 |  | 2 | 76 | 68 |

Reaction conditions: 1 mmol substrate, 0.005 mol % **5.8**, 2.5 mmol NaBH₄, 2 mL water, RT. ^bConversion and selectivity determined using ¹H NMR spectroscopy using dioxane as the internal standard, average of at least 3 runs. Selectivity = [% desired product / (% desired product + % other products)].

Gratifyingly, the reduction of 1-chloro-2-nitrobenzene proceeded smoothly to afford *N*-(2-chlorophenyl)hydroxylamine in 95% selectivity at 98% conversion (entry 1). Similarly, *N*-(4-chlorophenyl)hydroxylamine was obtained in 93% selectivity although the conversion was slightly lower, which suggests that the chloro group in the *para*- position is slightly more deactivating than the *ortho*- (entry 2). In stark contrast to the reduction catalysed by PIILP-stabilised PdNPs, no hydrodehalogenation products were detected, further highlighting the intrinsic differences associated with the activity of the two different supported metal catalysts. Excellent conversion and selectivity was observed for the reduction of 2-nitrotoluene and 4-nitrobenzotrifluoride (entries 3 and 4) as the corresponding

hydroxylamines were obtained in 97% selectivity together with only 3% of the over-hydrogenation products. 4-nitroanisole was chosen as a representative substrate bearing an electron donating substituent (entry 5), however, the reaction was slower, and selectivity was significantly lower due to the formation of 4-aminoanisole. Based on these results, further studies are currently underway with other members of the group to expand the range of substrates and develop a meaningful substrate-activity relationship.

5.4 Optimisation for selective formation of aniline

Preliminary studies have demonstrated that lower temperatures are crucial to prevent the further reduction of NHPA to aniline. Speculating that by adjusting the reaction conditions accordingly, high selectivity towards aniline could be achieved, a series of reactions were conducted at elevated temperatures to drive the complete reduction. Moreover, in this instance, the efficiency of PIILP catalysts could be more rationally evaluated, given that most systems reported in the literature tend to catalyse complete reduction of nitrobenzene to aniline. Reactions were carried out using 5 equivalents of NaBH_4 as even though earlier studies showed that optimum activity is achieved using 15 equivalents, this would reduce the accumulation of alkali metal by-product waste.

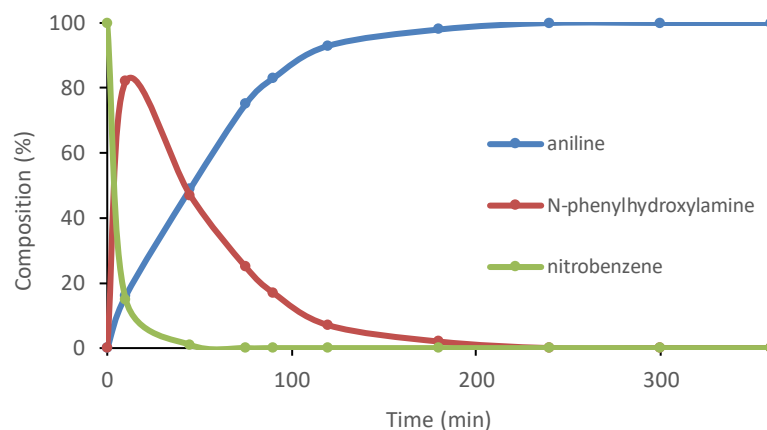


Figure 60: Time-composition profile for the reduction of nitrobenzene catalysed by 5.8. Reaction conditions: 1 mmol nitrobenzene, 5.0 mmol NaBH_4 , 0.005 mol% 5.8, 2 mL water, 60 °C. Relative composition determined by ^1H NMR spectroscopy using dioxane as the internal standard. Average of three runs. Selectivity for aniline = [% aniline / (% aniline + % N-phenylhydroxylamine)].

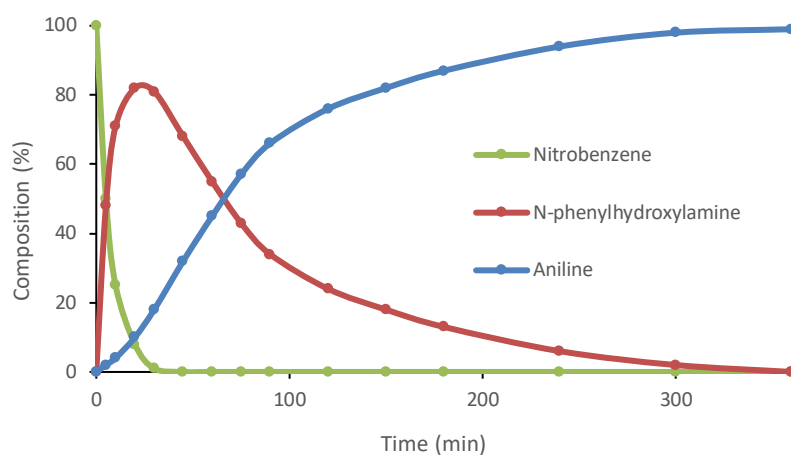
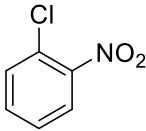
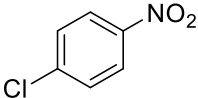
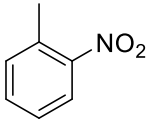
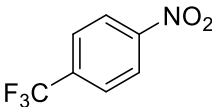
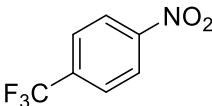


Figure 61: Time-composition profile for the reduction of nitrobenzene catalysed by **5.7**. Reaction conditions: 1 mmol nitrobenzene, 5.0 mmol NaBH₄, 0.005 mol% **5.7**, 2 mL water, 60 °C. Relative composition determined by ¹H NMR spectroscopy using dioxane as the internal standard. Average of three runs. Selectivity for aniline = [% aniline / (% aniline + % N-phenylhydroxylamine)].

Under these conditions, quantitative amounts of aniline were obtained after a reaction time of 3 hours. As expected, the reaction clearly proceeds through the direct route as NPHA is the major species (82%) after a reaction time of 20 minutes. For comparison, the reaction catalysed by **5.7** also gave complete reduction to aniline, although the reaction was slower and required 5 hours to reach completion (Figure 61). A reduced the catalyst loading of 0.0002 mol % **5.8** also gave complete reduction to aniline albeit after a reaction time of 8 h at 50 °C; this corresponds to TON of 500,000 and a TOF of 62,500 h⁻¹ based on the total gold content as determined by ICP-OES analysis. For comparison, AuNPs supported on a syndiotactic polystyrene-*cis*-1,4-polybutadiene multiblock copolymer catalysed the aqueous phase reduction of nitrobenzene to aniline in 96% selectively using 6 equivalents of NaBH₄ with a TOF of 2,130 h⁻¹.²⁸ Interestingly, in these systems, the polymer support facilitated the diffusion of reactants toward the AuNP centre thereby acting as the effective reaction medium and enhancing the reaction rate. **5.8** also outperforms other AuNP systems such as AuNPs supported on alumina which gave a TOF of 1.92 h⁻¹,²⁹ and AuNPs supported on nanocrystalline MgO which gave a TOF of 188 h⁻¹.⁷

These experiments therefore demonstrate that whilst the activation barrier for the reduction of NPHA to aniline is high enough to obtain NPHA quantitatively at room temperature, hydrogenation of NPHA is more facile at higher temperatures. The conditions above were then applied to selected nitroarene substrates, details of which are shown in Table 29.

Table 29: Reduction of selected nitroarenes to the corresponding anilines catalysed by 5.8.

| Entry ^a | Substrate | Time (hours) | Conversion (%) ^b | Selectivity (%) ^b |
|--------------------|---|-----------------|--------------------------------|---------------------------------|
| 1 |  | 5 | 100 | 100 |
| 2 |  | 5 | 100 | 100 |
| 3 |  | 5 | 99 | 100 |
| 4 |  | 4 | 98 | 100 |
| 5 |  | 5 | 98 | 100 |

^aReaction conditions: 1 mmol substrate, 0.005 mol % 5.8, 5.0 mmol NaBH₄, 2 mL water, 50 °C. ^b Conversion and selectivity determined using ¹H NMR spectroscopy using dioxane as the internal standard, average of at least 3 runs. Selectivity = [% desired product / (% desired product + % other products)].

Under these conditions both electron withdrawing and electron donating substrates could be reduced to the corresponding anilines in 4-5 hours with 100% selectivity. Moreover, no products of hydrodehalogenation were observed in the reduction of 1-chloro-2-nitrobenzene or 1-chloro-4-nitrobenzene (entries 1 and 2).

5.5 Optimisation for the selective formation of azoxybenzene

The unprecedented solvent-dependent behaviour observed earlier during the optimisation process for the transfer hydrogenation of nitrobenzene prompted a series of experiments to investigate whether azoxybenzene could be obtained in high conversion with high selectivity. Despite initially conducting the solvent screen with **5.7**, **5.8** was chosen as it is markedly more active and has already been used to generate two different reduction products selectively under appropriate conditions. To this end, the ethanol/water ratio was varied by gradually

decreasing the water content in order to identify the optimum solvent composition for obtaining AXB selectively.

Table 30: Optimisation of the relative ethanol/water content for the selective reduction of nitrobenzene to azoxybenzene catalysed by 5.8.

| Entry ^a | % ethanol | Conversion (%) ^b | Selectivity (%) ^{bc} |
|--------------------|-----------|--------------------------------|----------------------------------|
| 1 | 50 | 92 | 96 ^c |
| 2 | 75 | 85 | 95 ^c |
| 3 | 85 | 76 | 94 ^c |
| 4 | 95 | 74 | 94 ^c |
| 5 | 99 | 74 | 92 ^c |
| 6 | 100 | 70 | 100 |

^aReaction conditions: 1 mmol substrate, 0.005 mol % 5.8, 2.5 mmol NaBH₄, 2 mL total solvent, RT, reaction time = 45 mins.

^bConversion and selectivity determined using ¹H NMR spectroscopy using dioxane as the internal standard, average of at least 3 runs. ^cSelectivity for *N*-phenylhydroxylamine. Selectivity for azoxybenzene = [% azoxybenzene / (% azoxybenzene + % aniline + % *N*-phenylhydroxylamine + % azobenzene)]. Selectivity for *N*-phenylhydroxylamine = [% *N*-phenylhydroxylamine / (% *N*-phenylhydroxylamine + % aniline + % azoxybenzene + % azobenzene)].

Surprisingly, high selectivity for NHPA was obtained in ethanol/water mixtures even up to 99% ethanol (entries 1-5). As the ethanol content increased, conversion dropped and selectivity for NHPA decreased marginally due to the formation of AXB. Remarkably however, the use of neat ethanol gave a complete switch in selectivity, and azoxybenzene was obtained with 100% selectivity in 70% conversion (entry 6).

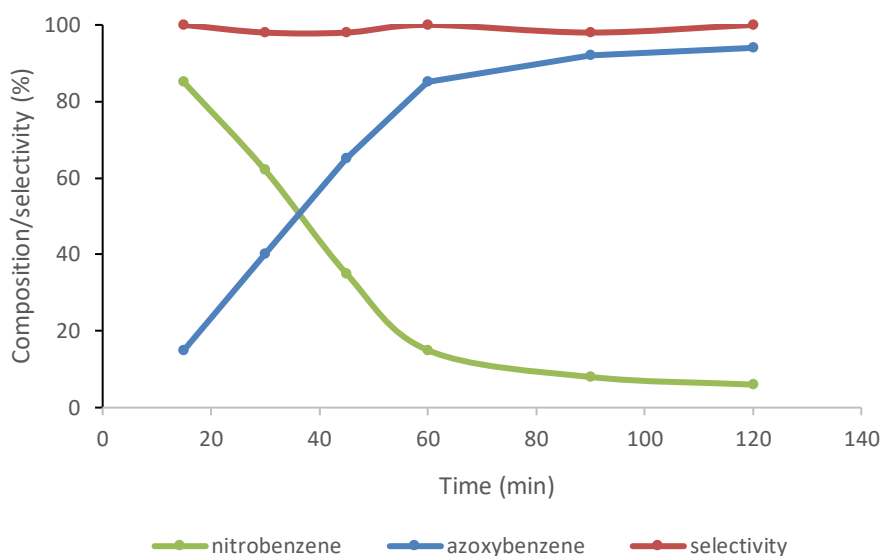


Figure 62: Time-composition profile for the reduction of nitrobenzene to azoxybenzene catalysed by 0.005 mol% **5.8**. Reaction conditions: 1 mmol nitrobenzene, 2.5 mmol NaBH₄, 2 mL ethanol, RT. Relative composition determined by ¹H NMR spectroscopy using dioxane as the internal standard. Average of three runs. Selectivity for azoxybenzene = [% azoxybenzene/ (% azoxybenzene + % aniline + % *N*-phenylhydroxylamine + % azobenzene)].

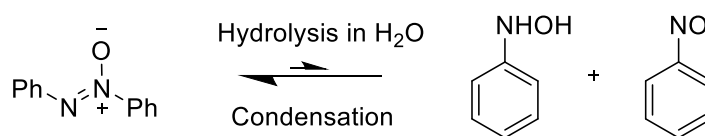
The time-conversion profile in Figure 62 demonstrates that AXB is obtained as the sole product for the reduction of nitrobenzene with catalyst **5.8** in neat ethanol and gratifyingly, can be obtained quantitatively after 2.5 hours. For comparison, the same reaction using catalyst **5.7** afforded 61% AXB, albeit in 100% selectivity. The phosphine modification proved to be key for achieving high selectivity as the reaction catalysed by **5.5** (AuNP@PIILP) gave only 23% conversion with 65% selectivity for AXB while catalyst **5.6** (AuNP@PEGPIILP) gave 26% conversion and 88% selectivity. Thus, it appears that the PEG modification also drastically improves the selectivity of the catalyst, as in this case conversion was similar to that of **5.5**. Interestingly, under identical conditions, AuNPs stabilised by sodium citrate were completely inactive and only starting material was recovered. Moreover, even after an extended reaction time of 2 days, only 10% conversion was achieved, which represented multiple reduction products further highlighting the advantages of the PIILP support.

A reduction in the catalyst loading of **5.8** to 0.0002 mol % resulted in a conversion of 11% with 100% selectivity for AXB, corresponding to a TON of 55,000 and TOF of 37,000 h⁻¹. The origin of this remarkable selectivity switch is difficult to elucidate based on the limited data available at this stage. However, as the reductions were conducted under otherwise identical conditions, it is tentatively suggested that since the solubility of nitrobenzene is markedly higher in ethanol than in water, it will be highly dispersed throughout the reaction media. In contrast, driven by the hydrophobic effect, the substrate is likely to concentrate close to the

surface of the catalyst in water. Should this be true, the effective concentrations of the reactant near the active site would be dramatically different in the two solvents, therefore imposing different mass transport constraints on the relative reaction kinetics. Another possible scenario is that the solvent may play a role in the mechanism by interacting with either the catalyst or other reactive species generated under the conditions of catalysis to promote a switch of the reaction pathway. Either way, clearly more studies will be required to examine the influence of the solvent on the selectivity of this reduction.

A survey of the literature revealed that catalysts for the selective reduction of nitrobenzene to azoxybenzene are scarce. On comparison with the few existing examples, **5.8** appears to offer substantial improvements with regards to catalyst performance and the environmental impact of the reaction credentials. For example, magnetically separable urchin-like Ni/graphene nanocomposites gave complete selectivity for the reduction of nitrobenzene to azoxybenzene and could be recycled, however, the maximum TOF of 32.6 h^{-1} is well below that of $37,000 \text{ h}^{-1}$ obtained with **5.8**.³⁰ Moreover, this system used hydrazine as the reducing agent which is considered extremely toxic. As discussed earlier in this chapter, AuNPs supported on mesostructured ceria also exhibit switchable selectivity based on solvent composition as the addition of water to 2-propanol resulted in a shift from azoxybenzene to azobenzene.¹³ However, the TOF of 20 h^{-1} obtained with 1 mol % catalyst is also markedly lower than that obtained with **5.8**. Ir/Rh nanosheets also proved to be active for this transformation and a maximum selectivity of 89% for azoxybenzene was reported with a TOF of 400 h^{-1} , which is almost 100-fold lower than that obtained with our optimum PIIL-stabilised AuNPs.³¹

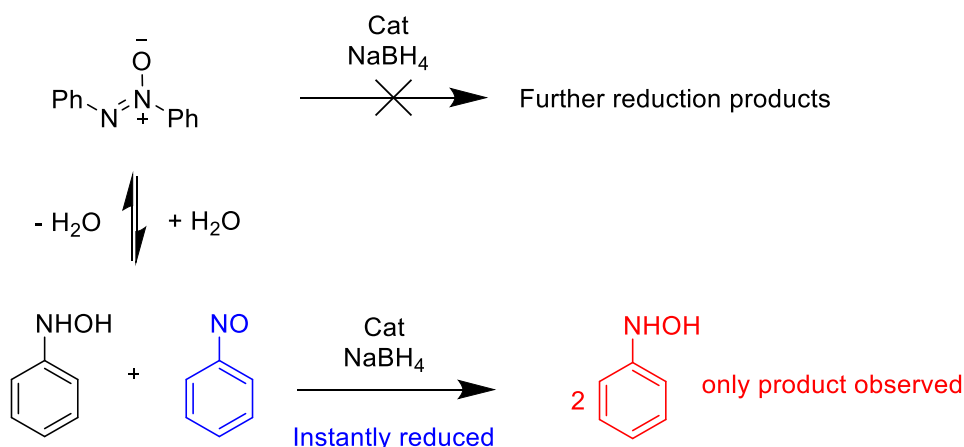
Surprisingly, whilst sampling of the reduction of nitrobenzene in ethanol using catalyst **5.8** showed that AXB was the sole product, a quantitative yield of NPHA was obtained after aqueous work-up. To further investigate this result, three control experiments were conducted by stirring an authentic sample of azoxybenzene under different conditions. Firstly, to examine whether hydrolysis was responsible for the formation of NPHA, AXB was stirred in ethanol under an inert atmosphere and water was added. After aging for 2 hours, AXB was still the only species present in solution, which suggests that the NPHA is not formed by hydrolysis.



Only product observed

Scheme 50: Addition of water to a solution of azoxybenzene in water resulting in no reaction.

In the next control experiment water was added to a solution of AXB in ethanol in the presence of **5.8**. Under these conditions there was no noticeable reaction which also suggests that the catalyst does not promote this transformation. However, in the final control, the addition of catalyst, reducing agent and water to a solution of AXB in ethanol resulted in the formation of a significant amount of NPHA. This indicates that catalyst, water, and reducing conditions are all required to generate NPHA. Furthermore, no AXB reduction products were observed suggesting the reduction of AXB is slow.



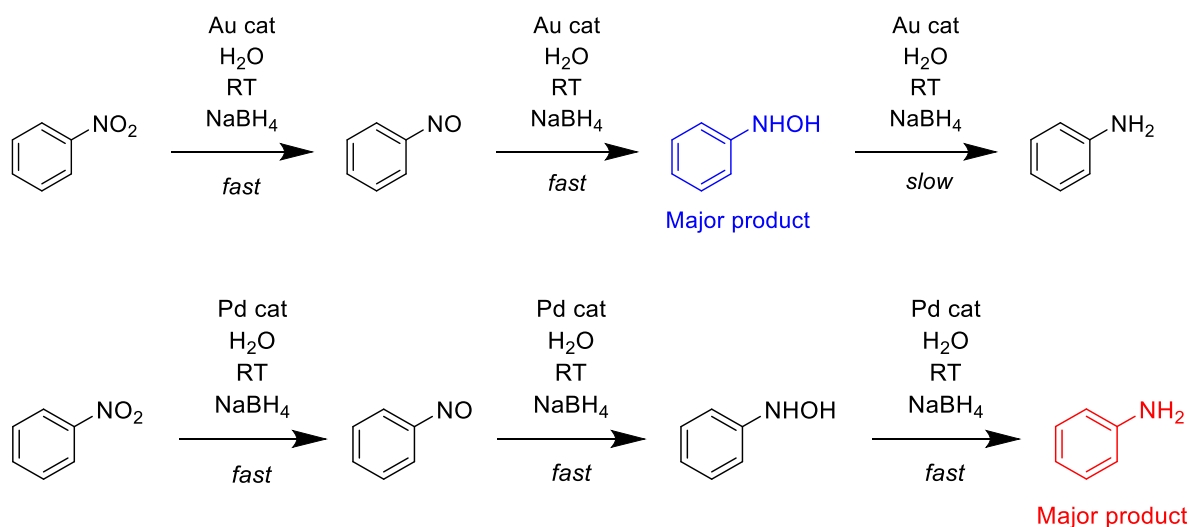
Scheme 51: Formation of two equivalents of *N*-phenylhydroxylamine *via* hydrolysis of azoxybenzene and reduction of nitrosobenzene.

Based on these results it is suggested that on the addition of water, azoxybenzene undergoes reversible hydrolysis to afford nitrosobenzene and NPHA, and the former is rapidly reduced to generate another equivalent of NPHA.

5.6 Conclusion

Whilst the reduction of nitrobenzene to aniline using AuNP-based catalysts supported on PIILP materials is much slower than the corresponding PdNP@R-PIILP-catalysed reduction, the utility of PIILP-stabilised gold NPs lies in the ability to obtain partially reduced commodity chemicals with remarkable selectivity under mild conditions and at extremely low catalyst loadings. Furthermore, as the active catalyst can be prepared by *in situ* reduction of the corresponding Au^(III) precursor, the overall protocol represents an improvement in the step

economic potential and further streamlines the process as sensitive NP systems do not need to be preformed, isolated and stored.



Scheme 52: Differences in the Pd and Au catalysed reduction of nitroarenes.

The NaBH₄-mediated reduction of nitrobenzene in water at room temperature catalysed by 0.005 mol% AuNP@PPh₂-PEGPIILP (**5.8**) results in quantitative conversion to *N*-phenylhydroxylamine (NPHA), and further reduction to aniline is completely suppressed. Such a high selectivity is unprecedented for a AuNP-based reduction and is tentatively attributed to the increase in the activation barrier for the reduction of NPHA due to the lower activity of the AuNPs compared with their Pd counterparts. However, complete reduction to the corresponding aniline could be obtained selectively by simply increasing the temperature and the concentration of the reducing agent. The reaction was also demonstrated to be solvent-dependant as a change to ethanol resulted in a switch in selectivity to afford quantitative conversion to azoxybenzene. Gratifyingly, the TOFs obtained for reduction to each of the respective species with catalyst **5.8** were substantially higher than any competing systems in the literature.

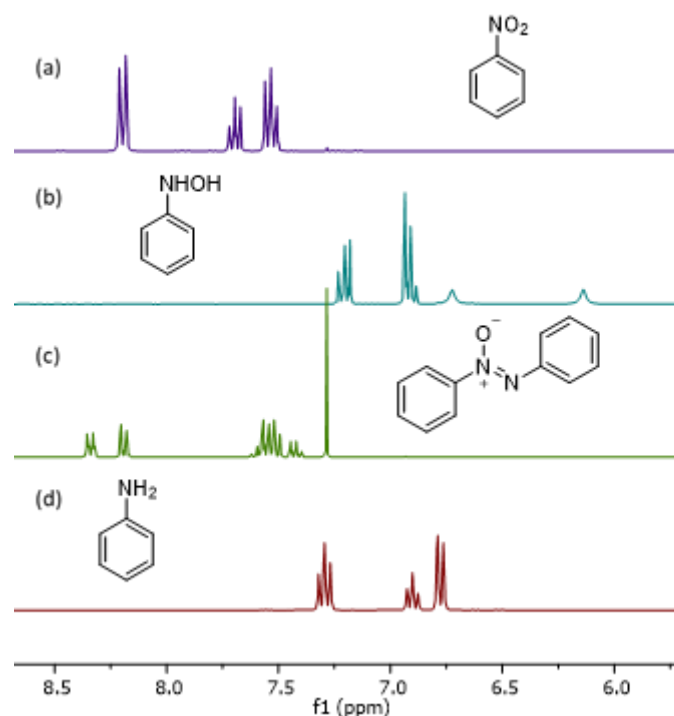


Figure 63: ^1H NMR spectra of nitrobenzene (a) and the post reaction mixtures of the reactions catalysed by 5.8 (b-d), showing the reduction products obtained selectively. Reaction conditions are; b) water, 2.5 equivalents NaBH_4 , 0.005 mol % catalyst, inert atmosphere, RT, 40 min. c) dry ethanol, 2.5 equivalents NaBH_4 , 0.005 mol % catalyst, inert atmosphere, RT, 150 min. d) water 5 equivalents of NaBH_4 , 0.005 mol % catalyst, inert atmosphere, 50 $^\circ\text{C}$, 6 hours.

The benefits of a single system capable of generating three distinct products selectively under such mild conditions at low catalyst loadings are numerous and this technology represents a sustainable method for the production of compounds that would otherwise be challenging to prepare and difficult to separate from non-selective mixtures.

It would be challenging to accurately identify the factors that govern this selectivity given the complexity of PIILP systems and the numerous possible interactions involving the solvent, reagent, support and catalyst that may influence performance. In this regard, experimentally, the PPh_2 and PEG modifications proved to be crucial for obtaining high selectivity. Thus, in combination with further computational, *in situ* spectroscopic and kinetic analysis, future studies will examine how the nature and density of the heteroatom(s) and overall dispersibility of the different supports influence the electronic structure of the active AuNP phase and overall catalyst efficacy. Furthermore, since the IL moiety may well direct the flow of charged substrates toward the catalyst surface, future studies will examine whether PIILP-based systems can be used as ‘smart’ catalysts that can discriminate between reagents and products to achieve highly selective systems for other transformations.

5.7 References

1. P. Zhao, X. Feng, D. Huang, G. Yang and D. Astruc, *Coord. Chem. Rev.*, 2015, **287**, 114-136.
2. M. Stratakis and H. Garcia, *Chem. Rev.*, 2012, **112**, 4469-4506.
3. H. Tang, J. Wei, F. Liu, B. Qiao, X. Pan, L. Li, J. Liu, J. Wang and T. Zhang, *J. Am. Chem. Soc.*, 2016, **138**, 56-59.
4. T. Mitsudome and K. Kaneda, *Green Chem.*, 2013, **15**, 2636-2654.
5. L. Luza, C. P. Rambor, A. Gual, J. Alves Fernandes, D. Eberhardt and J. Dupont, *ACS Catal.*, 2017, **7**, 2791-2799.
6. L. Wang, J. Zhang, H. Wang, Y. Shao, X. Liu, Y.-Q. Wang, J. P. Lewis and F.-S. Xiao, *ACS Catal.*, 2016, **6**, 4110-4116.
7. K. Layek, M. L. Kantam, M. Shirai, D. Nishio-Hamane, T. Sasaki and H. Maheswaran, *Green Chem.*, 2012, **14**, 3164-3174.
8. C. Wang, W. Zou, J. Wang, Y. Ge, R. Lu and S. Zhang, *New J. Chem.*, 2017, **41**, 3865-3871.
9. A. Corma, P. Concepción and P. Serna, *Angew. Chem. Int. Ed.*, 2007, **46**, 7266-7269.
10. G. Chen, C. Xu, X. Huang, J. Ye, L. Gu, G. Li, Z. Tang, B. Wu, H. Yang, Z. Zhao, Z. Zhou, G. Fu and N. Zheng, *Nature Mater.*, 2016, **15**, 564.
11. A. Grirrane, A. Corma and H. García, *Science*, 2008, **322**, 1661-1664.
12. H. Zhu, X. Ke, X. Yang, S. Sarina and H. Liu, *Angew. Chem. Int. Ed.*, 2010, **49**, 9657-9661.
13. X. Liu, S. Ye, H.-Q. Li, Y.-M. Liu, Y. Cao and K.-N. Fan, *Catal. Sci. Technol.*, 2013, **3**, 3200-3206.
14. S. Fountoulaki, V. Daikopoulou, P. L. Gkizis, I. Tamiolakis, G. S. Armatas and I. N. Lykakis, *ACS Catal.*, 2014, **4**, 3504-3511.
15. D. Andreou, D. Iordanidou, I. Tamiolakis, G. Armatas and I. Lykakis, *Nanomaterials*, 2016, **6**, 54.
16. R. Sharma, G. P. Holland, V. C. Solomon, H. Zimmermann, S. Schifffenhaus, S. A. Amin, D. A. Buttry and J. L. Yarger, *J. Phys. Chem. C*, 2009, **113**, 16387-16393.
17. H. Kitagawa, N. Kojima, N. Matsushita, T. Ban and I. Tsujikawa, *J. Chem. Soc., Dalton Trans.*, 1991, 3115-3119.
18. Y.-Y. Fong, B. R. Visser, J. R. Gascooke, B. C. C. Cowie, L. Thomsen, G. F. Metha, M. A. Buntine and H. H. Harris, *Langmuir*, 2011, **27**, 8099-8104.
19. K. R. J. Lovelock, E. F. Smith, A. Deyko, I. J. Villar-Garcia, P. Licence and R. G. Jones, *Chem. Commun.*, 2007, 4866-4868.
20. J. Zhao, S. Gu, X. Xu, T. Zhang, Y. Yu, X. Di, J. Ni, Z. Pan and X. Li, *Catal. Sci. Technol.*, 2016, **6**, 3263-3270.
21. A. C. Templeton, W. P. Wuelfing and R. W. Murray, *Acc. Chem. Res.*, 2000, **33**, 27-36.
22. C. P. Gulka, A. C. Wong and D. W. Wright, *Chem. Commun.*, 2016, **52**, 1266-1269.
23. E. Vasilikogiannaki, C. Gryparis, V. Kotzabasaki, I. N. Lykakis and M. Stratakis, *Adv. Synth. Catal.*, 2013, **355**, 907-911.
24. D. Andreou, D. Iordanidou, I. Tamiolakis, G. S. Armatas and I. N. Lykakis, *Nanomaterials*, 2016, **6**, 54.
25. J. H. Tyler, S. H. Nazari, R. H. Patterson, V. Udumula, S. J. Smith and D. J. Michaelis, *Tetrahedron Lett.*, 2017, **58**, 82-86.
26. A. K. Shil and P. Das, *Green Chem.*, 2013, **15**, 3421-3428.
27. S. Roy, A. Rao, G. Devatha and P. P. Pillai, *ACS Catalysis*, 2017, **7**, 7141-7145.
28. A. Noschese, A. Buonerba, P. Canton, S. Milione, C. Capacchione and A. Grassi, *J. Catal.*, 2016, **340**, 30-40.

29. K. Chaiseeda, S. Nishimura and K. Ebitani, *ACS Omega*, 2017, **2**, 7066-7070.
30. M. N. Pahalagedara, L. R. Pahalagedara, J. He, R. Miao, B. Gottlieb, D. Rathnayake and S. L. Suib, *J. Catal.*, 2016, **336**, 41-48.
31. Z.-P. Zhang, X.-Y. Wang, K. Yuan, W. Zhu, T. Zhang, Y.-H. Wang, J. Ke, X.-Y. Zheng, C.-H. Yan and Y.-W. Zhang, *Nanoscale*, 2016, **8**, 15744-15752.

Chapter 6 : Synthesis of PIILP-stabilised ruthenium nanoparticles and application in the hydrogenation of bioderived feedstock and model substrates

6.1 Introduction

Triggered by the heavy depletion of fossil fuel reservoirs and the global attempt to decrease CO₂ emissions, there has been increasing interest in the development of catalysts for the 'greener' production of fuels and fine chemicals from sustainable feedstock. In particular, the valorisation of lignocellulosic-based biomass is a key area for development as it is a cheap, abundant and accessible source of carbon.¹ Furthermore, the upgrading of the raw bioderived material yields a wide variety of organic sugars and acids with diverse functionality, which represents an environmentally responsible source of synthetic chemical building blocks.²

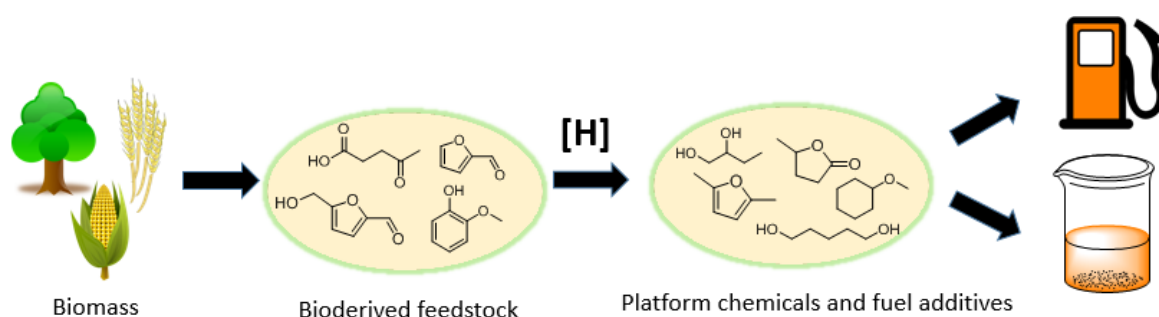
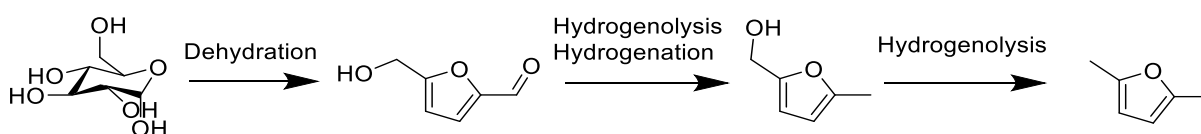


Figure 64: Schematic demonstration of the production of fuel and platform chemicals from bioderived resources.

Direct use of such feedstock as fuel additives is extremely limited due to their highly oxygenated nature and inherent combustion properties, which renders them inferior to conventional fuel sources. As such, to truly realise the potential of these resources, new catalyst technologies must be developed and methodically optimised to produce non-functionalised fuel-like substances with more appropriate physical properties in an energy efficient manner (Figure 64). Furthermore, the products must also be amenable to convenient and safe storage on larger scales.³ For example, 2,5-dimethylfuran, a potential biofuel, can be obtained from glucose, which is a direct product of lignocellulose-based biomass processing, through a series of metal and acid catalysed deoxygenation steps (Scheme 53).



Scheme 53: Stepwise deoxygenation of glucose yielding potential biofuel DMF.

Catalytic technologies are regarded as central for the development of such sustainable processes and whilst the existing fundamental chemical transformations will remain, it is becoming increasingly more important to develop greener and more energy efficient processes to achieve them. Nowadays, the principles of green chemistry – broadly, the reduction of waste, use of ubiquitous and renewable starting materials, avoidance of hazardous substances and reuse of reaction components, provides clear concepts for the design of sustainable processes. Despite the high activity and selectivity of homogenous catalysts, the arduous protocols required for catalyst recovery and the problems of metal leaching into product streams has hampered their implementation on an industrial scale. However, heterogeneous catalytic hydrogenations over metal nanoparticles are widely acknowledged as a scalable and sustainable technology due to their high efficiency, ease of separation and reuse and atom economy.

Currently, a wealth of different transition metal nanoparticle based catalysts have been utilised for similar operations such as Ni,⁴ Cu,⁵ Pd,⁶ Pt⁷ and Rh.⁸ However, due to its high oxophilicity, coupled with vast amounts of computational and experimental data, ruthenium nanoparticles have been frequently demonstrated to be the optimum metal for selective and efficient hydrogenation of carbonyls and arenes, which are amongst the key chemical transformations to be optimised for the valorisation of lignin-derived monomers.⁹

6.1.1 Aqueous phase ruthenium catalysed hydrogenation

Whilst traditionally Ru catalysts have proved to be inferior to their Pd and Pt counterparts for vapour phase hydrogenation,¹⁰ the activity of Ru catalysts has been shown to be highly sensitive to the local environment, particularly under liquid phase conditions; this has allowed for optimisation of the system to tailor the target selectivity.¹¹ For example, Dumesic *et al.* found that RuNPs supported on ceria, magnesia-zirconia and γ -alumina all outperformed the corresponding Pd and Pt catalysts under identical conditions for the selective liquid phase hydrogenation of bioderived 5-hydroxymethylfurfural.¹² Similar observations were reported by Huber *et al.* who demonstrated that alumina supported monometallic RuNPs exhibited higher activity for the aqueous phase hydrogenation of acetone, acetaldehyde, xylose and propanal than any other metal.¹³

Table 31: Comparison of different metal phases for the hydrogenation of propanal.

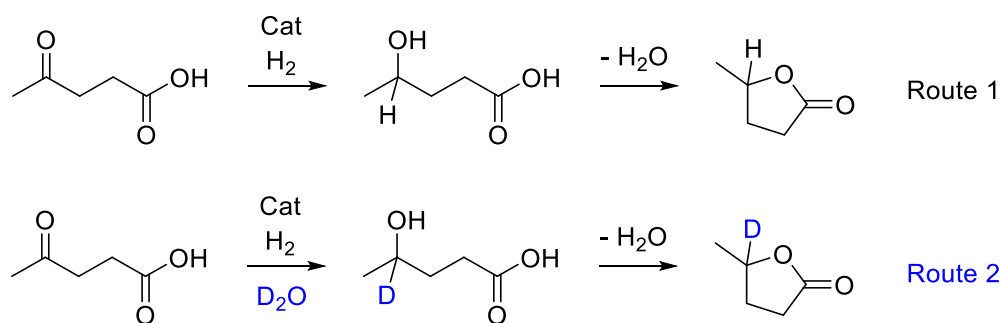
| Entry | Catalyst | Reaction time (mins) | Propanal Conversion (%) |
|-------|---|----------------------|-------------------------|
| 1 | 3 wt% Ru/Al ₂ O ₃ | 120 | 30.9 |
| 2 | 3 wt% Pd/Al ₂ O ₃ | 120 | 12.9 |
| 3 | 3 wt% Pt/Al ₂ O ₃ | 120 | 26.7 |
| 4 | 5 wt% Ni/Al ₂ O ₃ | 120 | 14.7 |
| 5 | 5 wt% Co/Al ₂ O ₃ | 120 | 0 |
| 6 | 5 wt% Rh/Al ₂ O ₃ | 120 | 0.9 |

Typically, aqueous phase catalysis is often preferred as it offers numerous advantages from both a practical engineering and sustainability perspective. The high solubility of the starting materials and immiscibility of the products in aqueous solution promotes efficient catalyst-substrate interactions as well as cost reduction of the overall process *via* facile downstream processing and selective recovery of catalyst, reagent and product. Moreover, as small molecules obtained *via* the depolymerisation of lignocellulosic based biomass are typically produced in aqueous solution, the need for further processing prior to reaction is eliminated, streamlining the overall process.¹⁴ Additionally, as discussed in earlier chapters, water is considered an environmentally benign solvent due to its high availability, low toxicity and low volatility. Therefore, water tolerance and compatibility are crucial aspects to consider during catalyst design.

In addition to sustainability, there is also now overwhelming evidence that water, either as bulk solvent or additive, is directly responsible for enhancements in activity for ruthenium catalysed hydrogenations.¹⁵ Many of these investigations indicate that role of the solvent is not limited to simply mediating the dissolution of reactants, but also that it may be involved in crucial mechanistic steps, or alter the product distribution by altering mass transfer rates and/or reaction kinetics. For example, molecular simulation using DFT methods and experimental data reported by Rooney *et al.* highlighted the crucial role of water in the hydrogenation of 2-butanone catalysed by Ru/SiO₂.¹⁶ A hydrogen bond interaction between a

water molecule and the hydroxybutyl intermediate was proposed to significantly lower the energy barrier for hydrogen insertion, thereby enhancing the rate of reaction. The same trend was also seen using other hydrogen bonding solvents, although the effect was somewhat diminished. Moreover, Ruppert *et al.* employed DFT calculations using acetone as a model substrate to rationalise the promotional effect of water on the relative rate of ketone hydrogenation over Ru(0001) surfaces.¹⁷ The authors reported that the addition of a chemisorbed water molecule to the calculation enabled the reaction to proceed through an alternative lower energy pathway mediated by a key hydrogen bond interaction between the solvent and the hydroxy intermediate. Interestingly, under identical conditions, this intermediate was not observed for the Pt-catalysed hydrogenation, which was controlled primarily by the formation of a hydroxy-alkyl intermediate.

There was also extensive evidence suggesting that exposure to water, followed by raising the temperature results in the partial desorption of adsorbed H₂O molecules on Ru surfaces, facilitating the formation of OH-H₂O-H mixed-monolayers and a H₂O monolayer at the interface.¹⁸ The interaction, and in particular, the acidity of water on ruthenium surfaces has recently been investigated¹⁹ and acidic protons were proposed to mediate proton transfer in heterogeneously catalysed hydrogenations. The two monolayers were characterised using low energy sputtering (LES) and reactive ion scattering (RIS). Using NH₃ molecules as a probe, spontaneous protonation was shown to occur exclusively as a result of the synergy between the metal and the adsorbed surface H₂O monolayer, indicating that the metal is crucial for the increase in acidity. Zhu and co-workers reported that the rate of hydrogenation of bio-derived levulinic acid to γ -valerolactone catalysed by Ru/TiO₂ was remarkably enhanced by the addition of water.²⁰ Detailed kinetic and isotopic labelling studies revealed that deuterium was incorporated in to the final product, suggesting that the solvent also acts as a source of hydrogen (Scheme 54).



Scheme 54: Isotopic labelling experiments demonstrating the incorporation of deuterium into γ -valerolactone.

6.1.2 Heteroatom promoted catalysis with electron-rich ruthenium nanoparticles

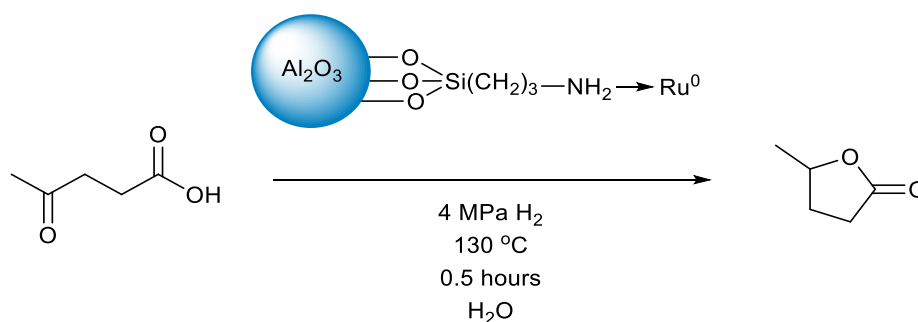
As well as favourable solvent effects, it is now also well-established that tuning of the interactions between functionality on the support and/or ligand additives can lead to vast improvements in selectivity and activity by modulation of the particle morphology and/or surface electronic structure.²¹ Moreover, alloying of the active catalyst with different metal phases has also been widely used to ‘dilute’ or partially deactivate catalysts to optimise the product selectivity, however, this method suffers the intrinsic disadvantage of higher overall precious metal loading.²² Although these techniques have been discussed in Chapter 1, this short sections aims to provide a more relevant overview.

As well as the results from Chapters 3 and 5, recent reports have shown that heteroatom doped materials can promote favourable electronic catalyst-support interactions to improve catalyst performance, without the need for expensive ligand additives that require multistep syntheses and are challenging to reuse.²³ Similar to ligand assisted homogeneous catalysis, the electronic properties of the metal centre in heterogeneous catalysts are known to exert considerable influence on the activity and selectivity.²⁴ This strategy largely employs carbon based supports as they are generally cheap, robust, non-reducible and are easily decorated. In particular, for the hydrogenation of carbonyl functionalities, electron rich metal centres have been demonstrated to increase catalyst activity. Enhanced activation of the carbonyl is thought to occur due to the increase in density at the metal available for π -backbonding into the accessible carbonyl π^* , which in turn promotes strong adsorption of the carbonyl onto the catalyst surface. This is commonly achieved by incorporating electron donor functionality into the support architecture such as amines, phosphines or carbenes. In agreement with these observations, Chaudret and co-workers demonstrated a strong ligand effect for the RuNP catalysed hydrogenation of aromatics.²⁵ It was found that the addition of strong electron donors such as *N*-heterocyclic carbenes (NHCs) dramatically enhanced the rate of reaction

with enhancements in the order $\text{NHC} > \text{PAlkyl}_2\text{Ar} > \text{PAr}_3$. More recently, Glorius *et al.* demonstrated that the addition of NHCs to RuNPs supported on $\text{K-Al}_2\text{O}_3$ resulted in a remarkable increase in selectivity for the partial hydrogenation of *trans*-stilbene.²⁶ Surface characterisation studies and ^{13}C labelling studies demonstrated that the NHCs bind strongly in a covalent manner to the particles rather than simply adsorb on the surface. The authors then demonstrated that selectivity can be optimised *via* irreversible blocking of active sites on the particle surface through NHC coordination, however, saturation of the surface as a result of high concentration of NHC led to complete deactivation of the catalyst. Additionally, the same group later demonstrated that the strong electron donating ability of NHCs activated PdNPs towards the Buchwald-Hartwig amination of bromobenzene.²⁷ The addition of NHCs was reported to facilitate formation of highly electron rich PdNPs which lowered the barrier for hydrogenolysis of bromobenzene, thus allowing the amination to proceed; in stark contrast, the unmodified PdNPs were inactive.

As well as NHCs, amines have also been shown to improve the efficacy of RuNP-based catalysts *via* interaction of the nitrogen with the particle surface. On comparison with carbenes, amines represent a more synthetically convenient modification, as they are easier to handle and do not require any additional selective deprotonation steps in the presence of other reactive functionality. For example, Zhu *et al.* investigated the influence of amine donors on the stability and activity of RuNPs supported on NH_2 -modified $\gamma\text{-Al}_2\text{O}_3$ for the aqueous phase hydrogenation of levulinic acid to γ -valerolactone.²⁸ Comparative catalyst testing against the unmodified support revealed a marked difference in catalyst performance. Whilst $\text{r-Ru-NH}_2\text{-}\gamma\text{-Al}_2\text{O}_3$ and $\text{Ru}/\gamma\text{-Al}_2\text{O}_3$ were both extremely selective for the hydrogenation of levulinic acid to γ -valerolactone, the former was markedly more active reaching 99.1% conversion after 13 hours at room temperature under 4MPa H_2 , whereas the non-functionalised catalyst only reached 43.1% conversion under the same conditions. The superior performance of $\text{r-Ru-NH}_2\text{-}\gamma\text{-Al}_2\text{O}_3$ was attributed to the amino modification on the basis that the -NH_2 σ -donor groups could bind the Ru precursor and facilitate the formation of highly dispersed small RuNPs in an electron rich state. This concept was supported by XPS analysis of the as-prepared unloaded support and precatalyst, which was used to probe the metal-support interaction. Analysis of the N1s region of the precatalyst, $\text{i-Ru-NH}_2\text{-}\gamma\text{-Al}_2\text{O}_3$, revealed a positive shift in binding energy of 0.24 eV on comparison with the free support, which is indicative of coordination of Ru(III) to the amine functionality. Furthermore, HRTEM analysis revealed that

the NH₂- modification was indeed responsible for the formation of smaller and more uniformly dispersed RuNPs compared with its non-functionalised counterpart (1.2 nm vs 12.3 nm). The authors also suggest that anchoring of the RuNPs to the surface of the support through the strong M-NH₂ interaction improved the stability and durability and as a result, the catalyst was able to be reused 10 times under harsh conditions with no loss of activity.



Scheme 55: Hydrogenation of levulinic acid to γ -valerolactone catalysed by i-Ru-NH₂- γ -Al₂O₃.

Zhou *et al.* reported a facile protocol for the fabrication of RuNPs supported on -NH₂ functionalised metal organic frameworks which were extremely efficient catalysts for the hydrolytic dehydrogenation of ammonia borane.²⁹ The authors suggested that the amino groups embedded within the architecture provided enhanced stabilisation and better dispersion of the more electron rich RuNPs throughout the support, which ultimately led to the higher efficiency of the catalyst on comparison against commercial Ru/C and the non-functionalised support. Moreover, Beller *et al.* reported a convenient, scalable and highly economic synthesis of RuNPs supported on a nitrogen doped carbon matrix.²¹ The presence of nitrogen donors within the support greatly improved catalyst performance for the selective hydrogenation of arenes.

6.2 Results and discussion

The work presented in this chapter aims to expand the scope of PIILP-stabilised nanoparticle catalysts to include ruthenium nanoparticles. Building on the encouraging results obtained with PIILP-stabilised PdNPs in Chapters 2, 3 and 4, as well as previously discussed PIILP-stabilised AuNPs, it is envisaged that the same systems could enable the fabrication of small, well dispersed and electron rich ruthenium nanoparticles for the selective hydrogenation of target industrially relevant bioderived compounds such as furaldehyde, levulinic acid and its esters. Given the low thermal stability of some of these compounds and the various intermediary products, to achieve this, it will be challenging but necessary to develop systems

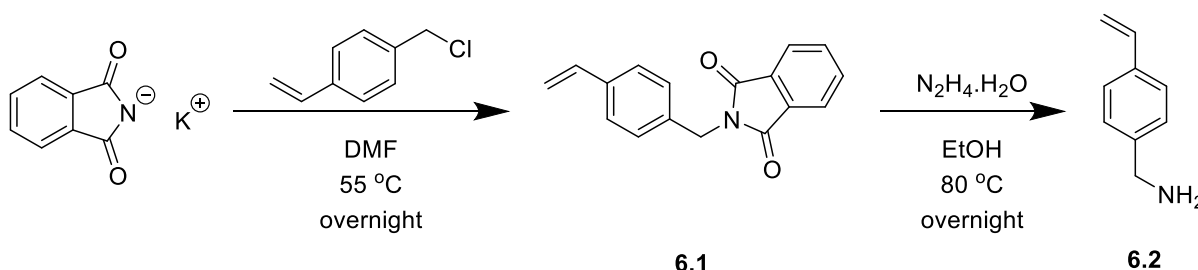
that operate efficiently under mild conditions. In particular, the PEG modification has been demonstrated to be vital for enhancing catalyst performance in the aqueous phase, therefore all catalysts in this project will bear this motif.

The results presented in earlier chapters have highlighted the crucial role of the heteroatom donor within the polymer architecture to achieve high selectivity. Based on a strong literature precedent for favourable interfacial electronic interactions of amino modified supports, this chapter will detail the synthesis of amino and phosphine modified catalysts, RuNP@NH₂-PEGPIILP and RuNP@PPh₂-PEGPIILP, respectively, as well as the benchmark non-functionalised counterpart RuNP@PEGPIILP. By conducting thorough and systematic catalyst testing in parallel with various structural and surface analysis, the influence of the heteroatom donor will be explored, and the relative merits evaluated for the aqueous phase hydrogenation of various carbonyl and aryl-based substrates.

6.3 Catalyst synthesis and characterisation

6.3.1 Monomer synthesis

Compound **6.2** was identified as a suitable target monomer to incorporate the amino functionality within the polymer scaffold. The synthesis of primary amine **6.2** was achieved using a Gabriel synthesis as reported by Bertini and coworkers.³⁰ The Gabriel adduct **6.1** was obtained as a white crystalline solid *via* *N*-alkylation of potassium phthalimide in DMF with 1-chloro-4-vinylbenzene (Scheme 56), which was then converted to monomer **6.2** *via* hydrazinolysis. After conducting a workup under basic conditions, **6.2** was isolated as a spectroscopically pure pale-yellow oil in 87% yield.



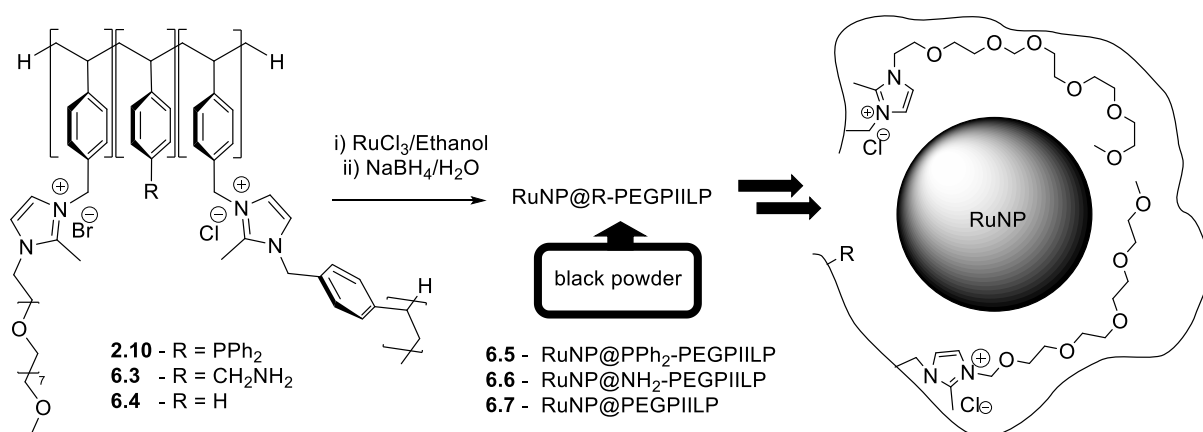
Scheme 56: Synthesis of 4-(vinylphenyl)methanamine **6.2**.

The heteroatom donor decorated PIILs were prepared as discussed in section **2.1.2** using AIBN-initiated free radical copolymerisation. Full characterisation data, which demonstrated

the amino functionalisation does not alter any structural or physical properties on comparison with previously prepared PIILP systems, is available in the appendix (A65, A66).

6.3.2 Immobilisation of RuNPs within PIILP frameworks

Based on literature precedent, and in the absence of readily available ionic ruthenium complexes, RuCl_3 was identified as the precursor of choice to impregnate the polymer as its reduction to RuNPs is well precededented.³¹ Furthermore, the strong electrostatic and covalent interactions provided from the IL and heteroatom donors within the support should provide sufficient driving force to enable efficient absorption of the metal onto the support. Ethanol was chosen as the appropriate solvent for impregnation on the basis that PEGylated PIILP materials tend to form a homogenous solution of large aggregates (as evidenced by DLS measurements in section 2.2.2), enabling a large surface area for absorption and efficient dispersion of the metal precursor throughout the PIIL. In this regard, the active catalysts were fabricated *via* a one-pot protocol depicted in Scheme 57.



Scheme 57: Synthesis and schematic representation of RuNP@R-PEGPIILP catalysts.

In a typical procedure, an ethanol dispersion of the polymer was treated with RuCl_3 and the resulting mixture stirred for 6 h to ensure complete impregnation. Following this, the Ru^{3+} loaded PIILPs were reduced *in situ* by dropwise addition of an aqueous sodium borohydride solution. After stirring the mixture for 2 hours under an N_2 atmosphere, PIILP stabilised RuNPs were obtained as black powders after centrifugation, filtration, washing and drying in high yields.

6.3.3 Characterisation of RuNP@R-PEGPIILP materials

ICP-OES analysis of the freshly prepared catalysts was used to determine their ruthenium content (Table 32). Interestingly, despite bearing no heteroatom donors, Ru uptake was more

efficient with the PEGPIILP support on comparison with the PPh₂ modified support (entries 1 and 3), whilst the amino functionalised support proved to be the most efficient for immobilisation of RuNPs (entry 2).

Table 32: Ruthenium content of PIILP catalysts as determined by ICP-OES.

| Entry | Catalyst | mmol Ru/ g PIILP | Ru wt% |
|-------|---------------------------------------|---------------------|--------|
| 1 | RuNP@PPh ₂ -PEGPIILP (6.5) | 0.10 | 1.01 |
| 2 | RuNP@NH ₂ -PEGPIILP (6.6) | 0.18 | 1.83 |
| 3 | RuNP@PEGPIILP (6.7) | 0.14 | 1.41 |

SEM analysis of the materials revealed that NH₂ and PPh₂ modified catalysts display similar granular surface morphology to that of previously prepared PIILP stabilised PdNPs (Figure 65). Moreover, both are not as smooth as the corresponding free PIILP supports, which may simply be a result of expulsion of residual solvent during later synthetic steps. However, the unmodified benchmark catalyst gives a more swollen appearance with salt-like deposits. It is possible that the interaction of the heteroatom donor with the solvent may alter the dynamic behaviour of the materials in solution during the metal loading stage and ultimately lead to changes in surface morphology after isolation of the catalyst.

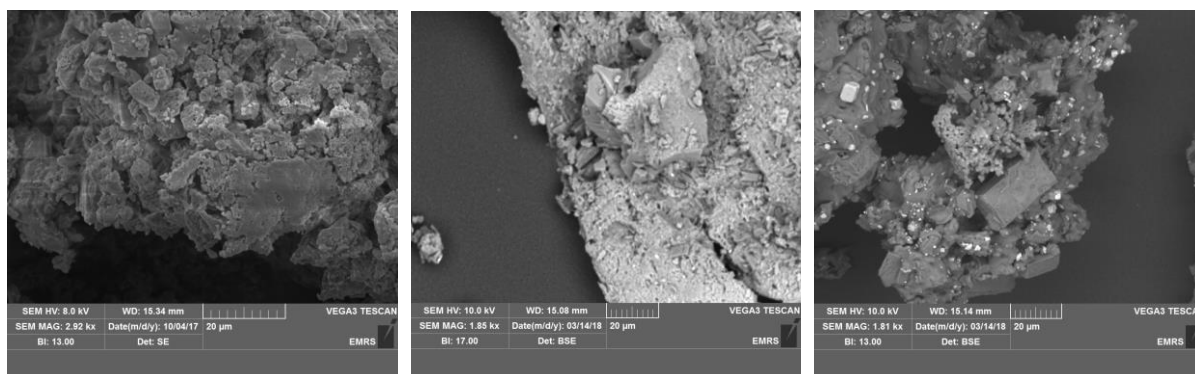


Figure 65: (left to right) SEM images of RuNP@PPh₂-PEGPIILP (5.5), RuNP@NH₂-PEGPIILP (5.6) and RuNP@PEGPIILP (5.7).

As expected, all the catalysts exhibited limited solubility in conventional deuterated solvents thus, solid state NMR spectroscopy was used to identify any interaction of the donor modified supports with the metal surface. The solid state ¹³C spectrum of **6.6** showed characteristic

signals associated with the imidazolium ring at δ 127 and 147 ppm. Additionally, the intense signal at δ 70 ppm was assigned to the PEG functionality, with aliphatic carbons signals observed at δ 10 and 50 ppm. The benzylic carbon atom adjacent to the amine groups showed a small downfield shift of 1.3 ppm (from δ 45.8 to 47.1 ppm) after metal loading, which although small, may be indicative of coordination of the nearby NH_2 group to the Ru surface (Figure 66).

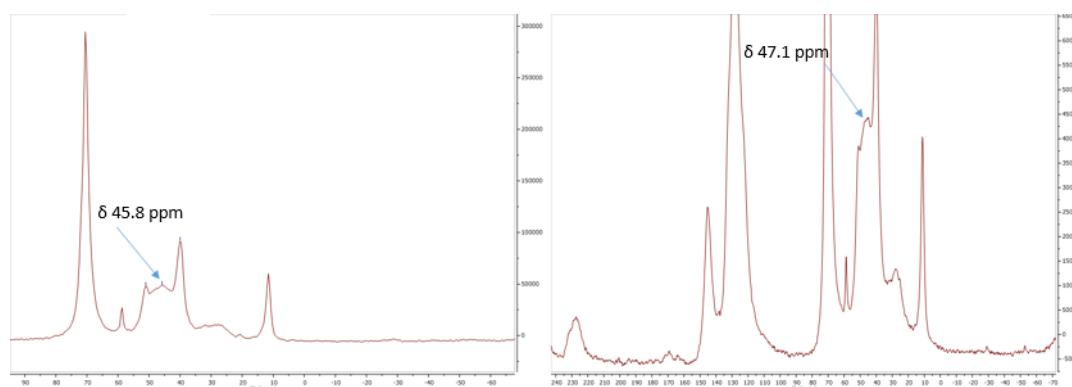


Figure 66: ^{13}C solid state NMR spectrum of $\text{NH}_2\text{-PEGPIILP}$ (left) and $\text{RuNP@NH}_2\text{-PEGPIILP}$ (right).

The ^{31}P solid state NMR spectrum of **6.5** confirmed the presence of a Ru-P interaction. Figure 67 clearly shows a single phosphine environment with spinning side bands and a clear downfield shift from δ - 7.24 to 24.18 ppm upon coordination of the PPh_2 moiety with the RuNPs.

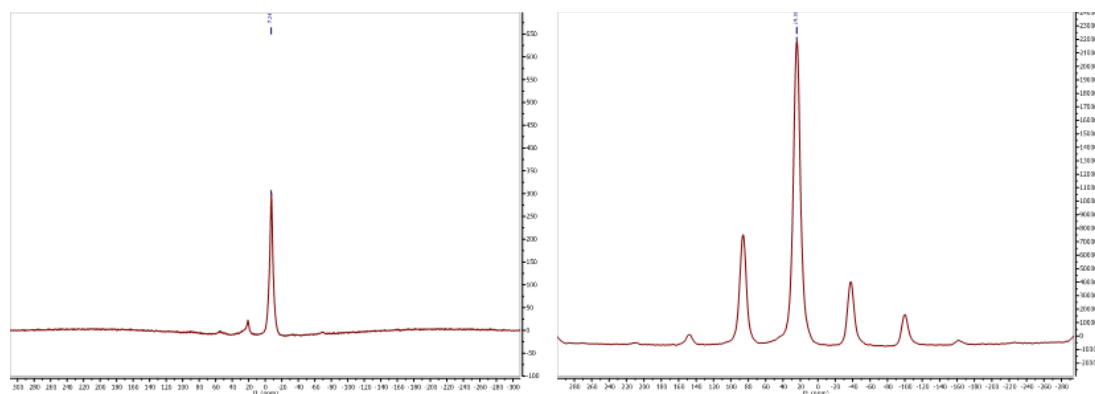


Figure 67: ^{31}P solid state NMR spectrum of $\text{PPh}_2\text{-PEGPIILP}$ (left) and $\text{RuNP@PPh}_2\text{-PEGPIILP}$ (right).

The presence of RuNPs embedded within the support was confirmed by TEM analysis. Figure 68 shows that all three catalysts contain discrete spherical particles which are well dispersed throughout the support. Particle size analysis revealed that the amino-functionalised support yielded the narrowest size distribution, as well as the smallest average diameter of 1.0 ± 0.2 nm. In contrast, the PPh_2 modified support exhibited a considerably broader size distribution and yielded larger particles of 2.2 ± 0.6 nm in size. Interestingly, the mean diameter of $1.5 \pm$

0.4 nm for the RuNPs stabilised by the benchmark PIIL support is slightly smaller than its phosphine-modified counterpart. This is somewhat surprising given that PPh₂-modified supports gave smaller particles exclusively for the corresponding PdNP-based systems.

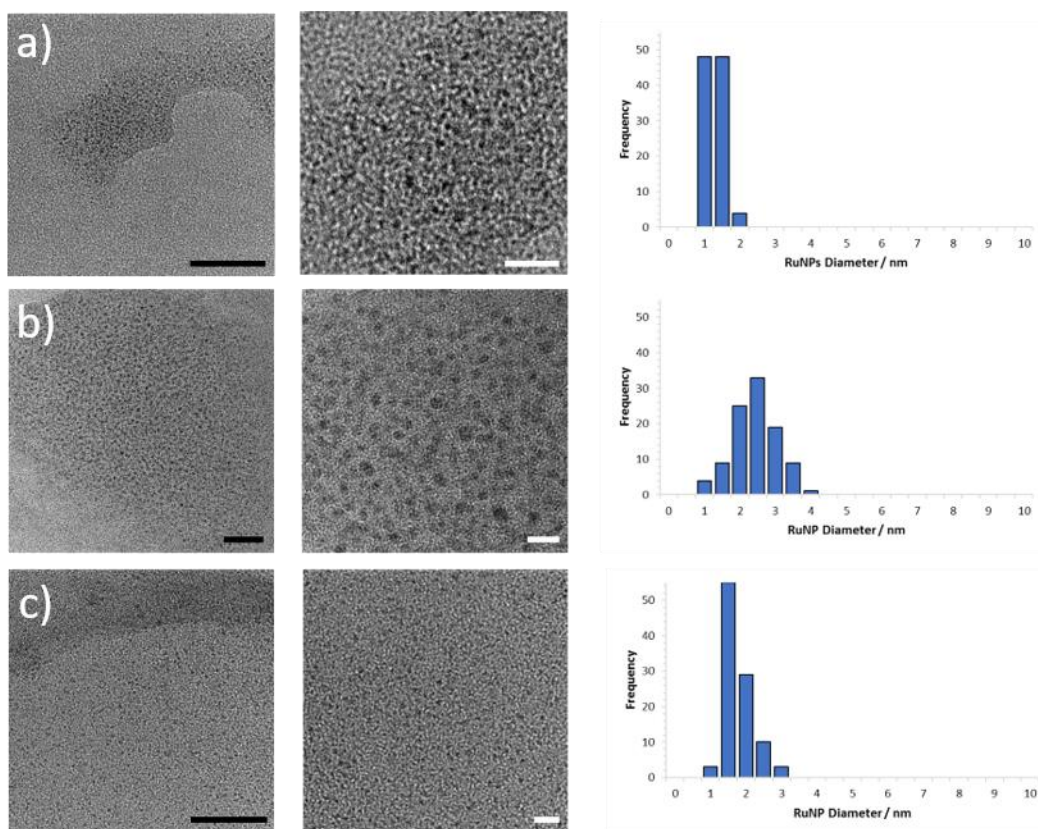


Figure 68: HRTEM images of a) RuNP@NH₂-PEGPIILP 6.6, b) RuNP@PPh₂-PEGPIILP 6.5, and c) RuNP@PEGPIILP 6.7. Average particle sizes of 1.0 ± 0.2 nm, 2.2 ± 0.6 nm and 1.5 ± 0.4 nm were determined based on >100 particles for a), b) and c) respectively. Scale bars are 25 nm (black) and 5 nm (white).

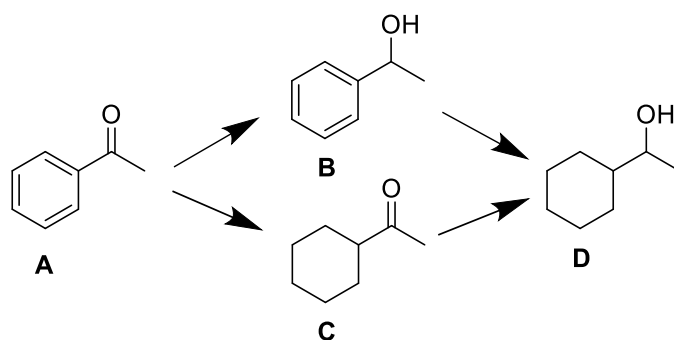
The data gathered in Figure 68 suggests that heteroatom donors anchored within the support may influence the kinetics of nanoparticle nucleation, as the ratio of heteroatom donors to Ru is the same as defined by the chosen monomer stoichiometry. However, it is noteworthy to add that relative nanoparticle size does not reflect differences in the relative electronic environments associated with the different supports. In this regard, further investigations and detailed chemisorption studies would be required to elucidate the true nature of the interfacial electronic metal-support effects.

No peaks associated with crystalline phases of Ru were observed in the XRD spectrum of any of the catalysts (data is presented in the appendix A67-69), which is a further indication that RuNP@R-PEGPIILP systems consist of small, well-dispersed particles throughout an amorphous support. This is also consistent with observations by Varma *et al.* who reasoned

that that low metal loading, in combination with high dispersion throughout the support was responsible for the absence of peaks in the XRD spectrum of RuNPs supported on silica.³²

6.4 Comparative catalyst testing

For the valorisation of biomass, there are two fundamental chemical transformations to be considered; the selective hydrogenation of carbonyls and aromatic functionalities, thus as a simple aromatic ketone, the aqueous phase hydrogenation of acetophenone is often regarded as an appropriate benchmark reaction and was used for preliminary catalyst optimisation. Furthermore, analysis of the reaction products is easily achieved using ^1H NMR spectroscopy. To this end, there have been several reports of the selective hydrogenation of model ketones catalysed by RuNP-based systems. For example, Chaudret *et al.* demonstrated a significant ligand effect of phosphine-stabilised RuNPs with a clear relationship between the basicity of the ligand stabiliser and catalyst activity.³³ Experimental results revealed that ketone hydrogenation was clearly more thermodynamically accessible than reduction of the aryl ring on isolated systems. However, in the case of acetophenone, where the ketone is directly attached to the arene ring, selectivity for C=O hydrogenation was markedly lower due to the increased possibility of simultaneous coordination of both the ketone and phenyl ring onto the RuNP surface.



Scheme 58: Possible products from the hydrogenation of acetophenone.

The main products from the reduction of acetophenone are depicted in Scheme 58. Selective hydrogenation of the aryl ring of acetophenone (**A**), results in the formation of cyclohexylmethylketone (**C**), whereas selective hydrogenation of the carbonyl results in the formation of 1-phenylethanol (**B**). Finally, both possible intermediates can then be further hydrogenated to the fully reduced product, cyclohexylethanol (**D**). To this end, initial catalyst screening focused on the selective formation of 1-phenylethanol (**B**).

6.5 Reaction optimisation

Catalyst screening was conducted in a 50 mL temperature-controlled Parr benchtop reactor. In a typical procedure, a glass insert was charged with 1 mmol acetophenone and 0.1 mol% catalyst, based on the Ru content as determined by ICP-OES analysis. After dilution with 13 mL of the appropriate solvent, hydrogen was successively introduced and released from the reactor five times to purge the apparatus, before pressurising to 70 psi and heating at 50 °C for the allocated time. The extent of conversion and reaction selectivity was determined by analysis of the resultant reaction mixture by ^1H NMR spectroscopy using 1,3-dinitrobenzene as the internal standard.

6.5.1 Solvent screen

Screening of the reaction solvent highlighted the ligand effect on catalyst performance, as higher conversion and selectivity was achieved with the PPh_2 -modified catalyst compared with its amino-modified counterpart in almost all cases. Interestingly, despite the limited solubility of the substrate, both heteroatom donor functionalised catalysts performed most efficaciously in water reaching moderate conversions with high selectivities, which is consistent with the promotional effect of water discussed earlier. For all solvents examined, **B** was the major product and trace amounts of **D** were obtained as the only other identifiable product. Furthermore, both catalysts exhibit a clear trend with regards to hydrogen donor ability such that activity increased in the order of ethanol < 1:1 ethanol/water < water. Reactions conducted in toluene and 2-methyl THF gave a slight improvement in selectivity, however, this is most likely associated with the low concentration of **B** available to hydrogenate further as conversions were extremely poor in both cases. In particular, the enhancement in selectivity obtained with **6.5** compared with **6.6** is further evidence that whilst intrinsically linked, catalyst performance is not ultimately dictated by the relative particle sizes and in these systems, may be more strongly linked to the influence of the heteroatom on the electronic properties of the metal surface.

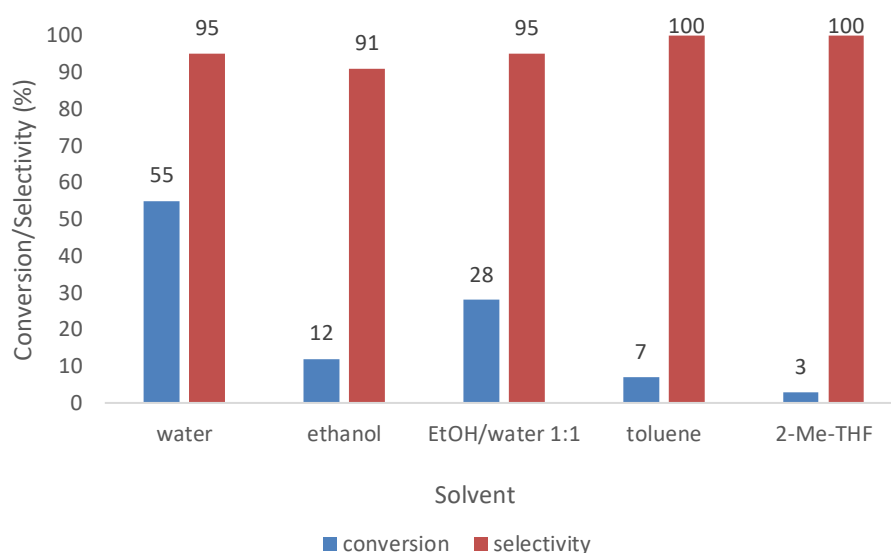


Figure 69: Conversion and selectivity for the hydrogenation of acetophenone as a function of solvent. Reaction conditions: 1 mmol acetophenone, 0.1 mol% RuNP@PPh₂-PEGPIILP (6.5), 70 psi H₂, 50°C, 13 mL solvent, reaction time = 3 hours. Conversion and selectivity determined by ¹H NMR spectroscopy with 1,3-dinitrobenzene as the internal standard. Selectivity for 1-phenylethanol = [% 1-phenylethanol / (% 1-phenylethanol + % cyclohexylethanol)].

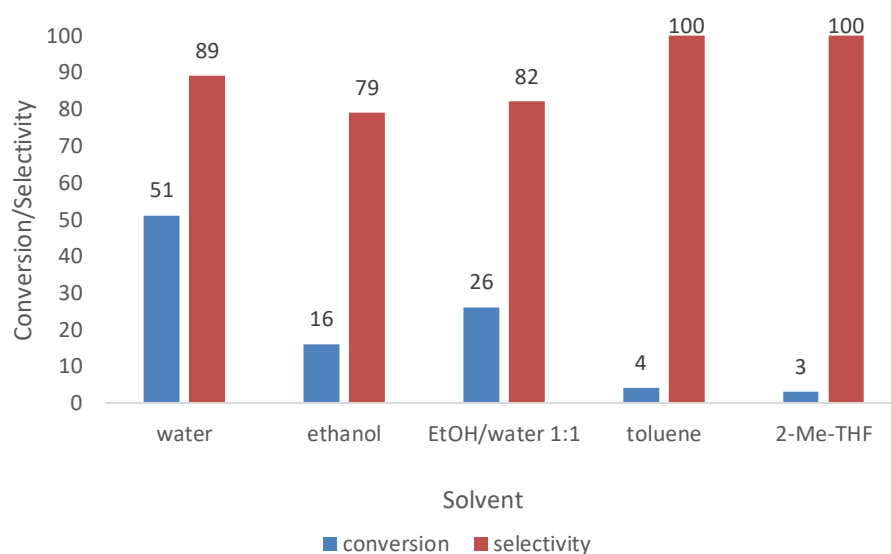
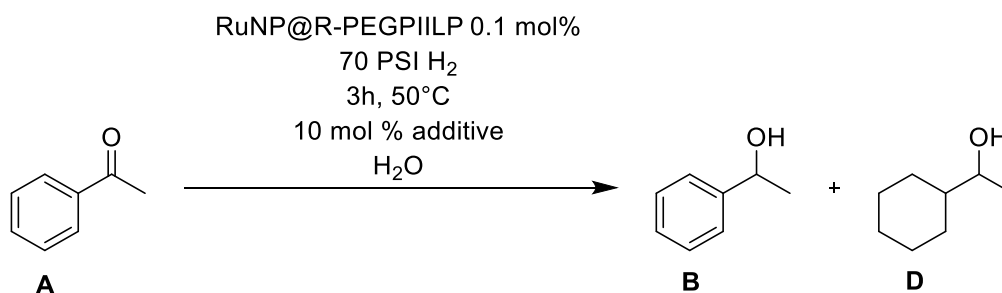


Figure 70: Conversion and selectivity for the hydrogenation of acetophenone as a function of solvent. Reaction conditions: 1 mmol acetophenone, 0.1 mol% RuNP@NH₂-PEGPIILP (6.6), 70 psi H₂, 50°C, 13 mL solvent, reaction time = 3 hours. Conversion and selectivity determined by ¹H NMR spectroscopy with 1,3-dinitrobenzene as the internal standard. Selectivity for 1-phenylethanol = [% 1-phenylethanol / (% 1-phenylethanol + % cyclohexylethanol)].

Although not definitive evidence, the superior catalyst performance under a purely aqueous environment also certainly highlights the possible activating role of water in the reaction as discussed above. However, whilst molecular simulation studies may provide deeper insight into any water-mediated activation, it would be challenging to accurately model the complex network of interactions between the substrate, catalyst, support and solvent.

6.5.1 Additive screen

Several recent literature reports have provided compelling evidence that the addition of base can improve selectivity for the ruthenium catalysed hydrogenation of ketones.^{34, 35} Based on this precedent, the influence on selectivity of various inorganic bases was investigated for the hydrogenation of acetophenone. Additionally, a series of water tolerant Lewis acids were also screened on the basis that activation of the carbonyl may enhance the rate of hydrogenation.



Scheme 59: Catalyst screening of base and Lewis acid additives for the selective hydrogenation of acetophenone.

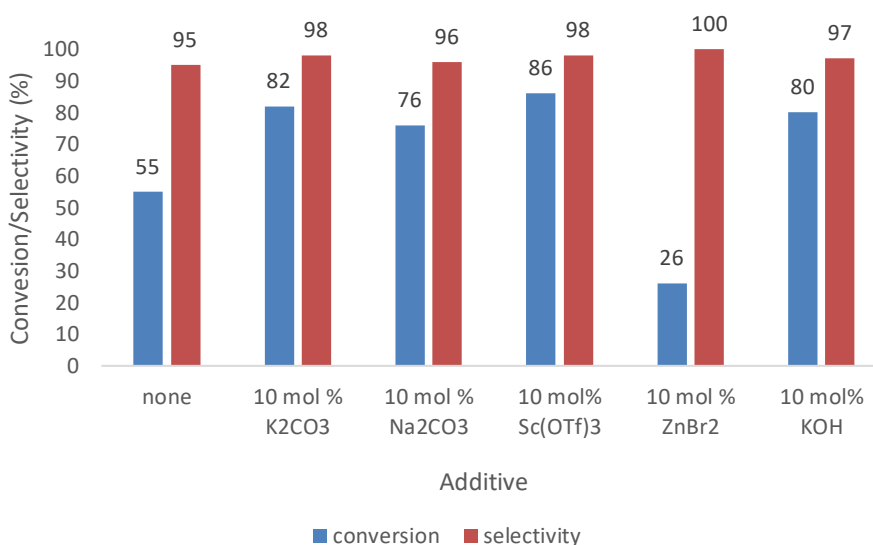


Figure 71: Effect of additives on the hydrogenation of acetophenone catalysed by 6.5. Reaction conditions: 1 mmol acetophenone, 0.1 mol% RuNP@PPh₂-PEGPIILP, 0.1 mmol additive, 13 mL water, 50°C, 70 psi H₂, reaction time = 3 hours. Conversion and selectivity determined by ¹H NMR spectroscopy with 1,3-dinitrobenzene as the internal standard. Selectivity for 1-phenylethanol = [% 1-phenylethanol / (% 1-phenylethanol + % cyclohexylethanol)].

The addition of various additives resulted in a remarkable improvement in catalyst performance for the selective hydrogenation of acetophenone catalysed by 6.5, with the most significant enhancement achieved with 10 mol % of the lewis acid, scandium triflate (31% and 3% improvement in conversion and selectivity, respectively). A similar improvement was also achieved for the addition of 10 mol % potassium carbonate (27% and 3% improvement on

conversion and selectivity, respectively). The addition of other inorganic bases such as sodium carbonate and potassium hydroxide also exhibited positive effects and a marked improvement on the benchmark reaction without any additive. At this stage it is difficult to rationalise this observation. However, an interaction between the ions and the Ru surface would inherently induce electronic changes to catalyst surface which may force changes in substrate adsorption modes or relative activation energies. Despite the improvements achieved with scandium triflate, the addition of zinc bromide resulted in a dramatic drop in catalyst activity, which may suggest that activation of the carbonyl with Lewis acids is not the underlying reason for the enhancement in activity.

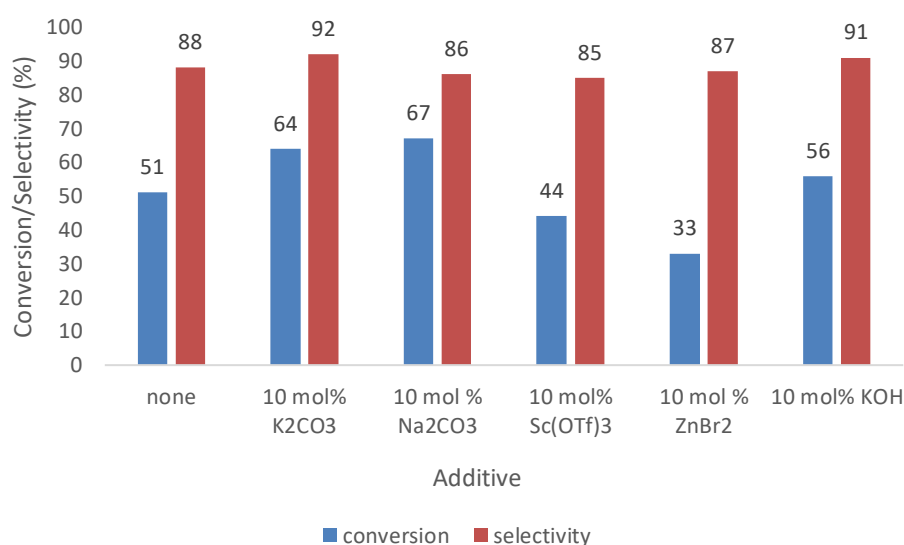


Figure 72: Effect of additives on the hydrogenation of acetophenone catalysed by **6.6**. Reaction conditions: 1 mmol acetophenone, 0.1 mol% RuNP@NH₂-PEGPIILP, 0.1 mmol additive, 13 mL water, 50°C, 70 psi H₂, reaction time = 3 hours. Conversion and selectivity determined by ¹H NMR spectroscopy with 1,3-dinitrobenzene as the internal standard. Selectivity for 1-phenylethanol = [% 1-phenylethanol / (% 1-phenylethanol + % cyclohexylethanol)].

Similar enhancements were also obtained for the selective hydrogenation of acetophenone catalysed by **6.6**, as the addition of potassium carbonate resulted in a marked improvement in conversion and selectivity of 13% and 4%, respectively. Catalyst performance was also improved on the addition of other additives, although the presence of 10 mol % of the Lewis acid zinc bromide was again detrimental to catalysis. However, in stark contrast, the addition of Sc(OTf)₃ to reactions catalysed by **6.6** resulted in a 7% drop in catalyst activity and 3% drop in selectivity compared with the positive effect obtained for catalyst **6.5**. These results again further confirm that **6.5** is a more efficient system for the selective hydrogenation of acetophenone.

In this regard, the base may well act as an electronic promoter and enable an alternative mechanism for the adsorption and/or activation of hydrogen on the ruthenium surface. Furthermore, the results in Figure 71 suggest that the cation of the additive may be more influential than the anion in promoting catalyst activity as hydrogenation catalysed by **6.5** proved to be more efficient in the presence of K_2CO_3 and KOH compared with Na_2CO_3 . This observation is perhaps not unprecedented as the DLVO theory reasons that the outer layer of the NPs is anionic in nature, thus a strong interaction with cationic species would be expected.

Whilst optimum performance was achieved in the presence of $Sc(OTf)_3$, potassium carbonate was considered to be the base of choice for further optimisation studies as it is a readily available and cheap additive and its use avoids the potential accumulation of lanthanide-based waste. To identify the optimum substrate:base ratio, a series of reactions were conducted in parallel to monitor the conversion and product distribution as a function of equivalents of potassium carbonate.

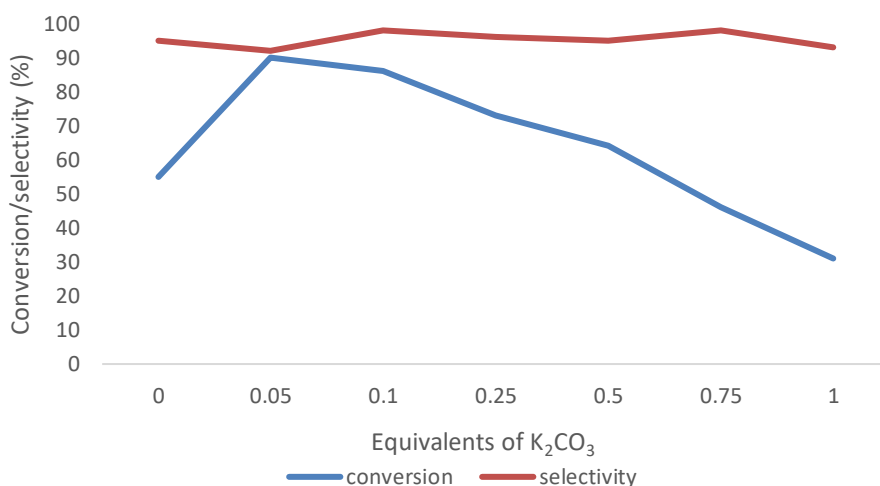


Figure 73: Conversion and selectivity for the hydrogenation of acetophenone catalysed by **6.5** in the presence of varying amounts of K_2CO_3 . Reaction conditions: 1 mmol acetophenone, 0.1 mol% $RuNP@PPh_2-PEGPIILP$ (**6.5**), 13 mL water, $50^\circ C$, 70 psi H_2 , reaction time = 3 hours. Conversion and selectivity determined by 1H NMR spectroscopy with 1,3-dinitrobenzene as the internal standard. Selectivity for 1-phenylethanol = [% 1-phenylethanol / (% 1-phenylethanol + % cyclohexylethanol)].

The profile depicted for the hydrogenation of acetophenone catalysed by **6.5** clearly demonstrates that only catalytic amounts of base are required to achieve optimum performance. The addition of 5 mol % K_2CO_3 resulted in a substantial increase in activity of 37%, although a minor drop in selectivity of 3% was observed. Selectivity peaks at 98% in the presence of 10 mol % base, which corresponds to an increase of 3%; this is also accompanied by a dramatic increase in conversion from 55% to 86%. Although selectivity remained high, a

substantial drop in catalyst activity occurred as the amount of base was increased above 10 mol % indicating that high concentrations of base is detrimental to catalysis.

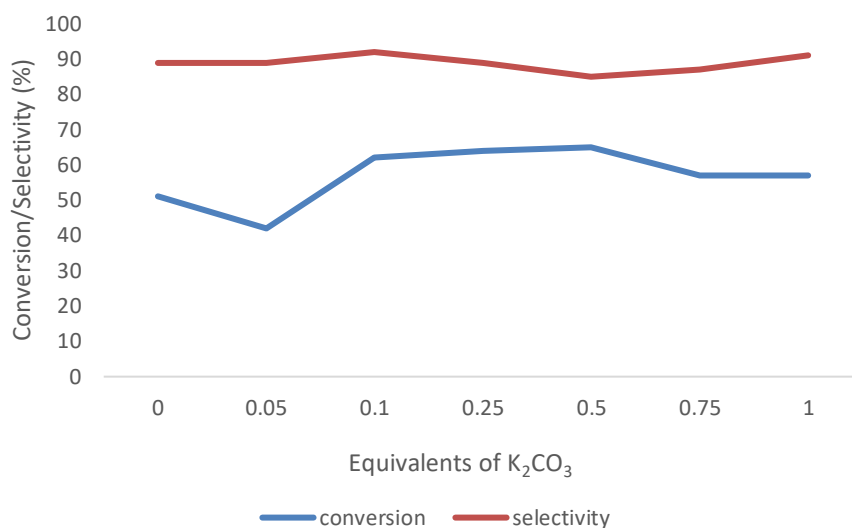
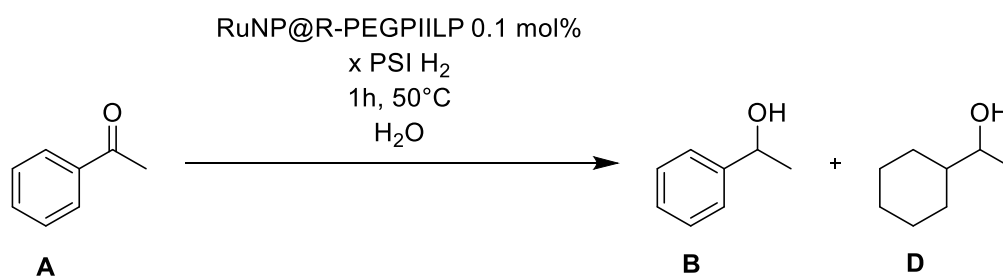


Figure 74: Conversion and selectivity for the hydrogenation of acetophenone catalysed by **6.5** in the presence of varying amounts of K_2CO_3 . Reaction conditions: 1 mmol acetophenone, 0.1 mol% $RuNP@NH_2-PEGPIILP$ (**6.6**), 13 mL water, $50^\circ C$, 70 psi H_2 , reaction time = 3 hours. Conversion and selectivity determined by 1H NMR spectroscopy with 1,3-dinitrobenzene as the internal standard. Selectivity for 1-phenylethanol = [% 1-phenylethanol / (% 1-phenylethanol + % cyclohexylethanol)].

Similarly, the amino-functionalised catalyst exhibited optimum performance in the presence of 10 mol % potassium carbonate, although the enhancement in conversion was only 11% with a 3% increase in selectivity. In contrast to the PPh_2 -functionalised catalyst **6.5**, the activity of **6.6** appears to gradually increase with the addition of base up to 50 mol%, representing a 14% increase in activity. Although the drop in activity was less marked than for the PPh_2 counterpart, the onset of catalyst deactivation begins after the addition of 75 mol % base.

6.5.2 Effect of Pressure

The conversion of acetophenone was then monitored as a function of pressure on the basis that under the reaction conditions, the low solubility of molecular hydrogen may limit the effective mass transfer. To prevent full consumption of the substrate at elevated pressure, the reaction time was decreased to 45 minutes. For both catalysts, increasing the hydrogen pressure resulted in an incremental increase in conversion up to 350 psi, at which point the reaction no longer appears to operate under dissolution control and the conversion begins to plateau.



Scheme 60: Reaction scheme for the hydrogenation of acetophenone with varied hydrogen pressure.

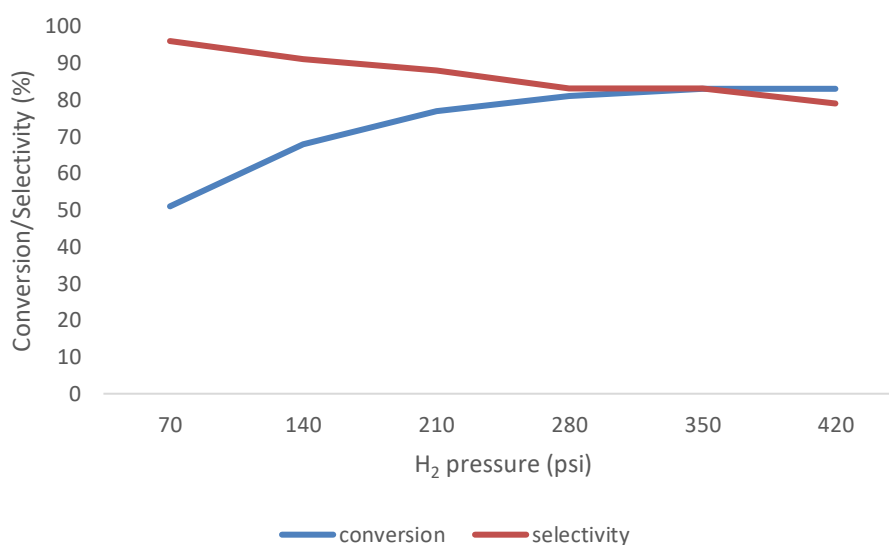


Figure 75: Conversion and selectivity for the hydrogenation of acetophenone as a function of hydrogen pressure. Reaction conditions: 1 mmol acetophenone, 0.1 mol% RuNP@PPh₂-PEGPIILP (6.5), 0.1 mmol K₂CO₃, 13 mL water, 50°C, reaction time = 45 mins. Conversion and selectivity determined by ¹H NMR spectroscopy with 1,3-dinitrobenzene as the internal standard. Selectivity for 1-phenylethanol = [% 1-phenylethanol / (% 1-phenylethanol + % cyclohexylethanol)].

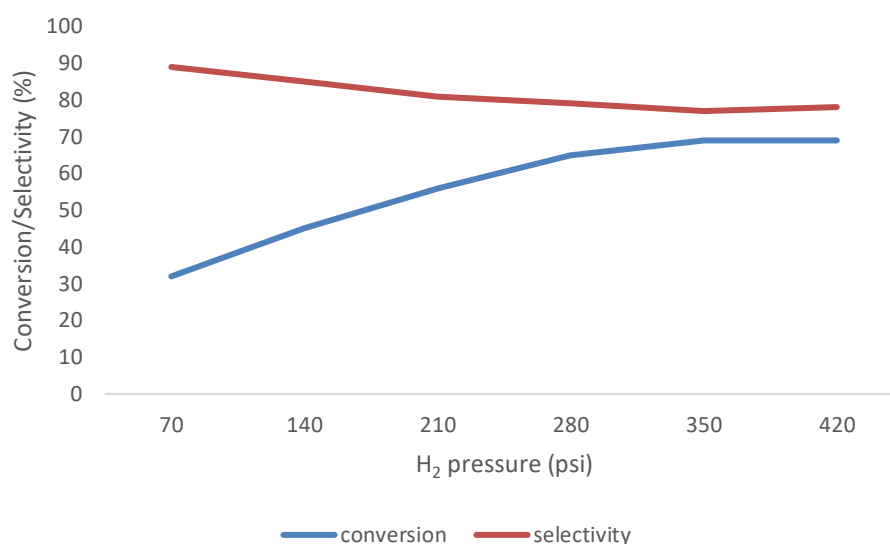


Figure 76: Conversion and selectivity for the hydrogenation of acetophenone as a function of hydrogen pressure. Reaction conditions: 1 mmol acetophenone, 0.1 mol% RuNP@NH₂-PEGPIILP (6.6), 0.1 mmol K₂CO₃, 13 mL water, 50°C, reaction time = 45 mins. Conversion and selectivity determined by ¹H NMR spectroscopy with 1,3-dinitrobenzene as the internal standard. Selectivity for 1-phenylethanol = [% 1-phenylethanol / (% 1-phenylethanol + % cyclohexylethanol)].

Whilst the activity of the catalyst can be maximised at higher hydrogen pressure, this is at the expense of selectivity which drops gradually over the pressure range. To investigate whether the high selectivity obtained at lower pressure was simply a result of lower conversion, a series of batch reactions catalysed by RuNP@PPh₂-PEGPIILP were conducted in order to compare selectivity at similar conversion (85-95%).

Table 33: Effect of H₂ pressure on selectivity for the 6.5 catalysed hydrogenation of acetophenone to 1-phenylethanol at high conversion.

| Entry ^a | H ₂ pressure (psi) | Time (hours) | Conversion (%) ^b | Selectivity (%) ^b | TOF (h ⁻¹) ^c |
|--------------------|-------------------------------|--------------|-----------------------------|------------------------------|-------------------------------------|
| 1 | 35 | 3.5 | 89 | 98 | 254 |
| 2 | 70 | 3 | 86 | 98 | 287 |
| 3 | 105 | 3 | 95 | 86 | 316 |
| 4 | 140 | 2.5 | 86 | 78 | 344 |
| 5 | 175 | 2.5 | 94 | 76 | 380 |
| 6 | 210 | 2 | 85 | 77 | 420 |

^aReaction Condition: 1 mmol acetophenone, 0.1 mol% RuNP@PPh₂-PEGPIILP, 0.1 mmol K₂CO₃, 13 mL water, 50°C. ^b Conversion and selectivity determined by ¹H NMR spectroscopy with 1,3-dinitrobenzene as the internal standard. ^c TOF = moles product per mole catalyst per hour based on total Ru content. Selectivity for 1-phenylethanol = [% 1-phenylethanol / (% 1-phenylethanol + % cyclohexylethanol)].

The results presented in Table 33 clearly demonstrate that higher selectivity is indeed achieved exclusively as a result of the lower pressure, which may impose a higher activation barrier for aryl hydrogenation, rather than an artefact of low conversion. Therefore, 70 psi was chosen as the optimum pressure for further studies as both high conversions and selectivity can be achieved even though the reaction is mass transfer limited with regards to the dissolution of H₂.

6.5.3 Catalyst comparison

Having established the optimum conditions, a series of batch reactions were conducted to compare the heteroatom modified supports against the benchmark unmodified catalyst, as well as a sample of the commercially available Ru/C.

Table 34: Comparison of catalysts for the Ru catalysed hydrogenation of acetophenone to 1-phenylethanol.

| Entry ^a | Catalyst | Conversion (%) ^b | Selectivity (%) ^b |
|--------------------|---------------------------------|-----------------------------|------------------------------|
| 1 | RuNP@PPh ₂ -PEGPIILP | 99 | 98 |
| 2 | RuNP@NH ₂ -PEGPIILP | 92 | 89 |
| 3 | RuNP@PEGPIILP | 90 | 83 |
| 4 | Ru/C | 69 | 80 |

^aReaction conditions: 1 mmol acetophenone, 0.1 mol% catalyst, 0.1 mmol K₂CO₃, 13 mL water, 50°C, 70 psi H₂, reaction time = 4 hours. ^b Conversion and selectivity determined by ¹H NMR spectroscopy with 1,3-dinitrobenzene as the internal standard. Selectivity for 1-phenylethanol = [% 1-phenylethanol / (% 1-phenylethanol + % cyclohexylethanol)].

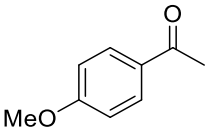
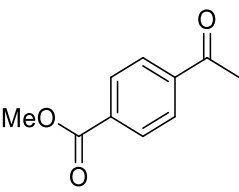
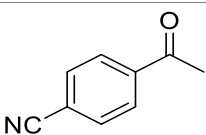
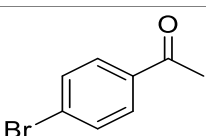
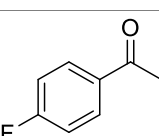
Gratifyingly, both heteroatom donor modified catalysts outperformed the benchmark catalyst **6.7** (Table 34, entries 1-3) and demonstrated a significant improvement over the commercially available catalyst (entry 4). The results presented in Table 34 demonstrate that PIILs can significantly enhance catalyst activity and even **6.7** which does not contain a heteroatom donor gives a 21% improvement in conversion compared to Ru/C. Whilst heteroatom donor modified PIIL supports provide only a marginal improvement in catalyst activity, the heteroatom donor appears crucial to obtaining high selectivity. Moreover, the nature of the

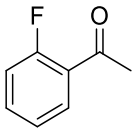
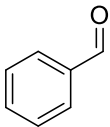
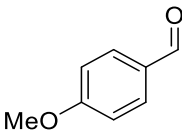
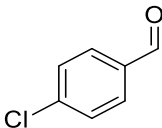
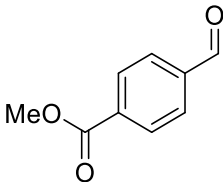
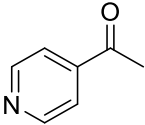
donor is also a key aspect, as the phosphine modification outperformed all other catalysts under the optimum conditions.

6.5.4 Substrate scope

To further investigate the influence of the stabilising heteroatom donors, comparative catalyst testing was conducted on the hydrogenation of a range of substrates.

Table 35: Selective hydrogenation of aromatic and heteroaromatic ketones and aldehydes catalysed by PIILP supported RuNPs.

| Entry ^a | Substrate | Catalyst | Time (hours) | Conversion (%) ^b | Selectivity (%) ^b |
|--------------------|---|----------|--------------|-----------------------------|------------------------------|
| 1 |  | 6.5 | 4 | 97 | 88 |
| | | 6.6 | 4 | 42 | 96 |
| | | 6.7 | 4 | 40 | 97 |
| 2 |  | 6.5 | 4 | 72 | 97 |
| | | 6.6 | 4 | 26 | 94 |
| | | 6.7 | 4 | 19 | 90 |
| 3 |  | 6.5 | 4 | 0 | 0 |
| | | 6.6 | 4 | 0 | 0 |
| | | 6.7 | 4 | 0 | 0 |
| 4 |  | 6.5 | 4 | 45 | 37 |
| | | 6.6 | 4 | 32 | 21 |
| | | 6.7 | 4 | 28 | 33 |
| 5 |  | 6.5 | 4 | 82 | 100 |
| | | 6.6 | 4 | 53 | 97 |

| | | | | | |
|-----------|---|------------|----------|-----------|------------|
| | | 6.7 | 4 | 50 | 97 |
| 6 |  | 6.5 | 4 | 99 | 98 |
| | | 6.6 | 4 | 63 | 95 |
| | | 6.7 | 4 | 67 | 94 |
| 7 |  | 6.5 | 2 | 97 | 100 |
| | | 6.6 | 2 | 67 | 100 |
| | | 6.7 | 2 | 85 | 100 |
| 8 |  | 6.5 | 6 | 90 | 100 |
| | | 6.6 | 6 | 47 | 100 |
| | | 6.7 | 6 | 62 | 100 |
| 9 |  | 6.5 | 2 | 80 | 100 |
| | | 6.6 | 2 | 32 | 100 |
| | | 6.7 | 2 | 12 | 100 |
| 10 |  | 6.5 | 3 | 73 | 100 |
| | | 6.6 | 3 | 30 | 100 |
| | | 6.7 | 3 | 61 | 100 |
| 11 |  | 6.5 | 4 | 97 | 100 |
| | | 6.6 | 4 | 30 | 100 |
| | | 6.7 | 4 | 36 | 100 |

^aReaction conditions: 1 mmol substrate, 0.1 mol % catalyst, 0.1 mmol K₂CO₃, 13 mL water, 50°C, 70 psi H₂. ^b Conversion and selectivity determined by ¹H NMR spectroscopy with 1,3-dinitrobenzene as the internal standard. Selectivity for 1-phenylethanol = [% 1-phenylethanol / (% 1-phenylethanol + % cyclohexylethanol)].

Preliminary catalyst testing focused on substituted acetophenones. Introducing a methoxy group at the *para*- position did not affect the conversion for the reaction catalysed by **6.5**, however, selectivity dropped from 98% to 88% suggesting that the electronic effect of the electron donating group alters the reactivity of both the carbonyl and aromatic ring (entry 1). Under the same conditions, **6.6** and **6.7** were less active than **6.5** and gave conversions of 42 and 40% respectively. While both catalysts gave markedly higher selectivities than **6.5**, it will be necessary to run the reaction to higher conversion to obtain a meaningful comparison. Hydrogenation of 4-acetylbenzoate was more challenging as conversions only reached 26% and 19% for **6.6** and **6.7**, respectively, and the high selectivities of 94% and 90% are again likely associated with the low concentration of the partially reduced product (entry 2). Gratifyingly though, **6.5** was more efficient and gave a conversion of 72% with 97% selectivity. No reduction products were obtained at all for the hydrogenation of 4-acetylbenzonitrile with any of the catalysts tested (entry 3). Since this result was not specific to any catalyst, it is likely that the nature of the substrate is responsible for the inactivity. In this regard, as the substrate is present in a 1000-fold excess, the nitrile group may well bind to the surface ruthenium atoms and saturate the active sites and deactivate the catalyst (*vide infra*).

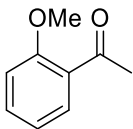
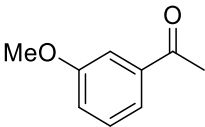
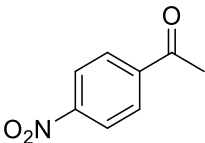
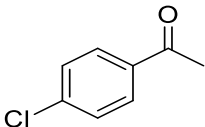
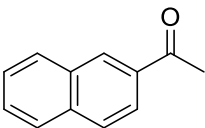
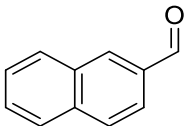
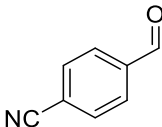
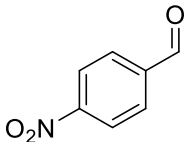
The hydrogenation of 4-bromoacetophenone gave poor selectivity in all cases due to the formation of acetophenone *via* dehalogenation (entry 4). For the reaction catalysed by **6.5**, the reaction mixture comprised of the starting material (65%), acetophenone (11%), the product 1-(4-bromophenyl)ethanol (9%), and 1-phenylethanol (15%). Whilst these results do not indicate whether 1-phenylethanol is formed *via* dehalogenation of 1-(4-bromophenyl)ethanol or *via* hydrogenation of acetophenone formed as the dehalogenation product of the starting material, this distribution suggests that overall, dehalogenation occurs at a similar rate to hydrogenation. Similar product distributions were also observed for the reaction catalysed by **6.6** and **6.7**. In contrast, the hydrogenation of 4-fluoroacetophenone showed no dehalogenation products as a result of an increase in carbon-halogen bond strength, and 100% selectivity for 1-(4-fluorophenyl)ethanol was achieved for the reaction catalysed by **6.5** (entry 5). However, the conversion of 82% was lower than that of 98% obtained with acetophenone suggesting that electron withdrawing groups deactivate the carbonyl toward hydrogenation. In this regard, the fluorine substituent may deactivate the carbonyl towards either adsorption and/or hydrogenation. Similar observations were made in the case of **6.6** and **6.7** as 97% selectivity was obtained but the conversions were much lower

than that obtained with **6.5**. Gratifyingly, **6.5** catalysed the hydrogenation of 2-fluoroacetophenone under the same conditions in near-quantitative conversion and 98% selectivity which suggests that substitution at this position does not deactivate the carbonyl (entry 6). In many cases, substitution at the *ortho*- position is often detrimental to catalysis due to steric effects, however, in this case the fluorine atom is likely too small to cause any such negative effect. The hydrogenation of 4-acetylpyridine was examined as a model heteroaromatic substrate. Fortunately, in contrast to the Pd-based systems discussed in Chapters 2 and 4 that were unable to catalyse reactions involving heteroaromatics, **6.5** catalysed this hydrogenation to afford 1-(4-pyridyl)ethanol in near-quantitative conversion and 100% selectivity after 4 hours (entry 11). Although the other Ru catalysts were sluggish in comparison, both showed some degree of activity.

The hydrogenation of a series of aromatic aldehydes was also investigated under the optimum conditions. For each of the substrates (entries 7-10), no reduction of the aromatic ring was observed, and the aromatic alcohols were obtained as the sole product. The origin of the exclusive selectivity is likely associated with the enhanced reactivity of the aldehydes, which are more sterically accessible than the corresponding ketones. Overall, the results clearly show that a heteroatom donor is beneficial for catalysis as it appears to enhance both catalyst activity and selectivity. As comparative testing has demonstrated that phosphine and amino functionalised supports can have a substantial impact on the performance, it would be useful to initiate an optimisation survey of a wider series of heteroatom donor-modified supports to rationalise and establish an activity relationship profile and thereby further improve the credentials of the system.

Given the superior performance of the phosphine-modified catalyst, the scope of substrates was further extended to provide a more comprehensive and thorough evaluation of the efficacy of **6.5** for the selective hydrogenation of challenging substituted aryl carbonyls and aldehydes.

Table 36: Hydrogenation of further aromatic aldehydes and ketones catalysed by 6.5.

| Entry ^a | Substrate | Catalyst | Time (hours) | Conversion (%) ^b | Selectivity (%) ^b |
|--------------------|---|----------|--------------|-----------------------------|------------------------------|
| 1 |  | 6.5 | 4 | 83 | 100 |
| 2 |  | 6.5 | 4 | 96 | 100 |
| 3 |  | 6.5 | 8 | 50 | 100 ^c |
| 4 |  | 6.5 | 4 | 92 | 95 |
| 5 |  | 6.5 | 24 | 96 | 100 |
| 6 |  | 6.5 | 8 | 90 | 100 |
| 7 |  | 6.5 | 8 | 7 | 100 |
| 8 |  | 6.5 | 8h | 26 | 100 ^d |

^aReaction conditions: 1 mmol substrate, 0.1 mol % catalyst, 0.1 mmol K₂CO₃, 13 mL water, 50°C, 70 psi H₂. ^b Conversion and selectivity determined by ¹H NMR spectroscopy with 1,3-dinitrobenzene as the internal standard. ^c Selectivity for 4-aminoacetophenone. ^dSelectivity for 4-aminobenzaldehyde. Selectivity = [% desired product / (% desired product + % other products)].

Gratifyingly, **6.5** proved to be a highly active and selective catalyst for the partial reduction of most substrates examined in this study. Whilst selectivity remained at 100%, a slightly lower conversion was obtained with 2-methoxyacetophenone (entry 1) on comparison to its *para*-substituted counterpart; this is most likely due to the increased steric hindrance in close proximity to the carbonyl. A slight increase of 6% conversion was observed for 3-methoxyacetophenone (entry 2) compared with its *para*-substituted counterpart, which was somewhat unexpected as this may cause a slight depolarisation of the electrophilic carbonyl carbon. The drop in selectivity to 95% for the hydrogenation of 4-chloroacetophenone catalysed by **6.5** was the result of competing hydrodechlorination to afford acetophenone. However, the extent of dehalogenation was markedly less than 4-bromoacetophenone due to the increased strength of the C-Cl bond compared with the C-Br bond. Sterically demanding naphthyl-based substrates were tolerated and gave the corresponding alcohol as the sole product in excellent yield albeit after longer reaction times (entries 5 and 6). The reaction with 4-formylbenzonitrile (entry 7) exhibited a similar reaction profile to that of 4-acetylbenzonitrile, as only 7% conversion was achieved even after extending the reaction to 24 hours, further suggesting that nitriles may poison the active catalyst.

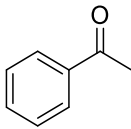
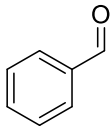
Interestingly, analysis of the post reaction mixture of the hydrogenation of 4-nitrobenzaldehyde (entry 8) revealed the presence of a single product, 4-aminoacetophenone which is formed by the selective reduction of the nitro fragment. As a weaker bond on comparison to the carbonyl, hydrogenation of the nitro group and formation of the amino ketone is not surprising. Inspection of the literature revealed that many Ru systems have been reported to catalyse the reduction of nitroarenes including RuNPs stabilised on modified Montmorillonite clay³⁶ and dendrimer encapsulated RuNPs.³⁷ However, even after prolonged reaction times of up to 24 hours, no further conversion of the starting material was observed, suggesting that the reaction may be self-inhibiting i.e. the product formed acts as a catalyst poison (*vide infra*). Not surprisingly, the same profile was also observed for 4-nitroacetophenone (entry 3) which gave 4-aminoacetophenone as the sole product in 50% yield after 8h. These observations are in keeping with the discussion in section 6.1 as excess of amines have been shown to be detrimental to catalyst activity. Overall, from a thorough survey of a range of substitute aldehydes and ketones, steric parameters appear to have a

strong influence on the catalyst activity, with bulkier substrates requiring longer reaction times. However, there is an absence of distinct trends with regard to the substrate's electronic parameters. In this regard, changes in the physical properties i.e. the state of matter and solubility may be the more dominant factor. For instance, some substrates are liquids and thus could be more homogeneously dispersed *via* efficient agitation, whereas insoluble solids would accumulate at the interface of the solution which would severely inhibit its accessibility to the active site.

6.5.5 Catalyst poisoning

Prompted by the unprecedentedly poor catalyst activity in the presence of nitrile-substituted substrates and amines accumulated by reduction of the corresponding nitro, a series of batch reactions were conducted to determine whether these substrates poison the catalyst or whether they are simply inactive under the reaction conditions. To this end, the hydrogenation of acetophenone and benzaldehyde (1 mmol) was catalysed by **6.5** in the presence of benzonitrile or aniline as model poisons. Furthermore, as the hydrogenation of 4-nitroacetophenone and 4-nitrobenzaldehyde reached only 50% and 26%, respectively, 0.5 and 0.26 mmol aniline was added to more accurately represent the reaction conditions under which poisoning occurred.

Table 37: Results of catalyst poisoning studies for the hydrogenation of acetophenone and benzaldehyde in the presence of amines and nitriles.

| Entry ^a | Substrate | Catalyst | Time (hours) | Conversion (%) ^b | Selectivity (%) ^b |
|--------------------|---|-------------------------|--------------|-----------------------------|------------------------------|
| 1 |  | 6.5 | 4 | 99 | 98 |
| | | 6.5 ^c | 4 | 0 | 0 |
| | | 6.5 ^d | 4 | 37 | 100 |
| 2 |  | 6.5 | 2 | 97 | 100 |
| | | 6.5 ^c | 2 | 30 | 100 |
| | | 6.5 ^e | 2 | 95 | 100 |

^aReaction conditions: 1 mmol substrate, 0.1 mol % RuNP@PPh₂-PEGPIILP, 0.1 mmol K₂CO₃, 13 mL water, 50°C, 70 psi H₂. ^bConversion and selectivity determined by ¹H NMR spectroscopy with 1,3-dinitrobenzene as the internal standard. ^c

Reaction conducted in the presence of 1 mmol benzonitrile. ^d Reaction conducted in the presence of 0.5 mmol aniline. ^e Reaction conducted in the presence of 0.26 mmol aniline. Selectivity = [% desired product / (% desired product + % other products)].

The results in Table 37 show that **6.5** is completely inhibited in the presence of stoichiometric amounts of benzonitrile, as a quantitative amount of acetophenone was isolated after the reaction (entry 1). This therefore suggests a poisoning mechanism as 98% conversion of acetophenone was obtained under identical reaction conditions in the absence of the nitrile. Activity was also markedly diminished for the hydrogenation of benzaldehyde (entry 2), although some activity was retained as 30% conversion was achieved compared with 100% in the absence of nitrile. This could be associated with the lower energetic barriers for the less challenging reduction of an aldehyde on comparison with a ketone. Interestingly while the addition of aniline to reaction mixture also resulted in a substantial drop in activity of 63% for the hydrogenation of acetophenone (entry 1), there was only a drop of 2% for the hydrogenation of benzaldehyde (entry 2). These results suggest that aniline can poison, but that nitrile substrates seemingly act as a stronger poison. Poisoning could potentially arise *via* binding of the nitrogen onto the catalyst surface thus saturating all the available active sites. Moreover, although the results suggest some sort of catalyst inhibition, they do not confirm whether this is due to competitive adsorption or whether they induce chemical changes to the active site rendering the catalyst inactive. Alternatively, this difference could be a result of hydrogen bonding between the amine and carbonyl, which may prevent complete saturation and allow some activity to be retained.

6.5.6 Recycling

Having established that **6.5** and **6.6** are both efficient catalysts for the hydrogenation of ketones and aldehydes, both systems were examined for recyclability. In this case, benzaldehyde was chosen as the test substrate to monitor recyclability due to its short reaction time. Each cycle was conducted for 1.5 hours and the extent of conversion and selectivity quantified using ¹H NMR spectroscopy. Following this, the reaction vessel was subsequently charged with one further equivalent of starting material and re-pressurised with hydrogen.

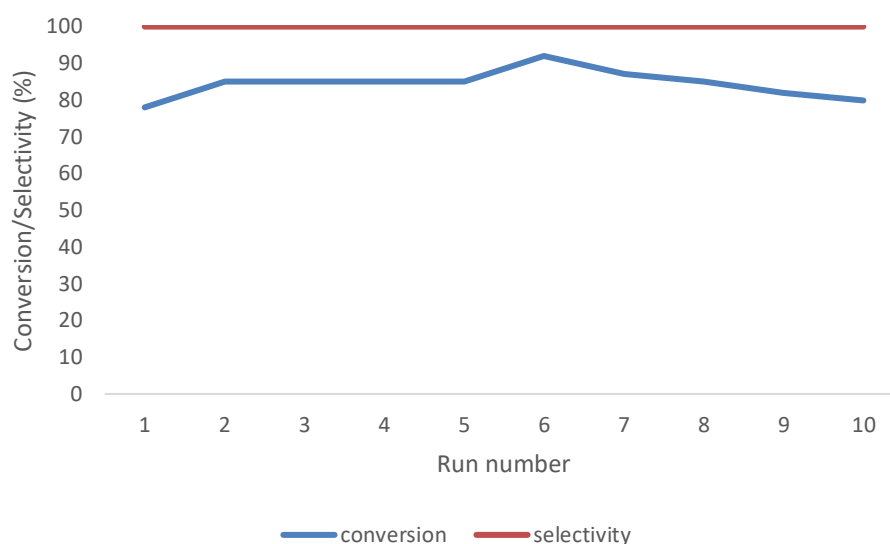


Figure 77: Recycling profile for the hydrogenation of benzaldehyde catalysed by **6.5**. Reaction conditions: 1 mmol substrate, 0.1 mol % RuNP@PPh₂-PEGPIILP, 0.1 mmol K₂CO₃, 13 mL water, 50°C, 70 psi H₂, reaction time = 90 mins. Conversion and selectivity determined by ¹H NMR spectroscopy with 1,3-dinitrobenzene as the internal standard. Selectivity for benzyl alcohol = [% benzyl alcohol / (% benzyl alcohol + % other products)].

The recycling profile for **6.5** (Figure 77) is encouraging and shows that despite an initial increase in conversion from 78% to 85% between the first and second runs, the catalyst reached a steady state between runs 2-5. Interestingly, between run 5 and 6, the aqueous layer was left overnight under a hydrogen atmosphere which resulted in a 7% increase in conversion to 92% for the subsequent recycle (run 6). After this point there was a gradual decline in activity up to run 10, at which point conversion was comparable to the first run (80%). The overall shape of the curve in the plot suggests that **6.5** may suffer an induction period or, is seemingly activated *via* continuous use. This increase in activity could be attributed to continuous leaching of Ru, enabling a parallel homogeneous type mechanism to proceed. However, ICP analysis of the Ru content in the organic phase was below the detection limit of the instrument, suggesting this was not the primary cause of activation. Alternatively, the activation could also be caused by successive reduction of any remaining surface RuO in the presence of hydrogen, thereby increasing the number of active sites available for catalysis. In this regard, post-reaction TEM analysis would be useful to identify whether particle morphology changes after prolonged exposure to the reaction conditions and vigorous agitation. Encouragingly, 100% selectivity for the carbonyl group was retained throughout the study.

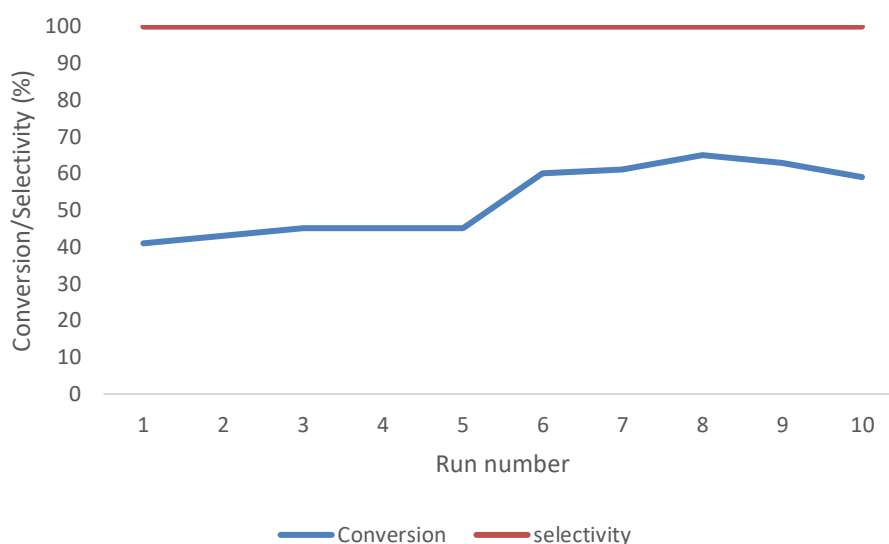


Figure 78: Recycling profile for the hydrogenation of benzaldehyde catalysed by **6.6**. Reaction conditions: 1 mmol substrate, 0.1 mol % RuNP@NH₂-PEGPIILP, 0.1 mmol K₂CO₃, 13 mL water, 50°C, 70 psi H₂, reaction time = 90 mins. Conversion and selectivity determined by ¹H NMR spectroscopy with 1,3-dinitrobenzene as the internal standard. Selectivity for benzyl alcohol = [% benzyl alcohol / (% benzyl alcohol + % other products)].

The recycle profile for **6.6** was qualitatively similar to that of **6.5** in that the selectivity remained constant at 100%, however, the catalyst activity was markedly lower. After a minor increase in conversion from 41% to 45% over the first two runs, conversions remained relatively constant over runs 2 to 5. As with **6.5**, the catalyst was left overnight under a hydrogen atmosphere which resulted in a marked increase in conversion from 45% to 60% between runs 5 and 6. If this ‘activation’ was also due to removal of surface ruthenium oxides, it suggests that reduction of the NH₂-functionalised catalyst may not have been as effective as its PPh₂-functionalised counterpart, i.e. more surface oxide was present. Alternatively, reoxidation of metallic Ru may be more facile in the case of **6.6**. There was a slight increase in conversion to 65% over runs 6-8 which was followed by a steady decline in activity to 59% conversion at run 10; however, this was still a notable improvement on the conversion of 41% in run 1 (41%).

To investigate this phenomenon further, pre and post-reaction XPS analysis coupled with the use of temperature-programmed reduction methods would allow a more realistic interpretation of the influence that heteroatom donors may exert on reduction of the catalyst. Similar observations were reported by Hutchings *et al.* who demonstrated that a decrease in the relative RuO content, and the associated morphological changes of the Ru crystallites containing better dispersity and increased content of metallic Ru, was responsible for an increase in activity of the spent catalysts.³⁸ In this regard, the application of the system within

a continuous flow protocol would both improve the recyclability and productivity of the system and eradicate the need for pre-activation of the catalyst in a one-off batch experiment once a steady state can be reached.

6.5.7 Complete reduction of acetophenone

As trace amounts of **D** was obtained in all reactions, it was envisaged that **D** could be obtained selectively as the sole product by judicious manipulation of the reaction conditions. Given the increased stability of the aryl ring with respect to hydrogenation under the previously optimised conditions, it was necessary to increase the reaction time, temperature and the hydrogen pressure to drive the reaction to completion. Having identified that the reaction occurs under dissolution control with regards to hydrogen solubility below 350 psi, reactions were performed at 420 psi on the basis that catalyst turnover and selectivity for **D** would be enhanced.

Table 38: Comparison of Ru catalysts for the selectivity hydrogenation of acetophenone to 1-cyclohexylethanol.

Reaction scheme: Acetophenone (**A**) reacts with Ru cat (0.1 mol%), K₂CO₃ (10 mol%), 420 PSI H₂, 20 h, 90°C, H₂O to produce 1-phenylethanol (**B**) and 1-cyclohexylethanol (**D**).

| Entry ^a | Catalyst | Conversion (%) ^b | Yield of D (%) ^b |
|--------------------|--|-----------------------------|------------------------------------|
| 1 | RuNP@PPh ₂ -PEGPIILP (6.5) | 100 | 100 |
| 2 | RuNP@NH ₂ -PEGPIILP (6.6) | 100 | 67 |
| 3 | RuNP@PEGPIILP (6.7) | 100 | 54 |
| 4 | Ru/C | 100 | 39 |

^aReaction conditions: 1 mmol substrate, 0.1 mol % catalyst, 0.1 mmol K₂CO₃, 13 mL water, 90°C, 420 psi H₂, reaction time = 20 hours. ^b Conversion and selectivity determined by ¹H NMR spectroscopy with 1,3-dinitrobenzene as the internal standard.

Remarkably, under these conditions, quantitative amounts of **D** were obtained albeit after a prolonged reaction time of 20 hours in the presence of 0.1 mol% **6.5**. Furthermore, the advantages of the cation-decorated support are clearly highlighted as all the PIILP catalysts

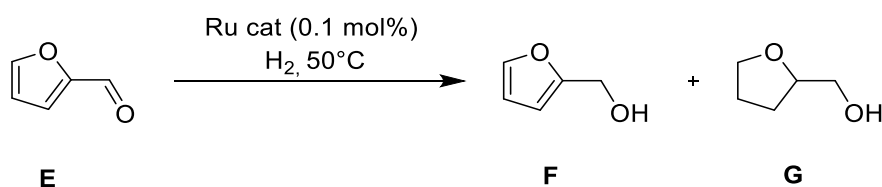
outperformed the commercial Ru/C. The data also suggests that catalyst performance is also related to the support functionality, as heteroatom donors enhanced the activity of the catalyst in comparison to **6.7** and Ru/C, and the PPh₂ modification proved crucial for optimum activity.

6.6 Application of RuNP@R-PIILP catalysts for the hydrogenation of bioderived substrates

In line with the ultimate aims of the project, the efficacy of PIILP-based catalysts for the production of fuel additives *via* the selective hydrogenation of renewable feedstock was investigated. In this regard, the selective production of the target products can be intrinsically difficult as hydrogenative transformations are often more challenging, requiring more extreme conditions.³⁹ Moreover, such conditions often give rise to extensive reaction networks including polyols and ring opening products formed due to the inherent instability of the intermediates and products. Even with clean feeds, as there is a myriad of products that may form under the reaction conditions, poisoning of the catalyst is often problematic. In a simplistic manner, the majority of reaction pathways involve two fundamental steps, consisting of metal catalysed hydrogenation/hydrogenolysis and various ring opening/closing or decarbonylation-based transformations. Chemistry on the support or particle surface such as acidic or basic sites can often accelerate these steps, and so methodical reaction optimisation is necessary.

6.6.1 PIILP-supported RuNP-catalysed hydrogenation of furfural

Having demonstrated that PIILP-stabilised RuNPs are efficient catalysts for the selective hydrogenation of acetophenone and its various derivatives, the substrate scope was extended to include furfural – a product obtained through processing of lignocellulosic-based biomass.⁴⁰ Furfural is highlighted as a sustainable source for the production of oxygen-containing value-added chemicals in the biorefinery sectors. Selective hydrogenation of the carbonyl in furfural (Scheme 61, **E**) yields furfuryl alcohol (**F**), a potential renewable source for resin production and more recently, a key intermediate for the sustainable generation of alkyl levulinates via acid catalysed alcoholysis.⁴¹ Further hydrogenation of the heteroaromatic ring affords tetrahydrofurfuryl alcohol (**G**).



Scheme 61: Products of the Ru catalysed hydrogenation of furfural.

Since the production of furfuryl alcohol consists of a single step and is more straightforward, it was chosen as an ideal benchmark transformation to investigate the performance of the PIILP catalysts. Given the structural and chemical differences between furfural and the model ketones previously investigated, the reaction parameters were optimised using the previously identified conditions as a lead (0.1 mol% catalyst, 70 psi H₂).

Table 39: Optimisation of the reaction parameters for the selective hydrogenation of furfural to furfuryl alcohol catalysed by 6.5.

| Entry ^a | Catalyst | Solvent | Additive | Conversion (%) ^b | Selectivity (%) ^b |
|--------------------|----------|----------------------|---|--------------------------------|---------------------------------|
| 1 | 6.5 | Water | None | 79 | 100 |
| 2 | 6.5 | Ethanol | None | 69 | 100 |
| 3 | 6.5 | Water/Ethanol 1:1 | None | 74 | 100 |
| 4 | 6.5 | Toluene | None | 44 | 100 |
| 5 | 6.5 | 2-Me-THF | None | 32 | 100 |
| 6 | 6.5 | Water | 0.1 eq K ₂ CO | 78 | 100 |
| 7 | 6.5 | Water | 0.25 eq K ₂ CO ₃ | 79 | 100 |
| 8 | 6.5 | Water | 0.5 eq K ₂ CO ₃ | 78 | 100 |

| | | | | | |
|-----------|-------------|-------|--|----|-----|
| 9 | 6.5 | Water | 1.0 eq K ₂ CO ₃ | 77 | 100 |
| 10 | 6.6 | Water | None | 63 | 100 |
| 11 | 6.7 | Water | None | 61 | 100 |
| 12 | Ru/C | Water | None | 28 | 100 |

^aReaction conditions: 1 mmol substrate, 0.1 mol % catalyst, 13 mL water, 50°C, 70 psi H₂, reaction time = 3 hours. ^b Conversion and selectivity determined by ¹H NMR spectroscopy with 1,3-dinitrobenzene as the internal standard. Selectivity for furfuryl alcohol = [% furfuryl alcohol / (% furfuryl alcohol + % tetrahydrofurfuryl alcohol)].

A survey of the solvent revealed that the catalyst performed best in the aqueous phase, achieving 79% conversion after a reaction time of 3 hours with complete selectivity for furfuryl alcohol (entry 1). Hydrogen bonding from the solvent appears to be crucial for enhanced activity as good conversions were also obtained in neat ethanol and in an ethanol-water mix, respectively (entries 2 and 3). Unlike the catalyst testing with acetophenone, moderate conversions were also achieved in the organic solvents; toluene and 2-methyl-THF, although these conversions were clearly markedly lower than the optimum (entry 4 and 5). The addition of potassium carbonate additive appeared to have no influence on conversion or selectivity, which is in stark contrast to the aromatic ketones and aldehydes studies above (entries 6-9). The results in Table 39 suggest that the aldehyde functionality is substantially more susceptible to hydrogenation than the heteroaromatic ring as no traces of the fully reduced tetrahydrofurfuryl alcohol were observed in any of the post-reaction mixtures. Ru-catalysed hydrogenation of the furan ring has been reported but this required much harsher conditions and temperatures in excess of 100°C.^{12,40} As anticipated, the PPh₂-modified catalyst performed the best whilst the two other PIILP-supported catalysts **6.6** and **6.7** substantially outperformed the commercial Ru/C sample (entries 10-12), further validating the advantages of the PIILP-based support.

On the basis that no reduction products derived from saturation of the heteroaromatic ring were observed, the conversion was measured as a function of pressure to investigate whether activity could be improved whilst maintaining 100% selectivity for **F**. To allow sufficient room for improvement in conversion, the reaction time was reduced to 45 minutes.

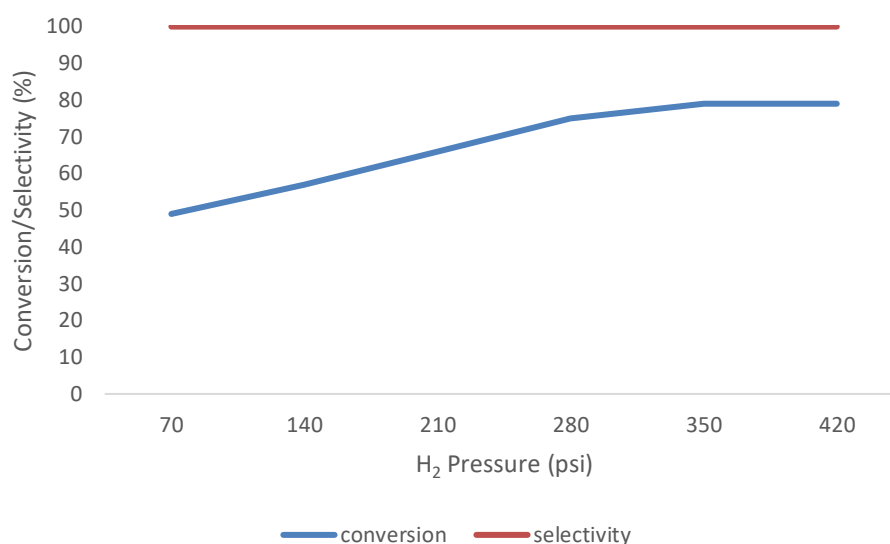
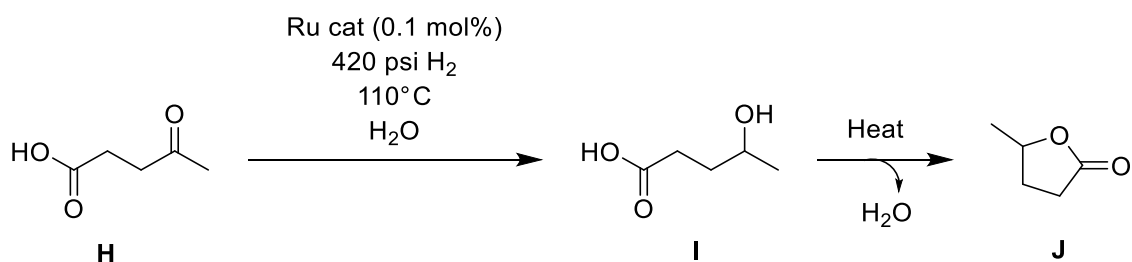


Figure 79: Conversion and selectivity for the hydrogenation of furfural as a function of pressure. Reaction conditions: 1 mmol substrate, 0.1 mol % RuNP@PPh₂-PEGPIILP, 13 mL water, 50°C, reaction time = 45 mins. ^b Conversion and selectivity determined by ¹H NMR spectroscopy with 1,3-dinitrobenzene as the internal standard. Selectivity for furfuryl alcohol = [% furfuryl alcohol / (% furfuryl alcohol + % tetrahydrofurfuryl alcohol)].

The plot in Figure 79 shows that increasing the hydrogen pressure results in a near-linear increase in conversion up to 350 psi, at which point conversion begins to plateau and any mass transfer limitations due to low solubility of hydrogen are surpassed. Interestingly, in stark contrast to the pressure survey conducted during the optimisation study for acetophenone, **F** was still obtained as the sole product indicating that reduction of the aromatic furan ring is more challenging than the phenyl ring of acetophenone. Under previously optimised conditions, and using a hydrogen pressure of 350 psi, quantitative conversion to **F** was obtained by increasing the reaction time to 90 minutes.

6.6.2 Levulinic acid and its ethyl ester

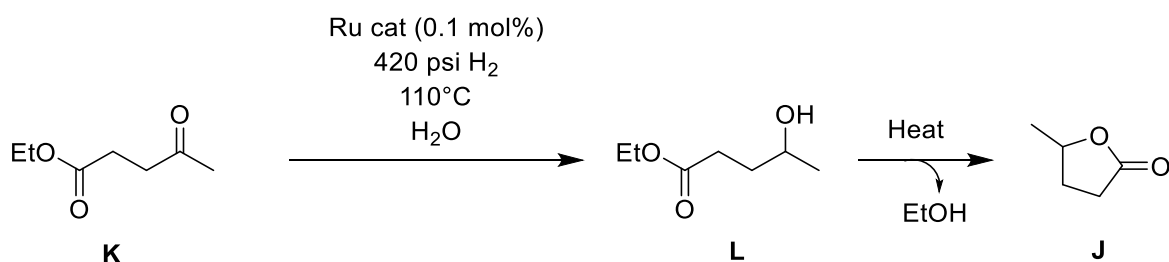
The encouraging results discussed above prompted an investigation into the selective hydrogenation of levulinic acid to γ -valerolactone. This particular transformation has been identified as one of the most fundamental challenges in the emerging area of green chemistry as successful strategies would present a new sustainable route to γ -valerolactone, which serves as a feedstock with diverse applications in the fine chemicals and fuel industries.⁴² The reaction begins with selective hydrogenation of the isolated ketone in levulinic acid (Scheme 62, **H**), to afford 4-hydroxypentanoic acid (**I**), which subsequently undergoes intramolecular cyclisation, liberating water and forming γ -valerolactone (**J**).



Scheme 62: Possible products of the Ru catalysed hydrogenation of levulinic acid.

Since molar equivalents of water accumulate as the reaction proceeds, it is important that the catalyst maintains its structural integrity and is hydrothermally stable. Due to the intrinsic nature of the reaction, a high temperature is required to drive the cyclisation towards completion. Alternatively, the cyclisation can also be promoted by a bifunctional catalyst containing Brønsted or Lewis acidic sites.⁴³ Whilst this technique can be favourable under certain reaction conditions, the substrate scope is often limited due to the sensitivity of some hydrogenation products and/or reaction intermediates towards undesired acid catalysed transformations, which may form catalyst poisons. As a result, the overall catalyst lifetime decreases, and reactors require more frequent recharging which increases the overall processing costs.

Another potential route to γ -valerolactone is the hydrogenation of levulinate esters, which can be readily obtained as a direct cellulosic product *via* acid catalysed esterification of the raw levulinic acid feed in alcoholic solvent.⁴⁴ The advantages of obtaining γ -valerolactone *via* this route lie upstream, as separation of the ester from aqueous depolymerisation streams which consist of an array of oxygenated water-soluble compounds is much less onerous.⁴⁵ Thus, a catalyst that can demonstrate versatility and is non-discriminative between levulinic acid and its esters would therefore improve the step economic benefits on a larger scale and simultaneously diversify the catalyst applications.



Scheme 63: Products of the Ru catalysed hydrogenation of ethyl levulinate.

Reactions were performed based on the previously identified optimum conditions (Scheme 63) although the hydrogen pressure was increased to 420 psi and the temperature was increased to enhance the rate of hydrogenation as well as promote the cyclisation, which is favoured at higher temperature. To ensure mass balance, after working up the reaction, the residual aqueous layer concentrated to dryness and 1,3-dinitrobenzene added as internal standard. The resultant residue was then analysed by ^1H NMR spectroscopy to quantify any reactants that were not extracted.

Table 40: Results of the Ru catalysed hydrogenation of levulinic acid.

| Entry ^a | Catalyst | Time (hours) | Conversion (%) ^b | Yield of I (%) ^b | Yield of J (%) ^b |
|--------------------|----------|----------------|--------------------------------|--------------------------------|--------------------------------|
| 1 | 6.5 | 4 | 100 | 23 | 77 |
| 2 | 6.5 | 8 | 100 | 0 | 100 |
| 3 | 6.5 | 8 ^c | 69 | 13 | 46 |
| 4 | 6.6 | 8 | 69 | 3 | 66 |
| 5 | 6.7 | 8 | 66 | 3 | 63 |
| 6 | Ru/C | 8 | 45 | 2 | 43 |

^aReaction conditions: 1 mmol substrate, 0.1 mol % catalyst, 13 mL water, 110°C, 420 psi H₂. ^b Conversion and selectivity determined by ^1H NMR spectroscopy with 1,3-dinitrobenzene as the internal standard. ^c Reaction performed in the presence of 0.1 mmol K₂CO₃. Selectivity for γ -valerolactone = [% γ -valerolactone / (% γ -valerolactone + % 4-hydroxypentanoic acid)].

The results for the hydrogenation of levulinic acid in Table 40 reveal that under these conditions, **I** is the only significant intermediate as confirmed by ^1H NMR analysis of the reaction mixture. Furthermore, under these conditions, intermolecular cyclisation is the clearly the rate-limiting step, as a reaction time of 4 hours resulted in complete consumption of **H** with 77% conversion to **J** and 23% conversion to **I** (entry 1). On extending the reaction time to 8 hours, **I** is fully cyclised to afford quantitative amounts of γ -valerolactone (entry 2). Interestingly, despite the positive effect of K₂CO₃ on the hydrogenation of model ketones, the addition of 10 mol% K₂CO₃ as additive appears to reduce activity under these conditions (entry 3). Comparative catalyst testing revealed that the PPh₂-functionalised catalyst outperformed all the other catalysts under identical conditions and gratifyingly, each of the PIILP-based

catalysts were markedly more efficient than commercial Ru/C (entries 4-6). These results compare favourably with recent literature examples as Luo *et al.* obtained a quantitative yield of γ -valerolactone with RuNPs supported on various metal oxides, however, it was necessary to perform these reactions at 200°C and 40 bar H₂ pressure.⁴⁶ Single Ru atoms confined within a nanotetragonal ZrO₂ support immobilised on amorphous carbon have also been reported to be highly selective catalysts for the hydrogenation of levulinic acid to γ -valerolactone.⁴⁷ The unique interaction between the Ru atoms and the well-defined ZrO₂ phase results in a durable and robust catalyst system that displayed vastly superior performance on comparison with commercial Ru/C, which suffered from severe degradation. However, the reaction medium was highly acidic (pH 1) and the reactions were conducted at 140°C. Electronic effects derived from a few layer graphene support have been reported to increase the relative content of metallic Ru on the catalyst surface which allowed the hydrogenation of levulinic acid to be conducted at room temperature, albeit a high hydrogen pressure and high concentration of starting material was required.⁴⁸

Unfortunately, the overall mass transfer limitations of the system under these conditions make accurate kinetic modelling challenging. Therefore, to provide a greater depth of understanding of the relative reaction rates, a series of reactions were conducted to generate a conversion-time profile.

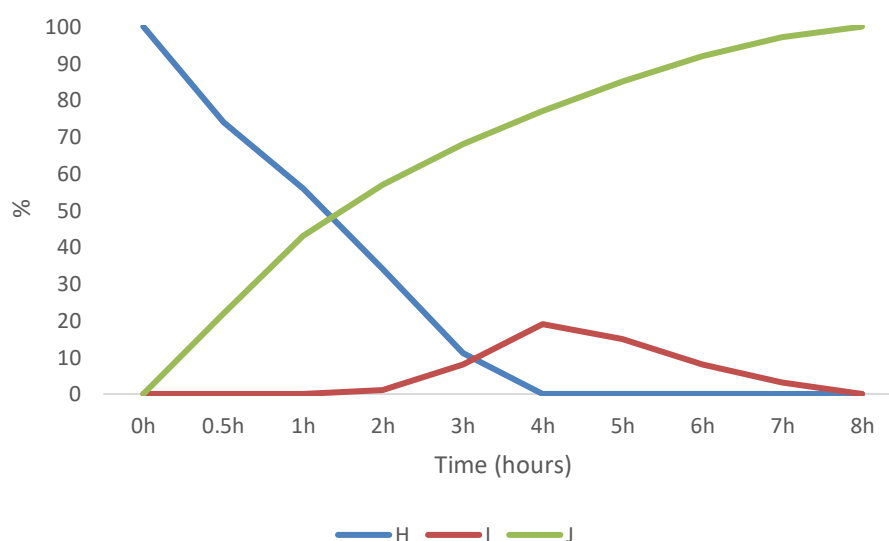


Figure 80: Product distribution for the hydrogenation of levulinic acid catalysed by 0.1 mol% 6.5 as a function of time. Reaction conditions: 1 mmol substrate, 0.1 mol % catalyst, 13 mL water, 110°C, 420 psi H₂. Conversion and selectivity determined by ¹H NMR spectroscopy with 1,3-dinitrobenzene as the internal standard.

The plot in Figure 80 supports the data presented in Table 40 and demonstrates that **H** is fully consumed after 4 hours, while 8 hours is required to achieve 100% conversion to **J**. Interestingly, at low conversions of **H** (below 45 %), the concentration of intermediate **I** is essentially zero, indicating that cyclisation occurs at a similar rate to hydrogenation. However, as the reaction proceeds, the rate of cyclisation begins to drop, hence the relative concentration of **I** begins to increase. The increase continues gradually until **H** is fully consumed at which point no more **I** can accumulate. Since cyclisation can be acid catalysed, residual molecules of **H** present at low conversion could be responsible for catalysing the cyclisation of **I**, however, as **H** is consumed over time, the concentration of acid is inherently depleted and, thus, the rate of cyclisation diminishes. However, more thorough kinetic experiments would be required to rationalise/validate this observation and elucidate the role of the acid.

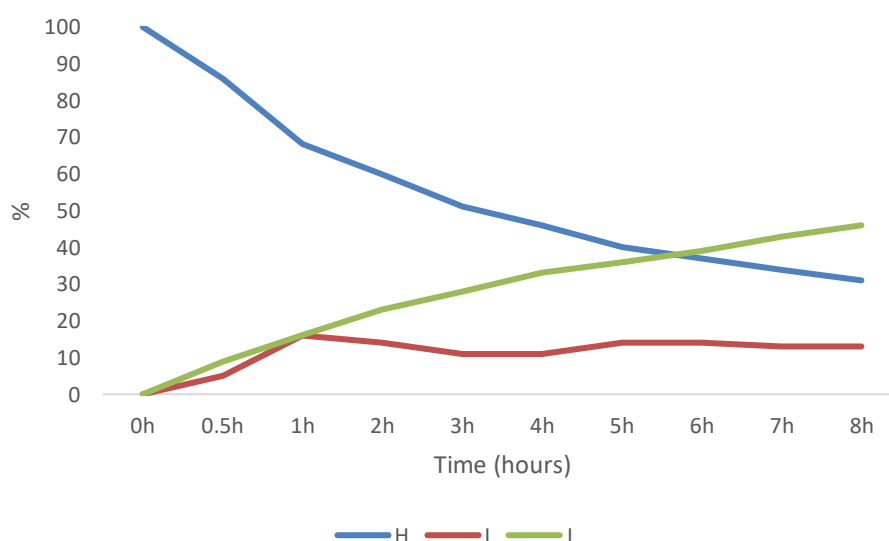


Figure 81: Product distribution for the hydrogenation of levulinic acid catalysed by 0.1 mol% **6.5** with base additive as a function of time. Reaction conditions: 1 mmol substrate, 0.1 mol % catalyst, 0.1 mmol K_2CO_3 , 13 mL water, 110°C, 420 psi H_2 . Conversion and selectivity determined by 1H NMR spectroscopy with 1,3-dinitrobenzene as the internal standard.

To understand how base affects the reaction, the hydrogenation of levulinic acid was catalysed by 0.1 mol% **6.5** under the same conditions but in the presence of 10 mol% K_2CO_3 . The resulting composition-time profile in Figure 81 revealed that in stark contrast to the profile in Figure 80, base appears to affect the Ru catalysed hydrogenation step as well as the cyclisation. Under these conditions, the conversion of **H** only reached 69% after 8h, with a product distribution of 46% **J** and 13% **I**, whereas 100% conversion was obtained in the absence of base. In this regard, the increase in pH caused by base additive may slow the acid

catalysed ring closure. Additionally, the base may also act as a poison, partially inhibiting the catalyst thus slowing down initial hydrogenation step.

A parallel study was also carried out for the hydrogenation of ethyl levulinate, the results of which are gathered below in Table 41.

Table 41: Results of the Ru catalysed hydrogenation of ethyl levulinate.

| Entry ^a | Catalyst | Time (hours) | Conversion (%) ^b | Yield of L (%) ^b | Yield of J (%) ^b |
|--------------------|----------|----------------|--------------------------------|--------------------------------|--------------------------------|
| 1 | 6.5 | 4 | 88 | 49 | 36 |
| 2 | 6.5 | 8 | 100 | 34 | 66 |
| 3 | 6.5 | 8 ^c | 100 | 0 | 100 |
| 4 | 6.6 | 8 ^c | 71 | 59 | 12 |
| 5 | 6.7 | 8 ^c | 57 | 49 | 8 |
| 6 | Ru/C | 8 ^c | 43 | 40 | 3 |

^aReaction conditions: 1 mmol ethyl levulinate, 0.1 mol % catalyst, 13 mL water, 110°C, 420 psi H₂. ^b Conversion and selectivity determined by ¹H NMR spectroscopy with 1,3-dinitrobenzene as the internal standard. ^c Reaction performed in the presence of 0.1 mmol K₂CO₃. Selectivity for γ -valerolactone = [% γ -valerolactone / (% γ -valerolactone % + ethyl 4-hydroxypentanoate)].

The reaction catalysed by 0.1 mol% **6.5** gave quantitative conversion to a 34:66 mixture of **L** and **J** after 8 h (entry 2). However, the addition of 10 mol% base resulted in a dramatic improvement in efficacy to afford **J** as the sole product (entry 3). As expected, **6.5** was much more efficient in comparison with all of the other catalysts tested (entries 4-6).

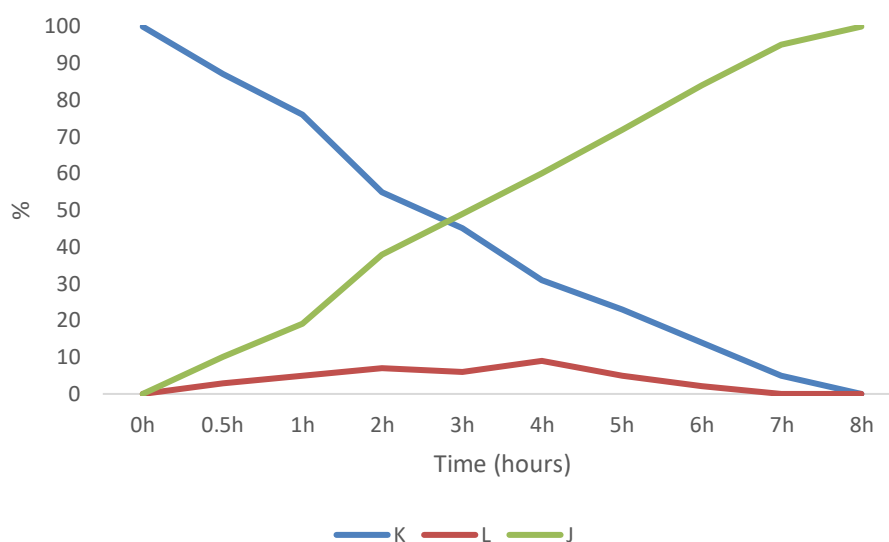


Figure 82: Product distribution for the hydrogenation of ethyl levulinate catalysed by 6.5 with base additive as a function of time. Reaction conditions: 1 mmol substrate, 0.1 mol % catalyst, 0.1 mmol K_2CO_3 , 13 mL water, 110°C, 420 psi H_2 . Conversion and selectivity determined by 1H NMR spectroscopy with 1,3-dinitrobenzene as the internal standard.

The corresponding composition-time profile in Figure 82 reveals that the initial hydrogenation of **K** is the slowest step as only minor amounts of intermediate **L** are present throughout the reaction. This scenario differs from that of **H**, as since the starting material is not acidic, its depletion does not cause marked changes in pH, allowing the cyclisation to proceed through a base catalysed route. To investigate further and to direct catalyst optimisation, it would be useful to obtain authentic samples of the intermediate to conduct control experiments and more efficiently monitor the effects of various reaction parameters on the cyclisation step.

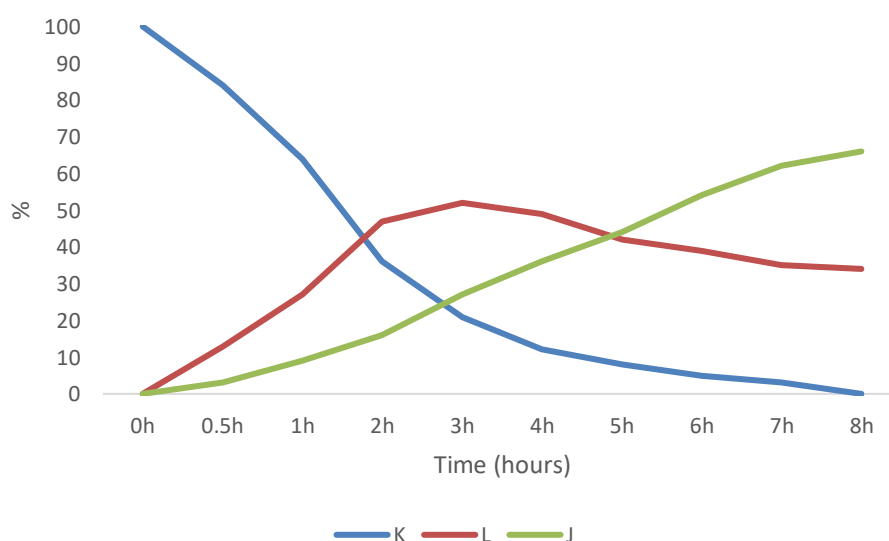


Figure 83: Product distribution for the hydrogenation of levulinic acid catalysed by 0.1 mol % 6.5 in the absence of base additive as a function of time. Reaction conditions: 1 mmol substrate, 0.1 mol % catalyst, 13 mL water, 110°C, 420 psi H_2 . Conversion and selectivity determined by 1H NMR spectroscopy with 1,3-dinitrobenzene as the internal standard.

In agreement with the results gathered in Table 41, the removal of base from the reaction clearly affects catalyst efficacy as only 66% of **J** is obtained after 8 hours. Moreover, in further agreement with the levulinic acid study, the removal of base appears to increase the rate of the hydrogenation step, further suggesting that base may indeed inhibit the catalyst; however, in contrast to levulinic acid this improvement is relatively minor.

The results presented at this stage are encouraging and indicate that PIILP technology could be a viable tool to produce fuel and platform chemicals in a more environmentally responsible manner. Moreover, the observations made in this chapter may serve as a platform for further optimisation of the system through alteration of the substrate:catalyst ratio, as well as surveying a range of additives in combination with careful modulation of the pH. For the latter, a carefully constructed continuous flow system may enable a more efficient approach to optimisation of the two fundamental chemical transformations, as well as improve scalability of the reaction and increase the potential for industrial use.

6.7 Conclusion

Ultra-small monodisperse ruthenium nanoparticles stabilised by heteroatom donor functionalised PEGylated polyionic liquids are highly active and selective catalysts for the aqueous phase hydrogenation of aldehydes, ketones and key biomass derived substrates under mild conditions relative to recent literature examples. Extrapolating PIILP methodology provided a convenient method to incorporate heteroatom donors into the support, and the influence of the heteroatom donor had pronounced effects on the both the performance and physical properties of the catalyst.

TEM analysis revealed that amino-modified PIIL support gave the smallest RuNPs (1.0 nm), and that removal of the NH₂ group resulted in a 50% increase in particle size as the average diameter of polymer immobilised ionic liquid-stabilised RuNPs were 1.5 nm. Remarkably, despite affording significantly larger particles (2.2 nm), the PPh₂-modified catalyst proved to be substantially more active and selective for each substrate tested. In line with the literature discussion, reaction optimisation highlighted the beneficial effects of the aqueous medium as both catalysts performed best for the hydrogenation of acetophenone, despite the limited solubility of the substrate. The selective hydrogenation of a series of acetophenone derived substrates with varied steric and electronic profiles revealed that the PPh₂ modification was necessary to achieve high activity and selectivity for the C=O bond. The inability of any PIILP

based catalyst to catalyse the hydrogenation of nitrile bearing substrates and the deactivation in the presence of excess amine prompted a more detailed investigation into the potential poisoning effects of nitrogen donors. By conducting the benchmark reaction in the presence of representative amounts of nitrile or amine, these substrates were shown to deactivate the catalyst, most likely through strong adsorption and saturation of the active site. Future studies may monitor poisoning as a function of substrate equivalents to identify whether the catalyst could be active under any conditions, or whether small amounts of the substrate could even be beneficial for selectivity.

Recycling experiments gave encouraging results, as both catalysts showed steady profiles in sequential batch experiments with no loss in activity. However, more sophisticated apparatus would be ideally required to investigate the activity/selectivity profiles over extended periods to increase catalyst turnover. Interestingly, stirring the catalyst in water under a hydrogen atmosphere overnight resulted in a substantial enhancement in activity and at this stage it is tentatively attributed to the reduction of surface oxide species. The optimum system, **6.5**, was demonstrated to be a versatile catalyst, as the challenging complete hydrogenation of acetophenone was successful, and quantitative amounts of cyclohexylethanol were recovered.

6.5 was then taken forward for evaluation in the more industrially relevant selective hydrogenation of biomass derived substrates; furfural, levulinic acid and ethyl levulinate. Gratifyingly, after optimisation, **6.5** proved to be extremely efficient and selective for the partial hydrogenation of furfural and gave furfuryl alcohol in 100% conversion and selectivity under mild conditions, in water with a low catalyst loading and in a short reaction time. Moreover, **6.5** also facilitated the selective formation of key intermediate, γ -valerolactone, in a clean, selective and sustainable protocol from both levulinic acid and its commercially important ethyl ester. Time-conversion profiles revealed that the hydrogenation of levulinic acid is faster in the absence of base and that cyclisation of the intermediate 4-hydroxypentanoic acid is accelerated in the presence of residual acidic starting material, which may catalyse this step. Conversely, the hydrogenation of ethyl levulinate occurs more readily in the presence of base additive which, in the absence of acidic starting material, may be responsible for catalysing the cyclisation in this instance.

On comparison with its amino counterpart **6.6**, as well as **6.7**, which had no heteroatom donors, **6.5** proved to be the most efficient system throughout the study, despite consisting of larger particles i.e. a lower active metal area. These results therefore suggest that the absolute volume of active sites is not the primary influence over catalyst enhancement or activation, and that interfacial electronic interactions may be a more dominant feature. In this regard, the nature of the donor may influence the kinetic and thermodynamic parameters associated with H₂ or substrate activation under conditions of catalysis.

Further surface studies using techniques such as *in situ* DRIFTS and XAS analysis would be required to probe responses in the local electronic structure of the catalyst on response to interactions with various heteroatom donors if we are to fully understand how these supports effect catalyst efficacy. Additionally, chemisorption measurements and temperature programmed desorption studies could also provide insight into differences in the nature of the particle surface. Once the optimum metal-support combination has been established, further optimisation of the heteroatom:metal ratio and reduction methodology may improve catalyst selectivity by yielding smaller and more active particles with the appropriate electronic profiles and ionic microenvironment. Indeed, adopting a homogeneous-type approach regarding further optimisation of the steric profile and basicity of the donor functionality may provide a handle for tuning the reaction selectivity. From first principles, computational analysis of the effects of Ru-P and Ru-N interactions on the barriers for either H₂ activation or different adsorption modes may also be beneficial and could direct future catalyst optimisation for screening other possible donors.

Finally, comparative catalyst testing against a sample of the commercially available heterogeneous catalyst, Ru/C, demonstrated that the surrounding ionic microenvironment provided by the cation decorated polymer support was crucial as all three PIILP catalysts outperformed this standard in both activity and selectivity.

6.8 Outlook

The results presented in this thesis have demonstrated that the concept of PIILP catalysis can be a useful tool for a range of transformations under mild and green conditions. Through advanced characterisation and methodical catalyst testing, progress has been made to establish a polymer composition-catalyst activity relationship. In particular, using benchmark substrates for catalyst testing and optimisation, the integration of heteroatom donors,

together with hydrophilic imidazolium-based ionic liquids was shown to lead to the formation of highly active catalysts that give partially reduced commodity products often in quantitative yield under purely aqueous conditions. The functionality embedded within the polymers was shown to affect both materials properties, including dispersivity and degree of swelling, as well as intrinsic catalyst performance as a result of different catalyst-support interactions which led to changes in particle size and metal dispersion. The optimum systems were then applied to more challenging and industrially relevant substrates, for example, bioderived substrates that can undergo a range of different transformations under conditions of catalysis.

However, to truly understand the behaviour of these systems as well as the origin of their activity and selectivity profiles, it would be beneficial to analyse them under conditions of catalysis using *in situ* techniques. Harvesting this information would aid the development of next generation systems by identifying optimum key parameters such as the presence of crucial interfacial electronic interactions, degree of catalyst dispersity and the nature of the metal-support interactions.

Furthermore, another possible avenue for further exploration would be to utilise the wide range of techniques available that have been shown to produce well-defined bimetallic composites as briefly described in Chapter 1. In this regard, it may be possible to design functional synergistic PIILP-based systems that efficiently catalyst multistep reactions.

The transfer from batch conditions to a continuous operation system using packed bed reactors is another challenge that could be addressed using PIILP catalysts. Building on the promising results in Chapter 4, it would be necessary to monitor catalyst lifetime at extended time on line. Furthermore, it may be necessary to develop more innovative support structures based on inorganic matrices such as MOFs, zeolites or mesoporous silicas to generate more robust systems that may improve catalyst lifetime.

6.9 References

1. Y. Kuwahara, H. Kango and H. Yamashita, *ACS Sus. Chem. Eng.*, 2017, **5**, 1141-1152.
2. M. J. Climent, A. Corma and S. Iborra, *Green Chem.*, 2014, **16**, 516-547.
3. Y. Román-Leshkov, C. J. Barrett, Z. Y. Liu and J. A. Dumesic, *Nature*, 2007, **447**, 982.
4. G. W. Huber, J. W. Shabaker and J. A. Dumesic, *Science*, 2003, **300**, 2075-2077.
5. K. Gupta, R. K. Rai and S. K. Singh, *ChemCatChem*, 2018, **10**, 2326-2349.
6. H. Li, W. Zhao, S. Saravanamurugan, W. Dai, J. He, S. Meier, S. Yang and A. Riisager, *Commun. Chem.*, 2018, **1**, 32.
7. M. J. Taylor, L. Jiang, J. Reichert, A. C. Papageorgiou, S. K. Beaumont, K. Wilson, A. F. Lee, J. V. Barth and G. Kyriakou, *J. Phys. Chem. C.*, 2017, **121**, 8490-8497.

8. Y. Yuan, N. Yan and P. J. Dyson, *ACS Catal.*, 2012, **2**, 1057-1069.
9. L. Corbel-Demailly, B.-K. Ly, D.-P. Minh, B. Tapin, C. Especel, F. Epron, A. Cabiach, E. Guillon, M. Besson and C. Pinel, *ChemSusChem*, 2013, **6**, 2388-2395.
10. N. N. Rimar and G. N. Pirogova, *Russ. Chem. Bull.*, 1998, **47**, 398-401.
11. C. Michel and P. Gallezot, *ACS Catal.*, 2015, **5**, 4130-4132.
12. R. Alamillo, M. Tucker, M. Chia, Y. Pagan-Torres and J. Dumesic, *Green Chem.*, 2012, **14**, 1413-1419.
13. J. Lee, Y. Xu and G. W. Huber, *Appl. Catal. B*, 2013, **140-141**, 98-107.
14. M. Saleheen and A. Heyden, *ACS Catal.*, 2018, **8**, 2188-2194.
15. S. Hou, C. Xie, H. Zhong and S. Yu, *RSC Adv.*, 2015, **5**, 89552-89558.
16. B. S. Akpa, C. D'Agostino, L. F. Gladden, K. Hindle, H. Manyar, J. McGregor, R. Li, M. Neurock, N. Sinha, E. H. Stitt, D. Weber, J. A. Zeitler and D. W. Rooney, *J. Catal.*, 2012, **289**, 30-41.
17. C. Michel, J. Zaffran, A. M. Ruppert, J. Matras-Michalska, M. Jędrzejczyk, J. Grams and P. Sautet, *Chem. Commun.*, 2014, **50**, 12450-12453.
18. A. Michaelides, A. Alavi and D. A. King, *J. Am. Chem. Soc.*, 2003, **125**, 2746-2755.
19. Y. Kim, E.-s. Moon, S. Shin and H. Kang, *Angew. Chem. Int. Ed.*, 2012, **51**, 12806-12809.
20. J. Tan, J. Cui, T. Deng, X. Cui, G. Ding, Y. Zhu and Y. Li, *ChemCatChem*, 2015, **7**, 508-512.
21. X. Cui, A.-E. Surkus, K. Junge, C. Topf, J. Radnik, C. Kreyenschulte and M. Beller, *Nature Commun.*, 2016, **7**, 11326.
22. G. Vilé, D. Albani, N. Almora-Barrios, N. López and J. Pérez-Ramírez, *ChemCatChem*, 2016, **8**, 21-33.
23. S. Gyergyek, A. Kocjan, A. Bjelić, M. Grilc, B. Likozar and D. Makovec, *Materials Research Letters*, 2018, **6**, 426-431.
24. Y.-K. Lee and S. T. Oyama, *J. Catal.*, 2006, **239**, 376-389.
25. D. Gonzalez-Galvez, P. Lara, O. Rivada-Wheelaghan, S. Conejero, B. Chaudret, K. Philippot and P. W. N. M. van Leeuwen, *Catal. Sci. Technol.*, 2013, **3**, 99-105.
26. J. B. Ernst, S. Muratsugu, F. Wang, M. Tada and F. Glorius, *J. Am. Chem. Soc.*, 2016, **138**, 10718-10721.
27. J. B. Ernst, C. Schwermann, G.-i. Yokota, M. Tada, S. Muratsugu, N. L. Doltsinis and F. Glorius, *J. Am. Chem. Soc.*, 2017, **139**, 9144-9147.
28. J. Tan, J. Cui, G. Ding, T. Deng, Y. Zhu and Y.-w. Li, *Catal. Sci. Technol.*, 2016, **6**, 1469-1475.
29. S. Zhang, L. Zhou and M. Chen, *RSC Adv.*, 2018, **8**, 12282-12291.
30. V. Bertini, S. Alfei, M. Pucci, F. Lucchesini, N. Picci and F. Iemma, *Tetrahedron*, 2004, **60**, 11407-11414.
31. L. M. Martínez-Prieto and B. Chaudret, *Acc. Chem. Res.*, 2018, **51**, 376-384.
32. R. B. Nasir Baig and R. S. Varma, *ACS Sus. Chem. Eng.*, 2013, **1**, 805-809.
33. D. González-Gálvez, P. Nolis, K. Philippot, B. Chaudret and P. W. N. M. van Leeuwen, *ACS Catal.*, 2012, **2**, 317-321.
34. F. Leng, I. C. Gerber, M. R. Axet and P. Serp, *Comptes Rendus Chimie*, 2017.
35. H.-y. Jiang and X.-x. Zheng, *Catal. Sci. & Technol.*, 2015, **5**, 3728-3734.
36. P. P. Sarmah and D. K. Dutta, *Green Chem.*, 2012, **14**, 1086-1093.
37. N. C. Antonels and R. Meijboom, *Langmuir*, 2013, **29**, 13433-13442.
38. S. Iqbal, S. A. Kondrat, D. R. Jones, D. C. Schoenmakers, J. K. Edwards, L. Lu, B. R. Yeo, P. P. Wells, E. K. Gibson, D. J. Morgan, C. J. Kiely and G. J. Hutchings, *ACS Catal.*, 2015, **5**, 5047-5059.
39. M. Besson, P. Gallezot and C. Pinel, *Chem. Rev.*, 2014, **114**, 1827-1870.
40. Y. Nakagawa, K. Takada, M. Tamura and K. Tomishige, *ACS Catal.*, 2014, **4**, 2718-2726.

41. G. Wang, Z. Zhang and L. Song, *Green Chem.*, 2014, **16**, 1436-1443.
42. A. S. Piskun, J. E. de Haan, E. Wilbers, H. H. van de Bovenkamp, Z. Tang and H. J. Heeres, *ACS Sus. Chem. & Eng.*, 2016, **4**, 2939-2950.
43. D. Albani, Q. Li, G. Vilé, S. Mitchell, N. Almora-Barrios, P. T. Witte, N. López and J. Pérez-Ramírez, *Green Chem.*, 2017, **19**, 2361-2370.
44. S. Saravanamurugan, O. Nguyen Van Buu and A. Riisager, *ChemSusChem*, 2011, **4**, 723-726.
45. B. Cai, X.-C. Zhou, Y.-C. Miao, J.-Y. Luo, H. Pan and Y.-B. Huang, *ACS Sus. Chem. Eng.*, 2017, **5**, 1322-1331.
46. W. Luo, U. Deka, A. M. Beale, E. R. H. van Eck, P. C. A. Bruijninx and B. M. Weckhuysen, *J. Catal.*, 2013, **301**, 175-186.
47. W. Cao, W. Luo, H. Ge, Y. Su, A. Wang and T. Zhang, *Green Chem.*, 2017, **19**, 2201-2211.
48. C. Xiao, T.-W. Goh, Z. Qi, S. Goes, K. Brashler, C. Perez and W. Huang, *ACS Catal.*, 2016, **6**, 593-599.

Chapter 7 Experimental

General comments

All reagents were purchased from commercial suppliers and used without further purification. ^1H and $^{13}\text{C}\{^1\text{H}\}$ NMR spectra were recorded on JEOL LAMBDA-500 or ECS-400 instruments. Solid-state ^{31}P spectra were recorded at 161.87 MHz using a Varian VNMRS 400 spectrometer and a 4 mm (rotor o.d.) magic-angle spinning probe. They were obtained using cross-polarization with a 2 s recycle delay, 3 ms contact time, at ambient probe temperature ($\sim 25^\circ\text{C}$) and at a sample spin-rate of 10 kHz. Between 1000 and 3600 repetitions were accumulated. Spectral referencing was with respect to an external sample of 85% phosphoric acid. Solid-state ^{13}C spectra were recorded at 100.562 MHz using a Varian VNMRS 400 spectrometer. They were obtained using cross-polarization with a 10 s recycle delay, 1 ms contact time, at ambient probe temperature ($\sim 25^\circ\text{C}$) and at a sample spin-rate of 6 kHz. Spectral referencing was with respect to an external sample of neat tetramethylsilane (carried out by setting the high-frequency signal from adamantane to 38.5 ppm). Thermogravimetric analysis (TGA) was performed using a TA TGA Q600 instrument, at a heating rate of $10^\circ\text{C min}^{-1}$ in air. The onset of the weight loss in each thermogram was used as a measure of the decomposition temperature. SEM images were acquired on a Tescan Vega 3LMU scanning electron microscope with digital image collection. XPS measurements were carried out using a Theta Probe system (Thermo Scientific, UK) equipped with a microfocused monochromatic $\text{AlK}\alpha$ source. The X-ray source was operated at 100 W and 15 kV. Samples for transmission electron microscopy (TEM) were dispersed in ethanol using an ultrasonic bath and deposited on lacey carbon film coated copper grids. TEM images were acquired on a FEI Tecnai TF20 field emission gun microscope operating at 200 kV. NP size distribution histograms were obtained from measurements of at least 100 different NPs assuming a spherical shape and with random distribution. Powder X-ray diffraction patterns (XRD) were recorded using a PANalytical X'Pert Pro Multipurpose Diffractometer (MPD) using $\text{Cu K}\alpha/\beta$ radiation of wavelength of 1.5418 \AA . The metal loadings were quantified using inductively coupled plasma optical emission spectroscopy (ICP-OES). FT-IR spectroscopy was performed on a Varian 800 FT-IR instrument (VarianInc.).

7.1 Chapter 2 experimental.

7.1.1 Synthesis of methyl octaethylene glycol chloride (2.1).

An oven-dried Schlenk flask was charged with polyethylene glycol monomethyl ether (7.0 g, 20 mmol), pyridine (3.16 g, 40 mmol) and anhydrous toluene (40 mL) under a nitrogen atmosphere. The solution was stirred and heated to 80 °C, at which point thionyl chloride (4.74 g, 40 mmol) was added dropwise over a 20-minute period. Following this, the mixture was heated to 110 °C and stirred for 2 days. After cooling to room temperature, water (10 mL) was added, and the organics were extracted with toluene (3 x 30 mL). The organic phases were combined and concentrated *in vacuo*. The crude pale-yellow product was then dissolved in dichloromethane (30 mL) and washed with water (3 x 30 mL). The organic fractions were then combined, dried over anhydrous MgSO₄, filtered and the solvent removed *in vacuo* to give the desired product as a pale-yellow liquid (6.3 g, 16.8 mmol) in 84% yield. ¹H NMR (300 MHz, CDCl₃, δ): 3.69 (t, *J* = 5.6 Hz, 2H), 3.67 – 3.52 (m, 24H), 3.50 (t, *J* = 4.8 Hz, 3H), 3.31 (s, 3H); ¹³C{¹H} NMR (75 MHz, CDCl₃, δ): 71.79, 71.20, 70.50, 70.44, 70.35, 58.83, 42.64. Anal. Calc. for C₁₅H₃₁ClO₇ (358.18): C, 50.21; H, 8.71. Found: C, 50.02; H, 8.73.

7.1.2 Synthesis of 2-methyl-1-(2,5,8,11,14,17,20,23-octaoxapentacosan-25-yl)-1H-imidazole (2.2).

An oven-dried Schlenk flask was charged with NaH (0.19 g, 8 mmol) dispersed in mineral oil. To remove the oil, hexane (10 mL) was added and the solution was stirred under N₂ for 10 minutes at room temperature. The solvent was removed *via* cannula filtration and this process was repeated three times. After this, the resultant white solid was suspended in anhydrous THF (30 mL) under a nitrogen atmosphere. The solution was cooled to 0 °C and 2-methylimidazole (0.66 g, 8 mmol) was added slowly, which resulted in the liberation of gas. After the exotherm had subsided, **2.1** (2.5 g, 6.7 mmol) was added slowly, and the dark brown mixture was heated to 75 °C and stirred for 16 hours. Once the solution had cooled, the solvent was removed using an external trap and water (20 mL) was added dropwise. The product was then extracted with ethyl acetate (4 x 40 mL) and the organic fractions were combined, dried over MgSO₄, filtered and the solvent removed *in vacuo* to give **2.2** as a viscous yellow oil (2.43 g, 18.9 mmol) in 87% yield. ¹H NMR (300 MHz, CDCl₃, δ): 7.11 (d, *J* = 1.3, 2H), 3.94 (t, *J* = 4.8 Hz, 2H), 3.90 – 3.76 (m, 22H), 3.73 (t, *J* = 5.0 Hz, 2H), 3.56 (s, 3H), 2.59 (s, 3H); ¹³C{¹H} NMR (75 MHz, CDCl₃, δ): 144.46, 121.24, 71.82, 71.80, 71.26, 71.23, 70.53, 70.46, 58.90, 58.87, 58.85,

42.68, 13.79; Anal. Calc. for $C_{21}H_{40}N_2O_8$ (448.3): C, 56.23; H, 8.99; N, 6.25%. Found: C, 58.02; H, 9.89; N, 7.01%.

7.1.3 Synthesis of 1-bromomethyl-4-vinyl-benzene (2.3).

An oven-dried Schlenk flask was charged with 4-chloromethyl styrene (1.86 mL, 13.2 mmol), sodium bromide (5.44 g, 52.8 mmol) and acetonitrile (50 mL) under a nitrogen atmosphere. The solution was heated to 88 °C and stirred for 16 hours. After this time, the reaction was left to cool to room temperature and then filtered. The filtrate was concentrated in vacuo, dissolved in dichloromethane (15 mL), filtered and the solvent was removed in vacuo to give a yellow oil (2.30 g, 11.6 mmol) in 88% yield. 1H NMR (399.78 MHz, $CDCl_3$, δ): 7.39 (m, 4H, Ar-H), 6.76 (dd, J = 17.4, 10.6 Hz, 1H, $H_aC=CH_bH_c$), 5.78 (d, J = 17.4 Hz, 1H, $H_aC=CH_bH_c$), 5.29 (d, J = 10.6 Hz, 1H, $H_aC=CH_bH_c$), 4.58 (s, 2H, Ar- CH_2 -Cl), 4.48 (s, 2H, Ar- CH_2 -Br). $^{13}C\{^1H\}$ NMR (100.52 MHz, $CDCl_3$, δ): 137.51, 137.43, 136.32, 129.14, 126.78, 114.39, 33.62. Anal. Calc. for C_9H_9Br (195.99): C, 54.85; H, 4.60. Found: C, 54.76; H, 4.61.

7.1.4 Synthesis of 2-methyl-1-(2,5,8,11,14,17,20,23-octaoxapentacosan-25-yl)-3-(4-vinylbenzyl)-1H-3 λ 4-imidazolium chloride (2.4).

An oven-dried Schlenk flask was charged with **2.2** (0.31 g, 1.57 mmol), **2.3** (0.55 g, 1.31 mmol) and anhydrous dichloromethane (20 mL) under a nitrogen atmosphere. The solution was heated to 35 °C and stirred for 16 hours. After this time, the solvent was removed *in vacuo* and the crude product was washed with diethyl ether (3 x 30 mL) and dried under high vacuum to afford the **2.4** as a viscous yellow oil (0.73 g, 1.23 mmol) in 94% yield. 1H NMR (300 MHz, $CDCl_3$, δ): 7.90 (s, 1H), 7.58 (s, 1H), 7.41 (d, J = 8.1 Hz, 2H), 7.28 (d, J = 7.9 Hz, 2H), 6.68 (dd, J = 17.6, 10.9 Hz, 1H), 5.76 (d, J = 17.6 Hz, 1H), 5.52 (s, 2H), 5.30 (d, J = 12.1 Hz, 2H), 4.53 (t, J = 4.8 Hz, 2H), 3.89 (t, J = 4.8 Hz, 2H), 3.73 – 3.41 (m, 19H), 3.34 (s, 3H), 2.79 (s, 3H); $^{13}C\{^1H\}$ NMR (75 MHz, $CDCl_3$, δ): 144.56, 144.53, 137.81, 135.57, 132.52, 132.49, 128.32, 128.17, 128.14, 126.67, 121.93, 121.87, 121.74, 114.89, 71.55, 71.47, 70.19, 70.14, 70.07, 69.95, 69.13, 58.65, 58.62, 51.52, 48.61, 10.99, 10.97, 10.95; Anal. Calc. for $C_{30}H_{49}BrN_2O_8$ (600.3): C, 59.94; H, 8.22; N, 4.66%. Found: C, 61.07; H, 8.98; N, 5.25%.

7.1.5 Synthesis of 1,2-dimethyl-3-(4-vinylbenzyl)-1H-imidazol-3-ium chloride. (2.5)

An oven-dried Schlenk flask was charged with 1,2-dimethylimidazole (5.32 g, 55.3 mmol) dissolved in anhydrous chloroform (60 mL). To this was added 4-chloromethylstyrene (10 mL, 71.0 mmol) and the resultant mixture was stirred at 55 °C for 16 hours. After this time, the

solution was left to cool to room temperature and the solvent removed *in vacuo*. The resultant residue was washed with ethyl acetate (4 x 50 mL) and dried under high vacuum to afford **2.5** as a white crystalline solid (12.41 g, 50.1 mmol) in 92% yield. ^1H NMR (300 MHz, CDCl_3 , δ): 2.76 (3H, s), 3.95 (3H, s), 5.25 (1H, d, J = 9 Hz), 5.56 (2H, s), 5.76 (1H, d, J = 12 Hz), 6.60-6.70 (1H, dd, J = 9 Hz, 12 Hz), 7.28-7.44 (4H, m), 7.44-7.77 (2H, q); $^{13}\text{C}\{^1\text{H}\}$ NMR (75 MHz CDCl_3 , δ): 10.79, 35.76, 51.93, 115.93, 121.94, 122.91, 126.94, 128.47, 132.45, 135.71, 138.19, 144.02. Anal. Calc. for $\text{C}_{14}\text{H}_{17}\text{ClN}_2$ (248.1): C, 67.60; H, 6.89; N, 11.27%. Found: C, 67.94; H, 7.22; N, 11.51%.

7.1.6 Synthesis of 2-methyl-1-(4-vinylbenzyl)-1H-imidazole (2.6)

An oven-dried Schlenk flask was charged with sodium hydride (1.46 g, 60.8 mmol) dispersed in mineral oil. To remove the oil, hexane (10 mL) was added and the solution was stirred under N_2 for 10 minutes at room temperature. The solvent was removed *via* cannula filtration and this process was repeated three times. After this, the resultant white solid was suspended in anhydrous dimethylformamide (30 mL) under a nitrogen atmosphere. The solution was cooled to 0 °C and 2-methylimidazole (6.0 g, 73.0 mmol) was added slowly resulting in the liberation of gas. After the exotherm had subsided, 4-chloromethylstyrene (8.58 mL, 60.8 mmol) was added dropwise and the resulting reaction mixture heated to 75 °C for 45 minutes. After this, the reaction was left to cool to room temperature and the mixture poured onto water (250 mL) and the product extracted with ethyl acetate (3 x 100 mL). The organic extracts were then combined, washed with water (200 mL), brine (100 mL) and the product extracted with 6N HCl (2 x 50 mL). The aqueous layer was washed with diethyl ether (2 x 50 mL) and then treated with 1M NaOH solution until pH 12.0 was reached. The product was then extracted with diethyl ether (3 x 100 mL), dried over MgSO_4 and the solvent removed *in vacuo* to give **2.6** as a pale-yellow oil (11.10 g, 54.72 mmol) in 90% yield. ^1H NMR (300 MHz δ): 2.15 (3H, s), 4.83 (2H, s), 5.09-5.12 (1H, d, J = 9 Hz), 5.55-5.61 (1H, d, J = 18 Hz), 6.48-6.57 (1H, dd, J = 9 Hz, 18 Hz), 6.84-6.86 (2H, d, J = 6 Hz), 7.20-7.22 (2H, d, J = 6 Hz); $^{13}\text{C}\{^1\text{H}\}$ NMR (75 MHz, CDCl_3 , δ): 12.85, 49.30, 114.32, 119.83, 126.60, 126.81, 126.96, 137.14, 135.77, 135.98, 144.77; Anal. Calc. for $\text{C}_{13}\text{H}_{14}\text{N}_2$ (198.1): C, 78.75; H, 7.12; N, 14.13%. Found: C, 79.17; H, 7.77 N, 14.57%.

7.1.7 Synthesis of 2-methyl-1,3-bis(4-vinylbenzyl)-1H-imidazol-3-ium chloride. (2.7)

An oven-dried Schlenk flask was charged with **2.6** (5.15 g, 26.0 mmol) anhydrous chloroform (40 mL) under a nitrogen atmosphere. To this solution was added 4-chloromethylstyrene (4.74

g, 31.2 mmol) and the resulting mixture was heated to 55 °C and stirred for 16 hours. The solution was then cooled to room temperature, then concentrated *in vacuo* (to ca. 5 mL), diethyl ether (250 mL) added and the resulting mixture stirred vigorously for 1 hour. After this time, the mixture was left to settle, and the product isolated *via* filtration through a frit, washed with diethyl ether (2 x 40 mL) and dried under high vacuum to afford the product as a white solid (8.97 g, 25.2 mmol) in 97% yield. ^1H NMR (300 MHz, CDCl_3 , δ): 1.97 (3H, s), 2.69 (4H, s), 5.19-5.23 (2H, d, J = 12 Hz), 5.64-5.70 (2H, d, J = 18 Hz), 6.54-6.63 (2H, dd, J = 12 Hz, 18 Hz), 7.20-7.22 (4H, d, J = 6 Hz), 7.29-7.31 (2H, d, J = 6 Hz); $^{13}\text{C}\{^1\text{H}\}$ NMR (75 MHz, CDCl_3 , δ): 11.42, 52.65, 113.28, 122.83, 128.51, 128.87, 133.65, 134.14, 136.09, 153.07; Anal. Calc. for $\text{C}_{22}\text{H}_{23}\text{ClN}_2$ (350.1): C, 75.31; H, 6.61; N, 7.98%. Found: C, 75.67; H, 9.93; N, 8.19%.

7.1.8 Synthesis of diphenyl(4-vinylphenyl)phosphine (2.8)

A 200 mL round bottom flask was charged with Mg turnings (3.54 g, 145.6 mmol) suspended in anhydrous THF (40 mL) under a nitrogen atmosphere and a crystal of iodine was added. The mixture was cooled to 0 °C and stirred for 10 minutes. An oven-dried Schlenk flask was charged with 4-chlorostyrene (9.4 mL, 79.8 mmol) dissolved in anhydrous THF (30 mL), and 20% of the solution was added dropwise to the Mg turnings. Once the reaction had initiated and began to generate heat, the remainder of the solution was added dropwise over 15 minutes before heating to 65 °C for 5 hours. Another 200 mL round bottomed flask was charged with chlorodiphenylphosphine (8 mL, 60 mmol) dissolved in anhydrous THF (30 mL) which was cooled to 0 °C. The Grignard solution was then added dropwise to this and the resultant mixture stirred for a further 16 hours at room temperature. The reaction was then quenched with degassed water (150 mL) and the product extracted with degassed diethyl ether (3 x 150 mL). The organic phases were stored under a nitrogen atmosphere then combined, dried over MgSO_4 , filtered and the solvent removed using an external trap to afford **2.8** as a white crystalline solid (10.52 g, 33.6 mmol) in 56% yield. The product was stored under nitrogen. ^1H NMR (300 MHz, CDCl_3 , δ): 7.25-7.29 (m, 14H, ArH), 6.63 (dd, J = 17.5, J = 10.9 Hz, 1H, ArCHCHH), 5.70 (d, J = 17.5, 1H, ArCHCHH) 5.20 (d, J = 10.9, 1H, ArCHCHH); $^{13}\text{C}\{^1\text{H}\}$ NMR (75 MHz, CDCl_3 , δ): 137.95, 137.23, 137.09, 136.4 (Ar) 134.09, 133.86, 133.83, 133.60 (Ar) 128.75 (CHCH₂), 126.35 (CHCH₂); $^{31}\text{P}\{^1\text{H}\}$ NMR (121 MHz, CDCl_3 , δ): -5.78.

7.1.9 General procedure for polymerisations.

An oven-dried Schlenk flask was charged with the appropriate monomers (mole ratio 1.86:1:0.14 imidazolium to phosphine to crosslinker) dissolved in a 1:1 mixture of anhydrous ethanol and anhydrous THF (8 mL solvent/g monomer) under a nitrogen atmosphere. To this was added AIBN (5 mol %) and the mixture degassed using the freeze-thaw method six times before heating to 70 °C for three days. After this time, the mixture was cooled to room temperature and an additional portion of AIBN (5 mol%) was added before repeating the degassing process and heating at 70 °C for a further 24 hours. The solution was cooled to room temperature and the solvent removed under reduced pressure. The resulting residue was dissolved in dichloromethane (5 mL/g polymer) and added dropwise to diethyl ether (250 mL) and stirred vigorously for 1 hour. After this time, the solution was left to settle, filtered and the solid was washed with diethyl ether and dried to afford the corresponding PIILP as an off white solid. ¹H NMR spectroscopy was used to confirm the disappearance of the vinyl protons in the starting material. Yield of **2.9** = 94%, and **2.10** = 97%.

7.1.10 General procedure for impregnation of PIILs with Na₂[PdCl₄].

A 100 mL round bottom flask was charged with a suspension of the appropriate PIIL (2.0 mmol) in water (20 mL). To this was added Na₂[PdCl₄] (0.58 g, 2.0 mmol) in a single portion, and the resultant mixture was stirred vigorously at room temperature for 5 hours. Following this, the precipitate was collected by filtration through a frit and the solid was washed with water (10 mL), ethanol (2 x 10 mL) and diethyl ether (2 x 20 mL) to yield free flowing orange/brown powders. Yield of **2.11** = 96%, yield of **2.12** = 93%.

7.1.11 General procedure for chemical reduction of [PdCl₄]²⁻ loaded PIILs with NaBH₄.

A 100 mL round bottom flask was charged with the appropriate [PdCl₄]²⁻ loaded precursor (1.5 mmol) and ethanol (20 mL) under a nitrogen atmosphere and cooled to 0 °C. To this was added NaBH₄ (0.40 g, 10.5 mmol) dissolved in water (3 mL), at which point the orange suspension rapidly turned black. The mixture was then allowed to warm to room temperature and stirred for 5 hours. After this time, the mixture was added dropwise to cold acetone (250 mL), stirred vigorously for 60 minutes and then centrifuged. The solution was then filtered and the solid washed with water (10 mL), ethanol (2 x 10 mL) and diethyl ether (2 x 20 mL) to yield the product as a black powder. Yield of **2.13** = 91%, yield of **2.14** = 90%.

7.1.12 General procedure for the Suzuki-Miyaura coupling.

A flame-dried Schlenk flask under N₂ was charged with aryl halide (1 mmol), phenylboronic acid (1.1 mmol), potassium carbonate (1.2 mmol) and catalyst (0.001 mmol, 0.1 mol % based on Pd content determined by ICP-OES). The reaction was initiated by the addition of EtOH (1.2 mL), and H₂O (1.2 mL) and the reaction mixture was stirred at room temperature for the appropriate length of time. Decane (1 mmol) was added as an internal standard and the reaction mixture was diluted with Et₂O (10 mL), washed with H₂O (5 mL) and the organic extract filtered through a plug of silica, washed with Et₂O (3 mL) and the solvent removed under reduced pressure. The resulting residue was analysed by GC and ¹H NMR spectroscopy. Gas chromatography was performed on a Shimadzu 2010 series gas chromatograph equipped with a split mode capillary injection system and flame ionisation detection using a Supleco Beta DEX column. Injection temperature = 200 °C, column conditions: 90 °C for 4 min, ramp to 120 °C at 4 °C/min, hold for 20 min, ramp to 180 °C at 7 °C/min, hold for 15 min. Total run time = 56 min. Error within results = 0.5%.

7.1.13 General procedure for Suzuki-Miyaura mercury poisoning experiments.

A flame-dried Schlenk flask under N₂ was charged with phenylboronic acid (1.1 mmol), potassium carbonate (1.2 mmol), catalyst (0.001 mmol, 0.1 mol %), EtOH (1.2 mL) and H₂O (1.2 mL). Mercury (0.2 mmol) was added and the resulting mixture was stirred for the appropriate length of time. Following poisoning the reaction was initiated by the addition of 4-bromotoluene (1 mmol), and the reaction was stirred at room temperature for the appropriate amount of time. Decane (1 mmol) was added to act as a standard and the reaction mixture was diluted with Et₂O (10 mL), washed with H₂O (5 mL) and the organic phase filtered through a plug of silica, washed with Et₂O (3 mL) and the solvent removed under reduced pressure. The resulting residue was analysed by GC and ¹H NMR spectroscopy. Error within results = 0.5%.

7.1.14 General procedure for Suzuki-Miyaura heteroaromatic poisoning experiments.

A flame-dried Schlenk flask under N₂ was charged with phenylboronic acid (1.1 mmol), potassium carbonate (1.2 mmol), catalyst (0.001 mmol, 0.1 mol %), EtOH (1.2 mL) and H₂O (1.2 mL). Pyridine (0.79 g, 1 mmol) was added and the resulting mixture stirred for the appropriate length of time. Following poisoning the reaction was initiated by the addition of 4-bromotoluene (1 mmol), and the mixture was stirred at room temperature for the appropriate amount of time. Decane (1 mmol) was added as internal standard and the

reaction mixture was diluted with Et₂O (10 mL), washed with H₂O (5 mL) and the organic phase filtered through a plug of silica, washed with Et₂O (3 mL) and the solvent removed under reduced pressure. The resulting residue was analysed by GC and ¹H NMR spectroscopy. Error within results = 0.5%.

7.2 Chapter 3 Experimental.

7.2.1 General procedure for the Pd catalysed hydrogenation of α,β -unsaturated aldehydes and ketones.

All hydrogenation reactions were conducted in a 50 mL temperature-controlled Parr benchtop reactor with a magnetically coupled stirrer and gas ballast. In a typical procedure, a 50 mL glass vessel was charged with substrate (1 mmol), the appropriate catalyst (0.5 mol % based on Pd content determined by ICP-OES) and diluted to 13 mL with the appropriate solvent. Reactions were conducted at 20 °C under 70 psi of hydrogen unless otherwise stated. Once assembled, the reactor was pressurised to 100 psi of hydrogen and left for 10 seconds, before releasing the gas through the outlet valve. After repeating the sequence five times, the reactor was pressurised to 70 psi and the solution stirred at room temperature for the desired amount of time. For reactions conducted in ethanol, 2-methyl-THF, toluene, hexane or ethyl acetate, the mixture was passed through a silica plug and the solvent removed. If the reaction was conducted in aqueous medium, the mixture was transferred to a dropping funnel and extracted with ethyl acetate (3 x 20 mL). The organic phases were combined, dried over MgSO₄, filtered and the solvent removed *in vacuo*. Conversion and selectivity were determined using ¹H NMR spectroscopy by quantifying the remaining starting material and products against an internal standard, 1,3-dinitrobenzene. In all reactions, mass balance was >99%. Well-resolved resonances were used to calculate the composition of the mixture by normalising the relative integrations according to the number of protons associated with the chosen peaks. For each substrate, ¹H NMR spectra were recorded at relaxation times of 10, 20 and 30 seconds to ensure that peaks integrated accurately. Error within results = 0.5%.

7.2.2 Synthesis of 1-(4-vinylphenyl)-2,5,8,11,14,17,20,23,26-nonaoxaheptacosane (para-PEG-styrene, for catalysis with modified neutral polymer supports).

An oven-dried Schlenk flask was charged with polyethylene glycol monomethylether (1.0 g, 2.85 mmol) dissolved in anhydrous THF (8 mL). The solution was added dropwise *via* cannula transfer to another Schlenk flask containing NaH (0.10 g, 4.3 mmol) suspended in THF (20 mL) over 15 minutes and the mixture was stirred at room temperature for 1 hour. After this, 4-

chloromethylstyrene (0.28 mL, 2 mmol) was added dropwise and the resultant mixture was stirred and heated at 60 °C for 16 h. After this time, the solution was cooled to room temperature and the mixtures transferred to a dropping funnel and diluted with water (80 mL). The mixture was brought to pH 7 by slow addition of 0.1 M HCl. The organic phase was collected, and the aqueous layer washed with diethyl ether (4 x 30 mL). The combined organic extracts were dried over MgSO₄, filtered and the solvent removed *in vacuo* to afford the product as a yellow oil (1.26 g, 2.80 mmol) in 98% yield.

7.2.3 Synthesis of PdNP@PPh₂-PEGPIILP via reduction of PdCl₄@PPh₂-PEGPIILP with hydrogen.

A glass insert was charged with PdCl₄@PPh₂-PEGPIILP (0.5 g, 0.33 mmol) and ethanol (25 mL). The reduction was conducted in a 50 mL temperature-controlled Parr benchtop reactor with a magnetically coupled stirrer and gas ballast. Once assembled, the reactor was pressurised with 100 psi of hydrogen and left for 10 seconds, before releasing the gas through the outlet valve. After repeating the sequence five times, the reactor was pressurised to 150 psi and the solution stirred at 70 °C for 16 hours. After this time, the reactor was cooled to room temperature, the gas was released through the outlet valve and the vessel removed from the reactor. After removal of the solvent, the product was obtained as a black powder (0.46 g, 3.2 mmol) in 98% yield.

7.3 Chapter 4 experimental.

7.3.1 Synthesis of tris(4-vinylphenyl)phosphine

A 250 mL three-necked round bottom flask was charged with Mg turnings (1.96 g, 81.7 mmol) suspended in anhydrous THF under a nitrogen atmosphere. A crystal of iodine was added, and the solution was stirred at room temperature for 10 minutes. After this, 4-chloromethylstyrene (7.49 g, 54.0 mmol) was added dropwise over 15 minutes and the resulting solution was heated to 60 °C and stirred for 5 hours. After this time the solution was cooled to 0 °C, PCl₃ (1.29 mL, 14.9 mmol) was added carefully over 10 minutes and the resultant mixture stirred at room temperature overnight. Following this, the solvent was removed from the flask under vacuum and degassed water (30 mL) was added carefully. The product was then extracted with degassed diethyl ether (3 x 30 mL) and the organic layer was decanted into a conical flask under a positive pressure of nitrogen. The combined layers were dried over MgSO₄, filtered and the solvent removed to give the product as a white solid in 62% yield (3.16 g). ³¹P NMR (162 MHz, CDCl₃, δ): -6.65. ¹H NMR (400 MHz, CDCl₃, δ): 7.40 – 7.08

(m, 12H), 6.67 – 6.60 (m, 3H). 5.67 (d, J = 16.8 Hz, 3H), 5.16 (d, J = 10.9 Hz, 3H); ^{13}C NMR (101 MHz, CDCl_3 , δ): 136.95, 135.61 (d, $J_{\text{C-P}}$ = 10.7 Hz, 3C), 135.63 (3C), 132.84 (d, $J_{\text{C-P}}$ = 19.6 Hz, 6C) 125.28 (d, $J_{\text{C-P}}$ = 7.13, 6C), 113.65 (3C).

7.3.2 Synthesis of highly crosslinked polymers 4.2 and 4.3

An oven-dried Schlenk flask was charged with **4.1** (4.0 g, 11.7 mmol), the appropriate IL-like monomer (23.4 mmol) and AIBN (0.16 g, 0.96 mmol) under a nitrogen atmosphere. The reagents were dissolved in a 1:1.5 mixture of anhydrous ethanol/THF (80 mL) and the solution was degassed using freeze-thaw cycles. After repeating the sequence 6 times to ensure complete exclusion of oxygen, the solution was heated to 65 °C and stirred for 3 days. After this time, the mixture was cooled to room temperature and a further equivalent of AIBN (0.16 g, 0.96 mmol) was added. The freeze-thaw cycle was then repeated 6 times before heating to 65 °C and stirring for a further 16 hours. The solution was then cooled to room temperature and concentrated *in vacuo*. The resultant residue was dissolved in the minimum volume of dichloromethane and added dropwise to a large volume of diethyl ether (300 mL) with rapid stirring. After 1 h, the mixture was left to settle, and the product was collected *via* filtration through a frit and washed with diethyl ether (2 x 20 mL) to give off-white powders. Yield of **4.2** = 98%, yield of **4.3** = 94% based on total mass of monomer. Catalysts were prepared using the impregnation technique and reduction method described in **7.2.10** and **7.2.11**, respectively.

7.3.3 General procedure for the catalytic hydrogenation of nitroarenes

All hydrogenation reactions were conducted in a 50 mL temperature-controlled Parr benchtop reactor with a magnetically coupled stirrer and gas ballast. In a typical procedure, a 50 mL glass vessel was charged with the substrate (1 mmol) and the appropriate catalyst (0.47-1.0 mol % based on Pd content determined by ICP-OES) and diluted to 13 mL with the appropriate solvent. Reactions were conducted at 20 °C under 70 psi of hydrogen unless otherwise stated. Once assembled, the reactor was pressurised to 100 psi of hydrogen and left for 10 seconds before releasing the gas through the outlet valve. After repeating the sequence five times, the reactor was pressurised to 70 psi and the solution was stirred at room temperature for the desired amount of time. For reactions conducted in ethanol, 2-methyl-THF, toluene, hexane or ethyl acetate, the mixture was passed through a silica plug and the solvent removed. If the reaction was conducted in aqueous medium, the mixture was transferred to a dropping funnel and extracted with ethyl acetate (3 x 20 mL). The organic phases were combined, dried over

MgSO₄, filtered and the solvent removed *in vacuo*. Conversion and selectivity were determined using ¹H NMR spectroscopy and GC analysis by quantifying the remaining starting material and products against dioxane and *n*-decane, respectively. In all reactions mass balance was >99%. When using ¹H NMR spectroscopy, well-resolved resonances were used to calculate the composition of the mixture by normalising the relative integrations according to the number of protons associated with the chosen peaks. For each substrate, ¹H NMR spectra were recorded at relaxation times of 10, 20 and 30 seconds to ensure that peaks were integrated accurately. Gas chromatography was performed on a Shimadzu 2010 series gas chromatogram equipped with a split mode capillary injection system and flame ionisation detector using a Supleco Beta DEX column. Injection temperature = 200 °C, column conditions: 90 °C for 4 min, ramp to 120 °C at 4 °C/min, hold for 20 min, ramp to 180 °C at 7 °C/min, hold for 15 min. Total run time = 56 min. Error within results = 0.5%.

7.3.4 General procedure for the catalytic transfer hydrogenation of nitroarenes

An oven-dried Schlenk flask was charged with the appropriate catalyst (0.047 mmol, 0.47 mol% based on Pd content determined by ICP-OES) suspended in water (2 mL). To this, NaBH₄ (95.4 mg, 2.5 mmol) was added and the mixture was stirred for 2 minutes. After this, the substrate (1.0 mmol) was added and the solution was stirred at 20 °C for 2 hours. After this time, the products were extracted with ethyl acetate (3 x 5 mL), dried over MgSO₄, filtered and the solvent was removed. Conversion and selectivity were determined using the same method as described in **7.4.3** for the hydrogenation of nitroarenes. Error within results = 0.5%.

7.3.5 Continuous flow reduction of nitrobenzene

Reagent reservoirs were prepared by dissolving nitrobenzene (6.155 g, 50 mmol) in ethanol (250 mL) and NaBH₄ (4.729 g, 125 mmol) in a 1.0 M NaOH_(aq) solution (250 mL) which was kept stirring on a hotplate. The feeds were pumped using JASCO PU980 dual piston HPLC pumps. The pump streams were mixed using a Swagelok SS-100-3 tee piece. In a typical run, a 2.5 mL aluminium tube was packed with **2.14** (0.092 g, 3.808 wt% Pd) and sand (3.92 g). The column was then placed in an aluminium block equipped with a Eurotherm temperature-controlled nickel heating element insert. The reactor was maintained under a fixed back pressure using an Upchurch Scientific 100 psi back pressure regulator. SS tubing (1/16" OD, 1/32" ID) was used throughout the reactor. The reaction was analysed using HPLC by collecting a 0.5 mL aliquot from the outlet which was diluted with 0.5 mL of a 0.02M solution of 1,3,5-trimethoxybenzene in ethanol. HPLC analysis was performed on an Agilent 1100 series LC

instrument using an Ascentis Express C18 reverse phase column (length = 5 cm, 4.6 mm ID, and 27 μm particle size) using a water acetonitrile (A/B) mixture as the mobile phase. Analysis was conducted based on normalisation of the response factors using 1,3,5-trimethoxybenzene as the internal standard. The method used was 10%:90% B (12 mins), 90%:10% B (0.1 min), 10% B (1 min), flow rate = 1.5 mL min⁻¹. Column temperature = 20 °C.

7.4 Chapter 5 experimental.

7.4.1 General procedure for impregnation of PIIL supports with $\text{K}[\text{AuCl}_4]$.

A 100 mL round bottom flask was charged with the appropriate PIIL support (2.0 mmol) suspended in water (15 mL) and potassium tetrachloroaurate (0.755 g, 2.0 mmol) was added in a single portion. The resultant mixture was stirred vigorously for 6 hours. The yellow precipitate was collected after centrifugation by filtration through a frit and the solid was washed with water (10 mL), ethanol (2 x 10 mL) and diethyl ether (3 x 10 mL) to afford the corresponding $[\text{AuCl}_4]^-$ loaded PIILs as free flowing yellow solids.

7.4.2 General procedure for the selective transfer hydrogenation of nitroarenes to the corresponding arylhydroxylamine

An oven-dried Schlenk flask was charged with the appropriate catalyst (0.5 μmol , 0.05 mol %) suspended in water (2 mL) under a nitrogen atmosphere. To this, NaBH_4 (0.096 g, 2.5 mmol) was added and the solution was stirred for 2 min at 20 °C. After this, the nitro substrate (1 mmol) was added and the mixture was stirred for the appropriate time at room temperature. The reaction was quenched by addition of water (7 mL), the products were extracted with ethyl acetate (2 x 10 mL) and the solvent removed under reduced pressure. The resulting residue was analysed by ¹H NMR spectroscopy using 1,4-dioxane as the internal standard to quantify the composition of starting material and products and determine the extent of conversion and selectivity. Error within results = 0.5%.

7.4.3 General procedure for the selective transfer hydrogenation of nitrobenzene to azoxybenzene

An oven-dried Schlenk flask was charged with the appropriate catalyst (0.5 μmol , 0.05 mol %) and ethanol (2 mL) under a nitrogen atmosphere. To this, NaBH_4 (0.096 g, 2.5 mmol) was added and the solution was stirred for 2 min at 20 °C. After this time, the nitrobenzene (102 μL , 1 mmol) was added and the mixture was stirred for the appropriate time at room temperature. After this, stirring was stopped and 1,4 dioxane (85 μL , 1 mmol) was added as the internal reference. A 0.05 mL aliquot was taken from the solution and diluted with CDCl_3

(0.15 mL). The reaction was analysed using ^1H NMR spectroscopy to quantify the composition of starting material and products and determine the extent of conversion and selectivity. Error within results = 0.5%.

7.4.4 General procedure for the selective transfer hydrogenation of nitroarenes to the corresponding arylamines

An oven-dried Schlenk flask was charged with the appropriate catalyst (0.5 μmol , 0.05 mol %) and water (2 mL) under a nitrogen atmosphere. To this, NaBH_4 (0.192 g, 5.0 mmol) was added and the solution was stirred for 2 min at 20 $^\circ\text{C}$. After this the nitro substrate (1 mmol) was added and the mixture heated to 50 $^\circ\text{C}$ with stirring for the appropriate time. After this, the reaction mixture was removed from the heat, left to cool and then quenched by the addition of water (7 mL). The products were then extracted with ethyl acetate (2 x 10 mL) and the solvent removed under reduced pressure. The resulting residue was analysed by ^1H NMR spectroscopy using 1,4-dioxane as the internal standard to quantify the composition of starting material and products and determine the extent of conversion and selectivity. Error within results = 0.5%.

7.5 Chapter 6 experimental.

7.5.1 Synthesis of *N*-[(4-vinylphenyl)methyl]phthalimide (6.1)

An oven-dried Schlenk flask was charged with potassium phthalimide (2.54 g, 13.7 mmol) and anhydrous dimethylformamide (20 mL) to afford a suspension. To this, 4-chloromethylstyrene (2.03 g, 13.3 mmol) was added dropwise. The mixture was then heated to 60 $^\circ\text{C}$ and stirred for 16 hours. The resultant pale-yellow solution was then diluted with dichloromethane (120 mL) and washed with water (6 x 100 mL). The organic phase was then washed with 0.2 M NaOH (25 mL) and water (25 mL), dried over MgSO_4 , filtered and the solvent removed under reduced pressure to afford the crude product as a white solid. The pure product was obtained as a white crystalline solid (1.32 g, 5.0 mmol) in 38% yield by crystallisation from methanol. ^1H NMR: (300 MHz, CDCl_3 , δ): 4.73 (2H, s), 5.11- 5.15 (1H, dd, J = 12 Hz, 3 Hz), 5.62- 5.68 (1H, dd, J = 18 Hz, 3 Hz), 6.55- 6.66 (1H, dd, J = 18 Hz, 12Hz), 7.20- 7.33 (4H, m), 7.62- 7.65 (2H, m), 7.77- 7.79 (2H, m); ^{13}C NMR: (300 MHz, CDCl_3 , δ): 40.86, 113.96, 123.38, 126.51, 129.02, 132.64, 134.10, 136.94, 136.49, 136.98, 167.78.

7.5.2 Synthesis of (4-vinylphenyl)methanamine (6.2)

An oven-dried Schlenk flask was charged with *N*-[(4-vinylphenyl)methyl]phthalimide (1.10 g, 4.16 mmol) dissolved in 95% ethanol (20 mL). To this, a solution of hydrazine hydrate (0.42 g, 8.32 mmol) dissolved in ethanol (3 mL) was added dropwise which resulted in the immediate precipitation of a white solid. After stirring for 5 minutes at room temperature, an additional portion of hydrazine hydrate (0.29 g, 5.94 mmol) in ethanol (3 mL) was added and the solution was heated to 80 °C and stirred for 16 hours. After this time, the solvent was removed *in vacuo* and the residue dissolved in chloroform (30 mL) and washed with 20% NaOH_(aq) (30 mL). The organic phase was collected, and the aqueous phase was then washed with chloroform (3 x 30 mL). The combined organic extracts were then dried over MgSO₄, filtered and the solvent was removed *in vacuo* to afford the product as a pale-yellow oil (0.49 g, 3.7 mmol) in 89% yield. ¹H NMR: (300 MHz, CDCl₃, δ): 1.41 (2H, s), 3.81 (2H, s), 5.14- 5.18 (1H, dd, *J* = 11 Hz, 3 Hz), 5.59- 5.66 (1H, dd, *J* = 17 Hz, 3 Hz), 6.59- 6.70 (1H, dd, *J* = 18 Hz, 12 Hz), 7.11- 7.31 (4H, m). ¹³C NMR: (300 MHz, CDCl₃, δ): 48.16, 114.53, 126.12, 124.59, 127.25, 137.84, 138.21.

7.5.3 Synthesis of NH₂-PEGPIILP (6.3)

Amine functionalised PEGylated PIIL **6.3** was prepared following the general protocol discussed in section 7.2.9 and was obtained as a pale-yellow solid in 88% yield.

7.5.4 Synthesis of PEGPIILP (6.4)

PEGylated PIIL **6.4** was prepared following the general protocol discussed in section 7.2.9 and was obtained as a pale-yellow solid in 92% yield.

7.5.5 General procedure for synthesis of PIIL-stabilised RuNPs.

A 100 mL round bottom flask was charged with the appropriate PIIL (0.5 mmol) suspended in ethanol (25 mL). To this, RuCl₃·3H₂O (0.13 g, 0.5 mmol) was added in a single portion and the mixture was stirred vigorously at room temperature for 4 hours. After this NaBH₄ (0.15 g, 4 mmol) dissolved in water (5 mL) was added dropwise. The mixture rapidly turned from dark brown to green then to black and the resulting mixture was stirred vigorously overnight at room temperature under a nitrogen atmosphere. After this, the solvent was concentrated under reduced pressure to ca. 5 mL and added dropwise to cold acetone (300 mL). After stirring for 1 hour the solids were collected by filtration through a frit and washed with water (10 mL), ethanol (2 x 10 mL) and diethyl ether (3 x 10 mL) to **6.5-6.7** as black powders. Yield of **6.5** = 87%, yield of **6.6** = 90%, yield of **6.7** = 89%.

7.5.6 General procedure for the selective hydrogenation of model aldehydes and ketones.

All hydrogenations were conducted in a 50 mL temperature-controlled Parr benchtop reactor with a magnetically coupled stirrer and gas ballast. In a typical procedure, a 50 mL glass vessel was charged with substrate (1 mmol), the appropriate catalyst (0.1 mol % based on Ru content determined by ICP-OES) and 13 mL of the appropriate solvent. Reactions were conducted at 50 °C under 70 psi of hydrogen unless otherwise stated. Once assembled, the reactor was pressurised to 100 psi of hydrogen and left for 10 seconds, before releasing the gas through the outlet valve. After repeating the sequence five times, the reactor was pressurised to 70 psi, heated to 50 °C and the solution was stirred at room temperature for the desired amount of time. For reactions conducted in ethanol, 2-methyl-THF, toluene, hexane or ethyl acetate, the mixture was passed through a silica plug and the solvent removed. If the reaction was conducted in aqueous medium, the mixture was transferred to a dropping funnel and extracted with ethyl acetate (3 x 20 mL). The organic phases were combined, dried over MgSO₄, filtered and the solvent removed *in vacuo*. Conversion and selectivity were determined using ¹H NMR spectroscopy by quantifying the remaining starting material and products against 1,3-dinitrobenzene. In all reactions mass balance was >99%. Well-resolved resonances were used to calculate the composition of the mixture by normalising the relative integrations according to the number of protons associated with the chosen peaks. For each substrate, ¹H NMR spectra were recorded at relaxation times of 10, 20 and 30 seconds to ensure that peaks were integrated accurately. Error within results = 0.5%.

7.5.7 General procedure for the hydrogenation of acetophenone to cyclohexylethanol

In a typical procedure, a 50 mL glass vessel was charged with acetophenone (0.12 g, 1 mmol), catalyst (0.1 mol % based on Ru content determined by ICP-OES) and the appropriate solvent (13 mL). Reactions were conducted at 110 °C under 450 psi of hydrogen unless otherwise stated. Once assembled, the reactor was pressurised to 100 psi of hydrogen and left for 10 seconds, before releasing the gas through the outlet valve. After repeating the sequence five times, the reactor was pressurised to 450 psi, heated to 110 °C and the solution stirred for the desired amount of time. After this, the reactor was cooled to room temperature and the reaction mixture transferred to a dropping funnel and extracted with ethyl acetate (3 x 20 mL). The organic phases were combined, dried over MgSO₄, filtered and the solvent removed *in vacuo*. Conversion and selectivity were determined using ¹H NMR spectroscopy by quantifying the remaining starting material and products against 1,3-dinitrobenzene. In all reactions mass

balance was >99%. Well-resolved resonances were used to calculate the composition of the mixture by normalising the relative integrations according to the number of protons associated with the chosen peaks. For each substrate, ^1H NMR spectra were recorded at relaxation times of 10, 20 and 30 seconds to ensure that peaks were integrated accurately. Error within results = 0.5%.

7.5.8 General procedure for the selective hydrogenation of furfural to furfuryl alcohol

In a typical procedure, a 50 mL glass vessel was charged with furfuryl alcohol (0.98 g, 1 mmol), catalyst (0.1 mol % based on Ru content determined by ICP-OES) and solvent (13 mL). Reactions were conducted at 50 °C under 70 psi of hydrogen unless otherwise stated. Once assembled, the reactor was pressurised to 100 psi of hydrogen and left for 10 seconds before releasing the gas through the outlet valve. After repeating the sequence five times, the reactor was pressurised to 70 psi, heated to 50 °C and the solution stirred for the desired amount of time. After this, the reactor was cooled to room temperature and the reaction mixture was transferred to a dropping funnel and extracted with ethyl acetate (3 x 20 mL). The organic phases were combined, dried over MgSO_4 , filtered and the solvent removed *in vacuo*. Conversion and selectivity were determined using ^1H NMR spectroscopy by quantifying the remaining starting material and products against 1,3-dinitrobenzene. In all reactions mass balance was >99%. Well-resolved resonances were used to calculate the composition of the mixture by normalising the relative integrations according to the number of protons associated with the chosen peaks. For each substrate, ^1H NMR spectra were recorded at relaxation times of 10, 20 and 30 seconds to ensure that peaks were integrated accurately. Error within results = 0.5%.

7.5.9 General procedure for the hydrogenation of levulinic acid to γ -valerolactone

In a typical procedure, a 50 mL glass vessel was charged with levulinic acid (0.12 g, 1 mmol), catalyst (0.1 mol % based on Ru content determined by ICP-OES) and solvent (13 mL). Reactions were conducted at 110 °C under 450 psi of hydrogen unless otherwise stated. Once assembled, the reactor was pressurised to 100 psi of hydrogen and left for 10 seconds before releasing the gas through the outlet valve. After repeating the sequence five times, the reactor was pressurised to 450 psi, heated to 110 °C and the solution stirred for the desired amount of time. After this, the reactor was cooled to room temperature and the reaction mixture was transferred to a dropping funnel and extracted with ethyl acetate (3 x 20 mL). The organic phases were combined, dried over MgSO_4 , filtered and the solvent removed *in vacuo*.

Conversion and selectivity were determined using ^1H NMR spectroscopy by quantifying the remaining starting material and products against 1,3-dinitrobenzene as the internal standard. In all reactions mass balance was >99%. Well-resolved resonances were used to calculate the composition of the mixture by normalising the relative integrations according to the number of protons associated with the chosen peaks. For each substrate, ^1H NMR spectra were recorded at relaxation times of 10, 20 and 30 seconds to ensure that peaks were integrated accurately. Error within results = 0.5%.

7.5.10 General procedure for the hydrogenation of ethyl levulinate to γ -valerolactone

In a typical procedure, a 50 mL glass vessel was charged with ethyl levulinate (0.14 g, 1 mmol), potassium carbonate (0.013 g, 0.1 mmol), catalyst (0.1 mol % based on Ru content determined by ICP-OES) and solvent (13 mL). Reactions were conducted at 110 °C under 450 psi of hydrogen unless otherwise stated. Once assembled, the reactor was pressurised to 100 psi of hydrogen and left for 10 seconds before releasing the gas through the outlet valve. After repeating the sequence five times, the reactor was pressurised to 450 psi, heated to 110 °C and the solution was stirred for the desired amount of time. After this, the reactor was cooled to room temperature and the reaction mixture was transferred to a dropping funnel and extracted with ethyl acetate (3 x 20 mL). The organic phases were combined, dried over MgSO_4 , filtered and the solvent removed *in vacuo*. Conversion and selectivity were determined using ^1H NMR spectroscopy by quantifying the remaining starting material and products against 1,3-dinitrobenzene as internal standard. In all reactions mass balance was >99%. Well-resolved resonances were used to calculate the composition of the mixture by normalising the relative integrations according to the number of protons associated with the chosen peaks. For each substrate, ^1H NMR spectra were recorded at relaxation times of 10, 20 and 30 seconds to ensure that peaks were integrated accurately. Error within results = 0.5%.

Appendix

List of Figures

A1 TEM images (a) and the associated particle size distribution (b) of PdNPs generated by the *in situ* reduction of PdCl₄@PPh₂-PIILP (**2.11**) with phenyl boronic acid. Scale bars are 5 nm (white) and 25 nm (black).

A2 TEM images (a) and the associated particle size distribution (b) of PdNPs generated from *in situ* reduction of PdCl₄@PPh₂-PIILP (**2.12**) with phenyl boronic acid. Scale bars are 5 nm (white) and 25 nm (black).

A3 TGA curve for PPh₂PEGstyrene wt% v temperature (green) and (b) derivative wt% v temperature (blue). Heating rate of 10 °C.

A4 SEM images of PPh₂PEGstyrene.

A5 Solid state ³¹P NMR spectrum of PPh₂PEGstyrene.

A6 TGA curve for PEGPIILP wt% v temperature (green) and (b) derivative wt% v temperature (blue). Heating rate of 10 °C.

A7 SEM images of PEGPIILP.

A8 TGA curve for PPh₂styrene wt% v temperature (green) and (b) derivative wt% v temperature (blue). Heating rate of 10 °C.

A9 SEM images of PPh₂styrene.

A10 Solid state ³¹P NMR spectrum of PPh₂styrene.

A11 TGA curve for PIILP wt% v temperature (green) and (b) derivative wt% v temperature (blue). Heating rate of 10 °C.

A12 SEM images of PIILP.

A13 Pd 3d core level XPS spectrum of [PdCl₂(MeCN)₂]@PPh₂PEGstyrene referenced to the hydrocarbon C 1s at 284.8 eV.

A14 SEM images of [PdCl₂(MeCN)₂]@PPh₂PEGstyrene.

A15 Solid state ³¹P NMR spectrum of [PdCl₂(MeCN)₂]@PPh₂PEGstyrene.

A16 Pd 3d core level XPS spectrum of [PdCl₄]@PEGPIILP referenced to the hydrocarbon C 1s at 284.8 eV.

A17 SEM images of [PdCl₄]@PEGPIILP.

A18 Pd 3d core level XPS spectrum of [PdCl₂(MeCN)₂]@PPh₂styrene referenced to the hydrocarbon C 1s at 284.8 eV.

A19 SEM images of [PdCl₂(MeCN)₂]@PPh₂styrene.

A20 Solid state ³¹P NMR spectrum of [PdCl₂(MeCN)₂]@PPh₂styrene.

A21 Pd 3d core level XPS spectrum of [PdCl₄]@PIILP referenced to the hydrocarbon C 1s at 284.8 eV.

A22 SEM images of [PdCl₄]@PIILP.

A23 Pd 3d core level XPS spectrum of PdNP@PPh₂PEGstyrene (**2.15**) referenced to the hydrocarbon C 1s at 284.8 eV.

A24 TEM micrographs (a-d) and associated particle size distribution (e) of PdNP@PPh₂PEGstyrene (**2.15**). Scale bars are 25 nm (black) and 5 nm (white).

A25 Solid state ³¹P NMR spectrum of [PdNP]@PPh₂PEGstyrene (**2.15**).

A26 SEM images of PdNP@PPh₂PEGstyrene (**2.15**).

A27 Pd 3d core level XPS spectrum of PdNP@PEGPIILP (**2.16**) referenced to the hydrocarbon C 1s at 284.8 eV.

A28 TEM micrographs (a-d) and the associated particle size distribution (e) of PdNP@PEGPIILP (**2.16**). Scale bars are 25 nm (black) and 5 nm (white).

A29 SEM images of PdNP@PEGPIILP (**2.16**).

A30 Pd 3d core level XPS spectrum of PdNP@PPh₂styrene (**2.17**) referenced to the hydrocarbon C 1s at 284.8 eV.

A31 TEM micrographs (a-d) and the associated particle size distribution (e) of PdNP@PPh₂styrene (**2.17**). Scale bars are 25 nm (black) and 5 nm (white).

A32 Solid state ³¹P NMR spectrum of [PdNP]@PPh₂styrene (**2.17**).

A33 SEM images of PdNP@PPh₂styrene (**2.17**).

A34 Pd 3d core level XPS spectrum of PdNP@PIILP (**2.18**) referenced to the hydrocarbon C 1s at 284.8 eV.

A35 TEM micrographs (a-d) and the associated particle size distribution (e) of PdNP@PIILP (**2.18**). Scale bars are 25 nm (black) and 5 nm (white).

A36 SEM images of PdNP@PIILP (**2.18**).

A37 XRD spectra of **2.13** - **2.18**.

A38 TGA curve for P(Sty)₃-PIILP (**4.2**).

A39 SEM images of P(Sty)₃-PIILP (**4.2**).

A40 Solution state ³¹P NMR spectrum of P(Sty)₃-PIILP (**4.2**).

A41 TGA curve for P(Sty)₃-PEGPIILP (**4.3**).

A42 SEM images of P(Sty)₃-PEGPIILP (**4.3**).

A43 Solid state ³¹P NMR spectrum of P(Sty)₃-PEGPIILP (**4.3**).

A44 XRD spectrum for PdNP@P(Sty)₃-PIILP (**4.6**).

A45 XRD spectrum for PdNP@P(Sty)₃-PEGPIILP (**4.7**).

A46 Time-composition profiles for the transfer hydrogenation of nitrobenzene catalysed by **2.13** (top), **4.6** (middle), and **4.7**. Reactions conditions: 1 mmol nitrobenzene, 0.047 mol% catalyst, 2.5 mmol NaBH₄, RT, 2 mL water.

A47 N 1s core level XPS spectrum of [AuCl₄]Cl@PPh₂PIILP (**5.3**) referenced to the hydrocarbon C 1s at 284.8 eV.

A48 P 2p core level XPS spectrum of $[\text{AuCl}_4]\text{Cl}@P\text{Ph}_2\text{-PIILP}$ (**5.3**) referenced to the hydrocarbon C 1s at 284.8 eV.

A49 SEM images of freshly prepared $[\text{AuCl}_4]\text{Cl}@P\text{Ph}_2\text{-PIILP}$ (**5.3**).

A50 N 1s core level XPS spectrum of $[\text{AuCl}_4]\text{Cl}@P\text{Ph}_2\text{-PEGPIILP}$ (**5.4**) referenced to the hydrocarbon C 1s at 284.8 eV.

A51 P 2p core level XPS spectrum of $[\text{AuCl}_4]\text{Cl}@P\text{Ph}_2\text{-PEGPIILP}$ (**5.4**) referenced to the hydrocarbon C 1s at 284.8 eV.

A52 SEM images of freshly prepared $[\text{AuCl}_4]\text{Cl}@P\text{Ph}_2\text{-PEGPIILP}$ (**5.4**).

A53 N 1s core level XPS spectrum of $[\text{AuCl}_4]\text{Cl}@P\text{Ph}_2\text{-PIILP}$ (**5.5**) referenced to the hydrocarbon C 1s at 284.8 eV.

A54 SEM images of freshly prepared $[\text{AuCl}_4]\text{Cl}@P\text{Ph}_2\text{-PIILP}$ (**5.5**).

A55 N 1s core level XPS spectrum of $[\text{AuCl}_4]\text{Cl}@P\text{Ph}_2\text{-PEGPIILP}$ (**5.6**) referenced to the hydrocarbon C 1s at 284.8 eV.

A56 SEM images of freshly prepared $[\text{AuCl}_4]\text{Cl}@P\text{Ph}_2\text{-PEGPIILP}$ (**5.6**).

A57 N 1s core level XPS spectrum of $\text{AuNP}@P\text{Ph}_2\text{-PIILP}$ (**5.7**) referenced to the hydrocarbon C 1s at 284.8 eV.

A58 P 2p core level XPS spectrum of $\text{AuNP}@P\text{Ph}_2\text{-PIILP}$ (**5.7**) referenced to the hydrocarbon C 1s at 284.8 eV.

A59 N 1s core level XPS spectrum of $\text{AuNP}@P\text{Ph}_2\text{-PEGPIILP}$ (**5.8**) referenced to the hydrocarbon C 1s at 284.8 eV.

A60 P 2p core level XPS spectrum of $\text{AuNP}@P\text{Ph}_2\text{-PEGPIILP}$ (**5.8**) referenced to the hydrocarbon C 1s at 284.8 eV.

A61 N 1s core level XPS spectrum of $\text{AuNP}@P\text{Ph}_2\text{-PIILP}$ (**5.9**) referenced to the hydrocarbon C 1s at 284.8 eV.

A62 TEM micrographs (a-d) and the associated particle size distribution (e) and EDX spectrum confirming the presence of Au in $\text{AuNP}@P\text{Ph}_2\text{-PIILP}$ (**5.9**). Scale bars are 25 nm (black) and 5 nm (white).

A63 N 1s core level XPS spectrum of $\text{AuNP}@P\text{Ph}_2\text{-PEGPIILP}$ (**5.10**) referenced to the hydrocarbon C 1s at 284.8 eV.

A64 TEM micrographs (a-d) and the associated particle size distribution (e) and EDX spectrum confirming the presence of Au in $\text{AuNP}@P\text{Ph}_2\text{-PEGPIILP}$ (**5.10**). Scale bars are 25 nm (black) and 5 nm (white).

A65 TGA curve for $\text{NH}_2\text{-PEGPIILP}$ (**6.3**).

A66 SEM images of $\text{NH}_2\text{-PEGPIILP}$ (**6.3**).

A67 XRD spectrum of $\text{RuNP}@P\text{Ph}_2\text{-PEGPIILP}$ (**6.5**).

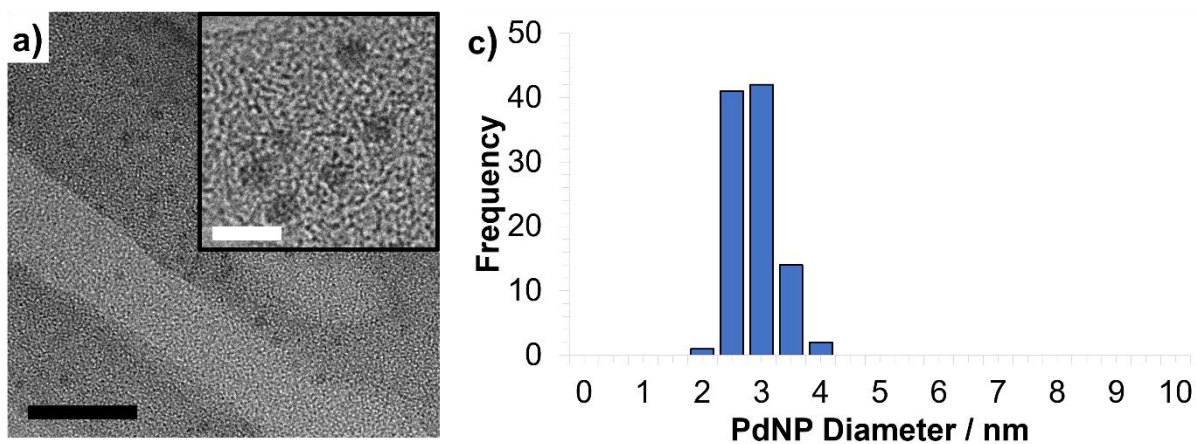
A68 XRD spectrum of $\text{RuNP}@P\text{Ph}_2\text{-PEGPIILP}$ (**6.6**).

A69 XRD spectrum of $\text{RuNP}@P\text{Ph}_2\text{-PEGPIILP}$ (**6.7**).

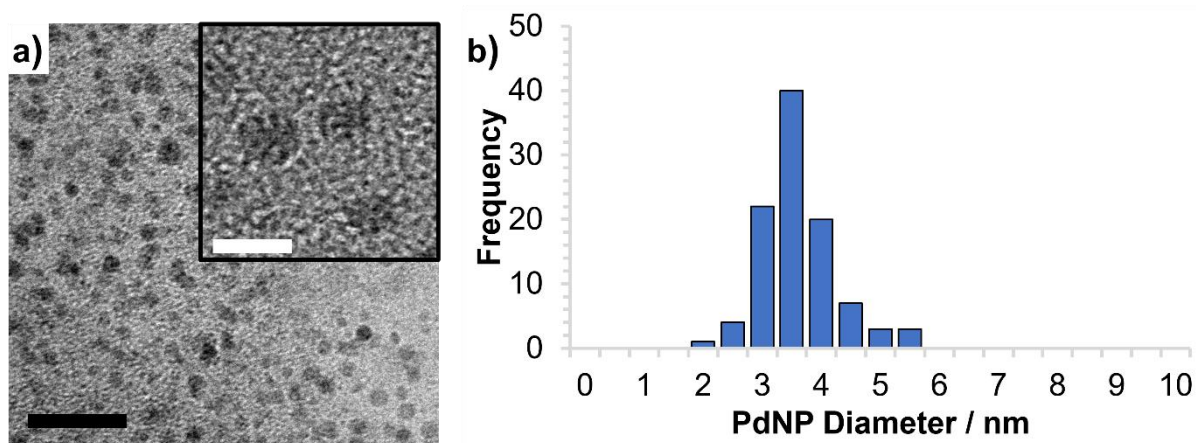
A70 Solid state ^{13}C NMR spectrum of $\text{RuNP}@P\text{Ph}_2\text{-PEGPIILP}$ (**6.7**).

Chapter 2 appendix.

A1 TEM images (a) and the associated particle size distribution (b) of PdNPs generated by the *in situ* reduction of PdCl₄@PPh₂-PIILP (**2.11**) with phenyl boronic acid. Scale bars are 5 nm (white) and 25 nm (black).

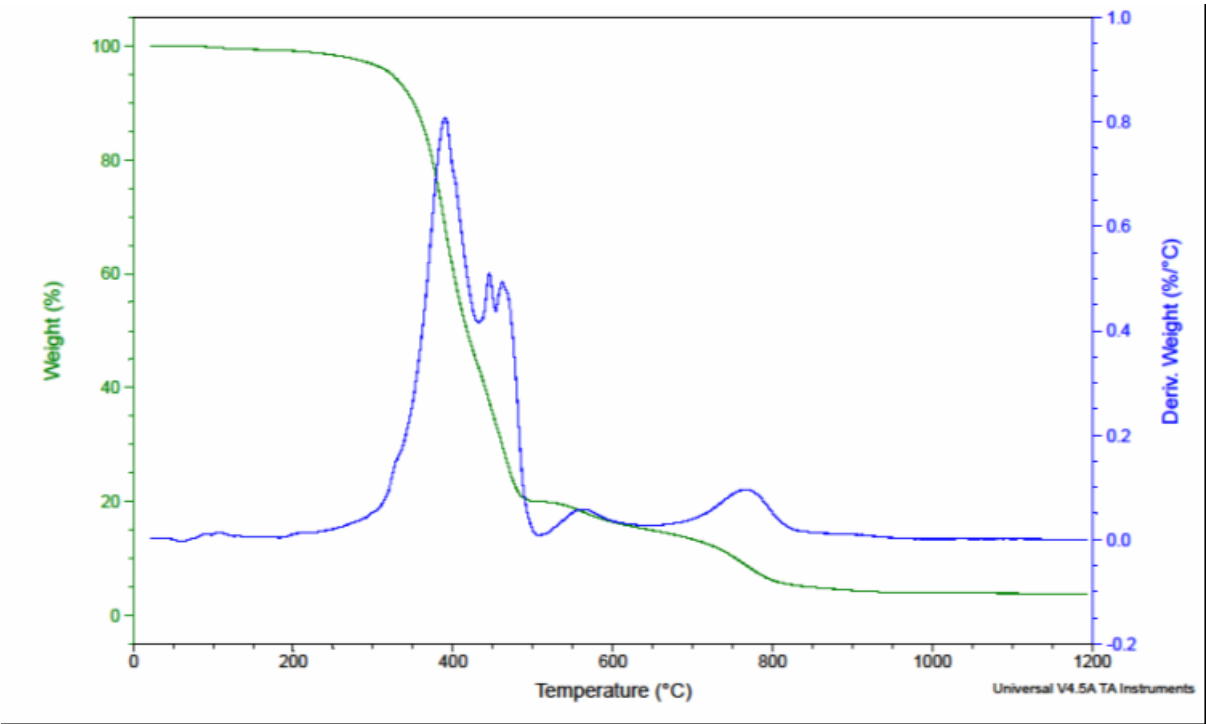


A2 TEM images (a) and the associated particle size distribution (b) of PdNPs generated from *in situ* reduction of PdCl₄@PPh₂-PIILP (**2.12**) with phenyl boronic acid. Scale bars are 5 nm (white) and 25 nm (black).

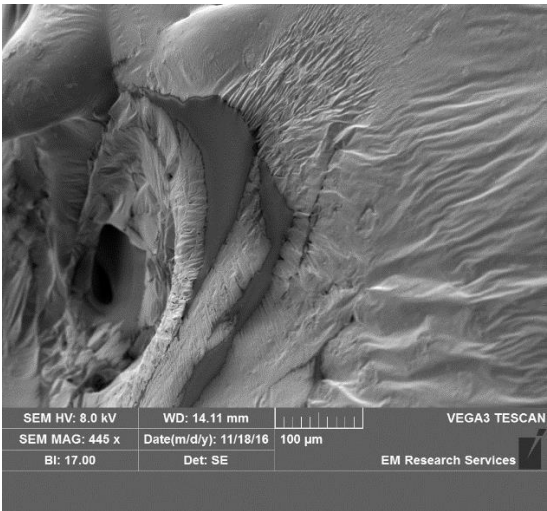
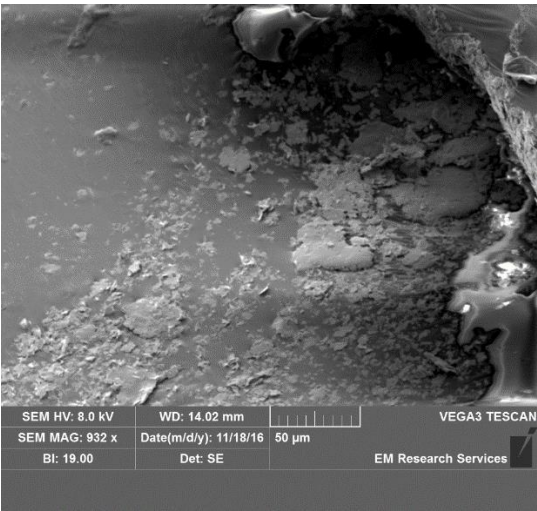


Chapter 3 appendix.

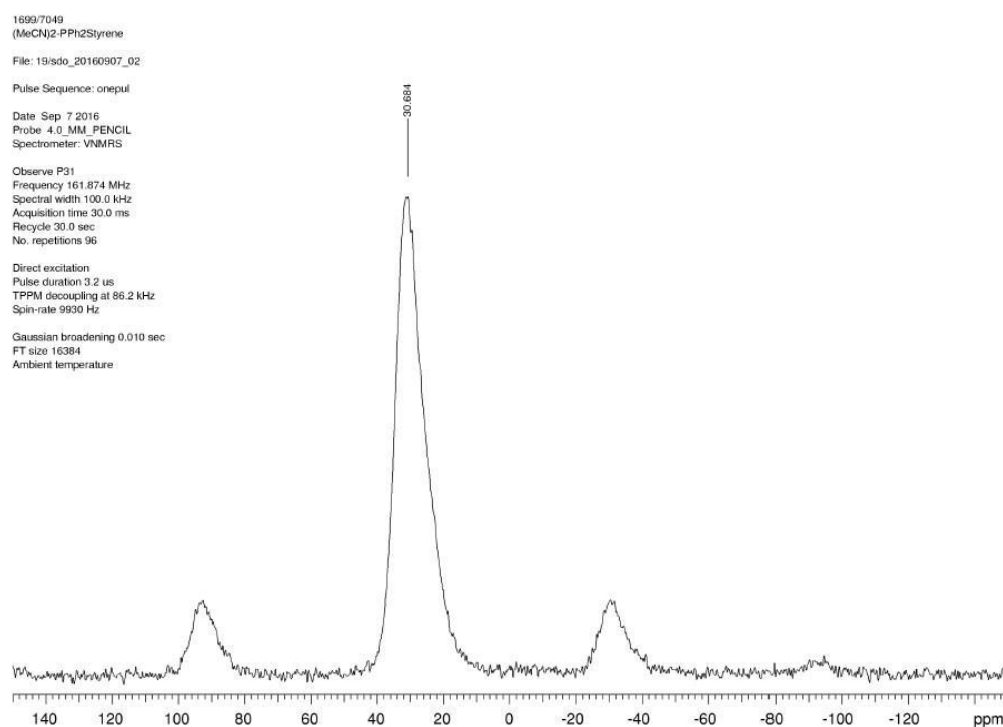
A3 TGA curve for PPh₂PEGstyrene wt% v temperature (green) and (b) derivative wt% v temperature (blue). Heating rate of 10 °C.



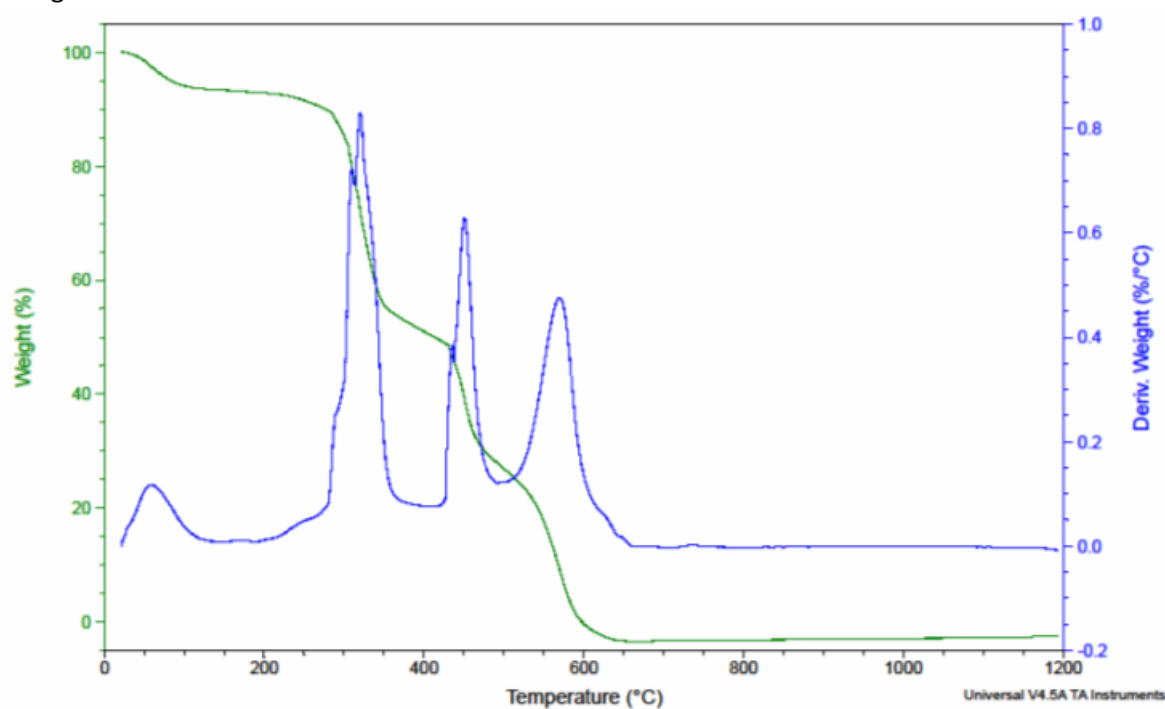
A4 SEM images of PPh₂PEGstyrene.



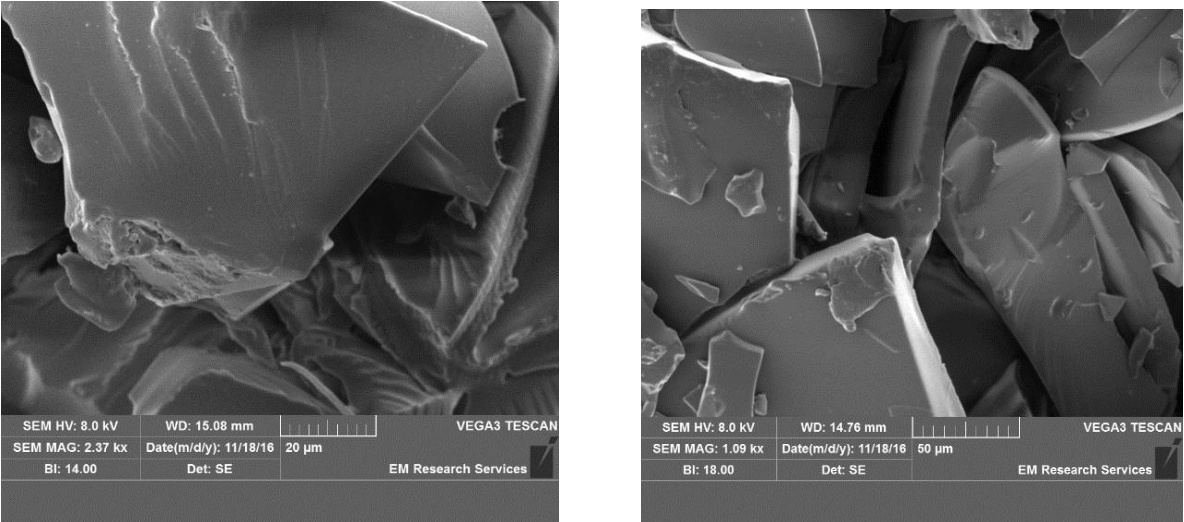
A5 Solid state ^{31}P NMR spectrum of $\text{PPh}_2\text{PEGstyrene}$.



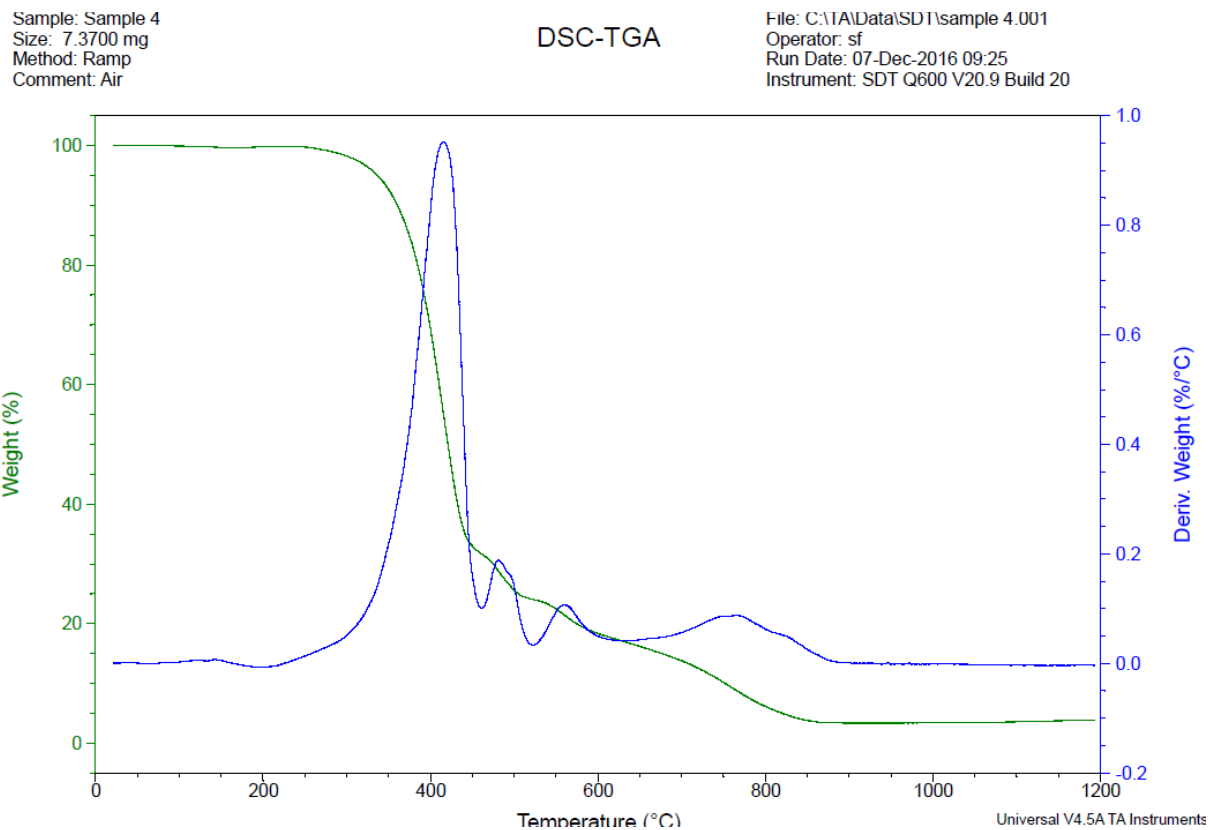
A6 TGA curve for PEGPIILP wt% v temperature (green) and (b) derivative wt% v temperature (blue). Heating rate of 10 $^{\circ}\text{C}$.



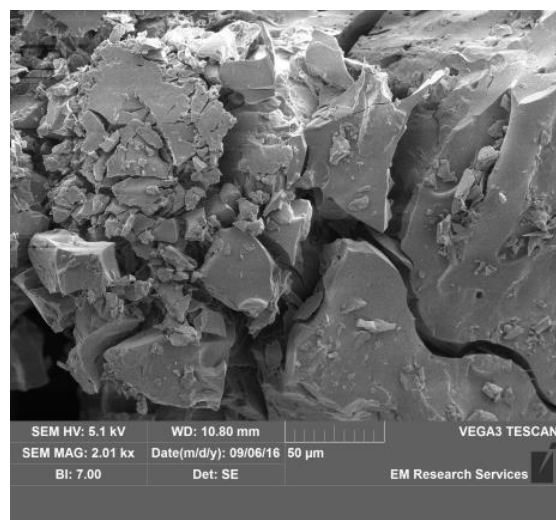
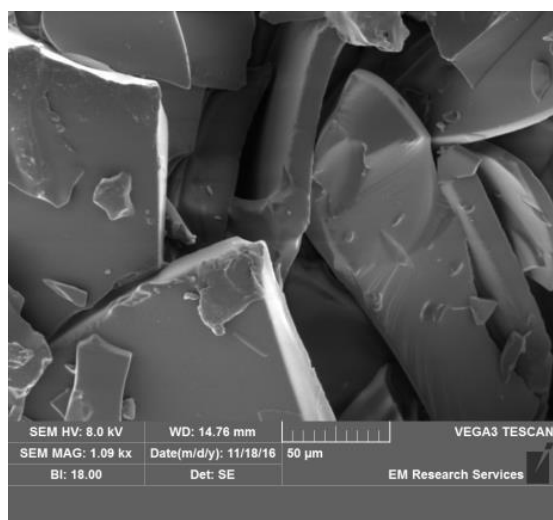
A7 SEM images of PEGPIILP.



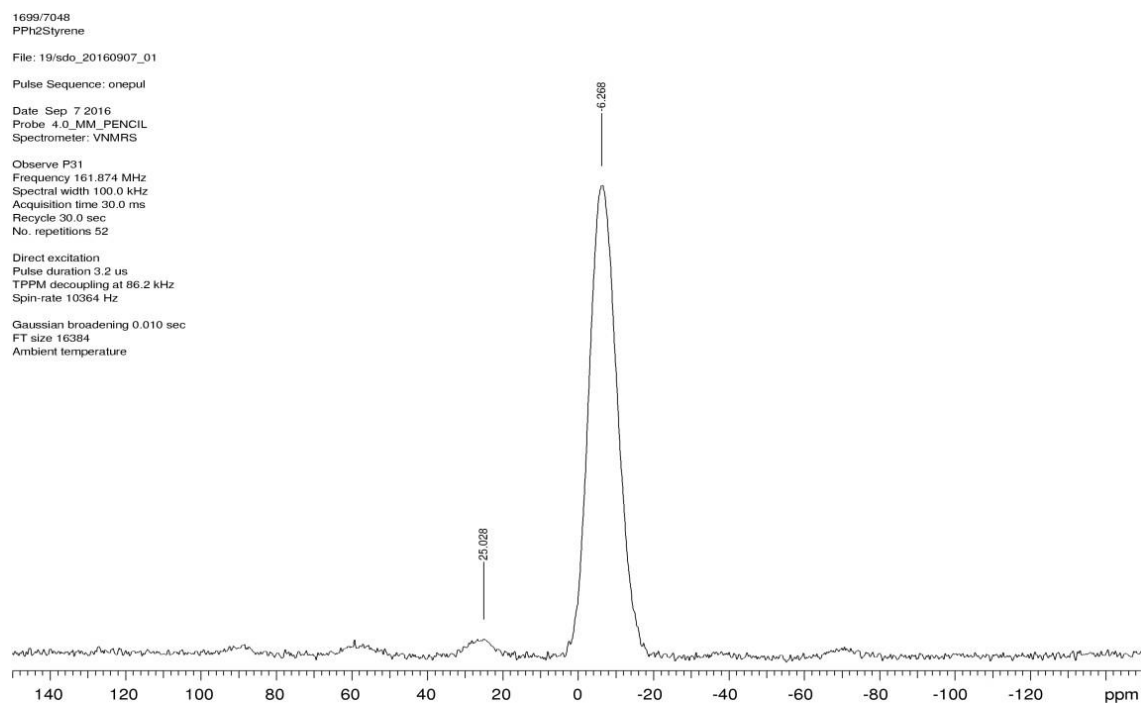
A8 TGA curve for PPh₂styrene wt% v temperature (green) and (b) derivative wt% v temperature (blue). Heating rate of 10 °C.



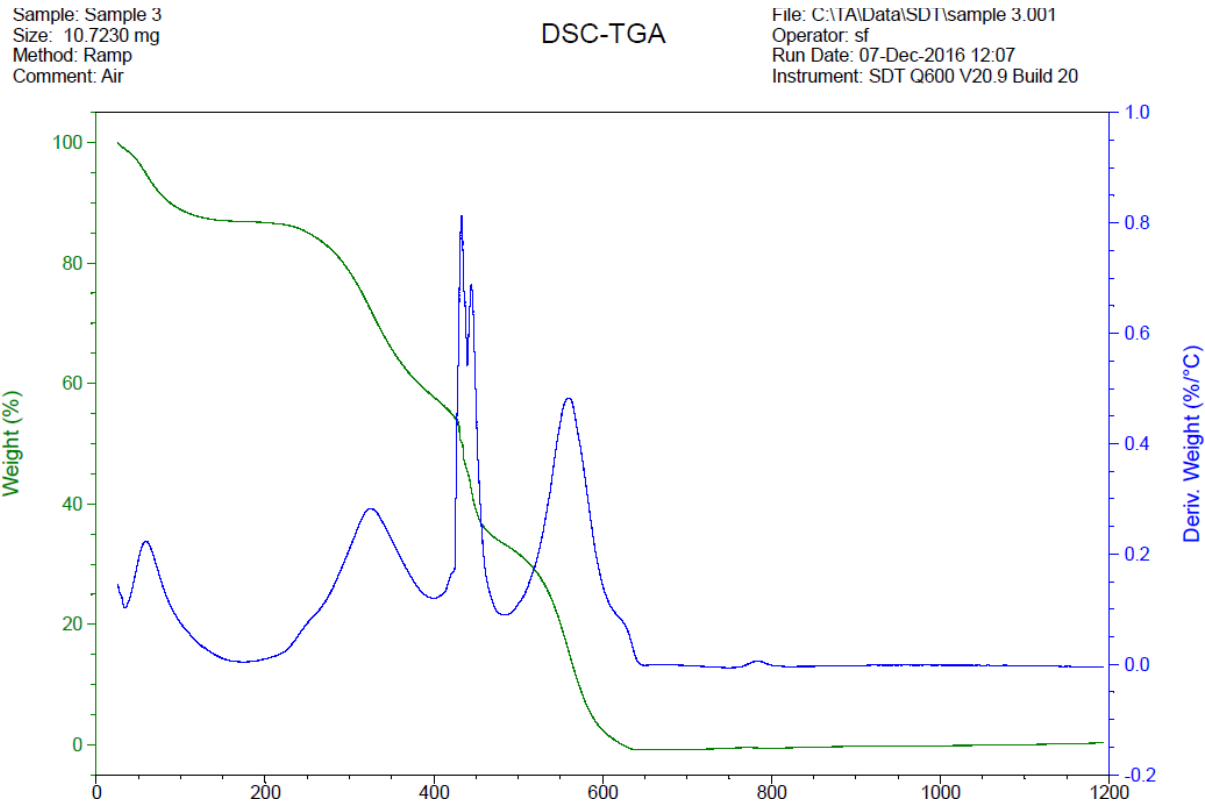
A9 SEM images of PPh₂styrene.



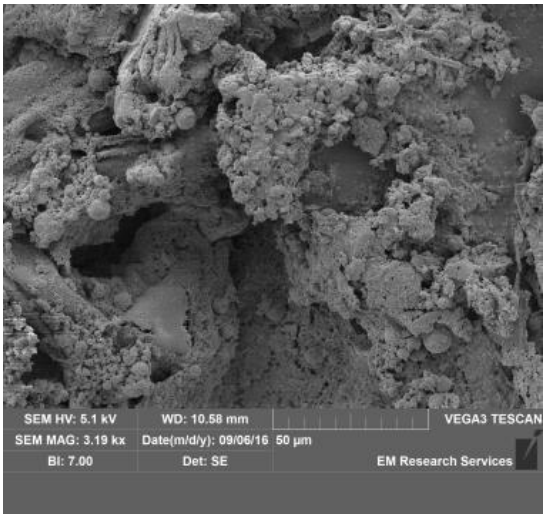
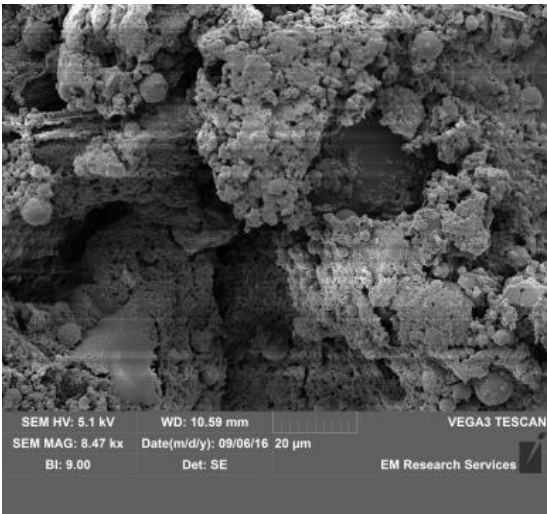
A10 Solid state ³¹P NMR spectrum of PPh₂styrene.



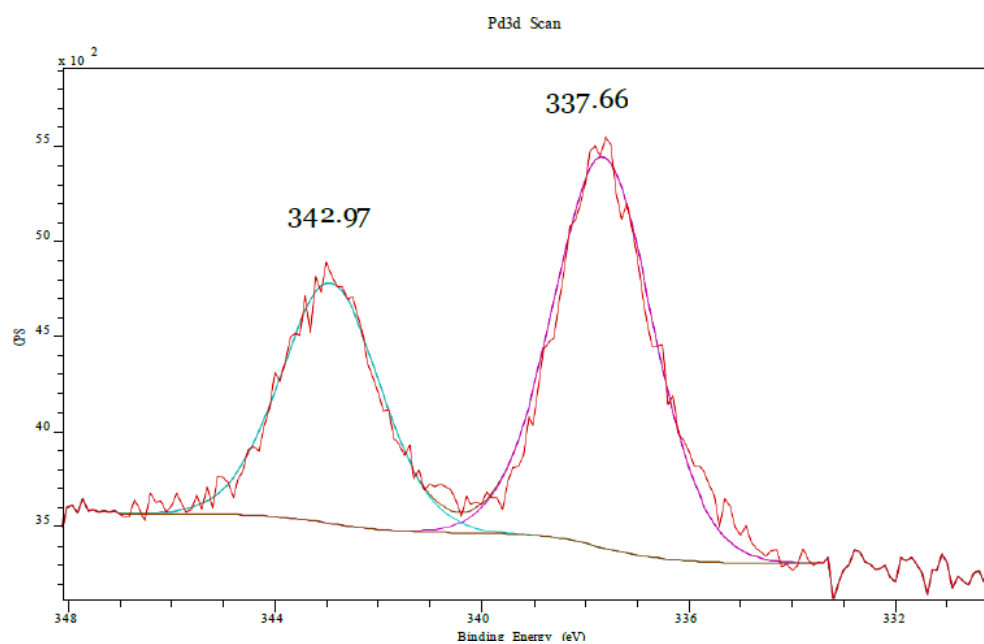
A11 TGA curve for PIILP wt% v temperature (green) and (b) derivative wt% v temperature (blue). Heating rate of 10 °C.



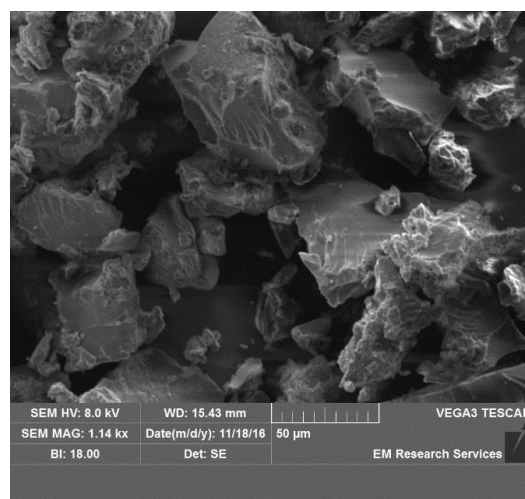
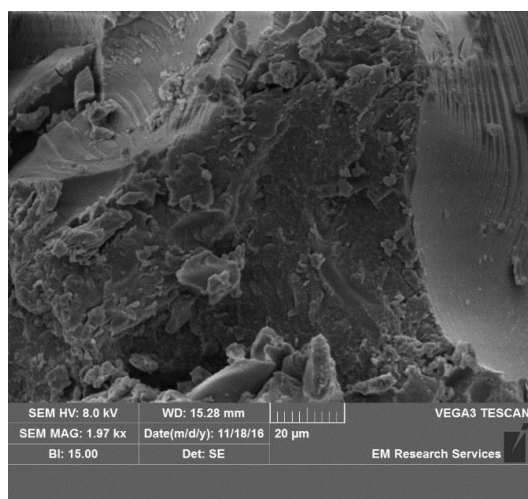
A12 SEM images of PIILP.



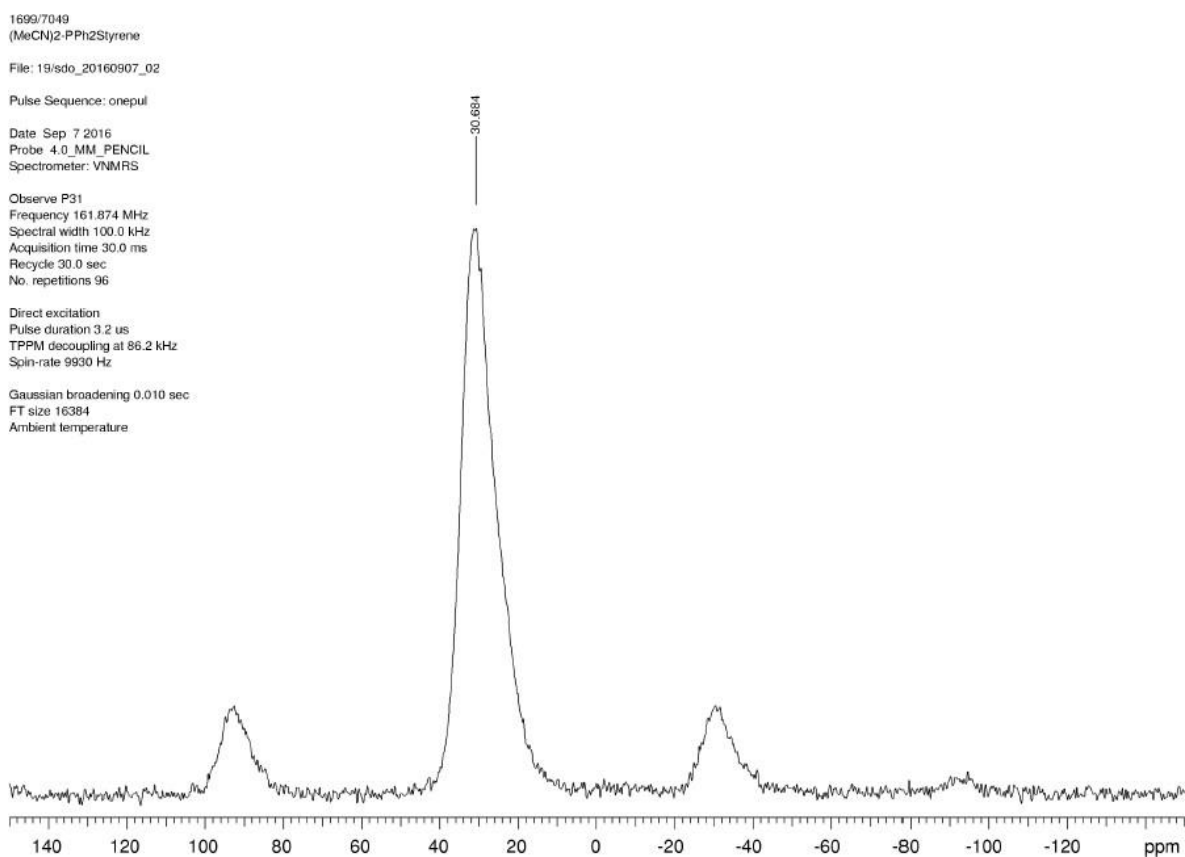
A13 Pd 3d core level XPS spectrum of $[\text{PdCl}_2(\text{MeCN})_2]@\text{PPh}_2\text{PEGstyrene}$ referenced to the hydrocarbon C 1s at 284.8 eV.



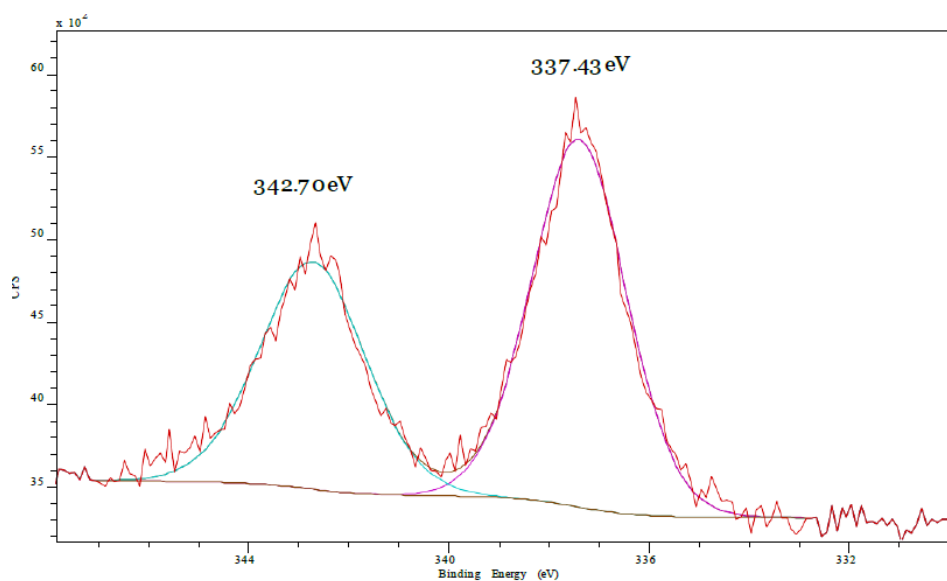
A14 SEM images of $[\text{PdCl}_2(\text{MeCN})_2]@\text{PPh}_2\text{PEGstyrene}$.



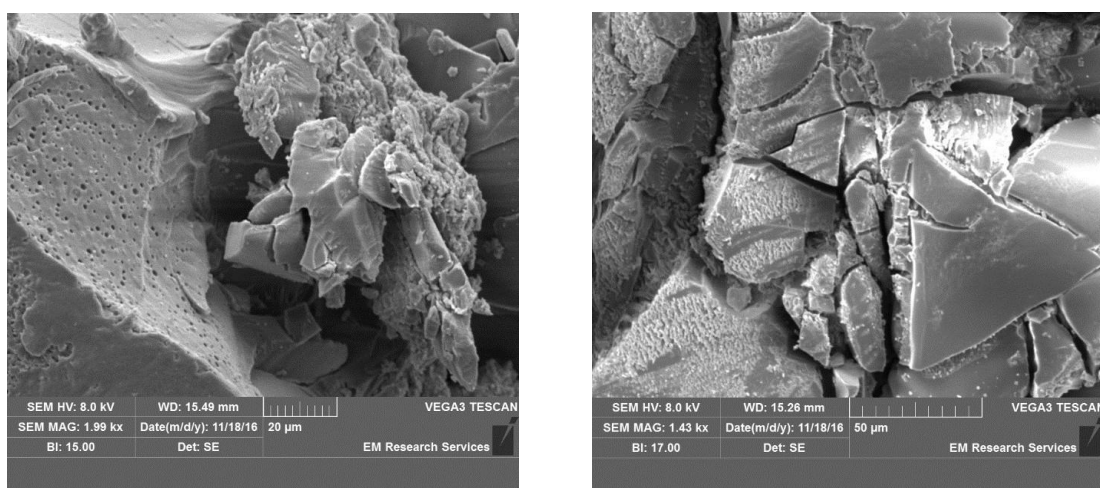
A15 Solid state ^{31}P NMR spectrum of $[\text{PdCl}_2(\text{MeCN})_2]@\text{PPh}_2\text{PEGstyrene}$.



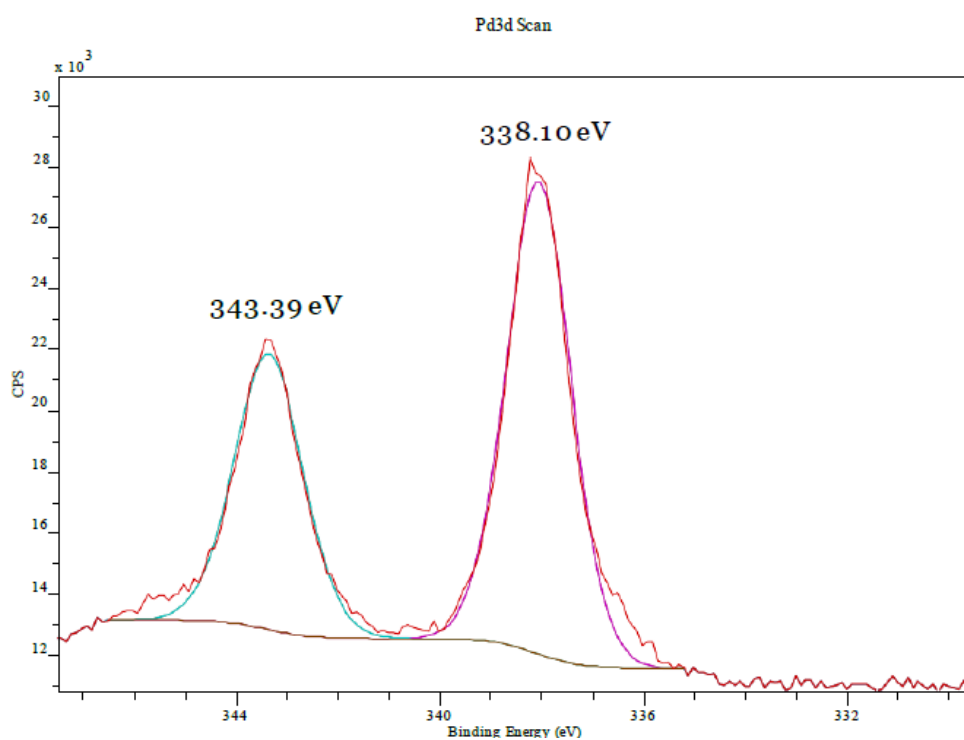
A16 Pd 3d core level XPS spectrum of $[\text{PdCl}_4]@\text{PEGPIILP}$ referenced to the hydrocarbon C 1s at 284.8 eV.



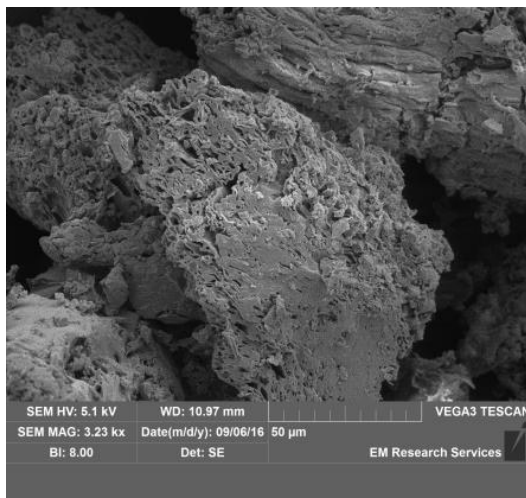
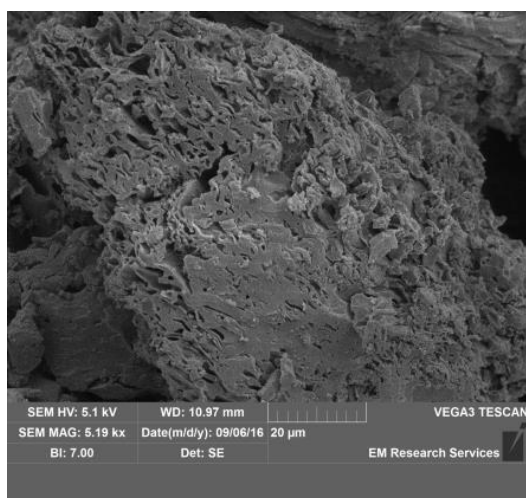
A17 SEM images of $[\text{PdCl}_4]@\text{PEGPIILP}$.



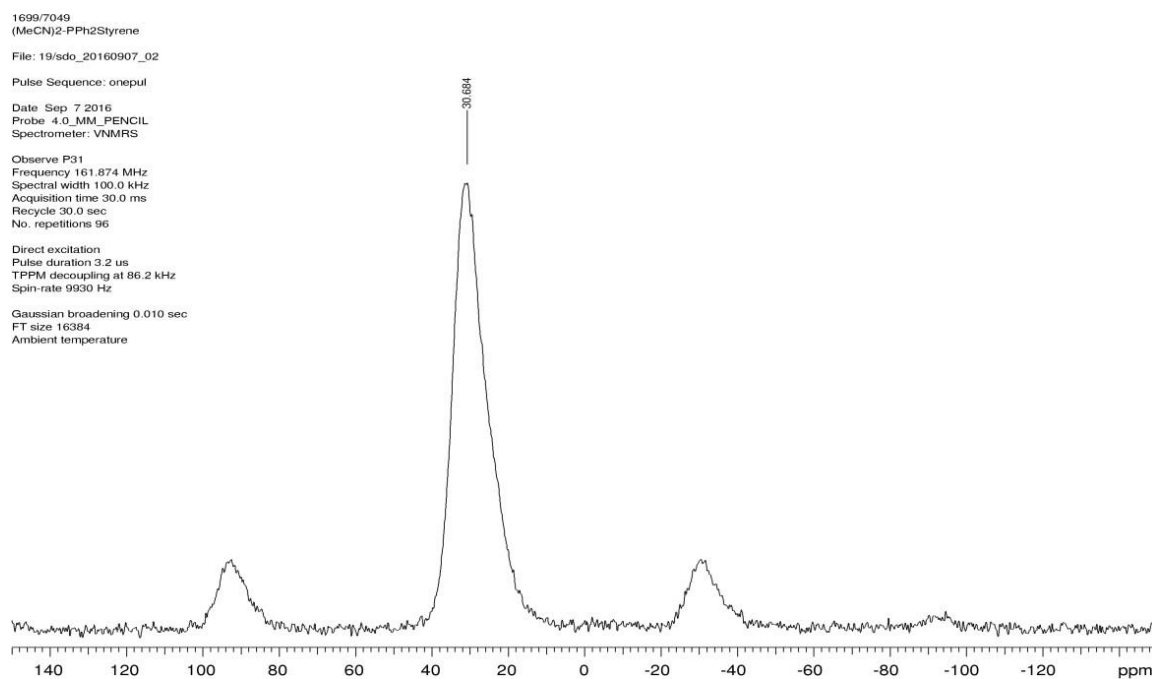
A18 Pd 3d core level XPS spectrum of $[\text{PdCl}_2(\text{MeCN})_2]@\text{PPh}_2\text{styrene}$ referenced to the hydrocarbon C 1s at 284.8 eV.



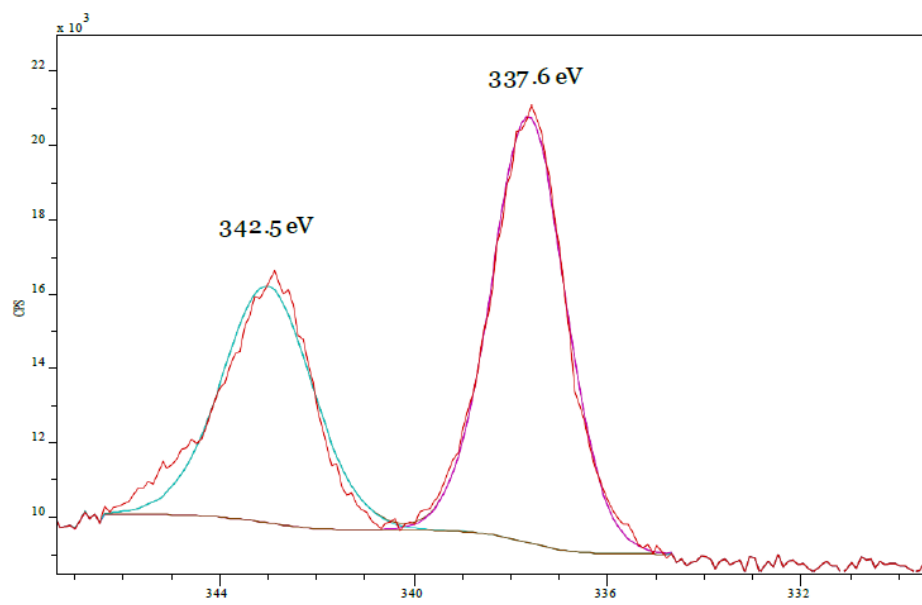
A19 SEM images of $[\text{PdCl}_2(\text{MeCN})_2]@ \text{PPh}_2\text{styrene}$.



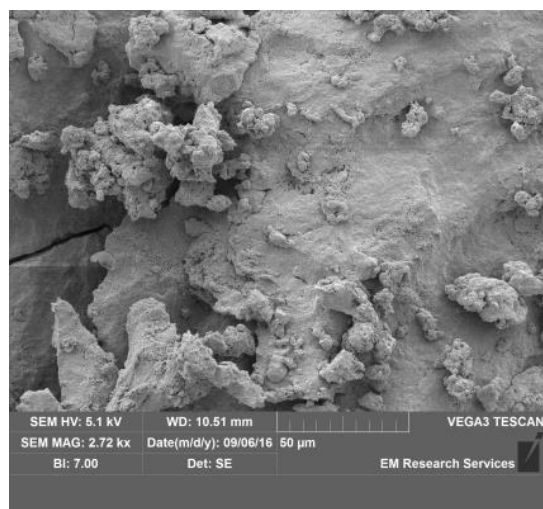
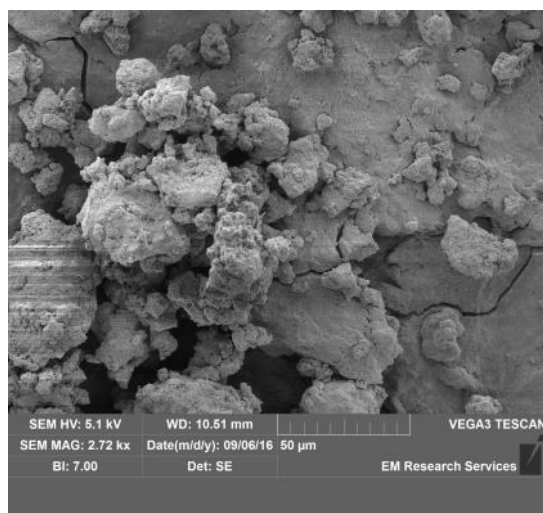
A20 Solid state ^{31}P NMR spectrum of $[\text{PdCl}_2(\text{MeCN})_2]@ \text{PPh}_2\text{styrene}$.



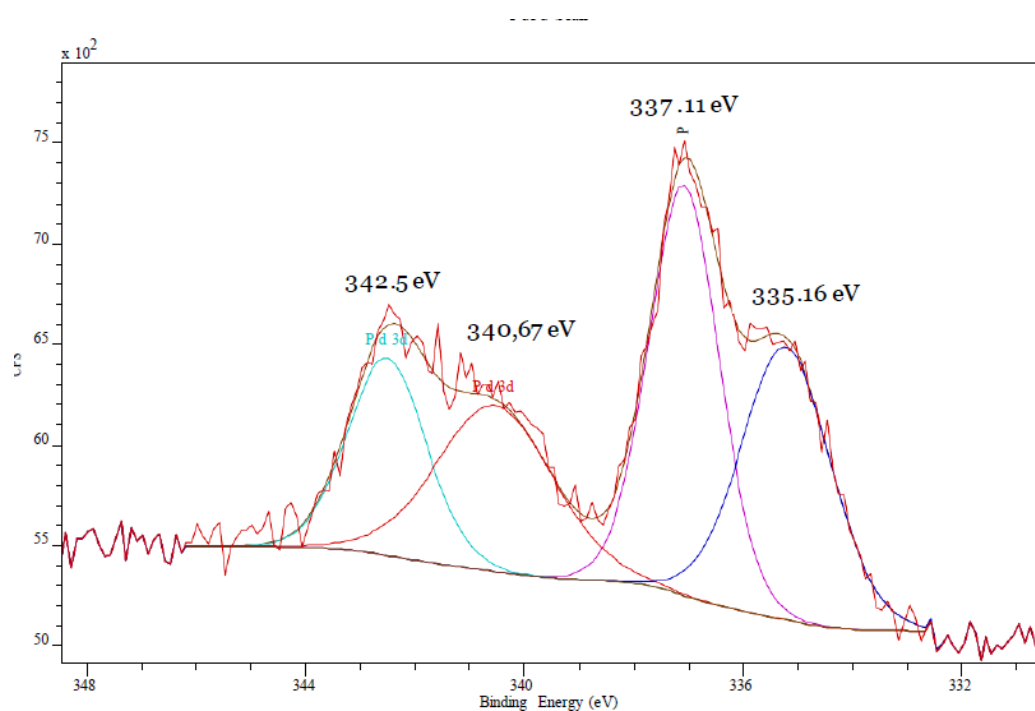
A21 Pd 3d core level XPS spectrum of [PdCl₄]@PIILP referenced to the hydrocarbon C 1s at 284.8 eV.



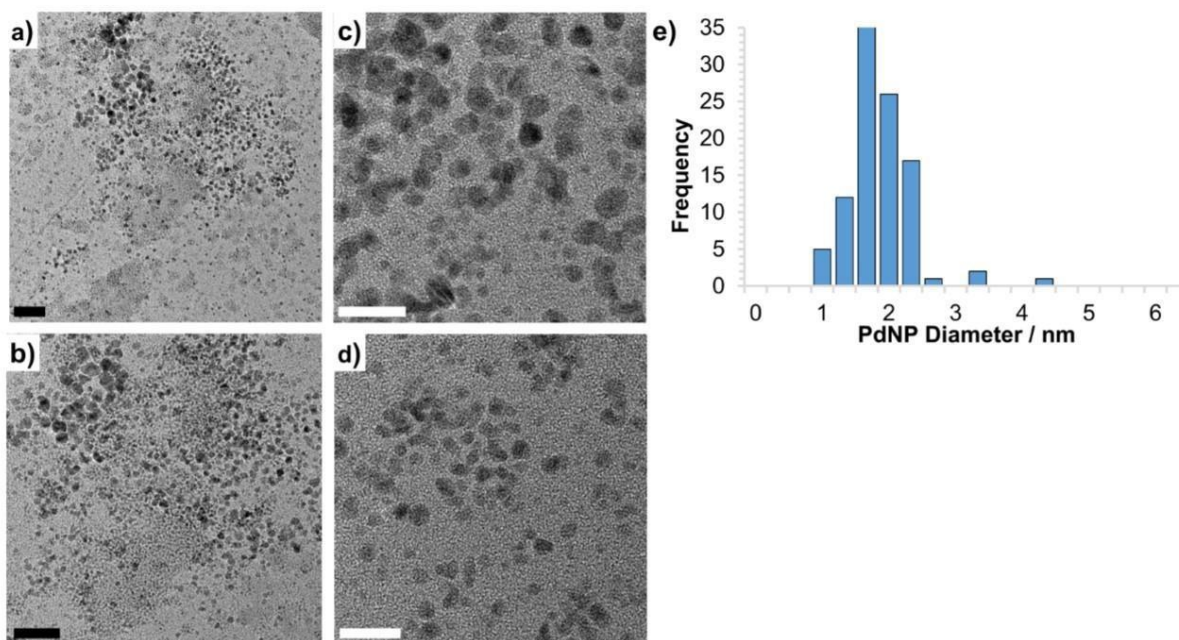
A22 SEM images of [PdCl₄]@PIILP.



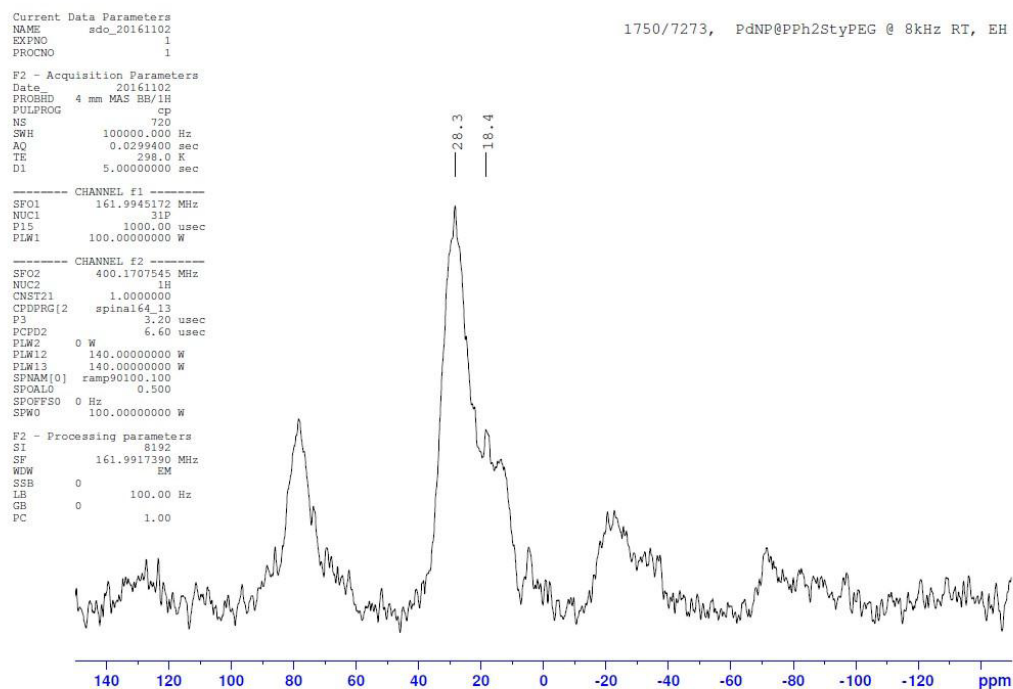
A23 Pd 3d core level XPS spectrum of PdNP@PPh₂PEGstyrene (**2.15**) referenced to the hydrocarbon C 1s at 284.8 eV.



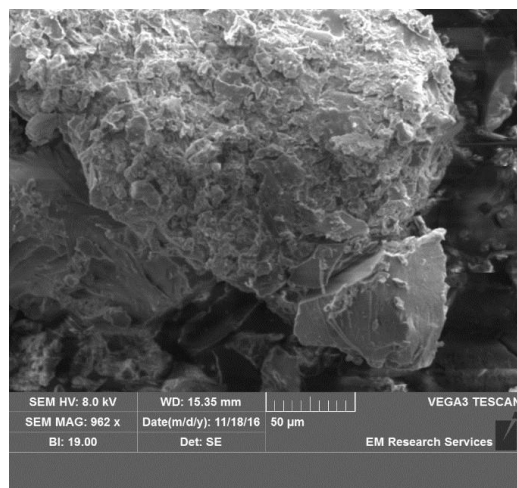
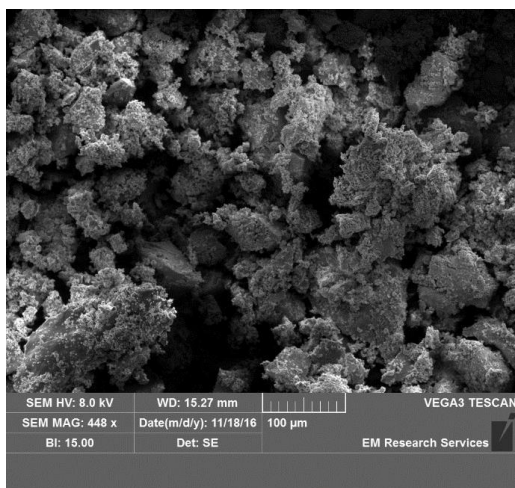
A24 TEM micrographs (a-d) and associated particle size distribution (e) of PdNP@PPh₂PEGstyrene (**2.15**). Scale bars are 25 nm (black) and 5 nm (white).



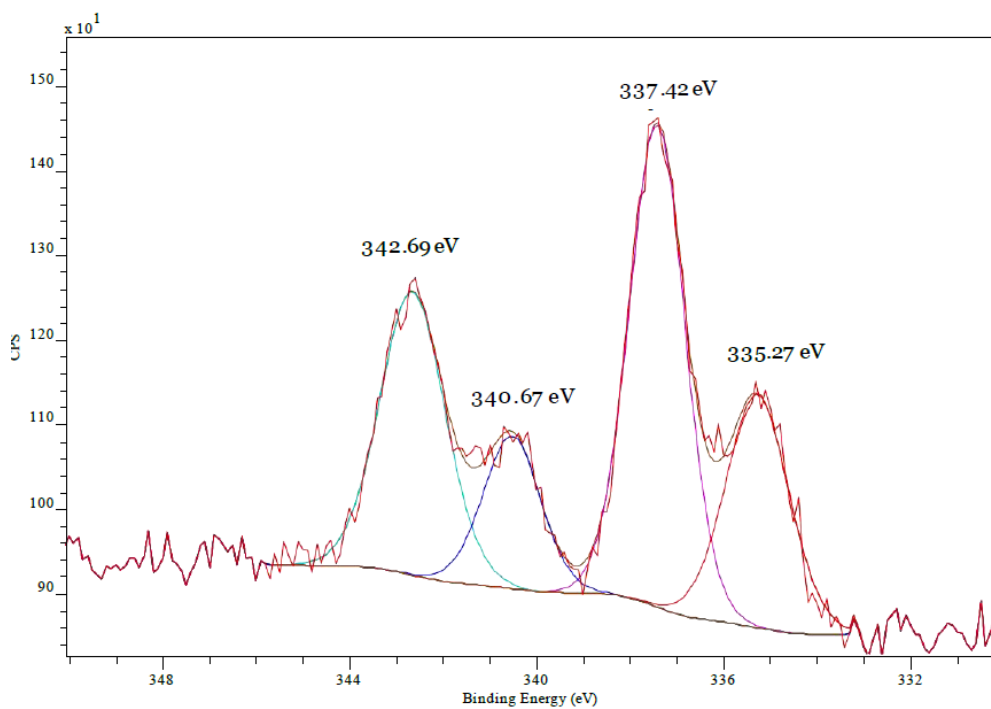
A25 Solid state ^{31}P NMR spectrum of $[\text{PdNP}]\text{@PPh}_2\text{PEGStyrene}$ (**2.15**).



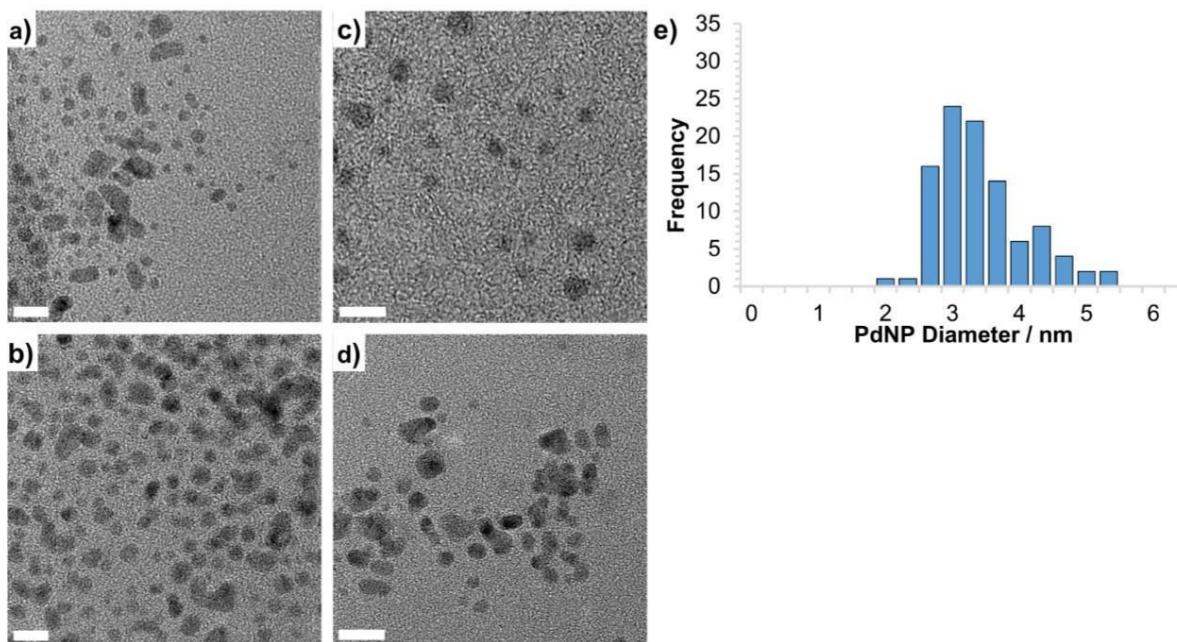
A26 SEM images of $[\text{PdNP}]\text{@PPh}_2\text{PEGStyrene}$ (**2.15**).



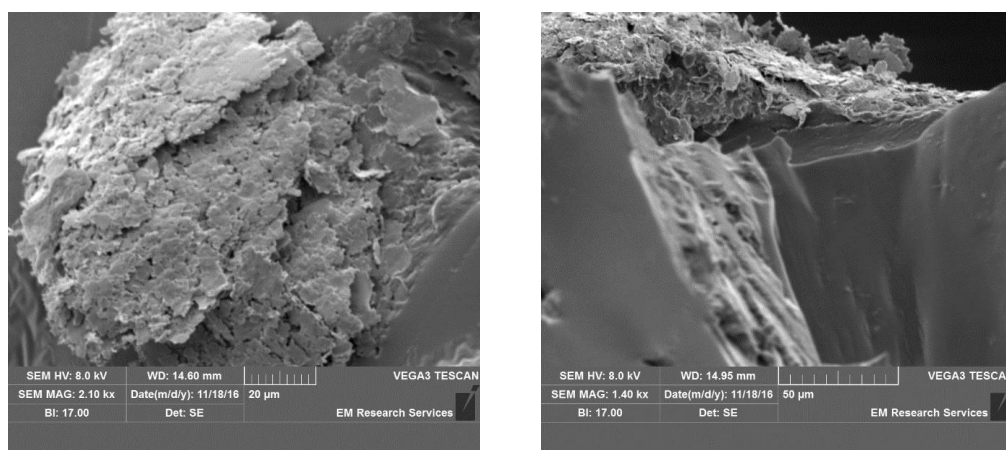
A27 Pd 3d core level XPS spectrum of PdNP@PEGPIILP (**2.16**) referenced to the hydrocarbon C 1s at 284.8 eV.



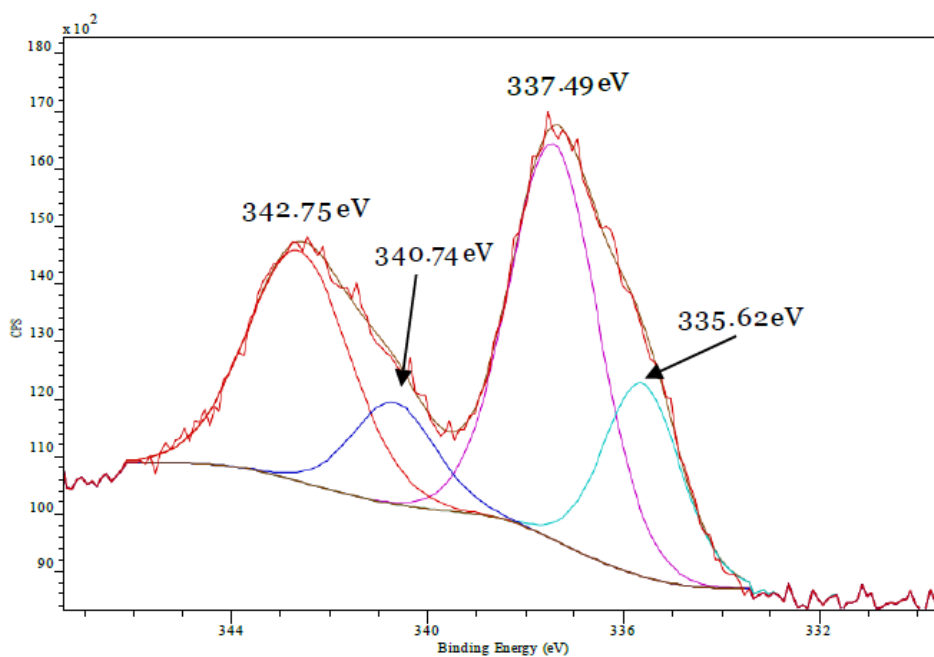
A28 TEM micrographs (a-d) and the associated particle size distribution (e) of PdNP@PEGPIILP (**2.16**). Scale bars are 25 nm (black) and 5 nm (white).



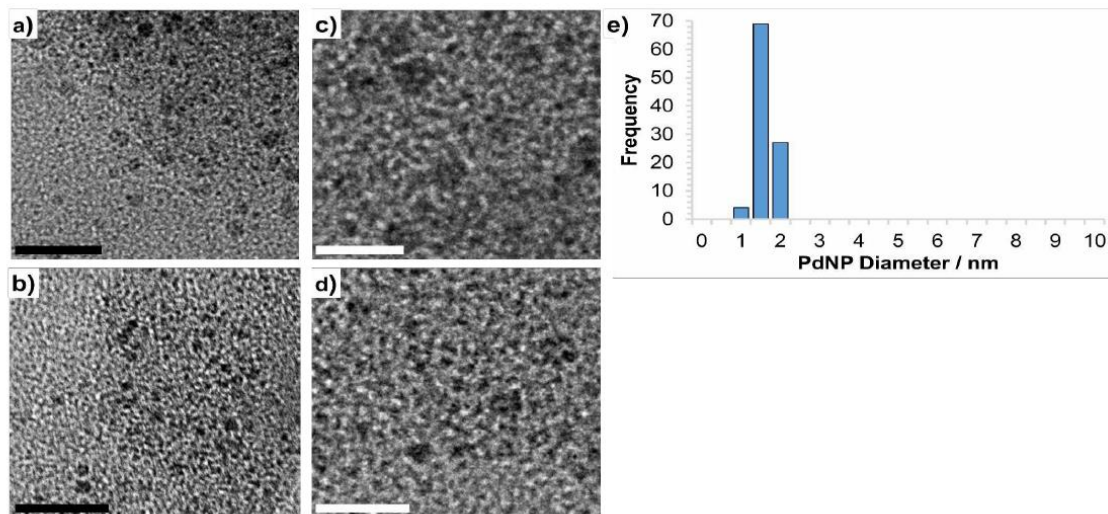
A29 SEM images of PdNP@PEGPIILP (**2.16**).



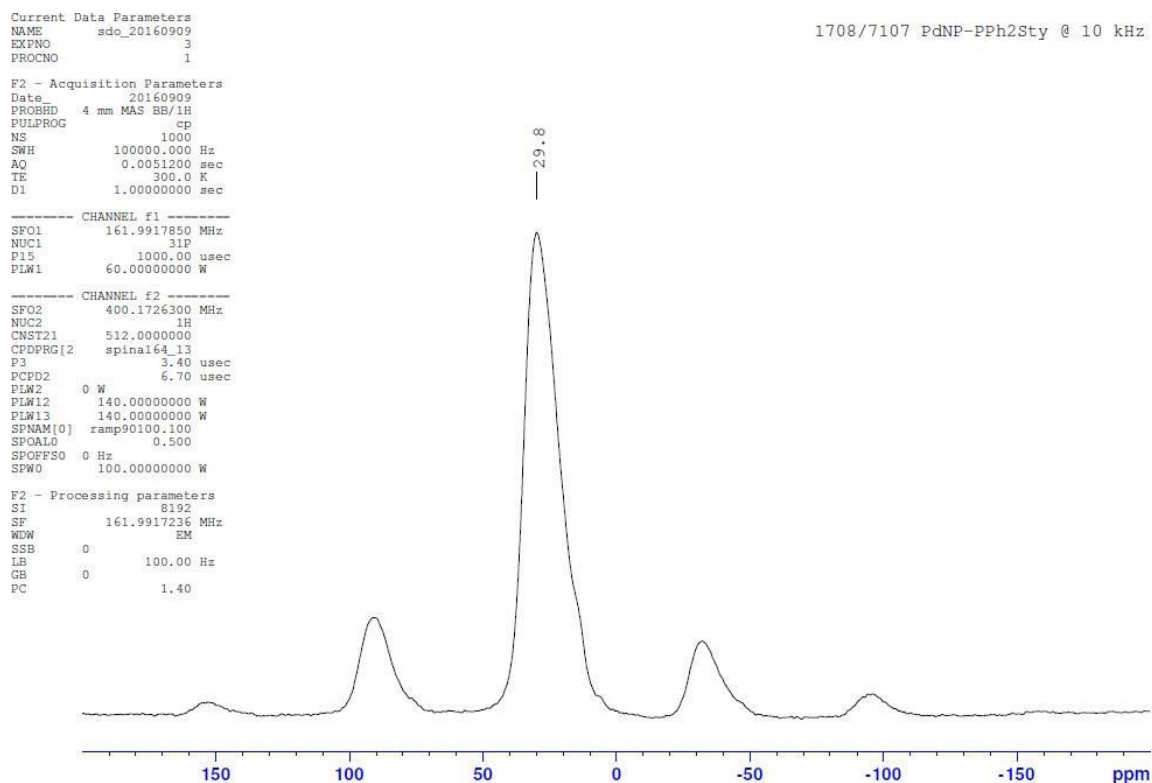
A30 Pd 3d core level XPS spectrum of PdNP@PPh₂styrene (**2.17**) referenced to the hydrocarbon C 1s at 284.8 eV.



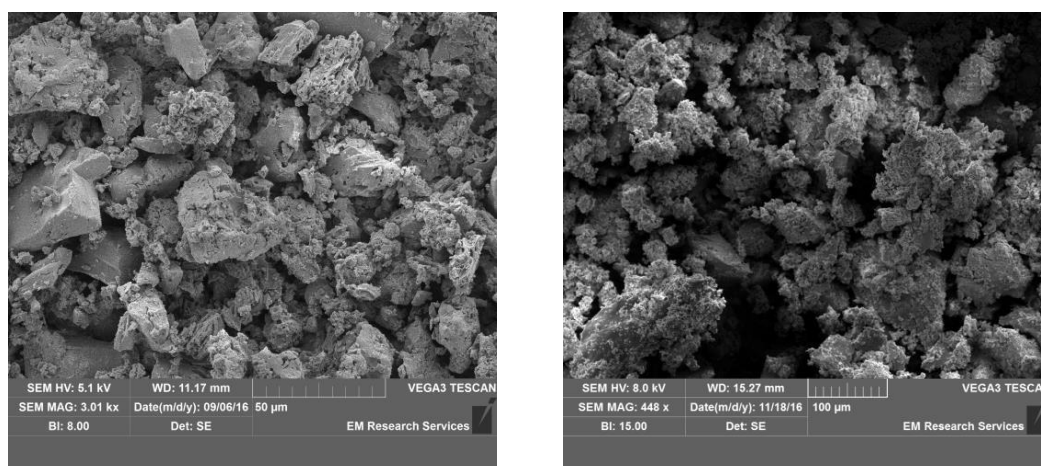
A31 TEM micrographs (a-d) and the associated particle size distribution (e) of PdNP@PPh₂styrene (**2.17**). Scale bars are 25 nm (black) and 5 nm (white).



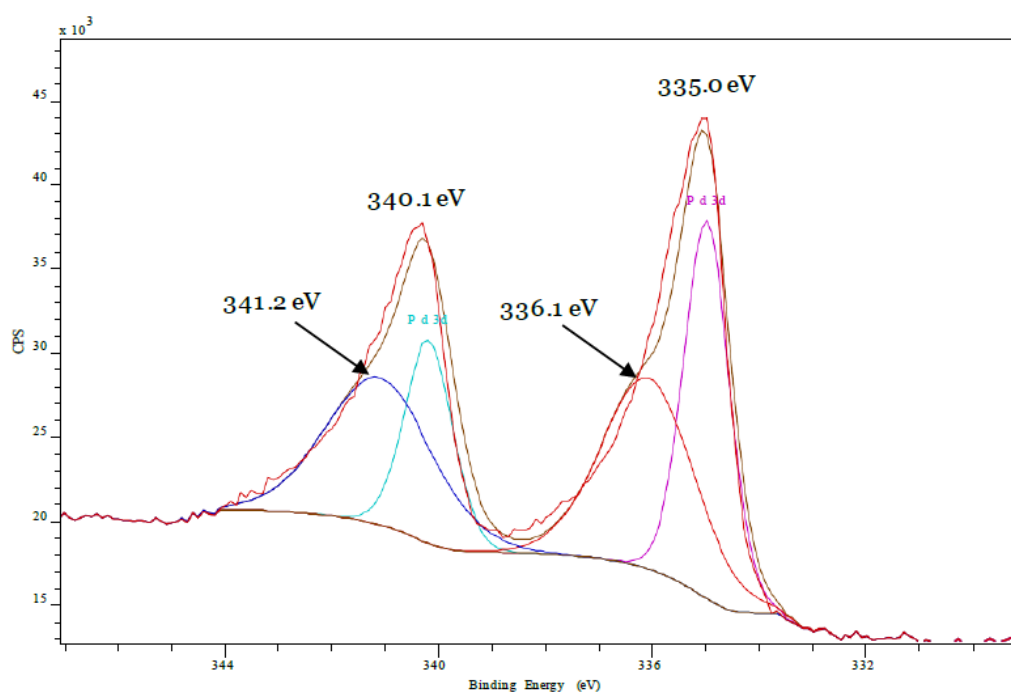
A32 Solid state ³¹P NMR spectrum of [PdNP]@PPh₂styrene (**2.17**).



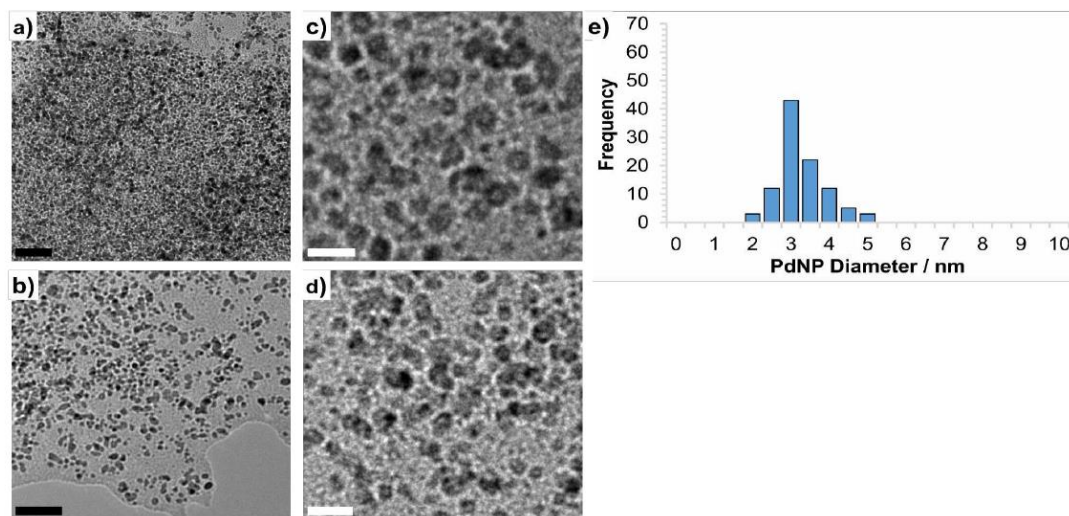
A33 SEM images of PdNP@PPh₂styrene (**2.17**).



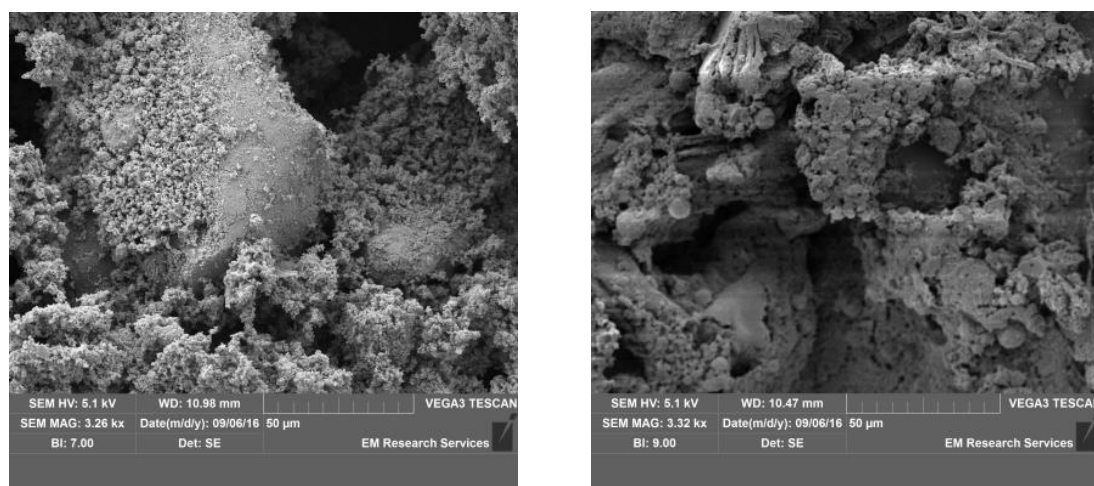
A34 Pd 3d core level XPS spectrum of PdNP@PIILP (**2.18**) referenced to the hydrocarbon C 1s at 284.8 eV.



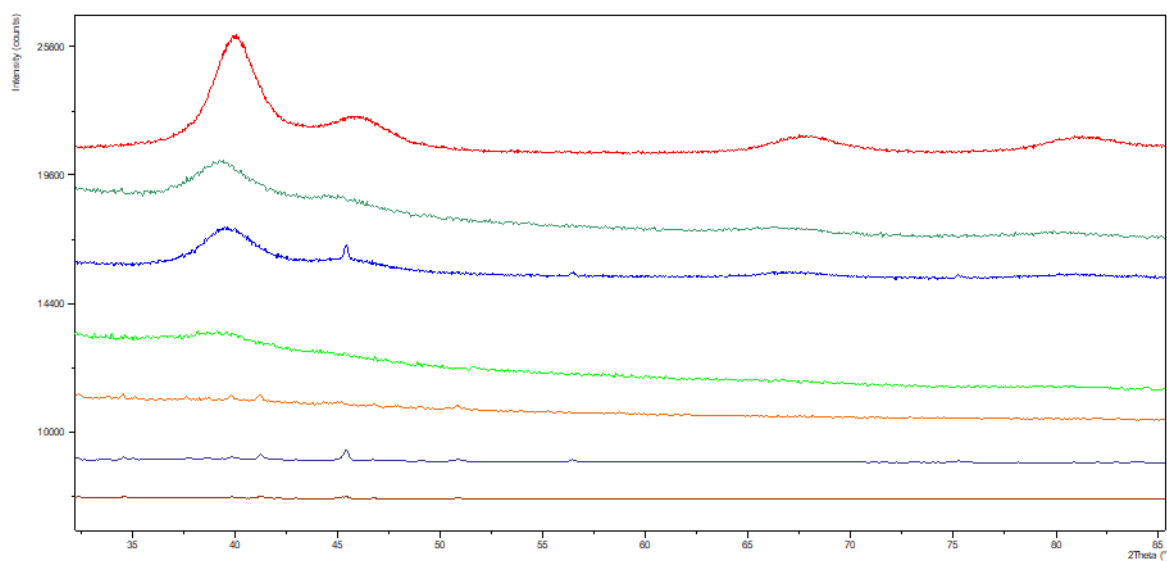
A35 TEM micrographs (a-d) and the associated particle size distribution (e) of PdNP@PIILP (**2.18**). Scale bars are 25 nm (black) and 5 nm (white).



A36 SEM images of PdNP@PIILP (**2.18**).

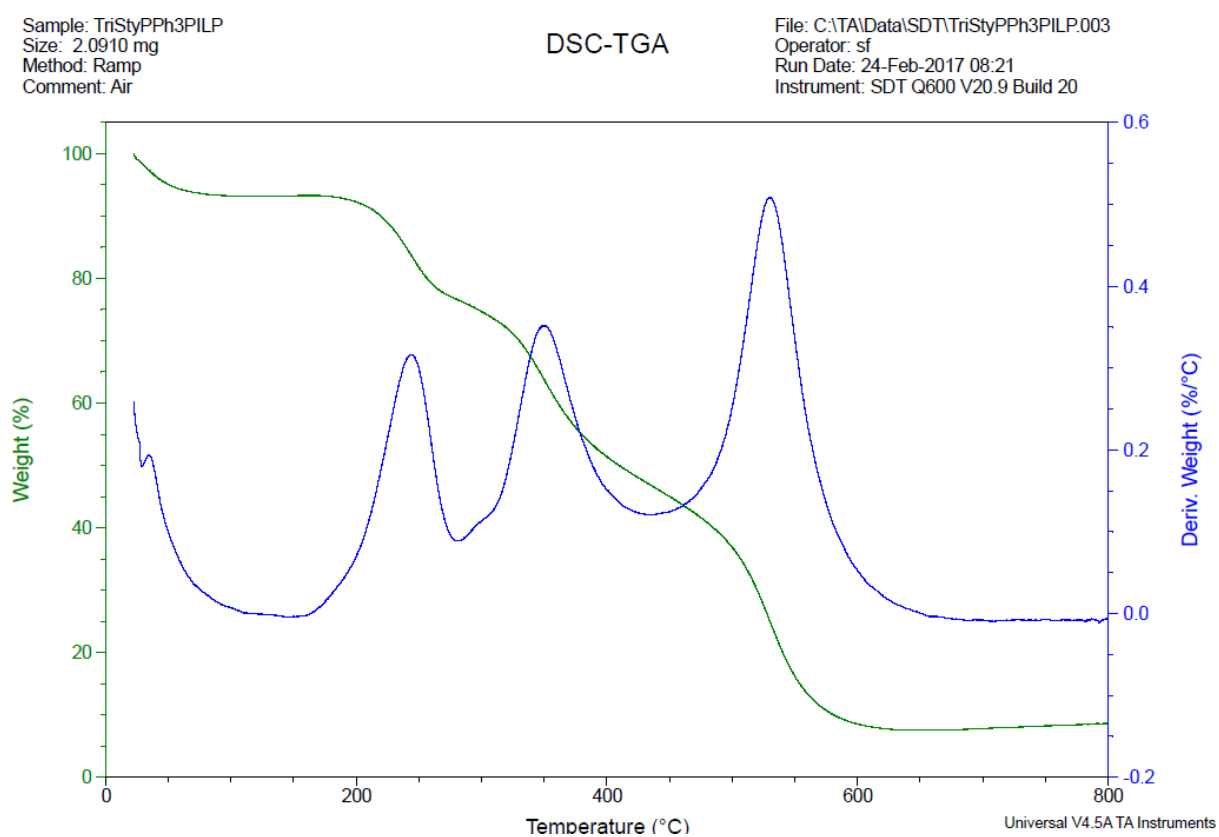


A37 XRD spectra of **2.13** - **2.18**. (Top to bottom: **2.18**, **4.6**, **2.16**, **2.13**, **2.17**, **2.14**, **2.15**).

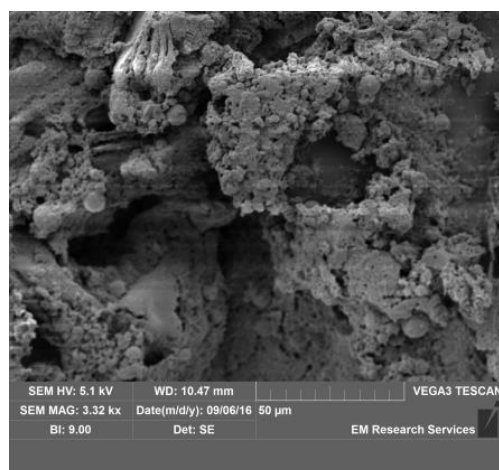
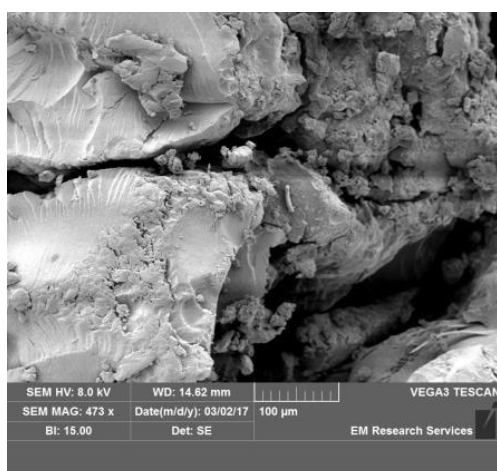


Chapter 4 appendix.

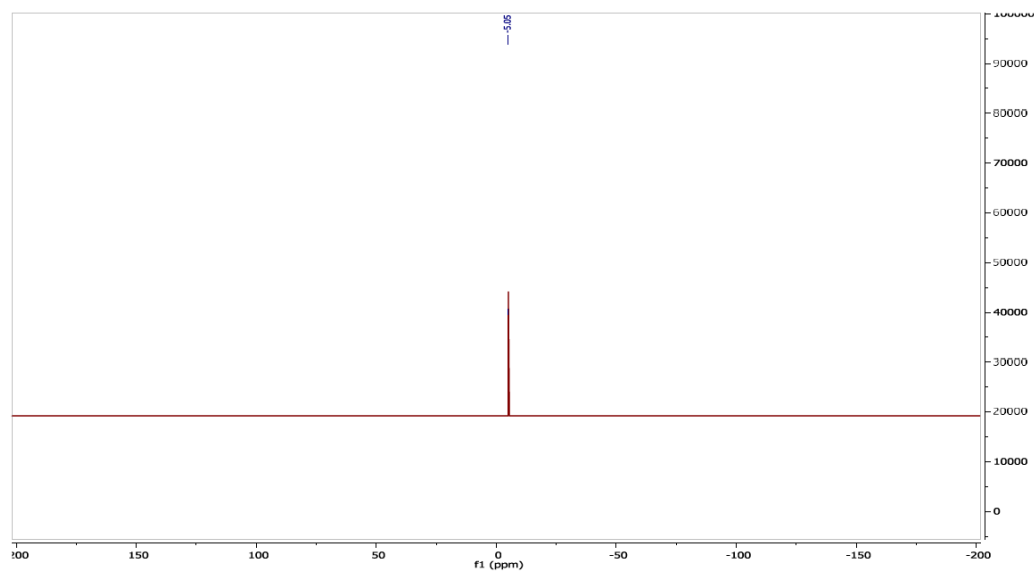
A38 TGA curve for P(Sty)₃-PIILP (**4.2**).



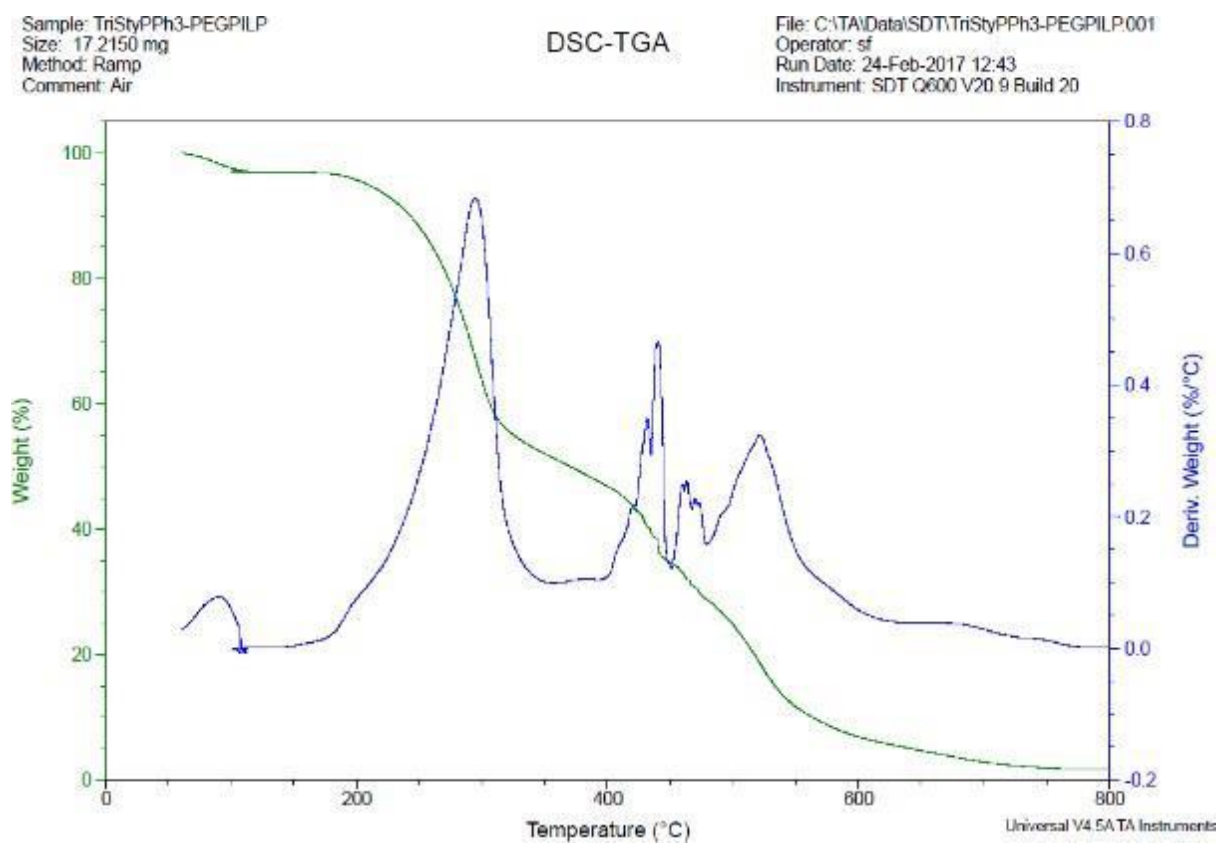
A39 SEM images of P(Sty)₃-PIILP (**4.2**).



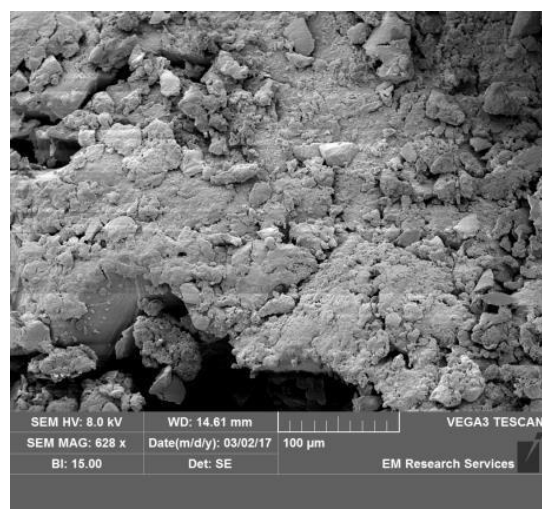
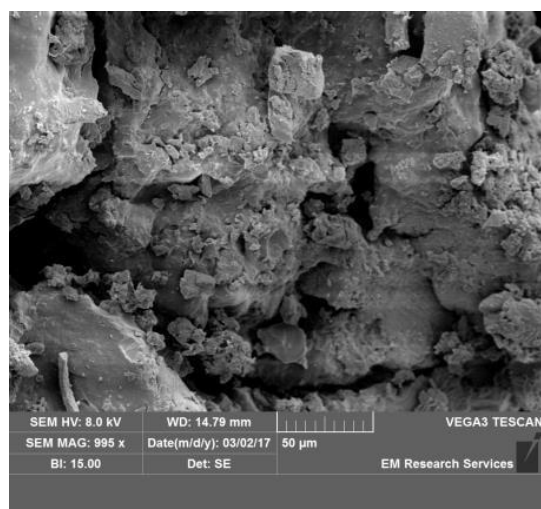
A40 Solution state ³¹P NMR spectrum of P(Sty)₃-PIILP (**4.2**).



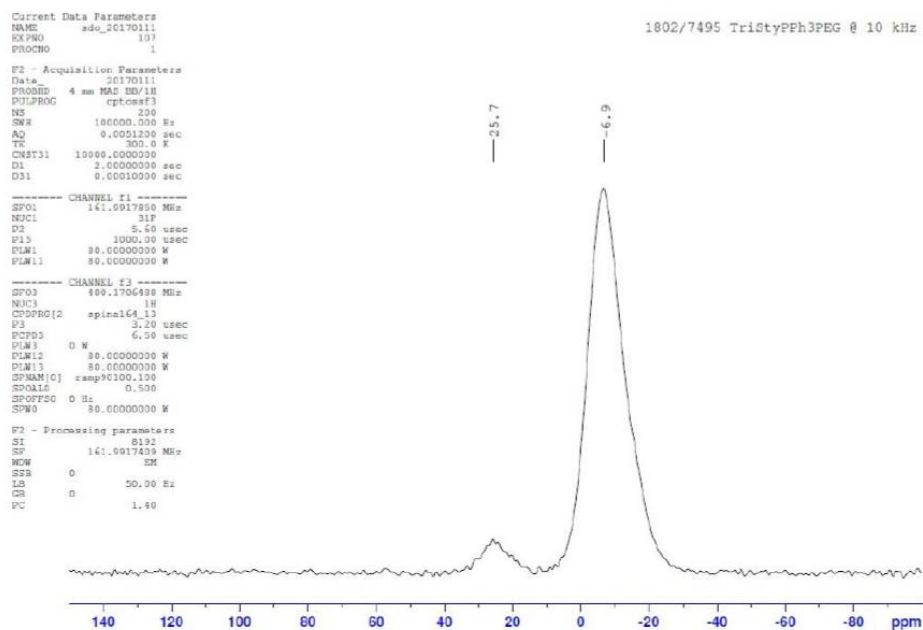
A41 TGA curve for P(Sty)₃-PEGPIILP (4.3).



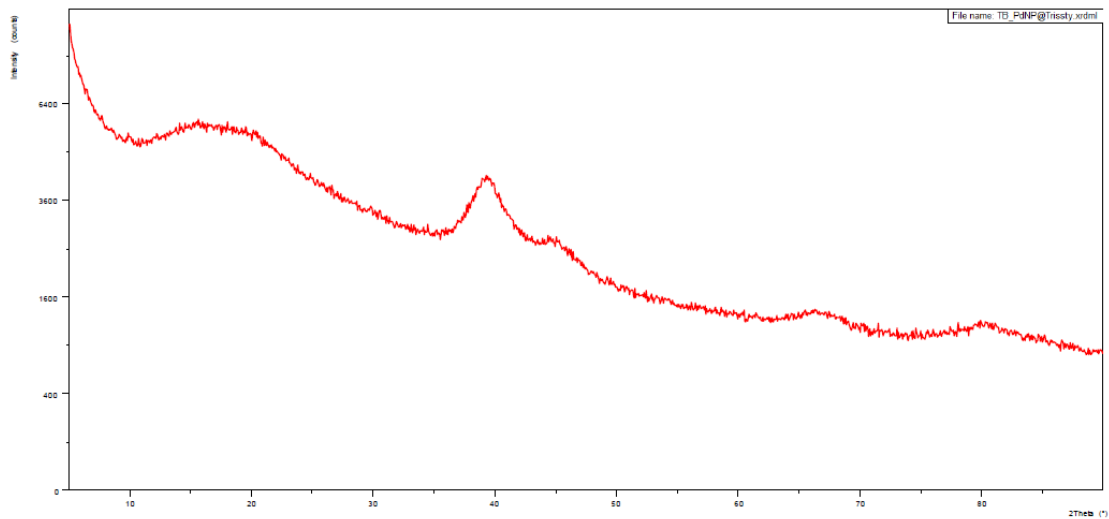
A42 SEM images of P(Sty)₃-PEGPIILP (4.3).



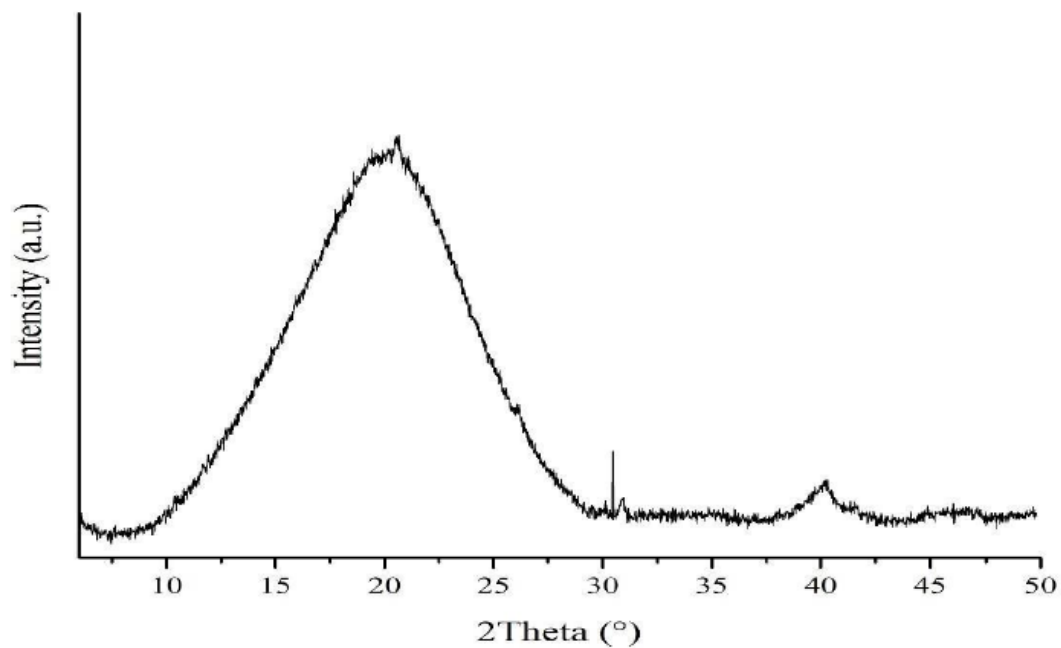
A43 Solid state ³¹P NMR spectrum of P(Sty)₃-PEGPIILP (4.3).



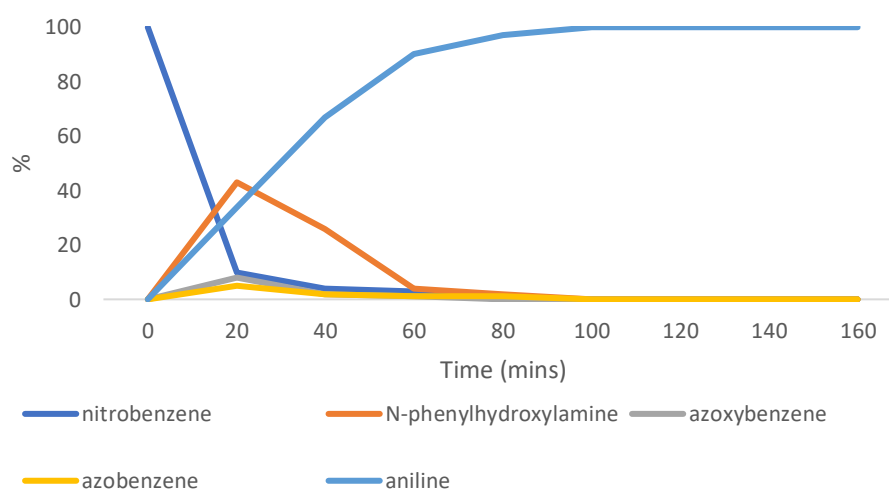
A44 XRD spectrum for PdNP@P(Sty)₃-PIILP (4.6).

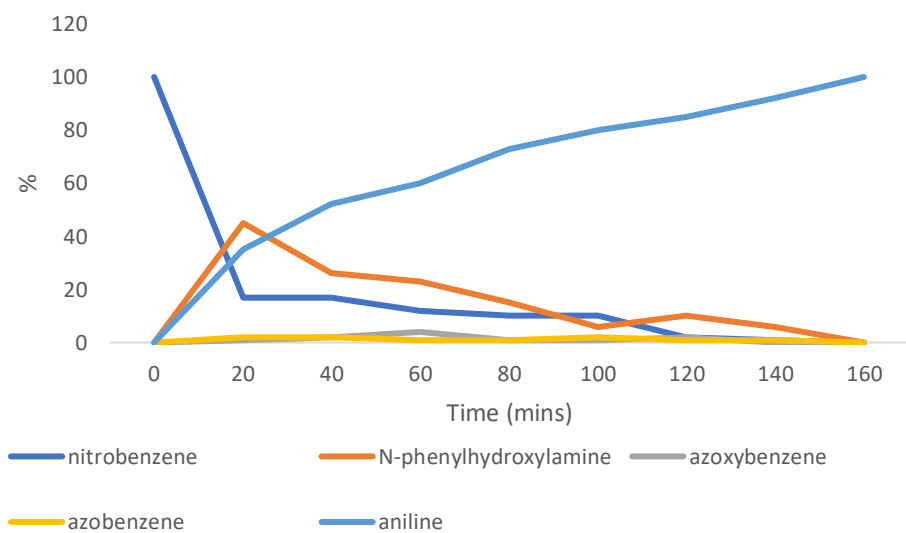
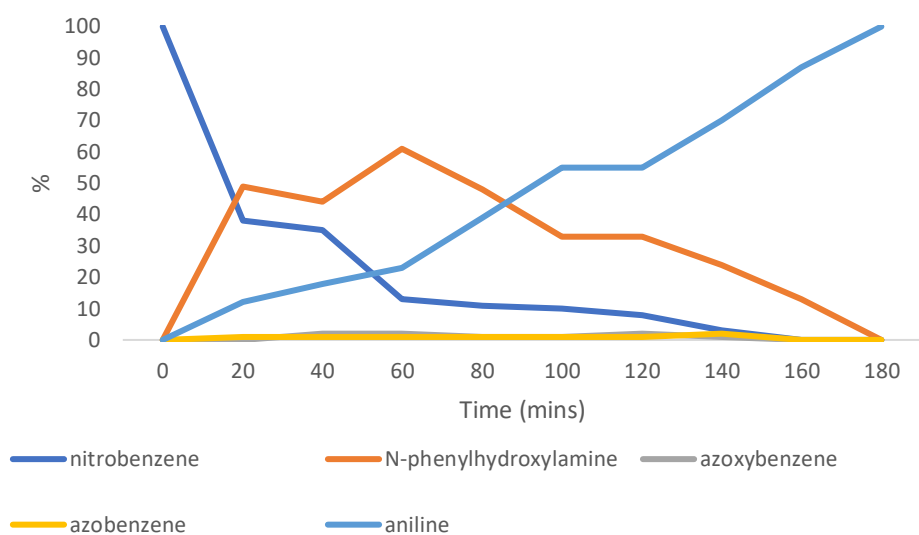


A45 XRD spectrum for PdNP@P(Sty)₃-PEGPIILP (**4.7**).



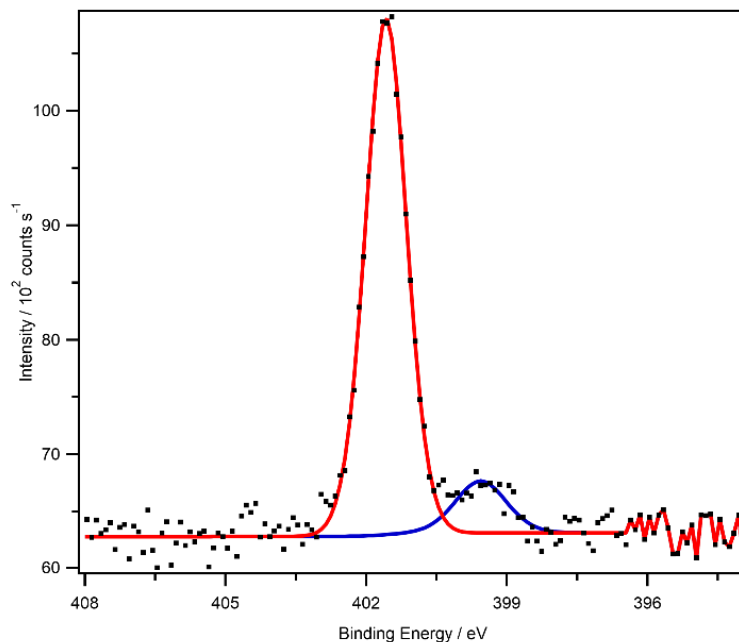
A46 Time-composition profiles for the transfer hydrogenation of nitrobenzene catalysed by **2.13** (top), **4.6** (middle), and **4.7**. Reactions conditions: 1 mmol nitrobenzene, 0.047 mol% catalyst, 2.5 mmol NaBH₄, RT, 2 mL water.



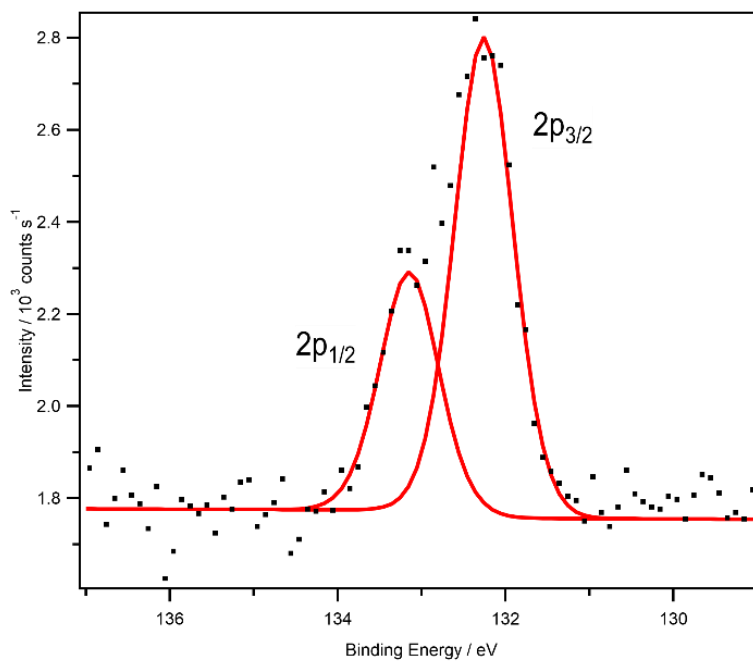


Chapter 5 appendix.

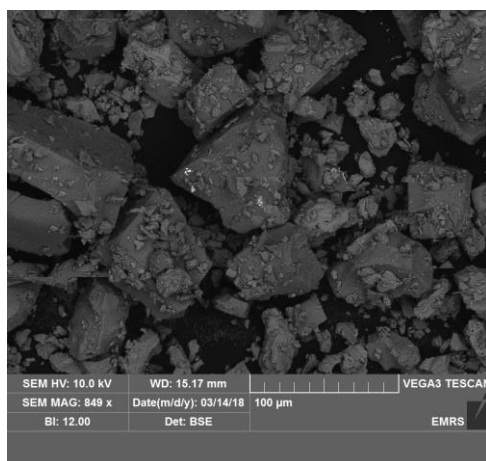
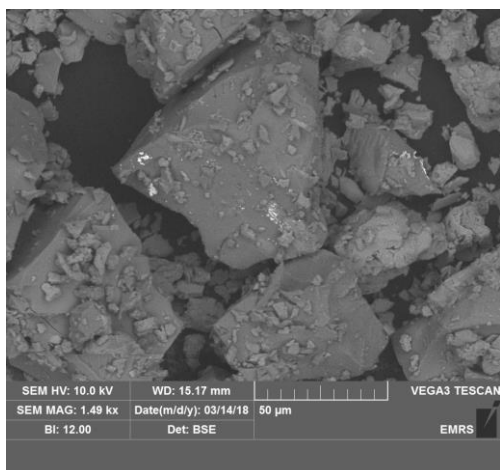
A47 N 1s core level XPS spectrum of $[\text{AuCl}_4]\text{Cl}@ \text{PPh}_2\text{PIILP}$ (**5.3**) referenced to the hydrocarbon C 1s at 284.8 eV.



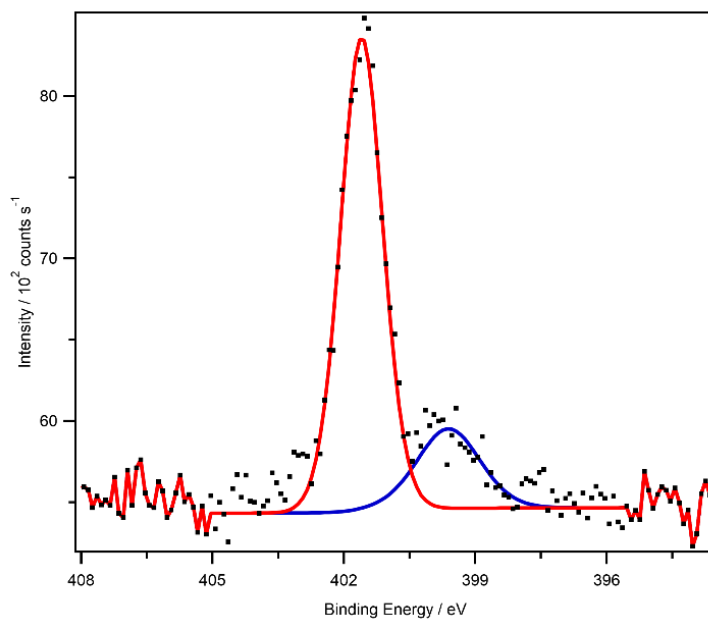
A48 P 2p core level XPS spectrum of $[\text{AuCl}_4]\text{Cl}@ \text{PPh}_2\text{PIILP}$ (**5.3**) referenced to the hydrocarbon C 1s at 284.8 eV.



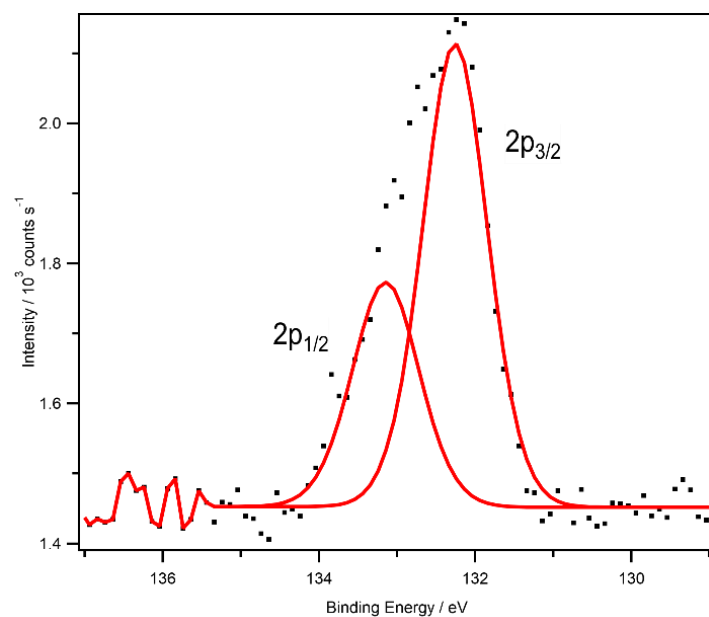
A49 SEM images of freshly prepared $[\text{AuCl}_4]\text{Cl}@P\text{Ph}_2\text{PIILP}$ (**5.3**).



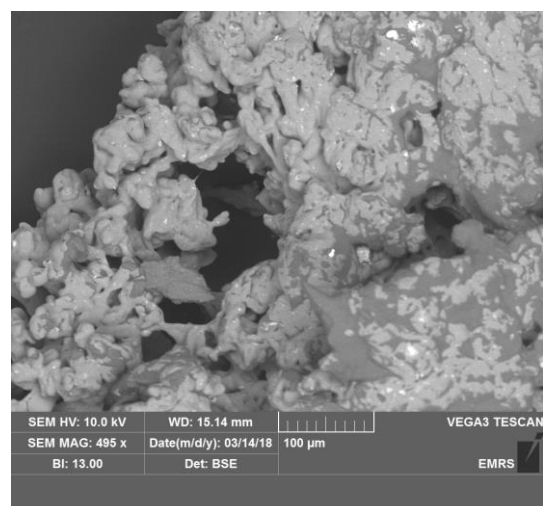
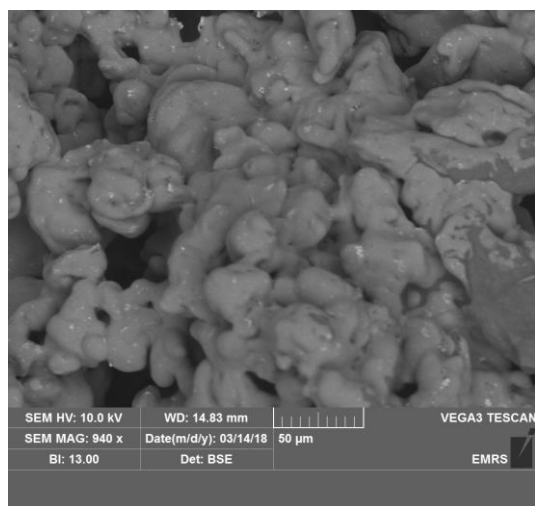
A50 N 1s core level XPS spectrum of $[\text{AuCl}_4]\text{Cl}@P\text{Ph}_2\text{-PEGPIILP}$ (**5.4**) referenced to the hydrocarbon C 1s at 284.8 eV.



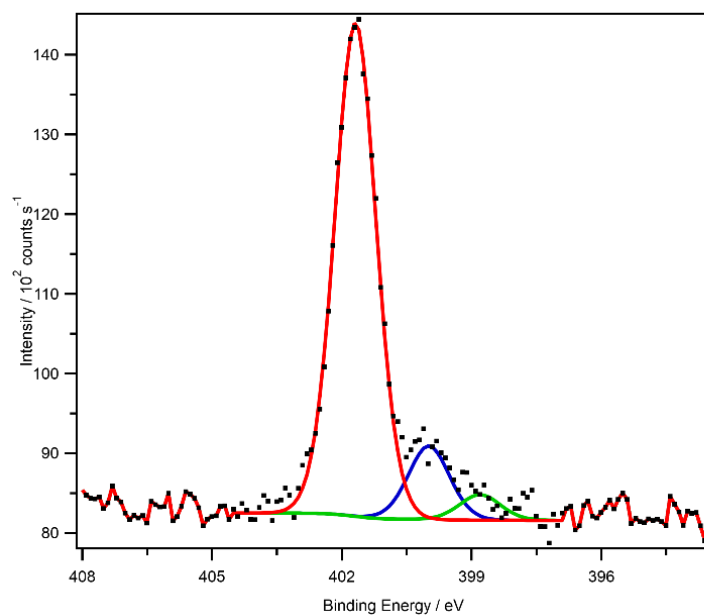
A51 P 2p core level XPS spectrum of $[\text{AuCl}_4]\text{Cl}@P\text{Ph}_2\text{-PEGPIILP}$ (**5.4**) referenced to the hydrocarbon C 1s at 284.8 eV.



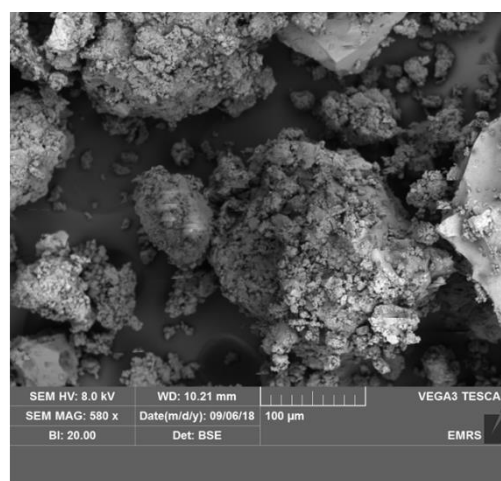
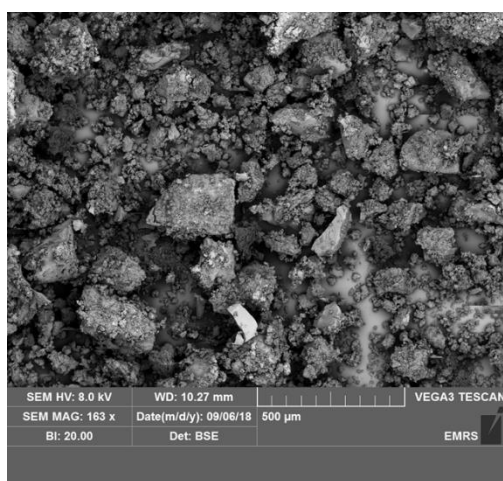
A52 SEM images of freshly prepared $[\text{AuCl}_4]\text{Cl}@P\text{Ph}_2\text{-PEGPIILP}$ (**5.4**).



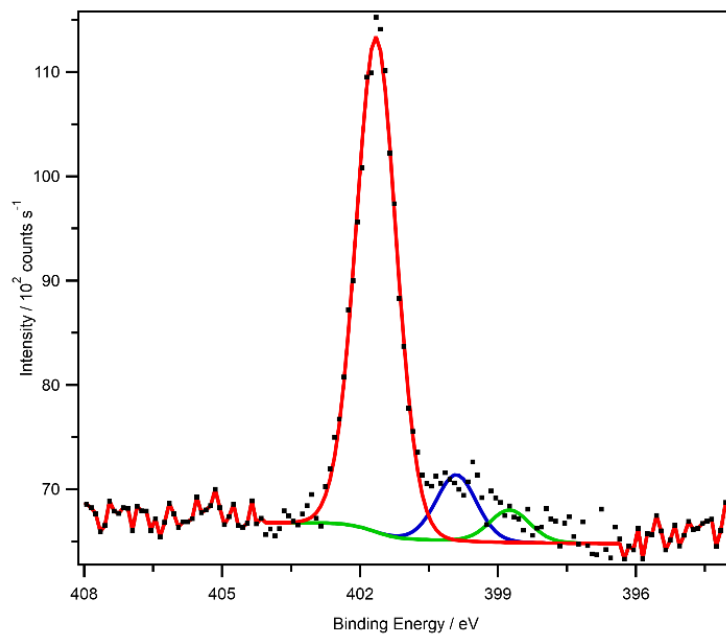
A53 N 1s core level XPS spectrum of $[\text{AuCl}_4]\text{Cl}@ \text{PIILP}$ (**5.5**) referenced to the hydrocarbon C 1s at 284.8 eV.



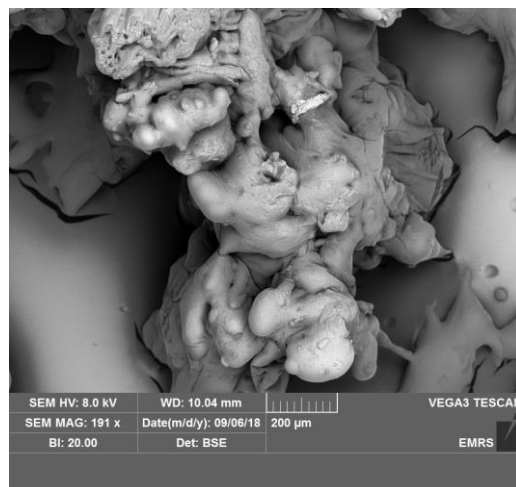
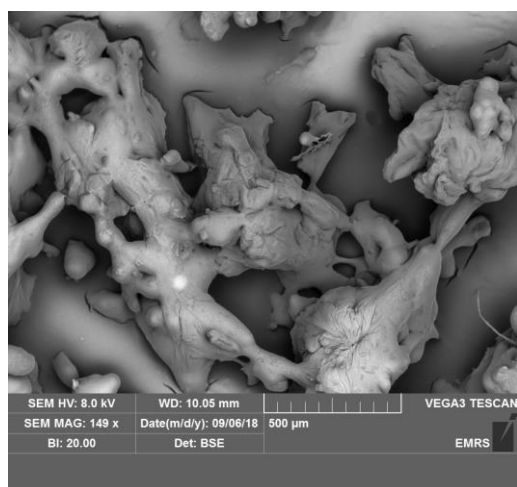
A54 SEM images of freshly prepared $[\text{AuCl}_4]\text{Cl}@ \text{PIILP}$ (**5.5**).



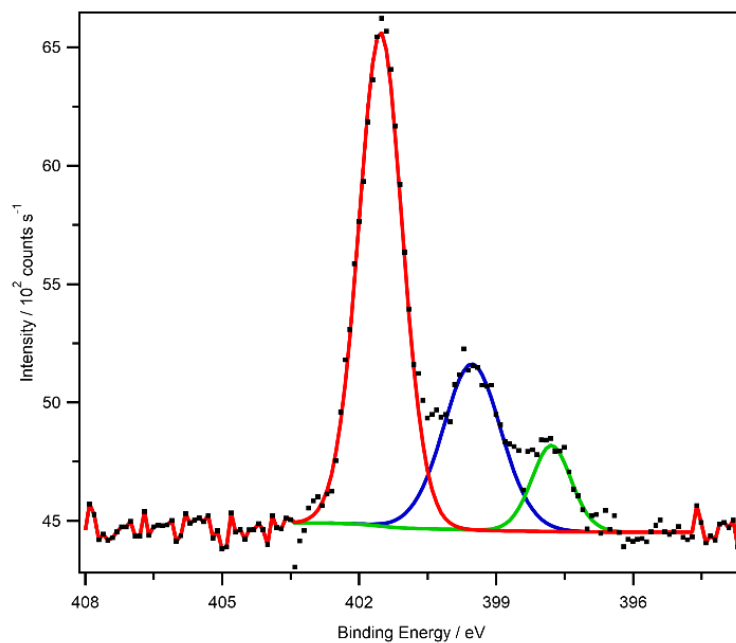
A55 N 1s core level XPS spectrum of $[\text{AuCl}_4]\text{Cl}@ \text{PEGPIILP}$ (**5.6**) referenced to the hydrocarbon C 1s at 284.8 eV.



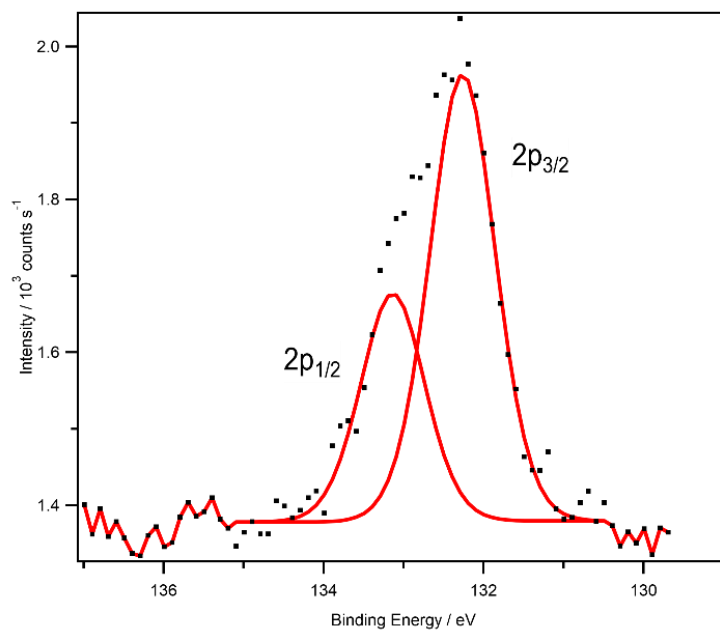
A56 SEM images of freshly prepared $[\text{AuCl}_4]\text{Cl}@ \text{PEGPIILP}$ (**5.6**).



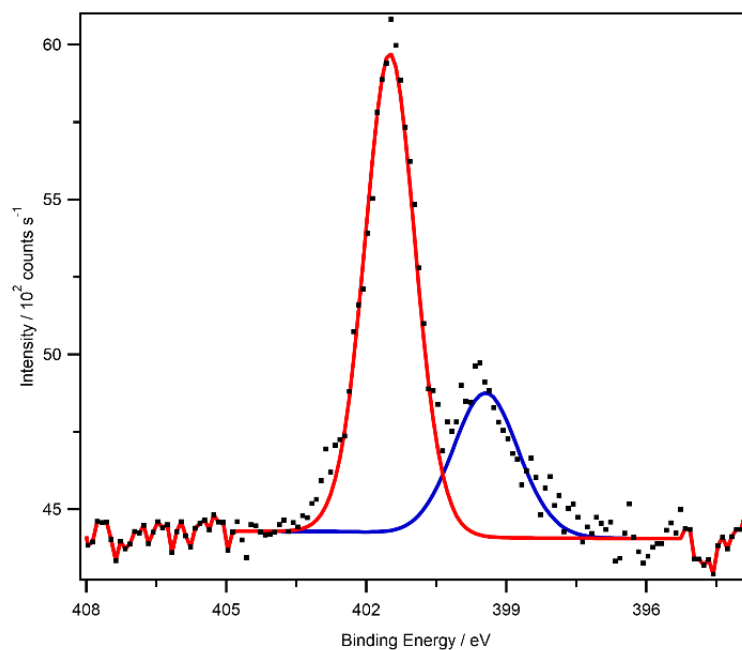
A57 N 1s core level XPS spectrum of AuNP@PPh₂-PIILP (**5.7**) referenced to the hydrocarbon C 1s at 284.8 eV.



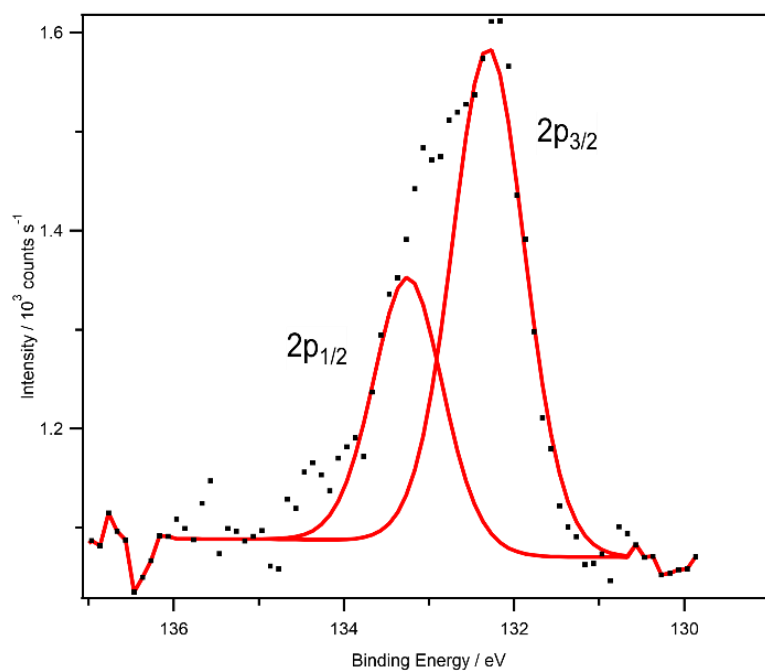
A58 P 2p core level XPS spectrum of AuNP@PPh₂-PIILP (**5.7**) referenced to the hydrocarbon C 1s at 284.8 eV.



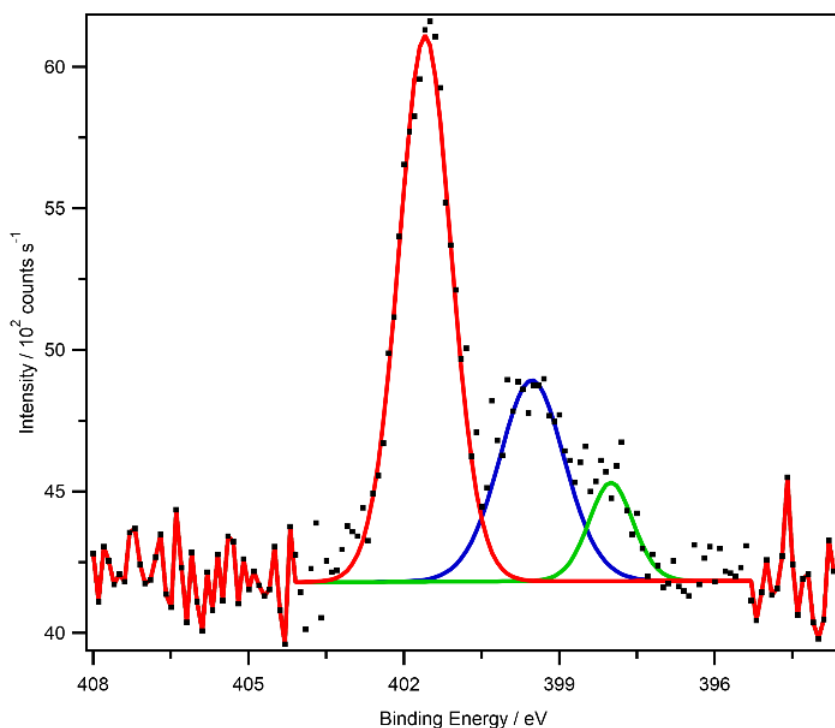
A59 N 1s core level XPS spectrum of AuNP@PEGPPH₂-PIILP (**5.8**) referenced to the hydrocarbon C 1s at 284.8 eV.



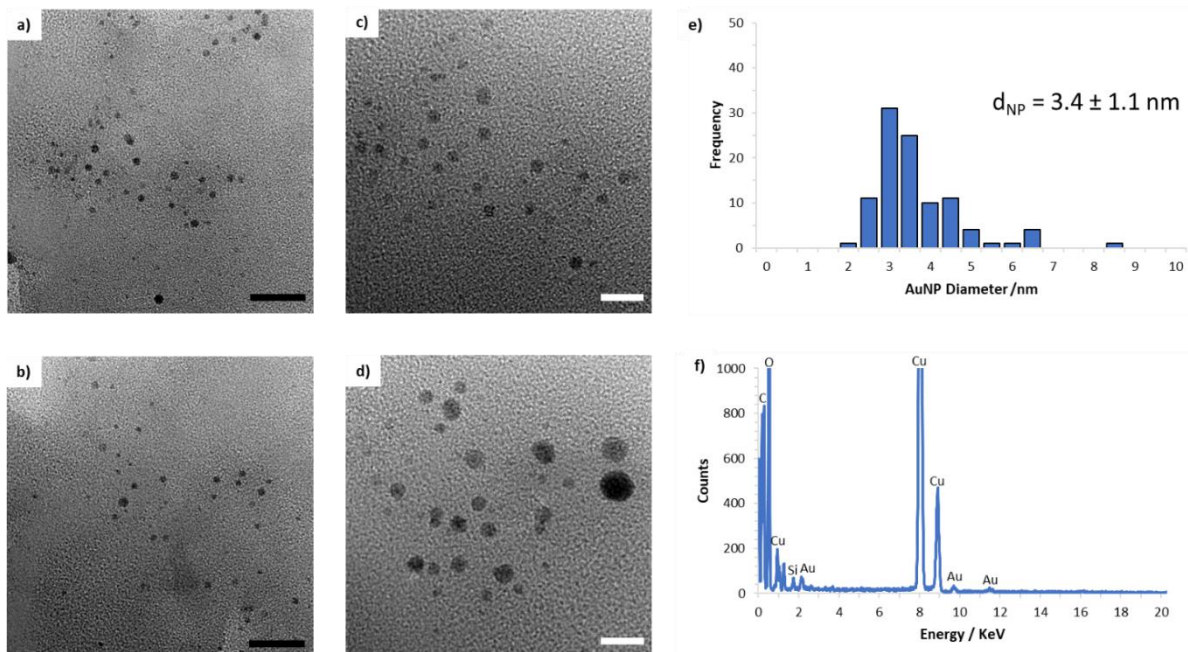
A60 P 2p core level XPS spectrum of AuNP@PPH₂-PEGPIILP (**5.8**) referenced to the hydrocarbon C 1s at 284.8 eV.



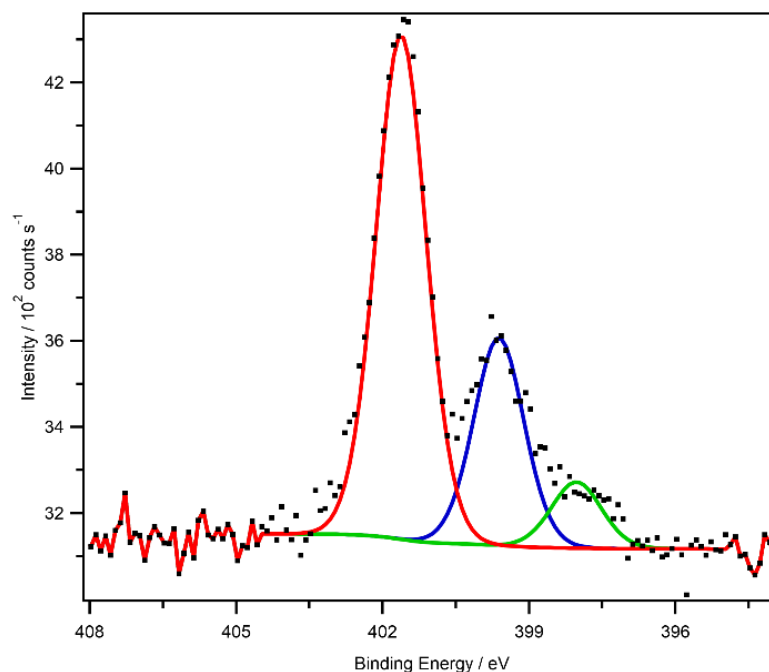
A61 N 1s core level XPS spectrum of AuNP@PIILP (**5.9**) referenced to the hydrocarbon C 1s at 284.8 eV.



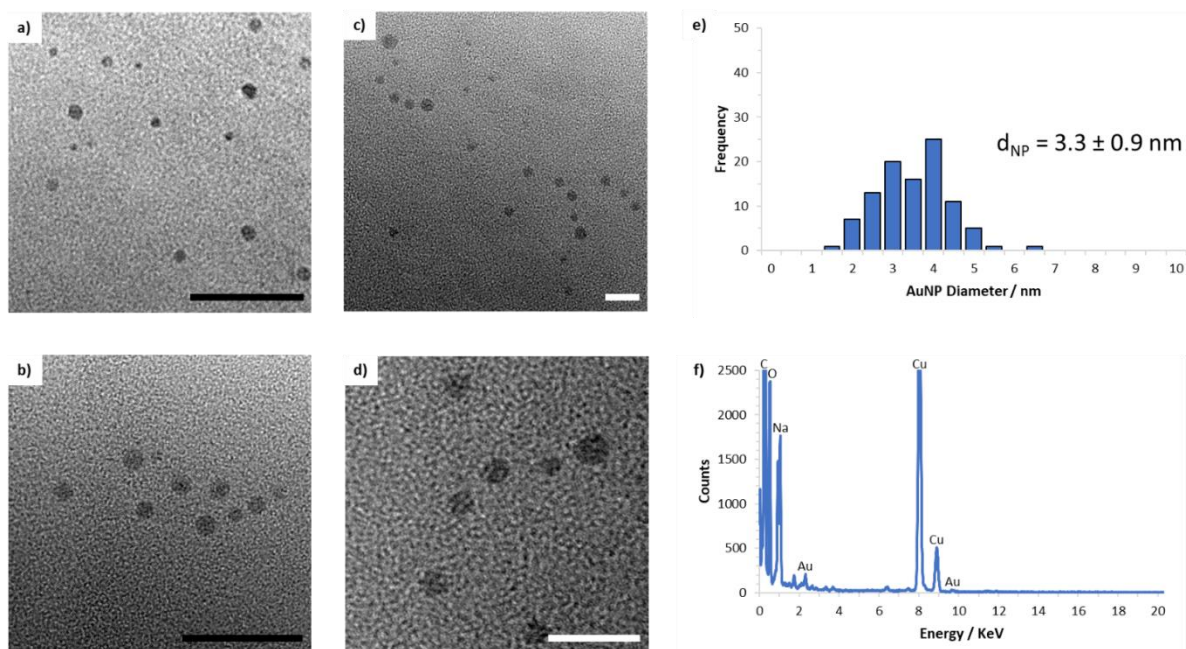
A62 TEM micrographs (a-d) and the associated particle size distribution (e) and EDX spectrum confirming the presence of Au in AuNP@PIILP (**5.9**). Scale bars are 25 nm (black) and 5 nm (white).



A63 N 1s core level XPS spectrum of AuNP@PEGPIILP (**5.10**) referenced to the hydrocarbon C 1s at 284.8 eV.

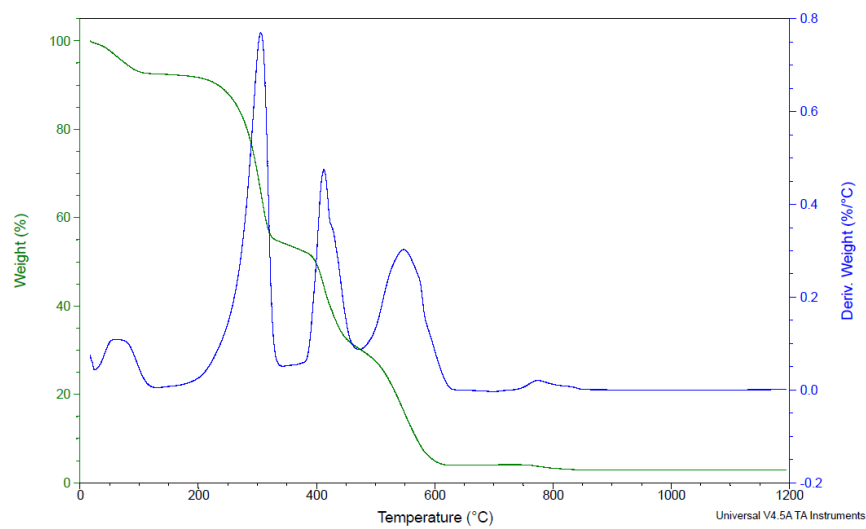


A64 TEM micrographs (a-d) and the associated particle size distribution (e) and EDX spectrum confirming the presence of Au in AuNP@PEGPIILP (**5.10**). Scale bars are 25 nm (black) and 5 nm (white).

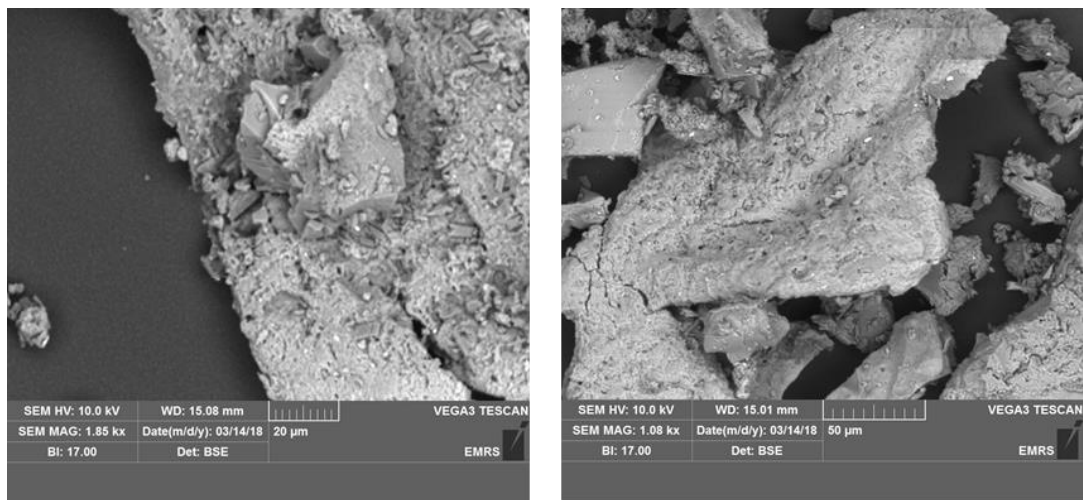


Chapter 6 appendix.

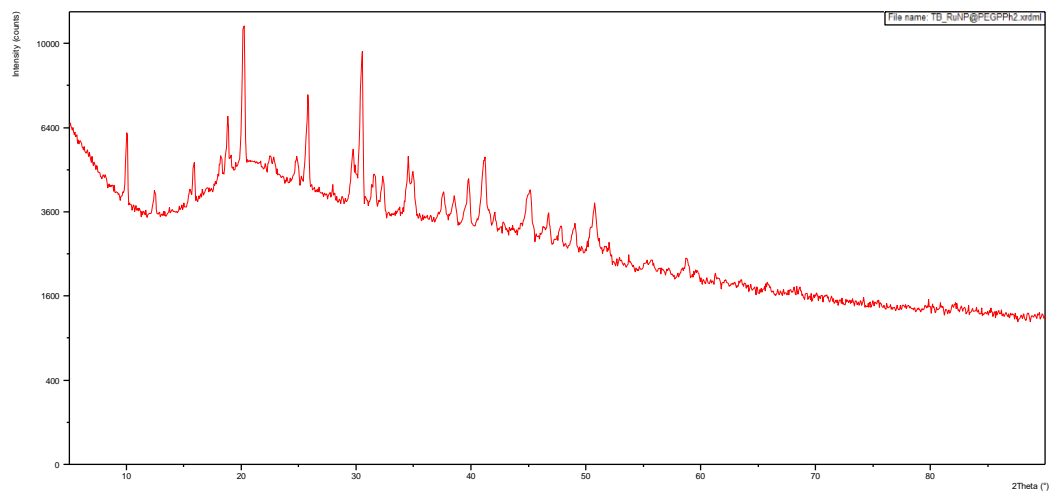
A65 TGA curve for NH₂-PEGPIILP (6.3).



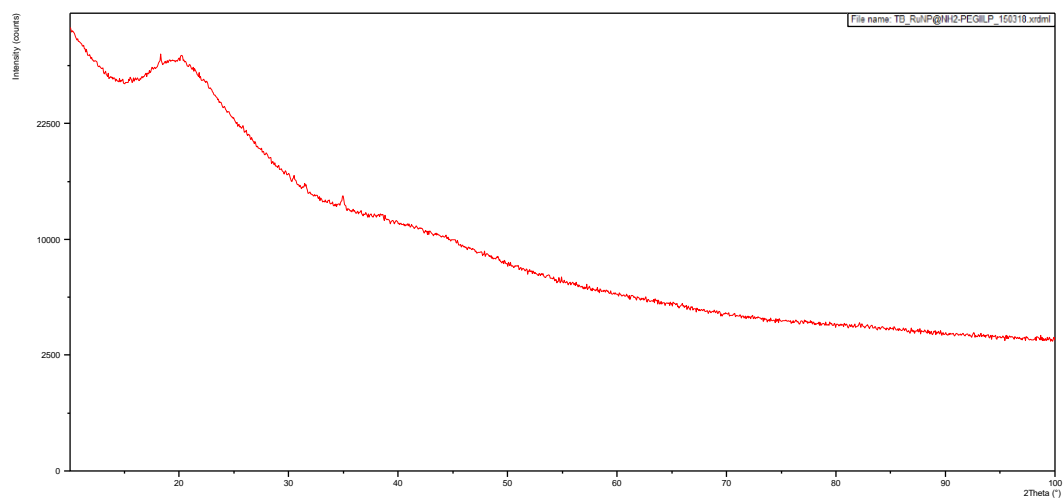
A66 SEM images of NH₂-PEGPIILP (6.3).



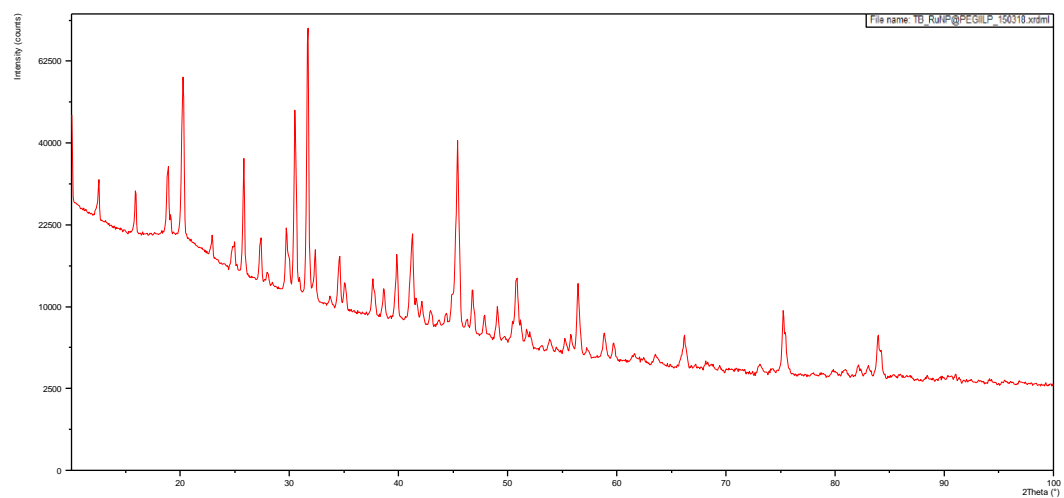
A67 XRD spectrum of RuNP@PPh₂-PEGPIILP (6.5).



A68 XRD spectrum of RuNP@NH₂-PEGPIILP (6.6).



A69 XRD spectrum of RuNP@PEGPIILP (6.7).



A70 solid state ^{13}C NMR spectrum of RuNP@PEGPIILP (6.7).

